

**IRIDIUM COMPLEXES AS HIGHLY ACTIVE
CATALYSTS FOR HYDROGEN ISOTOPE EXCHANGE
AND HYDROGEN BORROWING PROCESSES**

Philippa Kate Owens

Department of Pure and Applied Chemistry

University of Strathclyde

PhD Thesis

2017



Author Declaration

This thesis is the result of the author's original research. It has been composed by the author and has not been previously submitted for examination which has led to the award of a degree.

The copyright of this thesis belongs to the author under the terms of the United Kingdom Copyright Acts as qualified by University of Strathclyde Regulation 3.50. Due acknowledgement must always be made of the use of any material contained in, or derived from, this thesis.

Signed:

A handwritten signature in blue ink, consisting of a stylized 'P' followed by a large, rounded 'D'.

Date: 20th September 2017

Abstract

Over the last several decades, the organic chemistry community has become increasingly reliant upon iridium catalysis, with applications reported across a number of research areas. In recent years, the Kerr group has developed a series of iridium complexes, which were found to be excellent catalysts for hydrogen isotope exchange and olefin hydrogenation processes. The work described within this thesis centres upon the expansion of these catalysts' reactivity in hydrogen isotope exchange, as well as the synthesis and application of a series of novel iridium complexes, designed for use in hydrogen borrowing catalysis.

Chapter one focuses on the development of three efficient and selective methods for hydrogen isotope exchange. Iridium(I) catalysts previously developed within the group have been employed in the successful deuteration of *N*-heterocycles, which represent an important and relatively underexplored class of labelling substrates. The labelling of a large range of indole, pyrrole, and quinoline derivatives is reported, in which the regioselectivity can be controlled through careful choice of *N*-protecting group. Extensive practical and computational mechanistic investigations offered insight into the mechanism of indole C3 labelling, which is believed to proceed *via* an iridium–indoline intermediate.

In chapter two, the design and synthesis of a series of novel unsymmetrical NHC ligands, functionalised with electron donating substituents, is described. The corresponding neutral iridium NHC/halide complexes were prepared, and the steric and electronic properties of the ligands were investigated using a number of techniques. These novel complexes were then tested in the catalysis of hydrogen borrowing processes. Extensive optimisation led to the development of an efficient method for the room-temperature *N*-alkylation of anilines. This methodology was also expanded to include the synthesis of *N*-heterocycles *via* intramolecular C–N bond formation, albeit using more forcing conditions. Lastly, a small series of chiral NHC ligands was designed, and their corresponding iridium complexes prepared and used in a preliminary screening of asymmetric hydrogen borrowing.

Acknowledgements

First and foremost, I would like to thank my supervisor, Professor Billy Kerr, for welcoming me into your research group and for always motivating me to push myself. Your dedication to the training of your students is second to none, and I am endlessly grateful for the opportunities you have given me to develop as a researcher.

I would also like to offer particular thanks to Dr David Lindsay and Dr Laura Paterson, without whom life in the Kerr group would be infinitely more stressful! Your support and advice has been invaluable in directing my research to be as fruitful as possible. I am also grateful to a number of technical staff at Strathclyde, and especially to Craig Irving, who went out of his way to help me with some of the NMR work described in this thesis.

I have made some of my closest friends during my time in the Kerr group, and I could not have got through my PhD were it not for their support, advice, and constant entertainment. Goldie and R-Bo, you taught me the ways of the Kerr group, and kept me amused with your accidental insults and drunk dancing. To my conference buddy and fellow grammar enthusiast Marc, you have been an invaluable source of advice, and your encyclopaedic knowledge of chemistry has intimidated and inspired me in equal measure. Murali, your strange ways have been a constant source of amusement. I will remember our bizarre and often infuriating debates, and will forever flinch when palladium on carbon is mentioned. To Andy Malcolm, your collection of fun facts, your storytelling abilities, and your misadventures in the lab are unforgettable and have made my PhD so much more enjoyable. I doubt anyone I ever work with will be able to replicate our lunchtime debates or post-5pm ramblings! To Richard, at times you have infuriated me like nobody else can, but despite the endless eye-rolling, you have shown immense patience when dealing with my meltdowns, constant chattering, and atrocious knowledge of tadpole anatomy! You are one of my best friends and have cheered me up in my worst moments, and I value that immensely. To Peter, you have been a positive and calming figure in the lab, and I will miss your inquisitive passion for chemistry, strange Hungarian quirks, and irrational hatred for Pizza Hut! Renan, your dedication to your work is hugely admirable, and your patience in dealing with my computational ignorance has been greatly appreciated. John, your drunken misadventures have been a constant source of entertainment, and I hope that head of yours stays intact and full of chemistry. To my lab buddy Liam, you are a positive and helpful influence on the lab,

and our fumehood chats always cheer me up. Gary, you have always kept me entertained and have generously forgiven my many chemistry blonde moments. I'll try to forgive the stabbings in return! To Paul, your Sporce skills are ever impressive, and I remain proud of the three-second typing achievements! Adele, you have made yourself invaluable in the lab and I will miss your rants and, more importantly, your superior drink topping-up skills! Giorgia, you are a constant source of positive energy, and I will never fail to be amused and bemused by your strange ways! Raymond, you are becoming an excellent chemist, and I admire your resistance to being corrupted by the Kerr group influences – but sorry again for the Pasha night!.

Throughout my PhD, the group has welcomed a number of undergraduate students carrying out summer placements or final year projects, who have contributed to several projects while successfully making us all feel old and out of touch. Thanks to Gayle, Declan, Graeme, Rory, Fiona, Calum, Josh, Craig, Gemma, Fabien, Jemma, Harvey, and Kelly, as well as official Kerr group tagalongs Tim and Kirsty.

I was lucky enough to carry out a placement at GSK as part of my PhD program, and I thank Sebastien Campos for his help, encouragement, and for being so generous with the GSK chemical inventory! I am also grateful to Sam Dalton, Jake Bush, and Mike Barker for their assistance during my placement, and to Olivia and Carol for keeping me sane in Stevenage! We have also had a number of GSK students carry out placements in our lab in Glasgow, and I thank Craig, Storm, Chris, and Jason for bringing so much to our research projects and our pub quiz abilities.

I am of course grateful to my friends and family for their support, and especially to my mother Christabel, who has always been a phone call away, and whose own career has always inspired me. I could not have done it without your moral, and occasionally financial, support! Lastly, this thesis is dedicated to my wonderful father John, who cheered me up endlessly and who never failed to see the best in me.

Previously Published Work

Stated below is the work from (or associated with) this thesis that have been accepted for publication in the literature. A number of additional publications are planned for 2017–2018. Authorship is recorded alphabetically or by institution rather than by individual author contribution.

Hydrogen isotope exchange with highly active iridium(I) NHC/phosphine complexes: a comparative counterion study. W. J. Kerr, R. J. Mudd, P. K. Owens, M. Reid, J. A. Brown, S. Campos, *J. Labelled Compd. Radiopharm.* **2016**, *59*, 601–603.

Site-selective Deuteration of *N*-Heterocycles *via* Iridium-catalyzed Hydrogen Isotope Exchange. W. J. Kerr, D. M. Lindsay, P. K. Owens, M. Reid, T. Tuttle, S. Campos, *ACS Catal.* **2017**, *accepted*, DOI 10.1021/acscatal.7b02682.

Abbreviations

Ac	Acetyl
ADMET	Absorption, distribution, metabolism, excretion, and toxicology
aq.	Aqueous
Ar	Aryl
ATR	Attenuated total reflectance
BArF	Tetrakis[3,5-bis(trifluoromethyl)phenyl]borate
Boc	<i>Tert</i> -butoxy carbonyl
Bn	Benzyl
Bu	Butyl
BQC	Biquinoline dicarboxylic acid
Bz	Benzoyl
cat.	Catalyst
cod	Cyclooctadiene
COSY	Correlation spectroscopy
COX	Cyclooxygenase
CPME	Cyclopentyl methyl ether
CNS	Central nervous system
Cy	Cyclohexyl
<i>d</i>	Metal-ligand bond length
d (NMR)	Doublet
DCE	Dichloroethane
DCM	Dichloromethane
<i>d.e.</i>	Diastereomeric excess
DG	Directing group
DFT	Density functional theory
DMAP	<i>N,N</i> -Dimethylaminopyridine
DMF	<i>N,N</i> -Dimethylformamide
DMSO	Dimethylsulfoxide
DOE	Design of Experiments
DOSY	Diffusion-ordered spectroscopy
<i>e.e.</i>	Enantiomeric excess
EI	Electron ionisation

eq.	Equivalents
ESI	Electrospray ionisation
Et	Ethyl
FDA	Food and drug administration
FG	Functional group
g	gram(s)
h	hour(s)
HATU	1-[Bis(dimethylamino)methylene]-1H-1,2,3-triazolo[4,5-b]pyridinium 3-oxid hexafluorophosphate
HIE	Hydrogen isotope exchange
HPLC	High-performance liquid chromatography
HRMS	High resolution mass spectrometry
Hz	Hertz
IAd	1,3-Diadamantylimidazol-2-ylidene
IBn	1,3-Dibenzylimidazol-2-ylidene
IDiPhen	1,3-Bis(diphenylmethyl)imidazol-2-ylidene
IMes	1,3-Bis(2,4,6-trimethylphenyl)imidazol-2-ylidene
ⁱ Pr	<i>iso</i> -Propyl
IR	Infrared
<i>J</i>	Coupling constant
KHMDS	Potassium bis(trimethylsilyl)amide
KIE	Kinetic isotope effect
L	Ligand
LCMS	Liquid chromatography–mass spectrometry
LAC	Ligand acidity constant
m	Milli
<i>m</i> -	<i>Meta</i> -
M (concentration)	mol dm^{-3}
m (nmr)	Multiplet
<i>m/z</i>	Mass-to-charge ratio
<i>m</i> -CPBA	<i>meta</i> -chloroperbenzoic acid
Me	Methyl
Mes	Mesityl
min	Minute(s)

mmi	Membered metallocyclic intermediate
mol	Mole(s)
MP	Melting point
MPV	Meerwein-Ponndorf-Verley
MS	Molecular sieves
MTBE	Methyl <i>tert</i> -butyl ether
NHC	<i>N</i> -Heterocyclic carbene
NME	New molecular entity
NMP	<i>N</i> -Methyl-2-pyrrolidinone
NMR	Nuclear magnetic resonance
NOESY	Nuclear Overhauser effect spectroscopy
NSI	Nanospray ionisation
<i>o</i> -	<i>Ortho</i> -
OAc	Acetate
OTf	Triflate
<i>p</i> -	<i>Para</i> -
PES	Potential energy surface
Ph	Phenyl
PHOX	Phosphinooxazoline
Piv	Pivaloyl
ppm	Part(s) per million
PVP	Polyvinylpyrrolidone
Py	Pyridine
Pym	Pyrimidine
q (NMR)	Quartet
<i>r</i>	Radius
R	Substituent
RedAl	Sodium bis(2-methoxyethoxy)aluminumhydride
RuNP	Ruthenium nanoparticles
S _E Ar	Electrophilic aromatic substitution
SIMes	1,3-Bis(2,4,6-trimethylphenyl)imidazolin-2-ylidene
r.t.	Room temperature
t	Time
t (NMR)	Triplet

${}^t\text{Am}$	<i>tert</i> -Amyl
TBAF	Tetra- <i>n</i> -butylammonium fluoride
${}^t\text{Bu}$	<i>tert</i> -Butyl
<i>tert</i>	Tertiary
temp.	Temperature
TEP	Tolman electronic parameter
THF	Tetrahydrofuran
TLC	Thin layer chromatography
TOF	Turnover frequency
Tol	Tolyl
TON	Turnover number
TPAP	Tetrapropylammonium perruthenate
TS	Transition state
UV	Ultra-violet
Vis	Visible
5-HT	5-Hydroxytryptamine
δ	Chemical shift
μ	Micro
$\% V_{\text{bur}}$	Percentage buried volume

Contents

Author Declaration.....	ii
Abstract.....	iii
Acknowledgements.....	iv
Previously Published Work.....	vi
Abbreviations.....	vii
Contents	xi
Chapter 1: Selective Deuteration of N-Heterocycles.....	1
Introduction.....	1
Hydrogen Isotope Exchange	2
Transition Metal Catalysis of Hydrogen Isotope Exchange	4
Crabtree's Catalyst: Use in HIE and Modifications.....	7
Phosphines as Ligands	14
N-Heterocyclic Carbenes as Ligands.....	16
Kerr Group Investigations into HIE.....	19
Isotopic Labelling of N-Heterocycles	26
Proposed Work.....	34
Results and Discussion	36
C2 Labelling of N-Protected Indoles	36
C3 Labelling of N-Protected Indoles	56
N-Oxide-directed Labelling of N-Heterocycles.....	79
Conclusions.....	88
Future Work	91
Experimental.....	94
General Information.....	94
General Procedures	95
C2 Labelling of N-Protected Indoles	98

C3 Labelling of N-Protected Indoles	125
N-Oxide-directed Labelling of N-Heterocycles.....	155
Computational Studies	171
General Computational Details	171
Details of Optimised Structures	172
Summary of Calculated Energies.....	177
References.....	180
Chapter 2: Design and Synthesis of Novel Iridium(I) Catalysts for C–N Bond Formation via Hydrogen Borrowing	189
Introduction.....	189
Transfer Hydrogenation	189
Iridium Catalysis of Transfer Hydrogenation: Reduction of Carbonyls	192
Iridium Catalysis of Transfer Hydrogenation: Oxidation of Alcohols	201
C–C and C–N Bond Formation via Hydrogen Borrowing.....	205
Iridium Catalysis of Asymmetric Transfer Hydrogenation.....	210
Proposed Work.....	218
Results and Discussion	220
Design and Synthesis of Novel Ligands and Complexes.....	220
N-Alkylation of Amines via Hydrogen Borrowing	232
Synthesis of N-Heterocycles via Hydrogen Borrowing.....	238
Ligand Design for Asymmetric Transfer Hydrogenation	256
Conclusions.....	267
Future Work	269
Experimental.....	272
General Information.....	272
General Procedures	273
Design and Synthesis of Novel Ligands and Complexes.....	278
N-Alkylation of Amines via Hydrogen Borrowing	307

Synthesis of N-Heterocycles via Hydrogen Borrowing.....	320
Ligand Design for Asymmetric Transfer Hydrogenation	341
References.....	359

Chapter 1: Selective Deuteration of N-Heterocycles

Introduction

After an alarming decline in new drug approvals during the early 2000s, the number of new molecular entities (NMEs) approved by the FDA has risen dramatically over the last ten years.^{1,2} Approvals hit a 20-year high in 2015, with 45 drugs gaining approval compared to 22 in 2006. This improvement in productivity, while promising, is offset by the enormous financial burdens placed on the pharmaceutical industry when bringing new drugs to the market. Recent estimates put global R&D expenditure in 2016 at \$154 billion, with the average total cost per approved drug coming in at \$2.56 billion.^{3,4}

A large proportion of this staggering expenditure can be attributed to the lengthy drug development process, which regularly takes 10–15 years and during which failure is common. A recent report showed that from 2006–2015, less than 10% of drugs entering Phase I clinical trials progressed to final approval.⁵ One of the key challenges for medicinal chemists, therefore, is identifying any problems with the pharmacokinetic properties of a potential drug molecule as early in the drug discovery process as possible.

A key method for establishing the pharmacokinetic properties of a drug is the use of adsorption, distribution, metabolism, excretion, and toxicology (ADMET) studies, and efficient determination of these properties can dramatically reduce the overwhelming costs and high attrition rates that currently plague the pharmaceutical industry. Isotopic labelling plays a key role in the drug development process and offers an unparalleled insight into the metabolic pathways of a potential drug molecule.⁶ In recent years, the increase in sensitivity of NMR spectroscopic techniques and the widespread availability of high resolution mass spectrometry have provided new methods with which we are able to monitor the path of an isotopic label throughout the body and easily identify drug metabolites, even in complex samples such as blood or urine.

The kinetic properties offered by heavy hydrogen isotopes can further be exploited in the synthesis of deuterated drugs.^{7,8} The increased strength of the C–D bond means a deuterated drug molecule can have a slower rate of metabolism than its protio- analogue. Consequently, an improvement in the drug's half-life or a decrease in the required dose can be achieved

with minimal alteration of the drug's other properties. As far back as 1961, the pharmacokinetic profiles of deuterated drugs have been investigated,⁹ and a number are currently in clinical trials. April 2017 saw the FDA approval of Deutetrabenazine **1**, a Teva compound sold as Austedo.¹⁰ **1** is a deuterated analogue of Tetrabenazine, a popular drug which treats the symptoms of Huntington's disease. The relatively short half-life of Tetrabenazine means that multiple doses a day are often required. In clinical trials, Deutetrabenazine demonstrated comparable efficiency to Tetrabenazine in treating chorea, the involuntary movements often caused by Huntington's disease, and its slower rate of metabolism means that less frequent doses are required.^{11,12}

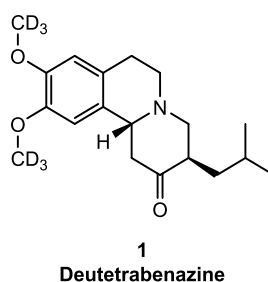


Figure 1.1

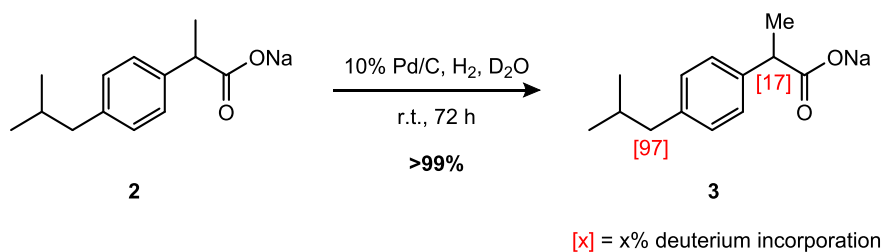
Traditional methods for the incorporation of an isotope, such as naturally-occurring ²H or ¹³C, or radioactive ³H or ¹⁴C, involve the use of isotopically-enriched starting materials in the drug synthesis. While such materials are commercially available, they often present significant extra costs or require additional synthetic steps. Moreover, any low yielding steps in the synthetic route represent a substantial loss of expensive labelled compounds to purification and waste. Given the clear incentives for avoiding such lengthy procedures, focus over the last few decades has turned to developing methods by which deuterium and tritium can be incorporated in the late stages of drug synthesis.

Hydrogen Isotope Exchange

Several of the early methods reported for the incorporation of radioactive labels into drug compounds involved the introduction of a ¹⁴C label, for which the only original source is barium ¹⁴C-carbonate.¹³ Evidently, the synthesis of even simple labelled aromatic building blocks would therefore present a massive challenge. Instead, hydrogen isotope exchange (HIE) emerged as a convenient alternative, allowing a hydrogen atom already present in a molecule to be exchanged for a heavier isotope. The advantages were twofold: deuterium

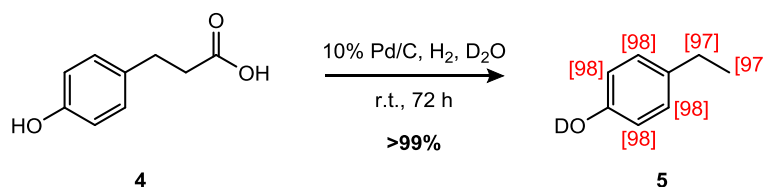
and tritium are significantly cheaper and more readily accessible than carbon isotopes, and the hydrogen isotope exchange procedure meant that incorporation could occur at the late stages of a synthesis and without having to rely upon labelled starting materials.

Perhaps unsurprisingly, several methods for the catalysis of hydrogen isotope exchange have grown from commonly used hydrogenation techniques. A prime example of this is the use of Pd/C, which, in combination with deuterium or tritium gas, was successfully used as a heterogeneous catalyst system for isotopic labelling for several years. For example, elegant work published by Sajiki and co-workers demonstrated high selectivity for benzylic labelling in aromatic compounds, using D₂O and H₂ to generate D₂ *in situ*, with an impressive 97% deuterium incorporation observed at the benzylic position in ibuprofen salt **2** (Scheme 1.1).¹⁴



Scheme 1.1

Despite several attractive examples of Pd/C-catalysed HIE being reported, there remained some key drawbacks to these methods. The use of harsh conditions, originally developed for use in hydrogenation methodology, means that regioselectivity can often be poor; moreover, reduction is often a competing side-reaction. As shown in Scheme 1.2, Matsubara and co-workers reported that the deuteration of substituted phenol **4** proceeded with labelling of all sites in the molecule as well as decarbonylation of the carboxylic acid functionality.¹⁵

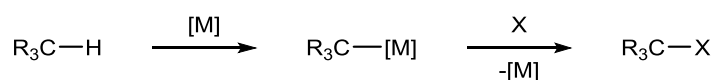


Scheme 1.2

Transition Metal Catalysis of Hydrogen Isotope Exchange

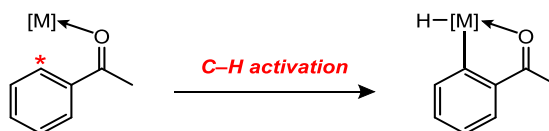
Over the last few decades, homogeneous transition metal catalysis has emerged as one of the most widely used methods for hydrogen isotope exchange. In comparison to earlier labelling methods, metal-catalysed processes typically offer mild reaction conditions and high functional group tolerance. As mentioned previously, one of the key advantages of hydrogen isotope exchange is the ability to install a label in the late stages of a compound's synthesis. It is vital, therefore, that any functional groups already present must remain intact during the labelling process, which is often not the case with many acid- or base-catalysed methods.

By far the most common approach to homogenous transition metal-catalysed HIE is directed *ortho*-labelling of substituted aromatic compounds. This process relies on a 'C–H activation' step, involving the cleavage of a C–H bond and subsequent formation of a much more reactive C–[M] bond (Scheme 1.3), which is poised for reaction with a source of deuterium or tritium. As an additional advantage from a pharmaceutical perspective, the ability to introduce a label at a normally inert C–H position means that it is more likely to remain intact throughout metabolism without being subject to uncatalysed exchange.



Scheme 1.3

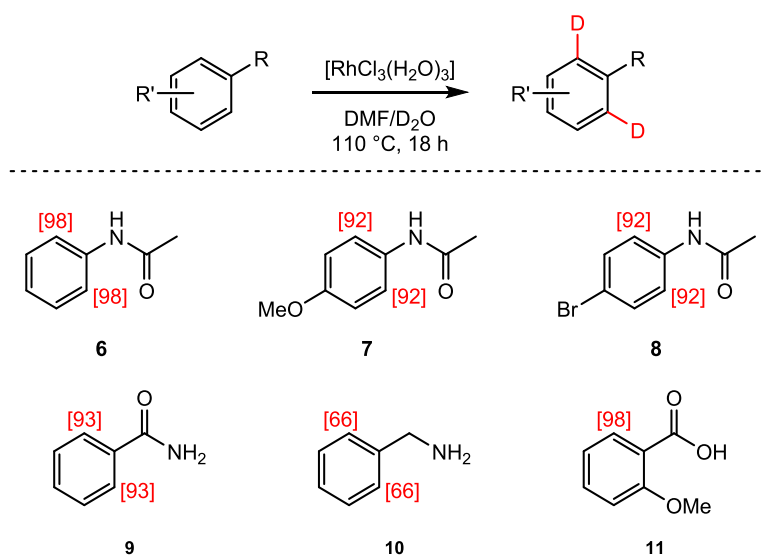
The ubiquity of C–H bonds means that selectivity is difficult to control, with many organic molecules having multiple potential functionalisation sites; approaches must therefore be developed to overcome this problem and allow the selective activation of one C–H bond in the presence of others. There are several key strategies that have been adopted to achieve selectivity in catalytic C–H bond activation processes.¹⁶ One of the most commonly used is directing group control, where a donor group, such as a nitrogen or oxygen atom, in the substrate is able to coordinate to the metal centre, resulting in cyclometallation *via* C–H activation, which dictates the site of C–H bond activation (Scheme 1.4).



Scheme 1.4

Seminal work by Garnett and co-workers demonstrated that $[\text{RhCl}_3(\text{H}_2\text{O})_3]$ was a suitable catalyst for hydrogen isotope exchange,¹⁷ and it quickly became one of the industry standards. Undoubtedly, one of the key early examples of homogenous transitional metal-catalysed HIE came from Lockley and co-workers, who in 1984 reported the use of $[\text{RhCl}_3(\text{H}_2\text{O})_3]$ in the *ortho*-labelling of carboxylic acids, amides, and amines.^{18,19}

A selection of Lockley's key results are shown in Scheme 1.5. Using DMF at 110 °C and D_2O as the deuterium source, a range of aromatic acids, amides, amines and anilides were labelled with up to 98% incorporation. Notably, highly regioselective *ortho*-exchange was observed in all cases. In contrast, Garnett's work with rhodium trichloride, while pioneering, had been completely non-selective. Lockley postulated that the presence of a carbonyl functional group in all the *ortho*-labelled substrates was responsible for the high selectivity observed. It was postulated that one of the lone pairs of electrons on the carbonyl oxygen atom was able to complex to the metal centre before C–H insertion, thus acting as a directing group and “steering” the rhodium atom to the desired C–H position.



Scheme 1.5

For several years, $[\text{RhCl}_3(\text{H}_2\text{O})_3]$ remained a mainstay of the isotopic labelling community, with the scope of catalysis being expanded to include benzyl amines and tetrazoles.^{13,19} This methodology was also applied to the tritium labelling of drug compounds such as Pentamidine **12** and Necrodomil sodium **13** with complete regioselectivity being observed (Figure 1.2).^{20,21}

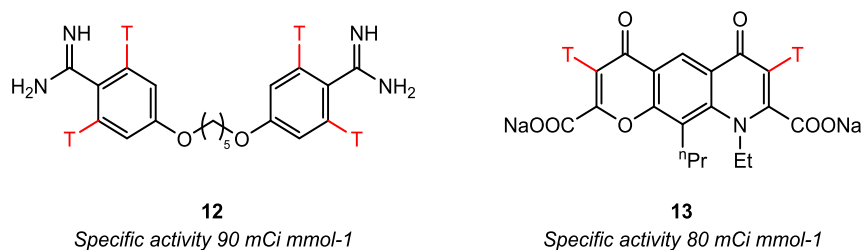
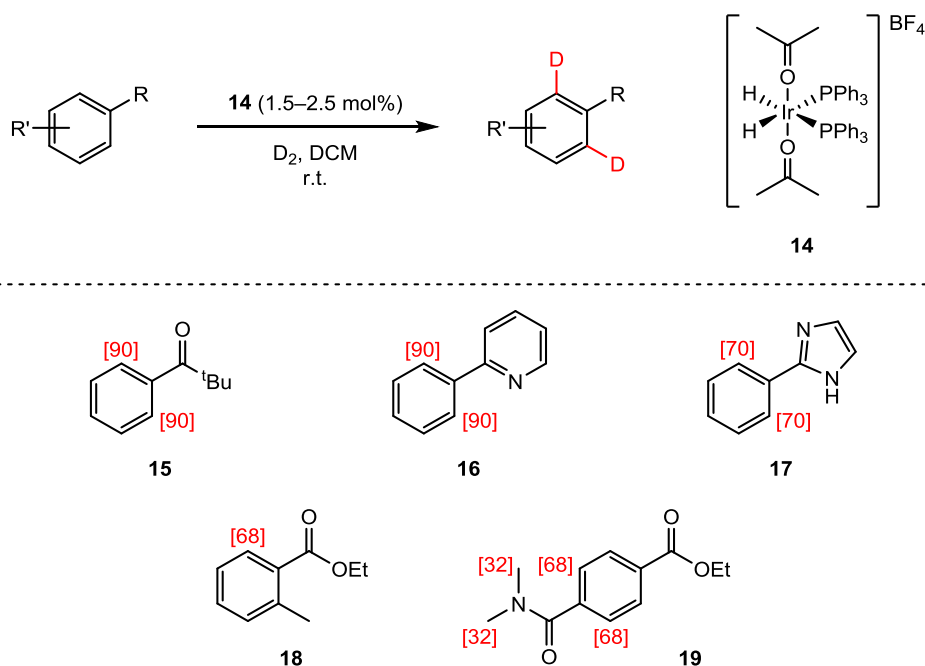


Figure 1.2

In the 1980s and 1990s, cationic iridium complexes emerged as excellent C–H activation catalysts,^{22,23} and as such, the field of homogeneous hydrogen isotope exchange has since become increasingly dominated by iridium catalysis. In 1992, a key paper published by Heys reported the use of 18-electron complex **14** as a successful HIE catalyst, with D₂ gas used as the deuterium source instead of D₂O.²⁴ As shown in Scheme 1.6, the labelling of a wide range of substrates was achieved, with oxygen or nitrogen donor groups being used as coordinating handles to direct HIE at the *ortho*-positions. Interestingly, the electronic and steric properties of the substrate were not seen to play a large role in labelling efficacy.



Scheme 1.6

It quickly became apparent that this early work into iridium catalysis of HIE offered several advantages over the previously reported systems involving rhodium catalysis. Firstly, the reaction conditions used by Heys were significantly milder than those reported by Lockley.

Labelling reactions were carried out at room temperature in dichloromethane, as opposed to the 110 °C used previously. Additionally, complex **14** could be employed at a catalyst loading of only 2 mol%, compared to the 50 mol% of rhodium chloride required under Lockley's conditions.

In the following years, Heys and co-workers demonstrated that the scope of labelling with **14** could be further expanded across a range of ethyl benzoate substrates.²⁵ A series of rate studies showed that substrates containing *para*-substituents underwent HIE faster than their unsubstituted analogues, and when similar studies were conducted with monosubstituted benzophenones, labelling on the *para*-substituted aryl ring occurred faster than on the unsubstituted ring. Since both sites are accessed by the same coordinating handle, Heys concluded that substrate coordination could not be the rate-determining step of the reaction; instead, it was postulated that some part of the C–H insertion process was rate-determining.

Crabtree's Catalyst: Use in HIE and Modifications

As discussed previously, many examples of transition metal catalysis of HIE came from commonly used hydrogenation techniques. Since initial reports published in 1977, one of the industry standards for alkene hydrogenation had been Crabtree's catalyst, **20** (Figure 1.3).^{26,27} With the emergence of iridium complexes as key tools for hydrogen isotope exchange catalysis, Hesk and co-workers investigated the use of **20** in labelling chemistry.²⁸

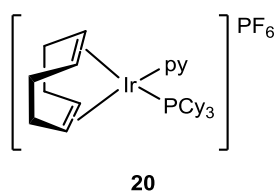
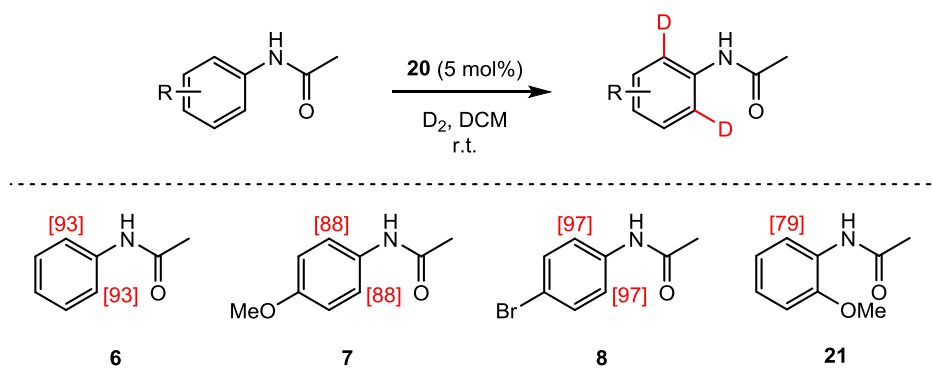


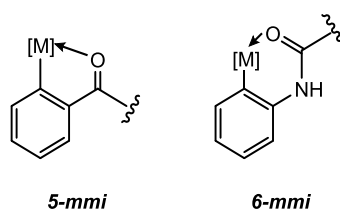
Figure 1.3

Hesk reported high levels of deuterium incorporation in a range of substituted acetanilides (Scheme 1.7). This was a notable expansion to the substrate scope analysed by Heys and co-workers, in that the carbonyl oxygen used to direct insertion in the acetanilides is 5 bonds away from the C–H bond undergoing exchange.



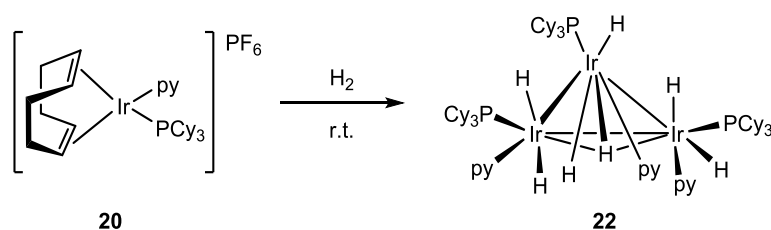
Scheme 1.7

The concept of intermediates varying in ring size had been widely accepted by the mid-1990s, with several researchers having proposed that directed C–H activation could, depending on substrate choice, occur with the formation of both 5- or 6-membered metallocyclic intermediates (*mmi*) (Scheme 1.8).



Scheme 1.8

Despite the widespread use of Crabtree's catalyst **20** in both hydrogenation and hydrogen isotope exchange chemistry, there remained some key issues with this complex.²⁹ One general drawback is the tendency of **20** to undergo thermal deactivation, forming iridium trimer species **22** (Scheme 1.9). **22** is catalytically inactive, and its formation under reaction conditions removes active iridium from the system, effectively poisoning the catalyst. As such, reactions employing **20** often require stoichiometric or superstoichiometric catalyst loadings.



Scheme 1.9

In order to combat the issues encountered with thermally inactive catalyst **20**, Heys designed complexes **23** and **24**, bearing two phosphine ligands (Figure 1.4).³⁰ It was thought that the presence of a bulkier ligand set could prevent trimerisation and therefore improve catalytic activity.

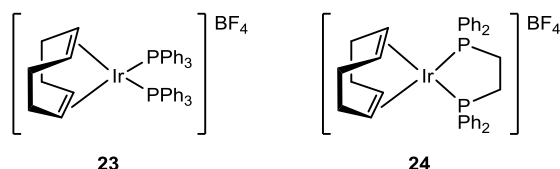
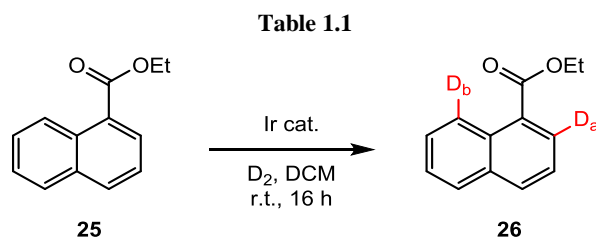


Figure 1.4

When **23** and **24** were employed as catalysts in the deuteration of ethyl 1-naphthoate **25**, levels of incorporation were considerably higher than for reactions carried out with Crabtree's catalyst **20** (Table 1.1). Even at catalyst loadings of 50 mol%, no more than 50% deuterium incorporation was observed with **20**. Notably, complex **24**, containing a bidentate phosphine ligand, was found to induce labelling at the C8 position (*via* a 6-mm) as well as the C2 position, *via* the more common 5-mm. When the substrate scope was further expanded, it was consistently observed that bidentate phosphine ligands were able to catalyse labelling of substrates which would proceed *via* a 6-membered metallocyclic intermediate, whereas monodentate phosphine complexes, including Crabtree's catalyst, showed complete regioselectivity for substrates requiring a 5-membered metallocyclic intermediate. Heys proposed that this trend implied that selectivity could be dependent on the steric bulk around the metal centre, with larger ligand sets favouring a 5-membered intermediate, and bidentate ligands, in which the two phosphine ligands are forced into a *cis*-arrangement, favouring the larger 6-membered intermediate.



Entry	Catalyst	Catalyst Loading / mol%	%D _a	%D _b
1	23	2.2	90	0
2	24	2.5	54	35
3	24	13	79	54
4	20	2.5	22	0
5	20	50	55	0

The concept of intermediates varying in ring size had been widely accepted by the mid-1990s, with several researchers having proposed that directed C–H activation could, depending on substrate choice, occur with the formation of both 5- or 6-membered metallocyclic intermediates (mmi) (Figure 1.5).

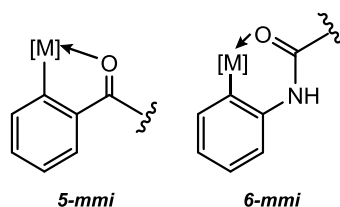
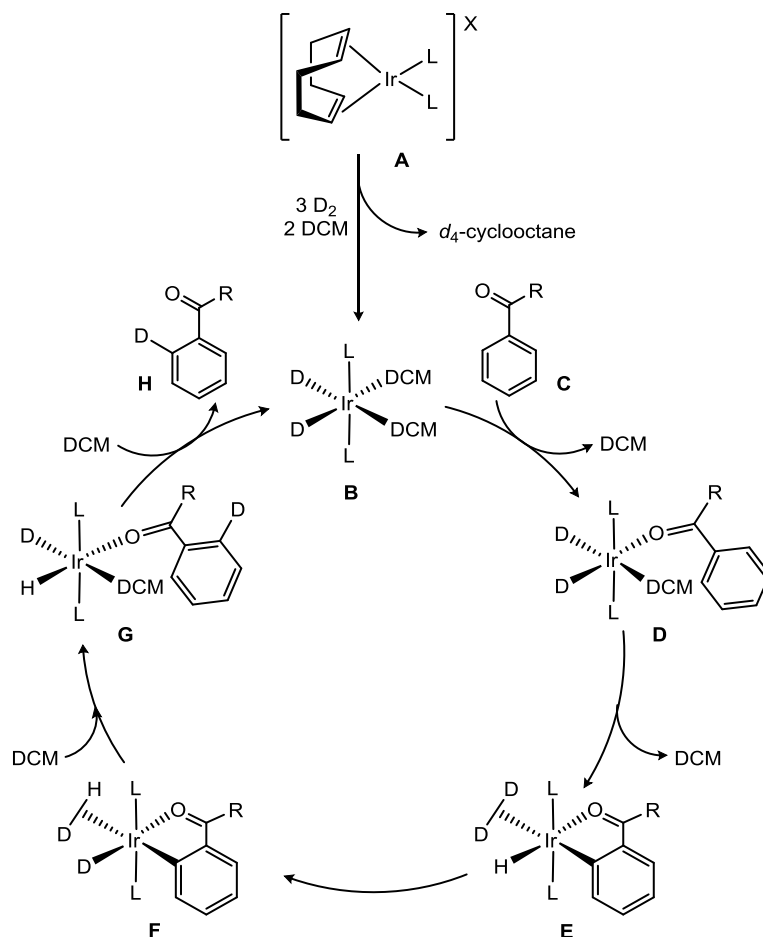


Figure 1.5

Upon consideration of these proposals, as well as the selectivity observed with mono- and bidentate phosphine ligands, Heys proposed a catalytic cycle through which Ir-mediated hydrogen isotope exchange could proceed (Scheme 1.10).³⁰ When deuterium gas is introduced to precatalyst **A**, the cyclooctadiene ligand is lost as cyclooctane-*d*₄ to generate complex **B**, which is believed to be the active species. The ligands, L, are assumed to occupy positions *trans*- to one another. S can represent either a loosely coordinated molecule of solvent or D₂. One solvent molecule is displaced upon complexation of substrate **C**'s donor group to the iridium centre, generating **D**. At this point, oxidative addition of the iridium centre into the nearby C–H bond is believed to occur, with concomitant formation of complexed deuterium from the two deuteride ligands to form intermediate **E**. Hydride

fluxionality is a key step in the proposed catalytic cycle, and generates compound **F**, bringing the iridium–carbon bond and iridium–deuteride bond into a *cis*-arrangement.³¹ These two groups are now suitably oriented for C–D bond-forming reductive elimination to occur, forming species **G**. Finally, dissociation of product **H** regenerates active species **B**.



Scheme 1.10

Heys proposed that the preference observed for the formation of a 5-mmi with complexes such as **23** was due to steric clash between ligand and substrate when a 6-mmi is formed (Figure 1.6). The use of a bidentate ligand brings the two phosphines *cis*- to one another, relieving some of the strain and allowing more space for the formation of a 6-mmi.

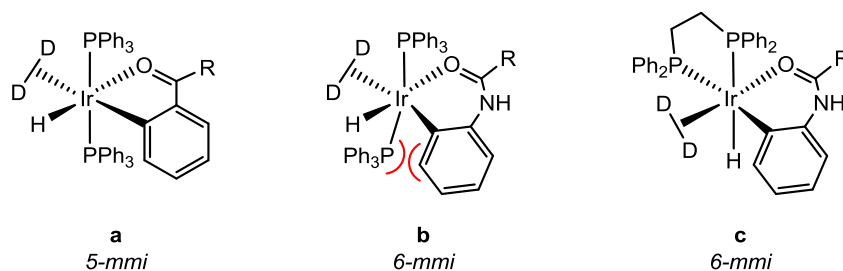
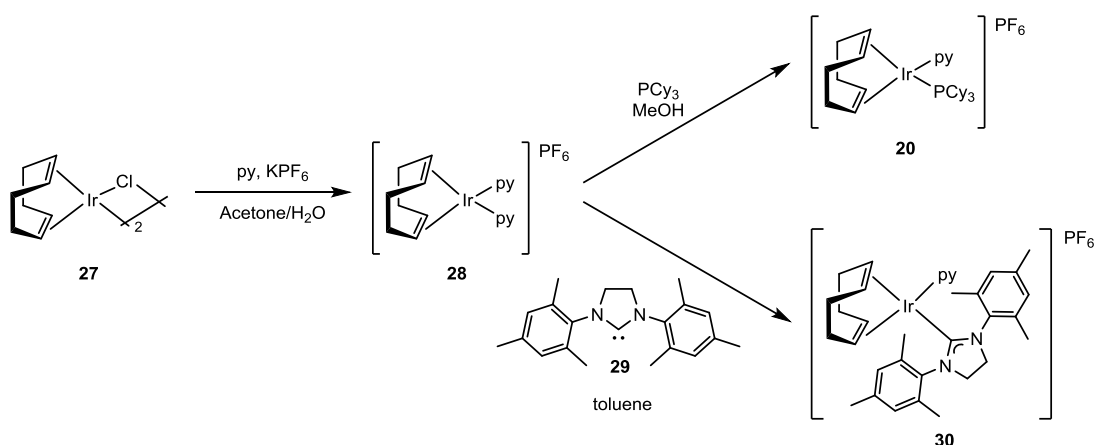


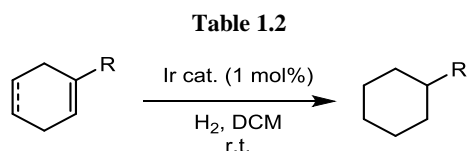
Figure 1.6

Extensive studies by Nolan and co-workers also aimed to develop alternatives to Crabtree's catalyst **20**, and in 2001 the synthesis of complex **30**, where one phosphine ligand had been replaced by an *N*-heterocyclic carbene (NHC) ligand, was reported.³² **30** was prepared *via* a similar procedure to that used for the synthesis of **20** (Scheme 8). After formation of dipyrindyl complex **28**, reaction with the NHC SIMes **29** instead of tricyclohexylphosphine leads to the displacement of a pyridine ligand and formation of **30**. The bulky SIMes NHC was selected to reduce the possibility of a bis-carbene species forming as a side product.



Scheme 1.11

When employed in the catalytic hydrogenation of simple alkenes at room temperature and atmospheric pressure, **30** was found to be less effective than **20** (Table 1.2). At elevated pressures of hydrogen, however, the catalytic activity of **30** was higher than that of Crabtree's catalyst. It was postulated that the presence of the bulky NHC SIMes offers increased thermal stability by hindering the formation of inactive iridium clusters.



Entry	Substrate	Catalyst	% Yield (15 psi H ₂)	% Yield (60 psi H ₂)
1		20	100	-
2	31 	30	100	-
3		20	77	34
4	32 	30	44	100
5		20	84	-
6	33 	30	57	-

Further expanding on the scope of alkene hydrogenation with modified versions of Crabtree's catalyst **20**, Buriak and co-workers reported in 2002 the successful synthesis of a range of complexes bearing both phosphine and NHC ligands (Figure 1.7).³³ Complexes **34**–**38** were tested as catalysts for the hydrogenation of simple alkenes and found to be highly active, with catalytic activities comparable to **20**, even for hindered olefins.

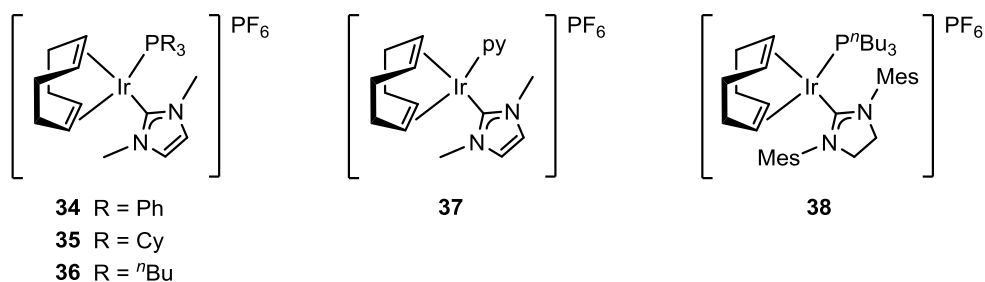


Figure 1.7

With the early 2000s seeing such promising developments in alkene hydrogenation catalysis, attention in the Kerr group turned to the application of modified versions of Crabtree's catalyst in hydrogen isotope exchange. The work of Nolan and Buriak, however, had emphasised the importance of ligand choice at the iridium centre.^{32,33} While Buriak had

encountered difficulties preparing complexes of the bulky IMes NHC with larger phosphines, it was clear that so far, the more sterically demanding ligand combinations had proved most active, and the synthesis of complexes containing two bulky ligands remained an attractive target. In order to develop an efficient route to such complexes, which were predicted to have high catalytic activity, a thorough understanding of the characteristics of the relevant ligands essential.

Phosphines as Ligands

Tertiary phosphines (PR_3) are among the most prevalent ligands in organometallic chemistry; the ability to tune the activity of their metal complexes through careful modification of the steric and electronic properties makes them ideal for use in catalysis. Phosphine ligands are excellent σ -donors and can also act as weak π -acceptors. The lone pair on the central phosphorous atom donates electron density to the metal centre (Figure 1.8a). Additionally, the σ^* -orbitals of the P–R bonds are suitably aligned for π -back donation from the metal d orbital (Figure 1.8b).

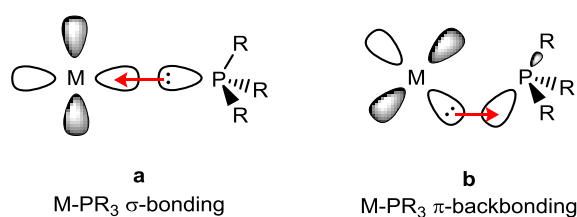


Figure 1.8

The π -acidity of tertiary phosphines increases according to substituent in the order shown in Figure 1.9.

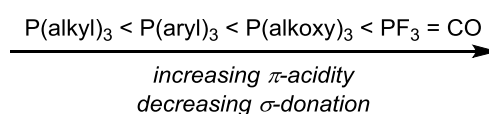


Figure 1.9

As the R group increases in electronegativity, both the σ and σ^* orbitals of the P–R bonds are stabilised. As the phosphorous atom contributes more to the empty σ^* orbitals, the lobes pointing towards the metal centre increase in size, allowing for greater overlap with the metal d orbitals and thus increased back-donation. The π -acidity of the PF_3 ligand roughly

equals that of the CO ligand, which is an excellent π -acceptor through donation from the metal centre into the CO π^* orbital.

In order to exploit the tuneable electronic and steric properties of phosphine ligands and use them to our best advantage in catalyst design, the need arose for methods by which to quantify these characteristics. In 1970, Chadwick Tolman proposed a simple way of measuring the electronic properties of ligands through infrared spectroscopy.³⁴ Through measurement of the carbonyl stretching frequency in nickel complexes of the type $[\text{Ni}(\text{CO})_3\text{L}]$, ligands could be ranked according to their σ -donor abilities.

The strong σ -donating capacity of a ligand gives rise to increased electron density at the nickel centre, which in turn increases the back donation from metal d orbitals into the CO π^* orbitals (Figure 1.10). This increase in π^* character weakens the C–O bond, causing its infrared stretching frequency to decrease. This frequency, $\nu(\text{CO})$, is known as the Tolman Electronic Parameter (TEP) and is one of the most widely used techniques for the quantification of a ligand's electronic properties. Over the last few decades, an increased interest in computational chemistry has led to the calculation of theoretical TEP values,^{35,36} which have proved to be in good agreement with those observed experimentally.

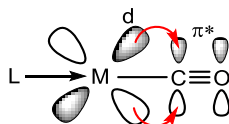


Figure 1.10

While the majority of early studies into ligand effects focused on the impact of a ligand's electronic properties, it soon became clear that the steric properties could play just as significant a role in a complex's reactivity. The introduction of a steric parameter, θ , by Tolman in 1976, provided a simple and quantitative method by which to assess the steric properties of phosphine ligands.³⁷

The cone angle (Figure 1.11) is a space-filling model of an M-PR_3 complex, in which the R substituents are “folded back” from the metal centre. If a cone is drawn, wherein the metal centre is the apex, the steric parameter, θ , is given as the angle of the cone required to contain the ligand. While at first glance this can seem like an approximate method,

experimental studies have shown it to be an excellent tool for predicting and rationalizing the behaviour of metal–phosphine complexes.³⁷

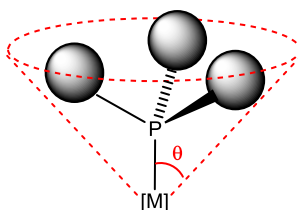


Figure 1.11

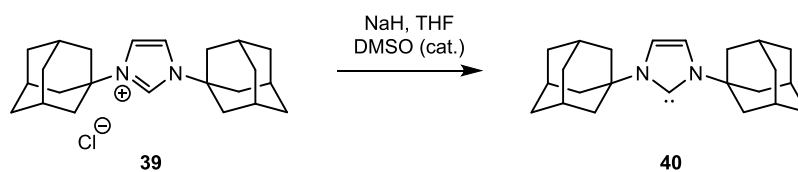
The increased steric demand of phosphine ligands compared to those with similar electronic properties, such as carbonyl ligands, offers a range of advantages for their use in catalysis. Phosphines are often bulky ligands, requiring more space around a metal centre and thus leaving limited room for the approach of other ligands. They can therefore be exploited in the preparation of low coordinate metal species. This can leave room for the binding of smaller, more weakly coordinating ligands, which would be out-competed when reacting with a carbonyl complex of the same type.

The versatility of phosphine ligands in catalysis is highlighted when we look at the subtle changes that can be made in a catalyst's activity through careful choice of the R group. For example, changing from $P(O^iPr)_3$ to PBu_3 alters the electronic properties of the ligand, with little effect on the steric environment. This sort of increase in σ -donor ability could, for example, promote the oxidative addition step of a catalytic cycle over the reductive elimination step. On the other hand, increasing the steric bulk of the ligand while maintaining similar electronic properties, for example by replacing a PMe_3 ligand with a $P(o-tol)_3$ ligand, could favour a lower coordination number species.

***N*-Heterocyclic Carbenes as Ligands.**

For a long time, carbenes were believed to be highly reactive species that were too short lived to be isolated. The successful isolation and characterisation of crystalline *N*-heterocyclic carbene (NHC) 1,3-diadamantylimidazol-2-ylidene (IAd) **40** by Arduengo and co-workers in 1991 (Scheme 1.12), therefore, was a remarkable achievement and paved the way for NHCs to become some of the most commonly used ligands in organometallic chemistry.³⁸ Despite previous assumptions about the high reactivity of carbenes, IAd was found to be remarkably stable. Since Arduengo's pioneering work, NHCs have become

ubiquitous as ligands in transition metal catalysis.^{39,40} As such, their electronic and steric properties have been extensively studied.



Scheme 1.12

The electronic properties of NHCs are responsible for their unexpected stability, and account for much of their behaviour. NHCs are singlet carbenes, with a lone pair of electrons occupying an sp^2 hybridised orbital in the plane of the ring (Figure 1.12). The empty p orbital on the sp^2 carbene centre is stabilized through π -donation by the lone pairs on the adjacent nitrogen atoms. NHCs form exceptionally stable metal–ligand bonds, meaning they are often able to act as spectator ligands during catalysis.



Figure 1.12

One of the key features of NHCs is their exceptionally electron-rich nature; save for a few exceptions, they are better σ -donors than even the most strongly donating phosphine ligands. As with their phosphine analogues, the electronic properties of NHCs can be quantified using the Tolman electronic parameter.⁴¹ Nickel complexes of the type $[\text{Ni}(\text{CO})_3(\text{NHC})]$ are prepared and the CO stretching frequency measured; the lower the value of $\nu(\text{CO})$, the better the σ -donating ability of the ligand.

A key issue, however, with the use of $[\text{Ni}(\text{CO})_3(\text{NHC})]$ species for the measurement of an NHC ligand's electronic properties arises from the fact that such complexes are highly toxic. Key results published by Nolan and co-workers in 2008 demonstrated that *cis*- $[\text{Ir}(\text{Cl})(\text{CO})_2(\text{NHC})]$ complexes can be used as an alternative;⁴² follow-up work by Crabtree and co-workers showed a simple correlation between TEP values collected from iridium complexes and those obtained from the traditional nickel complexes (Equation 1.1).⁴³ In a similar manner, Wolf and Plenio demonstrated that electronic data can be derived from examining the IR stretching frequencies of $[\text{Rh}(\text{Cl})(\text{CO})_2(\text{NHC})]$ complexes.⁴⁴

$$\text{TEP (cm}^{-1}\text{)} = 0.9485 \nu_{\text{CO}}^{\text{f}} \text{(cm}^{-1}\text{)} + 336.2 \text{(cm}^{-1}\text{)}$$

Equation 1.1

More recently, other techniques for quantifying the electronic properties of NHC ligands have begun to emerge. For example, the use of NMR spectroscopic techniques has been demonstrated by Ganter and co-workers to offer further insight into the electronic nature of NHCs. Specifically, the assessment of the ^{77}Se chemical shifts of selenium NHC adducts, such as **41** (Figure 1.13), allows quantification of the π -back donating abilities of these ligands.⁴⁵ These characteristics have also been measured through NMR spectroscopic analysis of NHC–phosphinidene complexes, such as **42**, by Bertrand and co-workers.⁴⁶ While TEP remains the most widely used method for analysis of the electronic properties of NHCs, the emergence of modern techniques offers us yet more tools for assembling a more holistic picture of their behaviour.

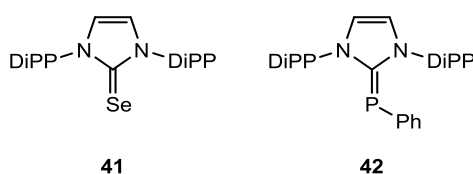


Figure 1.13

Just as with phosphines, the steric properties of NHC ligands are key to the role they play in catalysis; huge variations in metal–ligand distances and angles are observed depending on the steric demands of the NHC. These properties, however, are more challenging to quantify than they are for phosphines. While tertiary phosphines possess a C_3 symmetry axis, NHCs instead have a C_2 axis, rendering the cone angle model used for phosphines useless.

In order to overcome this problem, a new parameter, percentage buried volume ($\%V_{\text{bur}}$), was developed by Nolan and co-workers to describe the steric properties of NHC ligands. Through refinement by Nolan, Cavallo, and Clavier, $\%V_{\text{bur}}$ has become the most utilized method for describing NHC steric properties.⁴⁷ $\%V_{\text{bur}}$ is given as the percentage of a sphere, with a set radius r , around a metal centre that is occupied by the atoms in a ligand (Figure 1.14). One of the most attractive features of the $\%V_{\text{bur}}$ system is that its use is not limited to NHC ligands; using the same method, comparisons can be drawn with phosphines and cyclopentadienyl-derived ligands. As well as the radius, r , a metal–ligand bond length, d ,

must also be fixed. The most common choice has proved to be a bond length (d) of 2 Å and a radius (r) of 3.5 Å.

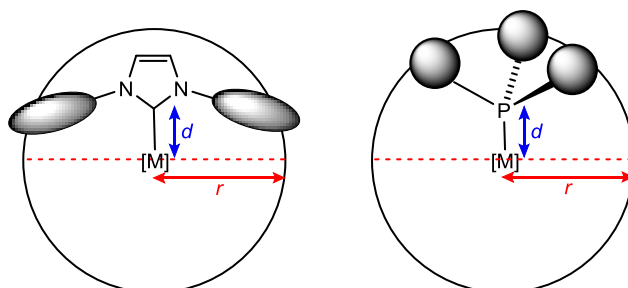


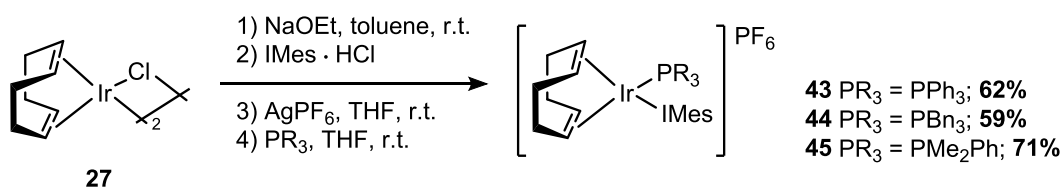
Figure 1.14

While the % V_{bur} model has provided us with a simple method for quantifying the steric bulk of a vast range of ligands, care must be taken when analysing this data. The structure of the NHC used in buried volume calculations can be derived either from crystallographic data or from data calculated computationally; it is important to note that these two methods can provide different results, meaning that not all % V_{bur} values can be directly compared.

Kerr Group Investigations into HIE

Over recent years, iridium-catalysed hydrogen isotope exchange has been extensively studied within the Kerr group.^{48–52} In an effort to combat some of the issues associated with Crabtree's catalyst, and following on from elegant studies by Nolan and Buriak,^{32,33,53} attention was focussed on the development of a new family of HIE and hydrogenation catalysts.

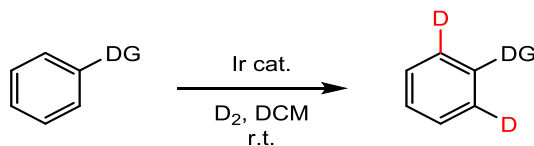
It was considered essential that any new catalyst system should employ low catalyst loadings, be tolerant of a wide range of functional groups, and offer excellent selectivity alongside high levels of deuterium incorporation. In 2008, the synthesis of iridium(I) complexes **43–45**, featuring a bulky ligand set containing phosphine and NHC ligands, was reported (Scheme 1.13).⁴⁹ Since Buriak had encountered difficulties in the preparation of compounds with sterically demanding phosphines and NHCs,³³ the synthesis involved generation of the IMes NHC *in situ*, according to a procedure earlier reported by Herrmann.⁵⁴ Conveniently, the synthesis of **43–45** did not require a glove box and the complexes were found to be air- and moisture-stable.



Scheme 1.13

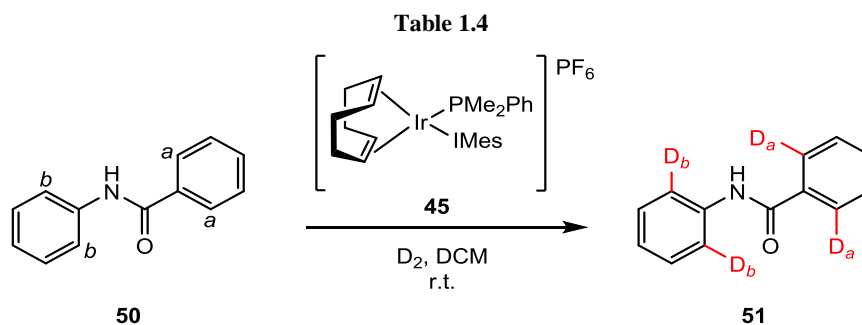
When the deuterium labelling of substituted aromatics was investigated, excellent levels of incorporation were observed, with selective labelling of the *ortho*- position (Table 1.3). Moreover, complexes **43–45** were shown to be significantly more active catalysts than Crabtree's catalyst **20**; loadings of 5 mol% were used throughout, including with substrates which had previously required either stoichiometric or superstoichiometric quantities of **20**.^{28,29} Notably, the successful labelling of acetanilide **48** demonstrated that these novel iridium complexes could also be used in the deuteration of substrates *via* a 6-mm as well as *via* the more energetically favoured 5-mm.

Table 1.3



Entry	Substrate	Catalyst	Catalyst Loading / mol%	%D _{ortho}
1		20	5	97
2	46 	43	5	97
3		20	100	100
4	47 	43	5	100
5		20	140	40
6	48 	43	5	97
7		20	100	0
8	49 	43	5	98

With such promising results having been observed for the deuteration of acetanilide **5**, further investigations were carried out into the selectivity of labelling *via* a 5-mmi *versus* a 6-mmi. The deuteration of benzanilide **50** using catalyst **45** was therefore studied (Table 1.4); here, two possible labelling sites are available, (*a*), which involves a 5-mmi and (*b*), which requires a 6-mmi. At a catalyst loading of 5 mol%, both sites are labelled to a similar extent. When the catalyst loading was dropped to 0.5 mol%, however, a clear preference for labelling *via* a 5-mmi was observed, as the levels of deuteration at position *a* were maintained, while the levels at position *b* decreased significantly.



Entry	Catalyst Loading / mol %	%D _a	%D _b
1	5	95	93
2	0.5	94	2

The mechanism of labelling of aromatic substrates with catalysts such as **43** has also been probed theoretically.⁵¹ The computational results obtained were in accordance with the mechanism proposed by Heys and co-workers,⁵⁵ with the additional observation that a complex such as **52** (Figure 1.15) could be implicated in the mechanism. Here, an agostic interaction between the metal centre and the *ortho* C–H bond is proposed to stabilise the initial substrate-bound catalyst species.

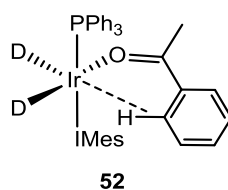
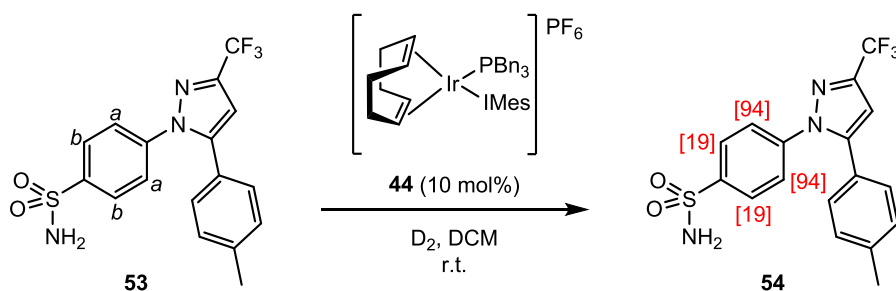


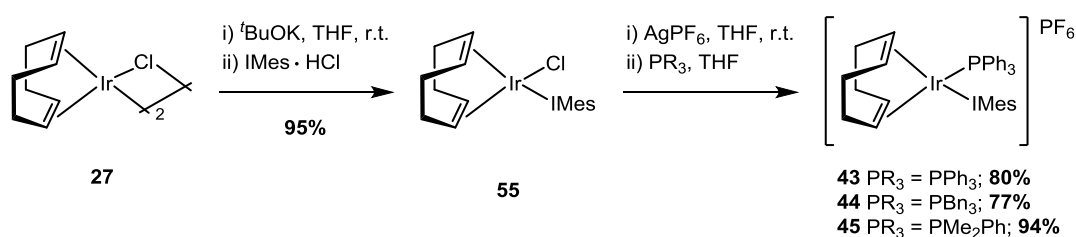
Figure 1.15

Selectivity in the deuteration of multiply functionalized compounds has also been probed through the labelling of compounds containing more than one directing group. For example, the labelling of Pfizer COX-2 inhibitor Celecoxib **53** with PBN₃ complex **44** showed preferential deuteration at position *a*, where the pyrazole unit acts as a functional handle (Scheme 1.14).⁵¹ Notably, the labelling observed at position *b* represents the first example of iridium-catalysed hydrogen isotope exchange *ortho*- to a primary sulfonamide.



Scheme 1.14

More recently, a novel and more efficient route to Kerr group complexes has been developed (Scheme 1.15).⁵⁶ Neutral complex **55** is a key intermediate in the synthesis of the NHC/phosphine complexes and its simplified synthesis afforded access to multigram quantities of **43–45**. These catalysts have since been commercialised and are now sold through Strem Chemicals.⁵⁷

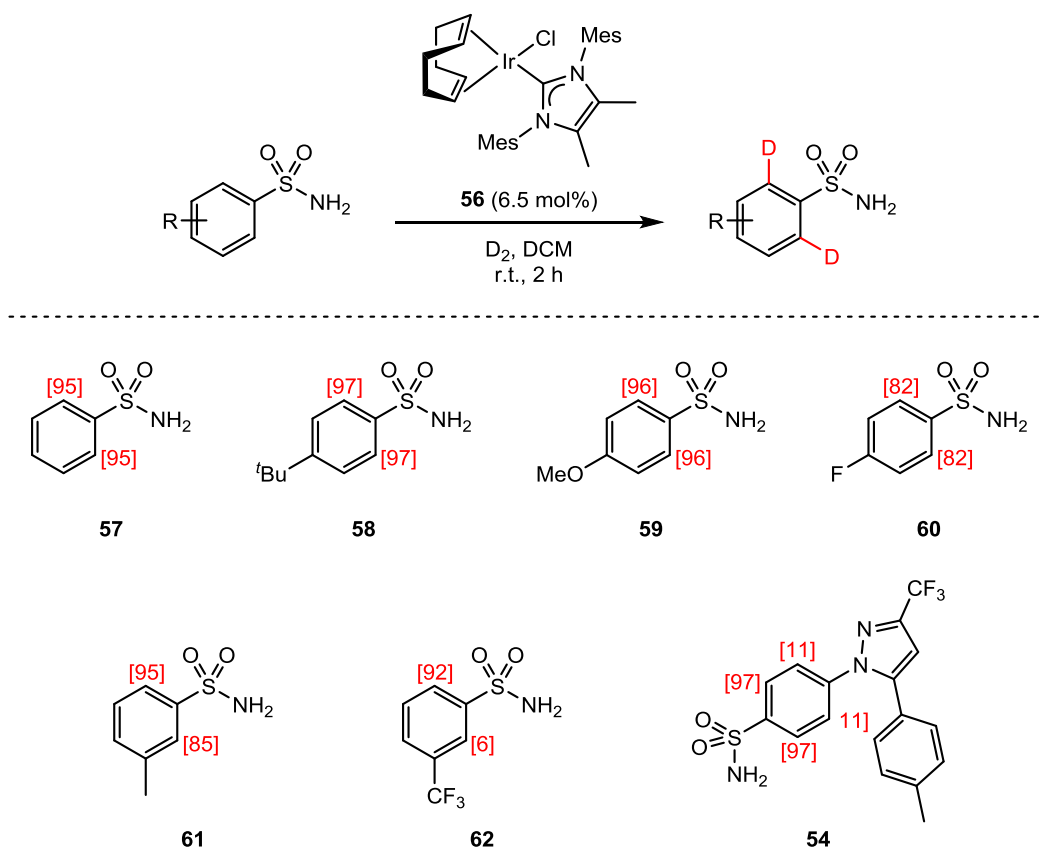


Scheme 1.15

With more efficient access to complex **55** having been established, it has since been employed as a catalyst in its own right. In the labelling of aromatic systems bearing ketone or *N*-heterocycle directing groups, **55** was shown to achieve deuterium incorporation comparable to that reported for phosphine–NHC complexes in some cases.⁵⁸ The most notable use of neutral NHC–chloride complexes, however, has been in the *ortho*-deuteration of primary sulfonamides.⁵⁹ While the combination of bulky NHC/phosphine ligands has proved highly effective in labelling reactions to date, it was thought that a smaller ligand set could offset some of the steric demands caused by the coordinating sulfonamide's tetrahedral geometry.

After a screening of complexes with varying NHC ligands, excellent levels of incorporation were observed with catalyst **56**, a more electron-rich analogue of **55**. Conditions were optimised and applied across a wide range of substrates (Scheme 1.16). When Celecoxib **53** was submitted to the reaction conditions, remarkable selectivity was observed for labelling

through the sulfonamide unit (Position *a*), while minimal labelling was observed next to the pyrazole group, which is typically an excellent directing group. These results are in notable contrast to those obtained for the labelling of Celecoxib with catalyst **44** (Scheme 1.14), meaning that complementary methods are now available for selective deuteration at two sites in the same molecule.

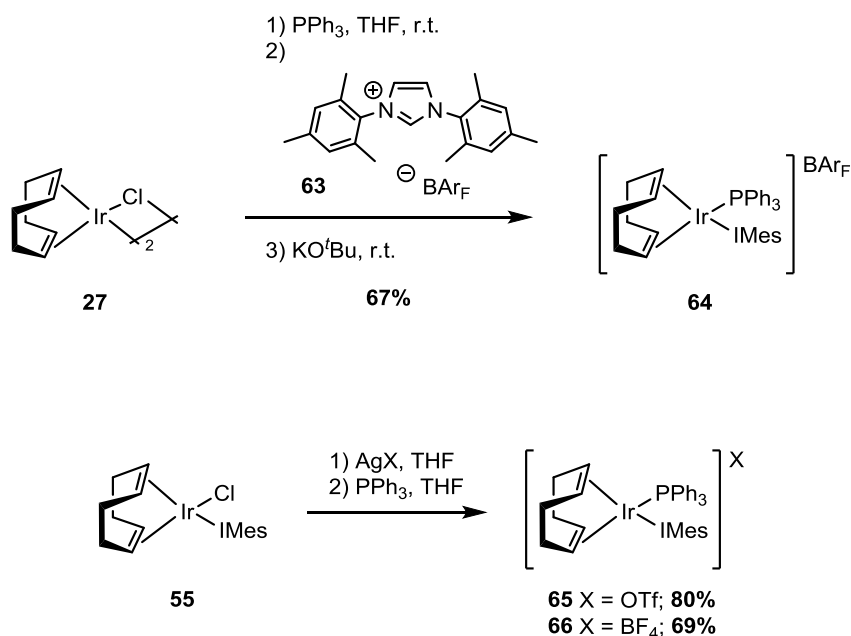


Scheme 1.16

With thorough investigations now having been carried out into the effects of ligand properties on catalytic activity, focus within the Kerr group turned to the effects of counterions in deuteration reactions.⁶⁰ In recent years, it has become apparent that the choice of anion can have a significant impact on the success of reactions catalysed by cationic transition metal complexes. Work published by the groups of Pfaltz and Nolan has demonstrated that using a larger counteranion, such as tetrakis[3,5-bis(trifluoromethyl)phenyl]borate (BArF) can dramatically increase catalyst efficacy.^{61–63}

With these studies in mind, a series of NHC/phosphine complexes with alternative counterions were prepared. Complex **64** was prepared in one step from chloride dimer **27**

with addition of IMes•HBArF **63** (Scheme 1.17). Complexes **65** and **66** were prepared in an analogous fashion to complex **43**, with the relevant AgX salts used in place of AgPF₆.



Scheme 1.17

When **64–66** were used as catalysts for the labelling of acetophenone **46**, improved catalytic activity was observed in the order X = BArF ≈ OTf > PF₆ > BF₄. These results are in line with other counterion studies published recently,^{61,63,64} and demonstrate that the use of larger, less coordinating anions results in more active catalysts (Figure 1.16).

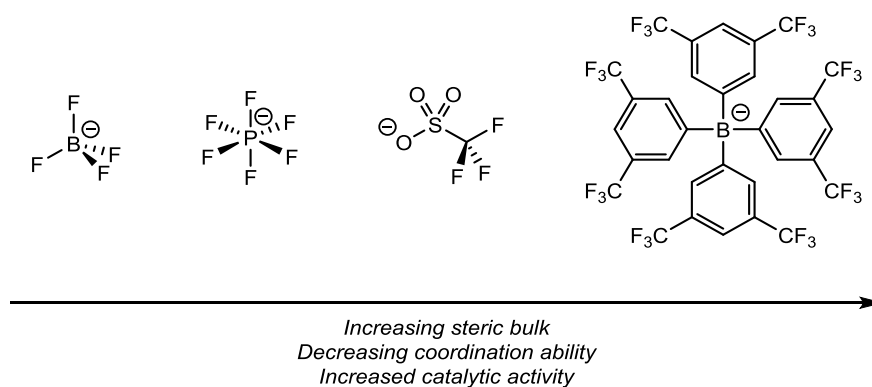
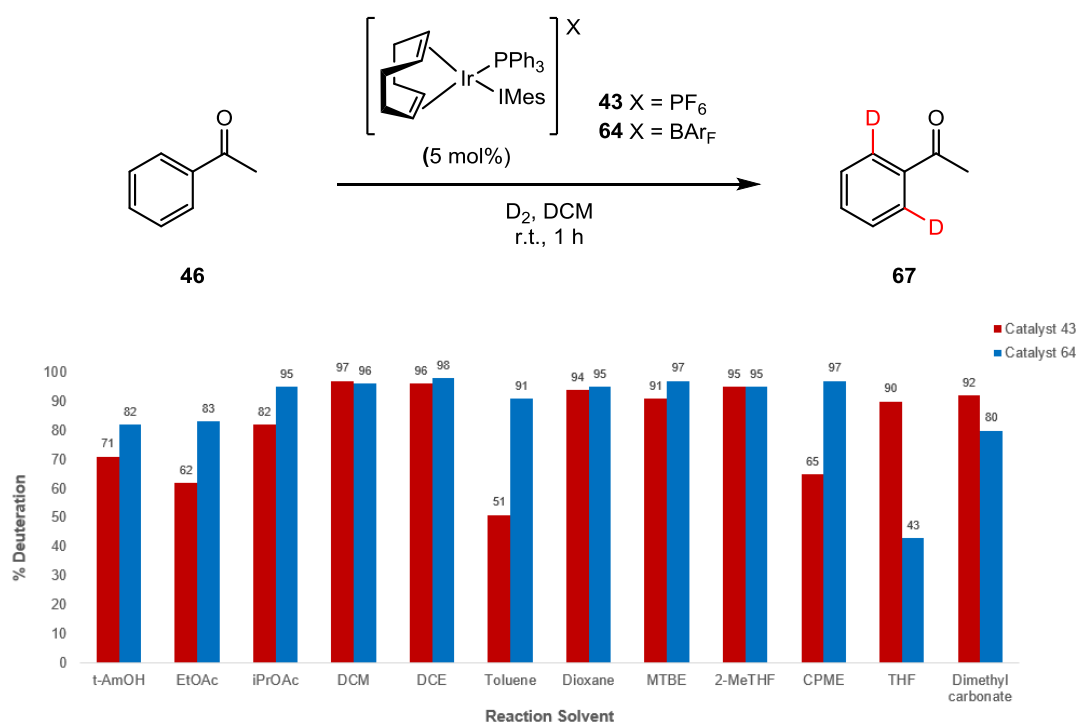


Figure 1.16

The increased utility of BArF catalyst **64** was demonstrated with a solvent screen comparing the labelling activity of **43** and **64**. One drawback of labelling methodology

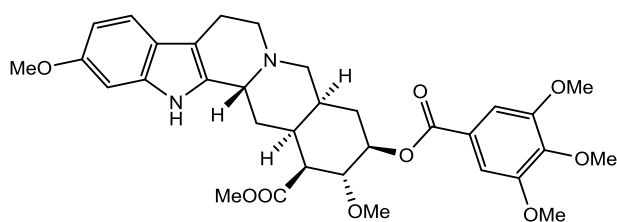
developed so far is the requirement for dichloromethane as solvent; the pharmaceutical industry is currently striving to eliminate the use of chlorinated solvents.⁶⁵ Previous work within the Kerr group showed that 2-methyltetrahydrofuran, methyl *tert*-butyl ether, and diethyl ether are viable alternative solvents for labelling with PF₆ complex **43**, but poor solubility of the catalyst remained a limitation.⁶⁶ When the more soluble BARF complex **64** was employed, however, the labelling of acetophenone proceeded to excellent levels of incorporation across a wide range of solvents, outperforming PF₆ complex **43** in almost all examples (Graph 1.1).⁶⁷



Graph 1.1

Isotopic Labelling of *N*-Heterocycles

As privileged structures in both the pharmaceutical and agrochemical industries, indoles and related *N*-heterocycles have been receiving increased attention over the last few decades.⁶⁸ A Scifinder survey in December 2016 showed that over the past 128 years, over 130,000 papers have been published of which indoles are the subject.⁶⁹ In the 1950s, the indole alkaloid Reserpine, **68**, (Figure 1.17) became one of the first central nervous system (CNS) drugs to be widely introduced to the marketplace. It quickly became an interesting target for natural product chemists, and between 1958 and 2003 was the subject of multiple total synthesis routes, which have been extensively reviewed by Chen.⁷⁰



68
Reserpine

Figure 1.17

Since the 1950s, the physiological importance of the indole moiety has expanded and it now represents one of the most important scaffolds in modern drug discovery, being found in a vast range of pharmaceutical compounds such as anti-inflammatory, antidepressant, anticancer or CNS drugs.⁷¹ Arguably, one of the most important classes of compounds in medicinal chemistry is the 5-hydroxytryptamine receptor family, which influences several neurological processes and has been implicated in treatments for depression and psychosis, amongst others.⁷² Notable examples of 5-HT receptor drugs include the triptan family, such as Sumatriptan **69** and Rizatriptan **70** (Figure 1.18), which are used to treat migraines and cluster headaches, and Ondansetron **71**, an anti-emetic which is used to combat the side effects of chemotherapy, and which featured in the 2015 World Health Organisation Essential Medicines List.⁷³

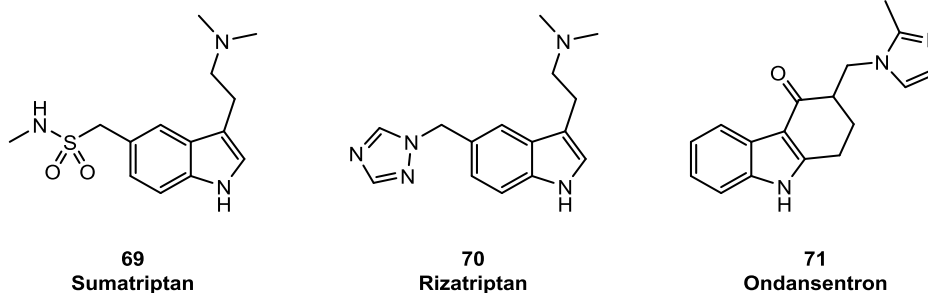
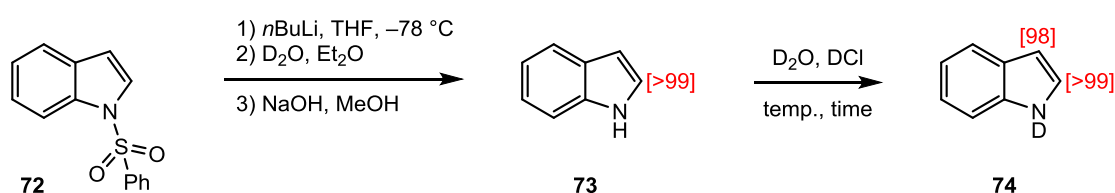


Figure 1.18

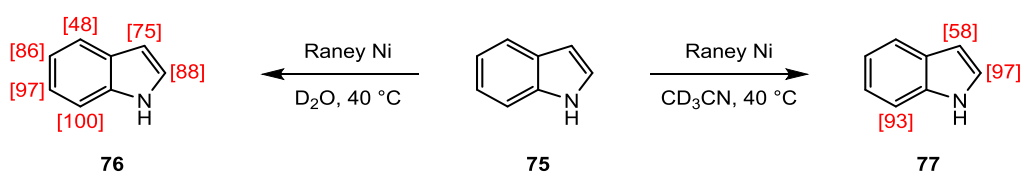
Over recent years, attention has focused on the use of transition metal catalysis for further functionalisation of the indole scaffold.^{68,74} With promising results being achieved for indole C–H activation with catalysts based on iridium, rhodium, palladium, and ruthenium,^{75–79} and given the enormous relevance of this family of compounds to the pharmaceutical industry, indole-containing compounds and related *N*-heterocycles represent an exciting class of substrates for the isotopic labelling community.

Early reports of hydrogen isotope exchange of indoles involved lithiation methodology, exploiting the nucleophilic character of the C2 and C3 positions.⁸⁰ For example, work published by Jackson and co-workers in 1987 demonstrated that 2-deuterioindole **73** could be prepared from *N*-phenylsulfonyl indole **72**, through lithiation and quenching with D₂O, followed by hydrolysis of the protecting group (Scheme 1.18).⁸¹ Furthermore, deuterium could then be introduced at the C3 position (as well as on the indole nitrogen) by treatment with DCl in D₂O. While acidic exchange can offer highly effective methods for deuterium incorporation, it suffers from the major drawback of a lack of selectivity. Additionally, the use of harsh lithiating reagents or acids can cause difficulties in the late stages of complex molecule synthesis, and as such milder conditions are often desirable.



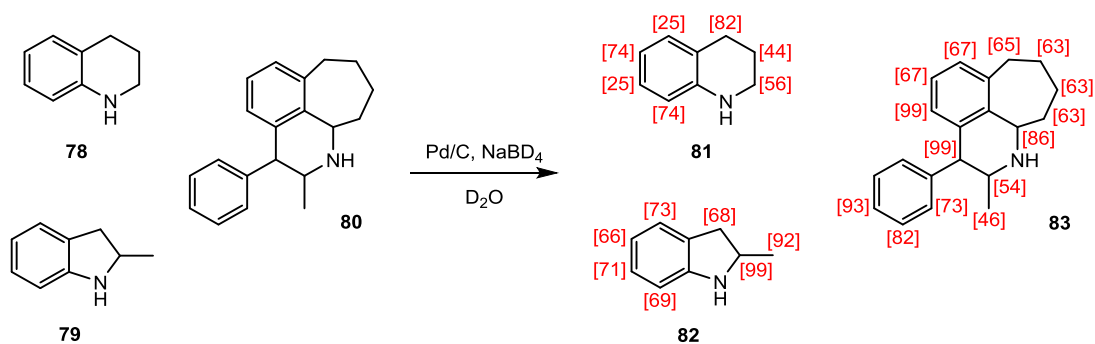
Scheme 1.18

In 1999, Yau and co-workers reported the deuteration of indole and *N*-methylindole with the use of Raney nickel catalysis, with the selectivity being determined by the reaction solvent, which is also the source of deuterium.⁸² Selectivity remained poor, however, with non-selective perdeuteration of indole **75** observed in D₂O, and labelling seen across three sites, albeit with varying success, with deuterated acetonitrile (Scheme 1.19).



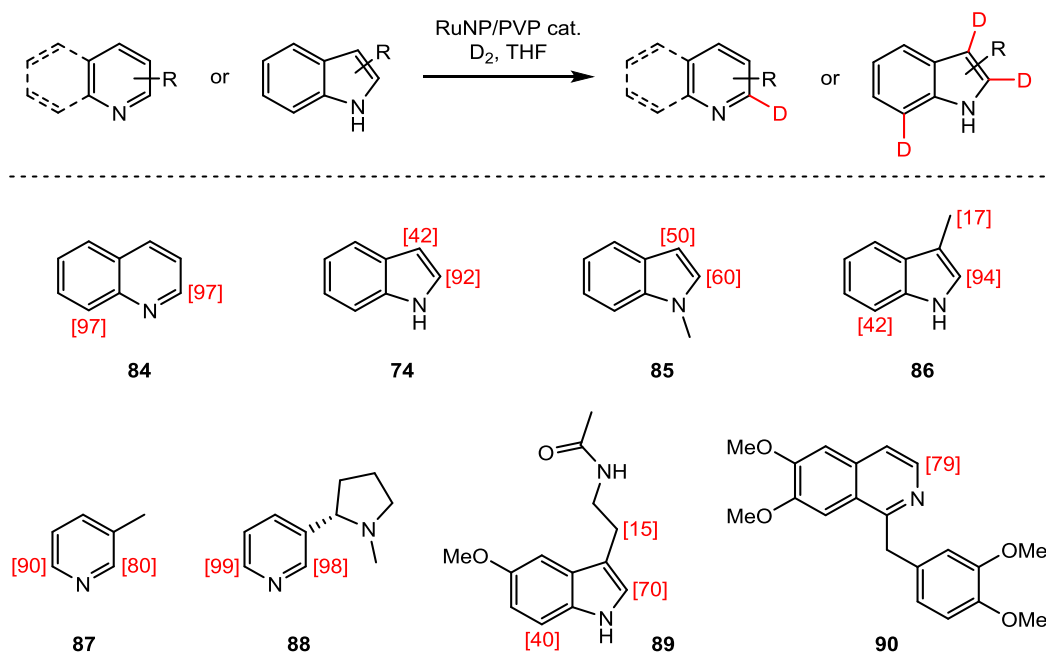
Scheme 1.19

The use of heterogeneous catalysis for *N*-heterocycle labelling was further examined by Atzrodt and Derdau, who in 2006 reported the use of Pd/C alongside NaBD₄ and D₂O (Scheme 1.20).⁸³ Once again, however, H/D exchange was non-selective, and although chiral substrates were screened, stereochemistry was not retained during the labelling process.



Scheme 1.20

Despite the increase in methodology for labelling of other *N*-heterocycles, the selective deuteration of indoles remained elusive. In 2014, however, the isotopic labelling of indoles, pyridines and quinolines catalysed by ruthenium nanoparticles was reported by Rousseau and co-workers.⁸⁴ Regioselective deuterium incorporation of up to 94% was observed for alkyl-substituted indoles, and similar results were achieved for quinoline and pyridine derivatives (Scheme 1.21).

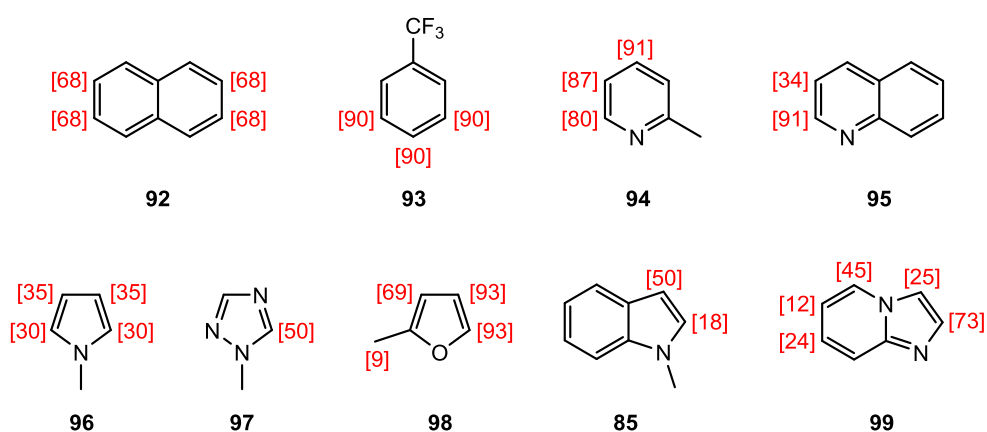
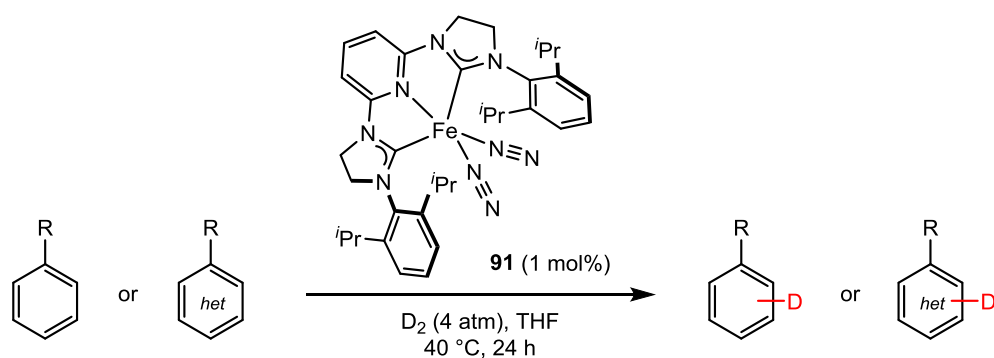


Scheme 1.21

In recent years, examples of homogeneous transition-metal catalysed labelling of indoles have begun to emerge. In 2016, Chirik and co-workers reported the use of a homogeneous

iron catalyst for the hydrogen isotope exchange of pharmaceuticals.⁸⁵ Complex **91**, previously shown to be a highly active catalyst for the hydrogenation of unfunctionalised alkenes,^{86,87} was found to deuterate a number of arenes and heteroarenes to high levels of incorporation (Scheme 1.22).

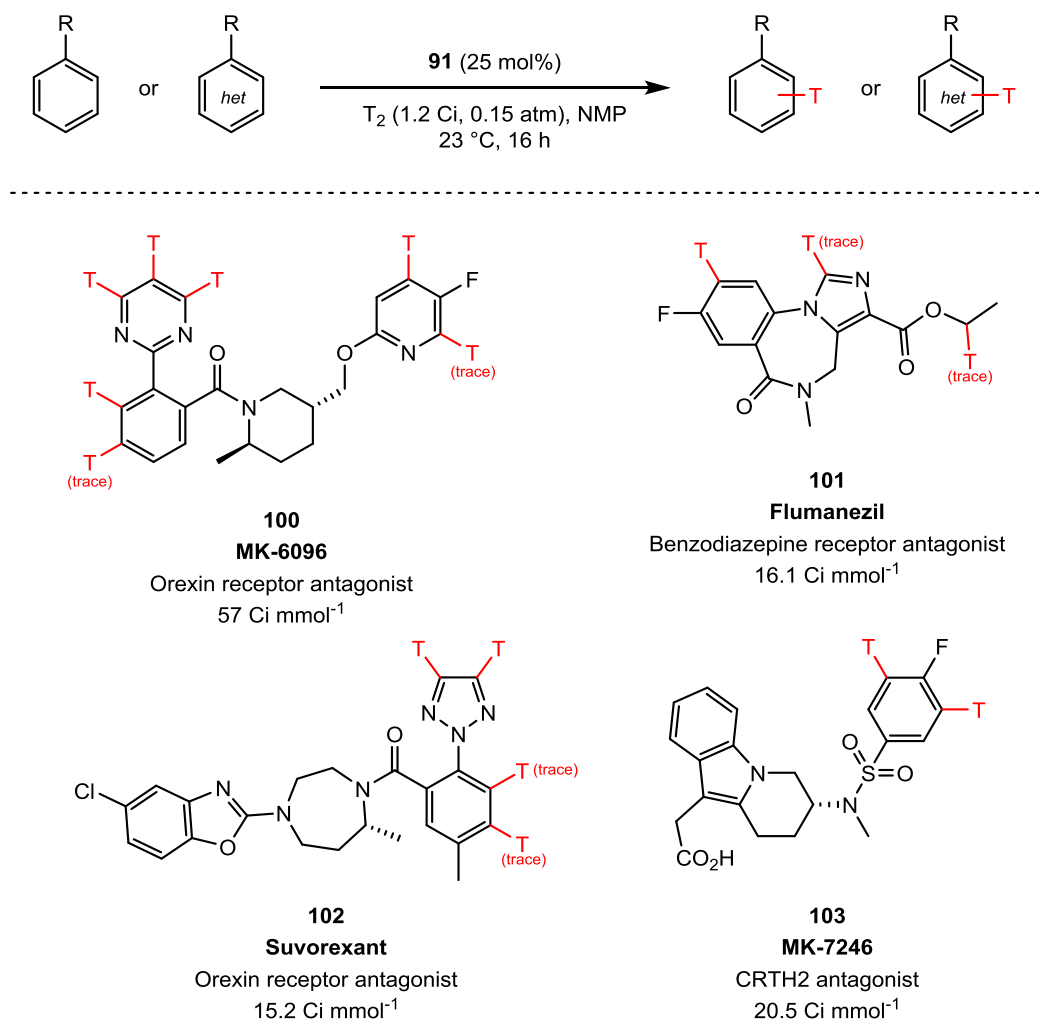
Two trends were observed upon examination of the site selectivity: substrates bearing electron-withdrawing substituents were found to undergo HIE more readily than those with electron-donating groups, and deuteration took place at the most sterically accessible positions. The selectivity observed for activation of less hindered C–H bonds makes this labelling process an impressive and complementary method to aromatic deuteration with Kerr group catalysts, which typically operate *via ortho*-activation by a donor directing group.



Scheme 1.22

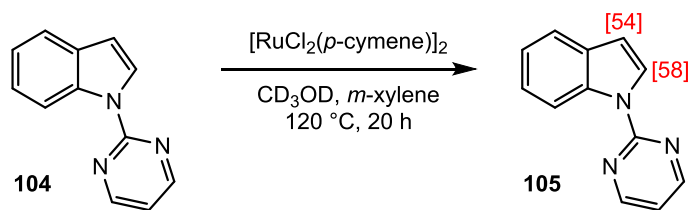
The utility of this novel labelling method was further highlighted with the tritiation of a range of drug molecules (Scheme 1.23). While the catalyst loading was increased to 25

mol%, reactions performed well at subatmospheric pressures of tritium gas, which is typically the most expensive component in practical tritiation chemistry.



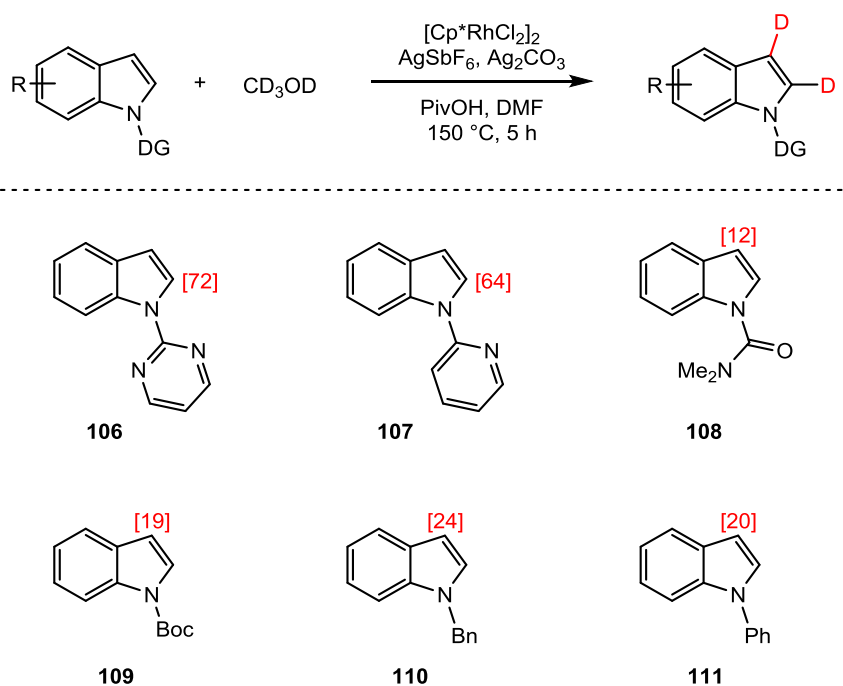
Scheme 1.23

Donor-directed hydrogen isotope exchange on *N*-heterocycles has also been reported. For example, Ackermann has published the direct C–H arylation of indoles and pyrroles catalysed by $[RuCl_2(p\text{-cymene})_2]$, where removable pyridine and pyrimidine moieties were used as directing groups.⁷⁶ In order to prepare deuterated starting materials for mechanistic investigations, the ruthenium complex was also used as an isotope exchange catalyst, along with methanol-*d*₄ as a deuterium source (Scheme 1.24). While levels of incorporation were moderate, Ackermann's work demonstrated that homogeneous HIE *via* directed C–H activation was a feasible route to deuterated indoles.



Scheme 1.24

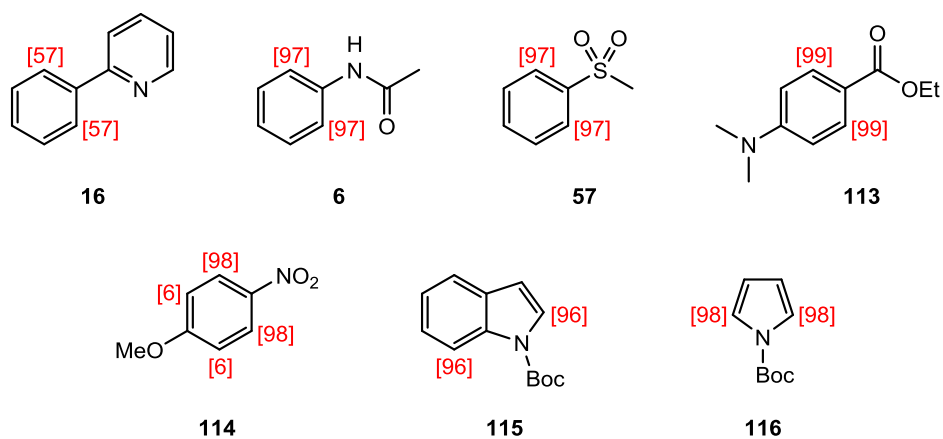
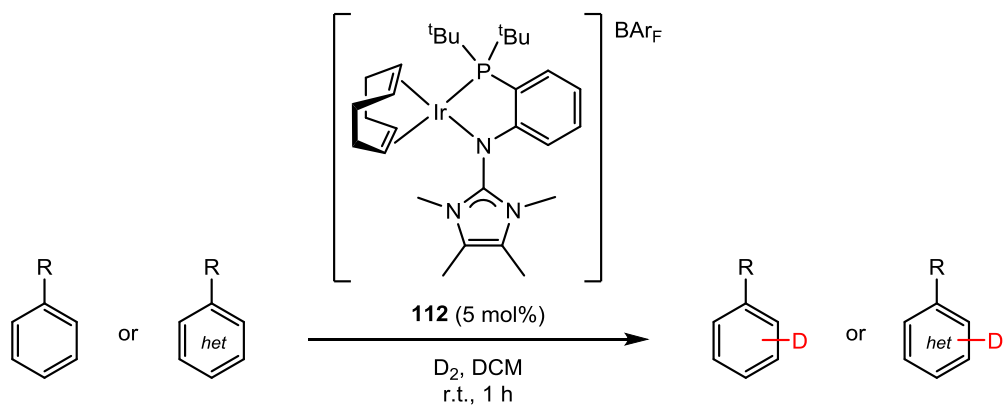
Further evidence of donor group-directed labelling of indoles came from the groups of You and Lan in 2013, who were investigating oxidative cross-coupling at the indole C2 position using a rhodium catalyst.⁷⁵ The treatment of *N*-substituted indoles with $[\text{Cp}^*\text{RhCl}_2]_2$ and methanol- d_4 led to selective deuterium incorporation at either the C3 or the C2 position (Scheme 1.25). While incorporations in some cases were only moderate, this was the first reported example where homogeneous transition metal-catalysed labelling of indoles could be achieved selectively at two different positions, through variation of the directing group.



Scheme 1.25

The labelling of the indole C2 position has been further reported in a very recent publication by Tamm and co-workers.⁸⁸ The deuteration of a series of aromatic and heteroaromatic substrates proceeded to excellent incorporations when catalysed by novel iridium complex **112**, bearing a bidentate phosphine-imidazolin-2-imine ligand (Scheme 1.26). As well as

demonstrating excellent activity for aromatic *ortho*-labelling directed by a range of functional handles, this methodology was also applied to the labelling of Boc-protected indole and pyrrole substrates.



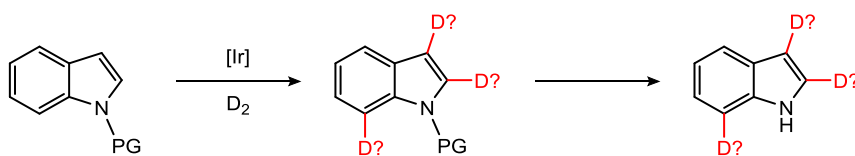
Scheme 1.26

When considered alongside the emergence of increasingly mild methods for iridium-catalysed hydrogen isotope exchange across a vast range of functional groups, the regioselectivity observed by You and Lan and the high activity observed by Tamm was extremely promising, offering insight into the labelling of what remains a highly attractive class of substrates.

Proposed Work

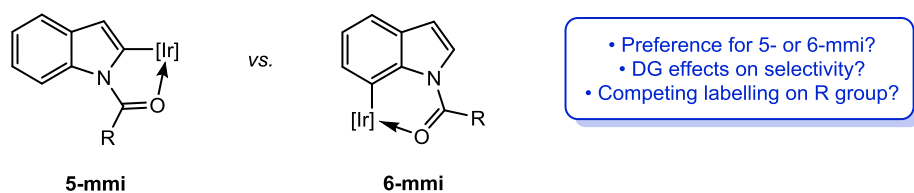
In recent years, Kerr group catalysts have shown high activity in hydrogen isotope exchange reactions of substituted aromatics and α,β -unsaturated systems.^{49,51,52,58-60} Within these studies, *N*-heterocyclic units such as pyrazoles and pyridines have been successfully employed as directing groups. However, there is still a demand for well-established methodology for metal-catalysed labelling on the ring of heteroaromatic moieties. The overarching aim of this project is the development of methodology for the selective deuteration of *N*-heterocycles.

In the first instance, the project will involve the preparation and deuteration of a large library of substituted indoles. It is essential that any methodology developed within this project should be suitable for application in the late stages of complex molecule synthesis, so common and removable *N*-protecting groups will be installed and used as functional handles. The capacity of Kerr group catalysts to carry out labelling on these indole substrates will be assessed and the selectivity observed for C2, C3 or C7 labelling will be investigated (Scheme 1.27). In order to demonstrate the versatility of our group's labelling methodology, methods for the deprotection of deuterated substrates, with retention of the isotopic label, will be developed to afford an overall traceless labelling process.



Scheme 1.27

When directing donor groups are used as protecting groups, the preference for formation of a 5- or 6-membered metallocyclic intermediate will be examined. The effects of catalyst and directing group choice will be probed in order to evaluate whether regioselectivity can be controlled (Scheme 1.28).

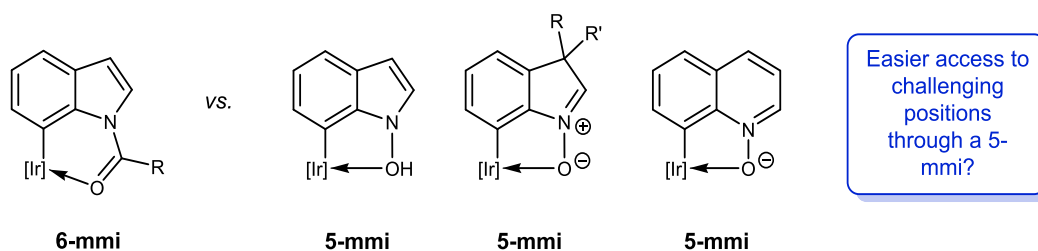


Scheme 1.28

In order to demonstrate the wide applicability of Kerr group catalysts, any methodology developed and optimised for indole substrates will be applied to a wider range of heterocycles, including substituted pyrroles and azaindoles. The application of any methodology developed to the labelling of *N*-heterocycle-containing drug compounds will also be targeted. The deuteration of members of the triptan family of anti-migraine drugs will be carried out with the aim of demonstrating the real-world utility of our mild labelling conditions.

As well as the introduction of directing donor groups onto the heterocycle nitrogen position, substrates containing non-coordinating protecting groups will be subjected to any labelling conditions developed; this will allow us to determine whether the presence of a coordinating functional handle is necessary, as well as to establish whether there are alternative deuteration mechanisms at play. Any investigations carried out into the mechanism of hydrogen isotope will be accompanied by complementary DFT studies.

Lastly, investigations will be carried out into the use of *N*-oxides or *N*-hydroxy indoles as directing groups. It is anticipated that the smaller metallocycle formed could allow C–H activation at alternative, more challenging positions, which could offer complementary site selectivity to acyl directing groups.

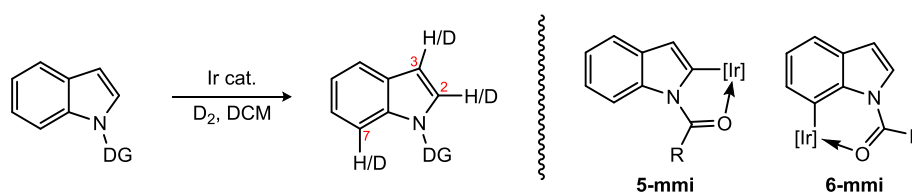


Scheme 1.29

Results and Discussion

C2 Labelling of *N*-Protected Indoles

As the first key aim of the project, we sought to prepare a range of substituted indoles to study as labelling substrates. As depicted in Scheme 1.30, for an indole bearing a donor group on the nitrogen atom, there are two potential sites for directed C–H activation. The overarching aim of the project was to develop a set of complementary techniques that would allow for the selective C–H activation and labelling of each of these positions.



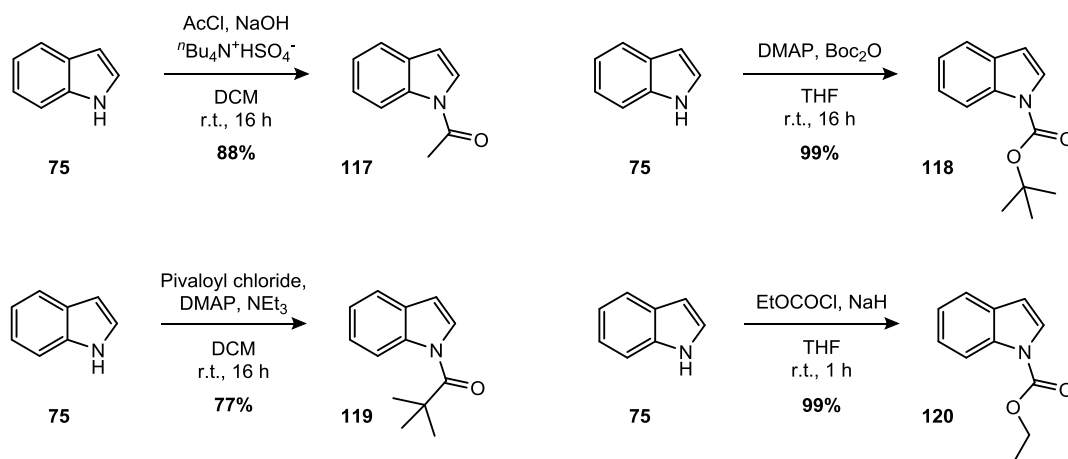
Scheme 1.30

Initially, it was decided to examine methods for inducing HIE at the C2 position. As shown in Scheme 1.30, the C2 position can be accessed *via* a 5-membered metallocyclic intermediate (mmi), whereas the C7 position requires the formation of a 6-mmi for activation. Previous work within the Kerr group has shown that C–H activation by iridium often occurs preferentially *via* a 5-mmi over a 6-mmi,⁴⁹ so it was decided that labelling of the C2 position would be best starting point for the project.

Establishing a thorough substrate scope of substituted indoles would involve varying the directing groups on the indole nitrogen atom, as well as the substituents on the benzene and pyrrole portions of the substrate. Initially, the synthesis of a range of *N*-protected indoles was carried out. We first focussed on the use of protecting groups containing a donor atom (*i.e.* N or O), which could act as a functional handle. Additionally, it was decided to employ protecting groups commonly used during organic synthesis; since one of the key advantages of hydrogen isotope exchange is the ability to introduce a heavy hydrogen label at the late stages of a complex molecule synthesis, it was imperative that any protecting groups used in this methodology could be installed and removed without the need for harsh conditions.

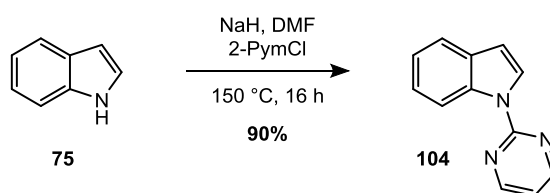
Given their prevalence in natural product chemistry, the use of acetamide and carbamate protecting groups was explored initially. With this in mind, substrates **117** and **118**, bearing

acetyl and *tert*-butoxycarbonyl (Boc) protecting groups, were prepared in excellent yields from 1*H*-indole **75** (Scheme 1.31). Additionally, and in order to gain an insight into the role played by the steric properties of the directing group, *N*-pivaloyl indole **119** was prepared as a bulkier analogue of **117**, and *N*-ethoxycarbonyl indole **120** was prepared as a less hindered analogue of Boc-protected substrate **118**.



Scheme 1.31

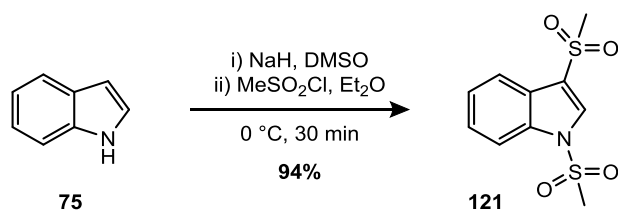
The potential labelling ability of substrates bearing less common directing groups was also of interest. Both pyridyl and pyrimidyl groups had been successfully used by You and co-workers as functional handles for Rh(III)-catalysed H/D exchange at the C2 position.⁷⁵ With promising results having been obtained within the group for pyridyl/pyrimidyl-directed *ortho*-HIE of aromatic systems,^{49,58} it was thought that these would be excellent candidates for heterocyclic labelling. As such, compound **104** was prepared in good yield following a literature procedure (Scheme 1.32).⁷⁶



Scheme 1.32

An additional example of a functionality that is of particular interest to our laboratory is the sulfonamide group. Despite their enormous relevance to the pharmaceutical industry, sulfones and sulfonamides remain especially difficult substrates for HIE. Recent work

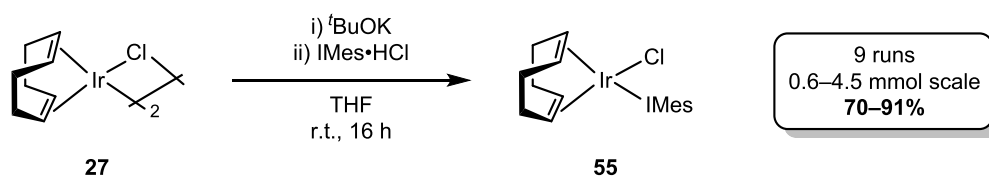
published by the Kerr group has demonstrated that the bulk of a tetrahedral sulfone group causes a significant steric clash upon approach to the iridium centre; the use of smaller NHC-chloride catalysts, such as **56**, has been shown to allow for HIE at the *ortho*- position of sulfonamide-substituted aromatic systems.⁵⁹ Additionally, ongoing work within the group is focussed upon the application of novel catalyst systems bearing chelating NHC-phosphine ligands in the labelling of sulfones and sulfonamides. Given the relevance of this functional group, it was decided to prepare an *N*-methylsulfonyl-substituted indole, to use as a labelling candidate, by reacting indole with methanesulfonyl chloride. Somewhat unexpectedly, 1,3-bis(methylsulfonyl)-substituted indole **121** was obtained in 94% yield (Scheme 1.33), with two additions of the sulfonyl group having taken place. It was decided, however, that **121** could still represent an interesting labelling substrate.



Scheme 1.33

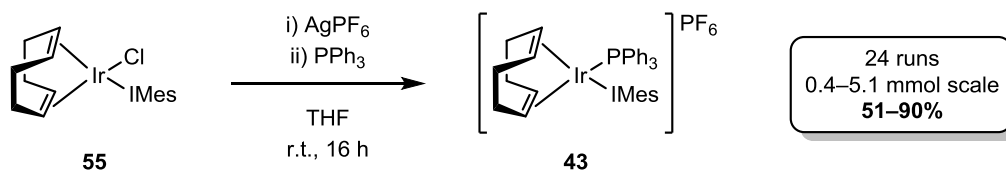
With a range of *N*-substituted indole substrates in hand, our attention turned to the choice of catalytic conditions to be employed. Numerous studies conducted within the Kerr group over the last decade have shown the combination of bulky IMes and PPh₃ ligands to be a highly efficient ligand set for HIE catalysis. With this in mind, it was decided that screening of the substrates prepared so far should be conducted using [Ir(cod)(PPh₃)(IMes)]PF₆ **43** as the model catalyst.

The widespread utility of **43** in hydrogen isotope exchange reactions means that it is now sold commercially through Strem Chemicals, along with its PMe₂Ph and PBN₃ analogues.⁵⁷ In order that sufficient quantities were prepared for sale, **43** and its precursor **55** were synthesized on over a 3 g scale. Firstly, **55** was prepared in good to excellent yield through the reaction of commercially available dimer [Ir(cod)Cl]₂ (**27**) with IMes (Scheme 1.34).



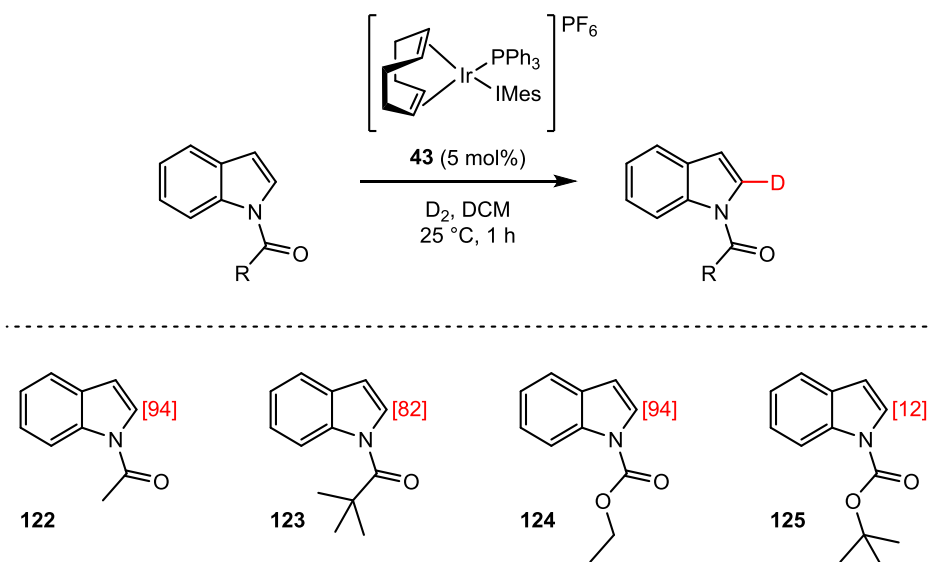
Scheme 1.34

Subsequent halide abstraction with silver hexafluorophosphate and reaction with triphenylphosphine afforded complex **43**. A total of 24 runs of this reaction proceeded in good to excellent yields (Scheme 1.35). As detailed previously, the synthesis of **43** is exceptionally mild and convenient; unlike preparations frequently reported for similar complexes, the use of a glove box is not required and all steps can be carried out under standard Schlenk conditions.



Scheme 1.35

Having been prepared in excellent yield, complex **43** could now be employed as a catalyst in the labelling of *N*-substituted indole substrates. Substrates **117–120**, bearing amide or carbamate protecting groups, were evaluated under mild HIE conditions using catalyst **43** (Scheme 1.36).

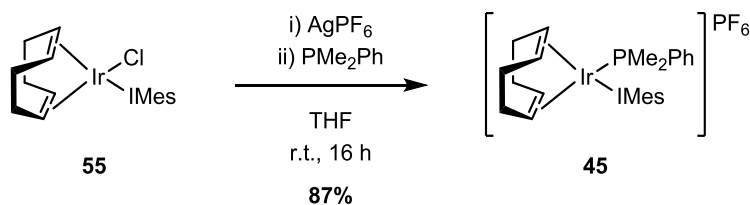


NB Incorporations are an average of two runs

Scheme 1.36

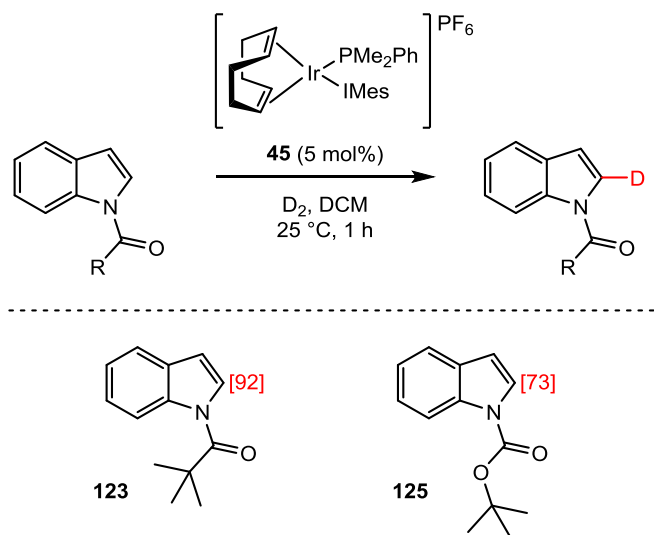
We were delighted to see that for *N*-acetyl indole **117**, labelling occurred exclusively at the C2 position, affording **122** with an excellent 94% deuterium incorporation. With the bulkier directing group in *N*-pivaloyl indole, labelling was reduced slightly to 82% (**123**). A similar drop-off in labelling ability was observed for the carbamate-protected indoles. For the ethyl carbamate derivative **120**, catalyst **43** delivered an impressive 94% labelling (**124**). Upon moving to the bulkier Boc protecting group, however, only 12% deuteration was observed in **125** with catalyst **43**.

For the pivaloyl- and Boc-protected indoles, it was thought that switching to a smaller catalyst motif might increase the labelling. Complex **45** was therefore prepared in an excellent yield using the method described previously (Scheme 1.37).



Scheme 1.37

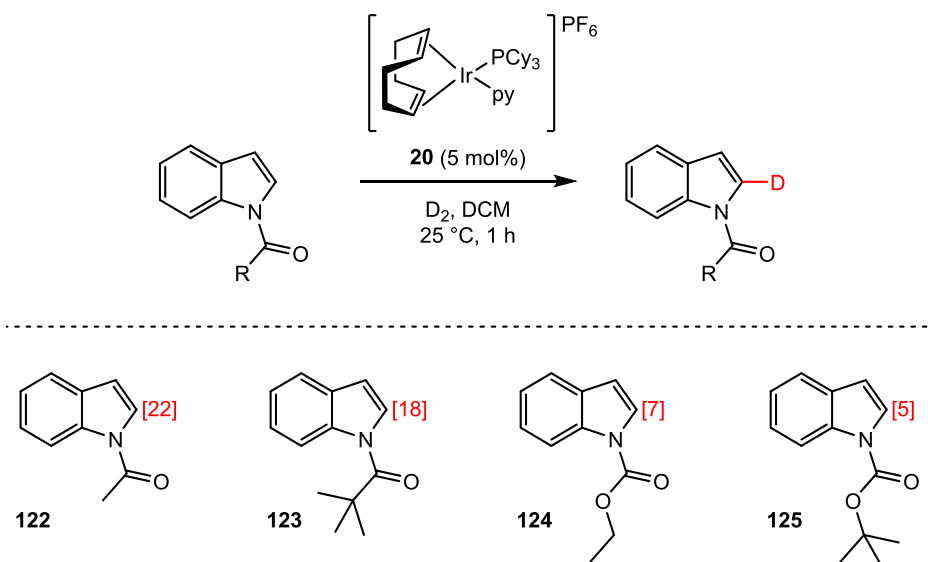
Pleasingly, when subjected to the HIE conditions with catalyst **45**, bearing a smaller phosphine ligand, deuterium incorporation in **123** and **125** increased to 92% and 73% respectively (Scheme 1.38).



NB Incorporations are an average of two runs

Scheme 1.38

In order to compare our catalyst system to the previous industry standard, reactions with substrates **117–120** were also conducted with Crabtree's catalyst **20**. We were pleased to see that complex **43** outperformed **20** as a catalyst in all reactions (Scheme 1.39), with only low levels of incorporation (up to 22%) observed with **20** under the conditions used for labelling with **43**.

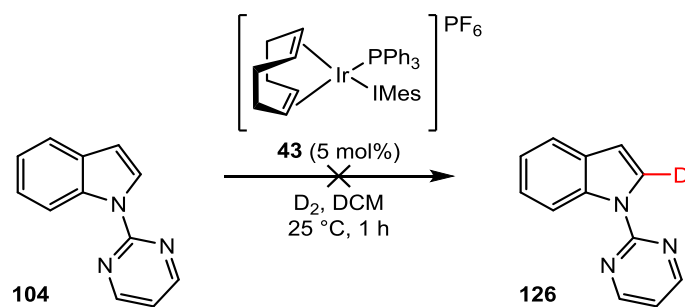


NB Incorporations are an average of two runs

Scheme 1.39

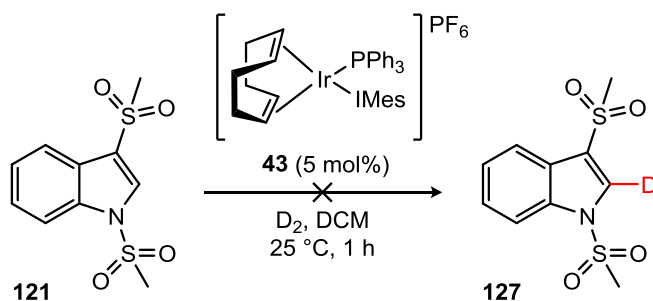
Having achieved such promising levels of deuterium incorporation with the acyl protecting groups used so far, we were keen to see if we could extend this methodology to the use of nitrogen-containing groups as functional handles. Pyridines and pyrimidines have been previously employed in aromatic directed HIE reported by the Kerr group, so there was a promising precedent.^{49,58}

Compound **104** was thus subjected to the reaction conditions used for the successful labelling of other *N*-protected indoles (Scheme 1.40). Disappointingly, deuterium incorporation was not observed. Despite both pyridyl and pyrimidyl directing groups having been previously used in labelling chemistry, we were not deterred by the lack of success in the indole system used here. One of the reasons for these heterocycles' widespread use as functional handles is their excellent ability to coordinate to metal centres such as iridium; such a trait, however, is not without its disadvantages. In some cases, coordination from the pyrimidyl nitrogen can be so strong that it binds irreversibly to the iridium centre, effectively "poisoning" the catalyst and removing any active species from the catalytic system.⁸⁹ We proposed that such a process could be occurring here.



Scheme 1.40

The last remaining substrate for testing was (bis)methylsulfonylindole **121**. Unfortunately, our previously successful labelling conditions resulted in no deuterium incorporation (Scheme 1.41).



Scheme 1.41

As mentioned before, this was not entirely surprising. It is highly likely that binding of either tetrahedral sulfonamide group to the iridium centre is not energetically favoured. As depicted in Figure 1.19, the presence of bulky phosphine and NHC ligands causes significant steric hindrance around the iridium centre, making substrate binding difficult. Ongoing work within the Kerr group is focusing on the development of a new family of chelating NHC-phosphine complexes, which aim to expand the applicability of our labelling methodology to bulky tetrahedral substrates by forcing the NHC and phosphine ligands to occupy positions *cis*- to one another. As such, it was decided to halt attempts at the labelling of substrate **121** at this point; this can be revisited when a more suitable chelating ligand is available.

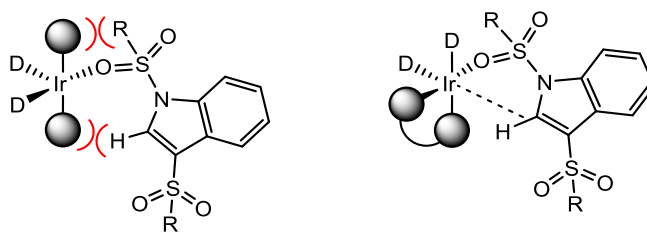
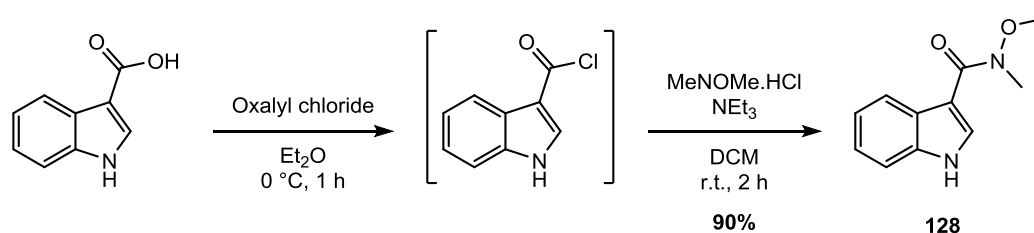


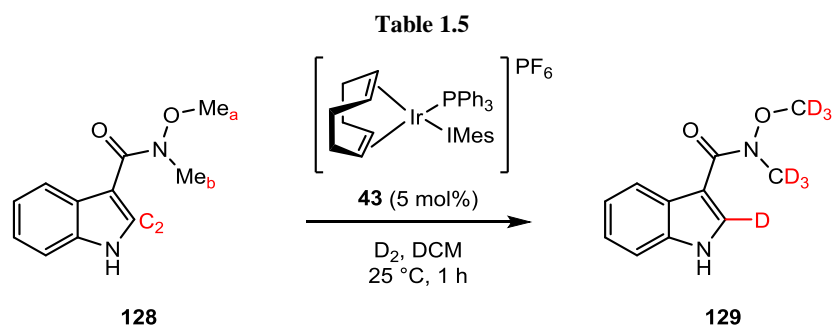
Figure 1.19

Having established an efficient method for the C2 labelling of acyl-protected indoles, we were keen to explore the use of directing groups at the C3 position of the indole ring. As such, Weinreb amide **128** was first prepared in a pleasing 90% yield (Scheme 1.42).



Scheme 1.42

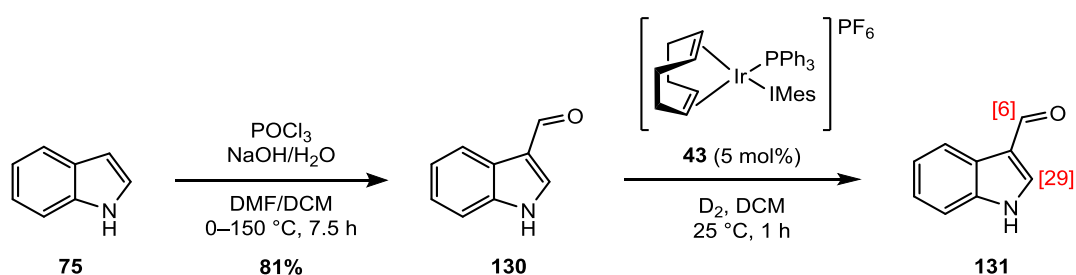
When **128** was subjected to our labelling conditions, we were delighted to see excellent labelling at the C2 position (Table 1.5, Entry 1). Some labelling of the two Weinreb amide methyl groups was also observed. When the reaction was repeated at a lower catalyst loading, methyl labelling was seen to decrease with minimal loss of C2 labelling (Entry 2).



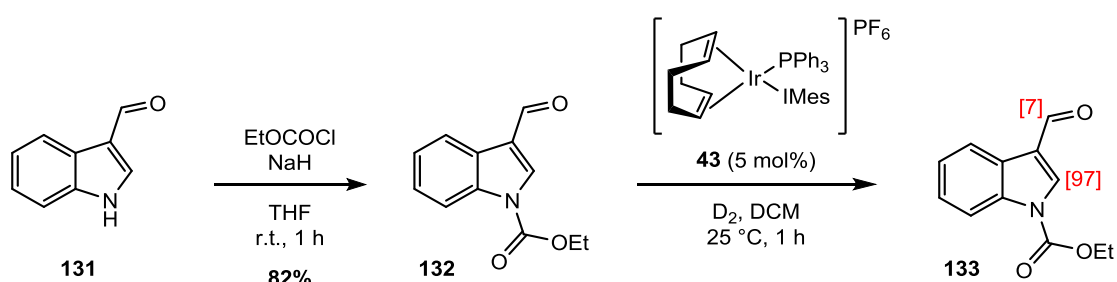
Entry	Catalyst Loading / mol%	%D _{C2}	%D _{Me^a}	%D _{Me^b}
1	5	99	27	27
2	2	96	8	11

NB Incorporations are an average taken over 2 runs

As a more challenging example, we sought to attempt labelling using an aldehyde directing group at the C3 position. The use of aldehydes as directing groups is more complicated than the previous functional handles explored; as well as the challenge of controlling selectivity between labelling on the aromatic ring and at the aldehydic position, decarbonylation presents itself as a competing reaction. 3-Formyl substituted indole **130** was prepared in a pleasing 81% yield to be used as a model substrate, and was then subjected to our standard labelling conditions (Scheme 1.43). We were pleased to observe selectivity for deuteration of the C2 position over the aldehydic position, though with only a moderate 29% incorporation at C2.

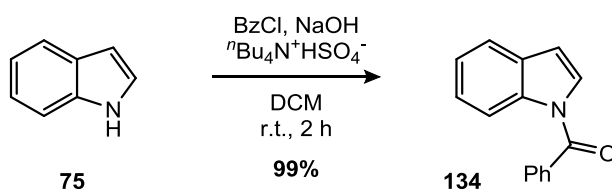


In order to examine the possibility of a double directing group effect, a carbamate group was installed onto the indole nitrogen atom. When the labelling of **132** was carried out (Scheme 1.44), we were delighted to observe 97% deuteration at the C2 position. Importantly, no decarbonylation and minimal aldehydic labelling was observed, confirming that our mild labelling conditions are tolerant of the aldehyde functionality.



For all substrates screened to this point, we had observed complete selectivity for activation and labelling of the C2 C–H bond. While we were delighted with these results, they were not

surprising. Previous work within the group has shown the formation of a 5-mmi to occur preferentially over the formation of a 6-mmi, so the fact that deuterium was incorporated into the C2 position over C3 or C7 positions was in keeping with previous results.⁴⁹ Next, we were keen to investigate the preference for the labelling of a heterocyclic substrate over a competing aromatic site. The ideal substrate by which to assess this selectivity was decided to be *N*-benzoylindole **134**, which was prepared easily in quantitative yield (Scheme 1.45).



Scheme 1.45

As depicted in Figure 1.20, substrate **134** has 3 possible sites for carbonyl-directed C–H activation. As well as the indole C2 position and more energetically challenging C7 position (accessed *via* a 6-mmi), the *ortho*-positions of the benzoyl group can be activated *via* a 5-mmi.

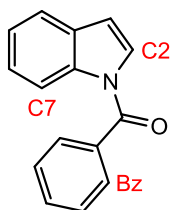
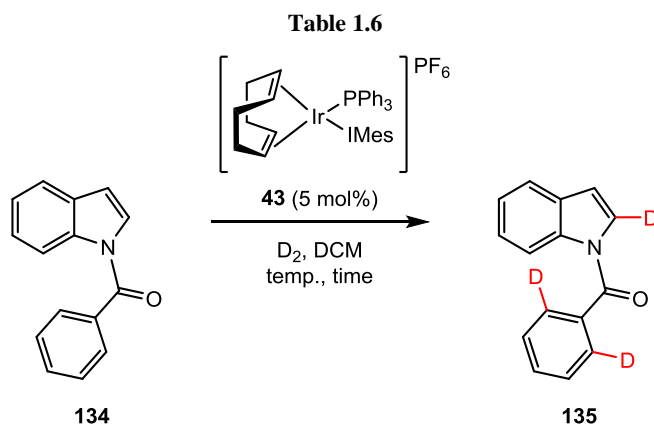


Figure 1.20

When the labelling of **134** was investigated, we were delighted to observe remarkable selectivity for deuteration at the C2 position over the aromatic *ortho*-protons in the benzoyl group (Table 1.6, Entry 1). Unsurprisingly, no C7 activation was observed whatsoever. Through tuning of the reaction conditions, deuterium incorporation at C2 was increased to 80–90%, maintaining only minimal labelling on the benzoyl group (Entries 2–3).



Entry	Temperature / °C	Time / h	%D _{C2}	%D _{Bz}
1	25	1	73	2
2	25	24	90	6
3	40	1	80	4

NB Incorporations are an average taken over 2 runs

To understand the origins of the remarkable selectivity observed, the reaction was studied computationally, in order to examine the relative energies of binding and C–H activation for each of the possible labelling sites. Work within the Kerr group has previously shown that in compounds containing more than one directing group, the binding energy for each group plays a key role in determining the selectivity.^{51,90} In **134**, however, all three potential labelling sites are accessed from the same directing group. In this case, the relative C–H bond activation energies for each binding conformer might be expected to influence the selectivity.⁵¹

Figure 1.21 shows the three potential energy surfaces (PESs) for C–H activation. At the initial binding phase, the conformer leading to C7 deuteration is the lowest in free energy ($G_{\text{rel}} = 0.0 \text{ kcal mol}^{-1}$), albeit only marginally more stable than the conformation for benzoyl activation (+ 0.4 kcalmol⁻¹). In contrast, the conformer leading to activation of the C2 position is significantly destabilised (+ 4.5 kcalmol⁻¹). Given that the C2 position is the preferred labelling site, these energy differences suggest that the lowest energy binding modes are not the most reactive; this is in contrast to our previously published results, which showed that the binding mode stability determined selectivity in substrates with more than one directing group.⁵¹

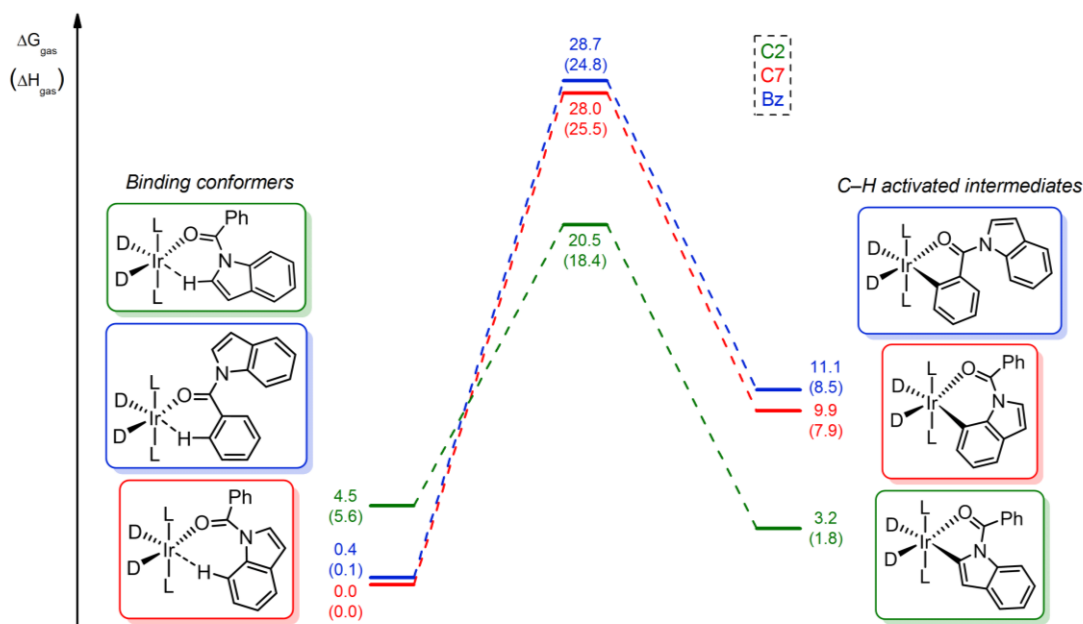


Figure 1.21

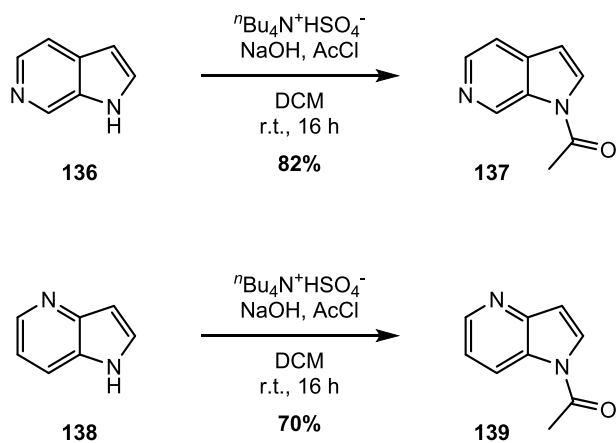
Instead, calculation of the energy barriers to the respective C–H activation processes reveals that the free energy barrier to activation of the C2 position is by far the lowest of the three processes. In addition, it is the only exothermic reaction coordinate of the three. The absolute free energy barriers to C–H activation of the three possible labelling sites are summarised in Table 1.7. Values were calculated using M06/6-31G* in the gas phase.

Table 1.7

Entry	Binding Conformer	ΔG^\ddagger / kcal mol ⁻¹	ΔG^0 / kcal mol ⁻¹
1	Bz	24.8	8.5
2	C7	25.5	7.9
3	C2	18.4	1.8

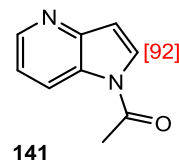
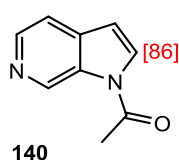
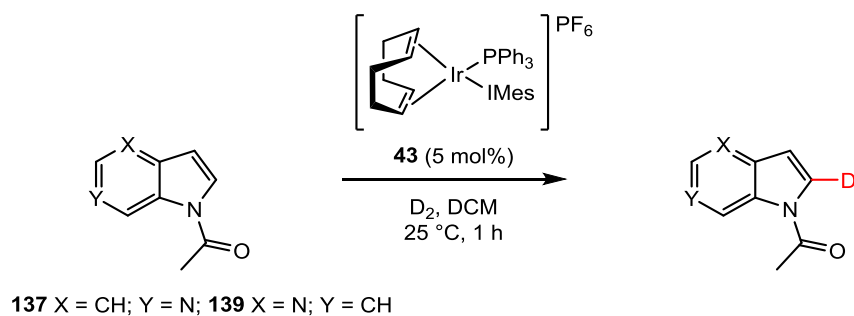
We can therefore conclude that the kinetic barrier to C–H activation of the C7 and benzoyl positions is the source of the remarkable labelling selectivity observed. These results are in keeping with the Kerr group's previous observations for the labelling on benzanilide, where two labelling sites are accessed *via* the same directing group and selectivity is governed by the preference for a 5- vs a 6-mmi.⁴⁹

With such promising results having been achieved for the labelling of indoles, we sought to expand the scope of our methodology to alternative heterocycle moieties. In the first instance, we looked to the labelling of indazoles and azaindoles. The presence of an extra heteroatom in each of these systems means that there is a competing coordination site; this can lead to “poisoning” of the catalyst by irreversible binding. To prepare suitable labelling substrates, azaindoles **136** and **138** each successfully underwent acetyl protection reactions (Scheme 1.46).



Scheme 1.46

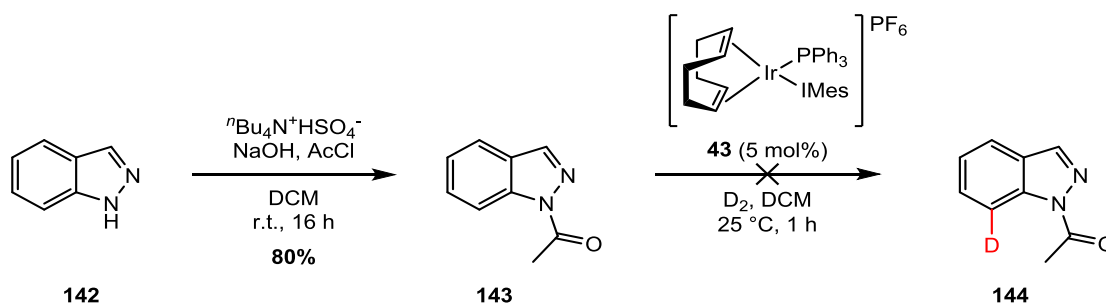
When subjected to our labelling conditions (Scheme 1.47), we were delighted to see high levels of deuteration at the C2 position, showing that the presence of an additional nitrogen atom had no negative effects on coordination.



NB Incorporations are an average of two runs

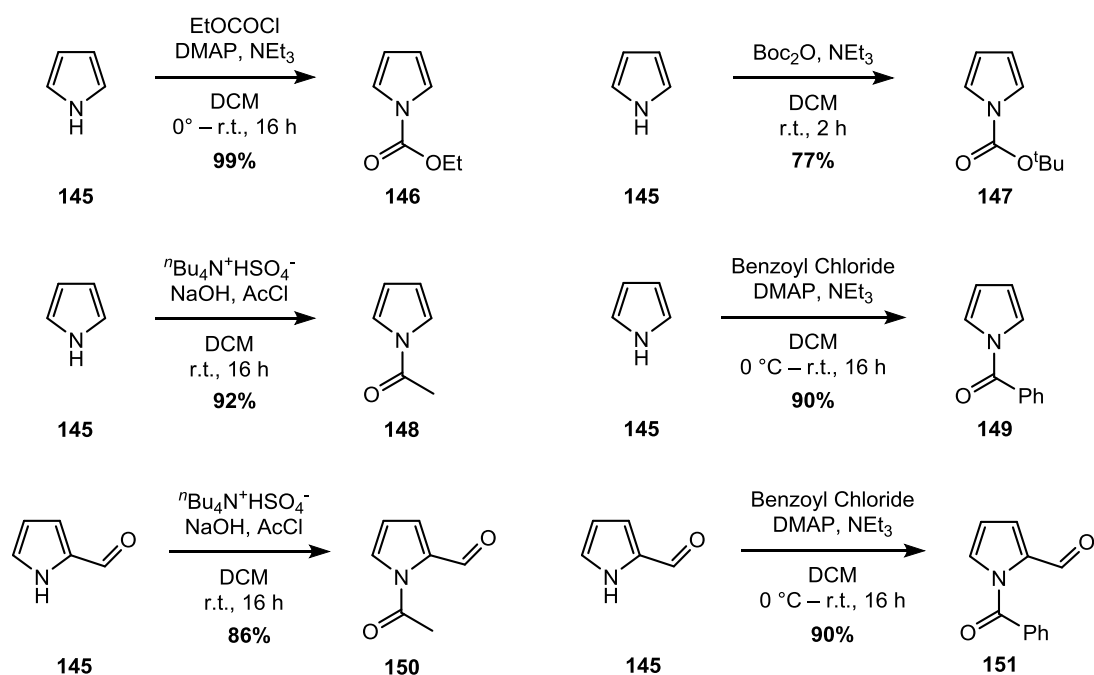
Scheme 1.47

In an attempt to bias the system towards labelling at the C7 position, *N*-acylindazole **143**, with the C–H unit at the C2 position replaced by a nitrogen, was employed as a substrate. **143** was prepared in good yield from the parent compound (Scheme 1.48). When subjected to our labelling conditions, however, no labelling whatsoever was observed.



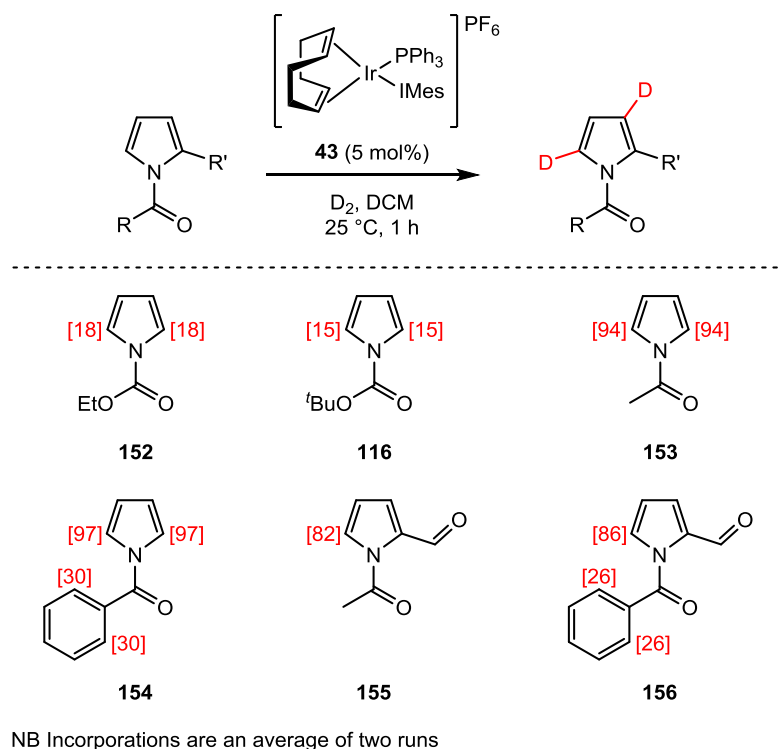
Scheme 1.48

Eager to extend our substrate scope to smaller heterocycles, we set about preparing a range of substituted pyrroles (Scheme 1.49). These were then subjected to our labelling conditions (Scheme 1.50).



Scheme 1.49

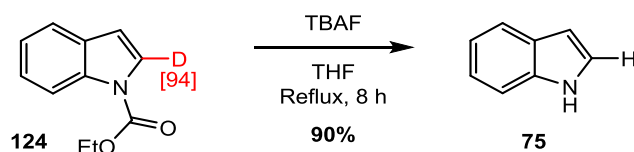
While the ethyl and *tert*-butyl carbamate-protected pyrroles, **146** and **147**, mediated labelling to less than 20%, we were pleased to observe that acetyl- and benzoyl-protected pyrroles, **148** and **149**, were labelled with high deuterium incorporation. Furthermore, their formyl-substituted analogues, **150** and **151**, were also labelled efficiently, with no decarbonylation or aldehyde labelling observed. In substrates **149** and **151**, selectivity was, again, observed for the C2 position over the competing benzoyl positions, though at a decreased level to that observed with *N*-benzoyl indole **134**. Whilst no computational studies were undertaken in order to assess this selectivity, it could be proposed that the smaller size of the pyrrole ring compared to the indole ring could have a significant effect on the flexibility and stability of the potential binding conformers, perhaps decreasing the free energy barrier for aromatic C–H activation.



Scheme 1.50

The work conducted up to this point had afforded us a mild and selective route to high deuterium incorporation at the C2 position of *N*-protected indoles. It was of paramount importance to us, however, that the protecting groups used as functional handles could be removed under mild conditions and without the loss of any deuterium label. As discussed previously, one of the key advantages of hydrogen isotope exchange is that it can be used in the late stages of complex molecule synthesis. Since total synthesis projects are often heavily dependent on the use of multiple protection and deprotection steps, it was considered essential that substitution on the indole nitrogen could be altered while maintaining high levels of deuterium incorporation.

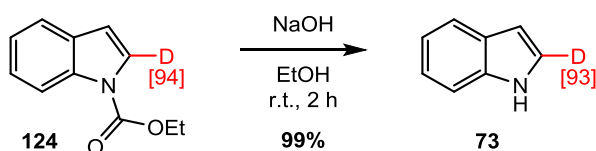
A deprotection strategy for the ethyl carbamate protecting group was first investigated. After C2 labelling, the deprotection of **124** with tetra-*n*-butylammonium fluoride was attempted, following a literature procedure (Scheme 1.51).⁹¹



Scheme 1.51

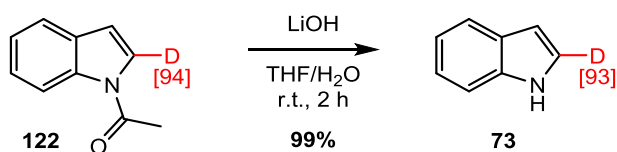
While the deprotection reaction proceeded in 90% yield, we were disappointed to see that the deuterium label had been replaced with hydrogen. Since the TBAF deprotection of carbamates is believed to occur *via* nucleophilic attack of the fluoride ion at the carbonyl unit to form a fluorocarbamate,⁹¹ hydrogen isotope exchange at the C2 position would not be expected to take place. It was noted, however, that “anhydrous” TBAF is often contaminated with the bifluoride species HF_2^- , which is generated *via* decomposition during the drying process.⁹² The bifluoride anion can act as a weak acid, and moreover is in equilibrium with HF, a much stronger acid. While most commercial sources of TBAF now contain water as a stabiliser, the presence of trace acid is still a very real possibility. As discussed previously, both the C2 and C3 positions of the indole moiety are nucleophilic, meaning that non-selective exchange can occur at both positions in the presence of acid. It was therefore decided to investigate basic conditions for deprotection instead.

Pleasingly, ethyl carbamate-protected deuterioindole **124** successfully underwent deprotection using sodium hydroxide in ethanol (Scheme 1.52). Most importantly, only negligible loss of the deuterium label was observed.



Scheme 1.52

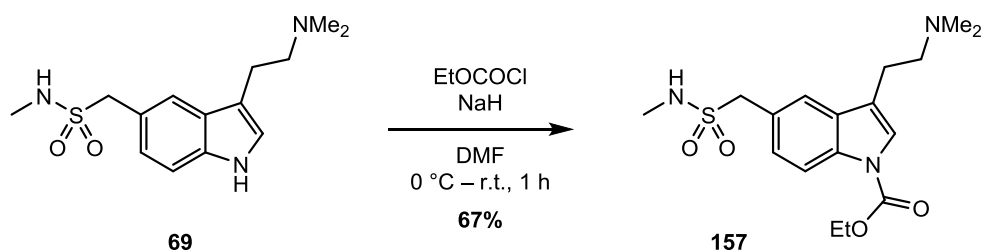
We next looked to the removal of the *N*-acetyl group from indole **122**. We were delighted to see that deprotection proceeded under basic conditions in quantitative yield, with retention of the deuterium label at the C2 position (Scheme 1.53).



Scheme 1.53

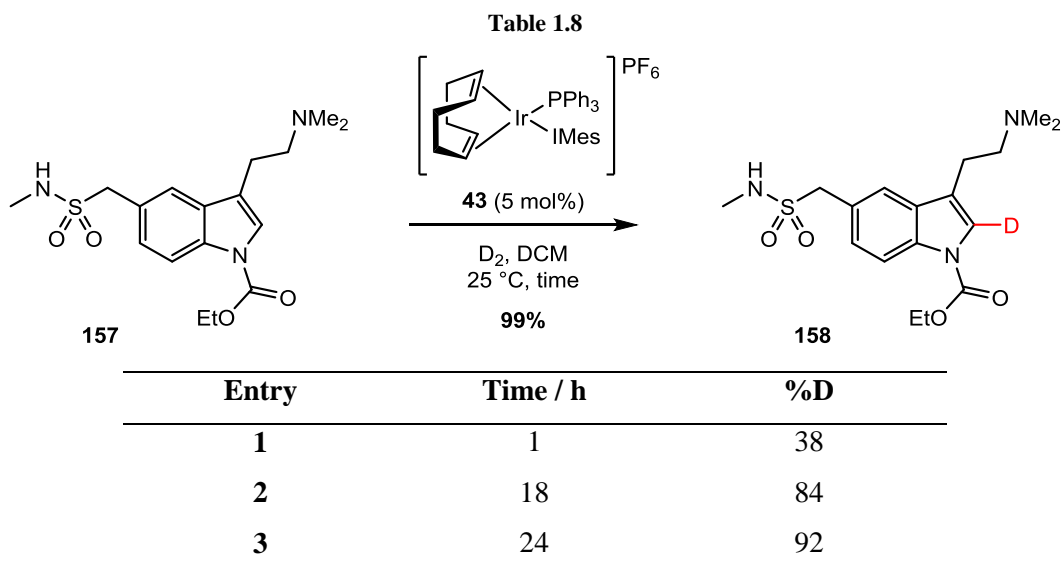
As a final C2 labelling example, we sought to apply our developed methodology to the deuteration of a drug molecule. As discussed previously, our motivation for achieving the selective labelling of indoles and related *N*-heterocycles lay in their physiological importance and prevalence as moieties in a range of pharmaceutical compounds, and we wished to highlight the potential applications of our methodology in the pharmaceutical industry.

We targeted the labelling of Sumatriptan **69**, a member of the triptan family of anti-migraine drugs.⁹³ Firstly, ethyl carbamate protection of **69** was carried out in order to introduce a C2 directing group (Scheme 1.54).

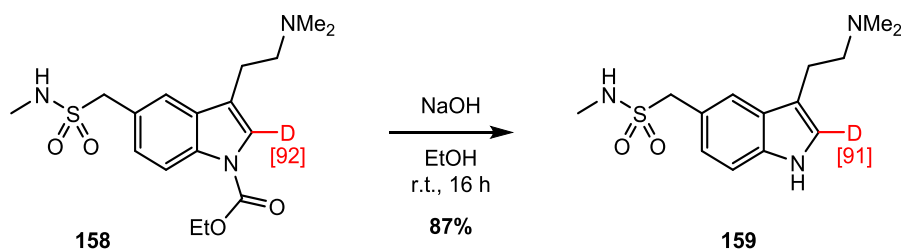


Scheme 1.54

Ethyl carbamate-protected substrate **157** was then subjected to our standard labelling conditions (Table 1.8). We were delighted to see that even in the presence of a sulfonamide and a tertiary amine, a moderate 38% deuterium incorporation was achieved after just 1 h (Entry 1). Increasing the reaction time led to an increase in labelling (Entry 2), and extending to 24 h led to an excellent 92% labelling at the C2 position (Entry 3), with the low catalyst loading and ambient pressure and temperature maintained.



Lastly, the deprotection of labelled compound **158** was carried out under our previously developed conditions (Scheme 1.55). Pleasingly, this proceeded in excellent yield with negligible degradation of the isotopic label, yielding 2-deuteriosumatriptan **159** in a 57% yield over the three steps of protection, labelling, and deprotection.



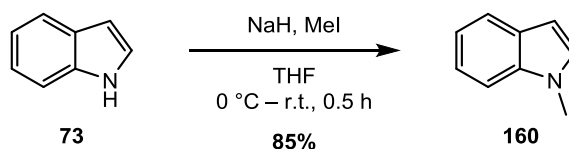
Scheme 1.55

In summary, we have established a mild and general method for the C2 deuteration of *N*-heterocycles. Using common *N*-protecting groups as removable functional handles, high levels of deuterium incorporation have been achieved on a wide range of substrates. Remarkable selectivity for C–H activation *via* a 5-*mmi* is observed, and the C2 position can be selectively labeled in the presence of benzoyl groups. The labelling and subsequent deprotection of the commercial migraine drug Sumatriptan serves to highlight the applicability of our mild and selective process to the pharmaceutical industry.

C3 Labelling of *N*-Protected Indoles

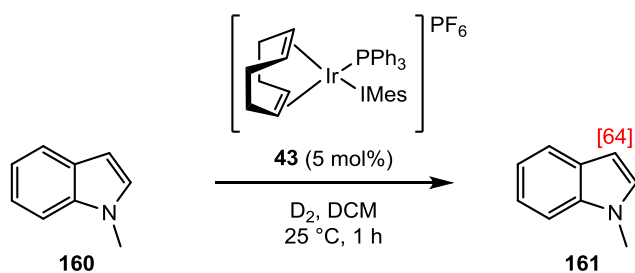
Having achieved such positive results with the use of *N*-protecting groups as directing groups for selective C2 labelling, we next sought to investigate the effects of the presence of alternate protecting groups, which did not possess a donor group, in our HIE reactions. Whilst conducting labelling reactions for the synthesis of substrates to be used in kinetic isotope effect studies, You and co-workers reported the C3-deuteration of indole substrates bearing an *N*-phenyl or *N*-benzyl group using a rhodium(III) catalyst, albeit achieving no more than 24% deuteration, and we wondered whether we would observe similar results in reactions catalysed by our group's iridium(I) catalysts.⁷⁵

As discussed previously, methodology for the selective C3 deuteration of indole is limited, and early methods often involved the use of strongly acidic conditions, which can cause problems in the late stages of complex molecule synthesis.⁸¹ While more recent methods, such as those reported by the groups of Rousseau and Chirik, have used milder conditions to achieve HIE at the C3 position, both of these examples still suffer from a lack of selectivity, with C2 labelling also observed in both cases.^{84,85} As such, methods for selective C3 deuteration of indoles are still required. As a model substrate, we first prepared *N*-methylindole **160** in an excellent 85% yield following a literature procedure (Scheme 1.56).⁹⁴



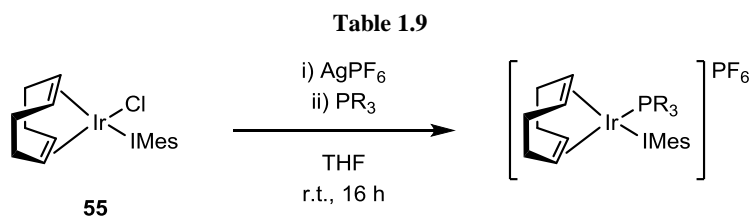
Scheme 1.56

When compound **160** was subjected to the previously-developed labelling conditions, we were delighted to see exclusive deuterium labelling at the C3 position (Scheme 1.57). The incorporation of 64% appeared incredibly promising, given that such mild conditions had been successfully employed with no optimisation yet carried out.



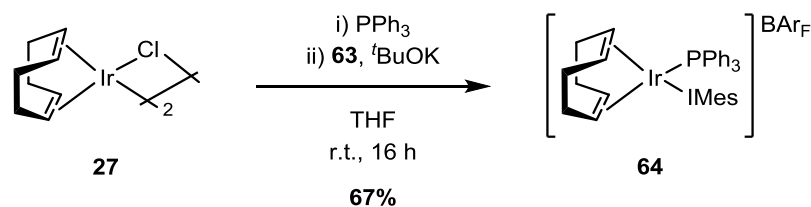
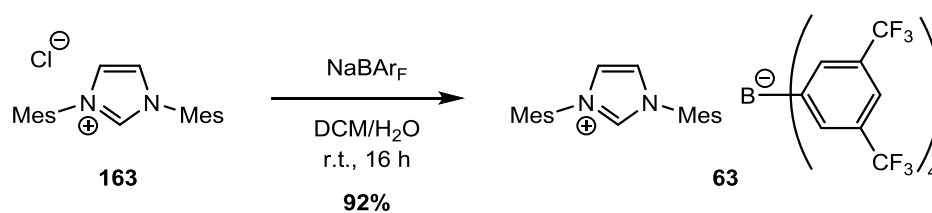
Scheme 1.57

We next sought to carry out a more thorough screening of our group's catalysts and, as such, synthesised a small range of complexes. Hexafluorophosphate complexes **46** and **162**, bearing alternative phosphine ligands, were prepared in excellent yields using the method described previously (Table 1.9).



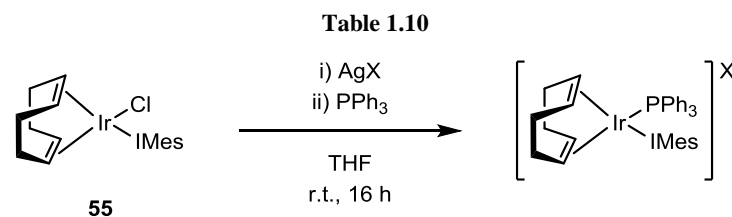
Entry	PR ₃	Product	Yield / %
1	PBn ₃	44	77
2	P ^{<i>i</i>} Bu ₃	162	73

It was also considered that the choice of counterion could have an effect on catalyst activity; our group's work has demonstrated that the use of a larger, more weakly coordinating anion, such as BAr_F, can offer more efficient catalysis.⁶⁰ With this in mind, BAr_F complex **64** was prepared in a two-step process (Scheme 1.58). Firstly, imidazolium BAr_F salt **63** was prepared through a salt metathesis reaction with NaBAr_F. Iridium(I) NHC-chloride complex **55** was then reacted with triphenylphosphine, before addition of **63** and potassium *tert*-butoxide, to afford complex **64** in a pleasing 67% yield.



Scheme 1.58

Lastly, complexes **65** and **66**, bearing smaller counterions, were also prepared using silver triflate and silver tetrafluoroborate salts (Table 1.10).

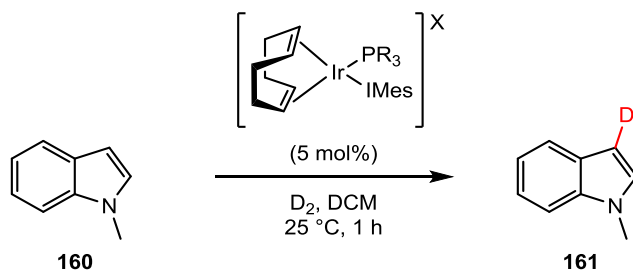


Entry	X	Product	Yield / %
1	OTf	65	69
2	BF ₄	66	80

With a range of alternative complexes in hand, a catalyst screening was carried out for the labelling of *N*-methylindole **160** (Table 1.11). While **45** and **162** were found to be poor labelling catalysts (Entries 1 and 3), complex **44**, bearing a more weakly σ -donating phosphine ligand, offered a promising incorporation of 54% (Entry 2).

BAR_F counterion catalyst **64** was tested, but was found to be less effective than **43** (Entry 4). Smaller counterions, such as those in catalysts **65** and **66**, however, also had a detrimental effect on deuterium incorporation (Entries 5 and 6).

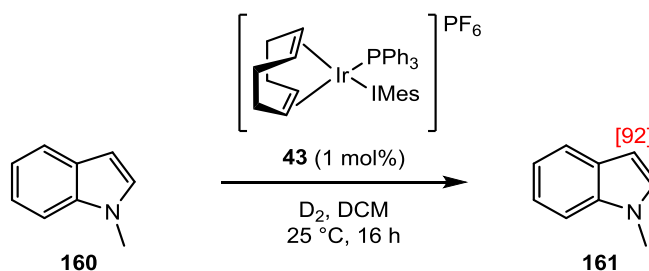
Table 1.11



Entry	Catalyst	PR ₃	X	%D
1	45	PMe ₂ Ph	PF ₆	25
2	44	PBn ₃	PF ₆	54
3	162	P ⁿ Bu ₃	PF ₆	7
4	64	PPh ₃	BAr _F	47
5	65	PPh ₃	OTf	38
6	66	PPh ₃	BF ₄	21

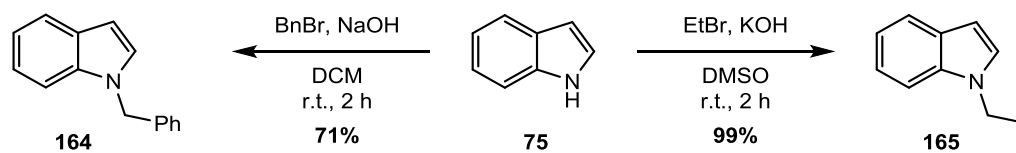
NB Incorporations are an average taken over 3 runs

Based on this initial screening, we chose to carry out further optimisation with catalyst **43**. In order to maximise the output of the screening process and assess the importance of multiple variables, optimisation was carried out using Design of Experiments.^{95,96} A 2-level, 3-factorial design was employed, in which the effects of catalyst loading, reaction time, and solvent volume were scrutinised. Examination of the data from this reaction indicated that catalyst loading and reaction time were the most important factors in achieving high incorporations. Pleasingly, by increasing the reaction time, we were able to achieve excellent deuterium incorporation at the C3 position at a low catalyst loading of 1 mol%. The optimised conditions are shown in Scheme 1.59.



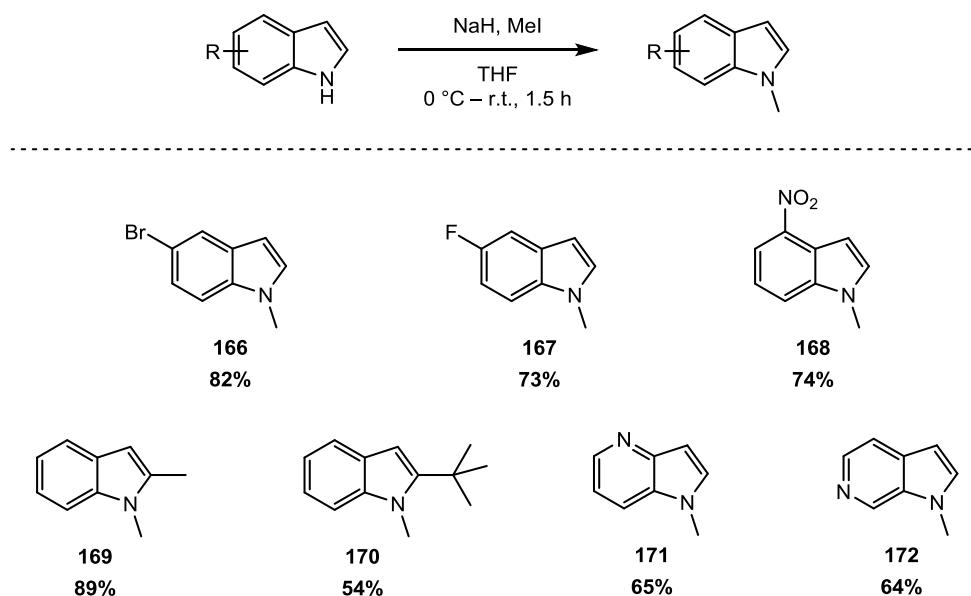
Scheme 1.59

In order to evaluate the applicability of this labelling process, we sought to prepare a larger series of substituted indoles for screening. *N*-benzyl- and *N*-ethylindole (**164** and **165**) were first prepared according to literature procedures (Scheme 1.60).



Scheme 1.60

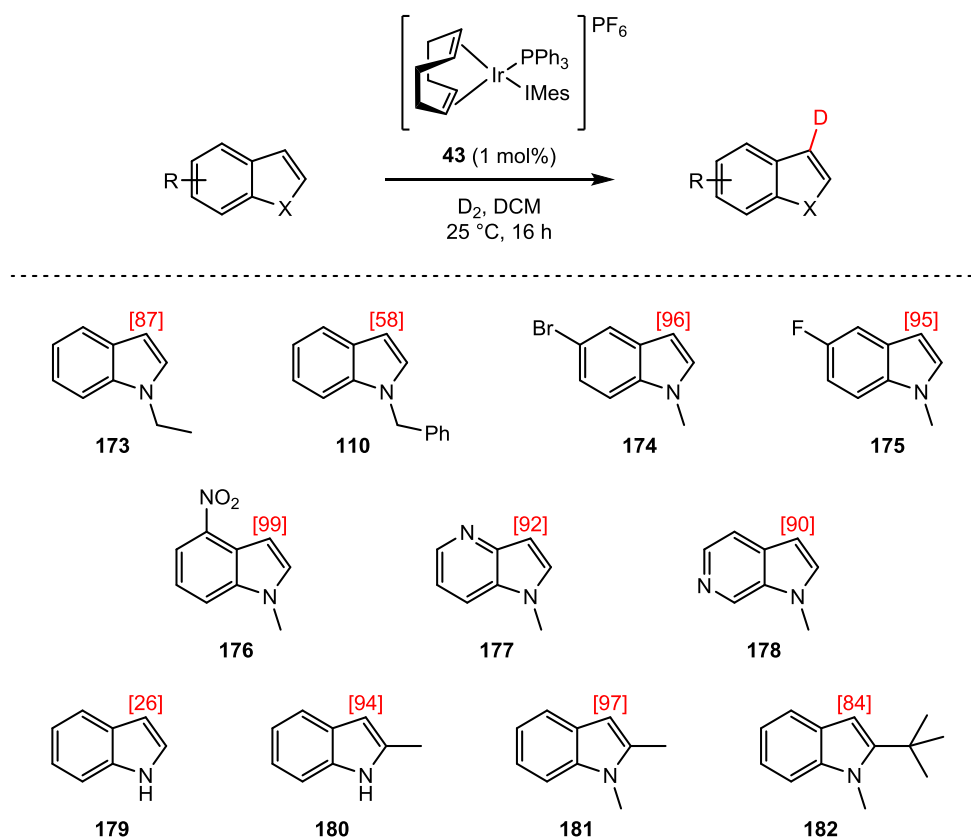
Next, *N*-methylation reactions were conducted on a range of free indoles (Scheme 1.61), including those with substitution at the C2 position, to afford *N*-methylindoles **166–172** in good to excellent yields.



Scheme 1.61

When these substrates were subjected to our optimised conditions, we found that altering the substitution on both the nitrogen atom and the heteroaromatic moiety was well tolerated (Scheme 1.62), affording a series of 3-deuterioindoles **173–182**, albeit with a small decrease in labelling efficiency for *N*-benzylindole **164**. Pleasingly, substrate **168**, bearing a coordinating nitro- group which could direct C–H activation at the indole C5 position, underwent quantitative and exclusive C3 labelling to afford **176**. We were encouraged, once again, to observe that azaindoles **171** and **172** were also labelled efficiently, with no catalyst

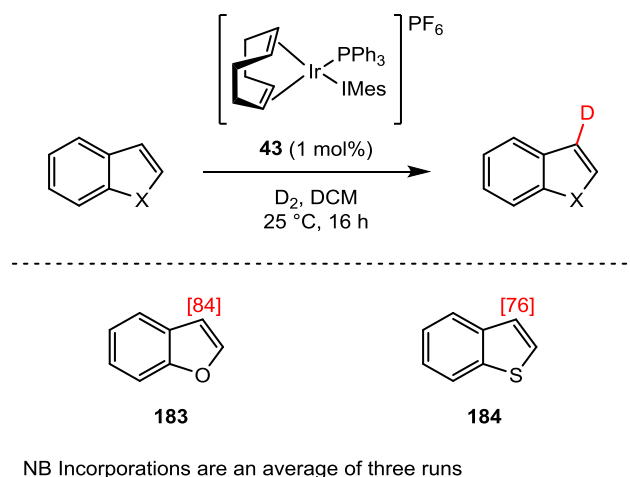
poisoning observed as a result of the pyridine unit present. As a control and to probe whether the presence of a functional group at the indole nitrogen position was necessary, the reaction was also conducted with free indole and 2-methylindole. While **179** only underwent 26% deuteration, the high incorporation in **180** demonstrated that an absence of substitution at the nitrogen position was not detrimental to the reaction, and that substitution at the C2 position was also tolerated. This was further highlighted in the successful labelling of bulky 2-*tert*-butyl-*N*-methylindole **169**.



NB Incorporations are an average of three runs

Scheme 1.62

In a final demonstration of the utility of our C3 labelling process, benzofuran **183** and benzothiophene **184** were subjected to our deuteration conditions (Scheme 1.63). We were delighted to see that both substrates underwent C3-selective labelling to satisfactory levels of incorporation, representing an important progression into the labelling of heterocyclic substrates that are unable to bear a directing group on the heteroatom.



Scheme 1.63

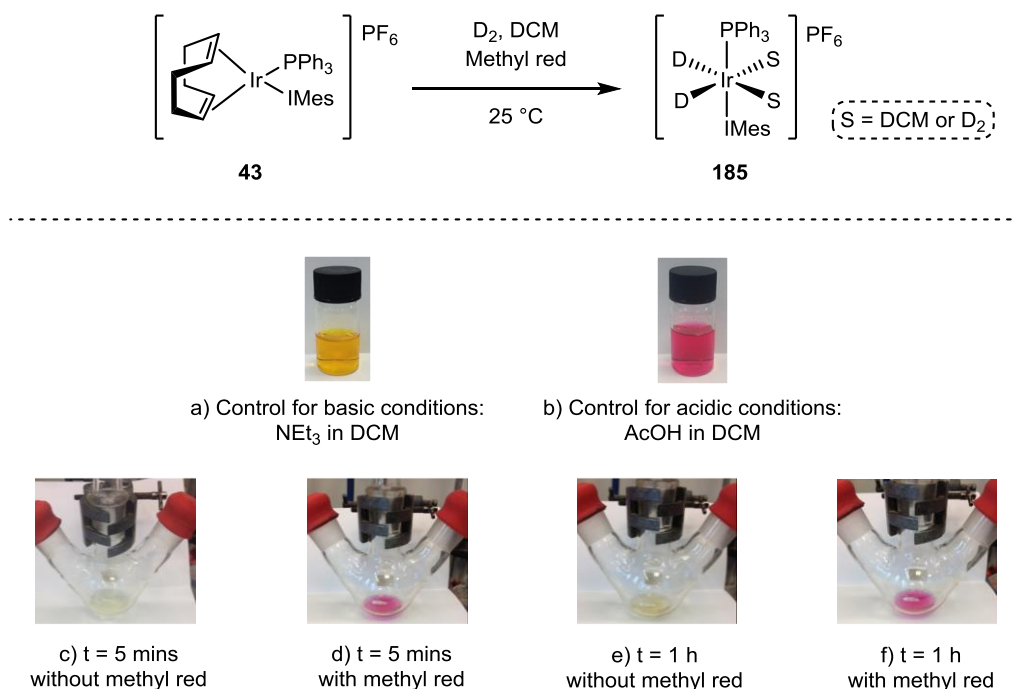
There is little precedent in the literature for iridium-catalysed HIE in the absence of a coordinating directing group, and we were keen to understand the mechanism of this novel C3 labelling process. Clearly, the reaction could not proceed *via* the same mechanism as our donor-directed C2 labelling; instead, our attention turned to the mechanisms of previously-reported processes for C3 labelling of indoles.^{81,97} As detailed previously, the majority of methods for installing a deuterium atom at the C3 position involve the use of deuterated acids, relying on the C3 carbon atom's inherent nucleophilicity for the reaction with an electrophilic deuterium atom.⁹⁸ The indole C3 position reacts 10^{13} times faster than benzene in S_EAr reactions, and while the C2 position reacts more slowly, it is also mildly nucleophilic. This reactivity is often responsible for the lack of selectivity observed in C3 deuteration reactions of indoles, such as that reported by Jackson and co-workers.⁸¹

We proposed that if the treatment of *N*-alkyl indoles with iridium catalyst **43** in the presence of D_2 caused the generation of an iridium complex bearing acidic deuteride ligands, then the nucleophilic C3 carbon atom could potentially react with one of these ligands through an S_EAr process. This hypothesis is consistent with the labelling results obtained for indole **75** and *N*-methylindole **160**; Mayr and co-workers have shown that the presence of an *N*-methyl group increases C3 nucleophilicity.⁹⁸

As a simple assessment of the viability of such a mechanism, we considered the use of an indicator that could confirm the presence of acidic intermediates. Employing a simple and elegant method developed by Burgess and co-workers in their comparison of hydride acidities in phosphine and NHC complexes,⁹⁹ catalyst **43** was subjected to the reaction

conditions in the absence of substrate (Scheme 1.64). Previous mechanistic studies within the Kerr group have shown that species **185** is rapidly generated under a deuterium atmosphere, and the intermediacy and catalytic competency of Ir^{III} dihydride complexes is well preceded.^{51,100}

Within a few minutes, a colour change from orange to pale yellow was observed; this is consistent with the formation of **185**.



Scheme 1.64

After 5 minutes, methyl red indicator was added to the reaction mixture. A colour change from yellow to pink was observed instantaneously (Scheme 1.64d), indicating an acidic medium with a pH < 4.4.¹⁰¹ In order to confirm that the observed species were long lasting, the mixture was left to stir at room temperature for 1 h, after which the vivid pink colour remained (Scheme 1.64f).

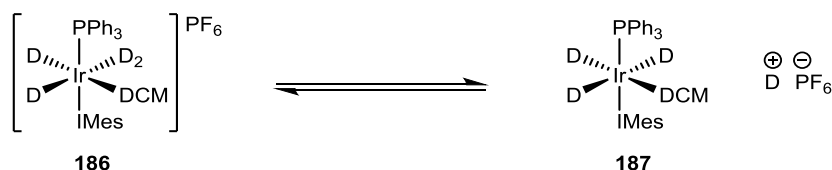
The effects of hydride ligand acidity on catalysis have been the subject of extensive discussion during recent years, and advances in computational chemistry have allowed for theoretical pK_a values of transition metal hydrides to be calculated.^{26,102,103} Morris and co-workers have demonstrated that the acid dissociation constants of transition metal hydride complexes can be estimated through the use of an additive ligand acidity constant (LAC)

equation.¹⁰⁴ The calculation of the pK_a in THF for a metal hydride complex is shown in Equation 1.2, and is based on the sum of acidity constants for each of the ligands in the conjugate base of the hydride or dihydrogen acid ($\Sigma(A_L)$). Corrections are then added to account for the charge on the conjugate base (C_{charge}) and the periodic row of the transition metal centre (C_{nd}). A final correction (C_{d6}) is added if formation of the conjugate base leads to a loss of octahedral geometry.

Equation 1.2

$$pK_a^{\text{THF}} = \Sigma(A_L) + C_{\text{charge}} + C_{\text{nd}} + C_{\text{d6}}$$

Having shown that our active iridium system is, indeed, acidic, it was thought that calculation of the pK_a of the proposed catalytically active species **186** would give further insight into its acidity, while perhaps also identifying which side of the equilibrium shown in Scheme 1.65 would be favoured.



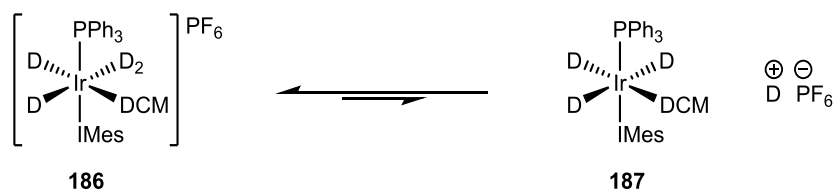
Scheme 1.65

For **186** and its conjugate base **187**, the pK_a was calculated as shown in Equation 1.3. The ligand acidity constants used have been reported previously for a range of common ligand classes.¹⁰⁴ The value of C_{charge} is 0 since conjugate base **187** is neutral, C_{nd} is assigned the value 2 as iridium is a 5d metal, and C_{d6} is 0 since formation of **187** occurs with the octahedral geometry maintained. This gives a value of 9.3 for the pK_a of **186** in THF; it has been demonstrated that the pK_a values in DCM are consistent with those calculated in THF.¹⁰⁵

Equation 1.3

$$\begin{aligned} pK_a^{\text{THF}} &= \Sigma(A_L) + C_{\text{charge}} + C_{\text{nd}} + C_{\text{d6}} \\ &= (0.2 + 0.2 + 0.2 + 4 + 2.7) + 0 + 2 + 0 \\ &= \mathbf{9.3} \end{aligned}$$

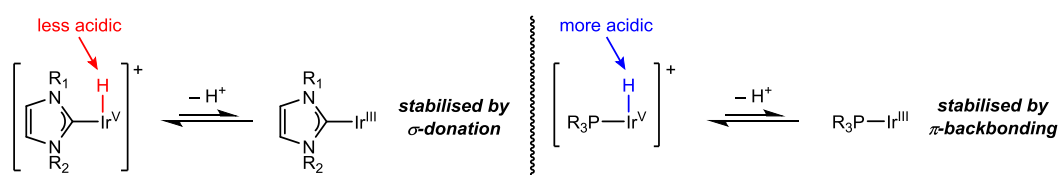
As well as confirming that **186** is, indeed, acidic, its pK_a of 9.3 suggests that the equilibrium shown in Scheme 1.66 is likely to lie to the left, with the active iridium complex being most likely to exist in the form of cationic dihydride species **187**.



Scheme 1.66

It was considered at this point that by careful selection of the ligands used for C3 labelling, the acidity of any hydride intermediates could be delicately tuned. In our previous work, we have demonstrated that the choice of phosphine and carbene ligands used in HIE reactions can have a significant effect on catalyst activity. Designing a range of catalysts with varying hydride acidities and comparing their catalytic activity would allow us to investigate our hypothesis that C3 labelling was occurring through an electrophilic substitution mechanism.

In 2010, Burgess and co-workers demonstrated that phosphine-ligated derivatives of Crabtree's catalyst were more acidic than the corresponding carbene analogues in an alkene hydrogenation reaction where the rate determining step is believed to be reductive elimination from Ir^{V} to Ir^{III} .⁹⁹ As shown in Scheme 1.67, the increased σ -donor capability of the carbene ligand compared to the phosphine was proposed to offer stabilisation of the higher oxidation state intermediate,⁴³ disfavoured the reductive elimination step. Additionally, the superior π -acceptor ability of the phosphine ligand allows it to stabilise the iridium(III) intermediate, driving reductive elimination and thus rendering the hydride ligands at iridium more acidic.

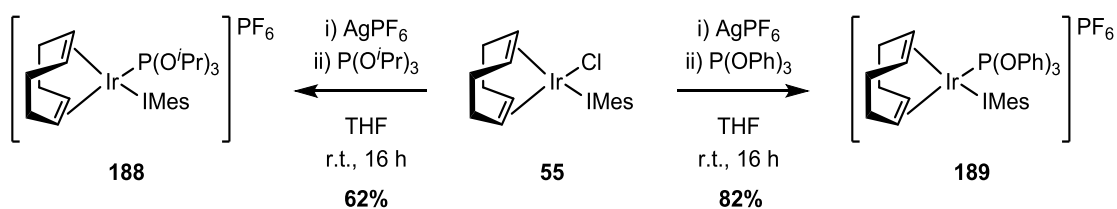


Scheme 1.67

Based on the reasoning applied by Burgess and co-workers for the differences in hydride acidity caused by phosphine π -backbonding and carbene σ -donating capabilities, we

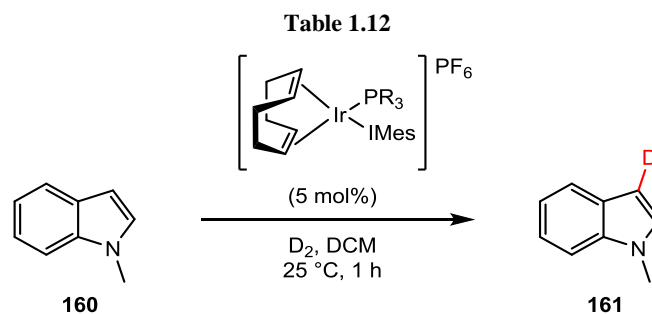
postulated that using a combination of weakly σ -donating ligands could allow us to increase the acidity of intermediate complexes bearing deuteride ligands. When TEP values are compared for common NHC and phosphine ligands,⁴¹ it is immediately apparent that even the most electron-poor NHCs still exhibit $\nu(\text{CO})$ values significantly higher than all common phosphines. With this in mind, it was thought that the greatest changes in deuteride acidity would be observed through variation of the phosphine ligand.

The results shown in Table 1.11, and discussed previously, confirmed that a reduction in ligand σ -donor capability led to the highest levels of labelling. As such, we sought to further investigate this using phosphite ligands, which are significantly weaker σ -donors than their phosphine analogues. Catalysts **188** and **189** were prepared from **55**, as described previously, in good yields (Scheme 1.68).



Scheme 1.68

With two phosphite catalysts in hand, the labelling of *N*-methylindole was carried out under our initial screening conditions (Table 1.12). For comparison, results obtained for all phosphine/phosphite ligands tested are shown, along with their TEP values.



Entry	Catalyst	PR ₃	PR ₃ TEP / cm ⁻¹	%D
1	162	P ^t Bu ₃	2060	7
2	45	PMe ₂ Ph	2065	25
3	44	PBn ₃	2066	54
4	43	PPh ₃	2069	64
5	188	P(O ⁱ Pr) ₃	2075	22
6	189	P(OPh) ₃	2085	14

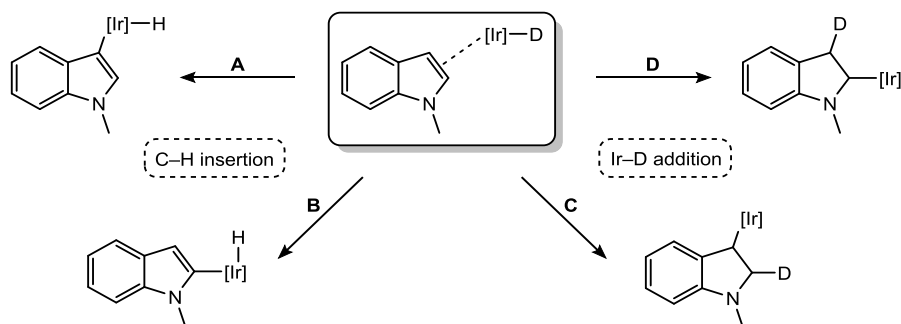
NB Incorporations are an average taken over 3 runs

We were disappointed, however, to see that the reactivity trend did not continue; in fact, the use of phosphite ligands caused a significant decrease in deuterium incorporation. These results did not directly invalidate our hypothesis that C3 labelling was occurring *via* reaction with an acidic deuteride ligand. The steric properties of the phosphine and phosphite ligands tested, for example, vary significantly across the series. However, the increased deuteration observed when using PBn₃ compared to P(OPh)₃, which has a similar percentage buried volume, suggests that the steric properties of the phosphite ligands tested are not the source of their hindered catalytic activity.

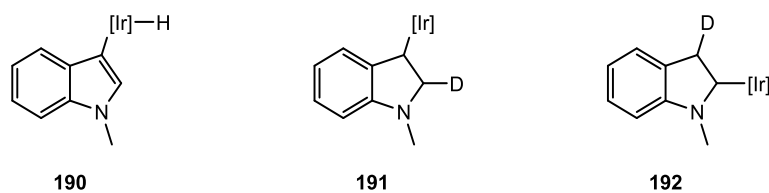
It appeared, therefore, that the mechanism was more complicated than previously anticipated and could involve an inner-sphere process. For example, the poor σ -donating capabilities of the phosphite ligands may well increase deuteride acidity, but in an inner-sphere process could similarly destabilise any high oxidation state intermediates formed.

At this stage, we considered the likely iridium-bound intermediates that might form through an inner-sphere mechanism. After initial coordination of the indole double bond to the iridium centre, we proposed that the reaction would proceed one of two ways: 1) C–H insertion of the iridium centre into one of the indole C–H bonds, as per the mechanism of our directed labelling; or 2) Deuterometallation of the indole double bond by the addition of

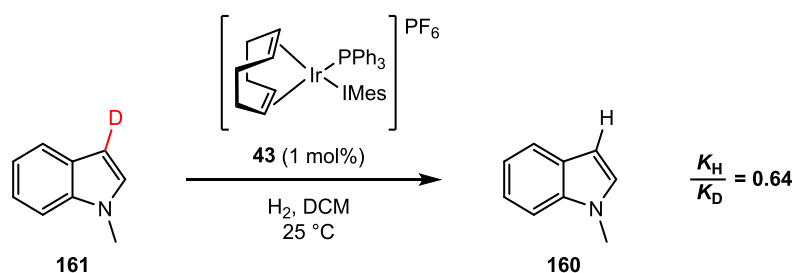
Ir–D. Taking into account the available regiochemistry, this gives four potential pathways for the formation of an iridium-bound intermediate, shown in Scheme 1.69.



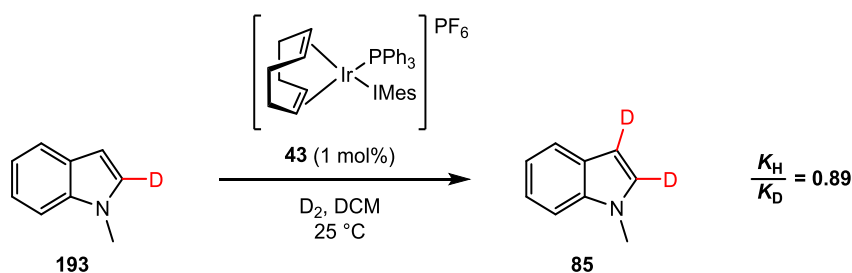
We were able to rule out C–H insertion at the C2 position (pathway **B**) as the major pathway due to the high levels of labelling observed with 2-methylindole. This allowed us to propose three plausible iridium-bound intermediates (Figure 1.22).



In order to investigate the likelihood of iridium C–H insertion *versus* deuteration, we looked to the use of kinetic isotope effect (KIE) experiments; firstly, the rates of reaction were measured for the forward and reverse deuteration reactions of **160** (Scheme 1.70).



A primary inverse kinetic isotope effect of 0.64 was observed, with the reverse reaction occurring approximately a factor of 1.6 times faster than the forward reaction. This rules out the possibility of C–H/C–D bond cleavage being the rate-determining step, and in fact suggests that the formation of a C–H/C–D bond could be implicated in the RDS. To gain further insight, the forward reaction was also carried out with 2-deutero-*N*-methylindole **161** (Scheme 1.71). Interestingly, a secondary inverse KIE of 0.89 was observed, with the reaction once again proceeding faster with a deuterated starting material.

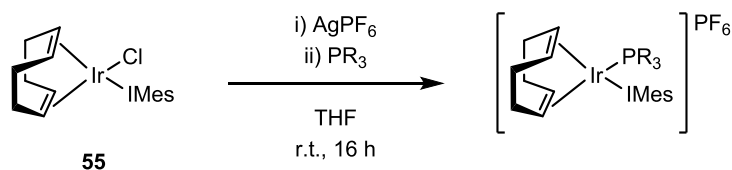


Scheme 1.71

The magnitude of the KIE observed here, where the reverse reaction occurs only 1.1 times faster than the forward reaction, reaffirmed our conclusion that the major pathway could not proceed through insertion into the C2 C–H bond. We postulated, however, that the presence of an inverse KIE could be indicative of a change in hybridisation from sp^2 to sp^3 at the C2 carbon, perhaps suggesting the formation of an indoline intermediate.

It was envisaged that we could gain additional insight into the mechanism taking place by investigating the electronics at the iridium centre. *Para*-substituted aryl phosphines have previously been used as a tool for monitoring electronic effects on reaction rates across a ligand series with minimal alteration of the steric properties.^{106–108} A range of novel *para*-substituted analogues of complex **43** were therefore prepared for use (Table 1.13).

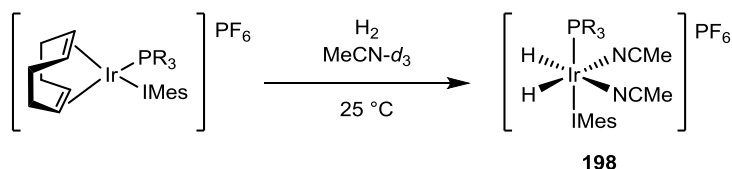
Table 1.13



Entry	PR ₃	Product	Yield / %
1	P(<i>p</i> -C ₆ H ₄ Cl) ₃	194	66
2	P(<i>p</i> -C ₆ H ₄ F) ₃	195	54
3	P(<i>p</i> -C ₆ H ₄ CH ₃) ₃	196	58
4	P(<i>p</i> -C ₆ H ₄ OCH ₃) ₃	197	62

The effects on aryl phosphine substitution on the electronic properties of the catalysts were probed by activating the complexes, as a solution in acetonitrile-*d*₃, with H₂ gas. As a strongly coordinating solvent, acetonitrile offers intermediate **198** enough stabilisation that the iridium hydride signals can be observed by ¹H NMR spectroscopy. The hydride resonances are listed in Table 1.14, and are seen to shift upfield as electron density at the phosphorous atom decreases, indicating that the iridium centre can, indeed, be affected by a change in electronics at the aryl phosphine *para*-position.

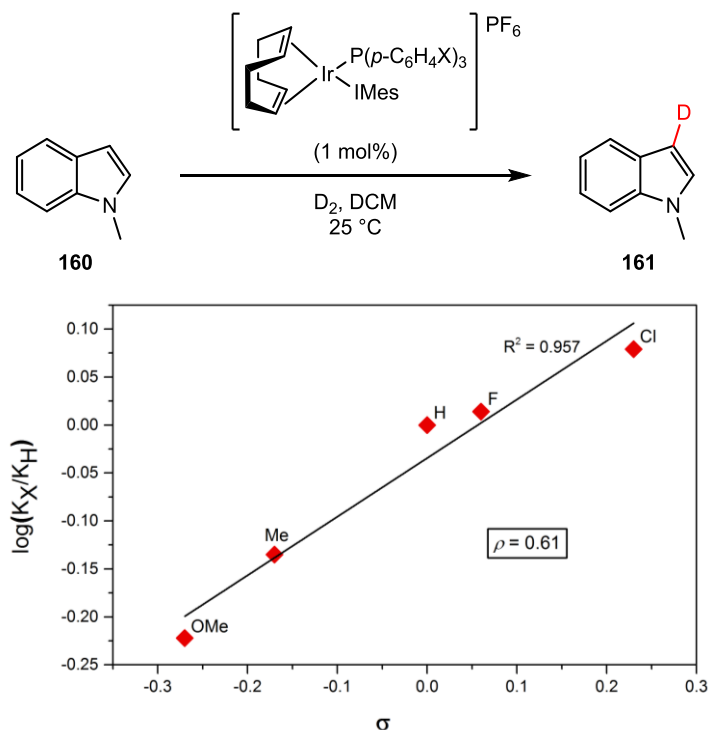
Table 1.14



Entry	Catalyst	PR ₃	PR ₃ TEP / cm ⁻¹	Hydride δ / ppm
1	43	PPh ₃	2069	-21.56
2	194	P(<i>p</i> -C ₆ H ₄ Cl) ₃	2073	-21.33
3	195	P(<i>p</i> -C ₆ H ₄ F) ₃	2070	-21.48
4	196	P(<i>p</i> -C ₆ H ₄ CH ₃) ₃	2067	-21.61
5	197	P(<i>p</i> -C ₆ H ₄ OCH ₃) ₃	2066	-21.65

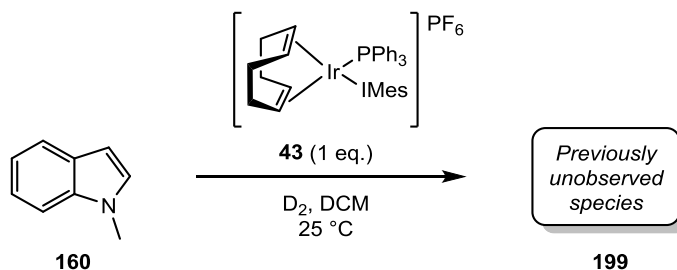
Kinetic analysis was then carried out on the labelling of *N*-methylindole **160** with [Ir(cod)(P(*p*-C₆H₄X)₃)(IMes)]PF₆ (catalysts **43** and **194–197**). When plotted against Hammett σ-parameters, the rate constants exhibited a linear relationship (Graph 1.2), further indicating that the electronic properties associated with the phosphine ligands are transmitted

to the iridium centre. The positive ρ value of 0.61 obtained suggests that the reaction pathway involves a build-up of electron density at the iridium centre during the rate-determining step.



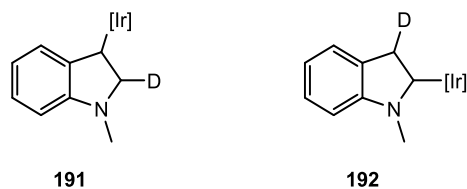
Graph 1.2

We next sought to observe and characterise the proposed intermediates through a series of NMR experiments. In the first instance, the activation of catalyst **43** with D₂ gas was carried out in the presence of an equimolar amount of *N*-methylindole **160** (Scheme 1.72) and the reaction followed by ¹H NMR spectroscopy. After 10 minutes, the formation of a new species, exhibiting several new alkyl signals, was observed.



Scheme 1.72

Figure 1.23 shows a comparison of the spectra taken before activation, at $t = 10$ min, and at $t = 80$ min. The complete loss of the COD signals confirms successful activation of the catalyst. At $\delta = 3.30\text{--}1.02$ ppm, the appearance of several new alkyl signals can be observed. We proposed that these signals could be attributed to an indoline intermediate such as **191** or **192**.



Scheme 1.73

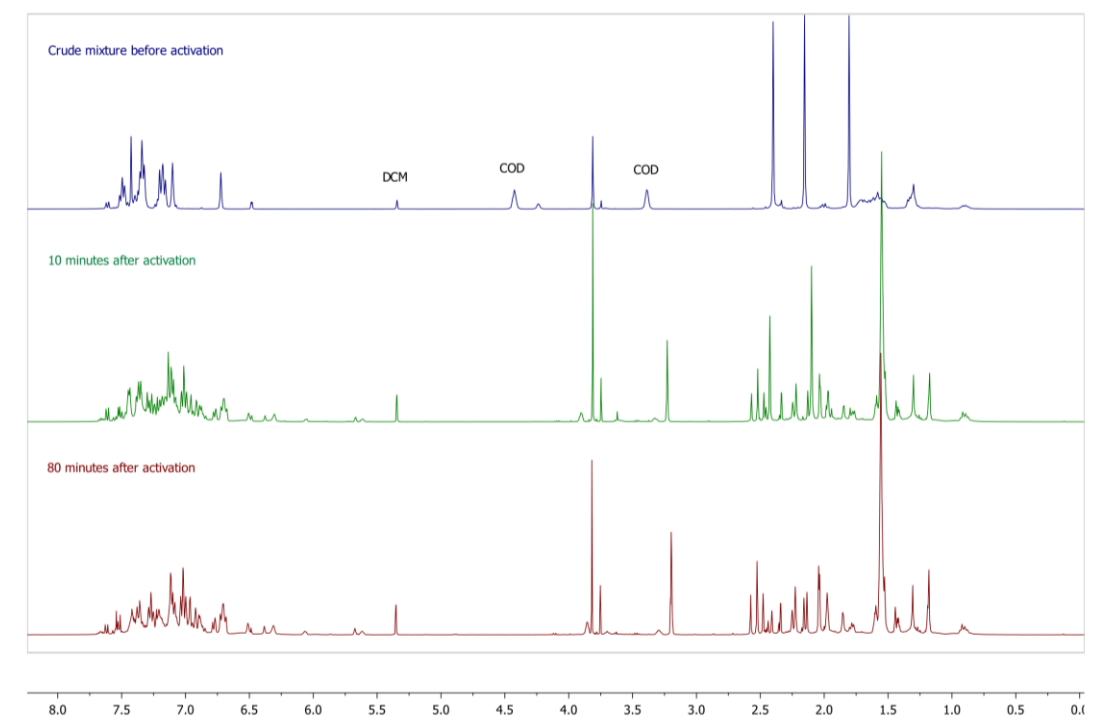


Figure 1.23

The structure of the unknown intermediate observed during the stoichiometric reaction was further assessed using diffusion-ordered NMR spectroscopy (DOSY). The diffusion coefficient of unknown species **199** was measured and was not consistent with the measured values for **43** or **200**. As a model system, the diffusion coefficient of **52**, a known intermediate in the directed labelling of acetophenone, was measured and found to be similar to that of **199**, suggesting that the presence of a substrate-bound iridium intermediate was plausible, and lending support to the proposal of an inner-sphere mechanism. Structures, molecular weights, and diffusion coefficients for **160**, **43**, **200**, **52**, and **199** are shown in

Figure 1.24. It should be noted that for all complexes, the PF₆ anion is discounted; we have previously demonstrated that the cation and anion move independently in solution.⁵⁶

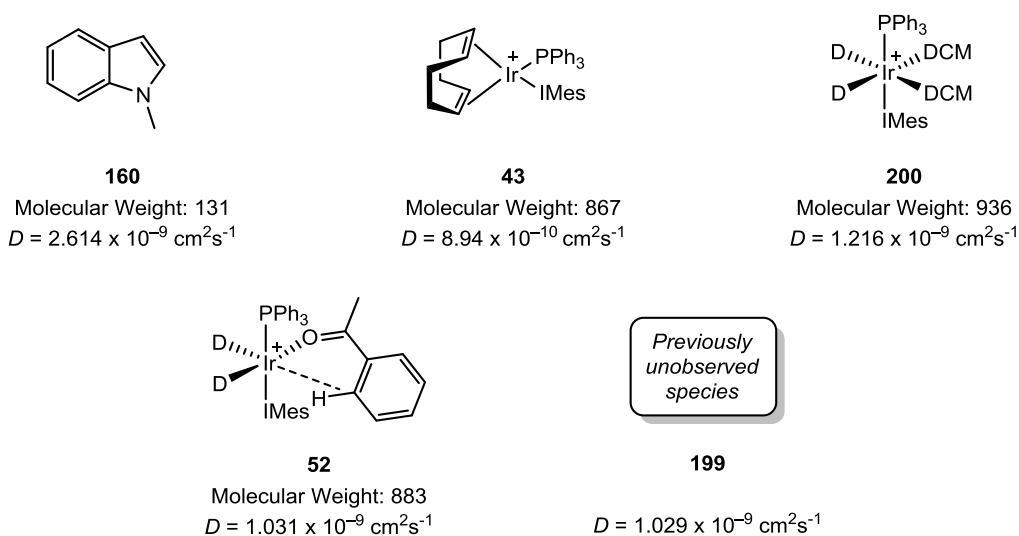
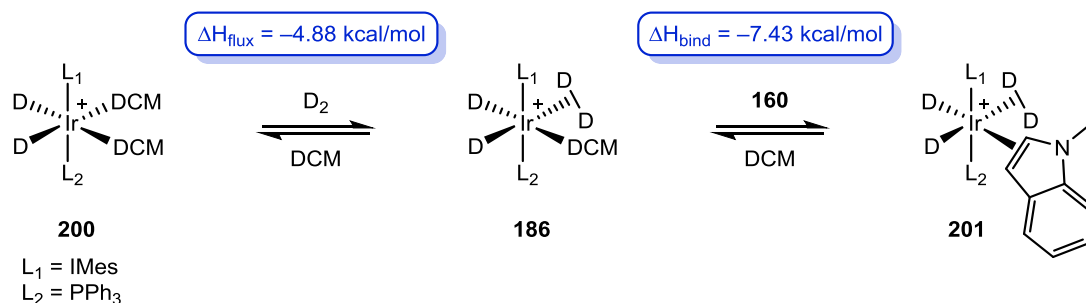


Figure 1.24

Having employed a series of practical mechanistic studies, we sought to complement our experimental data with a theoretical investigation into the viability of our proposed intermediates. The ability of known activated complex **200** to undergo the fluxional exchange of a loosely bound dichloromethane ligand for a deuterium molecule was first modelled, and found to be favourable, with a ΔH_{flux} value of -4.88 for the lowest energy isomer (Scheme 1.74). With NMR spectroscopic data having suggested a substrate-bound intermediate, we then calculated a binding energy of -7.43 kcal/mol for coordination of the indole moiety to active species **186** through the C2–C3 π -system (ΔH_{bind} , Scheme 1.74).



Scheme 1.74

At this stage, we sought to model complexes **202–204** (Figure 1.25), which we proposed as possible intermediate species resulting from reaction of **201**.

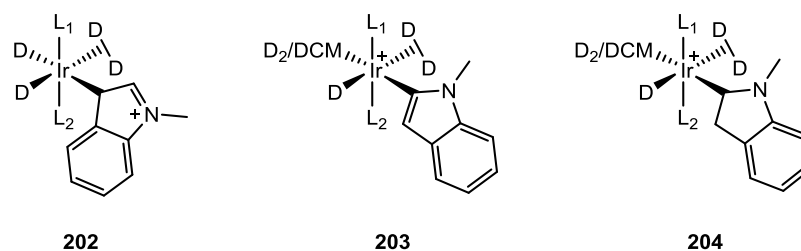


Figure 1.25

C3-bound indole compound **202** was considered to be the likely result of nucleophilic attack from the indole C3 position into the electrophilic iridium centre. To give an estimation of the viability of such an intermediate, the optimisation of **202** was carried out with a truncated ligand set of $L_1 = \text{Ime}$ and $L_2 = \text{PMe}_3$. All attempted optimisations, however, converged to a complex with a similar geometry to **201**, where the substrate is bound through the indole double bond. In order to see the plausibility of ‘forcing’ a formal Ir–C3 bond, electronic density difference plots were calculated. These are shown in Figure 1.26, where (a) shows the optimised geometry of **202**, (b) shows the electronic density difference when an η^2 interaction between the C2–C3 alkene and the iridium centre is in play, and (c) shows the electronic density difference when a C3–Ir σ -bond is enforced. These show clearly that significant disruption of the indole’s aromaticity would be required to create a formal carbon–iridium bond at this position.

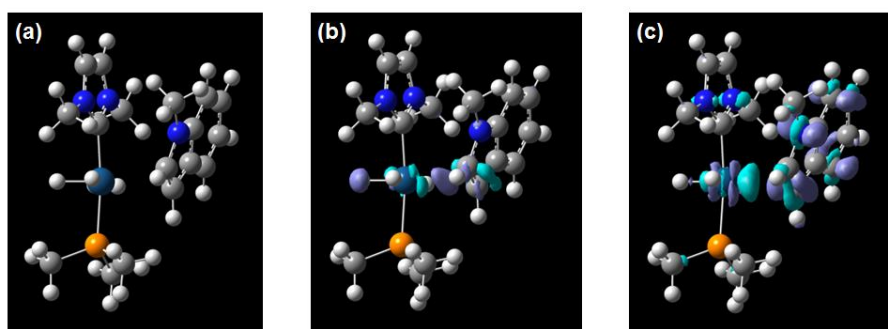


Figure 1.26

Of the three species proposed above, compound **203** was ruled out as an intermediate due to the successful labelling of substrates **169** and **170**, which lack a C–H bond at the C2 position. Saturated compound **204**, however, which is bound to iridium through the C2 position, was found to be much more energetically favourable, with the lowest energy isomer having a relative energy of -0.9 kcal/mol compared to intermediate **186**. The

plausibility of **204** as an intermediate is in keeping with our kinetic isotope effect studies, which suggested a change of hybridisation at the C2 carbon. These conclusions are summarised in Figure 1.27

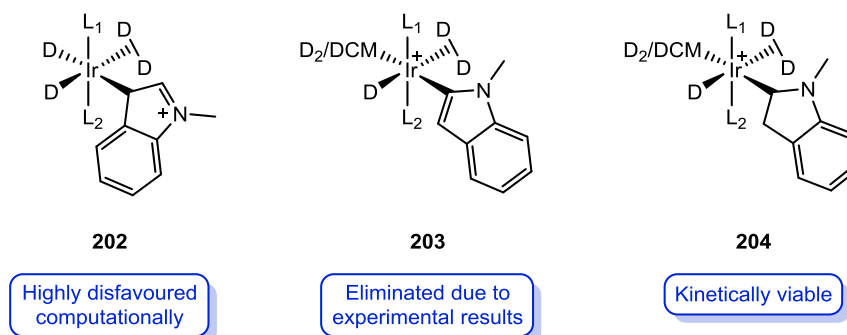


Figure 1.27

Concentrating on compound **204** as a likely intermediate, we calculated the full potential energy surface (PES) for the C3 labelling of **160**. This is shown in Figure 1.28; the energies of all complexes implicated are given relative to **186**. After initial stabilisation of activated intermediate **186** through coordination of the indole unit to generate **201**, deuterometallation across the C2–C3 double bond was found to be the most energetically demanding and therefore rate-determining step. The Ir^V trideuteride species expected to result from this step was found not to be viable, and instead converged to the coordinatively unsaturated intermediate **205**, with one of the deuteride ligands moving to regenerate the loosely-bound dideuterium molecule through a fluxional process. The resulting vacant coordination site is likely to be occupied by a solvent molecule, which is shown to stabilise the complex, meaning that **204** is the more likely species to exist in solution. The transformation from **201** to **205**, via Ir^V species **TS-1**, was found to be the rate-determining step of the reaction, with an energy barrier of 7.4 kcal/mol. This is consistent with the inverse kinetic isotope effect observed for the HIE of 3-deutero-*N*-methylindole **161**.

From intermediate **205**, cleavage of the C2–Ir bond and subsequent dissociation, rotation, and reassociation of the indole unit is required to generate a suitable configuration for removal of the C3 proton. This step is believed to proceed through **TS-2**, in which the positive charge on the iridium centre is quenched through participation of the indole nitrogen's lone pair, generating a loosely-bound cationic indolinium species. The energy barrier of +4.9 kcal/mol for this step is in keeping with the positive ρ value observed in our

Hammett analysis. The indolinium species is then able to dissociate, before reassociating through the other face of the N–C2 double bond.

Once intermediate **205'** is generated *via* **TS-2'**, transfer of the C3 hydrogen atom to form **201'** through **TS-1'** is endothermic, almost mirroring the earlier deuterium transfer through **TS-1**. Finally, dissociation of the indole unit generates **186'**, and the deuterium labelled substrate.

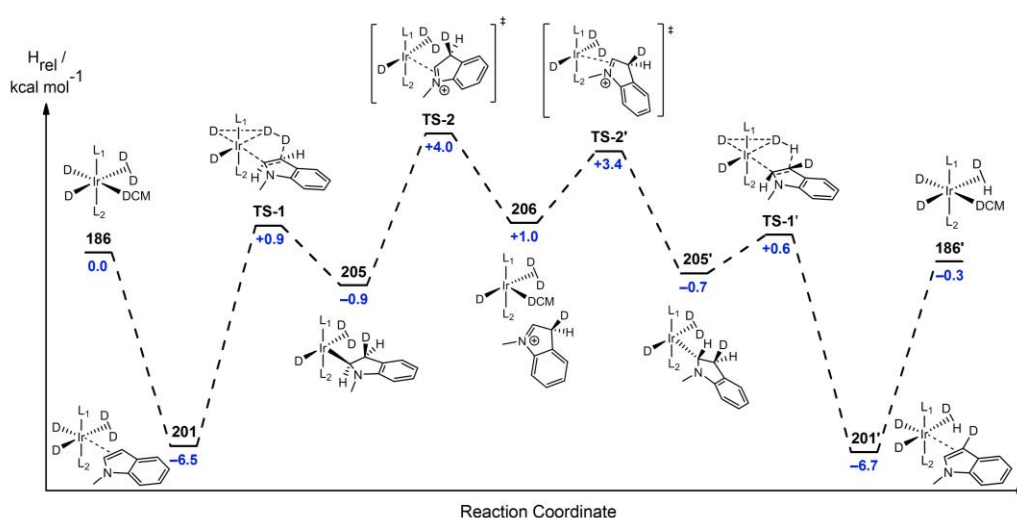
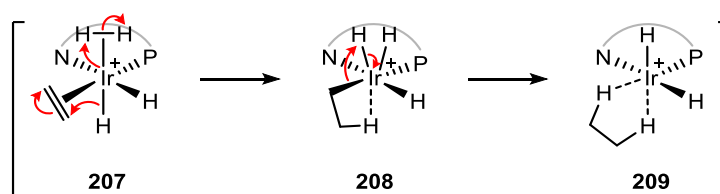


Figure 1.28

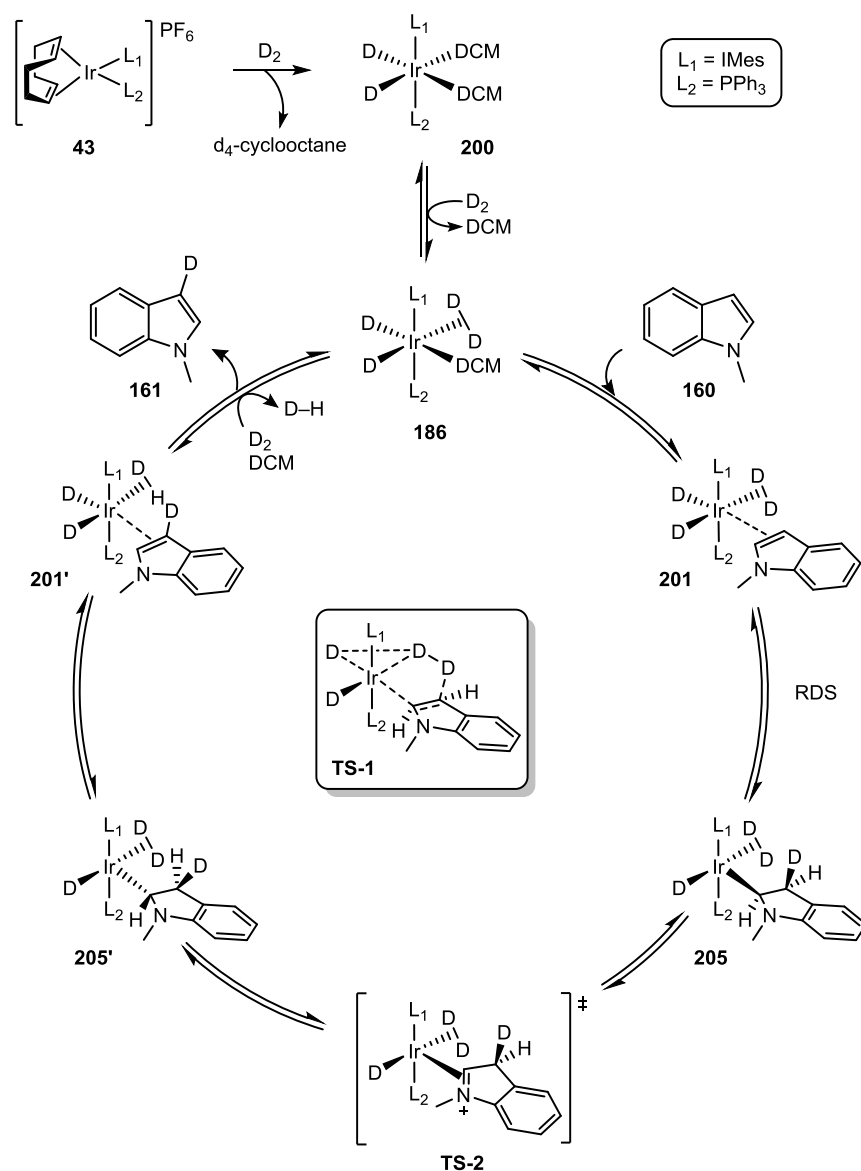
While **TS-1** and **TS-1'** exist as transient Ir^V complexes, all reaction intermediates are believed to be in the Ir^{III} oxidation state. This is in interesting contrast to the results of recent investigations into the mechanism of iridium-catalysed hydrogenation reactions.¹⁰⁹ Hopmann and Bayer carried out a comprehensive computational study into the hydrogenation of alkenes and imines by iridium-PHOX catalysts and found that the preferred mechanism proceeds *via* a key Ir^V trihydride intermediate (**208**, Scheme 1.75).



Scheme 1.75

It should be noted, however, that their investigations focussed only on bidentate ligands. The nitrogen and phosphorous atoms are forced to occupy mutually *cis*- positions, and the three hydride ligands can then also occupy positions *cis*- to one another. In our system, however, the NHC and phosphine are positioned *trans*- to one another. This means that any trihydride/trideuteride species would require two hydride ligands to occupy mutually *trans*- coordination sites; this is typically disfavoured due to the strong *trans*- influence exerted by the hydride ligand.¹¹⁰

Based on our experimental and theoretical mechanistic investigations, we propose the catalytic cycle shown in Scheme 1.76. After generation of the active species **200**, through reductive loss of cyclooctadiene, and ligand fluxionality, coordination of **160**'s double bond π -system proceeds to generate **201**. The rate-determining formation of indoline intermediate **205** occurs through **TS-1**, after which **205'** is formed *via* **TS-2**. Subsequent C2–Ir bond cleavage and removal of the C3 hydrogen atom proceed to regenerate the active catalyst species and furnish labelled compound **161**.

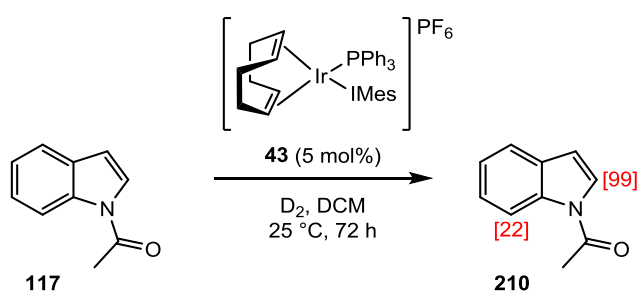


In summary, we have developed a mild and selective protocol for the C3 deuteration of *N*-alkyl indoles. Substrate scope expansion demonstrated excellent functional group tolerance, and the ambient temperature and low catalyst loading provide remarkably mild condition for directing group-free HIE. Extensive practical and theoretical mechanistic investigations indicate that the reaction most likely occurs through an inner-sphere pathway, and we can now propose a mechanism where rate-determining formation of an indole intermediate delivers the deuterium label to the C3 position.

N-Oxide-directed Labelling of N-Heterocycles

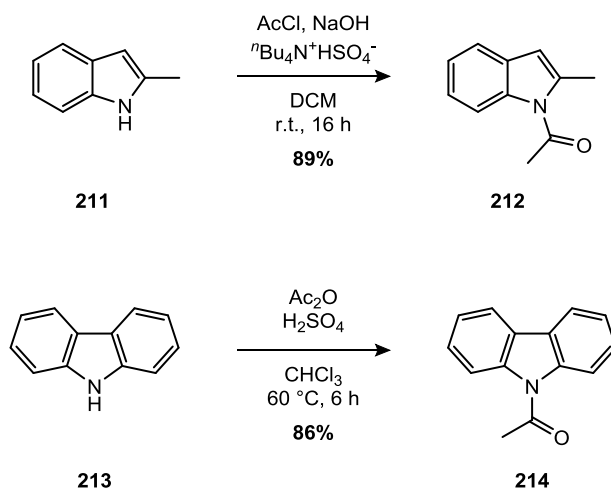
At this stage of the project, we were delighted to have obtained such promising results in the labelling of indoles at the C2 and C3 positions, and we were interested in achieving HIE at the more challenging C7 position. While this position is, in theory, accessible *via* a 6-membered metallocyclic intermediate, activation of the C7 C–H bond is notoriously difficult due to its inherently poor reactivity, and reports of C–H functionalisation at the C7 position are limited. As such, this remains a highly desirable objective that would be of enormous importance to the pharmaceutical industry as well as the wider organic chemistry community.

As discussed previously, despite excellent levels of directed C2 activation having been achieved with the range of protecting groups selected, no labelling of the C7 position had been observed. This was hardly surprising; even without taking into consideration the difficult electronics associated with C7 activation, Kerr group catalysts are well known to form a 5-mmI preferentially over 6-mmI. However, while investigating deprotection conditions, we carried out a large-scale C2 deuteration of *N*-acetyl indole **117**, with the reaction subjected to our labelling conditions for a three-day period to achieve maximum deuterium incorporation (Scheme 1.77). Upon analysis, we were surprised to observe 22% deuterium incorporation at the C7 position, as well as the expected high levels of deuteration at C2.



Scheme 1.77

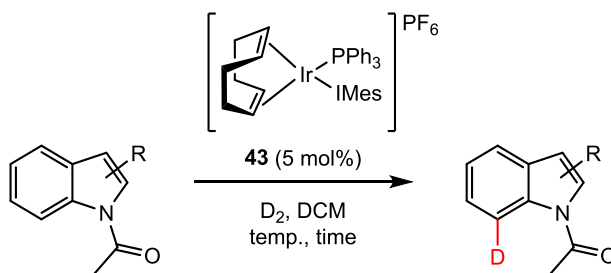
We reasoned that incorporation at C7 could be increased by the introduction of a group at the C2 position to block the formation of a 5-mmI. As such, *N*-acylation reactions were carried out on 2-methylindole **211** and carbazole **213** (Scheme 1.78), affording **212** and **214** in excellent yields.



Scheme 1.78

Disappointingly, when **212** was subjected to our previously optimised conditions, no HIE was observed whatsoever (Entry 1, Table 1.15). When the reaction time was increased to 72 h (Entry 2), 23% deuteration was achieved, in line with our observation for **117**. An increase in temperature saw no improvement (Entry 3). In all cases, no incorporation was observed whatsoever for carbazole **214**.

Table 1.15



Entry	Substrate	Temp. / °C	Time / h	%D
1		25	1	0
2		25	72	23
3	212	40	72	22
4		25	1	0
5		25	72	0
6	214	40	72	0

NB Incorporations are an average taken over 3 runs

While the C7 labelling of **212** was encouraging, the low levels of deuteration observed, especially with such a long reaction time, were considered insufficient for further studies into the labelling of this system. It was thought that even with the more accessible C2 position blocked, the formation of a 6-mmi was likely to be highly disfavoured for such an electronically challenging labelling substrate. It was therefore decided that a suitable strategy could involve the development of a system allowing C7 activation *via* a 5-mmi (Figure 1.29).

We anticipated that an *N*-hydroxy indole or an indole *N*-oxide would make an ideal substrate. There is little precedence in the literature, however, for the preparation and use of stable *N*-hydroxy indole or indole *N*-oxide compounds. Furthermore, *N*-oxides represent a new class of substrates for isotopic labelling within the Kerr group. It was therefore thought prudent to use a more stable substrate for the development of a system for the labelling of *N*-oxides.

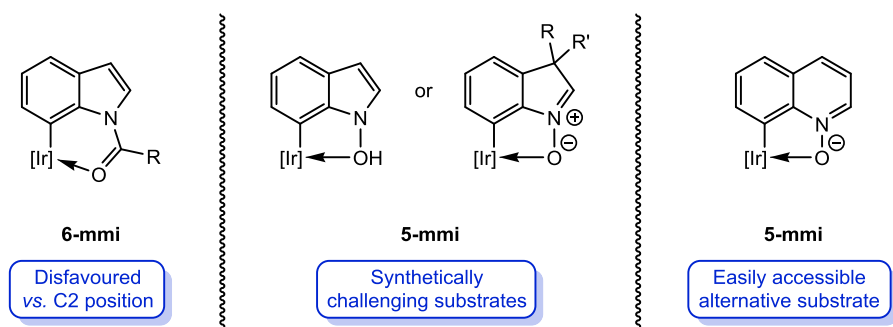
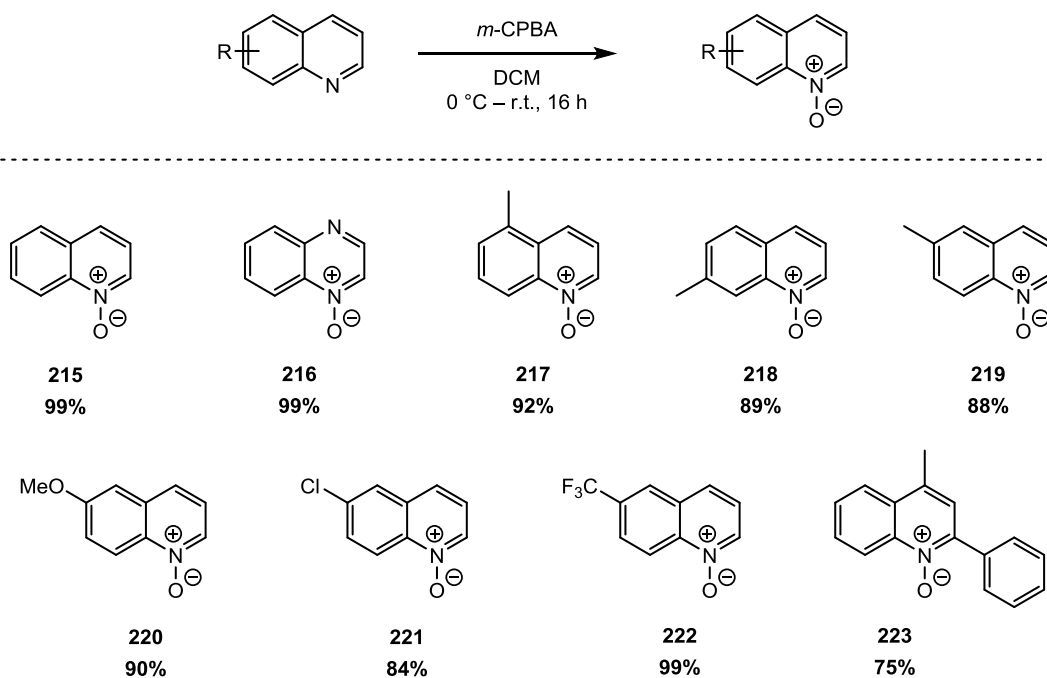


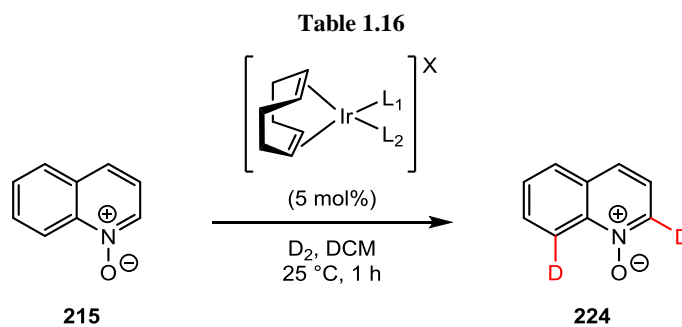
Figure 1.29

In recent years, reports have emerged demonstrating the use of *N*-oxides as functional handles for the C–H activation of the quinoline C8 position.^{111–114} We postulated that a similar system would make an excellent model for iridium-catalysed HIE. As such, a range of quinoline *N*-oxides were prepared in excellent yields (Scheme 1.79).



Scheme 1.79

Since this would represent the first use of Kerr group catalysts with the *N*-oxide moiety as a directing group, quinoline *N*-oxide **215** was used as a benchmark substrate and a full catalyst screening was carried out for its labelling (Table 1.16). A range of phosphines, NHCs, and counterions were screened, and the use of neutral chloro-carbene complex **55** was also investigated. Deuterium incorporation was measured at both the C2 and C8 positions.

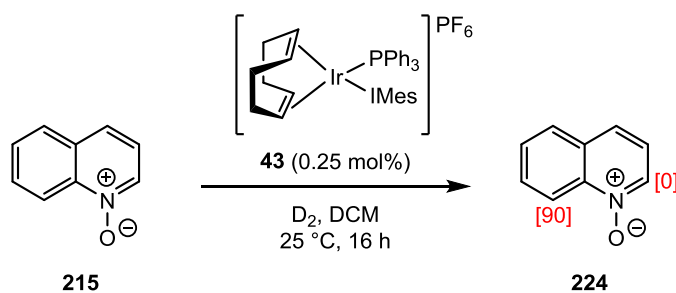


Entry	Catalyst	L ₁	L ₂	X	%D _{C8}	%D _{C2}
1	43	PPh ₃	IMes	PF ₆	80	0
2	45	PMe ₂ Ph	IMes	PF ₆	85	13
3	44	PBn ₃	IMes	PF ₆	86	9
4	64	PPh ₃	IMes	BAr _F	83	3
5	225	PMe ₂ Ph	IMes	BAr _F	84	5
6	226	PBn ₃	IMes	BAr _F	83	7
7	227	PPh ₃	IBn	PF ₆	10	18
8	55	Cl	IMes	-	45	0

NB Incorporations are an average taken over 3 runs

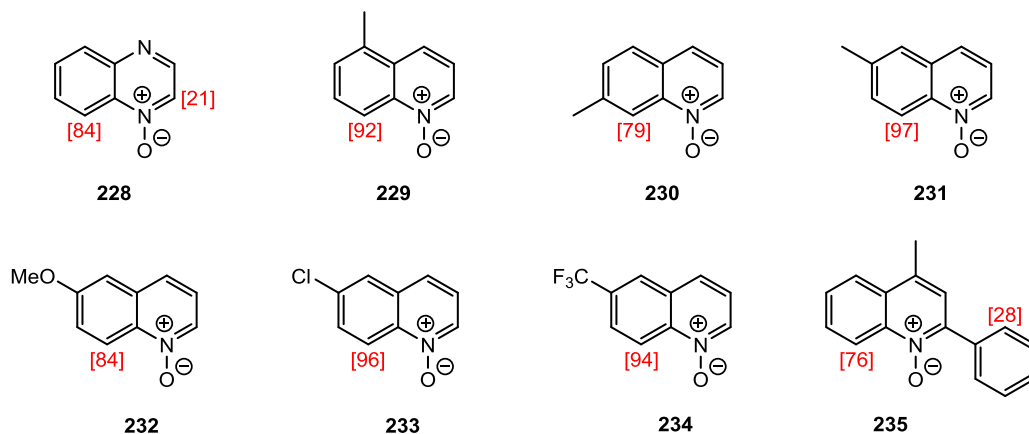
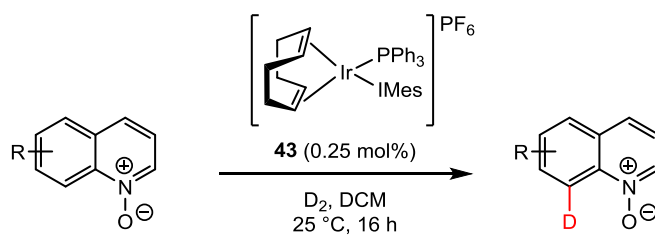
Pleasingly, several catalysts showed high labelling activity, and excellent levels of selectivity were observed for activation of the C8 position over the competing C2 position. It was decided to use catalyst **43** for further optimisation; while its labelling efficiency at the C8 position was marginally lower than some of its analogues, no C2 labelling was observed at all with this catalyst.

The labelling of **215** was optimised through Design of Experiments, and the optimised conditions are shown in Scheme 1.80. A 2-level, 3-factorial design was employed, with the effects of catalyst loading, reaction time, and solvent volume being investigated. Pleasingly, we were able to reduce the catalyst loading to just 0.25%, with a reaction time of 16 h.



Scheme 1.80

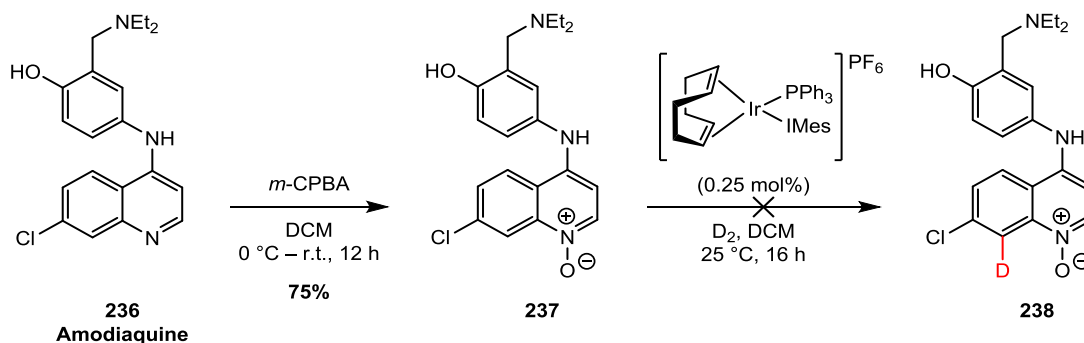
With these exceptionally mild conditions in hand, we sought to expand this labelling methodology across a range of quinoline-*N*-oxide substrates (Scheme 1.81). We were delighted to see that high levels of deuteration were observed for a number of substrates. For quinoxaline-*N*-oxide, low levels of C2 labelling were also observed in **228**, but in all other cases the C2 C–H bond was left intact. Altering the substitution pattern around the ring was well tolerated (**229–231**), as were both electron-withdrawing and electron-donating substituents (**232–234**). Compound **235** allowed us to investigate the competition between aromatic labelling sites; the *ortho*- C–H bond of the 2-phenyl substituent is accessible through a 6-*mmi*. Despite a small amount of labelling at the *ortho*- position, we were pleased to see excellent selectivity for labelling at the quinoline C8 position. Additionally, this result showed that the presence of a sterically-demanding substituent at the C2 position had only a minor effect on labelling efficiency.



NB Incorporations are an average of three runs

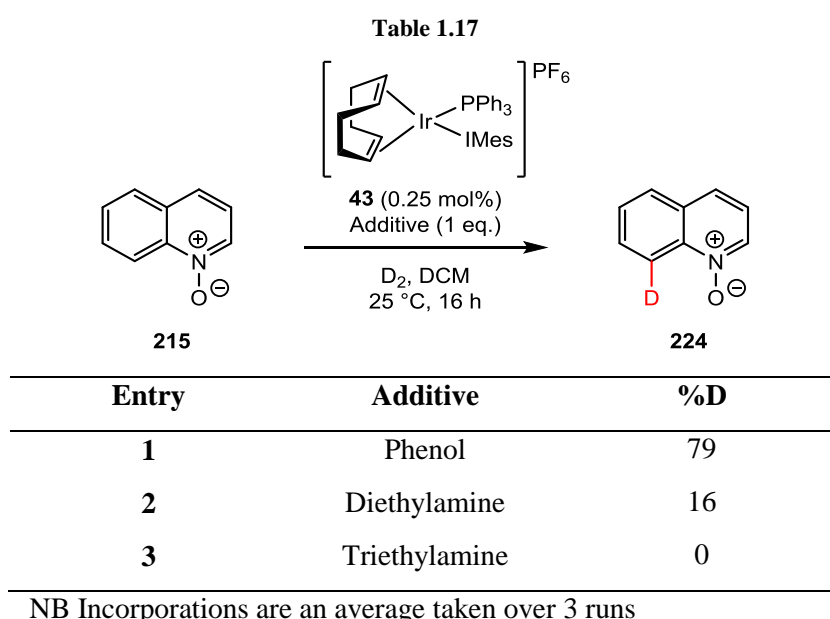
Scheme 1.81

As a final substrate, we sought once again to employ our new methodology in the labelling of a drug molecule. In this instance, we targeted the labelling of Amodiaquine **236**, an antimalarial and anti-inflammatory agent that is listed on the World Health Organisation's List of Essential Medicines.⁷³ The *N*-oxide of **236** was prepared as described previously (Scheme 1.82). When subjected to our labelling conditions, however, we were disappointed to observe no deuterium incorporation whatsoever.



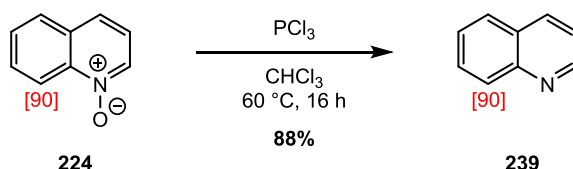
Scheme 1.82

We postulated that the lack of incorporation could be attributed to the presence of other functional groups that could bind competitively to the iridium centre. To probe this hypothesis, labelling reactions of quinoline-*N*-oxide **215** were carried out in the presence of a phenol, a secondary amine, and a tertiary amine (Table 1.17). While a small drop in reactivity was observed in the presence one equivalent of phenol, deuteration still proceeded to a high level (Entry 1). The two amines tested, however, had significant detrimental effects on labelling efficiency (Entries 2 and 3), with no deuteration observed whatsoever in the presence of triethylamine. On the basis of these results, we propose that the activity of catalyst **43** was hampered by the preferential binding of one or both amine moieties present in Amodiaquine.



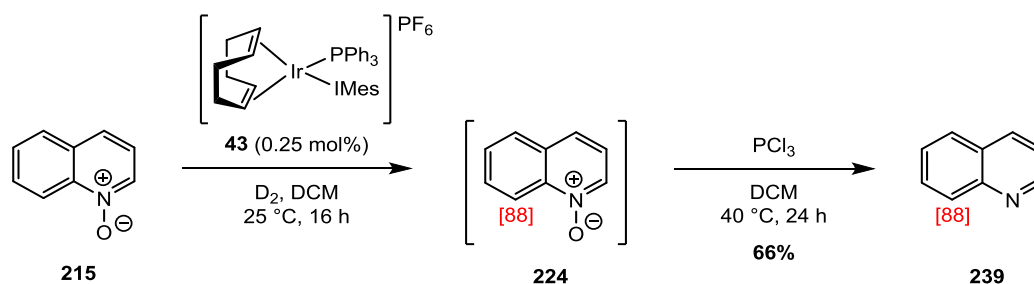
As a final objective, and to demonstrate the utility of our quinoline labelling protocol for generating versatile building blocks, we sought to develop a strategy for reduction of the *N*-oxide group with retention of the deuterium label. This would allow us to offer an overall traceless labelling process, generating a deuterated quinoline with no sign of the directing group.

We were delighted to see that 8-deutero-quinoline-*N*-oxide **224** could be reduced in good yield using phosphorus trichloride. Importantly, no depletion of the deuterium label at the C8 position was observed.



Scheme 1.83

Since the reduction was carried out in chloroform, we envisaged that if the solvent could be changed to dichloromethane, the labelling and reduction steps could be carried out in one-pot. As such, the deuteration of quinoline-*N*-oxide **215** was carried out as described previously. After 16 h, NMR spectroscopic analysis showed that deuteration had proceeded to 88%; at this stage, the deuterium atmosphere was exchanged for argon and the reaction subjected to the reduction conditions *in situ*. While the yield for the *N*-oxide cleavage was slightly lower than observed previously, we were delighted to see that even at a lower temperature, the reaction proceeded in good yield to afford 8-deuteroquinoline **239** in a one-pot, traceless labelling procedure (Scheme 1.84).



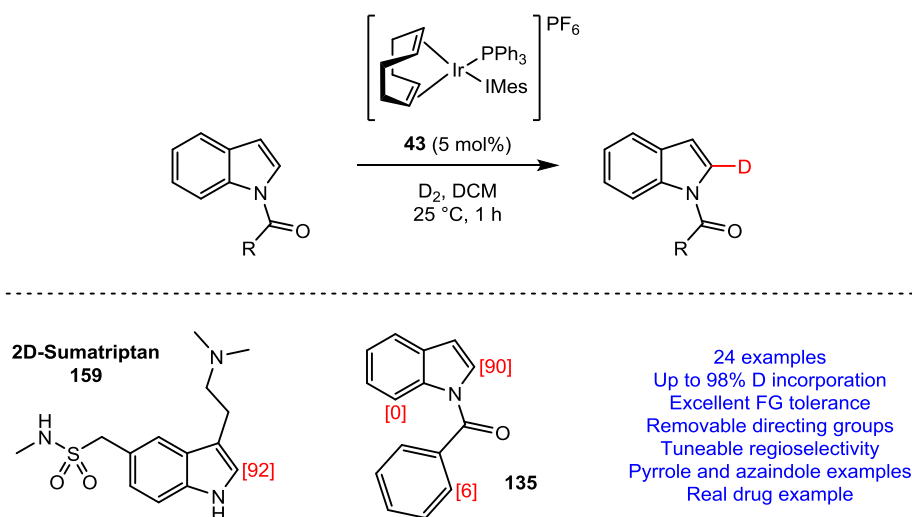
Scheme 1.84

To conclude, the use of the *N*-oxide moiety as a directing group for iridium-catalysed HIE has enabled the efficient deuteration of the C8 position of quinolines. The switch from acyl to *N*-oxide directing groups means that this new methodology is complementary to that developed earlier in the chapter, allowing the challenging positions on the quinoline's benzene ring to be accessed through manipulation of the size of the metallocyclic intermediate formed. Expansion of the substrate scope has shown excellent tolerance for a range of substituents, and we have demonstrated that *in situ* reduction of the *N*-oxide moiety can be carried out, affording an overall traceless labelling process.

Conclusions

In conclusion, we have developed three distinct and highly selective processes for the deuteration of indole, azaindole, pyrrole, and quinoline *N*-heterocycles, in which the regioselectivity is determined by the choice of *N*-protecting group. Using stable iridium(I) catalysts developed within our group, which are now commercially available, the processes described in this chapter allow for high deuterium incorporation at ambient conditions across a varied range of substrates

Firstly, common acyl *N*-protecting groups have been used to selectively direct C–H activation at the C2 position *via* a 5-membered metallocyclic intermediate (5-mmi), and can be removed under mild conditions with retention of the deuterium label. Our methodology is exemplified by the selective deuteration of the anti-migraine drug Sumatriptan. Complementary DFT studies have been used to rationalise the remarkable preference for C2 deuteration observed in substrates such as *N*-benzoyl indole, and have demonstrated that regioselectivity is determined by the kinetic barrier to C–H activation. Our C2 labelling methodology is summarised in Scheme 1.85.

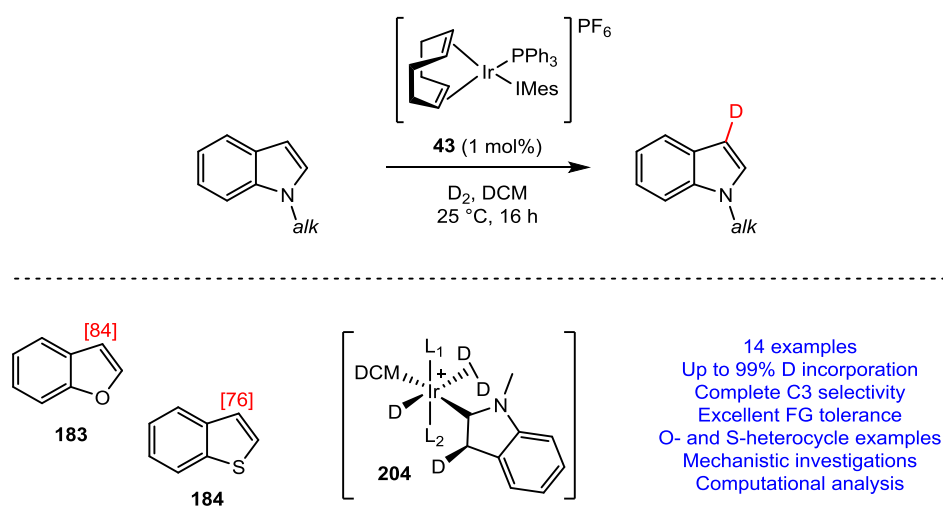


Scheme 1.85

A mild and efficient protocol for the C3 deuteration of *N*-alkyl indoles has also been developed. Substrate scope expansion demonstrated excellent functional group tolerance, with the presence of bulky C2 substituents or competing donor groups having no deleterious

effects on labelling efficiency. Additionally, the successful deuteration of benzofuran and benzothiophene represents an important step away from *N*-heterocyclic substrates.

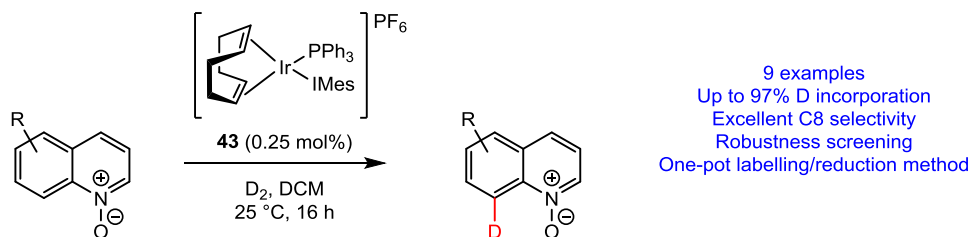
In addition to the development of a novel and notably mild technique for the selective C3 labelling of heterocycles, which provides the research community with expedient access to valuable deuterated compounds, we have rigorously explored the overall reaction in terms of its mechanism. Extensive experimental and computational investigations have been carried out, and this novel and notably mild procedure is now believed to proceed *via* an inner-sphere mechanism. Our studies indicate that an indoline σ -complex is the most likely iridium-bound intermediate, with its formation *via* *syn*-deuterometallation of the indole C2–C3 double bond being the rate-limiting step. Interestingly, all catalytic cycle intermediates are believed to be in the Ir^{III} oxidation state. Scheme 1.86 summarises this developed C3 labelling methodology.



Scheme 1.86

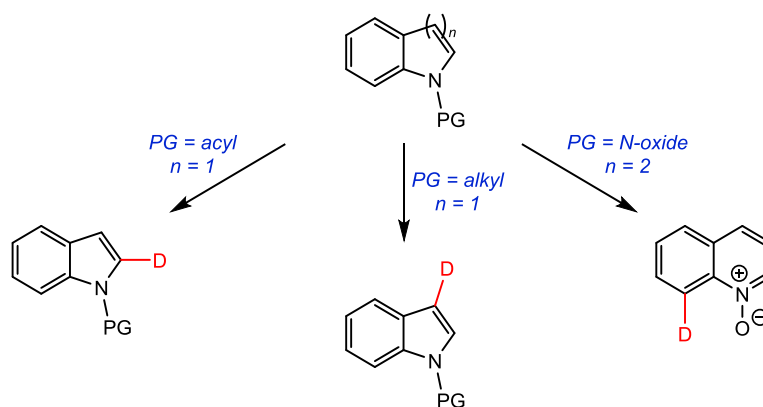
Lastly, our labelling methodology has also been extended to activation of the challenging C8 position of quinolines, using *N*-oxides as traceless directing groups which can be reduced after labelling. This methodology is complementary to our indole C2 and C3 methodology, where a change in metallocycle size enables C–H activation at the C8 position, while leaving the C2 position untouched. The scope of this protocol has been expanded, showing excellent tolerance for a number of substituents. While attempts to label a drug example were unsuccessful, robustness screening experiments demonstrated the tolerance of our catalyst to

the presence of competing Lewis basic donor substituents. Finally, a method for one-pot labelling and reduction of quinoline-*N*-oxides has been disclosed, offering expedient and convenient access to deuterated quinolines.



Scheme 1.87

All of the methods described within this chapter proceed under remarkably mild conditions, with low catalyst loadings and at ambient temperature and pressure. Our methods are also highly complementary, with the careful choice of directing group allowing complete regioselectivity for C–H activation at one of three sites. Overall, the development and understanding of these three novel and notably mild HIE procedures, summarised in Scheme 1.88, offers the research community expedient access to a broad range of valuable labelled heterocycles.

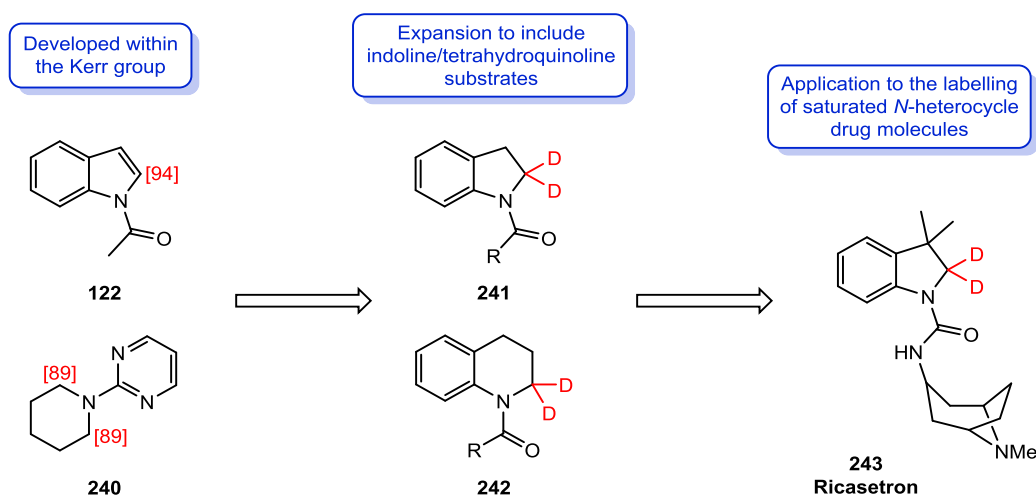


Scheme 1.88

Future Work

The first part of this chapter describes the development of methodology for acyl-directed labelling at the C2 position of indoles and pyrroles. All of the examples described herein relate to C–H activation at an sp^2 centre. There is increasing interest in the research community, however, in C–H activation at sp^3 centres, and future work could involve the expansion of our developed methodology to saturated *N*-heterocycles.

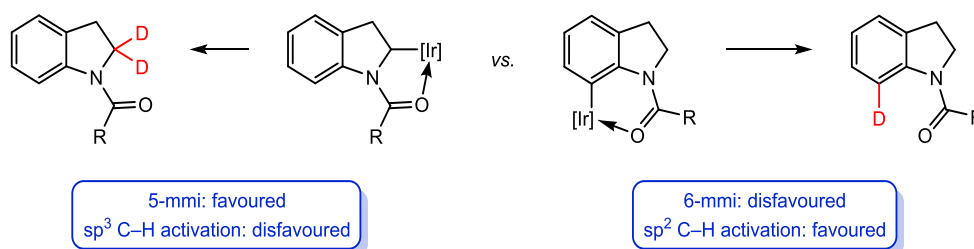
An sp^3 C–H bond is particularly difficult to activate due to its inert nature, but the presence of an adjacent heteroatom increases its pK_a and can make it more readily disposed to C–H activation.¹¹⁵ Recent work within our group has explored the use of Kerr group catalysts to activate sp^3 centres on heterocycles such as piperidine or morpholine.⁶⁷ Until now, this has been most successful with heterocyclic directing groups. It is anticipated, however, that future work in this field could improve the efficiency of this process with acyl directing groups; this methodology could then be adapted to involve removable protecting groups as functional handles, as described in this chapter. Subsequent investigations could include the application of these processes to the labelling of protected indoline or tetrahydroquinoline substrates (Scheme 1.89). This work could be further expanded in the deuteration of drug compounds such as anti-emetic Ricasetron **243**, which contains a urea functional group that could be used as a directing handle.



Scheme 1.89

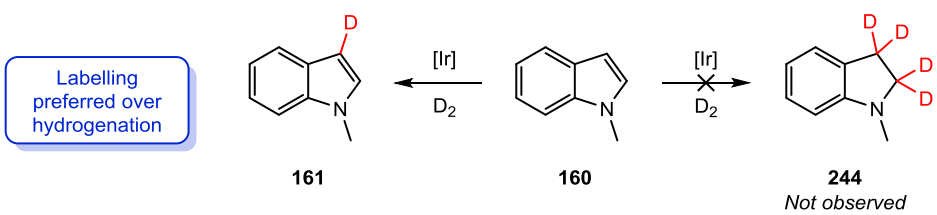
The expansion of this methodology into the labelling of sp^3 centres will raise a number of interesting selectivity questions. For example, we have demonstrated in this chapter that for

N-acyl indoles, C–H activation at the C2 position, *via* a 5-mmi, is preferred to C7 activation, which is accessed through a 6-mmi. However, early investigations into sp^3 labelling have shown that activation of sp^2 bonds C–H bonds is still preferred to sp^3 C–H activation.⁶⁷ Application of our labelling methodology to indoline derivatives would allow us to investigate whether the preference for a 5-mmi allows for the more difficult activation of the α - sp^3 C–H bonds, or whether the preference for sp^2 over sp^3 activation allows access to deuteration of the challenging C7 position (Scheme 1.90).

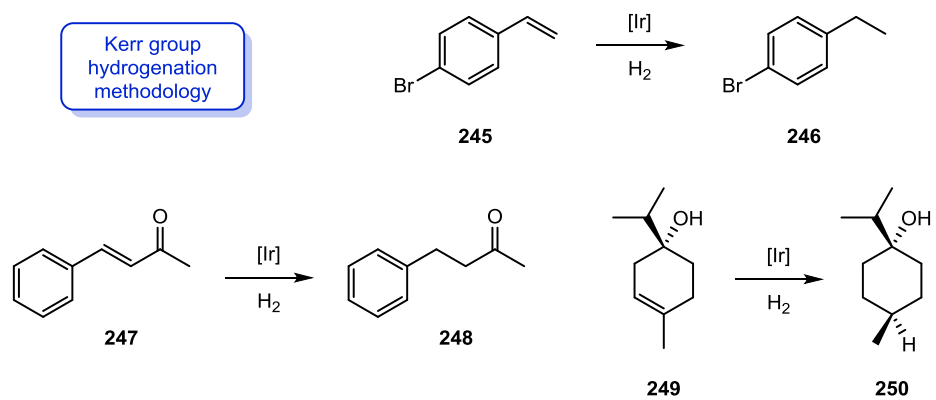


Scheme 1.90

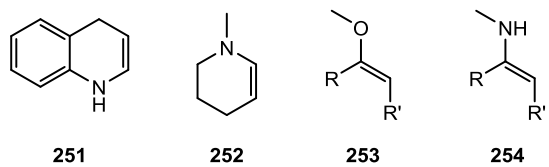
The C3 deuteration methodology developed within this chapter is distinct from previous Kerr group HIE procedures in that it does not require the presence of a Lewis basic directing group. Interestingly, while the key metal–substrate interactions occur through the indole C2–C3 double bond, the olefin reduction product was not observed at any stage, despite our knowledge that complexes such as **43** are excellent hydrogenation catalysts.⁵⁰ This indicates that after deuteration, participation of the nitrogen atom's lone pair is more favourable than reductive elimination. An investigation into the factors that determine reactivity of a double bond in the presence of Kerr group catalysts could be carried out by subjecting a series of test substrates to our labelling conditions. The screening of a number of nucleophilic olefins with donating substituents (Scheme 1.91), would allow us to investigate the preference for alkene reduction vs. lone pair interaction and provide us with a reliable method for predicting olefin reactivity with our catalysts.



Kerr group hydrogenation methodology



Preference for labelling vs. hydrogenation when substituents bear a lone pair?



Scheme 1.91

Experimental

General Information

All reagents were obtained from commercial suppliers (Alfa Aesar, Sigma Aldrich, Apollo Scientific or Strem) and used without further purification, unless otherwise stated. Purification was carried out according to standard laboratory methods.¹¹⁶

Tetrahydrofuran was purified by heating to reflux over sodium wire, using benzophenone ketyl as an indicator, before distilling under nitrogen. Dichloromethane was purified by heating to reflux over calcium hydride, before distilling under nitrogen. Diethyl ether and toluene were obtained from a PureSolv SPS-400-5 Solvent Purification System. Triphenylphosphine was purified by recrystallisation from ethanol, followed by drying under vacuum.

Thin layer chromatography was carried out using Camlab silica plates coated with fluorescent indicator UV254. The plates were analysed using a Mineralight UVGL-25 lamp, or developed using vanillin or KMnO_4 solution.

Flash column chromatography was carried out using Prolabo silica gel (230-400 mesh).

IR spectra were obtained on a Shimadzu IRAffinity-1 Spectrophotometer machine and are reported in cm^{-1} unless stated otherwise.

^1H , ^{13}C , ^{19}F , and ^{31}P NMR spectra were recorded on a Bruker DPX 400 spectrometer at 400 MHz, 101 MHz, 376 MHz, and 162 MHz, respectively. Chemical shifts are reported in ppm. Coupling constants are reported in Hz, and refer to $^3J_{\text{H-H}}$ interactions unless otherwise stated.

High resolution mass spectrometry was carried out by the EPSRC National Mass Spectrometry Facility at the University of Swansea.

General Procedures

General procedure A – Preparation of complexes of the type [Ir(cod)Cl(NHC)]

Bis(1,5-cyclooctadiene)diiridium(I) dichloride (1 eq.) and potassium *tert*-butoxide (2 eq.) were added to a flame-dried and Ar-cooled Schlenk tube and stirred under vacuum for 10 min. THF (20 mL / mmol) was added and the mixture stirred for 10 min. The relevant imidazolium chloride (2 eq.) was added and the resulting solution stirred at room temperature for 18 h. The solvent was removed *in vacuo*, and column chromatography (50% ethyl acetate in petrol) afforded the title compound.

General Procedure B – Preparation of complexes of the type [Ir(PR₃)(IMes)]X⁴⁹

A round-bottom flask, fitted with a stopcock sidearm, was flame-dried and cooled under an atmosphere of argon. (1,5-Cyclooctadiene)(1,3-dimesitylimidazol-2-ylidene)iridium(I) chloride **55** (1 eq.) was added and dissolved in dry THF (20 mL / mmol). On formation of a yellow solution, the silver salt (1 eq.) was added, and the resulting yellow suspension stirred at room temperature for 15 min. The reaction mixture was filtered through Celite under an argon atmosphere, rinsing the Celite with dry THF (5 mL / mmol). The requisite phosphine (1 eq.) was added and the reaction mixture then stirred at room temperature for 16 h before being concentrated *in vacuo*. The residue was dissolved in DCM and filtered through Celite. After removal of the DCM *in vacuo*, the product was triturated with ethyl acetate and collected by filtration. The product was then dried in a vacuum oven (40 °C, 0 bar) for 24 h.

General Procedure C – Deuteration of N-Heterocyclic Substrates

A 100 mL round-bottom flask bearing two stopcocks was flame dried and cooled under argon., The substrate (0.215 mmol), catalyst and dichloromethane (2.5 mL) were then added and the flask was cooled to -78 °C in a dry ice/acetone bath. The flask was then evacuated and refilled with deuterium gas from a balloon, and this vacuum/refilling cycle repeated one further time. The stopcocks were closed and the flask was placed in an oil bath. The reaction mixture was heated (25 °C unless otherwise noted), and was observed to change from an orange to a pale yellow solution after about 5 min. After the specified time, the stopcocks were opened to release the deuterium atmosphere. The solvent was removed *in vacuo* and the resulting residue was flushed through a plug of silica with diethyl ether. The solution was concentrated *in vacuo* and incorporation was determined by ¹H NMR spectroscopic analysis.

Equation 1.4 was used to determine the level of deuterium incorporation; peaks were calibrated against a signal corresponding to a position where labelling was not expected to occur.

Equation 1.4

$$\% \text{ Deuteration} = 100 - \left[\left(\frac{\text{residual integral}}{\text{no. labelling sites}} \right) \times 100 \right]$$

General Procedure D – Synthesis of N-Methylindoles

Prepared according to a literature procedure.⁹⁴ To a solution of the relevant indole (1 eq.) in THF (15 mL) at 0 °C was added sodium hydride (60% in mineral oil, 1.5 eq.). The reaction mixture was stirred for 15 min at 0 °C and then for 1 h at room temperature. Upon cooling to 0 °C, methyl iodide (1.3 eq.) was added and the reaction was stirred at room temperature for 30 min. The reaction was cooled to 0 °C and quenched with a saturated ammonium chloride solution (20 mL). The organic products were extracted into diethyl ether, washed with brine, dried over sodium sulfate and concentrated *in vacuo*. Column chromatography (8% ethyl acetate in petrol unless otherwise specified) afforded the product.

General Procedure E – Measurement of the Rate of Deuteration of N-Methylindole

An NMR tube was charged with a solution of *N*-methylindole (14.2 mg, 0.108 mmol) and the relevant catalyst (1 mol%) in DCM-*d*₂ (0.75 mL), before being sealed with a rubber septum and cooled to 0 °C. The tube was fitted with a D₂ balloon and an exit needle. D₂ gas was bubbled through the mixture for 3 min at 0 °C, during which a colour change from orange to pale yellow was observed. The tube was sealed under 1 atm of D₂ and immediately placed in a Bruker DPX 400 spectrometer with the sample temperature set to 298 K. Deuterium incorporation was assessed using ¹H NMR spectra, taken every 3 min, and used to determine reaction rates.

General Procedure F – Formation of MeCN-stabilised Ir^{III} Hydride Complexes

An NMR tube was charged with a solution of the relevant Ir(I) complex (0.01 mmol) in acetonitrile-*d*₃ (0.6 mL), before being sealed with a rubber septum and cooled to 0 °C. The tube was fitted with a H₂ balloon and an exit needle. H₂ gas was bubbled through the mixture for 3 min at 0 °C, during which a colour change from orange to pale yellow was observed. The tube was sealed under 1 atm of H₂ and placed in a Bruker DPX 400 spectrometer with

the sample temperature set to 298 K. The resulting hydride intermediates were analysed by ^1H (wide spectrum: sw = 60 ppm, o1p = -20 ppm) and ^{31}P NMR spectra

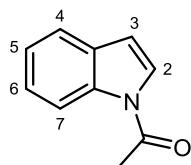
General Procedure G – Synthesis of Heterocycle N-Oxides

Carried out according to a literature procedure.¹¹⁷ A solution of the relevant *N*-heterocycle (3 mmol) in DCM (10 mL) was prepared and cooled to 0 °C. *meta*-Chloroperbenzoic acid (77 wt%, 173 mg, 4.5 mmol, 1.5 eq.) was added and the reaction mixture was heated to room temperature and stirred for 16 h. The reaction was cooled to room temperature and saturated sodium bicarbonate solution (20 mL) was added. The organics were extracted into DCM (3 × 20 mL), dried over sodium sulfate and concentrated *in vacuo*. The residue was purified by flash column chromatography (5% DCM in acetone).

C2 Labelling of *N*-Protected Indoles

Scheme 1.31

N-Acetylintole **117**¹¹⁸



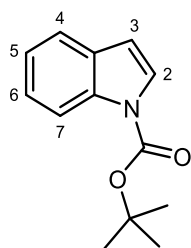
Prepared according to a literature procedure.¹¹⁹ To a flask charged with indole (500 mg, 4.26 mmol), sodium hydroxide (430 mg, 10.75 mmol), and tetrabutylammonium hydrogensulfate (29 mg, 0.08 mmol) was added DCM (11 mL). A solution of acetyl chloride (460 μ L, 6.45 mmol) in DCM (6 mL) was then added dropwise. The reaction mixture was stirred at room temperature for 16 h, filtered through a plug of silica and concentrated *in vacuo* to yield *N*-acetylintole **117** as a colourless oil (606 mg, 88% yield).

¹H NMR (400 MHz, CDCl₃) δ 8.47 (d, J = 8.1 Hz, 1H, H⁷), 7.60 (ddd, J = 7.8, ⁴ J = 1.0, 0.7 Hz, 1H, H⁴), 7.44 (d, J = 4.0 Hz, 1H, H²), 7.39 (ddd, J = 8.4, 7.3, ⁴ J = 1.6 Hz, 1H, H⁶), 7.33–7.28 (m, 1H, H⁵), 6.67 (dd, J = 3.8, ⁴ J = 0.6 Hz, 1H, H³), 2.66 (s, 3H, CH₃).

¹³C NMR (100 MHz, CDCl₃) δ 168.2, 135.0, 129.8, 124.8, 124.7, 123.2, 120.3, 116.0, 108.7, 23.4.

IR (ATR, cm⁻¹) 2980, 1699, 1450, 1323.

tert-Butyl indole-1-carboxylate **118**¹²⁰



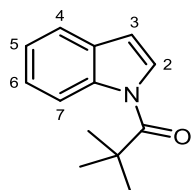
To a solution of indole (500 mg, 4.26 mmol) in THF (30 mL) was added 4-(dimethylamino)pyridine (5.2 mg, 0.04 mmol) and di-*tert*-butyl dicarbonate (1.022 g, 4.69 mmol). The reaction mixture was stirred at room temperature for 16 h, after which the solvent was removed *in vacuo*. The residue was purified by flash column chromatography (10% ethyl acetate in petrol) to afford product **118** as a yellow oil (916 mg, 99% yield).

¹H NMR (400 MHz, CDCl₃) δ 8.14 (d, *J* = 8.5 Hz, 1H, H⁷), 7.59 (d, *J* = 3.7 Hz, 1H, H²), 7.57–7.54 (m, 1H, H⁴), 7.30 (td, *J* = 7.5, ⁴*J* = 1.0 Hz, 1H, H⁶), 7.21 (t, *J* = 7.7, 1H, H⁵), 6.56 (d, *J* = 3.7 Hz, 1H, H³), 1.66 (s, 9H, (CH₃)₃).

¹³C NMR (100 MHz, CDCl₃) δ 149.5, 134.7, 130.0, 125.4, 123.8, 122.1, 120.3, 114.5, 106.7, 83.0, 27.7.

IR (ATR, cm⁻¹) 2978, 1730, 1450, 1328.

***N*-Pivaloylindole 119**¹²¹



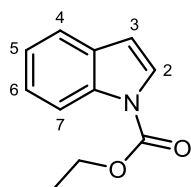
To a two-necked flask charged with indole (500 mg, 4.26 mmol), 4-(dimethylamino)pyridine (52 mg, 0.43 mmol) and triethylamine (879 μL, 6.3 mmol), was added DCM (8 mL), and the resulting solution cooled to 0 °C. Pivaloyl chloride (614 μL, 5 mmol) was added dropwise, and the reaction mixture was stirred at room temperature for 16 h. The solvent was removed *in vacuo*, and the residue was extracted into EtOAc (3 × 10 mL). The combined extracts were washed with saturated ammonium chloride solution and brine. The organic phase was then dried over sodium sulfate and concentrated *in vacuo*. The residue was purified by flash column chromatography (10% ethyl acetate in petrol), affording product **119** as a white solid (662 mg, 77% yield).

¹H NMR (400 MHz, CDCl₃) δ 8.50 (dd, *J* = 8.5, ⁴*J* = 0.8 Hz, 1H, H⁷), 7.72 (d, *J* = 3.9 Hz, 1H, H²), 7.55 (dd, *J* = 7.7, ⁴*J* = 1.4 Hz, 1H, H⁴), 7.36–7.31 (m, 1H, H⁶), 7.28–7.26 (m, 1H, H⁵), 6.61 (d, *J* = 3.9 Hz, 1H, H³), 1.51 (s, 9H, (CH₃)₃).

¹³C NMR (100 MHz, CDCl₃) δ 176.5, 136.3, 128.9, 125.2, 124.6, 123.0, 120.0, 116.7, 107.7, 40.7, 28.3.

IR (ATR, cm⁻¹) 2976, 1678, 1448, 1308.

Ethyl indole-1-carboxylate 120¹²²



To a solution of indole (500 mg, 4.26 mmol) in THF (8 mL) at 0 °C, was added sodium hydride (60% in mineral oil, 255 mg, 6.39 mmol) in portions. The reaction mixture was stirred for 30 min before ethyl chloroformate (488 μ L, 5.11 mmol) was added. The mixture was allowed to reach room temperature and was then stirred for 1 h. The reaction mixture was quenched with water (10 mL) and extracted into ethyl acetate (3 \times 10 mL). The organic phases were combined, dried over sodium sulfate and concentrated *in vacuo*. The residue was purified by flash column chromatography (20% ethyl acetate in petrol) to afford product **120** as a pale yellow oil (805 mg, 99% yield).

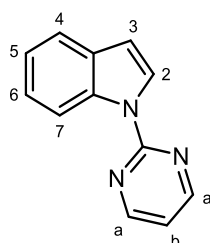
^1H NMR (400 MHz, CDCl_3) δ 8.17 (d, J = 8.4 Hz, 1H, H^7), 7.60 (d, J = 3.8 Hz, 1H, H^2), 7.57 (ddd, J = 7.9, 4J = 0.9, 0.9 Hz, 1H, H^4), 7.33–7.28 (m, 1H, H^6), 7.23 (td, J = 7.5, 4J = 1.0 Hz, 1H, H^5), 6.58 (dd, J = 3.8, 4J = 0.6 Hz, 1H, H^3), 4.48 (q, J = 7.3 Hz, 2H, CH_2CH_3), 1.46 (t, J = 7.3 Hz, 3H, CH_2CH_3).

^{13}C NMR (100 MHz, CDCl_3) δ 151.2, 135.5, 130.8, 125.9, 124.7, 123.2, 121.3, 115.5, 108.3, 63.5, 14.7.

IR (ATR, cm^{-1}) 2982, 1607, 1483, 1274.

Scheme 1.32

N*-Pyrimidylindole **104*¹²³



Prepared according to a literature procedure.¹²³ To a solution of indole (500 mg, 4.26 mmol) in DMF (10 mL) was added sodium hydride (60% in mineral oil, 255 mg, 6.39 mmol), and the reaction mixture was stirred at room temperature for 30 min, after which 2-chloropyrimidine (731 mg, 6.39 mmol) was added. The reaction mixture was heated at 150 °C for 16 h, and the reaction was quenched with water (15 mL). The organic products were extracted into ethyl acetate, dried over sodium sulfate, and concentrated *in vacuo*. Column chromatography (12% ethyl acetate in petrol) afforded product **104** (748 mg, 90% yield).

^1H NMR (400 MHz, CDCl_3) δ 8.80 (d, J = 8.1 Hz, 1H, H^7), 8.70 (d, J = 4.7 Hz, 2H, H^a), 8.26 (d, J = 3.4 Hz, 1H, H^2), 7.61 (dd, J = 7.8, 1.4 Hz, 1H, H^4), 7.33 (ddd, J = 8.5, 7.0, 1.4

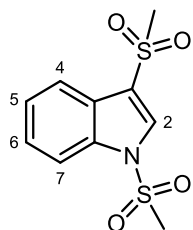
Hz, 1H, H⁶), 7.26–7.19 (m, 1H, H^b), 7.04 (t, *J* = 4.8 Hz, 1H, H⁵), 6.69 (d, *J* = 3.4 Hz, 1H, H³).

¹³C NMR (100 MHz, CDCl₃) δ 157.6, 134.9, 130.8, 125.3, 123.2, 121.6, 120.3, 115.7, 115.6, 106.5.

IR (ATR, cm⁻¹) 3117, 1578, 1433, 1307.

Scheme 1.33

1,3-bis(methylsulfonyl)indole **121**



To a suspension of sodium hydride (60% in mineral oil, 204 mg, 5.11 mmol) in DMSO (5 mL) at 0 °C was added a solution of indole (500 mg, 4.26 mmol) in diethyl ether (25 mL). The reaction mixture was stirred at room temperature for 30 min, before methanesulfonyl chloride (396 μL, 5.11 mmol) was added dropwise at 0 °C. The reaction mixture was stirred for a further 30 min, then poured into water and extracted with DCM. The organic extracts were washed with water, dried over sodium sulfate and concentrated *in vacuo*. The product was purified by recrystallisation from methanol to afford product **121** as an off-white crystalline solid (653 mg, 94% yield).

¹H NMR (400 MHz, CDCl₃) δ 8.13 (s, 1H, H²), 8.00–7.90 (m, 2H, H⁴ & H⁷), 7.54–7.45 (m, 2H, H⁵ & H⁶), 3.27 (s, 3H), 3.19 (s, 3H).

¹³C NMR (100 MHz, CDCl₃) δ 136.4, 127.1, 125.2, 125.1, 119.7, 119.2, 114.9, 114.4, 115.1, 49.0, 42.1.

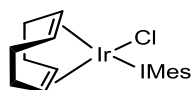
IR (ATR, cm⁻¹) 1604, 1364, 1189, 1121.

M.P. (°C) 78–81.

HRMS [M+NH₄] Expected 291.0468; Observed 291.0465.

Scheme 1.34

(1,5-cyclooctadiene)(1,3-dimesitylimidazol-2-ylidene)iridium(I) chloride **55**⁴⁹



Prepared according to *General Procedure A*.

Entry	Amount of dimer 27		Amount of IMes·Cl		Amount of 'BuOK		Product yield	
	mg	mmol	mg	mmol	mg	mmol	mg	%
1	400	0.60	406	1.19	133	1.19	631	83
2	500	0.74	508	1.49	167	1.49	820	86
3	600	0.89	610	1.79	200	1.79	915	80
4	1000	1.49	1016	2.98	334	2.98	1334	70
5	1000	1.49	1016	2.98	334	2.98	1523	80
6	2000	2.98	2032	5.96	669	5.96	3039	80
7	2000	2.98	2032	5.96	669	5.96	3282	86
8	2000	2.98	2032	5.96	669	5.96	3081	81
9	3000	4.47	3048	8.94	1004	8.94	5209	91

Product appearance: Yellow solid.

¹H NMR (400 MHz, CDCl₃) δ 6.99 (br s, 2H, ArH), 6.96 (br s, 2H, ArH), 6.93 (s, 2H, ArH, -NHC=CHN-), 4.15–4.11 (m, 2H, COD CH), 2.97–2.92 (m, 2H, COD CH), 2.34 (s, 12H, ArCH₃), 2.14 (s, 6H, ArCH₃), 1.75–1.60 (m, 4H, COD CH₂), 1.37–1.17 (m, 4H, COD CH₂).

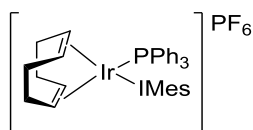
¹³C NMR (100 MHz, CDCl₃) δ 138.8, 138.5, 136.3, 134.6, 129.7, 128.3, 123.5, 82.7, 51.7, 33.7, 29.2, 21.3, 19.9, 18.4.

IR (ATR, cm⁻¹) 3089, 2910, 1604, 1481.

mp >200 °C (decomp.)

Scheme 1.35

(1,5-cyclooctadiene)(1,3-dimesitylimidazol-2-ylidene)(triphenylphosphine)iridium(I) hexafluorophosphate **43**⁴⁹



Prepared according to *General Procedure B*.

Entry	Amount of [Ir(cod)(IMes)Cl] 65		Amount of AgPF ₆		Amount of PPh ₃		Product yield	
	mg	mmol	mg	mmol	mg	mmol	mg	%
1	250	0.39	99	0.39	102	0.39	208	51
2	250	0.39	99	0.39	102	0.39	260	66
3	250	0.39	99	0.39	102	0.39	283	72
4	250	0.39	99	0.39	102	0.39	260	66
5	250	0.39	99	0.39	102	0.39	287	73
6	250	0.39	99	0.39	102	0.39	296	75
7	400	0.62	157	0.62	163	0.62	445	71
8	400	0.62	157	0.62	163	0.62	345	55
9	400	0.62	157	0.62	163	0.62	370	59
10	400	0.62	157	0.62	163	0.62	433	69
11	600	0.94	238	0.94	245	0.94	656	69
12	600	0.94	238	0.94	245	0.94	561	59
13	600	0.94	238	0.94	245	0.94	618	65
14	600	0.94	238	0.94	245	0.94	619	65
15	600	0.94	238	0.94	245	0.94	627	66
16	600	0.94	238	0.94	245	0.94	722	76
17	600	0.94	238	0.94	245	0.94	723	76
18	600	0.94	238	0.94	245	0.94	551	58
19	1000	1.56	397	1.56	408	1.56	1230	78
20	1000	1.56	397	1.56	408	1.56	1420	90
21	2000	3.12	793	3.12	816	3.12	2811	89
22	2000	3.12	793	3.12	816	3.12	2684	85
23	2000	3.12	793	3.12	816	3.12	2715	86
24	2000	3.12	793	3.12	816	3.12	2779	88

Product appearance: Orange-red solid.

¹H NMR (400 MHz, CDCl₃) δ 7.46–7.40 (m, 5H, ArH, NCH=CHN), 7.31–7.25 (m, 6H, ArH), 7.14–7.07 (m, 6H, ArH), 7.00 (s, 2H, ArH), 6.62 (s, 2H, ArH), 4.41–4.33 (m, 2H,

COD CH), 3.33–3.26 (m, 2H, COD CH), 2.33 (s, 6H, ArCH₃), 2.09 (s, 6H, ArCH₃), 1.74 (s, 6H, ArCH₃), 1.67–1.45 (m, 6H, COD CH₂), 1.31–1.22 (m, 2H, COD CH₂)

¹³C NMR (100 MHz, CDCl₃): δ 175.9, 138.3, 135.4, 135.0, 134.9, 134.3, 131.0, 130.4, 130.1, 129.5, 128.2, 126.0, 80.6, 79.8, 31.1, 30.2, 20.9, 20.6, 18.6

³¹P NMR (162 MHz, CDCl₃) δ 16.41 (PPh₃), -144.51 (septet, ¹J_{P,F} = 711 Hz, PF₆)

IR (ATR, cm⁻¹) 2991, 2314, 1628, 1487.

Scheme 1.36 – Substrates

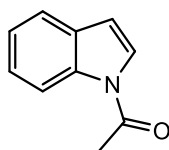
Deuteration of N-acetylindole 117

Carried out according to General Procedure C

Catalyst **43** (5 mol%), 25 °C, 1 h.

Incorporation expected at δ 7.44.

Determined against integral at δ 2.66.



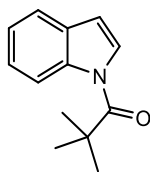
Deuteration of N-pivaloylindole 119

Carried out according to General Procedure C

Catalyst **43** (5 mol%), 25 °C, 1 h.

Incorporation expected at δ 7.72

Determined against integral at δ 1.51.



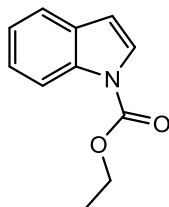
Deuteration of ethyl indole-1-carboxylate 120

Carried out according to General Procedure C

Catalyst **43** (5 mol%), 25 °C, 1 h.

Incorporation expected at δ 7.60.

Determined against integral at δ 1.45.



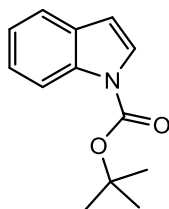
Deuteration of tert-butyl indole-1-carboxylate 118

Carried out according to General Procedure C

Catalyst **43** (5 mol%), 25 °C, 1 h.

Incorporation expected at δ 7.59.

Determined against integral at δ 1.66.

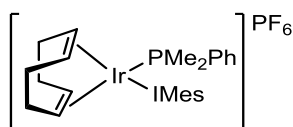


Scheme 1.36 – Results

Entry	Substrate	Mass Substrate / mg	Mass Catalyst / mg	Deuterium Incorporation / %		
				Run 1	Run 2	Average
1	117	34	10.1	94	93	94
2	119	43	10.1	82	82	82
3	120	41	10.1	93	94	94
4	118	47	10.1	11	12	12

Scheme 1.37

(1,5-cyclooctadiene)(1,3-dimesitylimidazol-2-ylidene)(dimethylphenylphosphine) iridium(I) hexafluorophosphate **45**⁴⁹



Prepared according to *General Procedure B*.

Amount of [Ir(cod)(IMes)Cl] **55**: 600 mg, 0.94 mmol.

Amount of THF: 15 mL.

Amount of AgPF₆: 237 mg, 0.94 mmol.

Amount of dimethylphenylphosphine: 126 μL, 0.94 mmol.

Product yield: 724 mg, 87%.

Product appearance: Bright red solid.

¹H NMR (400 MHz, CDCl₃) δ 7.42–7.32 (m, 3H, ArH) 7.28–7.21 (m, 4H, ArH, -NCH=CHN-), 7.06–7.00 (m, 2H, ArH), 6.93–6.87 (m, 2H, ArH), 4.34–4.22 (m, 2H, COD CH), 3.50–3.36 (m, 2H, COD CH), 2.36 (s, 6H, ArCH₃), 2.19 (s, 6H, ArCH₃), 2.12 (s, 6H, ArCH₃), 1.78–1.41 (m, 8H, COD CH₂), 1.49 (s, 3H, PCH₃), 1.47 (s, 3H, PCH₃).

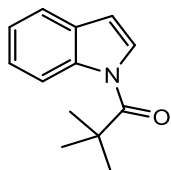
¹³C NMR (101 MHz, CDCl₃) δ 177.6, 139.3, 135.1, 134.2, 131.2, 130.5, 129.6, 129.3, 128.1, 125.3, 83.5, 82.6, 76.2, 75.2, 30.9, 29.9, 21.2, 20.5, 18.7, 16.5, 15.3.

³¹P NMR (162 MHz, CDCl₃) δ -14.1 (PMe₂Ph), -145.1 (septet, ¹J_{P-F} = 711 Hz, PF₆).

IR (ATR, cm⁻¹) 2980, 1609.

M.P. (°C) decomp. >180.

Scheme 1.38 – Substrates



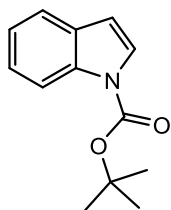
Deuteration of N-pivaloylindole 119

Carried out according to General Procedure C

Catalyst **45** (5 mol%), 25 °C, 1 h.

Incorporation expected at δ 7.72

Determined against integral at δ 1.51.



Deuteration of tert-butyl indole-1-carboxylate 118

Carried out according to General Procedure C

Catalyst **45** (5 mol%), 25 °C, 1 h.

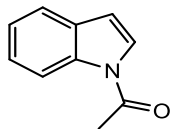
Incorporation expected at δ 7.59.

Determined against integral at δ 1.66.

Scheme 1.38 – Results

Entry	Substrate	Mass Substrate / mg	Mass Catalyst / mg	Deuterium Incorporation / %		
				Run 1	Run 2	Average
1	119	43	8.9	93	92	92
2	118	47	8.9	75	71	73

Scheme 1.39 – Substrates



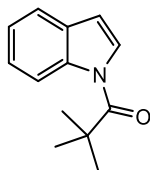
Deuteration of N-acetylindole 117

Carried out according to General Procedure C

Catalyst **20** (5 mol%), 25 °C, 1 h.

Incorporation expected at δ 7.44.

Determined against integral at δ 2.66.



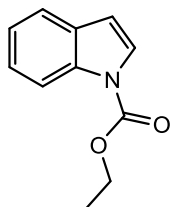
Deuteration of N-pivaloylindole 119

Carried out according to General Procedure C

Catalyst **20** (5 mol%), 25 °C, 1 h.

Incorporation expected at δ 7.72

Determined against integral at δ 1.51.



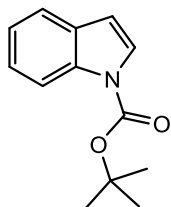
Deuteration of ethyl indole-1-carboxylate 120

Carried out according to General Procedure C

Catalyst **20** (5 mol%), 25 °C, 1 h.

Incorporation expected at δ 7.60.

Determined against integral at δ 1.45.



Deuteration of tert-butyl indole-1-carboxylate 118

Carried out according to General Procedure C

Catalyst **20** (5 mol%), 25 °C, 1 h.

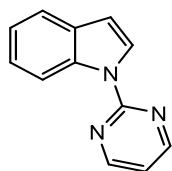
Incorporation expected at δ 7.59.

Determined against integral at δ 1.66.

Scheme 1.39 – Results

Entry	Substrate	Mass Substrate / mg	Mass Catalyst / mg	Deuterium Incorporation / %		
				Run 1	Run 2	Average
1	117	34	8.0	24	20	22
2	119	43	8.0	18	17	18
3	120	41	8.0	7	6	7
4	118	47	8.0	3	6	5

Scheme 1.40



Deuteration of *N*-pyrimidylindole **104**

Carried out according to General Procedure C

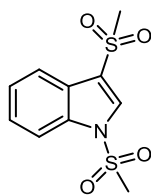
Catalyst **43** (5 mol%), 25 °C, 1 h.

Incorporation expected at δ 8.26.

Determined against integral at δ 7.61.

Entry	Mass Substrate / mg	Mass Catalyst / mg	Deuterium Incorporation / %		
			Run 1	Run 2	Average
1	42	10.1	0	0	0

Scheme 1.41



Deuteration of *N*-methylsulfonylindole **121**

Carried out according to General Procedure C

Catalyst **43** (5 mol%), 25 °C, 1 h.

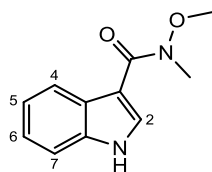
Incorporation expected at δ 8.13.

Determined against integral at δ 3.19.

Entry	Mass Substrate / mg	Mass Catalyst / mg	Deuterium Incorporation / %		
			Run 1	Run 2	Average
1	58	10.1	0	0	0

Scheme 1.42

N*-Methoxy-*N*-methyl-(1*H*-indol-3-yl)carboxamide **128*¹²⁴



Prepared following a reported procedure.¹²⁵ To a solution of 1*H*-indole-3-carboxylic acid (586 mg, 5 mmol) in diethyl ether (12 mL) at 0 °C was added oxalyl chloride (507 μ L, 6 mmol), and the reaction mixture was stirred for 1 h. The solvent was removed *in vacuo* and the residue dissolved in DCM (15 mL). The resulting yellow solution was added to a solution of *N,O*-dimethylhydroxylamine hydrochloride (512 mg, 5.25 mmol) and triethylamine (1.393 mL, 10 mmol) in DCM (15 mL) and the reaction mixture stirred at room temperature for 2 h. The solution was washed with water and saturated aqueous sodium bicarbonate, dried over sodium sulfate and concentrated *in vacuo*. The residue was purified by flash column chromatography (10% ethyl acetate in petrol) to afford **128** as a yellow solid (919 mg, 90% yield).

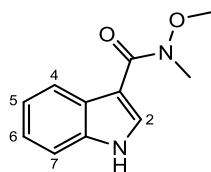
¹H NMR (400 MHz, CDCl₃) δ 8.26 (d, $J = 7.4$ Hz, 1H, H⁴), 7.94 (s, 0.2H, H²), 7.77 (s, 0.8H, H²), 7.38 (d, $J = 7.4$ Hz, 1 H, H⁷), 7.29–7.15 (m, 2H, H⁵ & H⁶), 3.76 (s, 0.6H, OCH₃), 3.60 (s, 2.4H, OCH₃), 3.26 (s, 3H, NCH₃).

Note: the peaks at 7.94 and 7.77 correspond to 1 proton (C2) and the peaks at 3.76 and 3.60 correspond to 3 protons (OCH₃). These signals are split due to rotameric effects.

¹³C NMR (100 MHz, CDCl₃) δ 184.6, 136.9, 135.4, 125.4, 124.3, 123.1, 122.0, 114.2, 112.2, 62.4, 31.8.

IR (ATR, cm⁻¹) 3269, 1662, 1425, 1163.

Table 1.5



Deuteration of *N*-methoxy-*N*-methyl-(1*H*-indol-3-yl)carboxamide **128**

Carried out according to General Procedure C

Catalyst **43** (5 mol%), 25 °C, 1 h.

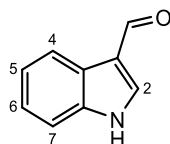
Incorporation expected at δ 7.94/7.77 (C2), 3.76/3.60 (OMe), and 3.26 (NMe).

Determined against integral at δ 7.41–7.34.

Entry	Mass Substrate / mg	Catalyst Loading / mol%	Mass Catalyst / mg	Deuterium Incorporation / %			
					Run 1	Run 2	Average
1	44	5	10.1	C2	99	99	99
				OMe	25	28	27
				NMe	27	26	27
2	44	2	4.0	C2	95	96	96
				OMe	7	9	8
				NMe	11	10	11

Scheme 1.43 – Synthesis

Indole-3-carboxaldehyde **130**¹²⁶



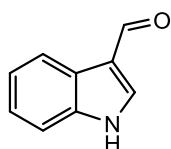
Phosphoryl chloride (1 mL, 10.8 mmol) was added dropwise to a flask containing DMF (7 mL) at 0 °C, and the resulting solution was stirred for 20 min. A solution of indole (1.172 g, 10 mmol) in DCM (3 mL) and added dropwise, and the mixture was then stirred at 35 °C for 1 h. Ice was added to the reaction mixture, followed by 20% aqueous sodium hydroxide, and the reaction mixture was then heated to reflux for 6 h. The mixture was poured into ice water and the resulting precipitate was collected by filtration, washed with water and dried, to yield **130** as a yellow fluffy solid (1.164 g, 81% yield).

¹H NMR (400 MHz, CDCl₃) δ 10.05 (s, 1H, CHO), 8.33–8.28 (m, 1H, H⁴), 7.85 (d, *J* = 3.0 Hz, 1H, H²), 7.45–7.40 (m, 1H, H⁷), 7.35–7.29 (m, 2H, H⁵ and H⁶).

^{13}C NMR (100 MHz, DMSO- d_6) δ 186.0, 137.8, 137.2, 124.5, 123.7, 122.2, 120.2, 118.4, 112.1.

IR (ATR, cm^{-1}) 2930, 1628, 1519, 1441.

Scheme 1.43 – Labelling



Deuteration of indole-3-carboxaldehyde **130**

Carried out according to General Procedure C

Catalyst **43** (5 mol%), 25 °C, 1 h.

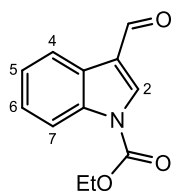
Incorporation expected at δ 7.87-7.83 (C2) and 10.05 (Ald).

Determined against integral at δ 7.35–7.29.

Entry	Mass Substrate / mg	Mass Catalyst / mg	Deuterium Incorporation / %			
				Run 1	Run 2	Average
1	31	10.1	C2	28	29	29
			Ald	4	7	6

Scheme 1.44 – Synthesis

Ethyl 3-formylindole-1-carboxylate **132**¹²⁷



Following the procedure for the ethoxycarbonylation of indole,¹¹⁹ to a solution of indole-3-carboxaldehyde **130** (250 mg, 1.72 mmol) in THF (4 mL) at 0 °C was added sodium hydride (60% in mineral oil, 103 mg, 2.58 mmol) in portions. After stirring for 30 min, ethyl chloroformate (198 μL , 2.07 mmol) was added then the reaction mixture was warmed to room temperature and stirred for 1 h. The reaction mixture was then quenched with water (5 mL) and extracted with ethyl acetate (3×5 mL). The organic phases were combined, dried over sodium sulfate and concentrated *in vacuo* to afford product **132** as a yellow solid (306 mg, 82% yield).

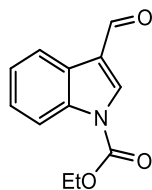
^1H NMR (400 MHz, CDCl_3) δ 10.09 (s, 1H, CHO), 8.28 (d, $J = 7.6$ Hz, 1H, H^4), 8.25 (s, 1H, H^2), 8.16 (d, $J = 8.3$ Hz, 1H, H^7), 7.42 (td, $J = 7.7$, $^4J = 1.6$ Hz, 1H, H^6), 7.39–7.35 (td, J

= 7.5, $^4J = 1.5$ Hz, 1H, H⁵), 4.56 (q, $J = 7.2$ Hz, 2H, CH₂CH₃), 1.50 (t, $J = 7.1$ Hz, 3H, CH₂CH₃).

¹³C NMR (100 MHz, CDCl₃) δ 185.9, 150.5, 136.3, 136.2, 126.5, 126.3, 125.1, 122.4, 122.3, 115.3, 64.6, 14.5.

IR (ATR, cm⁻¹) 2922, 2806, 1749, 1674, 1550, 1452.

Scheme 1.44 – Labelling



Deuteration of ethyl 3-formylindole-1-carboxylate 132

Carried out according to General Procedure C

Catalyst **43** (5 mol%), 25 °C, 1 h.

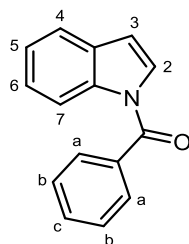
Incorporation expected at δ 8.25 (C2) and 10.09 (Ald).

Determined against integral at δ 4.59–4.52.

Entry	Mass Substrate / mg	Mass Catalyst / mg	Deuterium Incorporation / %			
				Run 1	Run 2	Average
1	47	10.1	C2	97	96	97
			Ald	6	8	7

Scheme 1.45

N-Benzoylindole 134¹¹⁹



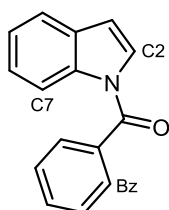
To a flask charged with indole (500 mg, 4.26 mmol), sodium hydroxide (426 mg, 10.65 mmol), and tetrabutylammonium hydrogensulfate (30 mg, 0.09 mmol) was added DCM (15 mL). Benzoyl chloride (741 μL, 6.39 mmol) was added dropwise and the reaction mixture was stirred at room temperature for 2 h. The reaction mixture was then concentrated *in vacuo* and purified by flash column chromatography (4% ethyl acetate in petrol) to afford product **134** as a white solid (933 mg, 99% yield).

^1H NMR (400 MHz, CDCl_3) δ 8.39 (d, $J = 8.0$ Hz, 1H, H^7), 7.74–7.71 (m, 2H, H^a), 7.59–7.57 (m, 2H, H^2 and H^4), 7.53–7.49 (m, 2H, H^b), 7.36–7.32 (m, 1H, H^c), 7.31 (dd, $J = 7.5$, $^4J = 1.0$ Hz, 1H, H^6), 7.30–7.28 (m, 1H, H^5), 6.60 (d, $J = 3.7$, 0.6 Hz, 1H, H^3).

^{13}C NMR (100 MHz, CDCl_3) δ 168.9, 136.3, 134.8, 132.1, 130.8, 129.3, 128.8, 127.8, 125.1, 124.1, 121.1, 116.6, 108.8.

IR (ATR, cm^{-1}) 3049, 1674, 1447, 1328.

Table 1.6



Deuteration of N-benzoylindole 134

Carried out according to General Procedure C

Catalyst **43** (5 mol%).

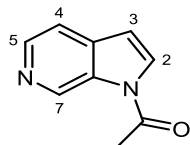
Incorporation expected at δ 7.59-7.57 (C2), 7.74-7.71 (Bz), and 8.39 (C7).

Determined against integral at δ 7.30-7.24.

Entry	Mass Substrate / mg	Mass Catalyst / mg	Conditions	Deuterium Incorporation / %			
				Run 1	Run 2	Average	
1	48	10.1	25 °C, 1 h	C2	75	70	73
				Bz	2	2	2
				C7	0	0	0
2	48	10.1	25 °C, 24 h	C2	89	91	90
				Bz	4	8	6
				C7	0	0	0
3	48	10.1	40 °C, 1 h	C2	82	77	80
				Bz	3	4	4
				C7	0	0	0

Scheme 1.46

1-Acetyl-6-azaindole 137¹²⁸



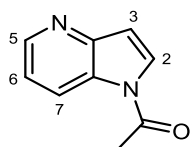
Following the procedure for the acetylation of indole,¹¹⁹ to a flask charged with 6-azaindole (500 mg, 4.23 mmol), sodium hydroxide (423 mg, 10.58 mmol), and tetrabutylammonium hydrogensulfate (29 mg, 0.08 mmol) was added DCM (11 mL). A solution of acetyl chloride (452 μ L, 6.35 mmol) in DCM (6 mL) was then added dropwise. The reaction mixture was stirred at room temperature for 16 h, filtered through a plug of silica and concentrated *in vacuo*. The residue was purified by flash column chromatography (4% methanol in DCM) to afford product **137** as a white solid (555 mg, 82% yield).

¹H NMR (400 MHz, CDCl₃) δ 9.69 (s, 1 H, H⁷), 8.45 (d, J = 5.4 Hz, 1H, H⁵), 7.56 (d, J = 3.6 Hz, 1H, H²), 7.49 (dd, J = 5.4, ⁴ J = 1.1 Hz, 1H, H⁴), 6.65 (d, J = 3.6 Hz, 1H, H³), 2.65 (s, 3H, CH₃).

¹³C NMR (100 MHz, CDCl₃) δ 168.0, 142.9, 138.6, 135.7, 132.8, 128.3, 115.4, 108.2, 23.5.

IR (ATR, cm⁻¹) 2980, 1705, 1435, 1307.

1-Acetyl-4-azaindole 139¹²⁹



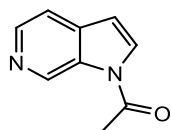
Following the procedure for the acetylation of indole,¹¹⁹ to a flask charged with 4-azaindole (500 mg, 4.23 mmol), sodium hydroxide (423 mg, 10.58 mmol), and tetrabutylammonium hydrogensulfate (29 mg, 0.08 mmol) was added DCM (11 mL). A solution of acetyl chloride (452 μ L, 6.35 mmol) in DCM (6 mL) was then added dropwise. The reaction mixture was stirred at room temperature for 16 h, filtered through a plug of silica and concentrated *in vacuo*. The residue was purified by flash column chromatography (4% methanol in DCM) to afford product **139** as a white solid (474 mg, 70% yield).

¹H NMR (400 MHz, CDCl₃) δ 8.67 (d, J = 8.3 Hz, 1H, H⁵), 8.55 (dd, J = 4.8, ⁴ J = 1.3 Hz, 1 H, H⁷), 7.65 (d, J = 3.8 Hz, 1H, H²), 7.25 (dd, J = 8.3, 4.7 Hz, 1H, H⁶), 6.82 (d, J = 3.8 Hz, 1H, H³), 2.64 (s, 3H, CH₃).

¹³C NMR (100 MHz, CDCl₃) δ 168.2, 147.9, 145.6, 128.7, 127.5, 123.3, 119.0, 109.5, 22.5.

IR (ATR, cm⁻¹) 3269, 2937, 1602, 1425.

Scheme 1.47 – Substrates



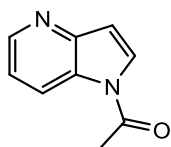
Deuteration of 1-Acetyl-6-azaindole **137**

Carried out according to General Procedure C

Catalyst **43** (5 mol%), 25 °C, 1 h.

Incorporation expected at δ 7.65.

Determined against integral at δ 2.65.



Deuteration of 1-Acetyl-4-azaindole **139**

Carried out according to General Procedure C

Catalyst **43** (5 mol%), 25 °C, 1 h.

Incorporation expected at δ 7.56.

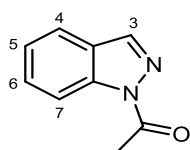
Determined against integral at δ 2.64.

Scheme 1.47 – Results

Entry	Substrate	Mass Substrate / mg	Mass Catalyst / mg	Deuterium Incorporation / %		
				Run 1	Run 2	Average
1	137	34	10.1	87	84	86
2	139	34	10.1	93	90	92

Scheme 1.48 – Synthesis

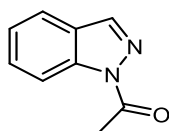
1-Acetylidazole **143**¹³⁰



Following the procedure for the acetylation of indole,¹¹⁹ to a flask charged with indazole (500 mg, 4.23 mmol), sodium hydroxide (423 mg, 10.58 mmol), and tetrabutylammonium hydrogensulfate (29 mg, 0.08 mmol) was added DCM (11 mL). A solution of acetyl chloride (452 μ L, 6.35 mmol) in DCM (6 mL) was then added dropwise. The reaction mixture was stirred at room temperature for 16 h, filtered through a plug of silica and concentrated *in vacuo*. The residue was purified by flash column chromatography (10% ethyl acetate in petrol) to afford product **143** as a white solid (542 mg, 80% yield).

¹H NMR (400 MHz, CDCl₃) δ 8.44 (dd, *J* = 8.0, ⁴*J* = 0.8 Hz, 1H, H⁷), 8.11 (s, 1H, H³), 7.72 (d, *J* = 7.4 Hz, 1H, H⁴), 7.57–7.52 (m, 1H, H⁶), 7.36–7.31 (m, 1H, H⁵), 2.65 (s, 3H, CH₃).
¹³C NMR (100 MHz, CDCl₃) δ 171.2, 140.0, 139.2, 129.7, 126.3, 124.6, 120.8, 115.4, 23.0.
IR (ATR, cm⁻¹) 2980, 1714, 1377, 1195.

Scheme 1.48 – Labelling



Deuteration of 1-Acetylimidazole 143

Carried out according to General Procedure C

Catalyst **43** (5 mol%), 25 °C, 1 h.

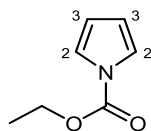
Incorporation expected at δ 8.44 (C7).

Determined against integral at δ 2.65.

Entry	Mass Substrate / mg	Mass Catalyst / mg	Deuterium Incorporation / %		
			Run 1	Run 2	Average
1	34	10.1	0	0	0

Scheme 1.49

Ethyl 1H-pyrrole-1-carboxylate 146¹³¹



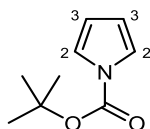
Following the procedure for the acylation of pyrroles,¹³² to a flask charged with pyrrole (520 μL, 7.5 mmol), triethylamine (780 μL, 5.6 mmol) and 4-(dimethylamino)pyridine (684 mg, 5.6 mmol) was added DCM (2 mL), and the resulting solution cooled to 0 °C. Ethyl chloroformate (535 μL, 5.6 mmol) was added slowly and the reaction mixture was then stirred at room temperature for 16 h. The reaction mixture was extracted with diethyl ether (3 × 5 mL), and the combined extracts were washed with aqueous potassium bisulfate, aqueous sodium bicarbonate and water. The organic phase was then dried over sodium sulfate and concentrated *in vacuo* to afford **146** as a yellow oil (770 mg, 99% yield).

¹H NMR (400 MHz, CDCl₃) δ 7.27 (t, *J* = 2.3 Hz, 2H, H²), 6.22 (t, *J* = 2.3 Hz, 2H, H³), 4.40 (q, *J* = 7.1 Hz, 2H, CH₂CH₃), 1.39 (t, *J* = 7.1 Hz, 3H, CH₂CH₃).

¹³C NMR (100 MHz, CDCl₃) δ 150.6, 120.2, 112.5, 63.6, 14.5.

IR (ATR, cm⁻¹) 2981, 1743, 1471, 1307.

tert*-Butyl 1H-pyrrole-1-carboxylate **147*¹³³



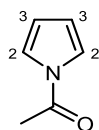
Following the reported procedure,¹³⁴ to a solution of pyrrole (500 μ L, 7.2 mmol) in DCM (5 mL) was added triethylamine (1.50 mL, 10.8 mmol) and di-*tert*-butyl dicarbonate (2.357 g, 10.8 mmol). The reaction mixture was stirred at room temperature for 2 h. The reaction mixture was then extracted with DCM (3 \times 10 mL), and the combined extracts washed with water, dried over sodium sulfate and concentrated *in vacuo*. The residue was then purified by flash column chromatography (5% diethyl ether in petrol) to afford product **15** as brown needles (928 mg, 77% yield).

¹H NMR (400 MHz, CDCl₃) δ 7.20 (t, J = 2.3 Hz, 2H, H²), 6.18 (t, J = 2.3 Hz, 2H, H³), 1.50 (s, 9H, (CH₃)₃).

¹³C NMR (100 MHz, CDCl₃) δ 147.3, 120.2, 111.9, 85.2, 27.1.

IR (ATR, cm⁻¹) 2983, 1799, 1755, 1371.

N*-Acetylpyrrole **148*¹³⁵



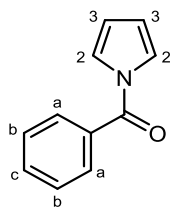
Following the procedure for the acetylation of indole,¹¹⁹ to a flask charged with pyrrole (292 μ L, 4.23 mmol), sodium hydroxide (423 mg, 10.58 mmol), and tetrabutylammonium hydrogensulfate (29 mg, 0.08 mmol) was added DCM (11 mL). A solution of acetyl chloride (452 μ L, 6.35 mmol) in DCM (6 mL) was then added dropwise. The reaction mixture was stirred at room temperature for 16 h, filtered through a plug of silica and concentrated *in vacuo*. The residue was purified by flash column chromatography (5% diethyl ether in petrol) to afford product **148** as a yellow oil (666 mg, 92% yield).

¹H NMR (400 MHz, CDCl₃) δ 7.31 (br. s, 2H, H²), 6.31 (t, J = 2.3 Hz, 2H, H³), 2.55 (s, 3H, CH₃).

¹³C NMR (100 MHz, CDCl₃) δ 168.1, 119.2, 112.8, 22.1.

IR (ATR, cm⁻¹) 2989, 1754, 1371, 1165.

N*-Benzoylpyrrole **149*¹³⁶



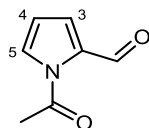
Following the literature procedure,¹³² to a flask charged with pyrrole (346 μ L, 5 mmol), triethylamine (515 μ L, 3.7 mmol) and 4-(dimethylamino)pyridine (452 mg, 3.7 mmol) was added DCM (2 mL) and the resulting solution was cooled to 0 °C. Benzoyl chloride (429 μ L, 3.7 mmol) was added slowly and the reaction mixture was stirred at room temperature for 16 h. The reaction mixture was extracted with diethyl ether (3 \times 5 mL), and the combined organic phases washed with aqueous potassium bisulfate, aqueous sodium bicarbonate and water, dried over sodium sulfate and concentrated *in vacuo*. The residue was purified by flash column chromatography (5% diethyl ether in petrol) to afford **149** as a colourless oil (570 mg, 90% yield).

¹H NMR (400 MHz, CDCl₃) δ 7.76–7.69 (m, 2H, H^a), 7.62–7.56 (m, 1H, H^c), 7.53–7.46 (m, 2H, H^b), 7.30–7.27 (m, 2H, H²), 6.37–6.33 m, 2H, H³).

¹³C NMR (100 MHz, CDCl₃) δ 168.0, 133.5, 132.5, 129.8, 128.7, 121.6, 113.3.

IR (ATR, cm⁻¹) 3147, 1691, 1466, 1323.

1-Acetyl-2-pyrrolecarboxaldehyde **150**^{137,138}



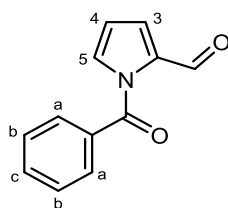
Following the procedure for the acetylation of indole,¹¹⁹ to a solution of pyrrole-2-carboxaldehyde (403 mg, 4.23 mmol) in DCM (10 mL) was added sodium hydroxide (423 mg, 10.58 mmol) and tetrabutylammonium hydrogensulfate (29 mg, 0.08 mmol). A solution of acetyl chloride (452 μ L, 6.35 mmol) in DCM (6 mL) was then added dropwise. The reaction mixture was stirred at room temperature for 16 h, filtered through a plug of silica and concentrated *in vacuo* to afford product **150** as a light brown solid (500 mg, 86% yield).

¹H NMR (400 MHz, CDCl₃) δ 10.31 (s, 1H, CHO), 7.38 (dd, $J = 3.0$, $^4J = 1.8$ Hz, 1H, H³), 7.22 (dd, $J = 3.8$, $^4J = 1.8$ Hz, 1H, H⁵), 6.32 (t, $J = 3.4$ Hz, 1H, H⁴), 2.63 (s, 3H, CH₃).

¹³C NMR (100 MHz, CDCl₃) δ 182.6, 169.3, 134.5, 128.0, 123.9, 112.8, 26.4.

IR (ATR, cm⁻¹) 2987, 2811, 1752, 1678, 1378.

1-Benzoyl-2-pyrrolecarboxaldehyde **151**¹³⁷



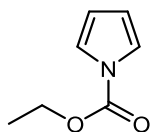
Following the procedure for benzylation of pyrrole,¹³² to a flask charged with pyrrole-2-carboxaldehyde (403 mg, 4.23 mmol), triethylamine (592 μ L, 4.23 mmol) and 4-(dimethylamino)pyridine (520 mg, 4.23 mmol) was added DCM (2 mL), and the resulting solution cooled to 0 °C. Benzoyl chloride (493 μ L, 4.23 mmol) was added slowly and the reaction mixture was stirred at room temperature for 16 h. The reaction mixture was extracted with diethyl ether (3 \times 5 mL), and the combined extracts washed with aqueous potassium bisulfate, aqueous sodium bicarbonate and water, dried over sodium sulfate and concentrated *in vacuo*. The residue was purified by flash column chromatography (5% diethyl ether in petrol) to afford **151** as a beige solid (758 mg, 90% yield).

¹H NMR (400 MHz, CDCl₃): δ 10.03 (s, 1H, CHO), 7.84–7.60 (m, 5H, H^a, H^b & H^c), 7.31 (dd, $J = 3.7$, $^4J = 1.5$ Hz, 1H, H⁵), 7.22 (dd, $J = 3.0$, $^4J = 1.5$ Hz, H³), 6.38 (dd, $J = 3.6$, 3.0 Hz, 1H, H⁴).

¹³C NMR (100 MHz, CDCl₃): δ 180.6, 172.0, 135.5, 133.8, 130.6, 129.4, 129.0, 128.6, 123.0, 112.3.

IR (ATR, cm⁻¹): 2989, 1758, 1689, 1471, 1326.

Scheme 1.50 – Substrates



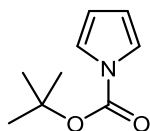
Deuteration of ethyl 1H-pyrrole-1-carboxylate **146**

Carried out according to General Procedure C

Catalyst **43** (5 mol%), 25 °C, 1 h.

Incorporation expected at δ 7.27.

Determined against integral at δ 4.40.



Deuteration of tert-butyl 1H-pyrrole-1-carboxylate **147**

Carried out according to General Procedure C

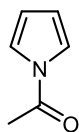
Catalyst **43** (5 mol%), 25 °C, 1 h.

Incorporation expected at δ 7.20.

Determined against integral at δ 1.50.

Deuteration of N-acetylpyrrole 148

Carried out according to General Procedure C



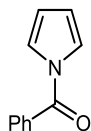
Catalyst **43** (5 mol%), 25 °C, 1 h.

Incorporation expected at δ 7.36–7.31.

Determined against integral at δ 2.71.

Deuteration of N-benzoylpyrrole 149

Carried out according to General Procedure C



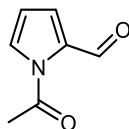
Catalyst **43** (5 mol%), 25 °C, 1 h.

Incorporation expected at δ 7.76–7.69 (Bz) and δ 7.27 (C2).

Determined against integral at δ 7.62–7.56.

Deuteration of 1-acetyl-2-pyrrolecarboxaldehyde 150

Carried out according to General Procedure C



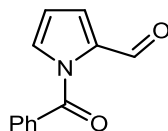
Catalyst **43** (5 mol%), 25 °C, 1 h.

Incorporation expected at δ 7.16 (C5) and δ 10.35 (Ald).

Determined against integral at δ 2.62.

Deuteration of 1-benzoyl-2-pyrrolecarboxaldehyde 151

Carried out according to General Procedure C



Catalyst **43** (5 mol%), 25 °C, 1 h.

Incorporation expected at δ 7.74–7.71 (C5), δ 7.92–7.84 (Bz) and δ 10.29 (Ald).

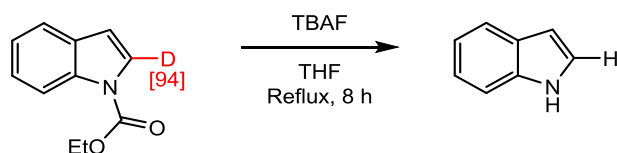
Determined against integral at δ 6.75–6.72.

Scheme 1.50 – Results

Entry	Substrate	Mass Substrate / mg	Mass Catalyst / mg	Deuterium Incorporation / %			
					Run 1	Run 2	Average
1	146	30	10.1	C2	16	19	18
2	147	36	10.1	C2	13	16	15
3	148	23	10.1	C2	90	97	94
4	149	37	10.1	C2	96	97	97
				Bz	32	29	30
6	150	29	10.1	C2	84	80	82
				Ald	0	0	0
5	151	43	10.1	C2	83	88	86
				Bz	30	22	26
				Ald	0	0	0

Scheme 1.51

Indole 75



Carried out following a literature procedure.⁹¹ To a solution of ethyl-1H-indole-1-carboxylate-2-²H **124** (41 mg, 0.215 mmol) in THF (3 mL) was added tetra-*n*-butylammonium fluoride (1.0 M in THF, 1.1 mL, 1.1 mmol). The mixture was heated at reflux for 8 h. The reaction mixture was then extracted with ethyl acetate (3 × 5 mL) and washed with water and brine, before being dried over sodium sulfate and concentrated *in vacuo* to afford indole **75** as an off-white solid (23 mg, 90% yield).

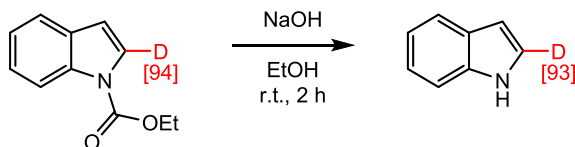
Deuterium incorporation in the desired product, [2-²H]-indole **73**, was expected at δ 7.28–7.20 (C2) and was determined against the integral at δ 7.17–7.14 (C5).

¹H NMR (400 MHz, CDCl₃) δ 8.21 (br s, 1H, NH), 7.70–7.66 (d, *J* = 7.5 Hz, 1H, H⁷), 7.45–7.41 (d, *J* = 7.5 Hz, 1H, H⁴), 7.28–7.20 (m, 2H, H⁶ and H²), 7.17–7.14 (m, 1H, H⁵), 6.60–6.57 (m, 1H, H³).

^{13}C NMR (100 MHz, CDCl_3) δ 135.9, 128.3, 124.6, 122.0, 121.3, 120.1, 111.4, 102.7, 101.9.

Scheme 1.52

2-Deuteroindole 73¹³⁹



To a solution of sodium hydroxide (100 mg, 2.5 mmol) in ethanol (15 mL) was added ethyl-1H-indole-1-carboxylate-2- ^2H **124** (190 mg, 1 mmol). The mixture was stirred at room temperature for 2 h. The reaction mixture was then extracted with ethyl acetate (3×20 mL), washed with brine, dried over sodium sulfate and concentrated *in vacuo* to yield [2- ^2H]-indole **73** as an off-white solid (118 mg, 99% yield).

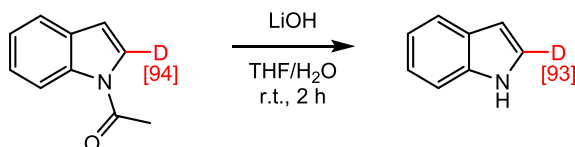
Deuterium incorporation in [2- ^2H]-indole **73** was expected at δ 7.28–7.20 (C2) and was determined against the integral at δ 7.17–7.14 (C5).

^1H NMR (400 MHz, CDCl_3) δ 8.21 (br s, 1H, NH), 7.70–7.66 (d, $J = 7.5$ Hz, 1H, H^7), 7.45–7.41 (d, $J = 7.5$ Hz, 1H, H^4), 7.28–7.20 (m, 1.07H, H^6 and H^2), 7.17–7.14 (m, 1H, H^5), 6.60–6.57 (m, 1H, H^3).

^{13}C NMR (100 MHz, CDCl_3) δ 135.9, 128.3, 124.6 (t, $^1J_{\text{C-D}} = 30$ Hz), 122.0, 121.3, 120.1, 111.4, 102.7, 101.9.

Scheme 1.53

2-Deuteroindole 73¹³⁹



To a solution of lithium hydroxide (60 mg, 2.5 mmol) in THF:H₂O (4:1, 15 mL) was added [2- ^2H]-*N*-acetylindole **122** (161 mg, 1 mmol). The mixture was stirred at room temperature for 2 h. The reaction mixture was then extracted with ethyl acetate, washed with brine, dried over sodium sulfate and concentrated *in vacuo* to yield [2- ^2H]-indole **73** as an off-white solid (117 mg, 99% yield).

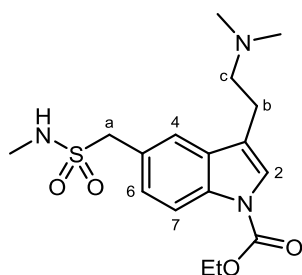
Deuterium incorporation in [2- ^2H]-indole **73** was expected at δ 7.28–7.20 (C2) and was determined against the integral at δ 7.17–7.14 (C5).

¹H NMR (400 MHz, CDCl₃) δ 8.21 (br s, 1H, NH), 7.70–7.66 (d, *J* = 7.5 Hz, 1H, H⁷), 7.45–7.41 (d, *J* = 7.5 Hz, 1H, H⁴), 7.28–7.20 (m, 1.08H, H⁶ and H²), 7.17–7.14 (m, 1H, H⁵), 6.60–6.57 (m, 1H, H³).

¹³C NMR (100 MHz, CDCl₃) δ 135.9, 128.3, 124.6 (t, ¹*J*_{C-D} = 30 Hz), 122.0, 121.3, 120.1, 111.4, 102.7, 101.9.

Scheme 1.54

Ethyl 3-[2-(dimethylamino)ethyl]-5-[methylsulfonylmethyl]-1H-indole-1-carboxylate
157



To a solution of 3-[2-(dimethylamino)ethyl]-*N*-methyl-1H-indole-5-methanesulfonamide (29 mg, 0.1 mmol) in DMF (1 mL) was added sodium hydride (60% dispersion in mineral oil, 12 mg, 0.3 mmol). The reaction mixture was allowed to stir at room temperature for 30 min, after which time it was cooled to 0 °C and ethyl chloroformate (9.2 μL, 0.1 mmol) was added. The reaction mixture was then stirred for 1 h at room temperature, before being quenched with saturated sodium bicarbonate (5 mL) and extracted with ethyl acetate (3 × 5 mL). The combined extracts were washed with brine (10 mL), dried over sodium sulfate and concentrated *in vacuo*. The residue was purified by flash column chromatography (5% methanol/1% triethylamine in DCM) followed by recrystallisation from ethanol, to afford **157** as a white solid (21 mg, 67% yield).

¹H NMR (400 MHz, CDCl₃) δ 7.72–7.65 (m, 1H, H⁴), 7.54–7.48 (m, 1H, H⁷), 7.38–7.33 (m, 1H, H⁶), 7.12–7.09 (s, 1H, H²), 4.93–4.88 (m, 2H, H^a), 4.04 (q, *J* = 6.6 Hz, 2H, CH₂CH₃), 2.85 (t, *J* = 7.7 Hz, 2H, H^c), 2.57 (t, *J* = 7.7 Hz, 2H, H^b), 2.32–2.27 (m, 3H, NHCH₃), 2.04–2.00 (m, 6H, N(CH₃)₂), 1.40–1.36 (m, 3H, CH₂CH₃).

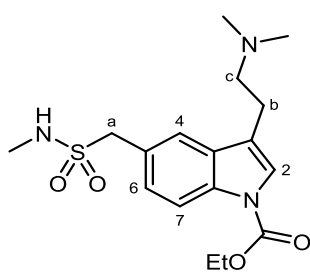
¹³C NMR (100 MHz, CDCl₃) δ 160.8, 132.2, 132.0, 127.4, 124.5, 120.7, 118.1, 117.6, 110.8, 66.5, 64.2, 63.7, 46.8, 26.0, 23.2, 14.2.

IR (ATR, cm⁻¹) 2981, 1743, 1471, 1360, 1167.

M.P. (°C) 170–173 °C

HRMS (NSI) *m/z* calculated for C₁₇H₂₆N₃O₄S [M+H]⁺: 368.1639; found: 368.1639.

Table 1.8



Deuteration of ethyl 3-[2-(dimethylamino)ethyl]-5-[methylsulfamoylmethyl]-1H-indole-1-carboxylate **157**

Carried out according to General Procedure C

Catalyst **43** (5 mol%), 25 °C.

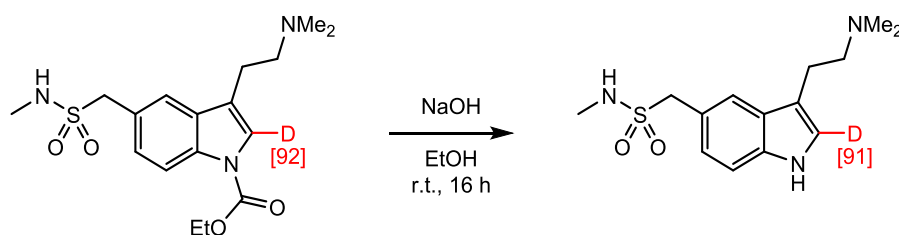
Incorporation expected at δ 7.12-7.09 (C2).

Determined against integral at δ 2.85 ($\text{CH}_2\text{-CH}_2\text{-N(CH}_3)_2$.)

Entry	Mass Substrate / mg	Mass Catalyst / mg	Time / h	Deuterium Incorporation / %
1	15	2.2	1	38
2	15	2.2	18	84
3	15	2.2	24	92

Scheme 1.55

[2-²H]-3-[2-(dimethylamino)ethyl]-5-[methylsulfamoylmethyl]-1H-indole **159**



To a solution of sodium hydroxide (4 mg, 0.1 mmol) in ethanol (0.6 mL) was added ethyl [2-²H]-3-[2-(dimethylamino)ethyl]-5-[methylsulfamoylmethyl]-1H-indole-1-carboxylate **158** (15 mg, 0.04 mmol). The reaction mixture was stirred at room temperature for 16 h, after which time the mixture was extracted with ethyl acetate (3×2 mL), and the combined extracts washed with brine, dried over sodium sulfate and concentrated *in vacuo* to yield **159** as a white solid (10 mg, 87% yield).

Deuterium incorporation in **159** was expected at δ 7.08–7.05 (C2) and was determined against the integral at δ 2.97–2.91 ($\text{CH}_2\text{-N(CH}_3)_2$).

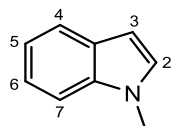
¹H NMR (400 MHz, CDCl₃) δ 7.59 (s, 1H, H⁴), 7.37–7.32 (m, 1H, H⁷), 7.21 (dd, $J = 8.3$, $^4J = 1.8$ Hz, 1H, H⁶), 7.08–7.05 (m, 0.09 H, H²), 4.36 (s, 2H, ArCH₂SO₂R), 2.97–2.91 (m, 2H, CH₂-N(CH₃)₂), 2.71 (s, 3H, NHCH₃), 2.68–2.62 (m, 2H, CH₂-CH₂-N(CH₃)₂), 2.36–2.33 (m, 6H, N(CH₃)₂).

¹³C NMR (100 MHz, CDCl₃) δ 134.2, 131.0, 126.9, 123.1 (t, $^1J_{\text{C-D}} = 29$ Hz), 119.9, 117.9, 113.5, 111.0, 66.7, 64.5, 47.3, 25.2, 23.8.

C3 Labelling of *N*-Protected Indoles

Scheme 1.56

1-Methylindole **160**⁹⁴



Prepared according to *General Procedure D*.

Amount of indole: 586 mg, 5 mmol.

Amount of sodium hydride: 300 mg, 7.5 mmol.

Amount of methyl iodide: 417 μ L, 6.7 mmol.

Product yield: 557 mg, 85%.

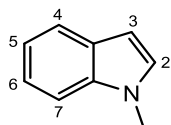
Product appearance: yellow oil.

¹H NMR (400 MHz, CDCl₃) δ 7.62 (d, J = 7.9 Hz, 1H, H⁴), 7.34–7.29 (m, 1H, H⁷), 7.23–7.19 (m, 1H, H⁶), 7.12–7.07 (m, 1H, H⁵), 7.04 (d, J = 3.2 Hz, 1H, H²), 6.48 (d, J = 3.2 Hz, 1H, H³), 3.78 (s, 3H, CH₃).

¹³C NMR (101 MHz, CDCl₃) δ 136.9, 129.0, 128.7, 121.8, 121.1, 119.5, 109.4, 101.1, 33.0.

IR (ATR, cm⁻¹) 2922, 1512, 1462, 1315.

Scheme 1.57



Deuteration of *N*-Methylindole **160**

Carried out according to *General Procedure C*

Catalyst **43** (5 mol%), 25 °C, 1 h.

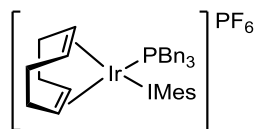
Incorporation expected at δ 6.48.

Determined against integral at δ 3.78.

Entry	Mass Substrate / mg	Mass Catalyst / mg	Deuterium Incorporation / %			
			Run 1	Run 2	Run 3	Average
1	34	10.1	64	68	60	64

Table 1.9

(1,5-cyclooctadiene)(1,3-dimesitylimidazol-2-ylidene)(tribenzylphosphine)iridium(I) hexafluorophosphate 44⁴⁹



Prepared according to *General Procedure B*.

Amount of [Ir(cod)(IMes)Cl] **55**: 700 mg, 1.09 mmol.

Amount of AgPF₆: 276 mg, 1.09 mmol.

Amount of tribenzylphosphine: 333 mg, 1.09 mmol.

Product yield: 888 mg, 77%.

Product appearance: Orange-red solid.

¹H NMR (400 MHz, CDCl₃) δ 7.79 (s, 2H, -NCH=CHN-), 7.41 (s, 2H, ArH), 7.34 (s, 2H, ArH), 7.30–7.28 (m, 9H, ArH), 6.99–6.97 (m, 6H, ArH), 4.72–4.70 (m, 2H, COD CH), 3.27–3.26 (m, 2H, COD CH), 3.02 (d, ²J_{P-H} = 8.8 Hz, 6H, PCH₂Ar), 2.57 (s, 6H, ArCH₃), 2.47 (s, 6H, ArCH₃), 2.39 (s, 6H, ArCH₃), 1.83–1.77 (m, 2H, COD CH₂), 1.60–1.48 (m, 4H, COD CH₂), 1.37–1.30 (m, 2H, COD CH₂).

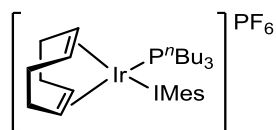
¹³C NMR (101 MHz, CDCl₃) δ 174.7, 141.1, 137.4, 137.0, 136.3, 134.4, 131.0, 130.7, 129.6, 128.8, 128.0, 127.9, 87.2, 75.8, 32.5, 31.2, 31.1, 21.1, 20.6, 20.0.

³¹P NMR (162 MHz, CDCl₃) δ -7.0 (PBn₃), -144.2 (septet, ¹J_{P-F} = 712 Hz, PF₆).

IR (ATR, cm⁻¹) 3040, 2995, 2319, 1631, 1495.

M.P. (°C) decomp. 170.

(1,5-cyclooctadiene)(1,3-dimesitylimidazol-2-ylidene)(tri-*n*-butylphosphine)iridium(I) hexafluorophosphate 162⁴⁹



Prepared according to *General Procedure B*.

Amount of [Ir(cod)(IMes)Cl] **55**: 400 mg, 0.62 mmol.

Amount of AgPF₆: 158 mg, 0.62 mmol.

Amount of tri-*n*-butylphosphine: 156 μL, 0.62 mmol.

Product yield: 433 mg, 73%.

Product appearance: Bright red solid.

¹H NMR (400 MHz, CDCl₃) δ 7.23 (s, 2H, -NCH=CHN-), 7.01 (s, 2H, ArH), 6.98 (s, 2H, ArH), 4.16–4.09 (m, 2H, COD CH), 3.68–3.62 (m, 2H, COD CH), 2.34 (s, 6H, ArCH₃), 2.28 (s, 6H, ArCH₃), 2.17 (s, 6H, ArCH₃), 1.91–1.81 (m, 2H, COD-CH₂), 1.72–1.61 (m, 2H, COD CH₂), 1.51–1.37 (m, 10H, COD CH₂, PⁿBu₃ CH₂), 1.26 (*app.* sextet, *J* = 7.2 Hz, 6H, PⁿBu₃ CH₂-CH₂-CH₃), 1.15–1.06 (m, 6H, PⁿBu₃ CH₂), 0.86 (t, *J* = 7.3 Hz, 9H, PⁿBu₃ CH₂-CH₃).

¹³C NMR (101 MHz, CDCl₃) δ 175.5, 133.9, 129.3, 129.2, 125.6, 81.5, 81.4, 73.2, 30.8, 30.41, 30.39, 26.13, 26.10, 23.9, 23.8, 23.7, 23.4, 20.5, 19.8, 18.9, 13.2.

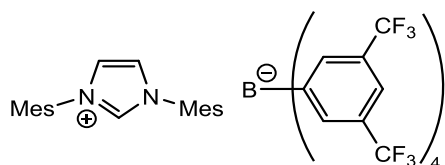
³¹P NMR (162 MHz, CDCl₃) δ -2.6 (PⁿBu₃), -144.4 (septet, ¹*J*_{P-F} = 711 Hz, PF₆).

IR (ATR, cm⁻¹) 2949, 2870, 1481, 1383.

M.P. (°C) decomp. >170.

Scheme 1.58

***N,N'*-Dimesitylimidazolium tetrakis[(3,5-trifluoromethylphenyl)]borate 63⁶⁰**



N,N-Dimesitylimidazolium chloride (0.269 g, 0.789 mmol) and NaBArF (0.700 g, 0.789 mmol) were added to a 50 mL round bottom flask and dissolved in a mixture of DCM and H₂O (20 mL). The reaction mixture was stirred overnight, before being transferred to a separating funnel and diluted with DCM (10 mL). The aqueous phase was washed with DCM and the combined organic phase washed with water then brine. After drying the DCM layer over anhydrous sodium sulfate and filtering through a Büchner funnel, the solvent was removed *in vacuo* and the residue purified through a short plug of silica, eluting with DCM. Concentration *in vacuo* gave the desired product as a white solid (0.840 g, 92% yield).

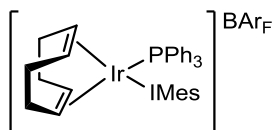
¹H NMR (400 MHz, CDCl₃) δ 8.11 (t, ⁴*J* = 1.6 Hz, 1H, NCHN), 7.70–7.68 (m, 8H, ArHBAr_F), 7.50 (s, 4H, ArHBAr_F), 7.40 (d, *J* = 1.6 Hz, 2H, -NCH=CHN-), 7.08 (s, 4H, ArH), 2.37 (s, 6H, ArCH₃), 2.04 (s, 12H, ArCH₃).

¹³C NMR (101 MHz, CDCl₃) δ 161.8 (q, *J*_{C-B} = 49.5 Hz), 143.1, 135.3, 134.8, 133.4, 130.4, 129.4–128.4 (unidentified multiplet), 125.0, 124.6 (q, *J*_{C-F} = 270.7 Hz), 117.4, 21.0, 16.9.

IR (ATR, cm⁻¹) 3156, 2994, 2968, 2928, 1609, 1545, 1479, 1352, 1273, 1115.

M.P. (°C) 136–137.

(1,5-cyclooctadiene)(1,3-dimesitylimidazol-2-ylidene)(triphenylphosphine)iridium(I) tetrakis[(3,5-trifluoromethylphenyl)]borate 64⁶⁰



To a flame-dried round bottom flask fitted with stopcock sidearm was added bis(1,5-cyclooctadiene)diiridium(I) dichloride (0.544 g, 0.81 mmol), and dry THF (5 mL). After all solids had dissolved, triphenylphosphine (0.426 g, 1.62 mmol) was added in one portion, causing an orange to yellow colour change. Having allowed the reaction mixture to stir at room temp. for 15 min, BArF salt **63** (1.894 g, 1.62 mmol) was added in one portion and allowed to dissolve completely. After a further 5 min stirring, KO^tBu (0.273 g, 2.43 mmol) was added in one portion. The reaction mixture was stirred for 1 h at r.t. before the THF was removed *in vacuo*. The red-black residue was dissolved in DCM and purified directly through a short plug of silica, eluting the bright red fraction with DCM. The combined fractions were concentrated under reduced pressure to reveal a red, oily solid, which was triturated with pentane to give the product as a grainy red solid (1.86 g, 67% yield).

¹H NMR (400 MHz, CDCl₃) δ 7.74–7.73 (m, 8H, ArHBAr_F), 7.53 (bs, 4H, ArHBAr_F), 7.46–7.42 (m, 3H, ArH), 7.32–7.27 (overlapping s and m, 8H, ArH, -NCH=CHN-), 7.16–7.11 (m, 6H, ArH), 7.05 (s, 2H, ArH), 6.69 (s, 2H, ArH), 4.40–4.37 (m, 2H, COD CH), 3.38–3.36 (m, 2H, COD CH), 2.36 (s, 6H, ArCH₃), 2.11 (s, 6H, ArCH₃), 1.77 (s, 6H, ArCH₃), 1.71–1.48 (m, 6H, COD CH₂), 1.33–1.27 (m, 2H, COD CH₂).

¹³C NMR (101 MHz, CDCl₃) δ 178.0 (d, *J*_{C-P} = 10.0 Hz), 161.8 (q, *J*_{C-B} = 50.0 Hz), 140.1, 135.4, 135.1, 134.8, 134.7, 131.3, 131.2, 130.7, 130.4, 129.8, 129.0, 128.7, 128.5, 124.5 (q, *J*_{C-F} = 270.0 Hz), 117.4, 80.5, 80.4, 78.5, 31.8, 21.1, 20.7, 18.9.

³¹P NMR (162 MHz, CDCl₃) δ 16.4 (PPh₃).

¹⁹F NMR (376 MHz, CDCl₃): δ -62.5 (BAr_F ArCF₃).

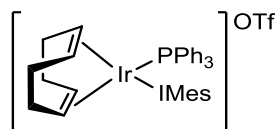
¹¹B NMR (128 MHz, CDCl₃): δ -6.60.

IR (ATR, cm⁻¹) 3024, 2978, 1610, 1539, 1479, 1467, 1426, 1352, 1271, 1187.

M.P. (°C) decomp. >150.

Table 1.10

(1,5-cyclooctadiene)(1,3-dimesitylimidazol-2-ylidene)(triphenylphosphine)iridium(I) trifluoromethylsulfonate 65⁶⁰



Prepared according to General Procedure B.

Amount of [Ir(cod)(IMes)Cl] **55**: 500 mg, 0.78 mmol.

Amount of THF: 20 mL.

Amount of AgOTf: 201 mg, 0.78 mmol.

Amount of triphenylphosphine: 204 mg, 0.78 mmol.

Product yield: 545 mg, 69%.

Product appearance: Orange-red solid.

¹H NMR (400 MHz, CDCl₃) δ 7.50 (s, 2H, -NCH=CHN-), 7.49–7.45 (m, 3H, ArH), 7.34–7.28 (m, 6H, ArH), 7.16–7.11 (m, 6H, ArH), 7.05 (s, 2H, ArH), 6.67 (s, 2H, ArH), 4.31–4.38 (m, 2H, COD CH), 3.34–3.32 (m, 2H, COD CH), 2.37 (s, 6H, ArCH₃), 2.13 (s, 6H, ArCH₃), 1.77 (s, 6H, ArCH₃), 1.70–1.50 (m, 6H, COD CH₂), 1.33–1.25 (m, 2H, COD CH₂).

¹³C NMR (101 MHz, CDCl₃) δ 176.2 (d, ³J_{C-P} = 8.0 Hz), 139.2, 135.2, 135.1, 134.7, 134.3, 134.2, 130.8, 130.2, 129.8, 129.2, 128.1, 128.0, 126.4, 80.0, 79.9, 77.5, 31.4, 29.7, 20.8, 20.4, 18.6.

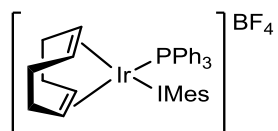
³¹P NMR (162 MHz, CDCl₃) δ 16.4 (PPh₃).

¹⁹F NMR (376 MHz, CDCl₃) δ -78.0 (OTf).

IR (ATR, cm⁻¹) 3174, 2951, 2924, 2887, 1477, 1437, 1381, 1267, 1140, 1032.

M.P. (°C) decomp. >170.

(1,5-cyclooctadiene)(1,3-dimesitylimidazol-2-ylidene)(triphenylphosphine)iridium(I) tetrafluoroborate 2g⁶⁰



Prepared according to General Procedure B.

Amount of [Ir(cod)(IMes)Cl] **55**: 250 mg, 0.39 mmol.

Amount of THF: 20 mL.

Amount of AgBF₄: 76 mg, 0.39 mmol.

Amount of triphenylphosphine: 99 mg, 0.39 mmol.

Product yield: 298 mg, 80%.

Product appearance: Orange-red solid.

¹H NMR (400 MHz, CDCl₃) δ 7.50 (s, 2H, -NCH=CHN-), 7.48–7.44 (m, 3H, ArH), 7.34–7.29 (td, *J* = 7.8, 2.5 Hz, 6H, ArH), 7.15–7.10 (m, 6H, ArH), 7.04 (s, 2H, ArH), 6.66 (s, 2H, ArH), 4.40–4.38 (m, 2H, COD CH), 3.33–3.31 (m, 2H, COD CH), 2.36 (s, 6H, ArCH₃), 2.12 (s, 6H, ArCH₃), 1.77 (s, 6H, ArCH₃), 1.68–1.49 (m, 6H, COD CH₂), 1.32–1.27 (m, 2H, COD CH₂).

¹³C NMR (101 MHz, CDCl₃) δ 176.1 (d, *J*_{C-P} = 8.0 Hz), 139.1, 135.2, 135.1, 134.7, 134.3, 134.2, 130.7, 130.3, 129.8, 129.2, 128.1, 128.0, 126.4, 79.9, 79.8, 77.5, 31.4, 29.7, 20.7, 20.4, 18.5.

³¹P NMR (162 MHz, CDCl₃) δ 16.3 (PPh₃).

¹⁹F NMR (376 MHz, CDCl₃) δ -153.8 (BF₄).

¹¹B NMR (128 MHz) δ -0.9 (BF₄).

IR (ATR, cm⁻¹) 3043, 2920, 2364, 1606, 1585, 1566, 1477, 1435, 1049.

M.P. (°C) decomp. >170.

Table 1.11

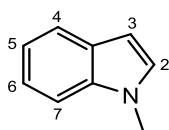
Deuteration of N-Methylindole 160

Carried out according to General Procedure C

5 mol% catalyst, 25 °C, 1 h.

Incorporation expected at δ 6.48.

Determined against integral at δ 3.78.



Entry	Mass Substrate / mg	Catalyst	Mass Catalyst / mg	Deuterium Incorporation / %			
				Run 1	Run 2	Run 3	Average
1	28	45	8.9	27	22	25	25
2	28	44	10.5	55	55	52	54
3	28	162	9.5	8	7	6	7
4	28	64	17.3	45	50	46	47
5	28	65	10.2	34	39	41	38
6	28	66	9.5	20	21	21	21

Scheme 1.59 – Reaction Optimisation with Design of Experiments

The effects of catalyst loading, reaction time and solvent volume were assessed using Design of Experiments (DOE).^{95,96} Design-Expert™ software v9.0.3 (Stat-Ease Inc., Minneapolis, MN) was used to generate a set of 11 experiments as part of a 2-level, 3-factorial design. For each factor, a range of values was specified; the eight combinations of high and low values were then run as individual experiments. Additionally, three centre point runs were carried out in order to: (a) assess any curvature in the response of deuteration to changes of the variables, and (b) ensure reproducibility of the labelling reaction. This design gave a total of 11 experiments (Table 1.18), with entries 3, 9, and 10 representing the centre points. Reactions were run according to *General Procedure C* with catalyst **43**, with deuterium incorporation (%) in *N*-methylindole **160** used as the response.

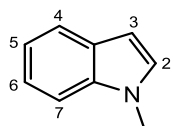
Table 1.18

Deuteration of N-Methylindole 160

Carried out according to General Procedure C

Incorporation expected at δ 6.48.

Determined against integral at δ 3.78.

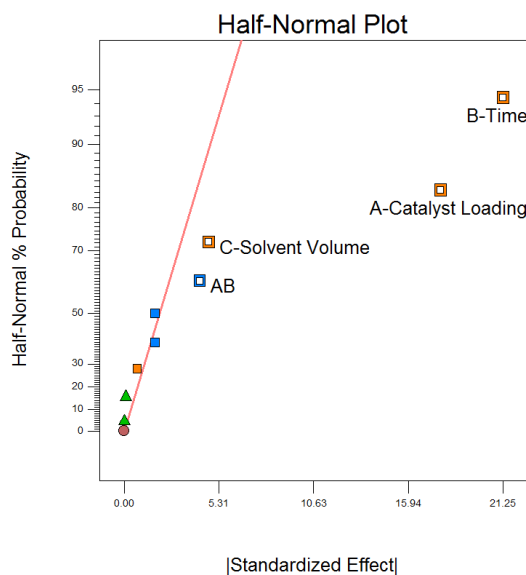


Run*	Factor A: Catalyst Loading / mol%	Factor B: Reaction Time / h	Factor C: Solvent Volume / mL	Response: % D Incorporation
1 (---)	0.1	0.5	1	52
2 (- - +)	0.1	0.5	5	56
3 (0 0 0) [‡]	2.55	8.25	3	86
4 (+ + -)	5	16	1	92
5 (- + -)	0.1	16	1	75
6 (+ - +)	5	0.5	5	78
7 (+ - -)	5	0.5	1	74
8 (+ + +)	5	16	5	94
9 (0 0 0) [‡]	2.55	8.25	3	87
10 (0 0 0) [‡]	2.55	8.25	3	86
11 (- + +)	0.1	16	5	84

* (+) = high value, (-) = low value, and (0) = centre point value of a variable.

[‡] These entries represent centre points.

The responses were entered into the same design program, and used to generate a half-normal plot (Graph 1.3), which suggested that both catalyst loading and reaction time had significant effects on reaction efficacy.



Graph 1.3

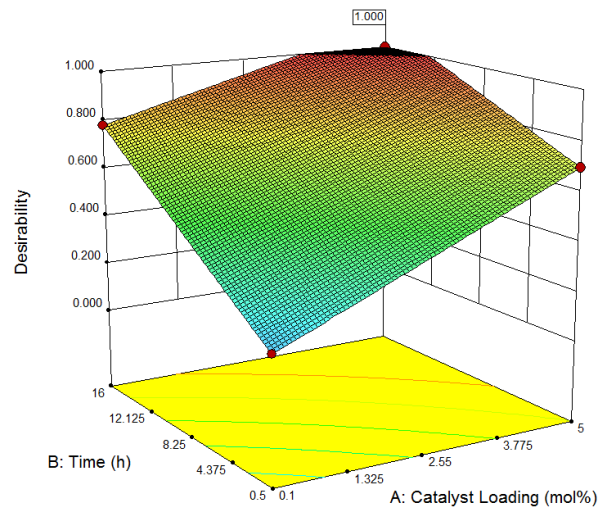
A numerical optimization model was then used to search the factor space for the best combination of variables to achieve specific goals. Two of these models were examined: one (Graph 1.4) was used to maximise desirability across the ranges initially specified by the design; the other (Graph 1.5) was set to maximise desirability as a top priority, while minimising catalyst loading as a secondary goal. The conditions at the top of the surface of Graph 1.5 (1 mol% catalyst, 16 h reaction time, 5 mL solvent) were taken forward for future reactions as optimum reaction conditions.

Design-Expert® Software
 Factor Coding: Actual
 Desirability



X1 = A: Catalyst Loading
 X2 = B: Time

Actual Factor
 C: Solvent Volume = 5



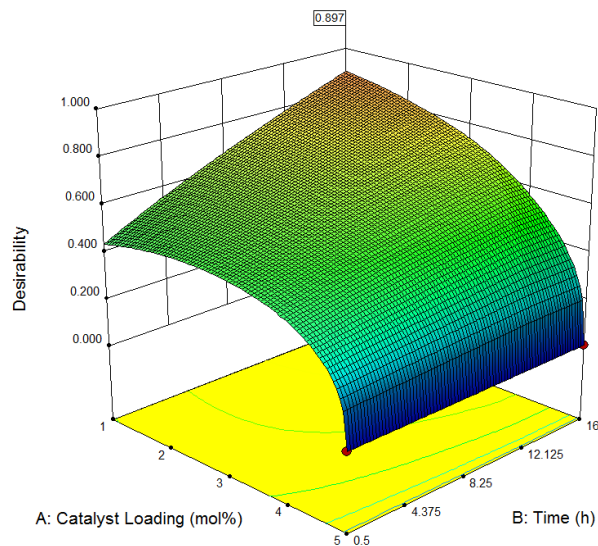
Graph 1.4

Design-Expert® Software
 Factor Coding: Actual
 Desirability



X1 = A: Catalyst Loading
 X2 = B: Time

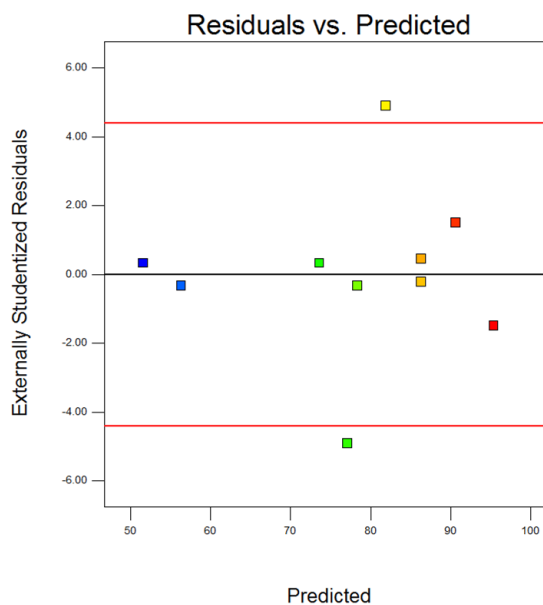
Actual Factor
 C: Solvent Volume = 4.99999



Graph 1.5

Lastly, a Residuals vs. Predicted graph was plotted (Graph 1.6). This plots residuals against the predicted response values and checks for constant variance across the range of data collected. A pattern in the plot indicates non-constant variance. In this case, the points appear randomly scattered and the assumption of constant variance can therefore be confirmed.

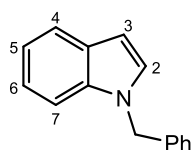
Design-Expert® Software
 R1
 (adjusted for curvature)
 Color points by value of
 R1:
 94
 52



Graph 1.6

Scheme 1.60

***N*-Benzylindole 164**¹⁴⁰



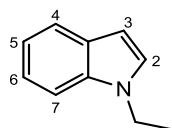
Prepared following a literature procedure.¹⁴¹ A solution of indole (586 mg, 5 mmol) and sodium hydroxide (400 mg, 10 mmol) in DCM (20 mL) was stirred at room temperature. After 30 min, benzyl bromide (831 μ L, 7 mmol) was added. The reaction mixture was stirred at room temperature for 2 h before being quenched with water (30 mL). The organic products were extracted into ethyl acetate (3 \times 20 mL), dried over sodium sulfate and concentrated *in vacuo*. Column chromatography (5% ethyl acetate in petrol) afforded product **164** (735 mg, 71% yield).

¹H NMR (400 MHz, CDCl₃) δ 7.67 (d, J = 7.8 Hz, 1H, H⁴), 7.31–7.23 (m, 4H, PhH, H², & H⁷), 7.18–7.10 (m, 5H, PhH, H⁵, & H⁶), 6.57 (d, J = 3.1 Hz, 1H, H³), 5.32 (s, 2H, CH₂).

¹³C NMR (100 MHz, CDCl₃) δ 137.5, 137.2, 129.5, 129.3, 129.0, 128.2, 126.2, 121.0, 119.7, 116.1, 100.8, 51.9 .

IR (ATR, cm⁻¹) 3029, 2920, 1486, 1465, 1311.

1-Ethylindole **165**¹⁴²



A solution of indole (586 mg, 5 mmol) and potassium hydroxide (561 mg, 10 mmol) in DMSO (20 mL) was stirred at room temperature for 30 min, after which time ethyl bromide (746 μ L, 10 mmol) was added. The resultant purple solution was stirred at room temperature for 2 h before being quenched with water (20 mL). The organic products were extracted into ethyl acetate (3 \times 50 mL), dried over sodium sulfate and concentrated *in vacuo*. Column chromatography (10% ethyl acetate in petrol) afforded product **165** as a yellow oil (722 mg, 99% yield).

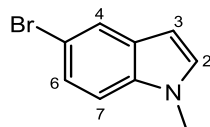
¹H NMR (400 MHz, CDCl₃) δ 7.64 (dt, $J = 7.8$, $^4J = 0.9$ Hz, 1H, H⁴), 7.35 (d, $J = 8.3$ Hz, 1H, H⁷), 7.23–7.16 (m, 1H, H⁶), 7.14–7.06 (m, 2H, H² & H⁵), 6.49 (d, $J = 3.0$ Hz, 1H, H³), 4.17 (q, $J = 7.3$ Hz, 2H, CH₂CH₃), 1.47 (t, $J = 7.3$ Hz, 3H, CH₂CH₃).

¹³C NMR (101 MHz, CDCl₃) δ 136.1, 128.9, 127.3, 121.7, 121.2, 199.3, 109.4, 101.1, 41.2, 15.7.

IR (ATR, cm⁻¹) 2916, 1510, 1450, 1311.

Scheme 1.61

1-Methyl-5-bromoindole **166**¹⁴³



Prepared according to General Procedure D.

Amount of 5-bromoindole: 980 mg, 5 mmol.

Amount of sodium hydride: 300 mg, 7.5 mmol.

Amount of methyl iodide: 417 μ L, 6.7 mmol.

Product yield: 861 mg, 82%.

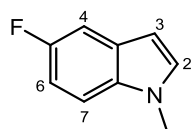
Product appearance: orange oil.

¹H NMR (400 MHz, CDCl₃) δ 7.75 (d, $^4J = 1.8$ Hz, 1H, H⁴), 7.30 (dd, $J = 8.7$, $^4J = 1.9$ Hz, 1H, H⁶), 7.18 (d, $J = 8.6$ Hz, 1H, H⁷), 7.05 (d, $J = 3.2$ Hz, 1H, H²), 6.42 (d, $J = 3.2$ Hz, 1H, H³), 3.77 (s, 3H, CH₃).

¹³C NMR (101 MHz, CDCl₃) δ 135.5, 130.3, 130.1, 124.5, 123.5, 112.9, 110.8, 100.7, 33.2.

IR (ATR, cm⁻¹) 2922, 1515, 1472, 1279.

1-Methyl-5-fluoroindole 167¹⁴³



Prepared according to General Procedure D.

Amount of 5-fluoroindole: 676 mg, 5 mmol.

Amount of sodium hydride: 300 mg, 7.5 mmol.

Amount of methyl iodide: 417 μ L, 6.7 mmol.

Product yield: 544 mg, 73%.

Product appearance: yellow oil.

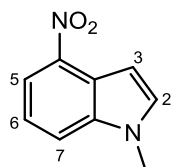
¹H NMR (400 MHz, CDCl₃) δ 7.28 (d, ⁴*J* = 2.5 Hz, 1H, H⁴), 7.25–7.20 (m, 1H, H⁷), 7.09 (d, *J* = 3.1 Hz, 1H, H²), 6.97 (td, *J* = 9.1, 2.5 Hz, 1H, H⁶), 6.44 (d, *J* = 3.1 Hz, 1H, H³), 3.79 (s, 3H, CH₃).

¹³C NMR (101 MHz, CDCl₃) δ 157.4 (d, ¹*J*_{CF} = 238 Hz), 132.8, 129.9, 128.2, 109.4 (d, ²*J*_{CF} = 22 Hz), 109.2 (d, ³*J*_{CF} = 9 Hz), 105.0 (d, ²*J*_{CF} = 24 Hz), 100.3 (d, ⁴*J*_{CF} = 4 Hz), 32.5.

¹⁹F NMR (376 MHz, CDCl₃) δ -125.9.

IR (ATR, cm⁻¹) 2926, 1493, 1426, 1240.

1-Methyl-4-nitroindole 168¹⁴⁴



Prepared according to General Procedure D.

Amount of 4-nitroindole: 811 mg, 5 mmol.

Amount of sodium hydride: 300 mg, 7.5 mmol.

Amount of methyl iodide: 417 μ L, 6.7 mmol.

Product yield: 651 mg, 74%.

Product appearance: yellow solid.

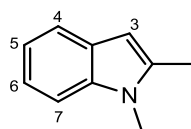
¹H NMR (400 MHz, CDCl₃) δ 7.64 (dd, *J* = 8.1, 0.7 Hz, 1H, H⁵), 7.31 (d, *J* = 3.2 Hz, 1H, H⁷), 7.29–7.25 (m, 1H, H²), 7.20 (dd, *J* = 3.0, ⁴*J* = 0.8 Hz, 1H, H⁶), 6.44–6.39 (m, 1H, H³), 3.88 (s, 3H, CH₃).

¹³C NMR (101 MHz, CDCl₃) δ 136.9, 129.0, 128.7, 121.8, 121.1, 119.5, 109.4, 101.1, 33.0.

IR (ATR, cm⁻¹) 2924, 1508, 1467, 1290.

M.P. (°C) 52–55 (lit. 54).

1,2-Dimethylindole 169¹⁴⁵



Prepared according to General Procedure D.

Amount of 2-methylindole: 655 mg, 5 mmol.

Amount of sodium hydride: 300 mg, 7.5 mmol.

Amount of methyl iodide: 417 μ L, 6.7 mmol.

Product yield: 646 mg, 89%.

Product appearance: orange-pink solid.

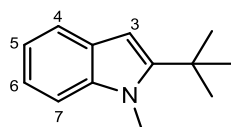
¹H NMR (400 MHz, CDCl₃) δ 7.53 (d, J = 8.3 Hz, 1H, H⁶), 7.27 (d, J = 7.3 Hz, 1H, H⁷), 7.16 (t, J = 7.7 Hz, 1H, H⁵), 7.07 (t, J = 7.3 Hz, 1H, H⁴), 6.26 (s, 1H, H³), 3.68 (s, 3H, N-CH₃), 2.44 (s, 3H, C²-CH₃).

¹³C NMR (101 MHz, CDCl₃) δ 137.5, 137.0, 128.1, 120.6, 119.8, 119.4, 108.9, 99.7, 29.6, 12.9.

IR (ATR, cm⁻¹) 2924, 1549, 1469, 1394.

M.P. (°C) 53–55 (lit. 54).

1-Methyl-2-tert-butylindole 170¹⁴⁶



Prepared according to General Procedure D.

Amount of 2-tert-butylindole: 866 mg, 5 mmol.

Amount of sodium hydride: 300 mg, 7.5 mmol.

Amount of methyl iodide: 417 μ L, 6.7 mmol.

Product yield: 505 mg, 54%.

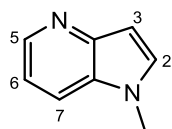
Product appearance: orange oil.

¹H NMR (400 MHz, CDCl₃) δ 7.59–7.53 (m, 1H, H⁶), 7.29–7.24 (m, 1H, H⁷), 7.19–7.13 (m, 1H, H⁵), 7.11–7.04 (m, 1H, H⁴), 6.31 (s, 1H, H³), 3.88 (s, 3H, N-CH₃), 1.48 (s, 9H, C(CH₃)₃).

¹³C NMR (101 MHz, CDCl₃) δ 121.3, 121.0, 120.4, 119.5, 118.8, 118.2, 106.7, 108.4, 98.2, 32.4, 31.9, 30.3, 29.8, 24.6.

IR (ATR, cm⁻¹) 2962, 1472, 1355, 1247.

1-Methyl-4-azaindole 171¹⁴⁷



Prepared according to General Procedure D.

Amount of 4-azaindole: 591 mg, 5 mmol.

Amount of sodium hydride: 300 mg, 7.5 mmol.

Amount of methyl iodide: 417 μ L, 6.7 mmol.

Product yield: 430 mg, 65%.

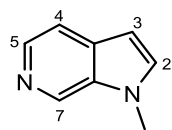
Product appearance: yellow oil.

¹H NMR (400 MHz, CDCl₃) δ 8.46 (d, J = 4.9 Hz, 1H, H⁵), 7.71–7.64 (m, 1H, H⁷), 7.56–7.51 (m, 1H, H⁶), 7.48–7.44 (m, 1H, H²), 6.68 (d, J = 3.2 Hz, 1H, H³), 3.83 (s, 3H, CH₃).

¹³C NMR (101 MHz, CDCl₃) δ 145.1, 142.9, 132.7, 129.0, 117.5, 115.4, 101.8, 33.2.

IR (ATR, cm⁻¹) 3101, 1513, 1415, 1294.

1-Methyl-6-azaindole 172¹⁴⁷



Prepared according to General Procedure D.

Amount of 6-azaindole: 591 mg, 5 mmol.

Amount of sodium hydride: 300 mg, 7.5 mmol.

Amount of methyl iodide: 417 μ L, 6.7 mmol.

Product yield: 428 mg, 64%.

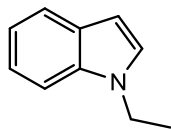
Product appearance: yellow oil.

¹H NMR (400 MHz, CDCl₃) δ 8.64 (s, 1H, H⁷), 8.23 (d, J = 4.9 Hz, 1H, H⁵), 7.46 (dd, J = 4.9, ⁴ J = 0.9 Hz, 1H, H⁴), 7.12 (dd, J = 3.1, ⁴ J = 1.0 Hz, 1H, H²), 6.58 (d, J = 3.2 Hz, 1H, H³), 3.83 (s, 3H, CH₃).

¹³C NMR (101 MHz, CDCl₃) δ 137.9, 133.9, 133.4, 132.7, 131.8, 115.7, 102.0, 33.2.

IR (ATR, cm⁻¹) 3105, 1515, 1410, 1293.

Scheme 1.62 – Substrates



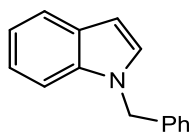
Deuteration of N-Ethylindole 165

Carried out according to General Procedure C

Catalyst **43** (1 mol%), 25 °C, 16 h.

Incorporation expected at δ 6.49.

Determined against integral at δ 4.17.



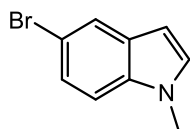
Deuteration of N-Benzylindole 164

Carried out according to General Procedure C

Catalyst **43** (1 mol%), 25 °C, 16 h.

Incorporation expected at δ 6.57.

Determined against integral at δ 5.32.



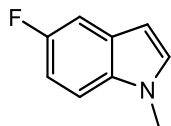
Deuteration of 1-Methyl-5-bromoindole 166

Carried out according to General Procedure C

Catalyst **43** (1 mol%), 25 °C, 16 h.

Incorporation expected at δ 6.42.

Determined against integral at δ 3.77.



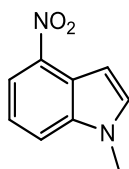
Deuteration of 1-Methyl-5-fluoroindole 167

Carried out according to General Procedure C

Catalyst **43** (1 mol%), 25 °C, 16 h.

Incorporation expected at δ 6.42.

Determined against integral at δ 3.79.



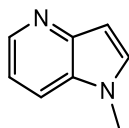
Deuteration of 1-Methyl-4-nitroindole 168

Carried out according to General Procedure C

Catalyst **43** (1 mol%), 25 °C, 16 h.

Incorporation expected at δ 6.44–6.39.

Determined against integral at δ 3.88.



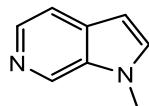
Deuteration of 1-Methyl-4-azaindole 171

Carried out according to General Procedure C

Catalyst **43** (1 mol%), 25 °C, 16 h.

Incorporation expected at δ 6.68.

Determined against integral at δ 3.83.



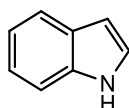
Deuteration of 1-Methyl-6-azaindole 172

Carried out according to General Procedure C

Catalyst **43** (1 mol%), 25 °C, 16 h.

Incorporation expected at δ 6.68.

Determined against integral at δ 3.83.



Deuteration of indole 75

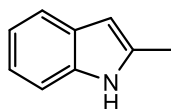
Carried out according to General Procedure C

Catalyst **43** (1 mol%), 25 °C, 16 h.

¹H NMR (400 MHz, CDCl₃) δ 8.21 (br s, 1H, NH), 7.70–7.66 (d, J = 7.5 Hz, 1H, H⁷), 7.45–7.41 (d, J = 7.5 Hz, 1H, H⁴), 7.28–7.20 (m, 2H, H⁶ and H²), 7.17–7.14 (m, 1H, H⁵), 6.60–6.57 (m, 1H, H³).

Incorporation expected at δ 6.60–6.57.

Determined against integral at δ 7.17–7.14.



Deuteration of 2-Methylindole 211

Carried out according to General Procedure C

Catalyst **43** (1 mol%), 25 °C, 16 h.

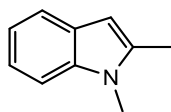
¹H NMR (400 MHz, CDCl₃) δ 7.80 (bs, 1H, NH), 7.55 (d, J = 7.9 Hz, 1H, H⁴), 7.28 (d, J = 7.9 Hz, 1H, H⁷), 7.17–7.07 (m, 2H, H⁶ & H⁵), 6.26–6.22 (m, 1H, H³), 2.44 (s, 3H, CH₃).

Incorporation expected at δ 6.26–6.22.

Determined against integral at δ 2.44.

Deuteration of 1,2-Dimethylindole 169

Carried out according to General Procedure C



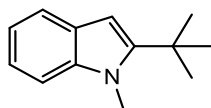
Catalyst **43** (1 mol%), 25 °C, 16 h.

Incorporation expected at δ 6.26.

Determined against integral at δ 2.44.

Deuteration of 1-Methyl-2-tert-butylindole 170

Carried out according to General Procedure C



Catalyst **43** (1 mol%), 25 °C, 16 h.

Incorporation expected at δ 6.31.

Determined against integral at δ 3.88.

Scheme 1.62 – Results

Entry	Substrate	Mass Substrate / mg	Mass Catalyst / mg	Deuterium Incorporation / %			
				Run 1	Run 2	Run 3	Average
1	165	31	2.18	88	89	84	87
2	164	45	2.18	60	55	58	58
3	166	45	2.18	98	97	92	96
4	167	32	2.18	95	95	96	95
5	168	38	2.18	99	99	99	99
6	171	28	2.18	90	97	88	92
7	172	28	2.18	87	91	92	90
8	75	25	2.18	22	27	29	26
9	211	28	2.18	95	94	92	94
10	169	31	2.18	95	99	96	97
11	170	40	2.18	81	85	86	84

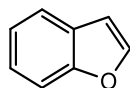
Scheme 1.63 – Substrates

Substrates **255** and **256** were obtained commercially and used as received.

Deuteration of Benzofuran 255

Carried out according to General Procedure C

Catalyst **43** (1 mol%), 25 °C, 16 h.



¹H NMR (400 MHz, CDCl₃) δ 7.66 (d, *J* = 2.1 Hz, 1H, H²), 7.63 (d, *J* = 7.8 Hz, 1H, H⁴), 7.54 (d, *J* = 7.9 Hz, 1H, H⁷), 7.30–7.23 (m, 2H, H⁵ & H⁶), 6.76 (dd, *J* = 2.1. 0.8 Hz, 1H, H³).

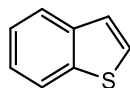
Incorporation expected at δ 6.76.

Determined against integral at δ 7.30–7.23.

Deuteration of Benzothiophene 256

Carried out according to General Procedure C

Catalyst **43** (1 mol%), 25 °C, 16 h.



¹H NMR (400 MHz, CDCl₃) δ 7.89 (d, *J* = 7.0 Hz, 1H, H⁷), 7.83 (dd, *J* = 6.5. 1.9 Hz, 1H, H⁴), 7.42 (d, *J* = 6.0 Hz, 1H, H²), 7.37–7.36 (m, 3H H², H⁵ & H⁶).

Incorporation expected at δ 7.37–7.36.

Determined against integral at δ 7.83.

Scheme 1.63 – Results

Entry	Substrate	Mass Substrate / mg	Mass Catalyst / mg	Deuterium Incorporation / %			
				Run 1	Run 2	Run 3	Average
1	255	25	2.18	82	87	83	84
2	256	29	2.18	75	76	77	76

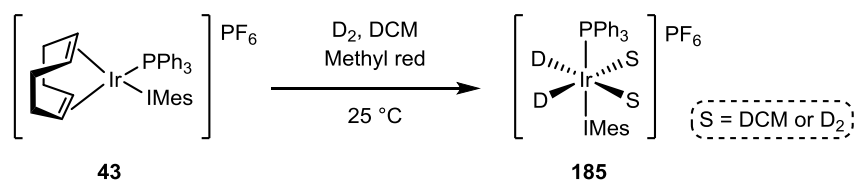
Scheme 1.64

Activation of 43 with Methyl Red Indicator

Control for Basic Conditions: Methyl red indicator (4 mg) was added to a solution of triethylamine (0.05 mL) in DCM (2 mL).

Control for Acidic Conditions: Methyl red indicator (4 mg) was added to a solution of acetic acid (0.05 mL) in DCM (2 mL).

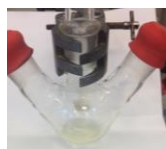
Catalyst Activation: A flame dried and Ar-cooled 3-necked round-bottom flask was fitted with two rubber seals and a stopcock. A solution of $[\text{Ir}(\text{cod})(\text{IMes})(\text{PPh}_3)]\text{PF}_6$ **43** (10 mg, 0.01 mmol) in DCM (2.5 mL) was prepared and added to the flask. The flask was cooled to -78°C in a dry ice/acetone bath, before being evacuated and refilled twice with deuterium gas from a balloon. The flask was left open to the D_2 balloon and allowed to warm to 25°C over 5 min, during which time a colour change from orange to pale yellow was observed. A solution of methyl red indicator (4 mg) in DCM (1 mL) was prepared and added to the flask *via* syringe, causing an immediate colour change to bright pink. The mixture was allowed to stir for 1 h, after which the vivid pink colour remained. As a control, the process was repeated in the absence of indicator and photographed at 5 min and 1 h.



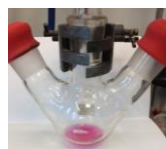
a) Control for basic conditions:
 NEt_3 in DCM



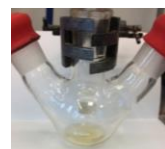
b) Control for acidic conditions:
AcOH in DCM



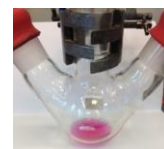
c) t = 5 mins
without methyl red



d) t = 5 mins
with methyl red



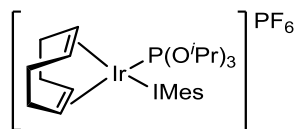
e) t = 1 h
without methyl red



f) t = 1 h
with methyl red

Scheme 1.68

(1,5-cyclooctadiene)(1,3-dimesitylimidazol-2-ylidene)(triisopropylphosphite)iridium(I) hexafluorophosphate 188



Prepared according to General Procedure B.

Amount of [Ir(cod)(IMes)Cl] **55**: 600 mg, 0.94 mmol.

Amount of THF: 15 mL.

Amount of AgPF₆: 238 mg, 0.94 mmol.

Amount of triisopropylphosphite: 196 mg, 0.94 mmol.

Product yield: 559 mg, 62%.

Product appearance: Red crystalline solid.

¹H NMR (400 MHz, CDCl₃) δ 7.21 (s, 2H, ArH), 7.03–6.98 (m, 4H, ArH, -NCH=CHN-), 4.55–4.44 (m, 5H, COD CH, isopropyl CH), 3.81–3.76 (m, 2H, COD CH), 2.35 (s, 6H, ArCH₃), 2.33 (s, 6H, ArCH₃), 2.02 (s, 6H, ArCH₃), 1.63–1.52 (m, 4H, COD CH₂), 1.40–1.30 (m, 4H, COD CH₂), 1.25–1.10 (d, *J* = 6.3 Hz, 18H, isopropyl CH₃).

¹³C NMR (101 MHz, CDCl₃) δ 176.5, 139.4, 135.5, 135.1, 135.0, 128.9, 128.8, 125.2, 85.1, 84.9, 75.6, 71.7, 30.8, 29.4, 23.0, 19.5, 18.9, 17.0, 13.5.

³¹P NMR (162 MHz, CDCl₃) δ 100.2 (P(O^{*i*}Pr)₃), -144.7 (PF₆).

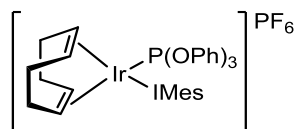
¹⁹F NMR (376 MHz, CDCl₃) δ -73.9 (PF₆).

IR (ATR, cm⁻¹) 3179, 2979, 2870, 1694, 1569, 1484, 1460.

HRMS (NSI, *m/z*): C₃₈H₅₇IrN₂O₃P [M - PF₆]⁺: expected 811.3736; observed 811.3732.

M.P. (°C) decomp. >170.

(1,5-cyclooctadiene)(1,3-dimesitylimidazol-2-ylidene)(triphenylphosphite)iridium(I) hexafluorophosphate 189



Prepared according to General Procedure B.

Amount of [Ir(cod)(IMes)Cl] **55**: 450 mg, 0.70 mmol.

Amount of THF: 20 mL.

Amount of AgPF₆: 181 mg, 0.70 mmol.

Amount of triphenylphosphite: 218 mg, 0.70 mmol.

Product yield: 611 mg, 82%.

Product appearance: Red crystalline solid.

¹H NMR (400 MHz, CDCl₃) δ 7.37 (2H, s, -NCH=CHN-), 7.23–7.12 (13H, m, ArH), 6.79–6.72 (6H, m, ArH), 4.94–4.84 (2H, m, COD CH), 3.74–3.67 (2H, m, COD CH), 2.49 (6H, s, ArCH₃), 2.40 (6H, s, ArCH₃), 2.23 (6H, s, ArCH₃), 1.46–1.04 (8H, m, COD CH₂).

¹³C NMR (101 MHz, CDCl₃) δ 200.3, 151.1, 150.9, 140.6, 136.2, 135.9, 135.1, 130.0, 129.9, 126.4, 125.8, 120.8, 120.7, 91.6, 91.4, 78.9, 31.3, 31.3, 30.6, 30.6, 21.4, 19.2, 18.7.

³¹P NMR (162 MHz, CDCl₃) δ 91.8 (P(OPh)₃, -144.4 (PF₆).

¹⁹F NMR (376 MHz, CDCl₃) δ -73.8 (d, *J*_{P-F} = 711 Hz, PF₆).

IR (ATR, cm⁻¹) 3138, 2978, 2359, 1609, 1585.

HRMS (NSI, *m/z*): C₄₇H₅₁¹⁹¹IrN₂O₃P [M - PF₆]⁺: expected 913.3238; observed 913.3230.

M.P. (°C) decomp. >190.

Table 1.12

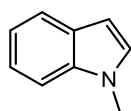
Deuteration of N-Methylindole 160

Carried out according to General Procedure C

5 mol% catalyst, 25 °C, 1 h.

Incorporation expected at δ 6.48.

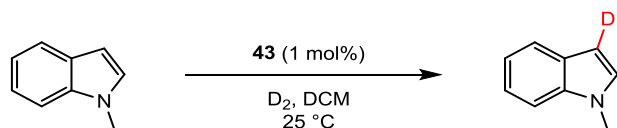
Determined against integral at δ 3.78.



Entry	Mass Substrate / mg	Catalyst	Mass Catalyst / mg	Deuterium Incorporation / %			
				Run 1	Run 2	Run 3	Average
1	28	188	2.06	23	20	23	22
2	28	189	2.28	14	16	12	14

Scheme 1.70

Forward Reaction – C3 Hydrogen Isotope Exchange of 1-Methylindole 160



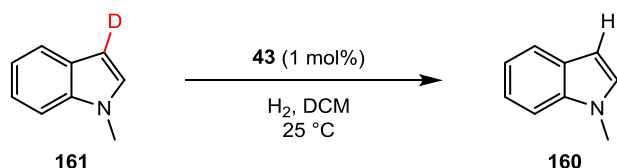
Carried out according to General Procedure E.

Incorporation expected at δ 6.48. Determined against integral at δ 3.78.

Entry	Time / min	% HIE	%HIE(t) – %HIE(t=3)	[SM] / M	Rate (t = 6 to t = 18) / M s ⁻¹
1	3	18	0	0.11808	-0.0000528
2	6	19	1	0.11664	
3	9	24	6	0.10944	
4	12	28	10	0.10368	
5	15	35	17	0.09360	
6	18	41	23	0.08496	

$$K(\text{H}) = -0.0000528 \text{ M s}^{-1}.$$

Reverse Reaction – C3 Hydrogen Isotope Exchange of 1-Methyl-3-deuterioindole 161



Carried out according to General Procedure E.

C₃-H signal expected at δ 6.48. Determined against integral at δ 3.78.

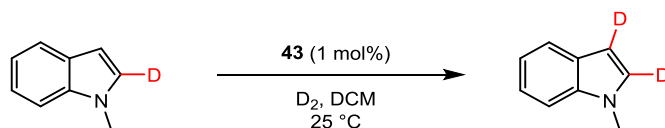
Entry	Time / min	% HIE	%HIE(t) – %HIE(t=3)	[SM] / M	Rate (t = 6 to t = 18) / M s ⁻¹
1	3	28	0	0.10368	-0.000084
2	6	34	6	0.09504	
3	9	50	22	0.07200	
4	12	55	27	0.06480	
5	15	60	32	0.05760	
6	18	63	35	0.05328	

$$K(\text{D}) = -0.000084 \text{ M s}^{-1}.$$

Kinetic Isotope Effect Calculation: $K(\text{H})/K(\text{D}) = (-0.0000528)/(-0.000084) = \mathbf{0.64}.$

Scheme 1.71

C3 Deuteration of 1-Methyl-2-deuteroindole 193



Carried out according to General Procedure E.

Incorporation expected at δ 6.48. Determined against integral at δ 3.78.

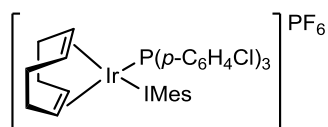
Entry	Time / min	% HIE	%HIE(t) – %HIE(t=3)	[SM] / M	Rate (t = 6 to t = 18) / M s ⁻¹
1	3	20	0	0.11520	-0.0000593
2	6	27	7	0.10512	
3	9	33	13	0.09648	
4	12	38	18	0.08928	
5	15	43	23	0.08208	
6	18	45	25	0.07920	

$$K(D) = -0.0000593 \text{ M s}^{-1}$$

Kinetic Isotope Effect Calculation: $K(H)/K(D) = (-0.0000528)/(-0.0000593) = \mathbf{0.89}$.

Table 1.13

(1,5-cyclooctadiene)(1,3-dimesitylimidazol-2-ylidene)(tri(4-chlorophenyl)phosphine) iridium(I) hexafluorophosphate 194



Prepared according to General Procedure B.

Amount of [Ir(cod)(IMes)Cl] **55**: 250 mg, 0.39 mmol.

Amount of THF: 15 mL.

Amount of AgPF₆: 99 mg, 0.39 mmol.

Amount of tri(4-chlorophenyl)phosphine: 143 mg, 0.39 mmol.

Product yield: 287 mg, 66%.

Product appearance: Orange solid.

¹H NMR (400 MHz, CDCl₃) δ 7.53 (s, 2H, -NCH=CHN-), 7.36–7.30 (m, 6H, ArH), 7.18–7.13 (m, 4H, ArH), 7.09–7.04 (m, 4H, ArH), 6.70 (s, 2H, ArH), 4.57–4.48 (m, 2H, COD)

CH), 3.29–3.26 (m, 2H, COD CH), 2.39 (s, 6H, ArCH₃), 2.10 (s, 6H, ArCH₃), 1.81 (s, 6H, ArCH₃), 1.66–1.58 (m, 6H, COD CH₂), 1.37–1.32 (m, 2H, COD CH₂).

¹³C NMR (101 MHz, CDCl₃) δ 140.2, 138.6, 136.1, 136.0, 135.8, 135.1, 130.5, 130.1, 129.4, 129.3, 127.6, 78.4, 78.2, 39.2, 36.9, 32.0, 30.4, 21.8, 21.1, 19.2 (N–C–N carbene signal not observed).

³¹P NMR (162 MHz, CDCl₃) δ 14.7 (PAr₃), –144.3 (septet, ¹J_{P-F} = 715 Hz, PF₆).

¹⁹F NMR (376 MHz, CDCl₃) δ 72.8 (d, J_{P-F} = 714 Hz, PF₆).

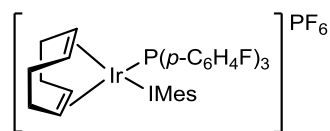
IR (ATR, cm⁻¹) 2922, 1577, 1483, 1388, 1083.

HRMS (NSI, m/z): C₂₉H₃₆¹⁹¹IrN₂ [M –PF₆ –PAr₃]⁺: expected 603.2507; observed 603.2505.

M.P. (°C) decomp. >160.

(1,5-cyclooctadiene)(1,3-dimesitylimidazol-2-ylidene)(tri(4-fluorophenyl)phosphine)

iridium(I) hexafluorophosphate **195**



Prepared according to General Procedure B.

Amount of [Ir(cod)(IMes)Cl] **55**: 250 mg, 0.39 mmol.

Amount of THF: 15 mL.

Amount of AgPF₆: 99 mg, 0.39 mmol.

Amount of tri(4-fluorophenyl)phosphine: 123 mg, 0.39 mmol.

Product yield: 224 mg, 54%.

Product appearance: Orange-red solid.

¹H NMR (400 MHz, CDCl₃) δ 7.52 (s, 2H, –NCH=CHN–), 7.20–7.00 (m, 14H, ArH), 6.67 (s, 2H, ArH), 4.51–4.47 (m, 2H, COD CH), 3.26–3.20 (m, 2H, COD CH), 2.36 (s, 6H, ArCH₃), 2.09 (s, 6H, ArCH₃), 1.79 (s, 6H, ArCH₃), 1.63–1.55 (m, 6H, COD CH₂), 1.36–1.24 (m, 2H, COD CH₂).

¹³C NMR (101 MHz, CDCl₃) δ 177.0, 161.2 (d, ¹J_{C-F} = 258 Hz), 138.9, 135.8, 135.7, 135.3, 135.0, 134.9, 129.8, 129.0, 126.5, 121.9, 121.3, 113.6, 113.4, 79.2, 79.0, 59.9, 55.0, 31.2, 29.6, 20.9, 20.3, 18.3, 13.7.

³¹P NMR (162 MHz, CDCl₃) δ 13.9 (PAr₃), –144.4 (septet, ¹J_{P-F} = 714 Hz, PF₆).

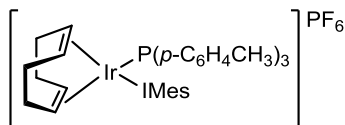
¹⁹F NMR (376 MHz, CDCl₃) δ –163.5 (d, ¹J_{F-C} = 257 Hz, P(ArF)₃) –73.3 (d, ¹J_{F-P} = 715 Hz, PF₆).

IR (ATR, cm⁻¹) 2922, 1591, 1496, 1232, 1165.

HRMS (NSI, m/z): $C_{39}H_{34}F_3^{191}IrN_2P$ [$M - PF_6 - COD$] $^+$: expected 807.2040; observed 807.2046.

M.P. (°C) decomp. >160.

(1,5-cyclooctadiene)(1,3-dimesitylimidazol-2-ylidene)(tri(4-methylphenyl)phosphine) iridium(I) hexafluorophosphate 196



Prepared according to General Procedure B.

Amount of [Ir(cod)(IMes)Cl] **55**: 250 mg, 0.39 mmol.

Amount of THF: 15 mL.

Amount of AgPF₆: 99 mg, 0.39 mmol.

Amount of tri(4-methylphenyl)phosphine: 118 mg, 0.39 mmol.

Product yield: 222 mg, 58%.

Product appearance: Orange solid.

¹H NMR (400 MHz, CDCl₃) δ 7.49 (s, 2H, -NCH=CHN-), 7.13–7.08 (m, 6H, ArH), 7.06–7.01 (m, 8H, ArH), 6.64 (s, 2H, ArH), 4.40–4.34 (m, 2H, COD CH), 3.36–3.30 (m, 2H, COD CH), 2.41 (s, 6H, ArCH₃), 2.37 (d, $J = 6.3$ Hz, 9H, P(ArCH₃)₃), 2.12 (s, 6H, ArCH₃), 1.80 (s, 6H, ArCH₃), 1.59–1.48 (m, 6H, COD CH₂), 1.31–1.26 (m, 2H, COD CH₂).

¹³C NMR (101 MHz, CDCl₃) δ 175.6, 141.8, 140.8, 139.7, 136.0, 135.9, 135.6, 135.0, 134.9, 133.7, 133.5, 130.4, 130.0, 129.9, 129.8, 129.5, 129.4, 129.0, 80.0, 79.9, 32.0, 30.4, 29.6, 21.6, 21.1, 19.2.

³¹P NMR (162 MHz, CDCl₃) δ 14.2 (PAr₃), -144.6 (septet, $^1J_{P-F} = 712$ Hz, PF₆).

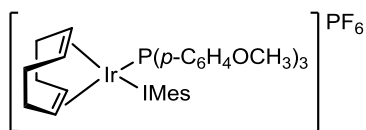
¹⁹F NMR (376 MHz, CDCl₃) δ -73.8 (d, $J_{P-F} = 709$ Hz, PF₆).

IR (ATR, cm⁻¹) 2921, 1483, 1388, 1307, 1091.

HRMS (NSI, m/z): $C_{42}H_{45}^{191}IrN_2P$ [$M - PF_6 - COD$] $^+$: expected 799.2949; observed 799.2957.

M.P. (°C) decomp. >180.

(1,5-cyclooctadiene)(1,3-dimesitylimidazol-2-ylidene)(tri(4-methoxyphenyl)phosphine) iridium(I) hexafluorophosphate 197



Prepared according to General Procedure C.

Amount of [Ir(cod)(IMes)Cl] **55**: 250 mg, 0.39 mmol.

Amount of THF: 15 mL.

Amount of AgPF₆: 99 mg, 0.39 mmol.

Amount of tri(4-methoxyphenyl)phosphine: 137 mg, 0.39 mmol.

Product yield: 266 mg, 62%.

Product appearance: Orange solid.

¹H NMR (400 MHz, CDCl₃) δ 7.50 (m, 2H, -NCH=CHN-), 7.12–7.06 (m, 6H, ArH), 7.05–6.97 (m, 8H, ArH), 6.66 (s, 2H, ArH), 4.51–4.45 (m, 2H, COD CH), 4.15 (s, 9H, P(ArOCH₃)₃), 3.26–3.20 (m, 2H, COD CH), 2.35 (s, 6H, ArCH₃), 2.07 (s, 6H, ArCH₃), 1.78 (s, 6H, ArCH₃), 1.62–1.54 (m, 6H, COD CH₂), 1.36–1.29 (m, 2H, COD CH₂).

¹³C NMR (101 MHz, CDCl₃) δ 139.4, 136.4, 136.2, 135.2, 135.1, 134.4, 129.8, 129.3, 126.7, 115.8, 115.7, 115.6, 115.5, 81.2, 77.3, 33.0, 31.3, 29.6, 28.4, 20.9, 20.6, 20.2, 18.3 (N–C–N carbene signal not observed).

³¹P NMR (162 MHz, CDCl₃) δ 12.5 (PAr₃), –144.1 (septet, ¹J_{P-F} = 711 Hz, PF₆).

¹⁹F NMR (376 MHz, CDCl₃) δ –73.5 (d, ¹J_{F-P} = 711 Hz, PF₆).

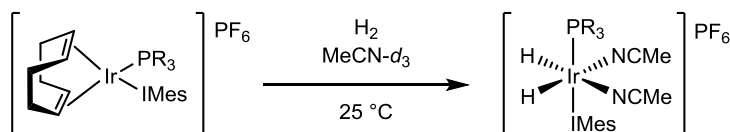
IR (ATR, cm⁻¹) 2924, 1735, 1595, 1502, 1256, 1180.

HRMS (NSI, m/z): C₅₀H₅₇¹⁹¹IrN₂O₃P [M – PF₆]⁺: expected 957.3736; observed 957.3742.

M.P. (°C) decomp. >190.

Table 1.14

Catalyst Activation and Observation of Iridium(III) Hydride Intermediates



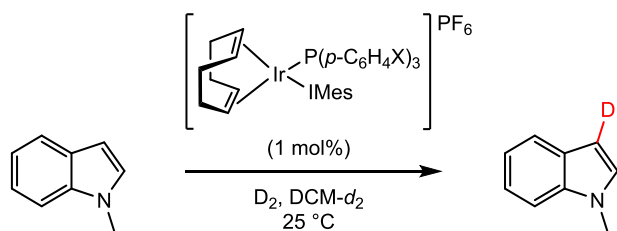
Carried out according to General Procedure F.

While full analysis of ^1H and ^{13}C NMR data is not provided for each derivative studied, a clear loss of the COD olefinic proton signals was observed in all cases. For ease of comparison, ^1H NMR hydride signals are tabulated alongside the major ^{31}P NMR triplet shift. For the sake of clarity, signals from counterions have been omitted.

Entry	Catalyst	PR ₃	PR ₃ TEP / cm ⁻¹	δH / ppm	δP / ppm	³ J _{P-H} / Hz
1	43	PPh ₃	2069	-21.56	18.6 (t)	16.1
2	194	P(<i>p</i> -C ₆ H ₄ Cl) ₃	2073	-21.33	18.8 (t)	16.0
3	195	P(<i>p</i> -C ₆ H ₄ F) ₃	2070	-21.48	18.7 (t)	16.1
4	196	P(<i>p</i> -C ₆ H ₄ CH ₃) ₃	2067	-21.61	18.1 (t)	16.1
5	197	P(<i>p</i> -C ₆ H ₄ OCH ₃) ₃	2066	-21.65	17.7 (t)	16.0

Graph 1.2

C3 Deuteration of 1-Methylindole 160 – Hammett Studies



Carried out according to General Procedure E.

Incorporation expected at δ 6.48. Determined against integral at δ 3.78.

Entry	Catalyst	X	Mass Catalyst / mg	X σ value	Rate / M ⁻¹ s ⁻¹	$\frac{K_X}{K_H}$	$\log \frac{K_X}{K_H}$
1	43	H	1.09	0.00	8.000×10^{-6}	1.000	0.000
2	194	Cl	1.20	0.23	-9.600×10^{-6}	1.200	0.079
3	195	F	1.15	0.06	-1.064×10^{-6}	0.133	0.014
4	196	CH ₃	1.14	-0.17	-5.840×10^{-6}	0.730	-0.135
5	197	OCH ₃	1.19	-0.27	-4.800×10^{-6}	0.600	-0.222

The calculated values for $\log(K_X/K_H)$ were plotted against Hammett σ -values to give the Graph 1.2. Rearranging the Hammett equation as follows shows that the slope of the graph gives Hammett ρ value:

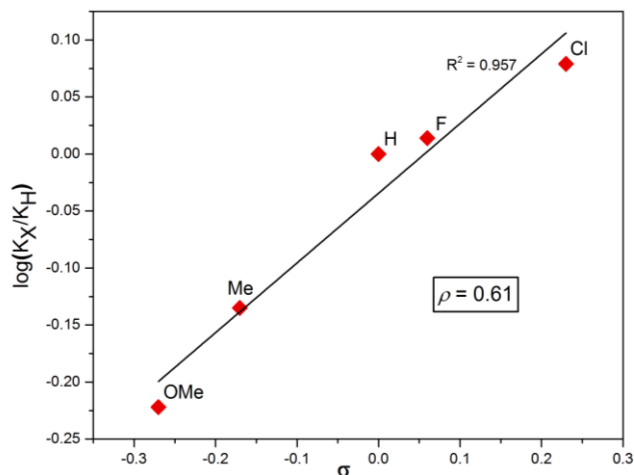
$$\log \frac{K_X}{K_H} = \sigma \cdot \rho$$

$$\log K_X = \rho \cdot \sigma + \log K_H$$

The graph parameters are as follows and show that $\rho = 0.61$:

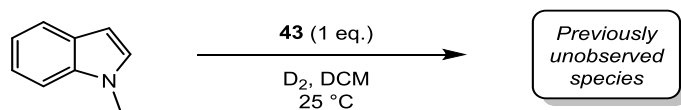
$$y = 0.6108x - 0.0344$$

$$R^2 = 0.9571$$



Scheme 1.72

Stoichiometric Reaction of *N*-Methylindole 160 with catalyst 43



An NMR tube was charged with a solution of *N*-methylindole (7.1 mg, 0.054 mmol) and catalyst **43** (1 eq., 54.6 mg, 0.054 mmol) in DCM-*d*₂ (0.75 mL), before being sealed with a rubber septum and cooled to 0 °C. A ¹H NMR spectrum was taken before activation of the reaction mixture. The tube was then fitted with a D₂ balloon and an exit needle. D₂ gas was bubbled through the mixture for 3 min at 0 °C, during which a colour change from orange to pale yellow was observed. The tube was sealed under 1 atm of D₂ and immediately placed in a Bruker DPX 400 spectrometer with the sample temperature set to 298 K. Spectra were taken 5, 10, 20, 30, 40, 50, 60, 80 and 100 minutes after activation. At *t* = 5 and *t* = 100 minutes, the hydride region was also analysed but no signals were observed.

Figure 1.30 shows a comparison of the spectra taken before activation, at *t* = 10 min, and at *t* = 80 min. Activation of the catalyst can be confirmed by the complete loss of COD signals at $\delta = 4.41\text{--}4.33$ and $3.33\text{--}3.26$ ppm. At $\delta = 3.30\text{--}1.02$ ppm, the appearance of several new alkyl signals can be observed, which we believe could be attributed to a saturated indoline intermediate. Figure 1.31 shows an expansion of the alkyl region.

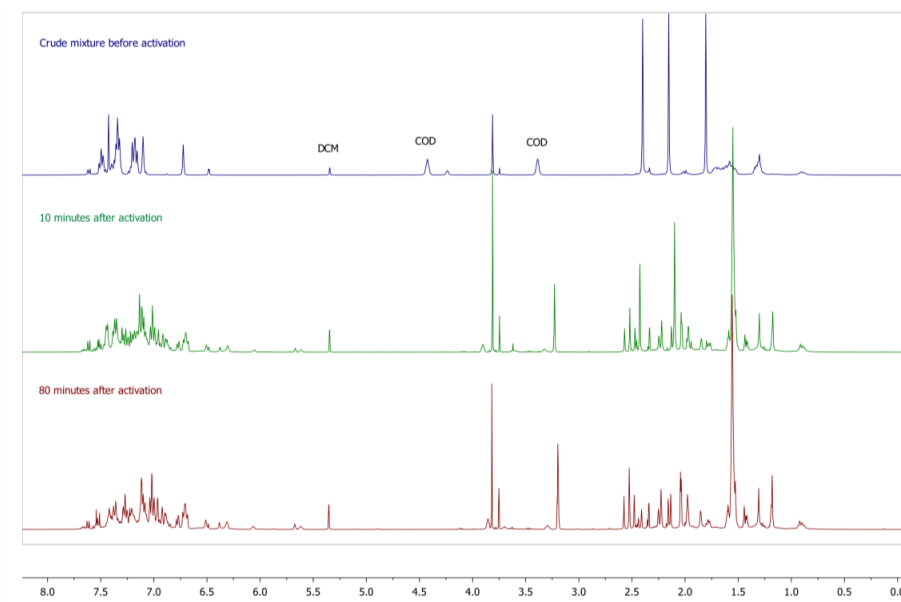


Figure 1.30

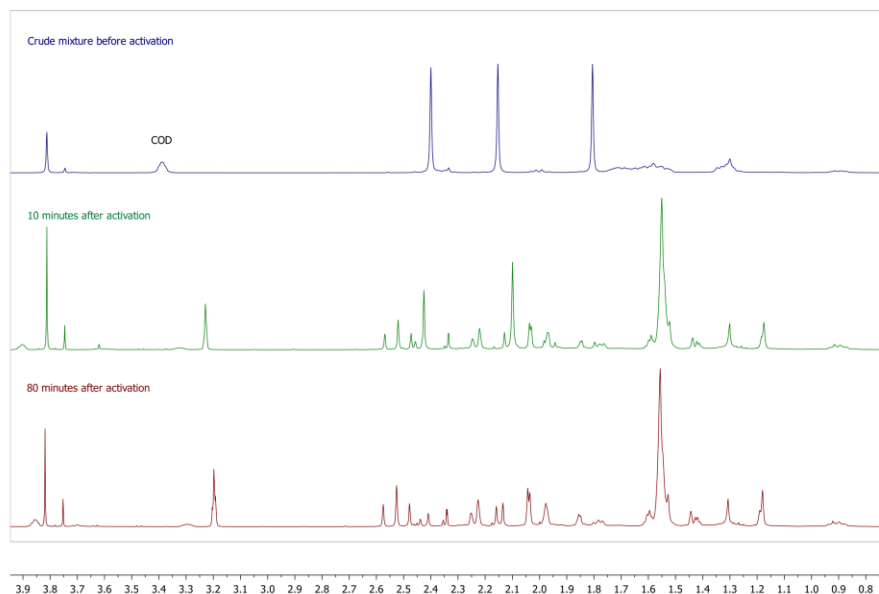
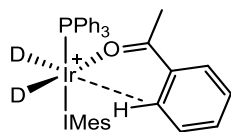


Figure 1.31

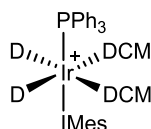
Figure 1.24

Formation of activated Ir^{III} complex **52**



An NMR tube was charged with a solution of acetophenone (6.5 mg, 0.054 mmol) and **43** (54.6 mg, 0.054 mmol) in DCM-*d*₂ (0.75 mL), before being sealed with a rubber septum and cooled to 0 °C. The tube was fitted with a D₂ balloon and an exit needle. D₂ gas was bubbled through the mixture for 3 min at 0 °C, during which a colour change from orange to pale yellow was observed. The tube was sealed under 1 atm of D₂ and immediately placed in a Bruker DPX 400 spectrometer with the sample temperature set to 298 K.

Formation of activated Ir^{III} complex **200**



Carried out as per the formation of **52**, but in the absence of acetophenone.

Formation of unknown intermediate **199** was carried out as described for Scheme 1.72.

DOSY NMR experiments were performed with ¹H NMR in CD₂Cl₂ at 300 K, according to reported procedures.¹⁴⁸

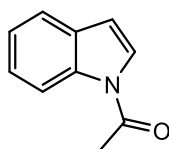
The raw values for relative diffusion rates are detailed below.

Entry	Compound	Molecular Weight	D ($\times 10^{-9} \text{ m}^2 \text{ s}^{-1}$)
1	160	131	2.614
2	43	867	0.894
3	200	936	1.216
4	52	883	1.031
5	199*	unknown	1.029

*N.B. The peak at $\delta = 3.20$ ppm (shown above in Figure 1.31) was used as the reference signal.

N-Oxide-directed Labelling of N-Heterocycles

Scheme 1.77



Deuteration of N-acetylindole **117**

Carried out according to General Procedure C

Catalyst **43** (5 mol%), 25 °C, 72 h.

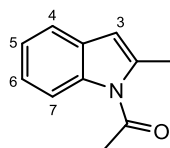
Incorporation expected at δ 7.44 (C2) and 8.47 (C7).

Determined against integral at δ 2.66.

Entry	Mass Substrate / mg	Mass Catalyst / mg	Time / h	Solvent Volume / mL	Deuterium Incorporation / %			
						Run 1	Run 2	Average
1	204	61	72	15	C2	99	99	99
					C7	22	21	22

Scheme 1.78

N-Acetyl-2-Methylindole **212**¹⁴⁹



To a suspension of 2-methylindole (1.31 g, 10 mmol) in DCM (20 mL) was added tetra-*n*-butylammonium hydrogensulfate (34 mg, 0.1 mmol, 0.01 eq.) and sodium hydroxide (1.0 g, 25 mmol, 2.5 eq.). Acetyl chloride (1.1 mL, 15 mmol, 1.5 eq.) was added dropwise at room

temperature. The resulting reaction mixture was stirred for 16 h at room temperature, after which it was quenched with saturated ammonium chloride solution (20 mL). The mixture was extracted with DCM (3 × 30 mL), dried over sodium sulfate and concentrated *in vacuo*. The crude residue was purified by flash column chromatography (10% ethyl acetate in petrol) to afford **212** as a white solid (1.541 g, 89% yield).

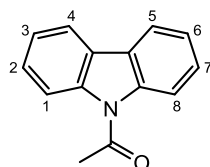
¹H NMR (400 MHz, CDCl₃) δ 7.98 (d, *J* = 7.8 Hz, 1H, H⁷), 7.45–7.36 (m, 1H, H⁴), 7.31–7.19 (m, 2H, H⁵ & H⁶), 6.37 (s, 1H, H³), 2.69 (s, 3H, CH₃), 2.64 (s, 3H, CH₃).

¹³C NMR (101 MHz, CDCl₃) δ 170.5, 137.4, 136.6, 129.9, 123.5, 123.2, 119.9, 115.4, 109.9, 27.4, 17.7.

IR (ATR) 2921, 1483, 1388, 1307, 1091.

MP (°C) 200–202 (lit. 201–202)¹⁵⁰

N*-Acetylcarbazole **214*¹⁵¹



Following a literature procedure,¹⁵² acetic anhydride (1.7 mL, 18 mmol, 1.8 eq.) was added to a solution of carbazole (1.673 g, 10 mmol) in chloroform (20 mL). 3 drops of concentrated sulfuric acid were added and the reaction mixture was heated at 60 °C for 6 h. The mixture was concentrated *in vacuo*, after which water was added (15 mL). The product was extracted into diethyl ether (3 × 20 mL) before being washed with saturated sodium bicarbonate solution, water, and brine. The organic layer was dried over sodium sulfate and concentrated *in vacuo*. Flash column chromatography (5% ethyl acetate in petrol) afforded **214** as an off-white solid (1.799 g, 86% yield).

¹H NMR (400 MHz, CDCl₃) δ 8.23 (d, *J* = 7.9 Hz, 2H, H⁴ & H⁵), 7.99–8.03 (d, *J* = 8.0 Hz, 2H, H¹ & H⁸), 7.50–7.46 (m, 2H, H² & H⁷), 7.42–7.38 (m, 2H, H³ & H⁶), 2.88 (s, CH₃).

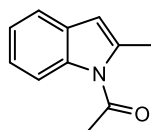
¹³C NMR (101 MHz, CDCl₃) δ 170.0, 138.6, 127.3, 126.4, 123.7, 119.8, 116.2, 27.7.

IR (ATR) 3049, 2918, 1678, 1446, 1368.

MP (°C) 76–78 (lit. 77.5–78.5)¹⁵³

Table 1.15 – Substrates

N-Acetyl-2-Methylindole **212**



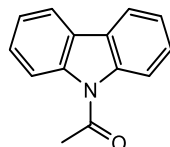
Carried out according to General Procedure C

Catalyst **43** (5 mol%).

Incorporation expected at δ 7.98.

Determined against integral at δ 2.69.

Deuteration of *N*-Acetylcarbazole **214**



Carried out according to General Procedure C

Catalyst **43** (5 mol%).

Incorporation expected at δ 7.99–8.03.

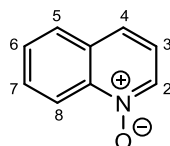
Determined against integral at δ 2.88.

Table 1.15 – Results

Entry	Substrate	Mass Substrate / mg	Mass Catalyst / mg	Conditions	Deuterium Incorporation / %			
					1	2	3	Average
1	212	37	10.1	25 °C, 1 h	0	0	0	0
2	212	37	10.1	25 °C, 72 h	21	23	24	23
3	212	37	10.1	40 °C, 72 h	20	23	23	22
4	214	45	10.1	25 °C, 1 h	0	0	0	0
5	214	45	10.1	25 °C, 72 h	0	0	0	0
6	214	45	10.1	40 °C, 72 h	0	0	0	0

Scheme 1.79

Quinoline *N*-Oxide **215**¹⁵⁴



Prepared according to General Procedure G.

Amount of quinoline: 387 mg, 3 mmol.

Product yield: 431 mg, 99%.

Product appearance: off-white solid.

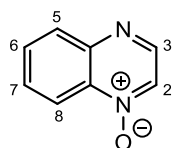
¹H NMR (400 MHz, CDCl₃) δ 8.78 (dd, *J* = 8.9, ⁴*J* = 1.2 Hz, 1H, H⁸), 8.66 (dd, *J* = 6.0, ⁴*J* = 1.0 Hz, 1H, H²), 7.89 (dd, *J* = 8.2, ⁴*J* = 1.2 Hz, 1H, H⁵), 7.84–7.76 (m, 2H, H⁴ & H⁷), 7.67 (ddd, *J* = 8.2, 6.9, ⁴*J* = 1.2 Hz, 1H, H⁶), 7.34 (dd, *J* = 8.5, 6.0 Hz, 1H, H³).

¹³C NMR (100 MHz, CDCl₃) δ 140.4, 135.4, 130.2, 130.1, 128.5, 128.0, 125.6, 120.7, 119.6.

IR (ATR, cm⁻¹) 2991, 1556, 1453, 1310, 1150.

MP (°C) 59–63 (lit. 60–62).¹⁵⁵

Quinoxaline *N*-Oxide 216¹⁵⁴



Prepared according to General Procedure G.

Amount of quinoxaline: 390 mg, 3 mmol.

Product yield: 435 mg, 99%.

Product appearance: red solid.

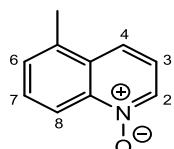
¹H NMR (400 MHz, CDCl₃) δ 8.70 (d, 1H, H²), 8.61 (d, *J* = 8.8 Hz, 1H, H³), 8.40 (d, *J* = 3.5 Hz, 1H, H⁸), 8.19 (d, *J* = 8.8 Hz, 1H, H⁵), 7.90–7.84 (m, 1H, H⁷), 7.83–7.75 (m, 1H, H⁶).

¹³C NMR (100 MHz, CDCl₃) δ 145.9, 145.8, 132.1, 130.7, 130.3, 129.5, 119.2.

IR (ATR, cm⁻¹) 2989, 1567, 1458, 1308, 1160.

MP (°C) 150–153 (lit. 152–155).¹⁵⁶

5-Methylquinoxaline *N*-Oxide 217¹⁵⁷



Prepared according to General Procedure G.

Amount of 5-methylquinoxaline: 430 mg, 3 mmol.

Product yield: 438 mg, 92%.

Product appearance: yellow solid.

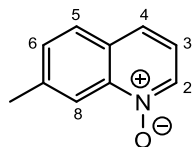
¹H NMR (400 MHz, CDCl₃) δ 8.74 (dd, *J* = 8.8, ⁴*J* = 1.1 Hz, 1H, H⁸), 8.60 (dd, *J* = 6.0, ⁴*J* = 1.0 Hz, 1H, H²), 8.04 (dd, *J* = 8.2, ⁴*J* = 1.0 Hz, 1H, H⁴), 7.91–7.88 (m, 1H, H⁷), 7.60 (dd, *J* = 8.8, 7.4 Hz, 1H, H⁶), 7.38 (dd, *J* = 8.8, 6.0 Hz, 1H, H³), 2.71 (s, 3H).

^{13}C NMR (100 MHz, CDCl_3) δ 141.8, 135.4, 135.3, 130.3, 130.2, 129.4, 123.1, 118.0, 19.3.

IR (ATR, cm^{-1}) 2984, 1560, 1452, 1309, 1148.

MP ($^{\circ}\text{C}$) 86–89.

7-Methylquinoline *N*-Oxide 218¹⁵⁷



Prepared according to General Procedure G.

Amount of 7-methylquinoline: 430 mg, 3 mmol.

Product yield: 424 mg, 89%.

Product appearance: yellow solid.

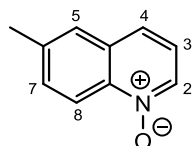
^1H NMR (400 MHz, CDCl_3) δ 8.56 (s, 1H, H^8), 8.52 (d, $J = 6.0$ Hz, 1H, H^2), 7.76–7.72 (m, 2H, H^4 & H^5), 7.49 (d, $J = 8.2$ Hz, 1H, H^6), 7.23 (dd, $J = 8.3, 6.0$ Hz, 1H, H^3), 2.61 (s, 3H).

^{13}C NMR (100 MHz, CDCl_3) δ 142.2, 141.4, 136.2, 135.6, 131.2, 128.8, 127.0, 120.1, 118.8, 22.3.

IR (ATR, cm^{-1}) 2983, 1560, 1452, 1311, 1153.

MP ($^{\circ}\text{C}$) 68–70.

6-Methylquinoline *N*-Oxide 219¹⁵⁸



Prepared according to General Procedure G.

Amount of 6-methylquinoline: 430 mg, 3 mmol.

Product yield: 419 mg, 88%.

Product appearance: off-white solid.

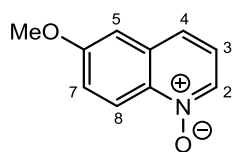
^1H NMR (400 MHz, CDCl_3) δ 8.71–8.64 (m, 1H, H^8), 8.48 (dd, $J = 6.0$ Hz, 1H, H^2), 7.67–7.56 (m, 3H, H^4 , H^5 & H^7), 7.24–7.27 (m, 1H, H^3), 2.54 (s, 3H).

^{13}C NMR (100 MHz, CDCl_3) δ 142.4, 141.7, 135.7, 135.3, 130.1, 130.0, 129.1, 122.2, 118.4, 20.1.

IR (ATR, cm^{-1}) 2984, 1556, 1451, 1308, 1148.

MP ($^{\circ}\text{C}$) 75–77 (lit. 76–78).¹⁵⁸

6-Methoxyquinoline *N*-Oxide 220¹⁵⁹



Prepared according to General Procedure G.

Amount of 6-methoxyquinoline: 477 mg, 3 mmol.

Product yield: 473 mg, 90%.

Product appearance: light yellow solid.

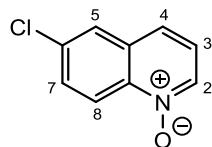
¹H NMR (400 MHz, CDCl₃) δ 8.67 (d, *J* = 9.3 Hz, 1H, H⁸), 8.41 (d, *J* = 6.1 Hz, 1H, H²), 7.64 (d, ⁴*J* = 2.3 Hz, 1H, H⁵), 7.43–7.36 (m, 1H, H⁴), 7.27–7.24 (m, 1H, H⁷), 7.09 (dd, *J* = 8.1, 6.1 Hz, 1H, H³), 3.97 (s, 3H).

¹³C NMR (100 MHz, CDCl₃) δ 159.5, 136.8, 134.1, 131.8, 125.4, 123.0, 121.4, 121.3, 106.2, 55.8.

IR (ATR, cm⁻¹) 2995, 2814, 1564, 1314, 1222.

MP (°C) 84–86 (lit. 80–82).¹⁶⁰

6-Chloroquinoline *N*-Oxide 221¹⁶¹



Prepared according to General Procedure G.

Amount of 6-chloroquinoline: 491 mg, 3 mmol.

Product yield: 474 mg, 84%.

Product appearance: off-white solid.

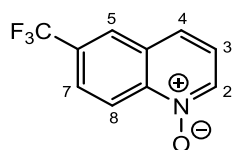
¹H NMR (400 MHz, CDCl₃) δ 8.70 (d, *J* = 9.2 Hz, 1H, H⁸), 8.50 (d, *J* = 6.1 Hz, 1H, H²), 7.87 (d, ⁴*J* = 2.2 Hz, 1H, H⁵), 7.69 (dd, *J* = 9.2, ⁴*J* = 2.2 Hz, 1H, H⁷), 7.65 (d, *J* = 8.6 Hz, 1H, H⁴), 7.33 (dd, *J* = 8.6, 6.1 Hz, 1H, H³).

¹³C NMR (100 MHz, CDCl₃) δ 140.5, 135.9, 135.1, 131.6, 131.3, 127.0, 124.9, 122.6, 122.1.

IR (ATR, cm⁻¹) 2341, 1562, 1440, 1301, 1175.

MP (°C) 105–108 (lit. 108).¹⁶¹

6-Trifluoromethylquinoline *N*-Oxide 222¹⁶²



Prepared according to General Procedure G.

Amount of 6-trifluoromethylquinoline: 591 mg, 3 mmol.

Product yield: 633 mg, 99%.

Product appearance: pale yellow solid.

¹H NMR (400 MHz, CDCl₃) δ 8.74 (d, *J* = 9.0 Hz, 1H, H⁸), 8.20–8.02 (m, 2H, H² & H⁵), 7.74 (dd, *J* = 8.2, ⁴*J* = 1.4 Hz, 1H, H⁴), 7.64 (dd, *J* = 9.0, ⁴*J* = 1.6 Hz, 1H, H⁷), 7.48–7.43 (m, 1H, H³).

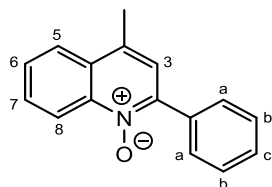
¹³C NMR (100 MHz, CDCl₃) δ 147.1, 135.7, 135.0 (q, ²*J*_{C-F} = 32 Hz), 130.9, 130.8, 124.7 (q, ³*J*_{C-F} = 4.1 Hz), 123.8 (q, ¹*J*_{C-F} = 268 Hz), 123.5, 123.4, 123.2 (q, ³*J*_{C-F} = 3.9 Hz).

¹⁹F NMR (376 MHz, CDCl₃) δ -63.0.

IR (ATR, cm⁻¹) 2924, 1467, 1331, 1294, 1160.

MP (°C) 79–82.

2-Phenyl-4-methylquinoline *N*-Oxide 223¹⁶³



Prepared according to General Procedure G.

Amount of 2-phenyl-4-methylquinoline: 657 mg, 3 mmol.

Product yield: 529 mg, 75%.

Product appearance: white solid.

¹H NMR (400 MHz, CDCl₃) δ 8.44 (dd, *J* = 8.2, ⁴*J* = 1.2 Hz, 1H, H⁸), 7.97 (dd, *J* = 8.0, ⁴*J* = 1.5 Hz, 2H, H^a), 7.68–7.64 (m, 2H, H^b), 7.61 (dd, *J* = 8.2, 7.9 Hz, 1H, H⁷), 7.52–7.47 (m, 1H, H^c), 7.41–7.36 (m, 2H, H⁶ & H³), 2.64 (s, 3H).

¹³C NMR (100 MHz, CDCl₃) δ 148.9, 141.7, 138.6, 136.0, 132.1, 130.4, 128.9, 128.7, 127.6, 126.8, 124.7, 118.9, 20.0.

IR (ATR, cm⁻¹) 2928, 1470, 1260, 1156.

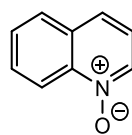
MP (°C) 116–120 (lit. 121).¹⁶³

Table 1.16

Deuteration of quinoline N-oxide **215**

Carried out according to General Procedure C

5 mol% catalyst, 25 °C, 1 h.

Incorporation expected at δ 8.78 (C8), and 8.66 (C2).Determined against integral at δ 7.67.

Entry	Mass Substrate / mg	Catalyst	Mass Catalyst / mg	Deuterium Incorporation / %				
					Run 1	Run 2	Run 3	Average
1	31	43	10.1	C8	82	78	80	80
				C2	0	0	0	0
2	31	45	8.9	C8	85	85	84	85
				C2	13	10	16	13
3	31	44	10.5	C8	85	89	83	86
				C2	9	8	9	9
4	31	64	17.3	C8	85	84	81	83
				C2	4	2	4	3
5	31	225	16.1	C8	85	86	82	84
				C2	4	7	4	5
6	31	226	17.7	C8	86	81	83	83
				C2	8	9	5	7
7	31	227	9.5	C8	12	9	10	10
				C2	18	20	15	18
8	31	55	6.4	C8	46	46	44	45
				C2	0	0	0	0

Scheme 1.80 – Reaction Optimisation with Design of Experiments

The effects of catalyst loading, reaction time and solvent volume were assessed using Design of Experiments (DOE).^{95,96} As described above, Design-Expert™ software v9.0.3 was used to

generate a set of 11 experiments as part of a 2-level, 3-factorial design. This design gave a total of 11 experiments (Table 1.19), with entries 2, 5, and 10 representing the centre points. Reactions were run according to *General Procedure C* with deuterium incorporation (%) in quinoline *N*-oxide **215** used as the response.

Table 1.19

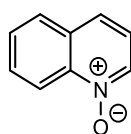
*Deuteration of quinoline *N*-oxide 215*

Carried out according to General Procedure C

Catalyst **43**, 25 °C.

Incorporation expected at δ 8.78 (C8), and 8.66 (C2).

Determined against integral at δ 7.67.

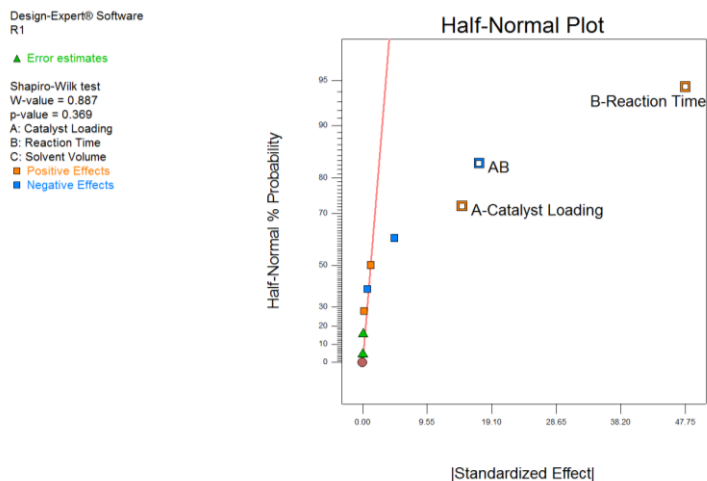


Run*	Factor A: Catalyst Loading / mol%	Factor B: Reaction Time / h	Factor C: Solvent Volume / mL	Response: % D Incorporation
1 (+ - -)	5	1	1	58
2 (0 0 0) [‡]	2.625	8.5	3	64
3 (- + -)	0.25	16	1	90
4 (- + +)	0.25	16	5	87
5 (0 0 0) [‡]	2.625	8.5	3	64
6 (- - -)	0.25	1	1	27
7 (+ + -)	5	16	1	88
8 (- - +)	0.25	1	5	20
9 (+ - +)	5	1	5	53
10 (0 0 0) [‡]	2.625	8.5	3	65
11 (+ + +)	5	16	5	84

* (+) = high value, (-) = low value, and (0) = centre point value of a variable. (+ - -) = combination of high A, low B, and low C.

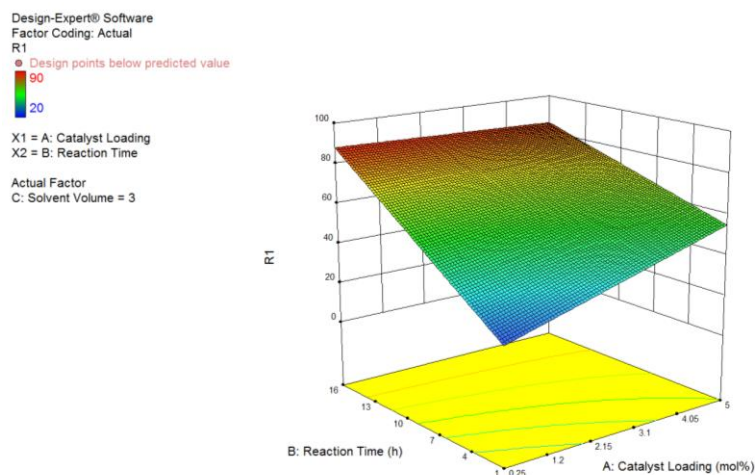
[‡] These entries represent centre points.

The responses were entered into the same design program, and used to generate a half-normal plot (Graph 1.7), which suggested that reaction time and catalyst loading affected reaction efficacy, with time having the most significant effect.



Graph 1.7

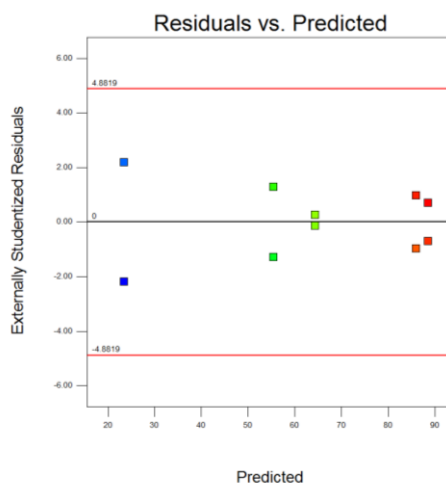
A numerical optimization model was then used to search the factor space for the best combination of variables to achieve the maximum response. The optimised conditions shown in Scheme 1.80 were selected from the top left of the plot shown in Graph 1.8 (0.25 mol% Ir, 16 h, 3 mL solvent).



Graph 1.8

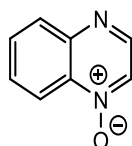
Lastly, a Residuals vs. Predicted graph was plotted (Graph 1.9), which confirmed constant variance.

Design-Expert® Software
R1
(adjusted for curvature)
Color points by value of
R1:
90
20



Graph 1.9

Scheme 1.81 – Substrates



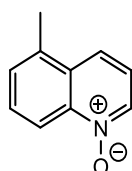
Deuteration of Quinoxaline N-oxide 216

Carried out according to General Procedure C

Catalyst **43** (0.25 mol%), 25 °C, 16 h.

Incorporation expected at δ 8.40 (C8) and 8.70 (C2).

Determined against integral at δ 7.83–7.75.



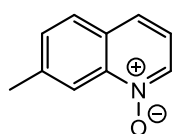
Deuteration of 5-Methylquinoxaline N-oxide 217

Carried out according to General Procedure C

Catalyst **43** (0.25 mol%), 25 °C, 16 h.

Incorporation expected at δ 8.74.

Determined against integral at δ 2.71.



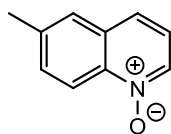
Deuteration of 7-Methylquinoxaline N-oxide 218

Carried out according to General Procedure C

Catalyst **43** (0.25 mol%), 25 °C, 16 h.

Incorporation expected at δ 8.56.

Determined against integral at δ 2.61.



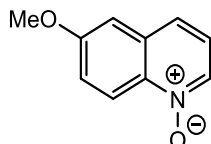
Deuteration of 6-Methylquinoline N-oxide 219

Carried out according to General Procedure C

Catalyst **43** (0.25 mol%), 25 °C, 16 h.

Incorporation expected at δ 8.71–8.64.

Determined against integral at δ 2.54.



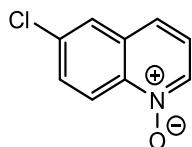
Deuteration of 6-Methoxyquinoline N-oxide 220

Carried out according to General Procedure C

Catalyst **43** (0.25 mol%), 25 °C, 16 h.

Incorporation expected at δ 8.67.

Determined against integral at δ 3.97.



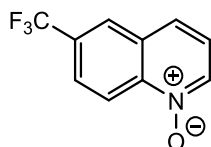
Deuteration of 6-Chloroquinoline N-oxide 221

Carried out according to General Procedure C

Catalyst **43** (0.25 mol%), 25 °C, 16 h.

Incorporation expected at δ 8.70.

Determined against integral at δ 7.87.



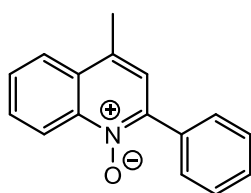
Deuteration of 6-Trifluoromethylquinoline N-oxide 222

Carried out according to General Procedure C

Catalyst **43** (0.25 mol%), 25 °C, 16 h.

Incorporation expected at δ 8.74.

Determined against integral at δ 7.74.



Deuteration of 2-Phenyl-4-methylquinoline N-oxide 223

Carried out according to General Procedure C

Catalyst **43** (0.25 mol%), 25 °C, 16 h.

Incorporation expected at δ 8.44 (C8) and 7.97 (Ph).

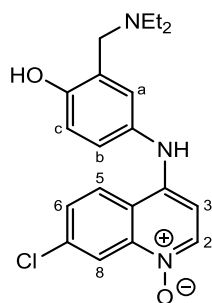
Determined against integral at δ 2.64.

Scheme 1.81 – Results

Entry	Substrate	Mass Substrate / mg	Mass Catalyst / mg	Deuterium Incorporation / %				
					Run 1	Run 2	Run 3	Average
1	216	31	0.54	C8	87	83	82	84
				C2	22	22	19	21
2	217	34	0.54	C8	91	89	94	92
3	218	34	0.54	C8	80	79	78	79
4	219	34	0.54	C8	97	98	95	97
5	220	35	0.54	C8	86	83	83	84
6	221	39	0.54	C8	95	94	98	96
7	222	46	0.54	C8	94	95	92	94
8	223	51	0.54	C8	78	71	79	76
				Ph	29	25	28	28

Scheme 1.82 – Synthesis

7-chloro-4-((3-((diethylamino)methyl)-4-hydroxyphenyl)amino)quinoline 1-oxide **237**¹⁶⁴



Prepared according to General Procedure G.

Amount of 7-chloro-4-((3-((diethylamino)methyl)-4-hydroxyphenyl)amino)quinoline (Amodiaquine): 1.017 g, 3 mmol.

Product yield: 837 mg, 75%.

Product appearance: white solid.

¹H NMR (400 MHz, CDCl₃) δ 8.47 (d, *J* = 5.3 Hz, 1H, H²), 8.00 (d, ⁴*J* = 2.1 Hz, 1H, H⁸), 7.81 (d, *J* = 8.9 Hz, 1H, H⁵), 7.42 (dd, *J* = 8.9, 2.2 Hz, 1H, H⁶), 7.08 (dd, *J* = 8.5, 2.7 Hz, 1H, H^b), 6.92 (d, *J* = 2.6 Hz, 1H, H^a), 6.86 (d, *J* = 8.5 Hz, 1H, H^c), 6.62 (d, *J* = 5.3 Hz, 1H, H³),

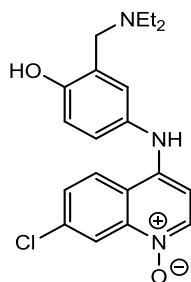
6.52 (s, 1H, NH), 3.78 (s, 2H, CH₂), 2.65 (q, *J* = 7.2 Hz, 4H, N(CH₂)₂), 1.14 (t, *J* = 7.2 Hz, 6H, N(CH₂)₂).

¹³C NMR (100 MHz, CDCl₃) δ 151.6, 143.5, 137.6, 136.3, 132.7, 130.8, 130.7, 128.2, 124.93, 124.2, 122.8, 122.7, 120.2, 115.6, 103.3, 53.9, 47.1, 11.7.

IR (ATR, cm⁻¹) 2996, 1594, 1506, 1360, 1258.

MP (°C) 222–225 (lit. 226).¹⁶⁴

Scheme 1.82 – Labelling



Deuteration of 7-chloro-4-((3-((diethylamino)methyl)-4-hydroxyphenyl)amino)quinoline 1-oxide 237

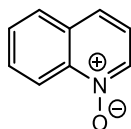
Carried out according to General Procedure C

Incorporation expected at δ 8.00.

Determined against integral at δ 3.78.

Entry	Mass Substrate / mg	Mass Catalyst / mg	Deuterium Incorporation / %			
			Run 1	Run 2	Run 3	Average
1	80	0.54	0	0	0	0

Table 1.14



Deuteration of quinoline N-oxide 215

Carried out according to General Procedure C

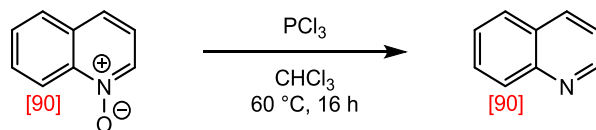
Incorporation expected at δ 8.78 (C8), and 8.66 (C2).

Determined against integral at δ 7.67.

Entry	Mass Substrate / mg	Mass Catalyst / mg	Mass Additive / mg	Deuterium Incorporation / %			
				Run 1	Run 2	Run 3	Average
1	31	0.54	20	81	78	77	79
2	31	0.54	16	18	12	17	16
3	31	0.54	22	0	0	0	0

Scheme 1.83

[8-²H]-Quinoline **239**¹⁶⁵



Carried out according to a literature procedure.¹⁶⁶ To a solution of 8-²H-quinoline *N*-oxide **224** (100 mg., 0.68 mmol) in chloroform (5 mL), was added phosphorous trichloride (87 μ L, 1 mmol, 1.5 eq.). The reaction mixture was heated to 60 °C for 16 h, after which it was concentrated *in vacuo*. The residue was diluted with diethyl ether (10 mL) and neutralised with saturated sodium bicarbonate solution (10 mL). The layers were separated and the aqueous portion extracted with diethyl ether (3 \times 10 mL). The organic fraction was dried over sodium sulfate and concentrated *in vacuo* to yield [8-²H]-quinoline **239** as a pale yellow oil (68 mg, 88% yield).

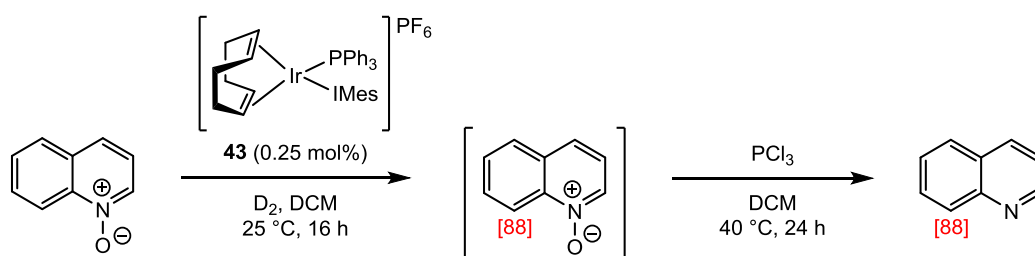
Deuterium incorporation in [8-²H]-quinoline **239** was expected at δ 8.12–8.07 (C8) and was determined against the integral at δ 7.74 (C5).

¹H NMR (400 MHz, CDCl₃) δ 8.89 (dd, J = 4.3, ⁴ J = 1.6 Hz, 1H, H²), 8.15 (dd, J = 8.2, ⁴ J = 1.6 Hz, 1H, H⁴), 8.12–8.07 (m, 0.1H, H⁸), 7.74 (dd, J = 8.2, ⁴ J = 1.7 Hz, 1H, H⁵), 7.72–7.68 (m, 1H, H⁷), 7.52 (dd, J = 8.2, 6.9 Hz, 1H, H⁶), 7.38 (dd, J = 8.3, 4.3 Hz, 1H, H³).

¹³C NMR (100 MHz, CDCl₃) δ 150.8, 148.6, 136.0, 130.2, 129.6 (t, ¹ J_{C-D} = 25 Hz), 128.4, 127.9, 126.3, 122.1.

Scheme 1.84

One-pot Labelling and Reduction of Quinoline *N*-Oxide **215**



The deuteration of **215** was set up according to *General Procedure C*. A 100 mL round-bottom flask bearing two stopcocks was flame dried and cooled under argon., Quinoline *N*-oxide **215** (73 mg, 0.5 mmol), catalyst **43** (1.26 mg, 0.00125 mmol, 0.25 mol%), and dichloromethane (5 mL) were then added and the flask was cooled to -78 °C in a dry ice/acetone bath. The flask was then evacuated and refilled with deuterium gas from a balloon, and this vacuum/refilling cycle repeated one further time. The stopcocks were

closed and the flask was left at 25 °C for 16 h, after which crude NMR analysis of an aliquot showed 88% deuterium incorporation. The deuterium atmosphere was exchanged for argon and phosphorous trichloride (65 μ L, 0.75 mmol, 1.5 eq.) was added. The reaction mixture was heated to 40 °C for 24 h, after which it was concentrated *in vacuo*. The residue was diluted with diethyl ether (10 mL) and neutralised with saturated sodium bicarbonate solution (10 mL). The layers were separated and the aqueous portion extracted with diethyl ether (3 \times 10 mL). The organic fraction was dried over sodium sulfate and passed through a pipette silica plug, eluting with diethyl ether. Concentration *in vacuo* yielded [8-²H]-quinoline **239** as a pale yellow oil (43 mg, 66% yield).

Deuterium incorporation in [8-²H]-quinoline 239 was expected at δ 8.12–8.07 (C8) and was determined against the integral at δ 7.74 (C5).

¹H NMR (400 MHz, CDCl₃) δ 8.89 (dd, $J = 4.3$, $^4J = 1.6$ Hz, 1H, H²), 8.15 (dd, $J = 8.2$, $^4J = 1.6$ Hz, 1H, H⁴), 8.12–8.07 (m, 0.1H, H⁸), 7.74 (dd, $J = 8.2$, $^4J = 1.7$ Hz, 1H, H⁵), 7.72–7.68 (m, 1H, H⁷), 7.52 (dd, $J = 8.2$, 6.9 Hz, 1H, H⁶), 7.38 (dd, $J = 8.3$, 4.3 Hz, 1H, H³).

¹³C NMR (100 MHz, CDCl₃) δ 150.8, 148.6, 136.0, 130.2, 129.6 (t, $^1J_{C-D} = 25$ Hz), 128.4, 127.9, 126.3, 122.1.

Computational Studies

This section gives broad details of how calculations were carried out, and summarises the energies discussed within this chapter. Output structures generated are included in the *Appendix*.

General Computational Details

Density functional theory (DFT) was employed to calculate the gas-phase electronic structures and energies for all species involved in H/D exchange reactions.¹⁶⁷ All structures thus far have been optimised with the hybrid meta-GGA exchange correlation functional M06.¹⁶⁸ The M06 density functional was used in conjunction with the 6-31G(d)¹⁶⁹ basis set for main group non-metal atoms and the Stuttgart RSC¹⁷⁰ effective core potential along with the associated basis set for Ir. The participating transition states (TS) are located at the same level of theory. Harmonic vibrational frequencies are calculated (with the incorporation of deuterium wherever stated) at the same level of theory to characterize respective minima (reactants, intermediates, and products with no imaginary frequency) and first order saddle points (TSs with one imaginary frequency). All calculations using the M06 functional have been performed using Gaussian 09 quantum chemistry program package.¹⁷¹ All coordinates provided are listed in Cartesian format, with charge and multiplicity of each system given at the top of the coordinate list (*i.e.* 0 1 = neutral singlet; 1 1 = 1+ charged singlet).

Potential Energy Surfaces

When constructing reaction coordinate diagrams from calculated energies, the number of atoms must remain constant for each structure considered. For each potential energy surface, one structure is set to a relative energy of 0 kcal/mol, and the energies for all other structures are given relative to the reference structure. Therefore, each PES will contain one structure with a reported relative energy of 0 kcal/mol.

Counterpoise-corrected Binding Energy Calculations

For binding energy calculations, counterpoise corrections and basis set superposition errors were calculated according to reported methods.^{172,173} Only final, corrected energies for these calculations are reported herein.

Details of Optimised Structures

Figure 1.21 – Calculation of the PES for *N*-Benzoylindole Labelling

The binding energy conformers for benzoyl labelling (**257**), C2 labelling (**258**), and C7 labelling (**259**) were calculated and analysed (Figure 1.32). Isomers possessing imaginary frequencies were discounted from further investigation, and the lowest energy conformers of the three respective binding modes were used for further calculation of the potential energy surface. Energies of all isomers are summarised in Table 1.20 (*vide infra*).

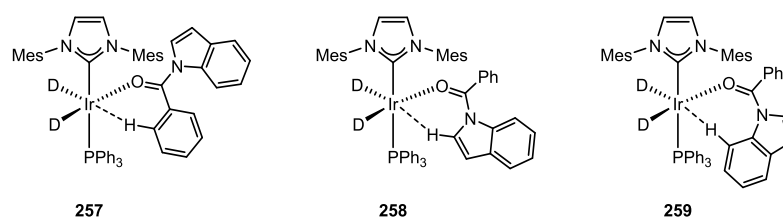


Figure 1.32

The gas-phase energies for the C–H activated intermediates and the transition states were next calculated. Energies of **260**, **261**, and **262** are shown in Figure 1.33 and summarised in Table 1.20 (*vide infra*).

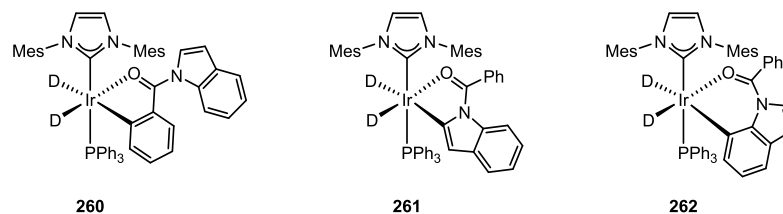
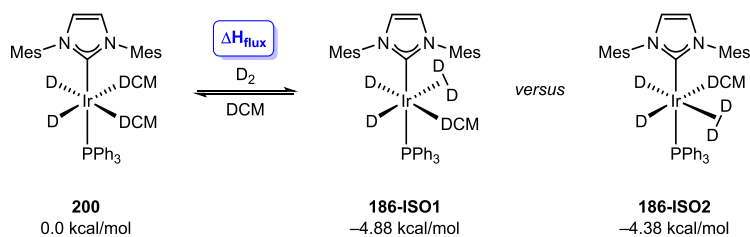


Figure 1.33

A Polarizable Continuum Model (PCM)¹⁷⁴ for DCM was then applied to the binding conformer, transition state, and C–H activated intermediate structures generated thus far. This generated the PES shown in Figure 1.21. The overall effect of solvation is a destabilisation of the activation barrier to benzoyl and C2 labelling, and a stabilisation of that for C7 labelling. However, solvation causes no changes to the interpretation of the results; C2 selectivity is predicted almost exclusively.

*Scheme 1.74 – Calculation of ΔH values for Binding of *N*-Methylindole with Complex **186**.*

Firstly, the ability of known activated complex **200** to undergo the fluxional exchange of a loosely bound dichloromethane ligand for a deuterium molecule was investigated. The relative enthalpies of **200** and the two D_2 -bound isomers of **186** are summarised below in Scheme 1.92.



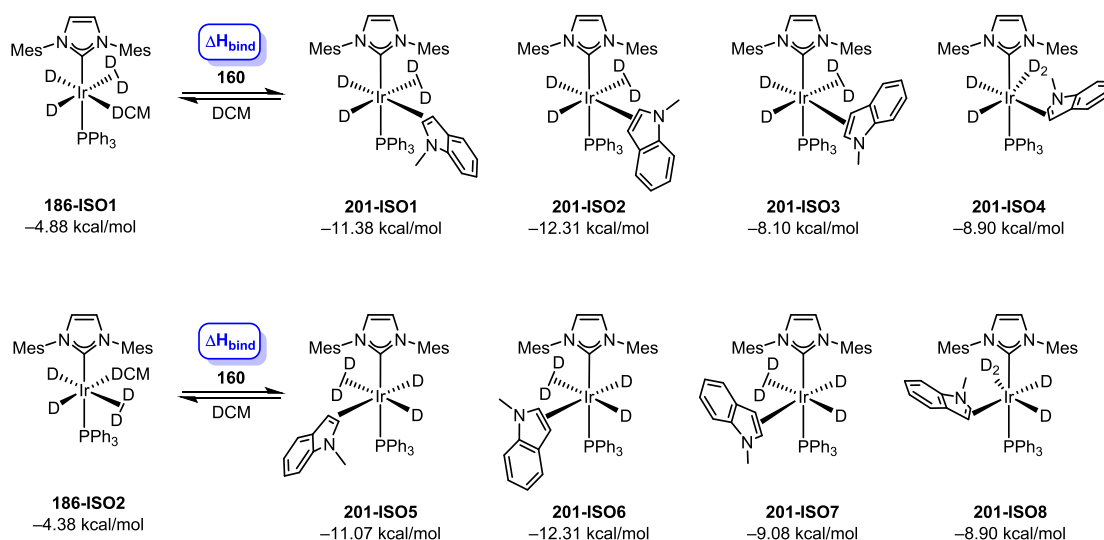
Scheme 1.92

The enthalpy change for the transformation of **200** into **186** through ligand fluxionality, ΔH_{flux} , was calculated according to Equation 1.5, below:

Equation 1.5

$$\Delta H_{flux} = [H(\mathbf{186}) + H(\text{DCM})] - [H(\mathbf{200}) + H(D_2)]$$

The binding modes of *N*-methylindole **160** to active catalyst **186** were then investigated. Scheme 1.93 summarises the enthalpies of the 8 binding isomers relative to **200**. It should be noted that complexes resulting from the reaction of both isomers of **186** were calculated here due to the relatively small (0.5 kcal/mol) energy difference between **186-ISO1** and **186-ISO2**.



Scheme 1.93

For the 8 isomers of complex **201**, enthalpy of binding (ΔH_{bind}) of *N*-methylindole **160** was calculated according to Equation 1.6, below:

Equation 1.6

$$\Delta H_{\text{bind}} = [\text{H}(\mathbf{201}) + \text{H}(\text{DCM})] - [\text{H}(\mathbf{186}) + \text{H}(\mathbf{160})]$$

Figure 1.25 – Modeling of Potential Intermediate **202**

As discussed above, complex **202**, with a formal Ir–C3 bond, was considered to be the likely product of nucleophilic attack of the indole C3 position on the iridium centre. To give an estimation of the viability of such an intermediate, the optimization of **202** was carried out with a truncated ligand set of $L_1 = \text{IMe}$ and $L_2 = \text{PMe}_3$. All attempts to calculate this, however, converged to a complex with a similar geometry to **201**, where the substrate is bound through the C2–C3 double bond. In order to see the plausibility of ‘forcing’ a formal Ir–C3 bond, electronic density difference plots were calculated using the Gaussian CubeGen utility. These are shown in Figure 1.34, where (a) shows the optimized geometry of **202**, (b) shows the electronic density difference when a η^2 interaction between the C2–C3 alkene and the iridium centre is in play, and (c) shows the electronic density difference when a C3–Ir σ -bond is enforced. These electronic plots clearly show that formation of a formal iridium–carbon bond at the C3 position causes significant disruption of the aromaticity in the benzene portion of the indole unit, and thus is likely to be highly disfavoured.

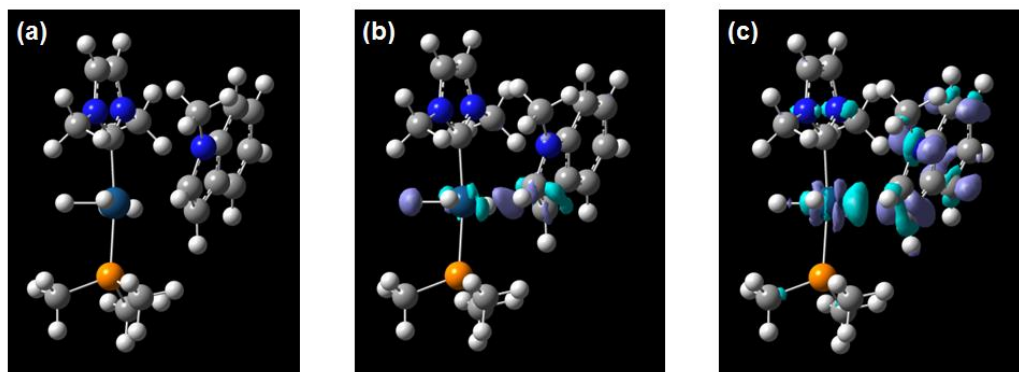


Figure 1.34

Figure 1.25 – Modelling of Potential Intermediate **205**

The enthalpy for deuterometallation of the *N*-methylindole C2–C3 bond was next calculated. While the lowest energy substrate-bound isomers of **201** had already been found (**201-ISO2** and its enantiomer **201-ISO6**), it was noted that several isomers were very close in energy. It was therefore decided to optimise the deuterometallation products for all isomers. Moreover, since our earlier calculations had shown some differences in energy between enantiomers, all enantiomeric forms of **205** were calculated. Assuming *syn*-addition of iridium and deuterium atoms, this gave 8 isomers for complex **205**. The structures and relative enthalpies are summarised in Figure 1.35.

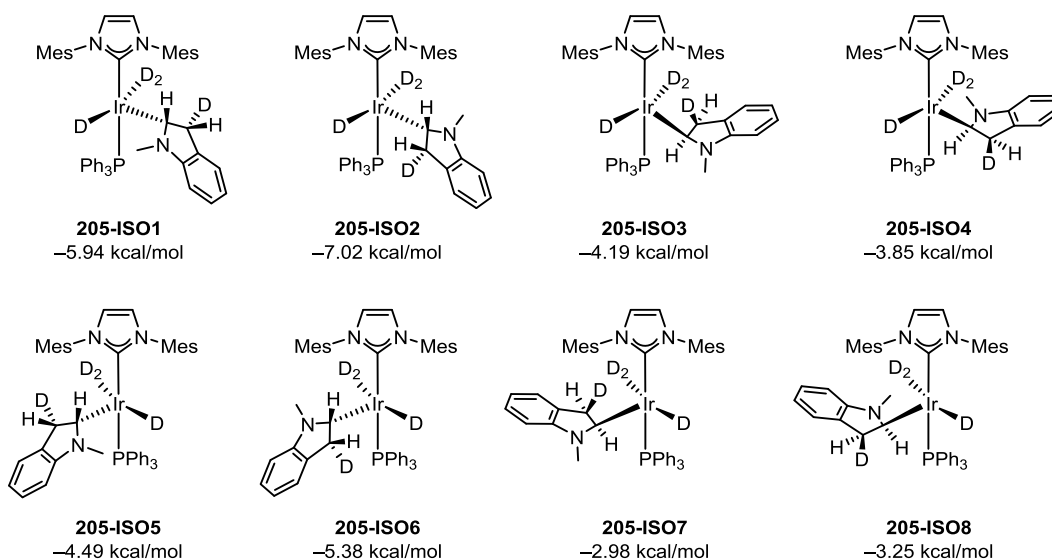


Figure 1.35

Figure 1.28 – Calculation of the PES for Deuteration of *N*-Methylindole **160** with Catalyst **43**

The potential energy surface shown in Figure 1.28 refers to the optimized geometries of **201-ISO1** and **205-ISO1**. This selection was made despite **201-ISO2** and **205-ISO2** having the lowest energy isomers, because when calculating the transition state geometries it was noted that the indole unit must be positioned with the C3 carbon facing the D₂ ligand.

The energies of all complexes implicated in the PES are given relative to **186-ISO1**. Transition state calculations were carried out using the QST3 method and their intermediacy confirmed with forward and reverse IRC calculations. To complete the PES, structures **201**, **TS-1**, **205**, and **186** were re-optimized with deuterium/hydrogen in the appropriate locations to give structures **201'**, **TS-1'**, **205'**, and **186'**. Energies of all optimised geometries are given in Table 1.22 (*vide infra*).

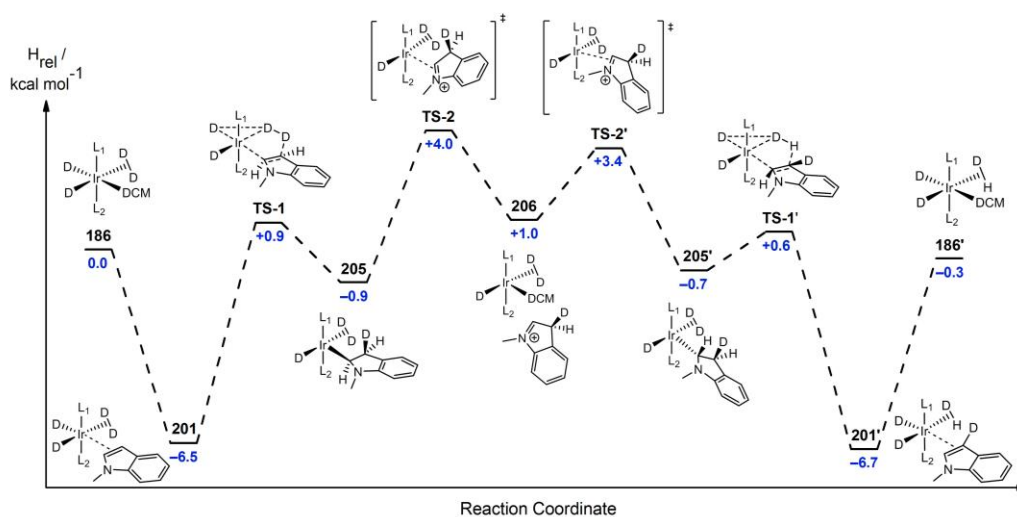


Figure 1.36

Summary of Calculated Energies

Labelling of *N*-Benzoylindole 134

Table 1.20

	Entry	Structure	H _{rel} / kcal mol ⁻¹
<i>Figure 1.32</i> (Gas-phase)	1	257-ISO1	0.1
	2	257-ISO2	5.8
	3	257-ISO3	4.8
	4	257-ISO4	1.7
	5	258-ISO1	5.9
	6	258-ISO2	4.0
	7*	259-ISO1	0.0
	8	259-ISO2	6.0
<i>Figure 1.33</i> (Gas-phase)	9	Bz-TS	24.8
	10	C2-TS	18.4
	11	C7-TS	25.5
	12	260	8.5
	13	261	1.8
	14	262	7.9
<i>Figure 1.21</i> (DCM)	15	257-ISO1	0.1
	16	258-ISO1	4.1
	17	259-ISO1	0.0
	18	Bz-TS	25.7
	19	C2-TS	21.8
	20	C7-TS	19.5
	21	260	9.1
	22	261	2.8
	23	262	8.3

* Reference energy

Labelling of *N*-Methylindole **160** – Optimisation

Table 1.21

	Entry	Structure	H _{rel} / kcal mol ⁻¹
<i>Scheme 1.92</i>	1*	200	0.0
	2	186-ISO1	-4.9
	3	186-ISO2	-4.4
<i>Scheme 1.93</i>	4	201-ISO1	-11.4
	5	201-ISO2	-12.3
	6	201-ISO3	-8.1
	7	201-ISO4	-8.9
	8	201-ISO5	-11.1
	9	201-ISO6	-12.3
	10	201-ISO7	-9.1
	11	201-ISO8	-8.9
<i>Figure 1.35</i>	13	205-ISO1	-5.9
	14	205-ISO2	-7.0
	15	205-ISO3	-4.2
	16	205-ISO4	-3.9
	17	205-ISO5	-4.5
	18	205-ISO6	-5.4
	19	205-ISO7	-3.0
	20	205-ISO8	-3.3

* Reference energy

Labelling of *N*-Methylindole **160** – PES

Table 1.22

<i>Figure 1.36</i>	1*	186-ISO1	0.0
	2	201-ISO1	-6.5
	3	TS-1	0.9
	4	205-ISO1	-0.9
	5	TS-2	4.0
	6	206	1.0
	7	TS-2'	3.4
	8	205'	-0.7
	9	TS-1'	0.6
	10	201'	-6.7
	11	186'	-0.3

* Reference energy

References

- (1) US Food and Drug Administration. *Novel Drugs 2015*; 2016.
- (2) Hay, M.; Thomas, D. W.; Craighead, J. L.; Economides, C.; Rosenthal, J. *Nat. Biotechnol.* **2014**, *32*, 40–51.
- (3) EvaluatePharma. *World Preview 2014, Outlook to 2020*; 2014.
- (4) DiMasi, J. A.; Grabowski, H. G.; Hansen, R. W. *J. Health Econ.* **2016**, *47*, 20–33.
- (5) Biotechnology Innovation Organization (BIO); Biomedtracker; AMPLION. *Clinical Development Success Rates 2006-2015*; 2016.
- (6) Unkefer, C. J.; Martinez, R. A. *Drug Test. Anal.* **2012**, *4*, 303–307.
- (7) Gant, T. G. *J. Med. Chem.* **2014**, *57*, 3595–3611.
- (8) Timmins, G. S. *Expert Opin. Ther. Pat.* **2014**, *24*, 1067–1075.
- (9) Belleau, B.; Burba, J.; Pindell, M.; Reiffenstein, J. *Science* **1961**, *133*, 102–104.
- (10) US Food and Drug Administration. NDA 208082 Approval Letter https://www.accessdata.fda.gov/drugsatfda_docs/applletter/2017/208082Orig1s000ltr.pdf (accessed Apr 13, 2017).
- (11) Geschwind, M. D.; Paras, N. *JAMA* **2016**, *316*, 33–35.
- (12) Citrome, L. *Int. J. Clin. Pract.* **2016**, *70*, 298–299.
- (13) Allen, P. H.; Hickey, M. J.; Kingston, L. P.; Wilkinson, D. J. *J. Labelled Compd. Radiopharm.* **2010**, *53*, 731–738.
- (14) Sajiki, H.; Hattori, K.; Aoki, F.; Yasunaga, K.; Hirota, K. *Synlett* **2002**, *2002*, 1149–1151.
- (15) Matsubara, S.; Yokota, Y.; Oshima, K. *Org. Lett.* **2004**, *6*, 2071–2073.
- (16) Neufeldt, S. R.; Sanford, M. S. *Acc. Chem. Res.* **2012**, *45*, 936–946.
- (17) Blake, M. R.; Garnett, J. L.; Gregor, I. K.; Hannan, W.; Hoa, K.; Long, M. A. *J. Chem. Soc., Chem. Commun.* **1975**, 930–932.
- (18) Lockley, W. J. S. *J. Labelled Compd. Radiopharm.* **1984**, *21*, 45–57.
- (19) Lockley, W. J. S. *J. Labelled Compd. Radiopharm.* **1985**, *22*, 623–630.
- (20) Hesk, D.; Jones, J. R.; Lockley, W. J. S.; Wilkinson, D. J. *J. Labelled Compd. Radiopharm.* **1990**, *28*, 1309–1320.
- (21) Hesk, D.; Jones, J. R.; Lockley, W. J. S. *J. Pharm. Sci.* **1991**, *80*, 887–890.
- (22) Buchanan, J. M.; Stryker, J. M.; Bergman, R. G. *J. Am. Chem. Soc.* **1986**, *108*, 1537–1550.
- (23) Arndtsen, B. A.; Bergman, R. G. *Science* **1995**, *270*, 1970–1973.
- (24) Heys, R. *J. Chem. Soc., Chem. Commun.* **1992**, 680–681.

- (25) Heys, J. R.; Shu, A. Y. L.; Senderoff, S. G.; Phillips, N. M. *J. Labelled Compd. Radiopharm.* **1993**, *33*, 431–438.
- (26) Crabtree, R. H.; Felkin, H.; Morris, G. E. *J. Organomet. Chem.* **1977**, *141*, 205–215.
- (27) Crabtree, R. *Acc. Chem. Res.* **1979**, *12*, 331–337.
- (28) Hesk, D.; Das, P. R.; Evans, B. *J. Labelled Compd. Radiopharm.* **1995**, *36*, 497–502.
- (29) Ellames, G. J.; Gibson, J. S.; Herbert, J. M.; McNeill, A. H. *Tetrahedron* **2001**, *57*, 9487–9497.
- (30) Shu, A. Y. L.; Chen, W.; Heys, J. R. *J. Organomet. Chem.* **1996**, *524*, 87–93.
- (31) Gusev, D. G.; Burke, H. *Chem. Ber.* **1996**, *129*, 1143.
- (32) Lee, H. M.; Jiang, T.; Stevens, E. D.; Nolan, S. P. *Organometallics* **2001**, *20*, 1255–1258.
- (33) Vázquez-Serrano, L. D.; Owens, B. T.; Buriak, J. M. *Chem. Commun.* **2002**, 2518–2519.
- (34) Tolman, C. A. *J. Am. Chem. Soc.* **1970**, *92*, 2953–2956.
- (35) Gusev, D. G. *Organometallics* **2009**, *28*, 763–770.
- (36) Tonner, R.; Frenking, G. *Organometallics* **2009**, *28*, 3901–3905.
- (37) Tolman, C. A. *Chem. Rev.* **1977**, *77*, 313–348.
- (38) Arduengo, A. J.; Harlow, R. L.; Kline, M. *J. Am. Chem. Soc.* **1991**, *113*, 361–363.
- (39) Dröge, T.; Glorius, F. *Angew. Chem. Int. Ed.* **2010**, *49*, 6940–6952.
- (40) Herrmann, W. A. *Angew. Chem. Int. Ed.* **2002**, *41*, 1290–1309.
- (41) Gusev, D. G. *Organometallics* **2009**, *28*, 6458–6461.
- (42) Kelly, R. A.; Clavier, H.; Giudice, S.; Scott, N. M.; Stevens, E. D.; Bordner, J.; Samardjiev, I.; Hoff, C. D.; Cavallo, L.; Nolan, S. P. *Organometallics* **2008**, *27*, 202–210.
- (43) Chianese, A. R.; Li, X.; Janzen, M. C.; Faller, J. W.; Crabtree, R. H. *Organometallics* **2003**, *22*, 1663–1667.
- (44) Wolf, S.; Plenio, H. *J. Organomet. Chem.* **2009**, *694*, 1487–1492.
- (45) Liske, A.; Verlinden, K.; Buhl, H.; Schaper, K.; Ganter, C. *Organometallics* **2013**, *32*, 5269–5272.
- (46) Back, O.; Henry-Ellinger, M.; Martin, C. D.; Martin, D.; Bertrand, G. *Angew. Chem. Int. Ed.* **2013**, *52*, 2939–2943.
- (47) Jacobsen, H.; Correa, A.; Poater, A.; Costabile, C.; Cavallo, L. *Coord. Chem. Rev.* **2009**, *253*, 687–703.
- (48) Nilsson, G. N.; Kerr, W. J. *J. Labelled Compd. Radiopharm.* **2010**, *53*, 662–667.

- (49) Brown, J. A.; Irvine, S.; Kennedy, A. R.; Kerr, W. J.; Andersson, S.; Nilsson, G. N. *Chem. Commun.* **2008**, 1115–1117.
- (50) Bennie, L. S.; Fraser, C. J.; Irvine, S.; Kerr, W. J.; Andersson, S.; Nilsson, G. N. *Chem. Commun.* **2011**, 47, 11653–11655.
- (51) Brown, J. A.; Cochrane, A. R.; Irvine, S.; Kerr, W. J.; Mondal, B.; Parkinson, J. A.; Paterson, L. C.; Reid, M.; Tuttle, T.; Andersson, S.; Nilsson, G. N. *Adv. Synth. Catal.* **2014**, 356, 3551–3562.
- (52) Kerr, W. J.; Mudd, R. J.; Paterson, L. C.; Brown, J. A. *Chem. Eur. J.* **2014**, 20, 14604–14607.
- (53) Vazquez-Serrano, L. D.; Owens, B. T.; Buriak, J. M. *Inorganica Chim. Acta* **2006**, 359, 2786–2797.
- (54) Köcher, C.; Herrmann, W. A. *J. Organomet. Chem.* **1997**, 532, 261–265.
- (55) Shu, L.; Chen, W.; Heys, R. *J. Organomet. Chem.* **1996**, 524, 87–93.
- (56) Reid, M. PhD Thesis, University of Strathclyde, 2015.
- (57) Strem Chemicals. Iridium Catalysts for Hydrogen Isotope Exchange and Catalytic Hydrogenation Processes
<https://www.strem.com/uploads/resources/documents/iridiumcatalysts.pdf> (accessed Feb 17, 2017).
- (58) Cochrane, A. R.; Irvine, S.; Kerr, W. J.; Reid, M.; Andersson, S.; Nilsson, G. N. *J. Labelled Compd. Radiopharm.* **2013**, 56, 451–454.
- (59) Kerr, W. J.; Reid, M.; Tuttle, T. *ACS Catal.* **2015**, 5, 402–410.
- (60) Kennedy, A. R.; Kerr, W. J.; Moir, R.; Reid, M. *Org. Biomol. Chem.* **2014**, 12, 7927–7931.
- (61) Smidt, S. P.; Zimmermann, N.; Studer, M.; Pfaltz, A. *Chem. – A Eur. J.* **2004**, 10, 4685–4693.
- (62) Lightfoot, A.; Schnider, P.; Pfaltz, A. *Angew. Chem. Int. Ed.* **1998**, 37, 2897–2899.
- (63) Nelson, D. J.; Truscott, B. J.; Egbert, J. D.; Nolan, S. P. *Organometallics* **2013**, 32, 3769–3772.
- (64) Lightfoot, A.; Schnider, P.; Pfaltz, A. *Angew. Chem. Int. Ed.* **1998**, 37, 2897–2899.
- (65) Henderson, R. K.; Jiménez-González, C.; Constable, D. J. C.; Alston, S. R.; Inglis, G. G. A.; Fisher, G.; Sherwood, J.; Binks, S. P.; Curzons, A. D. *Green Chem.* **2011**, 13, 854.
- (66) Cochrane, A. R.; Idziak, C.; Kerr, W. J.; Mondal, B.; Paterson, L. C.; Tuttle, T.; Andersson, S.; Nilsson, G. N. *Org. Biomol. Chem.* **2014**, 12, 3598–3603.

- (67) Mudd, R. J. PhD Thesis, University of Strathclyde, 2016.
- (68) Bandini, M.; Eichholzer, A. *Angew. Chem. Int. Ed.* **2009**, *48*, 9608–9644.
- (69) *Based on a survey of SciFinder, CAPLUS, and MEDLINE databases (December 2016).*
- (70) Chen, F.-E.; Huang, J. *Chem. Rev.* **2005**, *105*, 4671–4706.
- (71) Kaushik, N. K.; Kaushik, N.; Attri, P.; Kumar, N.; Kim, C. H.; Verma, A. K.; Choi, E. H. *Molecules* **2013**, *18*, 6620–6662.
- (72) Nichols, D. E.; Nichols, C. D. *Chem. Rev.* **2008**, *108*, 1614–1641.
- (73) World Health Organisation. *WHO Model List of Essential Medicines, 19th List (April 2015)*; 2015.
- (74) Seregin, I. V.; Gevorgyan, V. *Chem. Soc. Rev.* **2007**, *36*, 1173–1193.
- (75) Qin, X.; Liu, H.; Qin, D.; Wu, Q.; You, J.; Zhao, D.; Guo, Q.; Huang, X.; Lan, J. *Chem. Sci.* **2013**, *4*, 1964–1969.
- (76) Ackermann, L.; Lygin, A. V. *Org. Lett.* **2011**, *13*, 3332–3335.
- (77) Deprez, N. R.; Kalyani, D.; Krause, A.; Sanford, M. S. *J. Am. Chem. Soc.* **2006**, *128*, 4972–4973.
- (78) Lane, B. S.; Brown, M. A.; Sames, D. *J. Am. Chem. Soc.* **2005**, *127*, 8050–8057.
- (79) Gong, B.; Shi, J.; Wang, X.; Yan, Y.; Li, Q.; Meng, Y.; Xu, H. E.; Yi, W. *Adv. Synth. Catal.* **2014**, *356*, 137–143.
- (80) Katritzky, A. R.; Akutagawa, K. *Tetrahedron Lett.* **1985**, *26*, 5935–5938.
- (81) Ibaceta-Lizana, J. S. L.; Jackson, A. H.; Prasitpan, N.; Shannon, P. V. R. *J. Chem. Soc. Perkin Trans. 2* **1987**, 1221–1226.
- (82) Yau, W.-M.; Gawrisch, K. *J. Labelled Compd. Radiopharm.* **1999**, *42*, 709–714.
- (83) Derdau, V.; Atzrodt, J. *Synlett* **2006**, 1918–1922.
- (84) Pieters, G.; Taglang, C.; Bonnefille, E.; Gutmann, T.; Puente, C.; Berthet, J. C.; Dugave, C.; Chaudret, B.; Rousseau, B. *Angew. Chem. Int. Ed.* **2014**, *53*, 230–234.
- (85) Pony Yu, R.; Hesk, D.; Rivera, N.; Pelczar, I.; Chirik, P. J. *Nature* **2016**, *529*, 195–199.
- (86) Yu, R. P.; Darmon, J. M.; Milsman, C.; Margulieux, G. W.; Stieber, S. C. E.; DeBeer, S.; Chirik, P. J. *J. Am. Chem. Soc.* **2013**, *135*, 13168–13184.
- (87) Yu, R. P.; Darmon, J. M.; Hoyt, J. M.; Margulieux, G. W.; Turner, Z. R.; Chirik, P. J. *ACS Catal.* **2012**, *2*, 1760–1764.
- (88) Jess, K.; Derdau, V.; Weck, R.; Atzrodt, J.; Freytag, M.; Jones, P. G.; Tamm, M. *Adv. Synth. Catal.* **2017**, *359*, 629–638.

- (89) Liu, Y.-J.; Xu, H.; Kong, W.-J.; Shang, M.; Dai, H.-X.; Yu, J.-Q. *Nature* **2014**, *515*, 389–393.
- (90) Atzrodt, J.; Derdau, V.; Kerr, W. J.; Reid, M.; Rojahn, P.; Weck, R. *Tetrahedron* **2015**, *71*, 1924–1929.
- (91) Jacquemard, U.; Bénéteau, V.; Lefoix, M.; Routier, S.; Mérour, J.-Y.; Coudert, G. *Tetrahedron* **2004**, *60*, 10039–10047.
- (92) Sharma, R. K.; Fry, J. L. *J. Org. Chem.* **1983**, *48*, 2112–2114.
- (93) Derry, C. J.; Derry, S.; Moore, R. A. In *Cochrane Database of Systematic Reviews*; Derry, S., Ed.; John Wiley & Sons, Ltd: Chichester, UK, 2014.
- (94) Saha, D.; Ghosh, R.; Sarkar, A. *Tetrahedron* **2013**, *69*, 3951–3960.
- (95) Brereton, R. *Applied Chemometrics for Scientists*; John Wiley & Sons, Ltd.: West Sussex, U.K., 2008.
- (96) Leardi, R. *Anal. Chim. Acta* **2009**, *652*, 161–172.
- (97) Saulnier, M. G.; Gribble, G. W. *J. Org. Chem.* **1982**, *47*, 757–761.
- (98) Lakhdar, S.; Westermaier, M.; Terrier, F.; Goumont, R.; Boubaker, T.; Ofial, A. R.; Mayr, H. *J. Org. Chem.* **2006**, *71*, 9088–9095.
- (99) Zhu, Y.; Fan, Y.; Burgess, K. *J. Am. Chem. Soc.* **2010**, *132*, 6249–6253.
- (100) Heys, J. R. *J. Labelled Compd. Radiopharm.* **2007**, *50*, 770–778.
- (101) Sigma-Aldrich. Methyl Red
<http://www.sigmaaldrich.com/catalog/product/sial/250198?lang=en®ion=GB>
 (accessed Mar 5, 2017).
- (102) Qi, X.; Liu, L.; Fu, Y.; Guo, Q. *Organometallics* **2006**, *25*, 5879–5886.
- (103) Morris, R. H. *Chem. Rev.* **2016**, *116*, 8588–8654.
- (104) Morris, R. H. *J. Am. Chem. Soc.* **2014**, *136*, 1948–1959.
- (105) Li, T.; Lough, A. J.; Morris, R. H. *Chem. Eur. J.* **2007**, *13*, 3796–3803.
- (106) Muller, J. G.; Acquaye, J. H.; Takeuchi, K. J. *Inorg. Chem.* **1992**, *31*, 4552–4557.
- (107) Hansch, C.; Leo, A.; Taft, R. W. *Chem. Rev.* **1991**, *91*, 165–195.
- (108) Ugo, R.; Pasini, A.; Fusi, A.; Cenini, S. *J. Am. Chem. Soc.* **1972**, *94*, 7364–7370.
- (109) Hopmann, K. H.; Bayer, A. *Organometallics* **2011**, *30*, 2483–2497.
- (110) Kawaguchi, S. *Variety in Coordination Modes of Ligands in Metal Complexes*; Inorganic Chemistry Concepts; Springer Berlin Heidelberg: Berlin, Heidelberg, 1988; Vol. 11.
- (111) Hwang, H.; Kim, J.; Jeong, J.; Chang, S. *J. Am. Chem. Soc.* **2014**.
- (112) Stephens, D. E.; Lakey-Beitia, J.; Atesin, A. C.; Ateşin, T. A.; Chavez, G.; Arman,

- H. D.; Larionov, O. V. *ACS Catal.* **2015**, *5*, 167–175.
- (113) Liu, J.-B.; Sheng, X.-H.; Sun, C.-Z.; Huang, F.; Chen, D.-Z. *ACS Catal.* **2016**, *6*, 2452–2461.
- (114) Iwai, T.; Sawamura, M. *ACS Catal.* **2015**, 5031–5040.
- (115) Campos, K. R. *Chem. Soc. Rev.* **2007**, *36*, 1069–1084.
- (116) Armarego, W. L. F.; Chai, C. L. L. *Purification of Laboratory Chemicals*; Elsevier, 2009.
- (117) Hwang, H.; Kim, J.; Jeong, J.; Chang, S. *J. Am. Chem. Soc.* **2014**, *136*, 10770–10776.
- (118) Özüdüru, G.; Schubach, T.; Boysen, M. M. K. *Org. Lett.* **2012**, *14*, 4990–4993.
- (119) Pan, S.; Ryu, N.; Shibata, T. *J. Am. Chem. Soc.* **2012**, *134*, 17474–17477.
- (120) de Koning, C. B.; Michael, J. P.; Rousseau, A. L. *J. Chem. Soc., Perkin Trans. 1* **2000**, 1705–1713.
- (121) Cornella, J.; Lu, P.; Larrosa, I. *Org. Lett.* **2009**, *11*, 5506–5509.
- (122) Hostier, T.; Ferey, V.; Ricci, G.; Pardo, D. G.; Cossy, J. *Chem. Commun.* **2015**, *51*, 13898–13901.
- (123) Nishino, M.; Hirano, K.; Satoh, T.; Miura, M. *Angew. Chem. Int. Ed.* **2012**, *51*, 6993–6997.
- (124) Stokes, B. J.; Liu, S.; Driver, T. G. *J. Am. Chem. Soc.* **2011**, *133*, 4702–4705.
- (125) King, F. D.; Gaster, L. M.; Mulholland, K. R. 5-HT₄ Receptor Antagonist. US 5741801 A, 1994.
- (126) Xu, H.; Fan, L. *Eur. J. Med. Chem.* **2011**, *46*, 364–369.
- (127) Chakrabarty, M.; Basak, R.; Harigaya, Y.; Takayanagi, H. *Tetrahedron* **2005**, *61*, 1793–1801.
- (128) Prokopov, A. A.; Yakhontov, L. N. *Chem. Heterocycl. Compd.* **1978**, *14*, 406–410.
- (129) Huestis, M. P.; Fagnou, K. *Org. Lett.* **2009**, *11*, 1357–1360.
- (130) Tono-oka, S.; Tone, Y.; Marquez, V. E.; Cooney, D. A.; Sekikawa, I.; Azuma, I. *Bull. Chem. Soc. Jpn.* **1985**, *58*, 309–315.
- (131) Heller, S. T.; Schultz, E. E.; Sarpong, R. *Angew. Chem. Int. Ed.* **2012**, *51*, 8304–8308.
- (132) D’Silva, C.; Iqbal, R. *Synthesis* **1996**, 1996, 457–458.
- (133) Duan, Y.-N.; Cui, L.-Q.; Zuo, L.-H.; Zhang, C. *Chem. Eur. J.* **2015**, *21*, 13052–13057.
- (134) You, H.; Youn, H.-S.; Im, I.; Bae, M.-H.; Lee, S.-K.; Ko, H.; Eom, S. H.; Kim, Y.-C. *Eur. J. Med. Chem.* **2011**, *46*, 1153–1164.

- (135) Scott, M. S.; Luckhurst, C. A.; Dixon, D. J. *Org. Lett.* **2005**, *7*, 5813–5816.
- (136) Chen, W.; Wang, J. *Organometallics* **2013**, *32*, 1958–1963.
- (137) Candy, C. F.; Jones, R. A.; Wright, P. H. *J. Chem. Soc. C* **1970**, 2563–2567.
- (138) Granchi, C.; Rizzolio, F.; Bordoni, V.; Caligiuri, I.; Manera, C.; Macchia, M.; Minutolo, F.; Martinelli, A.; Giordano, A.; Tuccinardi, T. *J. Enzyme Inhib. Med. Chem.* **2016**, *31*, 137–146.
- (139) Sevov, C. S.; Hartwig, J. F. *J. Am. Chem. Soc.* **2013**, *135*, 2116–2119.
- (140) Kim, J.; Kim, H.; Chang, S. *Org. Lett.* **2012**, *14*, 3924–3927.
- (141) Ottoni, O.; Cruz, R.; Alves, R. *Tetrahedron* **1998**, *54*, 13915–13928.
- (142) Zhang, L.; Peng, C.; Zhao, D.; Wang, Y.; Fu, H.-J.; Shen, Q.; Li, J.-X. *Chem. Commun.* **2012**, *48*, 5928–5930.
- (143) Nemoto, K.; Tanaka, S.; Konno, M.; Onozawa, S.; Chiba, M.; Tanaka, Y.; Sasaki, Y.; Okubo, R.; Hattori, T. *Tetrahedron* **2016**, *72*, 734–745.
- (144) Bergman, J.; Norrby, P.-O.; Sand, P. *Tetrahedron* **1990**, *46*, 6113–6124.
- (145) Klare, H. F. T.; Oestreich, M.; Ito, J.; Nishiyama, H.; Ohki, Y.; Tatsumi, K. *J. Am. Chem. Soc.* **2011**, *133*, 3312–3315.
- (146) Shimada, T.; Nakamura, I.; Yamamoto, Y. *J. Am. Chem. Soc.* **2004**, *126*, 10546–10547.
- (147) Van Baelen, G.; Hostyn, S.; Dhooghe, L.; Tapolcsányi, P.; Mátyus, P.; Lemièrre, G.; Dommissie, R.; Kaiser, M.; Brun, R.; Cos, P.; Maes, L.; Hajós, G.; Riedl, Z.; Nagy, I.; Maes, B. U. W.; Pieters, L. *Bioorg. Med. Chem.* **2009**, *17*, 7209–7217.
- (148) Martínez-Viviente, E.; Pregosin, P. S. *Inorg. Chem.* **2003**, *42*, 2209–2214.
- (149) Shang, R.; Ilies, L.; Nakamura, E. *J. Am. Chem. Soc.* **2016**, *138*, 10132–10135.
- (150) Ali, M.; Punniyamurthy, T. *Synlett* **2011**, 623–626.
- (151) Li, D.; Xu, N.; Zhang, Y.; Wang, L. *Chem. Commun.* **2014**, *50*, 14862–14865.
- (152) Berger, L.; Corraz, A. J.; Parrish, J. W. Hydroxy methyl carbazole acetic acid and esters. US4150031, 1979.
- (153) Bjørsvik, H.-R.; Elumalai, V. *Eur. J. Org. Chem.* **2016**, *2016*, 5474–5479.
- (154) Bering, L.; Antonchick, A. P. *Org. Lett.* **2015**, *17*, 3134–3137.
- (155) Stephens, D. E.; Chavez, G.; Valdes, M.; Dovalina, M.; Arman, H. D.; Larionov, O. V. *Org. Biomol. Chem.* **2014**, *12*, 6190–6199.
- (156) Larionov, O. V.; Stephens, D.; Mfuh, A. M.; Arman, H. D.; Naumova, A. S.; Chavez, G.; Skenderi, B. *Org. Biomol. Chem.* **2014**, *12*, 3026–3036.
- (157) Tröster, A.; Alonso, R.; Bauer, A.; Bach, T. *J. Am. Chem. Soc.* **2016**, *138*, 7808–

7811.

- (158) Sasaki, K.; Tsurumori, A.; Hirota, T. *J. Chem. Soc. Perkin Trans. 1* **1998**, 3851–3856.
- (159) Loska, R.; Szachowicz, K.; Szydlak, D. *Org. Lett.* **2013**, *15*, 5706–5709.
- (160) Avendaño, C.; Moreno, T.; Fernández, M.; de la Cuesta, E. *Heterocycles* **1996**, *43*, 817.
- (161) Wengryniuk, S. E.; Weickgenannt, A.; Reiher, C.; Strotman, N. A.; Chen, K.; Eastgate, M. D.; Baran, P. S. *Org. Lett.* **2013**, *15*, 792–795.
- (162) Ma, W.; Zhang, J.; Xu, C.; Chen, F.; He, Y.-M.; Fan, Q.-H. *Angew. Chem. Int. Ed.* **2016**, *55*, 12891–12894.
- (163) Kato, T.; Yamanaka, H. *J. Org. Chem.* **1965**, *30*, 910–913.
- (164) Elslager, E. F.; Gold, E. H.; Tendick, F. H.; Werbel, L. M.; Worth, D. F. *J. Heterocycl. Chem.* **1964**, *1*, 6–12.
- (165) Kuriyama, M.; Hamaguchi, N.; Yano, G.; Tsukuda, K.; Sato, K.; Onomura, O. *J. Org. Chem.* **2016**, *81*, 8934–8946.
- (166) Sylvester, K. T.; Wu, K.; Doyle, A. G. *J. Am. Chem. Soc.* **2012**, *134*, 16967–16970.
- (167) Kohn, W.; Sham, L. J. *Phys. Rev.* **1965**, *140*, A1133–A1138.
- (168) Zhao, Y.; Truhlar, D. G. *Theor. Chem. Acc.* **2008**, *120*, 215–241.
- (169) Francl, M. M.; Pietro, W. J.; Hehre, W. J.; Binkley, J. S.; Gordon, M. S.; DeFrees, D. J.; Pople, J. A. *J. Chem. Phys.* **1982**, *77*, 3654–3665.
- (170) Andrae, D.; Häußermann, U.; Dolg, M.; Stoll, H.; Preuß, H. *Theor. Chim. Acta* **1990**, *77*, 123–141.
- (171) Frisch, M. J.; Trucks, G. W.; Schlegel, H. B.; Scuseria, G. E.; Robb, M. A.; Cheeseman, J. R.; Scalmani, G.; Barone, V.; Petersson, G. A.; Nakatsuji, H.; Li, X.; Caricato, M.; Marenich, A.; Bloino, J.; Janesko, B. G.; Gomperts, R.; Mennucci, B.; Hratchian, H. P.; Ortiz, J. V.; Izmaylov, A. F.; Sonnenberg, J. L.; Williams-Young, D.; Ding, F.; Lipparini, F.; Egidi, F.; Goings, J.; Peng, B.; Petrone, A.; Henderson, T.; Ranasinghe, D.; Zakrzewski, V. G.; Gao, J.; Rega, N.; Zheng, G.; Liang, W.; Hada, M.; Ehara, M.; Toyota, K.; Fukuda, R.; Hasegawa, J.; Ishida, M.; Nakajima, T.; Honda, Y.; Kitao, O.; Nakai, H.; Vreven, T.; Throssell, K.; Montgomery Jr, J. A.; Peralta, J. E.; Ogliaro, F.; Bearpark, M.; Heyd, J. J.; Brothers, E.; Kudin, K. N.; Staroverov, V. N.; Keith, T.; Kobayashi, R.; Normand, J.; Raghavachari, K.; Rendell, A.; Burant, J. C.; Iyengar, S. S.; Tomasi, J.; Cossi, M.; Millam, J. M.; Klene, M.; Adamo, C.; Cammi, R.; Ochterski, J. W.; Martin, R. L.; Morokuma, K.; Farkas, O.;

Foresman, J. B.; Fox, D. J. *Gaussian 09, Revision A.02*; Gaussian, Inc.: Wallingford CT, 2016.

(172) Spek, A. L. *Acta Crystallogr., Sect. D: Biol. Crystallogr.* **2009**, *65*, 148–155.

(173) Kirschner, K. N.; Sorensen, J. B.; Bowen, J. P. *J. Chem. Educ.* **2007**, *84*, 1225–1229.

(174) Tomasi, J.; Mennucci, B.; Cammi, R. *Chem. Rev.* **2005**, *105*, 2999–3094.

Chapter 2: Design and Synthesis of Novel Iridium(I) Catalysts for C–N Bond Formation via Hydrogen Borrowing

Introduction

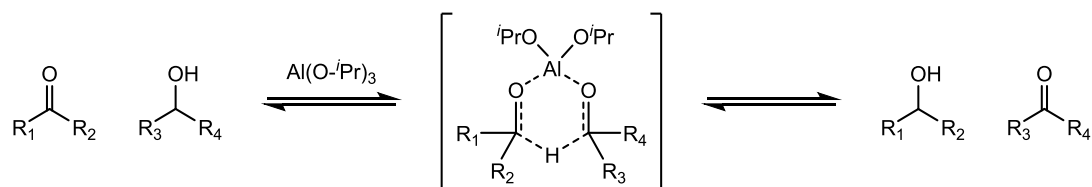
Hydrogenation reactions are among the most fundamental transformations in organic chemistry.^{1,2} Typically, reduction processes are carried out directly under a pressure of hydrogen gas or with stoichiometric amounts of a hydride reducing agent, but the advent of hydrogen transfer as an alternative reduction method has brought notable advantages over traditional methods.³ Transfer hydrogenation refers to the addition of hydrogen to a molecule from a source other than hydrogen gas. Typically, cheap and readily available organic compounds such as alcohols are used as the hydrogen donor. Transfer hydrogenation offers the atom efficiency of direct reduction by H₂, but without the safety issues or elaborate equipment often required when using gaseous hydrogen and, as such, has become a valuable tool for organic chemists wanting to access hydrogenated compounds.

Transfer Hydrogenation

Hydrogen transfer methods have been reported for over a century, and in a key 1954 survey, Braude and Linstead defined three categories into which hydrogen transfer reactions could be classified: 1) hydrogen migration taking place within one molecule; 2) hydrogen disproportionation, involving transfer where donor and acceptor are identical; and 3) transfer hydrogenation, where transfer occurs between different donors and acceptors.⁴ The first known example of hydrogen transfer, reported in 1903 by Knoevenagel, was the disproportionation of dimethyl 1,4-dihydroterephthalate catalysed by palladium black.⁵ Over the last century, however, the third category, transfer hydrogenation, has become by far the most widely used type of hydrogen transfer reaction.

The first example of carbonyl group reduction by transfer hydrogenation was published independently and almost simultaneously by Meerwein and Verley in 1925, who reported that a mixture of aluminium ethoxide and ethanol could facilitate the reduction of aldehydes to alcohols.^{6,7} Ponndorf soon expanded this methodology to include the reduction of ketones with a switch to aluminium *iso*-propoxide and *iso*-propanol,⁸ and the Meerwein-Ponndorf-Verley (MPV) reaction has since become one of the most used methods in transfer

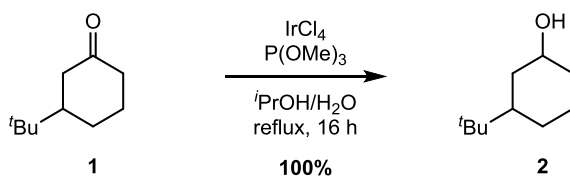
hydrogenation. The MPV reaction is proposed to take place *via* a 6-membered cyclic transition state, with both the carbonyl and alcohol oxygen atoms coordinated to the aluminium centre (Scheme 2.1).⁹



Scheme 2.1

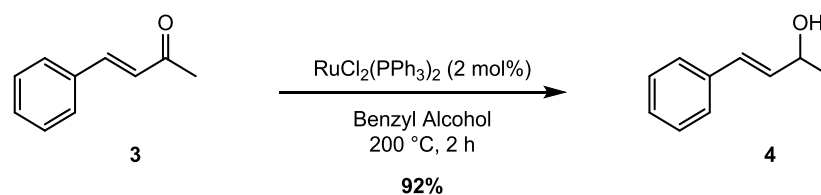
The reversibility of the MPV reaction has also been exploited, with the Oppenauer oxidation of alcohols in the presence of ketones offering another useful transformation.¹⁰ Since its discovery in the 1920s, the MPV reaction has been reported to proceed with a number of alternative organometallic reagents, including zirconium,¹¹ lanthanum,¹² and samarium reagents,¹² as well as with heterogeneous catalysts.¹³

Over the last 50 years or so, homogeneous transition metal catalysis has come to the forefront of transfer hydrogenation methodology. Pioneering research published in the 1960s by Henbest and Mitchell demonstrated the use of an iridium phosphite catalyst, generated *in situ*, for the reduction of cyclohexanones in the presence of *iso*-propanol (Scheme 2.2).^{14,15}



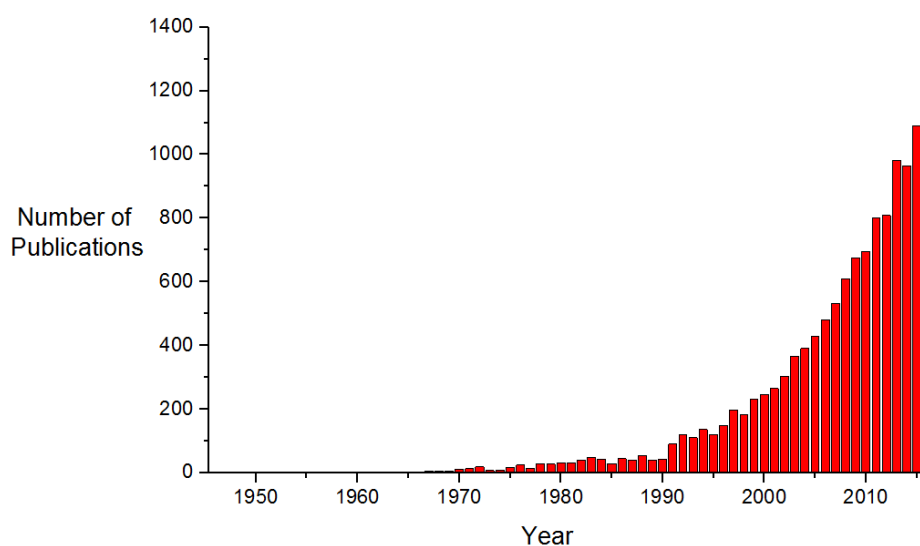
Scheme 2.2

Further developments in transition metal-catalysed transfer hydrogenation came from Sasson and Blum, who in the 1970s reported the reduction of a series of α,β -unsaturated ketones mediated by a $[\text{RuCl}_2(\text{PPh}_3)_3]$ complex (Scheme 2.3).¹⁶⁻¹⁸ It was later shown by Bäckvall that the addition of sodium hydroxide allowed this reaction to be carried out at a reduced temperature of 82 °C, with only 0.1 mol% of the ruthenium catalyst required.¹⁹



Scheme 2.3

Over the last few decades, the amount of transfer hydrogenation methodology published has been increasing exponentially. Graph 2.1 shows the results of a Web of Science search for papers classified under the topic of “Transfer Hydrogenation”, and shows an almost exponential increase over recent years, with 1225 papers published on the subject in 2016.²⁰

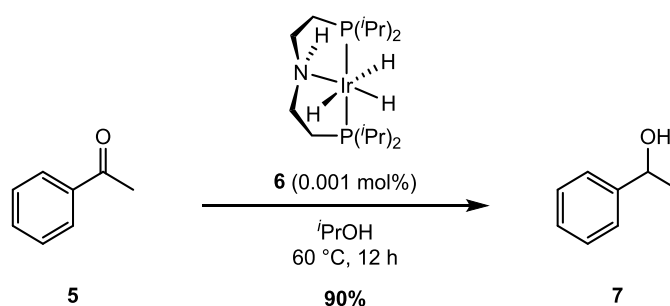


Graph 2.1

This increase in interest means that a vast array of methods for achieving transfer hydrogenation have been reported. More recent transition metal-catalysed processes have involved iron,^{21,22} ruthenium,^{23,24} cobalt,^{25,26} and palladium catalysis.^{27,28} Organocatalytic methods have also been reported.^{29,30} Undoubtedly, however, a considerable proportion of the most active catalysts are iridium-based, and iridium-catalysed transfer hydrogenation processes have received a vast amount of attention over the last decade.^{31,32} The increasing body of research on transfer hydrogenation has been extensively reviewed in recent years,^{3,33,34} and an exhaustive overview of modern methodology is beyond the scope of this section. For this reason, the next two sections will focus specifically on the use of iridium catalysts in transfer hydrogenation processes.

Iridium Catalysis of Transfer Hydrogenation: Reduction of Carbonyls

Following the report by Mestroni and co-workers on the use of an iridium phenanthroline complex in the reduction of ketones in 1980,^{35,36} significant attention has turned to the use of iridium catalysts for the reduction of carbonyl groups. In the majority of cases, reactions take place in *iso*-propanol, which acts both as solvent and as hydrogen donor. For example, in 2006 Abdur-Rashid and co-workers reported that the stable complex **6**, bearing a P^NP pincer ligand, was an exceptionally efficient catalyst for the reduction of ketones, even at loadings as low as 0.001 mol% (Scheme 2.4).³⁷ Notably, with an increase in catalyst loading to 0.5 mol%, the reaction could be carried out at room temperature; transfer hydrogenation processes are typically run at 80 °C or higher to encourage the removal of the acetone byproduct, which drives the reaction forward.



Scheme 2.4

While phosphine-based ligands have made frequent appearances in transfer hydrogenation methodology,³⁸ in recent years the field has been increasingly dependent on the use of iridium–NHC catalysts. For several decades, Crabtree’s catalyst **8** has been an industry standard catalyst for alkene hydrogenation, and in 2001 Nolan and co-workers reported the use of its NHC analogue **9**, as a transfer hydrogenation catalyst.³⁹

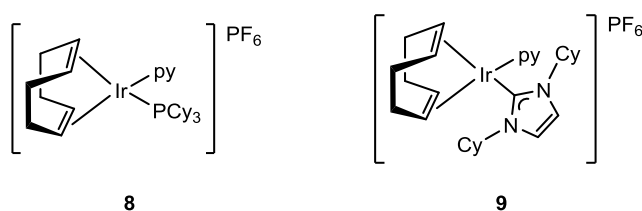
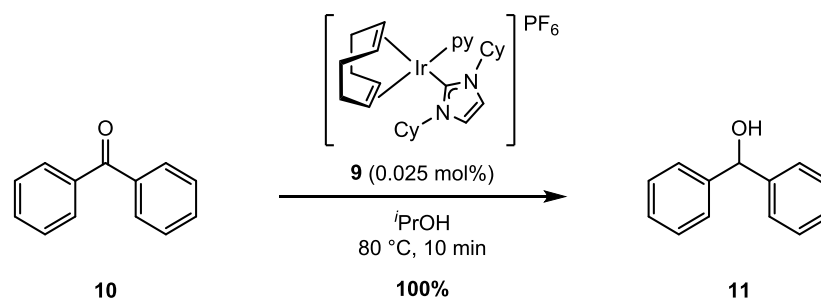


Figure 2.1

Complex **9**, which bears a cyclohexyl-substituted NHC in place of the phosphine ligand in **8**, exhibited high activity in the reduction of a range of ketones, with the reduction of benzophenone **10** proceeding to full conversion in just 10 minutes (Scheme 2.5). The reduction of alkenes and nitro- groups, also by transfer hydrogenation, was also reported to be catalysed by **9**.



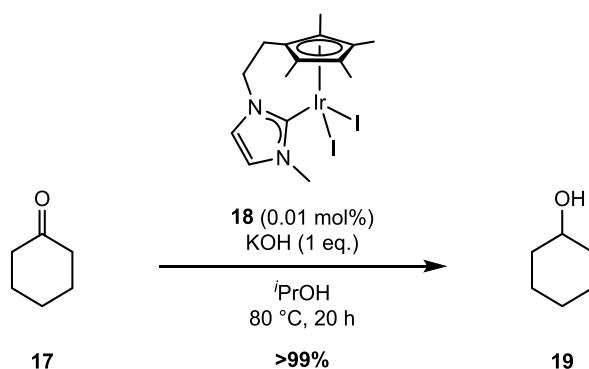
Scheme 2.5

The use of bis-NHC ligands was highlighted by Crabtree and co-workers, who in 2002 reported the use of neutral complexes **12–16** as highly active catalysts for ketone reduction (Table 2.1).⁴⁰ Tuning of the NHC wingtip substituents, R, had a notable effect on catalyst activity, with the greatest turnover frequency (TOF) being observed for catalyst **15**, bearing neopentyl substituents (Entry 4).

Table 2.1

Entry	Catalyst	R	Time / min	TOF / h ⁻¹
1	12	Me	90	2000
2	13	ⁿ Bu	90	2000
3	14	ⁱ Pr	120	1000
4	15	Neopentyl	4	50,000
5	16	Benzyl	>1200	<10

In an interesting expansion of iridium–NHC catalysis, Royo and co-workers prepared complex **18**, which contained the first NHC ligand functionalised with a Cp* unit.⁴¹ **18** was employed in the reduction of a series of ketones, exhibiting high activity with catalyst loadings as low as 0.01 mol% (Scheme 2.6).



Scheme 2.6

In a key 2013 paper, Gülcemal and co-workers disclosed the preparation of a series of iridium complexes bearing NHCs with high levels of steric congestion (Figure 2.2).⁴² Notably, while the NHC substituents are sterically demanding, due to their benzyl substituents, they remain relatively flexible when compared to bulky aryl-substituted NHCs.

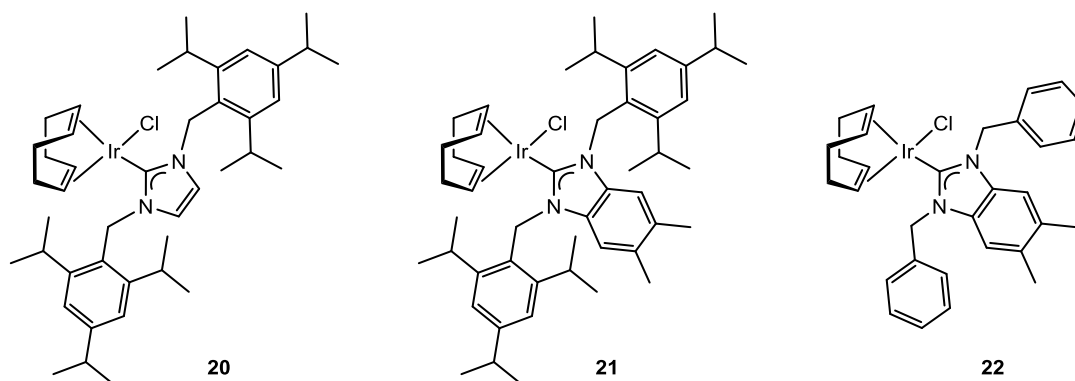
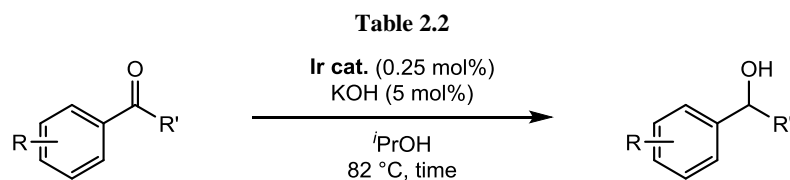


Figure 2.2

Complexes **20–22** were tested in the transfer hydrogenation of a range of ketones and their activity compared; selected results are displayed in Table 2.2.



Entry	Substrate	Catalyst	Time / min	Yield / %	TOF / h ⁻¹
1		20	2	95	11400
2		21	2	>99	12000
3	23	22	5	>99	4800
4		20	5	>99	4800
5	24	21	5	98	4800
6		22	10	>99	2400
7		20	10	>99	2400
8	25	21	5	>99	4800
9		22	10	95	2280
10		20	15	96	1536
11	10	21	15	>99	1600
12		22	20	>99	1200

The concept of “bulky yet flexible” NHC ligands was first introduced by Glorius,⁴³ and has been shown to offer increased catalytic activity in a number of processes catalysed by transition metal NHC complexes.^{44–46} The conformational flexibility of these ligands is proposed to facilitate the generation of catalytically active species and stabilise coordinatively unsaturated intermediates, through agostic interactions or chelate formation *via* a hemilabile bond.

The concept of hemilabile interactions in iridium–NHC catalysis has been further investigated in recent years, with focus turning to the use of NHCs bearing weakly coordinating substituents.^{47,48}

Cavell and co-workers prepared a series of large-ring NHCs with methoxy-functionalised aryl substituents (**26–29**, Figure 2.3).⁴⁹

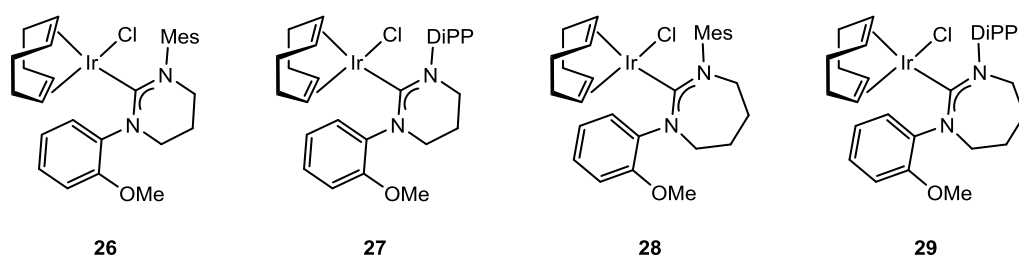
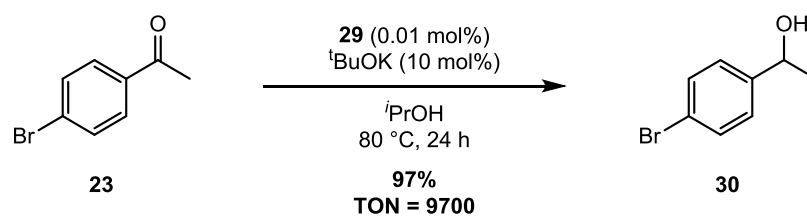


Figure 2.3

Complexes **26–29** were highly active in the transfer hydrogenation of a selection of acetophenone derivatives. While all 4 catalysts exhibited turnover numbers (TON) greater than 7000 at a loading of 0.01 mol%, complex **29**, bearing a 7-membered NHC with a di-*iso*-propylphenyl substituent, displayed the greatest activity in the reduction of 4-bromoacetophenone **23** (Scheme 2.7).



Scheme 2.7

The authors proposed that the catalytic activity was improved not only by the increased steric bulk of complex **29**, but also through a weak interaction between the methoxy oxygen atom and the iridium centre.

In a further, and thorough, investigation into the effect of donor atoms as NHC substituents, Jiménez and co-workers prepared a series of iridium(I) complexes with hemilabile NHC ligands bearing oxygen- or nitrogen-functionalised wingtips (**31–34**, Figure 2.4).⁵⁰

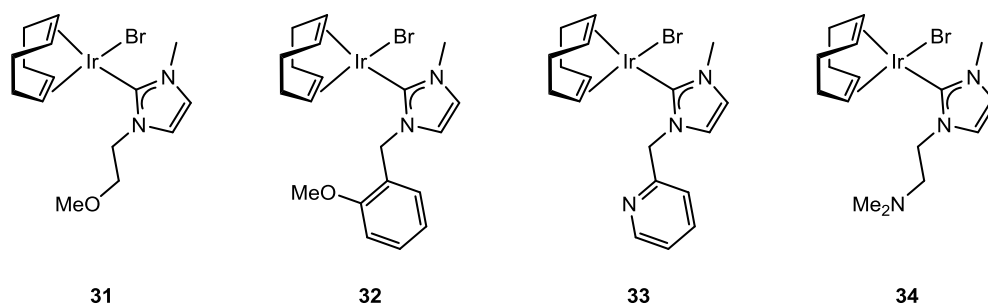
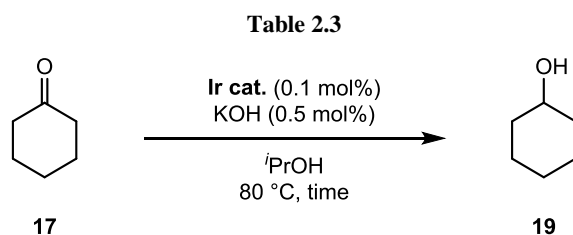


Figure 2.4

Complexes **31–34** were found to be efficient catalysts in the transfer hydrogenation of cyclohexanone (Table 2.3). Notably, complexes **31** and **32**, with oxygen-functionalised NHCs, displayed higher activity than **33** and **34**, bearing nitrogen-functionalised ligands. Of note is Entry 3, which demonstrates that oxygen-substituted catalyst **32** was able to catalyse the reaction at 40 °C, albeit with a longer reaction time required in this case. As discussed earlier, one drawback in many modern transfer hydrogenation methodologies is the requirement for temperatures of 80 °C or higher.



Entry	Catalyst	Time / min	Conversion / %	TOF / h ⁻¹
1	31	110	90	490
2	32	72	98	824
3*	32	1500	97	39
4	33	1730	90	31
5	34	408	94	138

* Carried out at 40 °C.

The authors speculated that while coordination of the oxygen or nitrogen donor atom can stabilise coordinatively unsaturated intermediates, dissociation of the hemilabile donor fragment is required for the formation of square planar alkoxide intermediates, and as such,

the increased chelating ability of the N-functionalised ligands could be responsible for their diminished activity. To probe this postulate further, cationic complexes **35** and **36** were prepared (Figure 2.5). The greater coordination ability of the nitrogen donor substituents was made clear by the successful formation of complex **36**, where the NHC is κ^2 -coordinated through the NHC carbon and the pyridine nitrogen. In complex **35**, on the other hand, the methoxy substituent remained uncoordinated, and the addition of acetonitrile was required to stabilise the resulting complex. Interestingly, the cationic complexes prepared showed greater efficiency as transfer hydrogenation catalysts than their neutral analogues; this was proposed to be due to their increased ability to generate alkoxide intermediates.

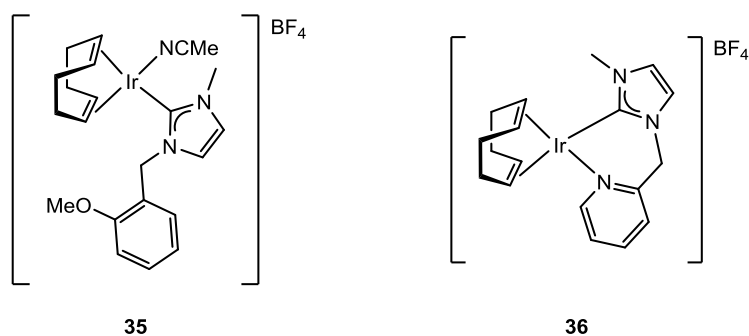
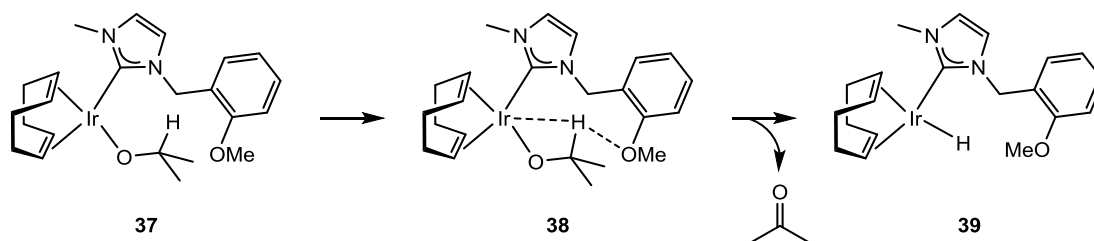


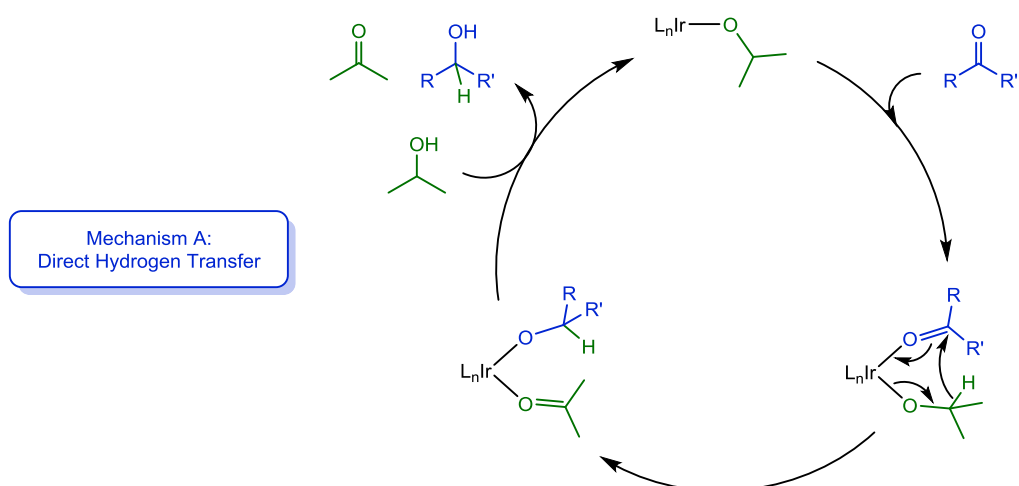
Figure 2.5

Mechanistic investigations supported the authors' proposal that the reduction of ketones catalysed by donor-functionalised NHC–Ir complexes proceeds *via* an iridium monohydride complex formed from *iso*-propoxide intermediate **37**. DFT studies were used to investigate the role of the donor substituents, and indicated the presence of an interaction between the methoxy substituent and the β -hydride of the alkoxide ligand (Scheme 2.8). This interaction serves to destabilise the intermediate alkoxide species, reducing the activation barrier to β -hydride elimination en route to the formation of the key iridium hydride intermediate **39**.



Scheme 2.8

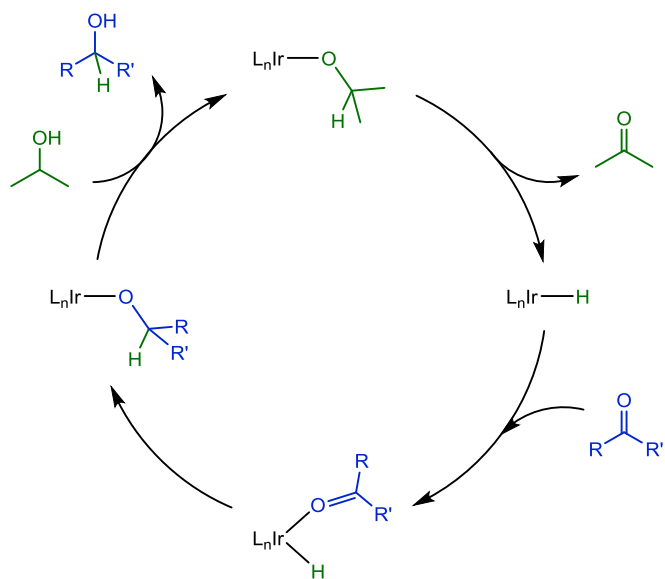
While mechanistic investigations lent support to the proposal that transfer hydrogenation catalysed by complexes **31–36** proceeded *via* an iridium monohydride intermediate, there are, in fact, three commonly proposed mechanisms for iridium-catalysed hydrogen transfer from alcohols to ketones.⁵¹ The first of these is shown in Scheme 2.9 and proceeds *via* direct hydride transfer from the alkoxide to the ketone, while both units are coordinated to the iridium centre. Computational studies carried out by Meijer and co-workers give support to the viability of this pathway.⁵²



Scheme 2.9

The second proposed mechanism is shown in Scheme 2.10, and is supported by deuterium labelling experiments conducted by Bäckvall and co-workers, who demonstrated that this was the favoured pathway for catalysis with iridium(I) complexes.⁵³ The pathway first proceeds *via* the formation of an iridium monohydride intermediate from an iridium *iso*-propoxide complex.⁵⁴ After coordination of the ketone, hydride transfer delivers the hydride to the carbonyl unit, and ligand exchange with the *iso*-propanol hydrogen donor regenerates the active alkoxide species.

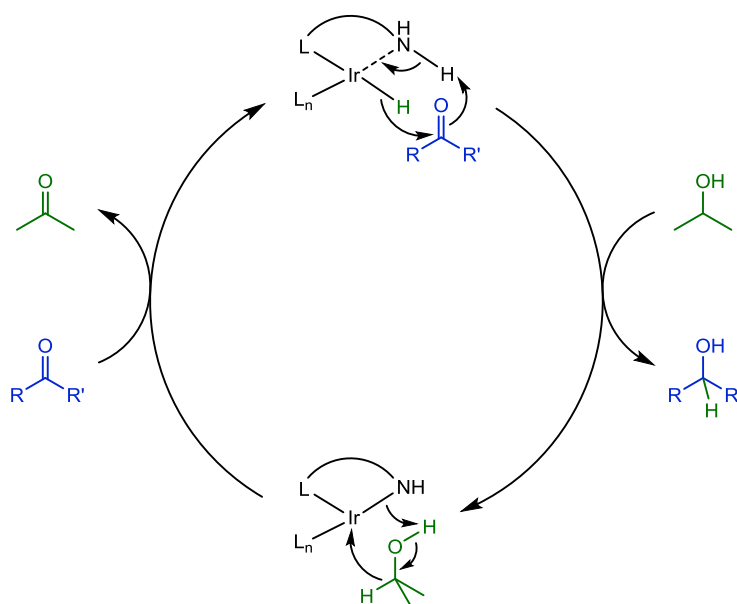
Mechanism B:
Monohydride Mechanism



Scheme 2.10

When one of the ligands present contains an available hydrogen atom, a third mechanism can take place; this is shown in Scheme 2.11. Here, the iridium hydride intermediate delivers a hydrogen atom to the carbonyl carbon; simultaneously, the ligand transfers the second hydrogen to the carbonyl oxygen. The reverse process then occurs to deliver one molecule of hydrogen to the iridium centre from the donor alcohol, regenerating the active catalyst.

Mechanism C:
Concerted Hydrogen Transfer



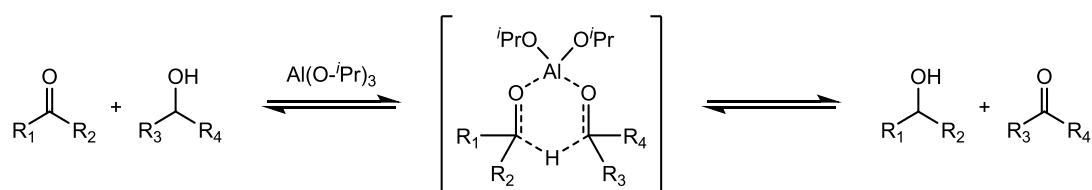
Scheme 2.11

While several groups have conducted mechanistic studies in order to understand the active pathway in the systems they have developed, at this stage all three mechanisms are still considered feasible. Indeed, it seems that the choice of ligand sphere determines which pathway will predominate for any particular iridium catalyst.

Iridium Catalysis of Transfer Hydrogenation: Oxidation of Alcohols

As discussed above, the use of metal-catalysed transfer hydrogenation processes offers mild and efficient methods to achieve the reduction of aldehydes and ketones. Of equal importance to the synthetic chemistry community, however, is the reverse process, involving the oxidation of alcohols to carbonyl compounds.⁵⁵ While alcohol oxidation is one of the most fundamental organic transformations, its methodology often requires stoichiometric quantities of harsh and toxic reagents, and as such, the development of milder, less harmful methods remains an attractive target. In recent years, the use of metal-catalysed hydrogen transfer processes has emerged as an efficient alternative to traditional oxidation methodology.

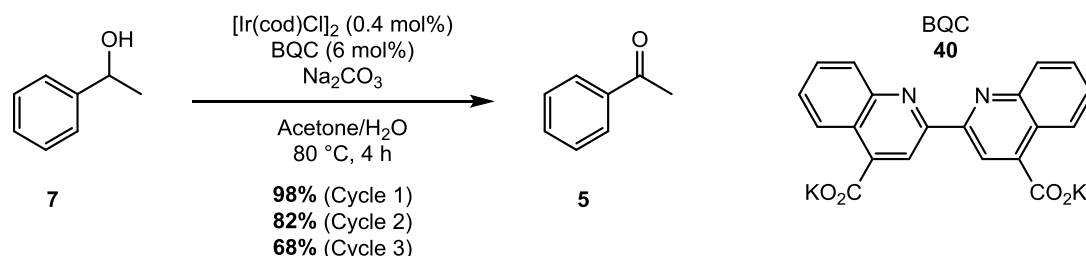
Originally described in 1937, the Oppenauer oxidation refers to the reverse reaction of the MPV reduction, and proceeds *via* the same transition state, as shown in Scheme 2.12.¹⁰ Just as MPV-type reductions are carried out with *iso*-propanol as the solvent and hydrogen donor, Oppenauer-type oxidations are typically carried out in acetone as the solvent and hydrogen acceptor.



Scheme 2.12

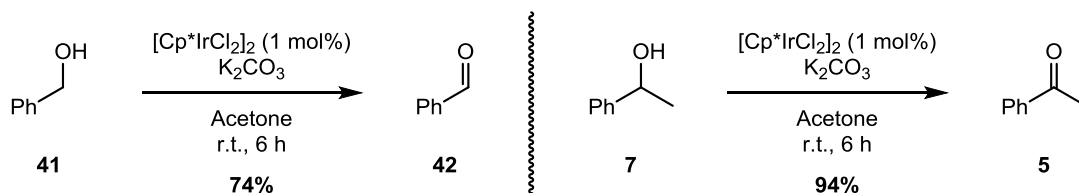
Since metal-catalysed hydrogen transfer reactions were first reported, a number of transition metal catalysts have been used successfully in the oxidation of alcohols. Since the development and widespread adoption of Crabtree's catalyst in the 1970s,⁵⁶ however, focus has shifted towards the use of iridium complexes as catalysts for alcohol oxidation *via* hydrogen transfer.^{31,57,58}

Ajjou reported the use of the $[\text{Ir}(\text{cod})\text{Cl}]_2$ dimer, in the presence of a biquinoline dicarboxylic acid salt **40** (BQC), as a successful catalyst system for the oxidation of secondary alcohols (Scheme 2.13).^{59,60} While the reaction was carried out using acetone as the oxidant, the catalyst system was soluble in water, and the aqueous phase could be recycled three times while maintaining high activity.



Scheme 2.13

Fujita and Yamaguchi demonstrated that the $[\text{Cp}^*\text{IrCl}_2]_2$ dimer could also be used as an effective catalyst for the oxidation of alcohols, again with acetone as both solvent and hydrogen acceptor (Scheme 2.14).⁶¹ While the transformation of both primary and secondary alcohols was successful, higher yields and lower catalyst loadings could be achieved with secondary alcohols.



Scheme 2.14

In a later publication, the authors reported that the inclusion of an *N*-heterocyclic carbene ligand improved the catalytic efficiency. For example, the use of complex **43** (Figure 2.6) was shown to allow notable reductions in catalyst loading with minimal decreases in yield, affording a catalyst system with a significantly improved turnover number.⁶² The increased nucleophilicity of the iridium monohydride intermediate generated is believed to be responsible for the improved activity of **43**. It was later noted that the use of complex **44**, in which the labile acetonitrile ligands have been replaced by chloride ligands, further increased yields at the same low catalyst loading of 0.025 mol%.⁶³

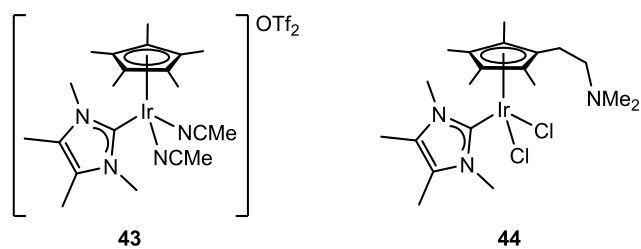
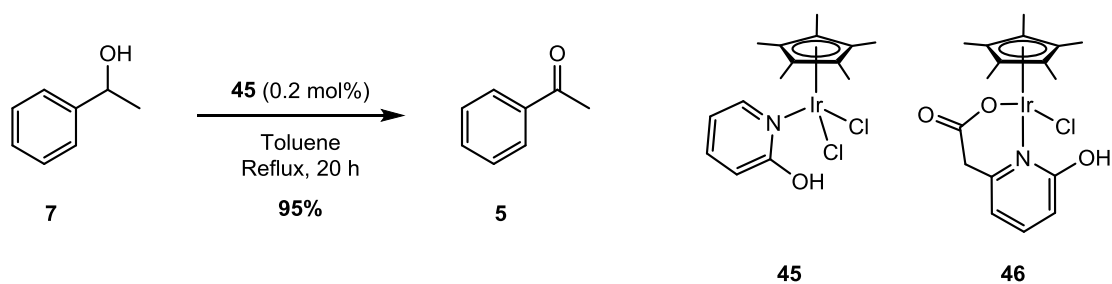


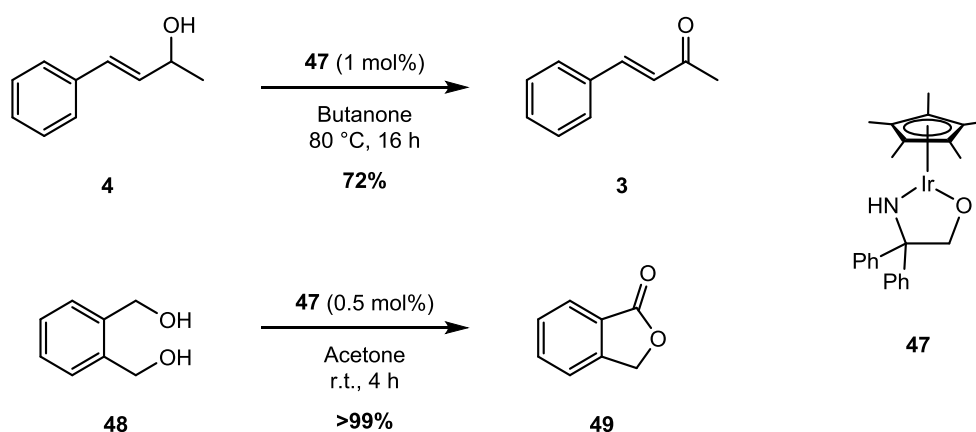
Figure 2.6

Fujita and Yamaguchi have also reported the use of complex **45**, a Cp*Ir catalyst bearing a 2-hydroxypyridine ligand, as an effective catalyst for the oxidation of secondary alcohols (Scheme 2.15).⁶⁴ A later modification of this ligand motif, reported by Rauchfuss and Wilson, was also found to be effective, with catalyst **46**, bearing a carboxylate-functionalised 2-hydroxypyridine unit, also found to be an efficient catalyst.⁶⁵



Scheme 2.15

In a further example of the use of an N,O chelating ligand, Suzuki and co-workers demonstrated the efficiency of iridium aminoalkoxide catalyst **47** in the oxidation of primary alcohols (Scheme 2.16).⁶⁶ Reactions proceeded cleanly even in the presence of oxidatively labile sulfide substituents, and with no over-oxidation of the aldehyde products observed. The authors also showed that the oxidation of diols could be carried out, leading to the formation of lactones from the corresponding intermediate hydroxy aldehydes.⁶⁷



Scheme 2.16

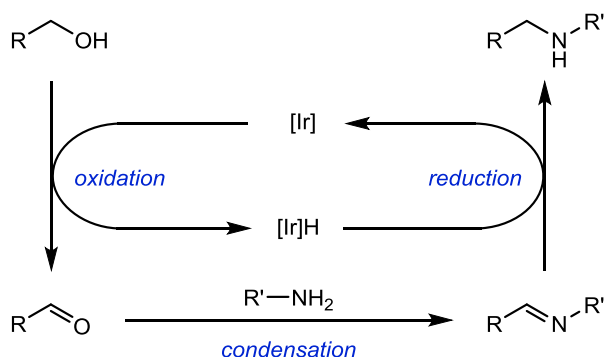
The advent of alcohol oxidation methodology *via* hydrogen transfer as an equally useful counterpart to carbonyl reduction has led to the development of a number of tandem reactions that combine oxidation and reduction methods. One key example of this is known as “hydrogen borrowing” or “hydrogen autotransfer”, which has emerged as an attractive technique for the activation and functionalisation of relatively inert substrate classes.^{68–72} For example, the metal-catalysed oxidation of alcohols *via* hydrogen transfer generates carbonyl compounds which can then react *in situ*. If the product of this reaction is another unsaturated species, reduction of this product can take place using the metal–hydride species generated by the initial oxidation step.

The versatility of the carbonyl group means it can be transformed into a range of alternative functional groups, such as imines, alkenes, and α -functionalised carbonyl compounds. The overall process, therefore, offers expedient access to amines, β -functionalised alcohols, and compounds containing new C–C bonds. The name “hydrogen borrowing” comes from the fact that the metal catalyst “borrows” two hydrogen atoms from the alcohol, before returning them to the reduction substrate. This results in an overall redox neutral process. This strategy has excellent atom efficiency; with no requirement for external oxidants or reductants, often the only byproduct is water. As an additional advantage, it allows for the transformation of alcohols, which are typically poor electrophiles, without the need for activation processes such as tosylation.

C–C and C–N Bond Formation *via* Hydrogen Borrowing

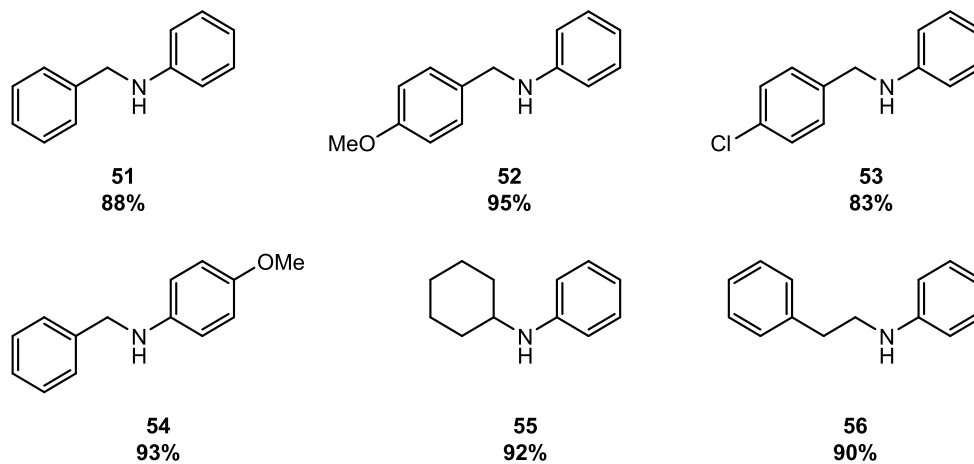
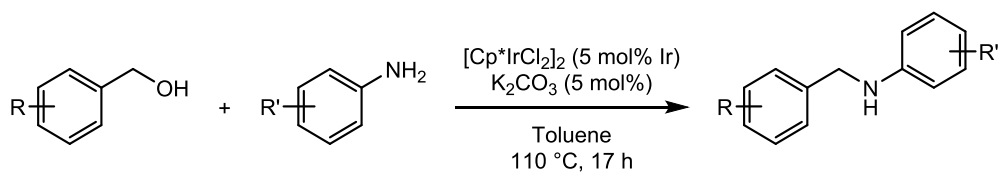
The synthesis of amines is of enormous importance to the organic chemistry community. The biological activity of nitrogenous molecules means that amines are extremely important pharmacophores in the field of drug discovery. Indeed, recent estimates show that approximately 90% of the top 200 best-selling drugs in the USA contain C–N bonds.⁷³ As a result, research activity remains focussed on the development of efficient methods for preparing amines.⁷⁴

While there are myriad procedures available for the synthesis of amines, which have been extensively reviewed,⁷⁴ a number of traditional methods are plagued with problems, such as the use of harsh alkylating agents or the formation of stoichiometric quantities of byproducts. The use of hydrogen borrowing methodology, however, offers an attractive method for the direct transformation of alcohols into amines without the need for stoichiometric additives and with no net change of oxidation state.^{31,71,72} As shown in Scheme 2.17, after activation of the alcohol *via* metal-catalysed oxidation, the generated carbonyl compound can undergo condensation to form an imine, which is then reduced. Overall, the formation of a new C–N bond occurs, with water as the only byproduct.



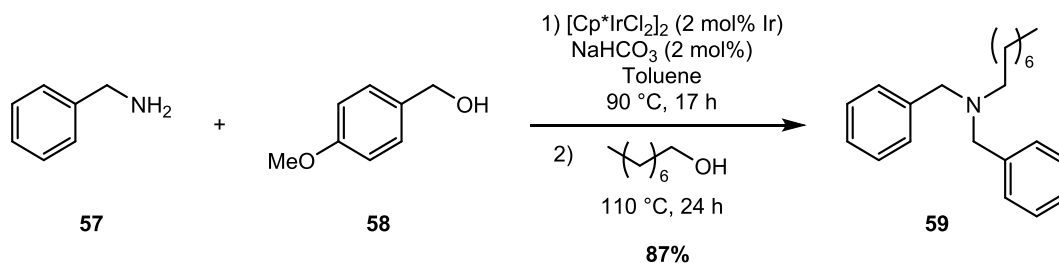
Scheme 2.17

Over the last few decades, C–N bond formation *via* hydrogen borrowing has been reported with a number of transition metal catalysts including ruthenium,^{68,75–77} rhodium,⁷⁸ and platinum.⁷⁹ In the field of iridium catalysis, the groups of Fujita and Yamaguchi are responsible for several key advances in the *N*-alkylation of amines with alcohols, and the most widely used catalyst is [Cp*IrCl₂]₂.^{80–83} The alkylation of aniline **50** and its derivatives was first reported with a series of primary, secondary, and benzylic alcohols, a selection of which are shown in Scheme 2.18.⁸¹



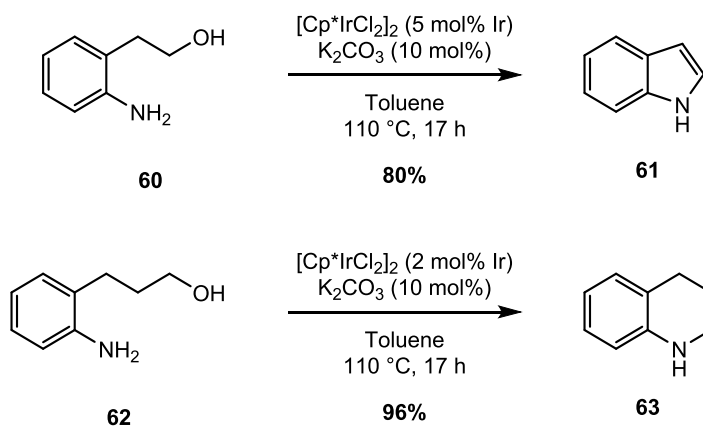
Scheme 2.18

This methodology has also been expanded to include the preparation of tertiary amines through sequential double *N*-alkylation, as shown in Scheme 2.19.⁸²



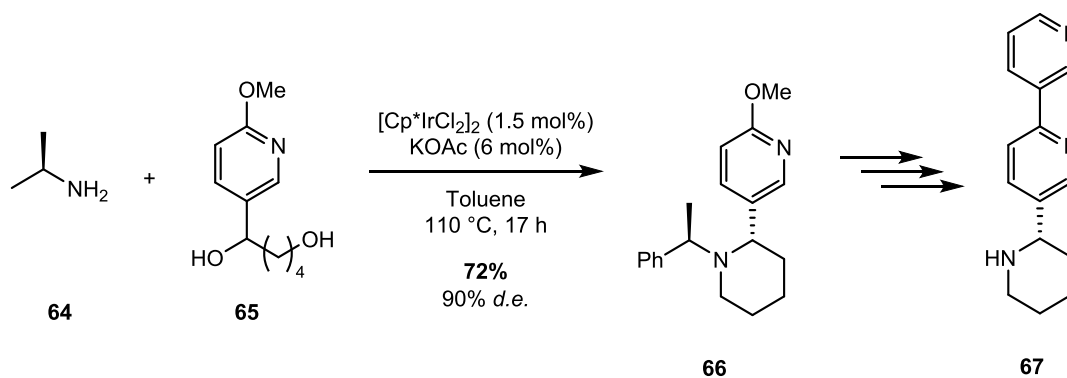
Scheme 2.19

In a further illustration of the utility of this process, the *N*-alkylation methodology was also applied to intramolecular cyclisation reactions. As shown in Scheme 2.20, indole **61** and tetrahydroquinoline **63** were prepared in excellent yields from the relevant amino alcohol starting materials. It should be noted that the formation of **61** does not involve a final reduction process; instead, tautomerisation of the generated imine, leading to rearomatisation, is favoured.



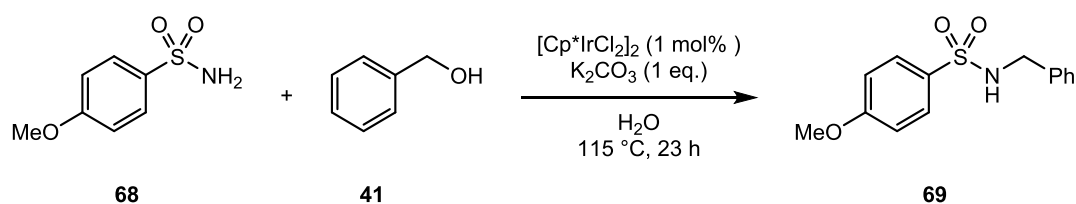
Scheme 2.20

Intermolecular cyclisation *via* the reaction of amines with diols such as ethylene glycol has also been carried out, with promising results.⁸⁴ In a particularly impressive example, this methodology was employed by Trudell and co-workers in the diastereoselective synthesis of noranabasamine **67**.⁸⁵ As depicted in Scheme 2.21, the reaction of diol **65** with chiral amine **64** proceeded to afford piperidine **66** in good yield. A further three steps were required to furnish the desired natural product, an alkaloid isolated from the Columbian poison dart frog.



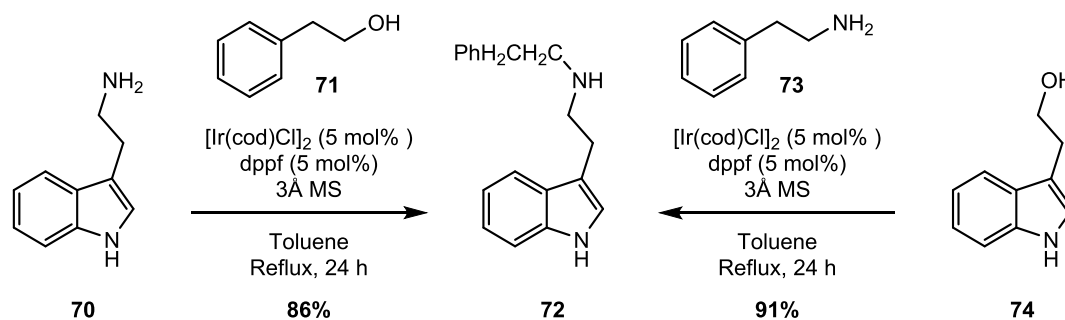
Scheme 2.21

The formation of C–N bonds *via* hydrogen borrowing is not limited to the use of amines as nucleophiles. For example, the alkylation of sulfonamides with alcohols has also been reported.⁸⁶ Williams and co-workers have demonstrated that this reaction proceeds efficiently using water as a solvent (Scheme 2.22).⁸⁷ Amine alkylation was also found to occur smoothly under these conditions, even in the absence of base.



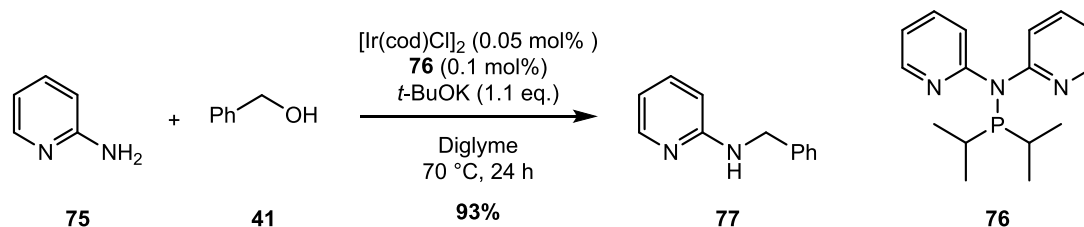
Scheme 2.22

The alternative iridium dimer $[\text{Ir}(\text{cod})\text{Cl}]_2$ has also found widespread use as a catalyst for *N*-alkylation reactions. Williams and co-workers reported the use of $[\text{Ir}(\text{cod})\text{Cl}]_2$, with a dpfp ligand, in the *N*-alkylation of phenylethylamine with alcohols.⁸⁸ In one particularly interesting example, this methodology was used for the preparation of *N*-alkyl tryptamine derivatives from both free tryptamine **70**, and the corresponding alcohol **74**, as shown in Scheme 2.23.



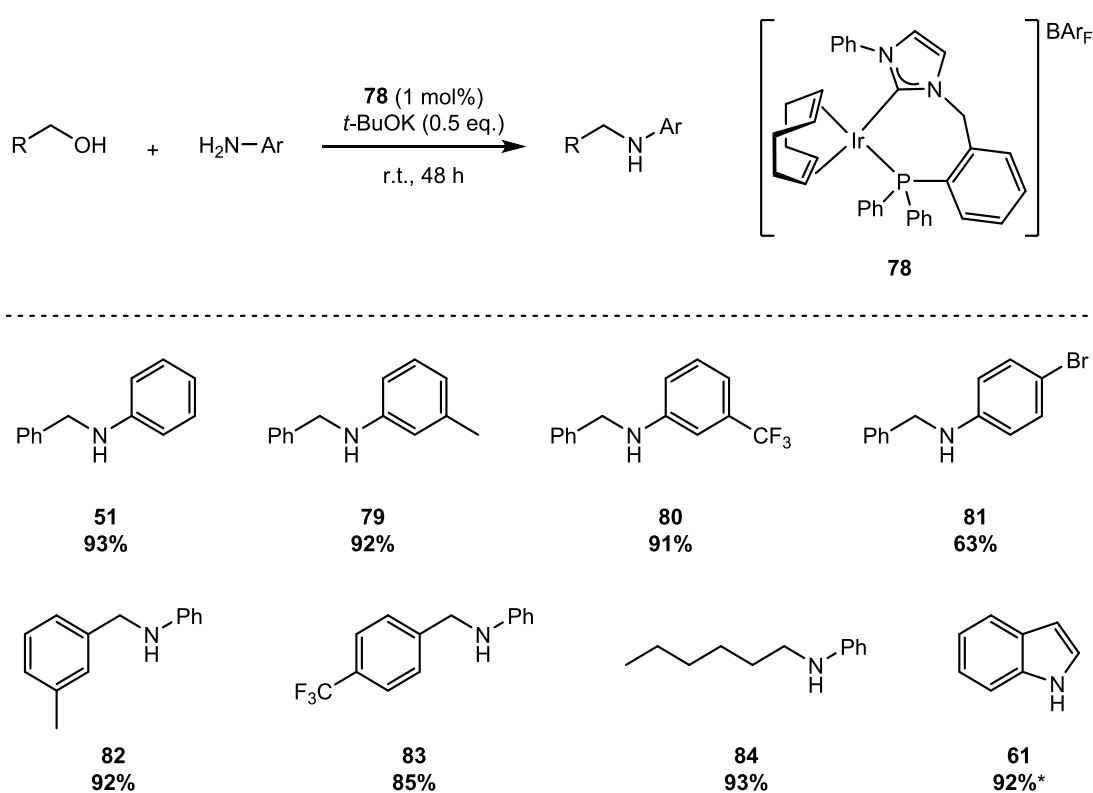
Scheme 2.23

Kempe and co-workers used a similar catalyst system in the *N*-alkylation of a series of amines.⁸⁹ It was demonstrated that the use of *N,P*-ligand **76** improved the reactivity of the iridium catalyst, and allowed the alkylation of 2-aminopyridine to proceed at a reduced temperature of 70 °C (Scheme 2.24).



Scheme 2.24

As discussed previously, the high temperatures that are often required are a major drawback to much modern transfer hydrogenation methodology, and the development of mild conditions for *N*-alkylation remains an attractive target. In 2013, Andersson and co-workers reported a solvent-free alkylation of anilines that proceeded efficiently at room temperature.⁹⁰ The iridium(I) catalyst used, **78**, features a bidentate NHC–phosphine ligand. As shown in Scheme 2.25, **78** was used to catalyse the conversion of a range of aromatic amines to their secondary amines with a series of alcohols. The reaction showed excellent functional group tolerance, proceeding smoothly with both electron-donating and electron-withdrawing substituents. Intramolecular cyclisation to form indole **61** was also carried out, albeit with the addition of diglyme solvent and with an increase in temperature to 80 °C.



* Carried out at 80 °C in diglyme

Scheme 2.25

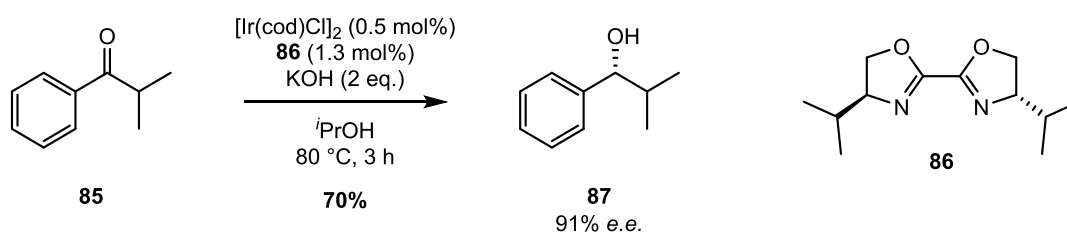
In summary, the use of iridium-catalysed hydrogen borrowing methodology in the activation of alcohols to electrophiles for amine alkylation offers a convenient and attractive route to the formation of new C–N bonds. The use of harsh alkylating reagents or stoichiometric oxidants can be avoided, and procedures are operationally simple. While many processes

still require high temperatures, Andersson's successful room temperature alkylation of amines with catalyst **78** is an important benchmark for C–N bond formation *via* hydrogen borrowing and offers exceptionally mild conditions for amine synthesis.

Iridium Catalysis of Asymmetric Transfer Hydrogenation

The asymmetric reduction of unsaturated compounds has long been regarded as one of the most useful transformations in synthetic organic chemistry.^{91,92} Typically, these reduction processes are carried out either catalytically, with the use of molecular hydrogen, or with the use of stoichiometric metal hydride reagents.¹ In recent years, however, transfer hydrogenation has emerged as a popular technique for the asymmetric reduction of unsaturated moieties.^{33,93–96} As discussed previously, metal-catalysed hydrogen transfer is a highly useful tool for the reduction of carbonyl compounds or imines, and its operational simplicity and reduced risks make it an attractive alternative to traditional reduction methods. The control of enantioselectivity in transfer hydrogenation reactions, therefore, offers a convenient route to enantioenriched alcohols or amines.

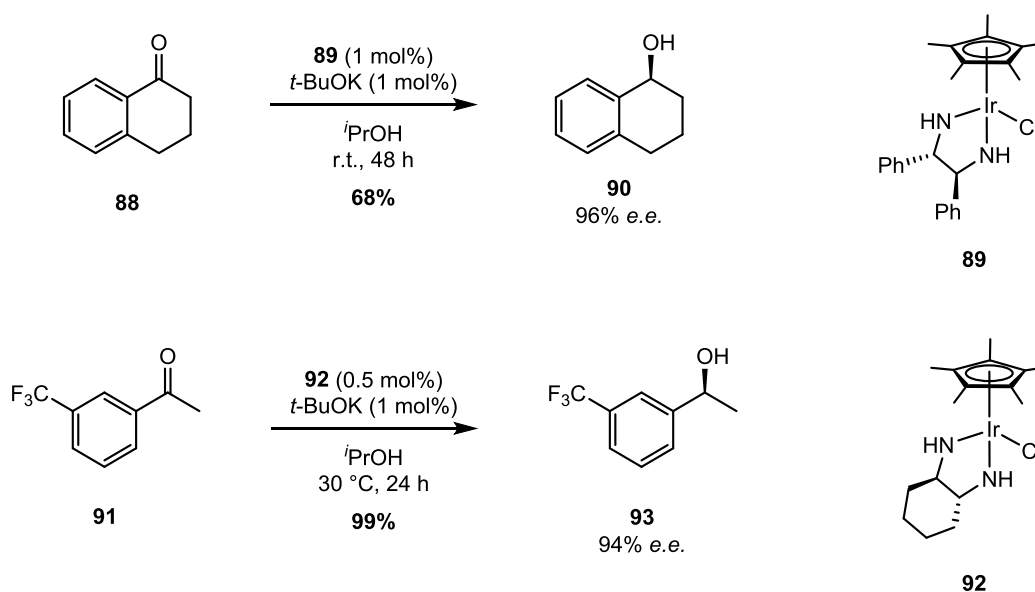
For many years, the field of asymmetric transfer hydrogenation was mostly dominated by the use of chiral ruthenium catalysts.^{97,98} A number of reports on the use of iridium catalysts for the asymmetric reduction of carbonyls or imines have, however, since emerged. As far back as 1991, Pfaltz and co-workers reported the asymmetric transfer hydrogenation of acetophenone derivatives with an $[\text{Ir}(\text{cod})\text{Cl}]_2$ catalyst and a bisoxazoline ligand (Scheme 2.26).⁹⁹



Scheme 2.26

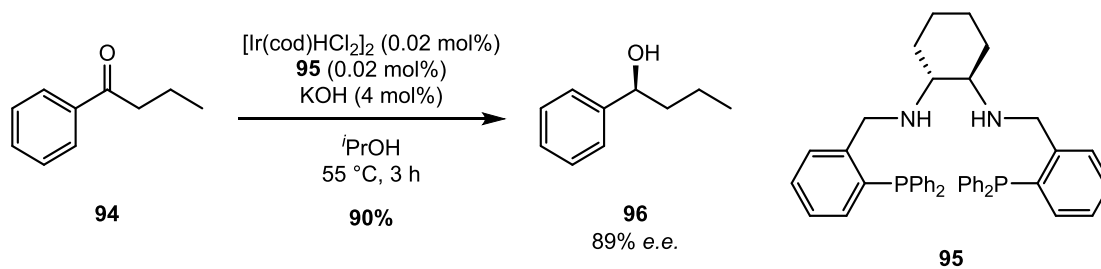
The majority of methods developed for iridium-catalysed asymmetric transfer hydrogenation have used either Ir(cod) or IrCp* complexes in conjunction with a chiral ligand. For example, chiral Cp* complexes **89** and **92** were reported, by Mashima and Ikariya, respectively, to be effective catalysts for the asymmetric reduction of ketones, as shown in

Scheme 2.27.^{100,101} Both catalysts were developed from the analogous rhodium complexes, which had also shown excellent activity.



Scheme 2.27

Excellent enantioselectivities were observed by Gao and co-workers, who reported the use of bidentate ligand **95** in the Ir(III)-catalysed reduction of propiophenone.^{102,103} As shown in Scheme 2.28, high yields and enantiomeric excesses were obtained at low catalyst loadings of 0.02 mol%. It was later reported that this reaction could also proceed without base.¹⁰⁴



Scheme 2.28

A number of other chiral bidentate ligands have been used for asymmetric transfer hydrogenation with an $[\text{Ir}(\text{cod})\text{Cl}]_2$ catalyst. These include bisoxazolines,^{105,106} aminooxazolines,¹⁰⁷ diamines,^{108,109} NHCs,¹¹⁰ and aminosulfides,¹¹¹ and a selection of these are shown in Figure 2.7. Ligands **100**, **104**, and **105** were found to be particularly efficient, with all three providing enantiomeric excesses well above 90%.^{111–113}

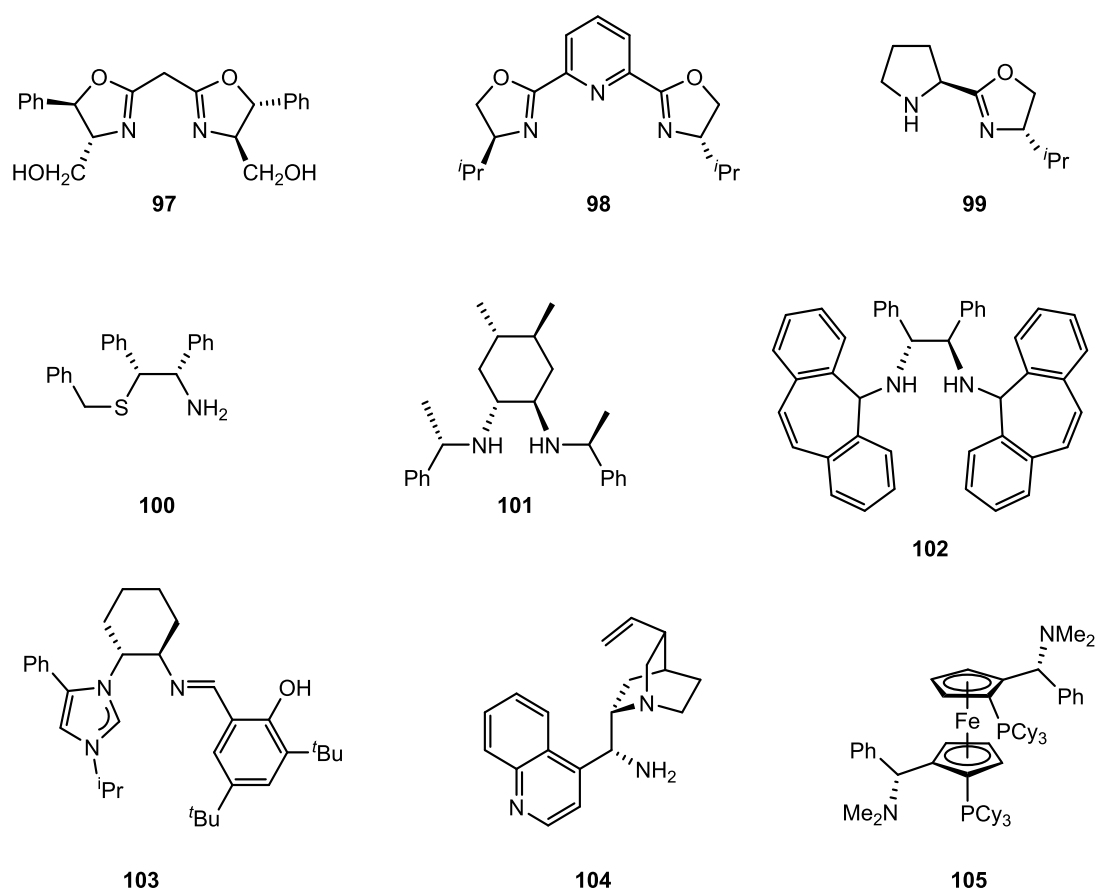
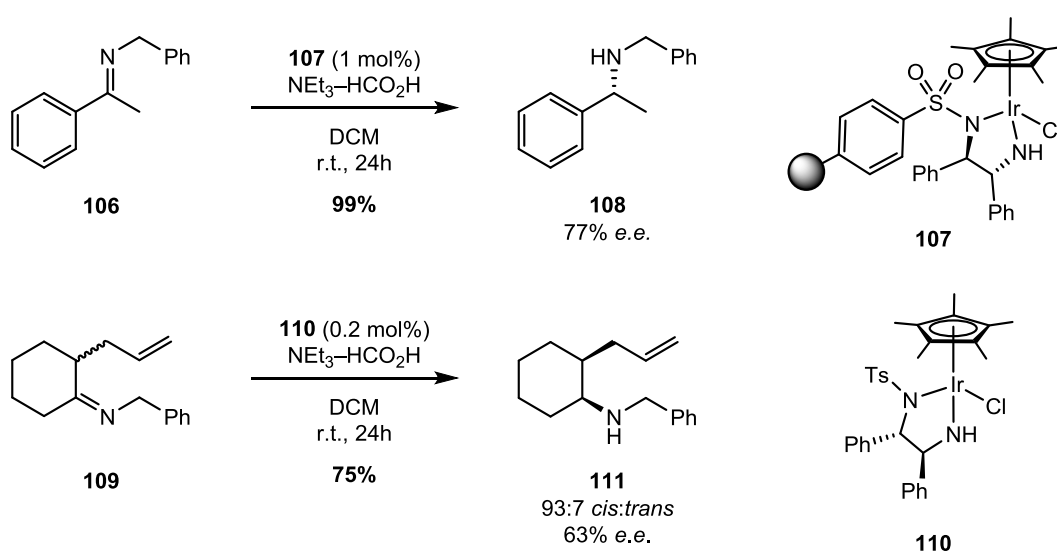


Figure 2.7

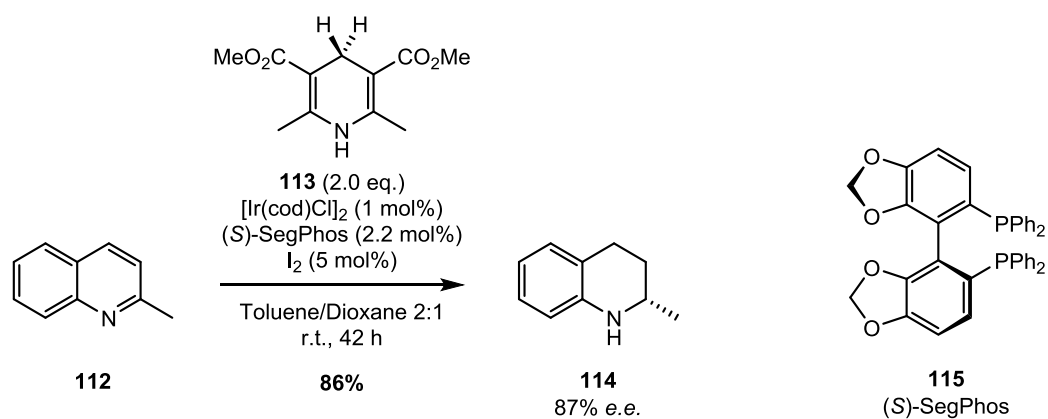
The importance of nitrogenous molecules as drug scaffolds, as well as the efforts being made by the pharmaceutical industry to increase the sp^3 character of drug candidates,¹¹⁴ means that the synthesis of chiral amines is an area of particular interest to synthetic organic chemists.¹¹⁵ The asymmetric reduction of imines is, therefore, an attractive transformation and remains the focus of significant research attention. While the asymmetric transfer hydrogenation of ketones was, for several years, dominated by catalysis by ruthenium or rhodium complexes, a varied selection of iridium-catalysed methods has since been developed. The asymmetric transfer hydrogenation of imines, on the other hand, remains largely dependent on ruthenium catalysis, and the use of analogous iridium complexes has often led to lower enantioselectivities.^{94,116} Nevertheless, in recent years progress has been made in the iridium-catalysed asymmetric reduction of imines *via* transfer hydrogenation, using a number of strategies.

Polymer-supported aminosulfonamide complex **107** was employed by Haraguchi and co-workers in the asymmetric reduction of imine **106**, as shown in Scheme 2.29.¹¹⁷ Instead of the typical *iso*-propanol hydrogen donor/solvent system, the reaction was carried out in dichloromethane with a triethylamine–formic acid mixture as the hydrogen donor. A similar system was used in the dynamic kinetic resolution of imine **109** with complex **110**.¹¹⁶ While moderate enantioselectivities were observed in both of the transformations shown in Scheme 2.29, in both examples selectivity could be improved by the use of the analogous ruthenium complex, and thus progress was still required in the field of iridium catalysis.



Scheme 2.29

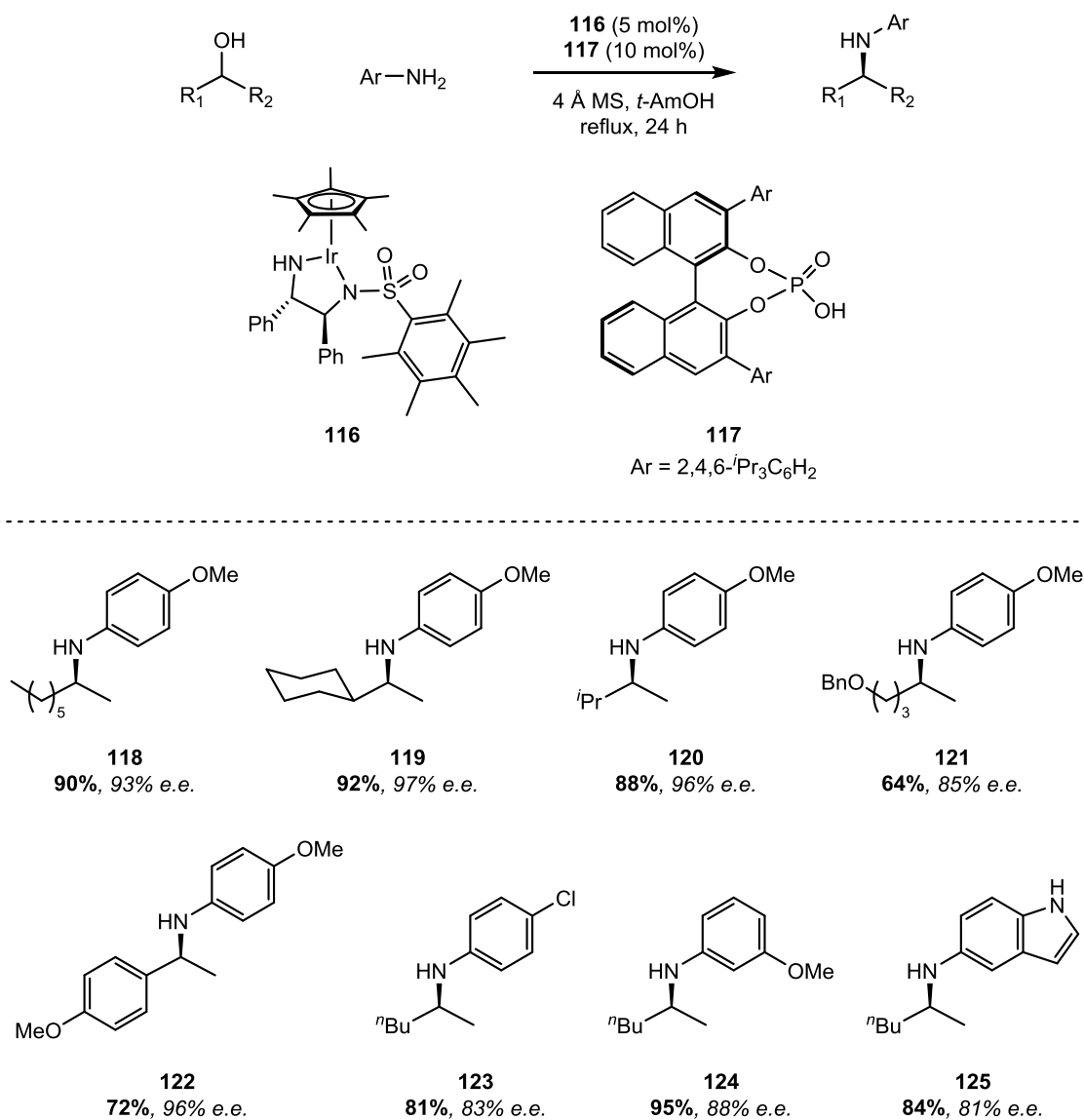
Zhou and co-workers have reported the use of Hantzsch esters as hydrogen donors in the asymmetric transfer hydrogenation of quinolines.¹¹⁸ Using a $[\text{Ir}(\text{cod})\text{Cl}]_2$ catalyst and a chiral SegPhos ligand, the reduction of 2-methylquinoline **112** proceeded smoothly, affording chiral amine **114** in good yield and with an 87% *e.e.* (Scheme 2.30).



Scheme 2.30

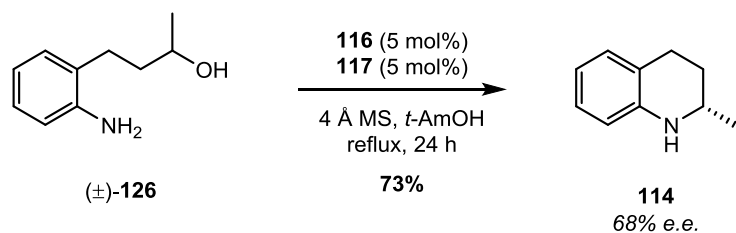
The asymmetric reduction of unsaturated moieties *via* transfer hydrogenation can also be used as part of a hydrogen borrowing strategy in the formation of new C–N, C–O, or C–C bonds. While the asymmetric transfer hydrogenation of imines remains relatively underdeveloped, reports on the synthesis of chiral amines *via* hydrogen borrowing have nevertheless emerged.

In 2014, Zhao and co-workers reported the use of chiral phosphoric acid **117**, along with an iridium aminosulfonamide complex **116**, in the first enantioselective formation of secondary aryl amines from alcohols (Scheme 2.31).



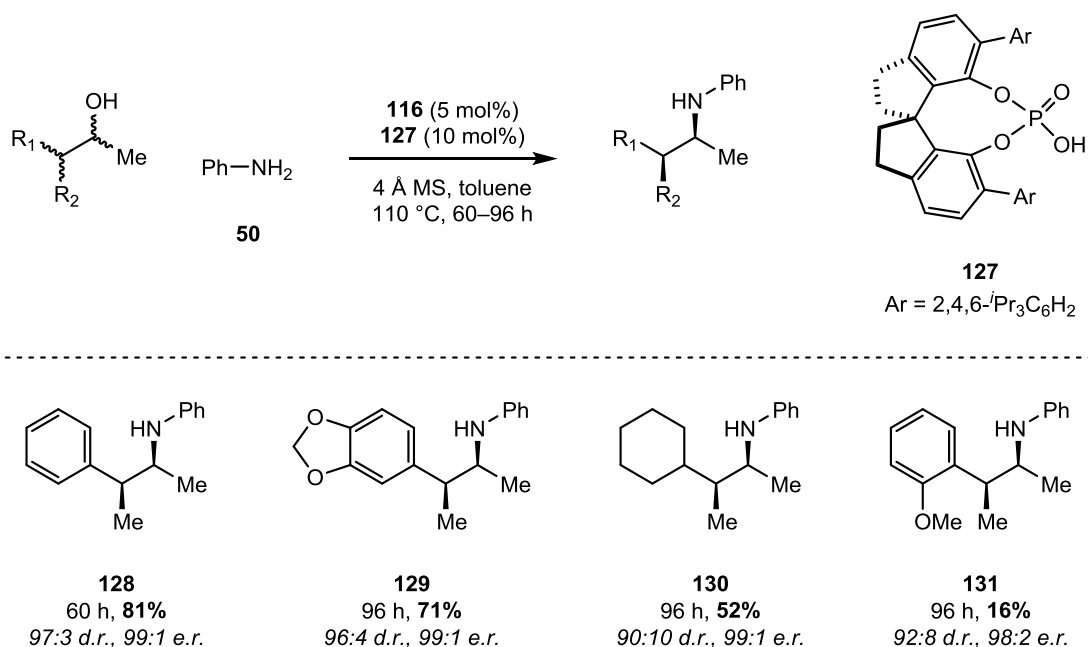
Scheme 2.31

As shown above, this methodology was used in the successful reaction of a series of alkyl and aryl substrates, with good functional group tolerance observed and enantiomeric excesses as high as 97% achieved. It was proposed that the high enantioselectivity observed in these processes could be attributed to cooperation between the iridium catalyst and the chiral phosphoric acid. The authors also applied their optimised conditions to the intramolecular cyclisation of **126**, affording tetrahydroquinoline **114** in good yield and a promising enantiomeric excess of 68% (Scheme 2.32).



Scheme 2.32

This methodology was further expanded in the use of a dynamic kinetic amination strategy, reported in 2015.¹¹⁹ Here, a series of α -branched alcohols, each a mixture of four isomers, underwent racemisation and were successfully converted to chiral amines with enantiomeric excesses as high as 97%, as shown in Scheme 2.33.



Scheme 2.33

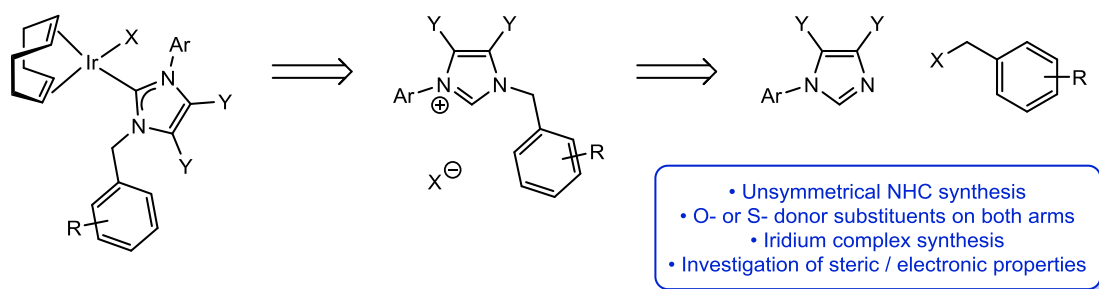
To conclude, iridium-catalysed transfer hydrogenation is an extremely useful method for the reduction or oxidation of organic compounds, proceeding with low catalyst loadings, and avoiding the toxic reagents often required in stoichiometric quantities for traditional oxidation or reduction methodology. The use of borrowing hydrogen methodology, in which a typically inert alcohol substrate can be activated through oxidation and can react as the corresponding carbonyl compound, before reduction of the product, is an attractive means by which to use alcohols as electrophiles. This strategy has been widely used in the *N*-

alkylation of amines with alcohols, offering expedient access to useful amine compounds without the requirement for harsh alkylating reagents. Over recent years, a number of iridium complexes have been reported to be excellent catalysts for the *N*-alkylation of amines *via* hydrogen borrowing. While one disadvantage of current methodology is that high temperatures are typically required, the development of milder conditions for transfer hydrogenation remains the focus of significant research attention. Recently, the use of chiral iridium complexes or ligands in asymmetric transfer hydrogenation has emerged as an attractive route by which to access chiral alcohols and amines. While methods for asymmetric iridium catalysis are still less widely reported than those for alternative transition metals, excellent progress has been made in recent years, and iridium-catalysed hydrogen borrowing is becoming a feasible strategy for the synthesis of chiral amines.

Proposed Work

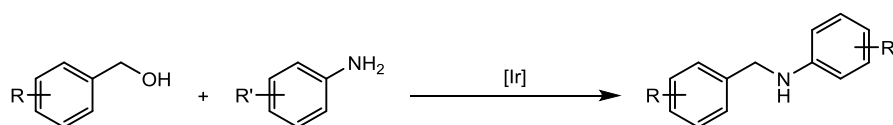
The last decade has seen transfer hydrogenation reactions become a useful tool in organic synthesis, allowing for the reduction and subsequent functionalisation of carbonyl or imine compounds without the requirement for gaseous H₂. Among the methods for homogeneous catalysis of hydrogen transfer, iridium-catalysed methodology has been seeing increased interest recently.^{3,31} In particular, there have been several key examples of the use of iridium NHC complexes as transfer hydrogenation catalysts.^{40,42,50} As discussed in more detail in Chapter 1, in recent years Kerr group catalysts have shown excellent activity in hydrogen isotope exchange and hydrogenation reactions.¹²⁰⁻¹²⁶ Within the group, however, work is ongoing to design and prepare analogues of our complexes and to further increase their reactivity. As part of this programme of work, we therefore aim to design a series of novel NHC ligands and test their corresponding complexes as catalysts in hydrogen borrowing methodology.

In the first instance, we will investigate the synthesis and reactivity of analogues of our group's neutral [Ir(cod)(NHC)X] complexes. Through our previous work, we have shown that the use of electron-rich and sterically demanding NHC ligands has increased catalytic activity. We aim to explore the use of ligands with similar properties in hydrogen borrowing reactions. Research by Jiménez and co-workers has demonstrated that donor-functionalised NHC ligands can offer increased activity in iridium-catalysed transfer hydrogenation processes.⁵⁰ A key part of our project, therefore, will involve the introduction of *N*-, *O*-, and *S*-donor substituents into our sterically demanding NHC ligands. We will first focus on the synthesis of unsymmetrical NHCs featuring one bulky aryl substituent and one benzyl substituent; this strategy will allow us to easily access a number of derivatives. The effects of hemilabile donor substituents on one or both arms of the NHC will be investigated. Our retrosynthetic strategy for the preparation of these ligands and complexes is shown in Scheme 2.34. As well as targeting the synthesis of a range of novel NHCs, we plan to thoroughly investigate their steric and electronic properties in the context of commonly used NHC ligands.



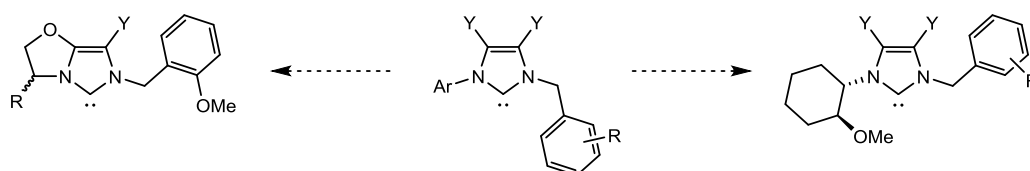
Scheme 2.34

Any novel NHCs prepared will be tested in iridium-catalysed hydrogen borrowing processes. We aim to focus on the use of neutral iridium(I) NHC/halide complexes; the lability of the halide ligands will be necessary in order to assess any hemilabile coordination from the NHC donor substituents. In the first instance, we aim to investigate the use of our complexes in the *N*-alkylation of anilines, as shown in Scheme 2.35, with the aim of developing a method that proceeds under milder conditions than those currently available within the literature.



Scheme 2.35

Lastly, a longer term aim is to expand any developed methodology to encompass asymmetric processes. Our focus will remain on the synthesis of NHCs with donor substituents, but the introduction of chirality will be targeted. We propose the use of the strategy outlined in Scheme 2.36, which will allow us to prepare chiral ligands with the hemilabile unit on either the chiral or achiral arm of the NHC. Any corresponding chiral iridium complexes synthesised will be screened in asymmetric variants of our hydrogen borrowing methodology.

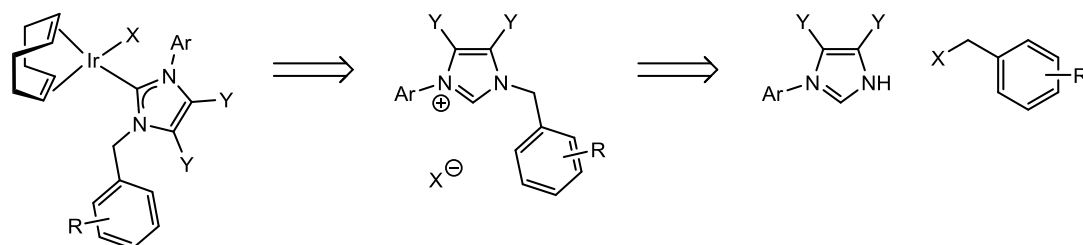


Scheme 2.36

Results and Discussion

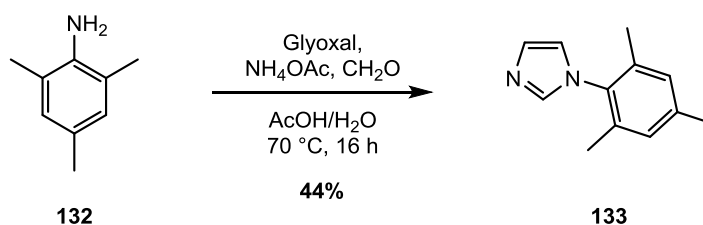
Design and Synthesis of Novel Ligands and Complexes

As the first step towards designing a range of transfer hydrogenation catalysts, we looked to synthesise a range of bulky, unsymmetrical NHC ligands containing donor substituents. In order to easily access a series of structurally diverse ligand motifs, it was initially decided to use the retrosynthetic strategy outlined in Scheme 2.37, focussing on NHCs with one aryl and one benzyl substituent. This would allow us to prepare a range of aryl imidazoles, which could then be coupled with various benzyl halides to afford a diverse series of imidazolium salts. A number of novel iridium complexes could then be prepared in a quick and efficient manner.



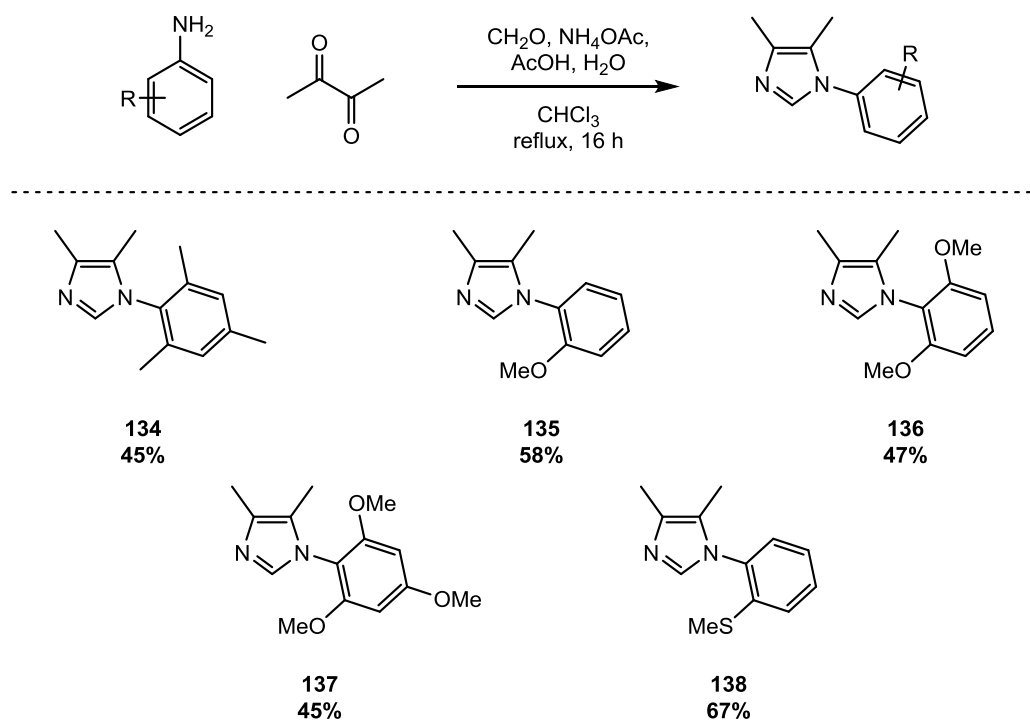
Scheme 2.37

We were keen to investigate the effects of the presence of donor substituents in both the aryl and benzyl units of the NHCs. In the first instance, therefore, a series of aryl imidazoles were prepared. As a benchmark example, mesityl imidazole **133** was first prepared as shown in Scheme 2.38. The moderate yield of 44% was considered sufficient here, given the capricious nature of such multicomponent reactions and the related difficulties associated with purification.



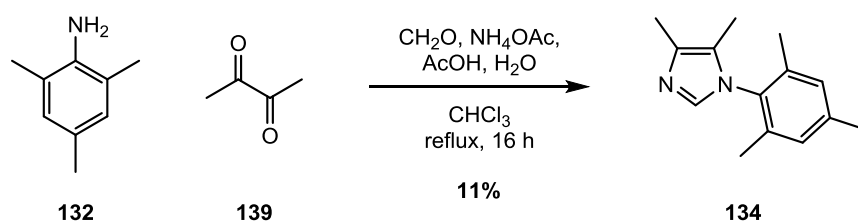
Scheme 2.38

As discussed previously, Kerr group investigations into the activity of neutral NHC/halide iridium complexes have shown that the introduction of two methyl groups on the NHC backbone can offer increased activity.¹²⁷ It has been widely reported in the literature that the electron-rich nature of NHC ligands is responsible for the high activity of their complexes in transfer hydrogenation reactions. It was therefore proposed to access a series of ligands based on a dimethyl imidazole motif, where the additional methyl substituents would offer increased electron donation from the NHC. As such, a range of aryl dimethyl imidazoles **134–138**, bearing oxygen- or sulfur-containing substituents, were prepared *via* multicomponent reaction as shown in Scheme 2.39.



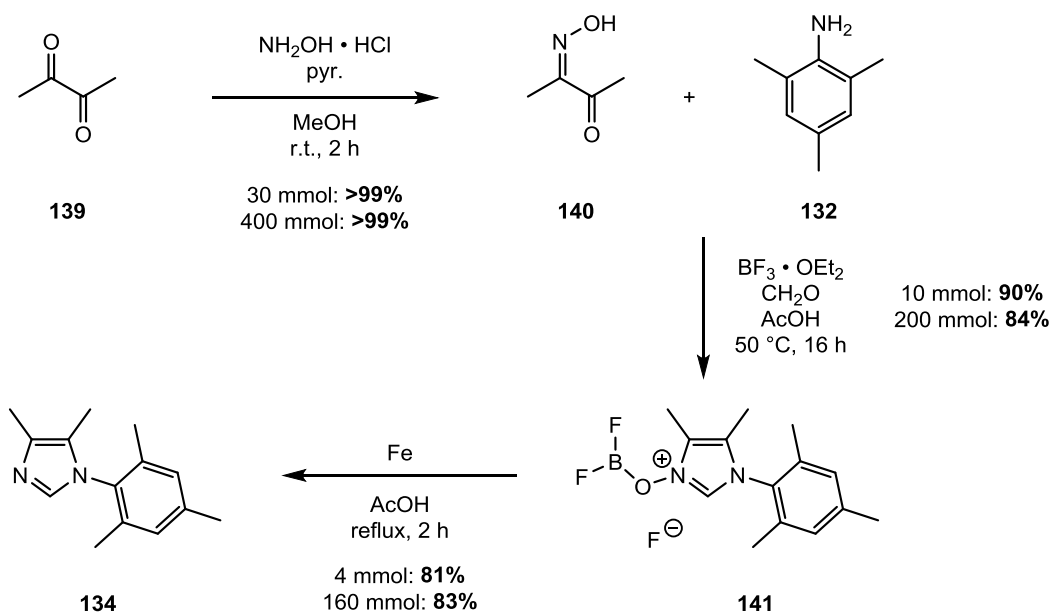
Scheme 2.39

At a later stage, the synthesis of mesityl dimethylimidazole **134** was repeated on a large scale of 180 mmol. Unfortunately, however, the yield was seen to drop to 11% (Scheme 2.40).



Scheme 2.40

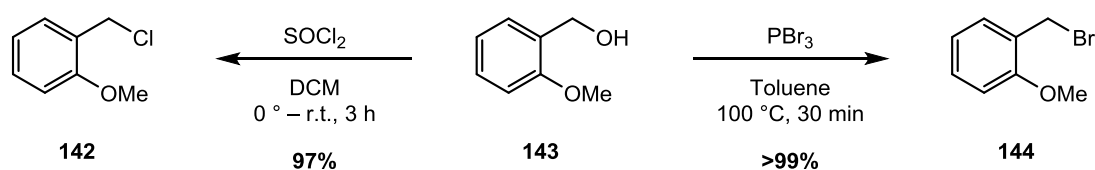
While low yields are common in multicomponent reactions such as this, a yield as low as 11% was considered unfeasible for future large scale imidazole synthesis. We therefore looked to the use of an alternative method for the preparation of **134**. Pleasingly, we were able to synthesise **134** in excellent yield following a method reported by Mityanov and co-workers.¹²⁸ This procedure, depicted in Scheme 2.41, involves the reaction of mesitylamine with 2,3-butanedione monooxime **140** to form an imidazole *N*-oxide, which is stabilised as a boron trifluoride adduct. Subsequent reduction over iron powder afforded mesityl dimethylimidazole **134** in a 72% yield over three steps. This synthesis was later repeated successfully on a much larger scale, with an overall yield of 69% achieved over three steps, affording 28 g of **134**.



Scheme 2.41

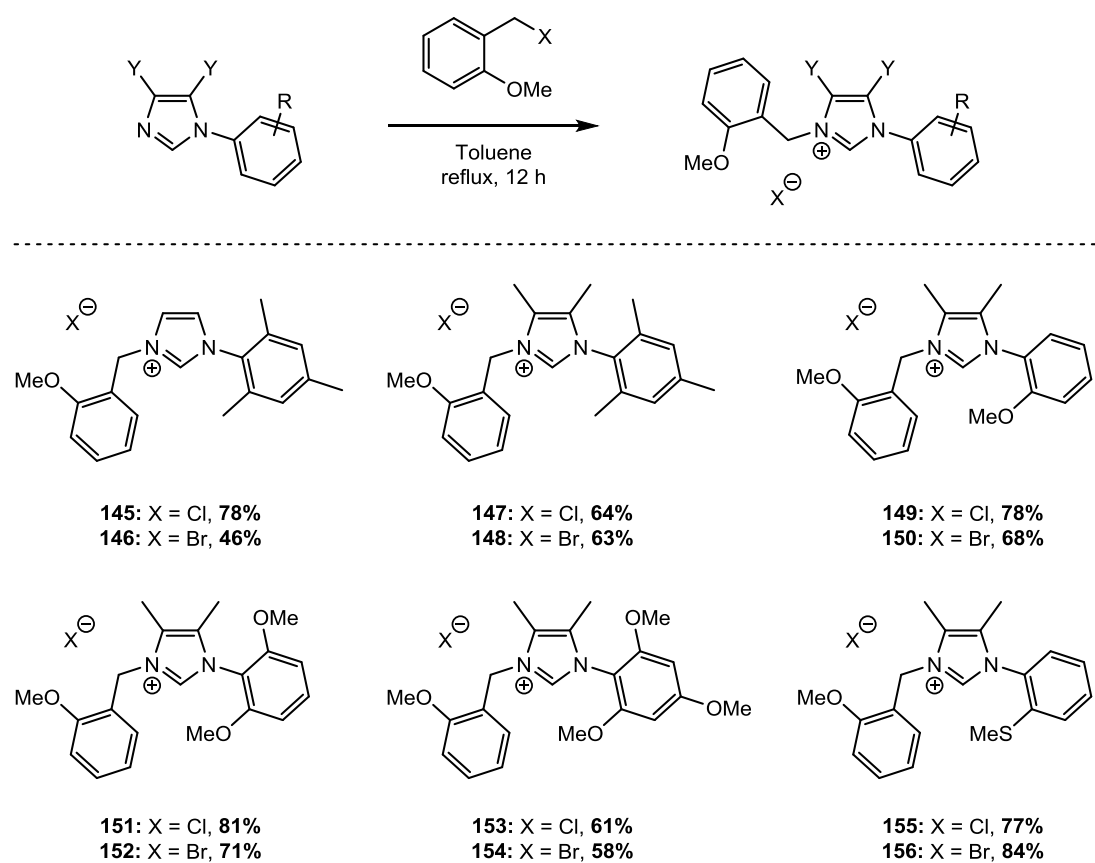
With a series of aryl imidazoles in hand, our next aim was to prepare the corresponding imidazolium salts. It was decided to use 2-methoxybenzyl halides as our initial choice for the alkyl arm of the NHC; these were prepared in excellent yields through treatment of the

corresponding benzyl alcohol with thionyl chloride or phosphorous tribromide, as shown in Scheme 2.42.



Scheme 2.42

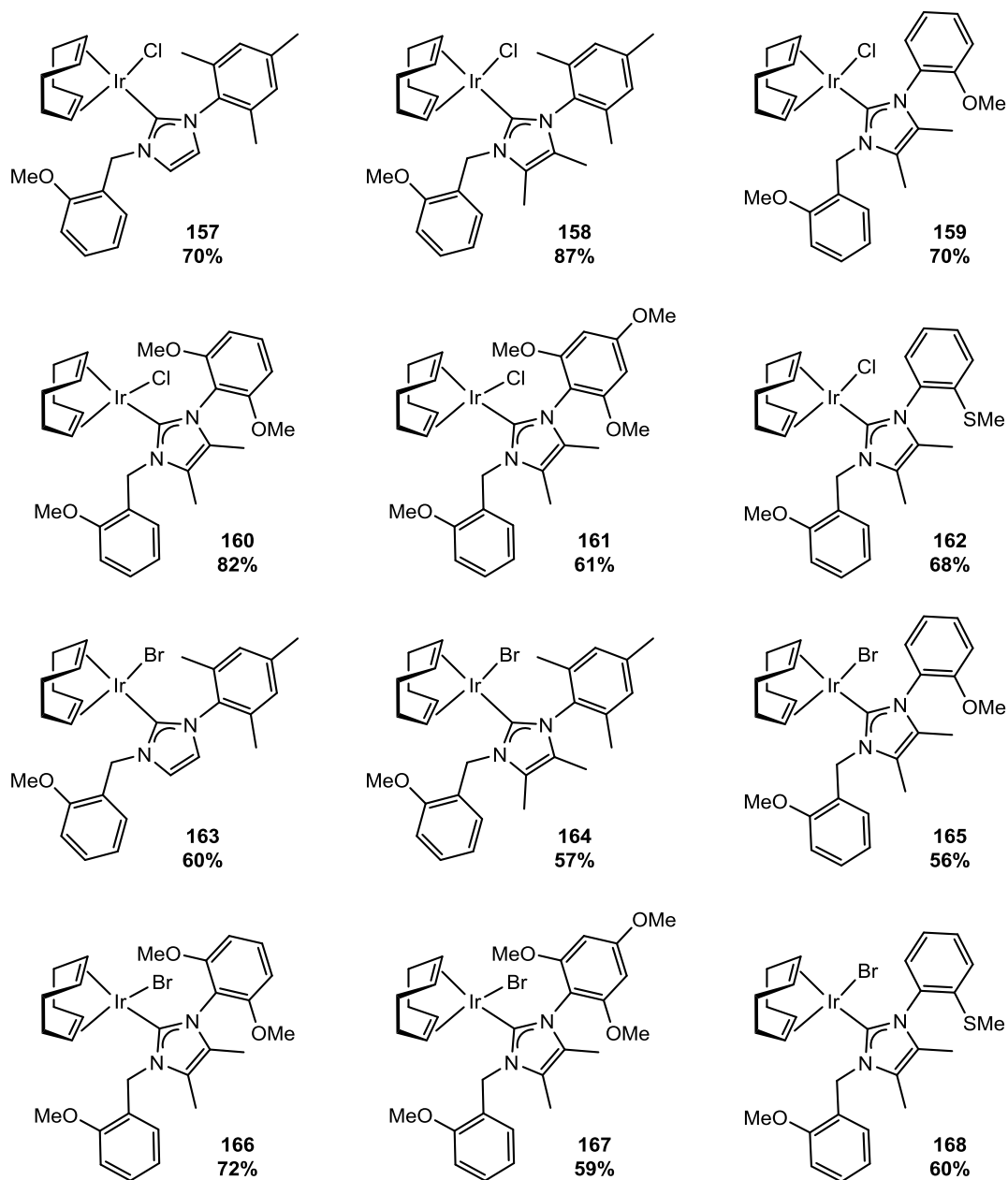
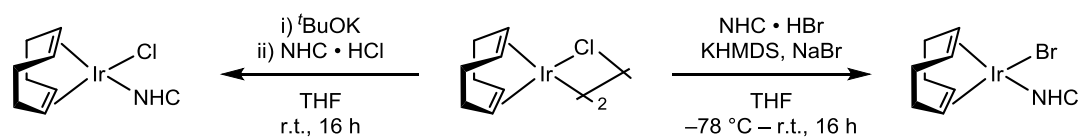
142 and **144** were next applied in the *N*-alkylation of our prepared imidazoles, as shown in Scheme 2.43. We were delighted to see that all of these reactions proceeded in good to excellent yields, affording 12 novel imidazolium salts, featuring 6 new NHC motifs.



Scheme 2.43

With a series of imidazolium salts now prepared successfully, the corresponding iridium complexes were synthesised. We were keen to use both the chloride and bromide salts in order to investigate the effects of altering the halide ligand when our complexes were used in catalysis. Neutral iridium halide complexes **157–168** were thus prepared, as shown in

Scheme 2.44. Chloride complexes were made *via* the same procedure used by the Kerr group to make $[\text{Ir}(\text{cod})(\text{IMes})\text{Cl}]$.¹²⁰ Bromide complexes, on the other hand, were prepared *via* an alternative method using KHMDS and a sodium bromide additive; this was to avoid the formation of a mixture of inseparable bromide and chloride complexes that could result when using an iridium chloride dimer as the starting material.¹²⁹



Scheme 2.44

We were delighted that our studies so far had provided us with expedient access to a range of 12 novel iridium(I) complexes. While some previous work has been carried out within the Kerr group into the use of unsymmetrical NHC ligands,¹³⁰ we had not yet investigated the

synthesis or behaviour of complexes bearing donor-substituted NHCs. It was therefore imperative that both the electronic and steric properties of our novel series of complexes were fully characterised.

In the first instance, the steric properties of our prepared NHCs were investigated using percentage buried volume (% V_{bur}) calculations.¹³¹ DFT calculations were used to establish the optimised geometry of the octahedral iridium(III) species **169** (Figure 2.8).

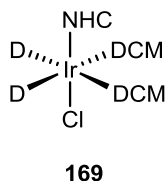


Figure 2.8

While this complex is not expected to exist under transfer hydrogenation conditions, the use of **169** for calculating % V_{bur} means that the values obtained could be compared with those calculated for NHC ligands used by our group in hydrogen isotope exchange.¹²⁵ After optimisation of the relevant complex, SambVca online software was used to calculate % V_{bur} from the output coordinates.¹³² The values obtained are shown in Figure 2.9, and are compared to those for a range of commonly used NHC ligands.

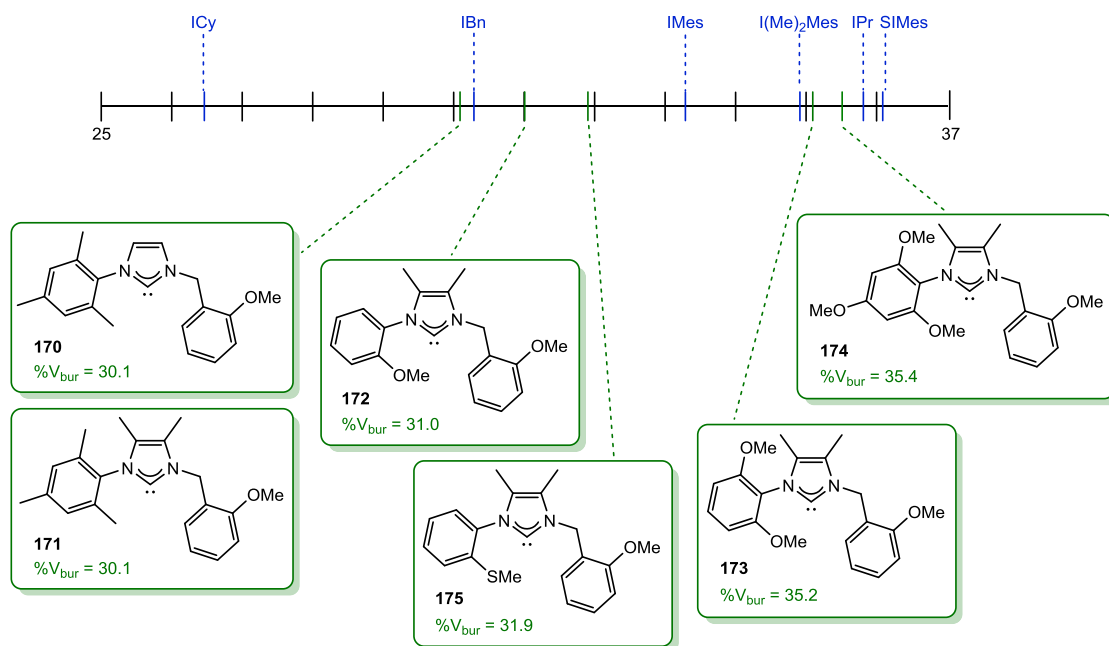


Figure 2.9

The SambVca software used to calculate the %V_{bur} values was also used to plot steric maps of each NHC ligand, which offer a visualisation of the steric components of the ligand. These are shown in Figure 2.10, with the darker blue sections representing the parts on the ligand furthest away from the metal centre.

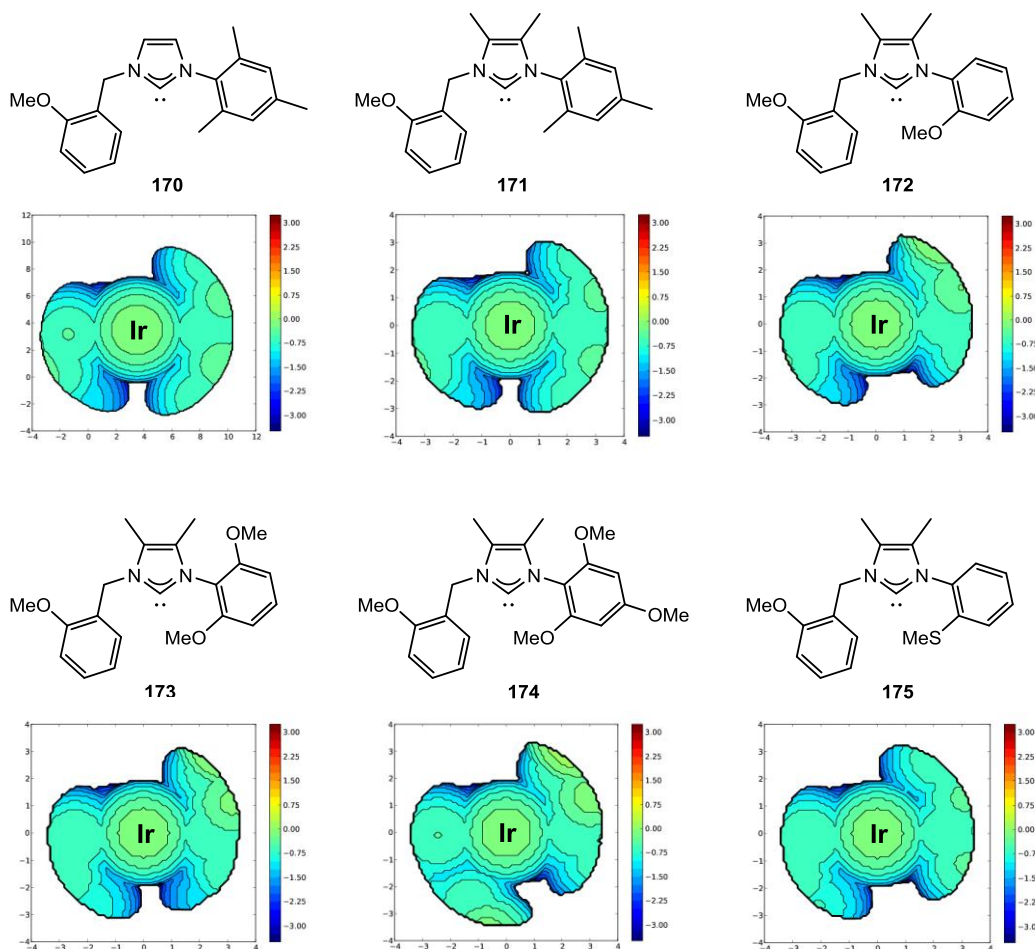


Figure 2.10

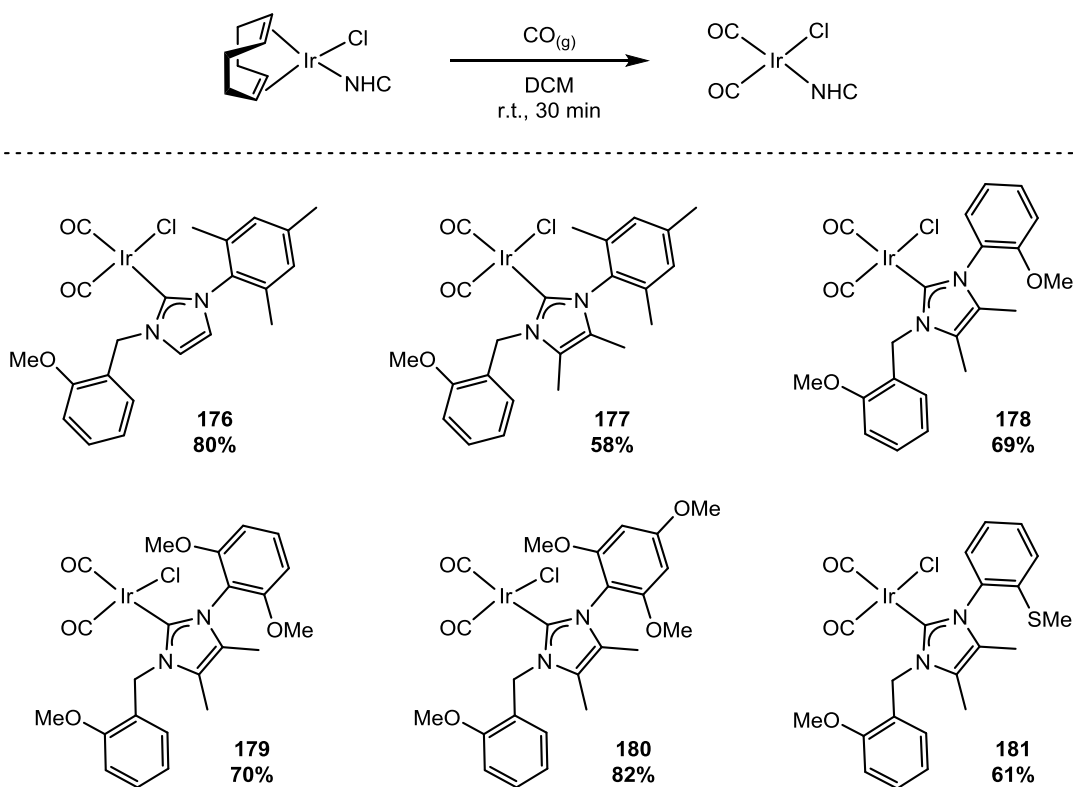
A number of interesting conclusions can be drawn from the steric calculations carried out. Firstly, the presence of two methyl substituents on the backbone had no effect on the $\%V_{\text{bur}}$; Figure 2.9 shows that **170** and **171** share the same value of 30.1%. Previous calculations, however, showed that IMes had a lower $\%V_{\text{bur}}$ when compared to its dimethyl-substituted analogue $\text{I}(\text{Me}_2)\text{Mes}$ (33.3% vs. 34.9%).¹²⁵ We considered it likely that the increased flexibility of the 2-methoxybenzyl substituent, compared to the mesityl group present in IMes and its derivatives, meant that the presence of additional bulk presented by the two methyl groups could be avoided somewhat *via* rotation of the benzyl unit.

It can also be observed that the presence of donor groups on the aryl unit of the NHC had significant effects on the steric demands of the ligand. Indeed, NHC **172**, bearing a 2-methoxyphenyl substituent, had a $\%V_{\text{bur}}$ larger than the corresponding mesityl-substituted NHC, which has three aryl substituents compared to one on **172**. Switching from a methoxy group at the *ortho*-position to a thiomethyl group (**175**) led to a further increase in $\%V_{\text{bur}}$.

Lastly, and as expected, increasing the number of methoxy substituents (**172–174**) increased the steric demands of the NHC, with **174** having a % V_{bur} of 35.4; this is almost as bulky as the IPr ligand, so **174** can be considered to be exceptionally sterically demanding for a benzyl-substituted NHC.

As discussed in Chapter 1, the many advantages of using NHCs as ligands include the fact that they are easily tuneable with regards to both their steric and electronic properties. Having obtained some insight into our novel ligands' steric properties, we therefore considered it essential that we also investigate their electronic parameters.

Starting from the chloride/NHC iridium complexes, we first prepared a series of dicarbonyl complexes in good yield *via* treatment with CO gas (Scheme 2.45).



Scheme 2.45

Complexes **176–181** were analysed by IR spectroscopy and their CO stretching frequencies noted. TEP values were then calculated by averaging the two CO frequencies and inputting them into Equation 2.1.¹³³ Both $\nu(\text{CO})$ and TEP values are listed in Table 2.4 (*vide infra*).

Equation 2.1

$$\text{TEP} = (0.847 \times \nu(\text{CO})_{\text{av}}) + 336 \text{ cm}^{-1}$$

The TEP values are also displayed in Figure 2.11, and are compared to examples of commonly used NHC ligands.¹³⁴ As expected, the addition of two methyl groups on the NHC backbone caused an increase in electron density, with **177** displaying a TEP value almost 3 cm⁻¹ smaller than that of **176**. Additionally, it was observed that increasing the number of methoxy groups on the aryl portion of the NHC rendered the ligand more electron rich. It was noticed, however, that the differences between CO stretching frequencies for **178–180** were very small, showing that substitution on the NHC backbone had a larger effect on ligand electronics. While **180**, bearing three methoxy substituents, had a lower TEP value than its mesityl analogue **177**, **178** and **179**, bearing fewer substituents, were still less electron rich than **177**. The small changes in $\nu(\text{CO})$ observed are in keeping with results reported by Nolan and co-workers in their investigation of methoxy-substituted derivatives of common symmetrical NHCs.¹³⁵

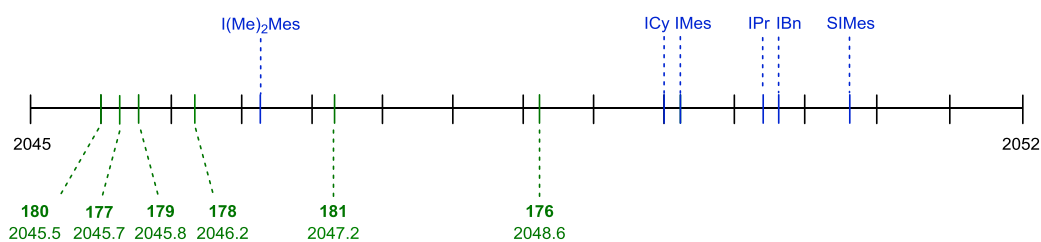
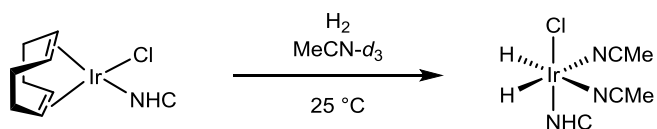


Figure 2.11

As an additional measure of the ligands' electronic properties, complexes **157–162** were activated, with H₂ gas, as a solution in acetonitrile-*d*₃, which offers the resultant octahedral complexes enough stabilisation that their hydride signals can be observed by ¹H NMR spectroscopy.

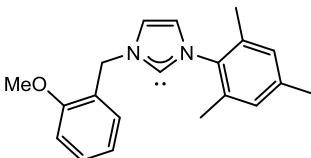
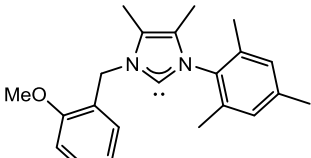
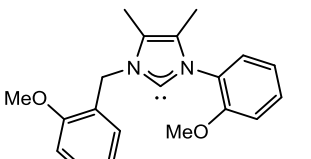
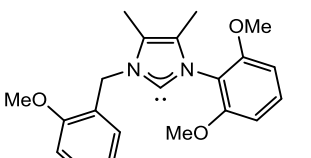
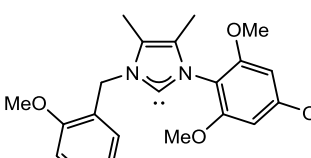
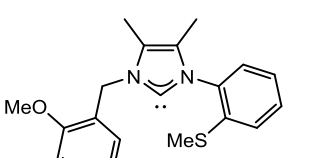


Scheme 2.46

The hydride resonances observed are listed in Table 2.4, and are seen to be in keeping with the $\nu(\text{CO})$ values obtained, with the addition of methoxy substituents on the aryl ring

rendering the ligands more electron rich than their mesityl analogues. All values of % V_{bur} , $\nu(\text{CO})$, and TEP, along with the hydride chemical shifts, are summarised in Table 2.4.

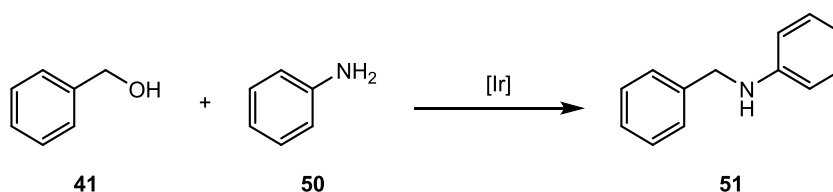
Table 2.4

Entry	NHC	% V_{bur}	$\nu(\text{CO})_{\text{DCM}}$ / cm^{-1}	TEP _{Ir} / cm^{-1}	Hydride δ / ppm
1	 170	30.1	2021.9	2048.6	-22.52
2	 171	30.1	2018.5	2045.7	-22.80
3	 172	31.0	2019.1	2046.2	-22.60
4	 173	35.2	2018.6	2045.8	-22.70
5	 174	35.4	2018.3	2045.5	-22.96
6	 175	31.9	2020.3	2047.2	n/a*

* Hydride signal not observed.

N-Alkylation of Amines *via* Hydrogen Borrowing

At this stage in the project, we were delighted to have synthesised and characterised a series of novel imidazolium salts and their corresponding iridium complexes and established their steric and electronic properties. Our next aim was to investigate the activity of our new complexes in transfer hydrogenation reactions. As a benchmark reaction, we chose the alkylation of aniline **50** with benzyl alcohol **41**, shown in Scheme 2.47. Using a hydrogen borrowing reaction would allow us to assess the ability of our complexes to facilitate both oxidation and reduction processes, and the use of relatively simple and activated substrates would allow us to compare our catalysts to a number of those reported in the literature.



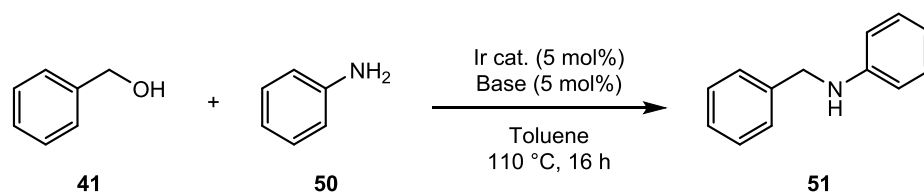
Scheme 2.47

In the first instance, we sought to carry out an initial screening to assess whether any of our catalysts were, indeed, active in the above process. For this assay, reactions were carried out in refluxing toluene. While our overall goal was to achieve hydrogen borrowing catalysis under milder conditions, it was thought that screening our catalysts initially under forcing conditions would give us the best initial overview of their activity. We also chose to test both carbonate and alkoxide bases, as both are frequently employed in similar reactions throughout the literature.

The results of our screening are shown in Table 2.5. We were delighted to see that all of our novel complexes showed some activity in the *N*-benzylation of aniline. There were some key findings, however, to be taken from the observed results. Comparing entries 1–12 with entries 13–24, it can be seen that in all cases, yields were higher when potassium *tert*-butoxide was used as a base. Very little difference was observed between the chloride complexes and their bromide analogues (Entries 1–6 and 13–18 *vs.* entries 7–12 and 19–24). Despite a number of the complexes we tested having donor substituents on both arms, higher yields were observed for those with a mesityl substituent as one arm of the NHC. The addition of two methyl groups on the NHC backbone was shown to increase reactivity, with the standout results coming from

reactions run with catalysts **158** and **164**, in which the NHC features a mesityl arm and a dimethyl-substituted imidazole backbone.

Table 2.5

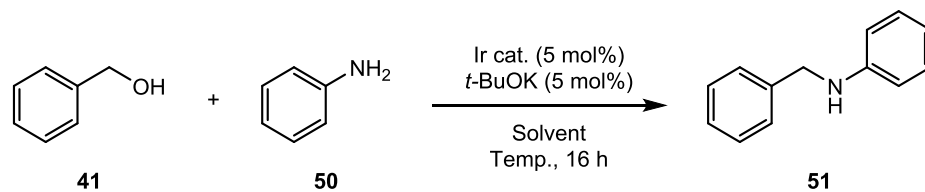


Entry	Catalyst	Base	Yield / %	Entry	Catalyst	Base	Yield / %
1	157	K ₂ CO ₃	59	13	157	^t BuOK	64
2	158	K ₂ CO ₃	80	14	158	^t BuOK	91
3	159	K ₂ CO ₃	71	15	159	^t BuOK	83
4	160	K ₂ CO ₃	50	16	160	^t BuOK	58
5	161	K ₂ CO ₃	46	17	161	^t BuOK	59
6	162	K ₂ CO ₃	6	18	162	^t BuOK	18
7	163	K ₂ CO ₃	53	19	163	^t BuOK	66
8	164	K ₂ CO ₃	82	20	164	^t BuOK	97
9	165	K ₂ CO ₃	70	21	165	^t BuOK	81
10	166	K ₂ CO ₃	51	22	166	^t BuOK	62
11	167	K ₂ CO ₃	52	23	167	^t BuOK	60
12	168	K ₂ CO ₃	8	24	168	^t BuOK	16

Having identified our most promising NHC ligand, at this stage we took both its chloride complex **158** and its bromide complex **164** for further optimisation. A solvent screening was next carried out, testing dioxane, which is another commonly used solvent for transfer hydrogenation reactions, as well as a series of lower boiling and ‘greener’ ethereal solvents, which are increasingly favoured within industry.¹³⁶ The results of our solvent screen are summarised in Table 2.6. For comparison, the results from our catalyst screen in toluene are also included.

Our catalysts showed comparable reactivity in dioxane to that observed in toluene (Entries 2 and 7 vs. entries 1 and 6). While little to no reactivity was observed in CPME or MTBE, we were pleased to see that reactions proceeded efficiently in 2-MeTHF (Entries 5 and 10), at a lower temperature of 80 °C.

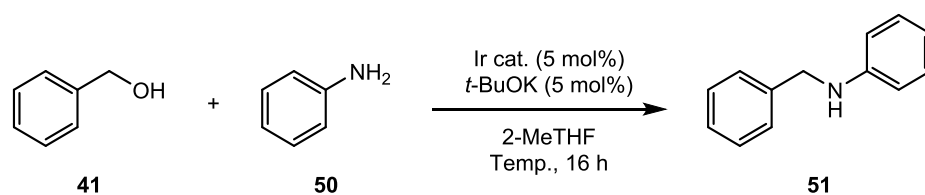
Table 2.6



Entry	Catalyst	Solvent	Temp. / ° C	Yield / %
1	158	Toluene	110	91
2	158	Dioxane	101	92
3	158	CPME	106	9
4	158	MTBE	55	15
5	158	2-MeTHF	80	93
6	164	Toluene	110	97
7	164	Dioxane	101	95
8	164	CPME	106	10
9	164	MTBE	55	18
10	164	2-MeTHF	80	94

With promising results having been observed for catalysts **158** and **164** at 80 °C, we were keen to carry out further screening in 2-MeTHF to identify whether the reaction would be amenable to even milder conditions. A temperature screening was carried out, and the results are shown in Table 2.7.

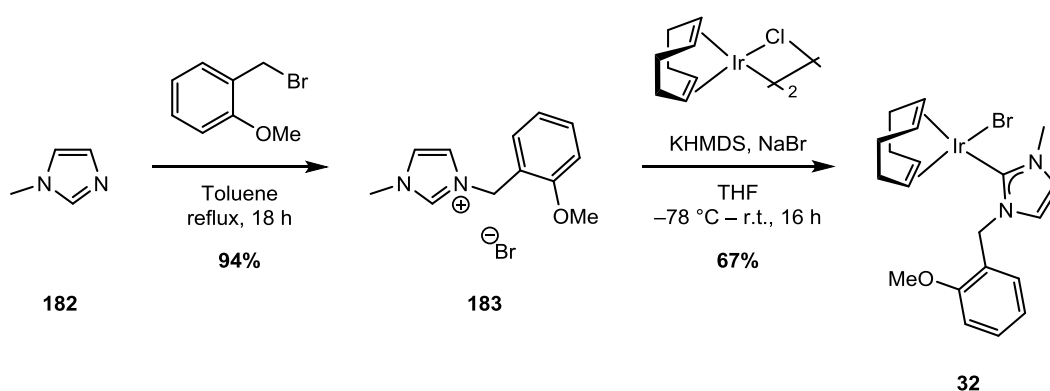
Table 2.7



Entry	Catalyst	Temp. / ° C	Yield / %
1	158	60	94
2	164	60	96
3	158	40	91
4	164	40	94
5	158	25	76
6	164	25	93

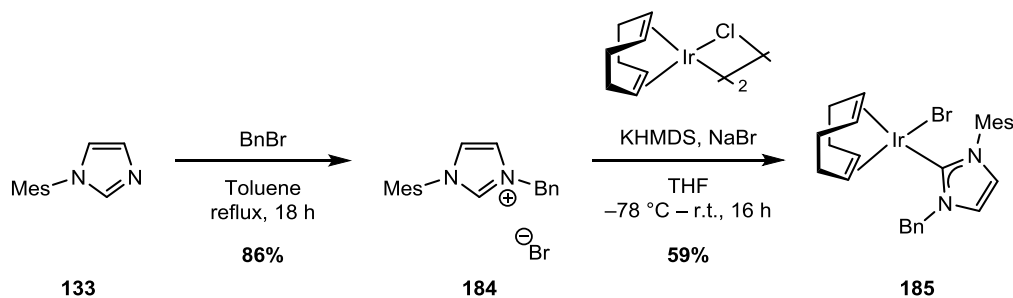
We were delighted to see that both catalysts maintained high levels of activity at lower temperatures. While a slight drop in the activity of **158** was observed as the temperature was decreased, only a very minor change in catalytic efficiency was observed with **164**, with an excellent yield of 93% obtained at 25 °C.

We were keen to explore whether the specific characteristics of our novel complex were responsible for its remarkable reactivity. As such, we looked to compare it with two key analogues. In the first instance, we looked to compare reactivity with complex **32**, used by Jiménez and co-workers and an excellent benchmark for hemilabile NHC–iridium complexes.^{50,137} **32** was prepared in good yield *via* the route shown in Scheme 2.48.



Scheme 2.48

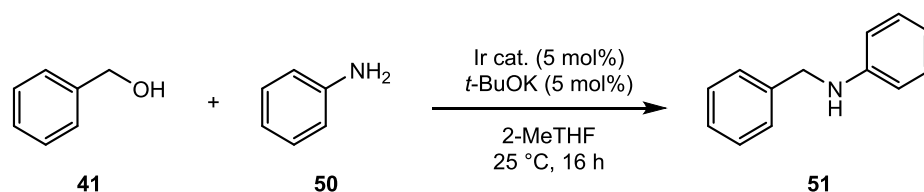
As an additional comparison, we also prepared complex **185**, an analogue of catalyst **164** without the presence of the methoxy substituent. **185** was synthesised as shown in Scheme 2.49.



Scheme 2.49

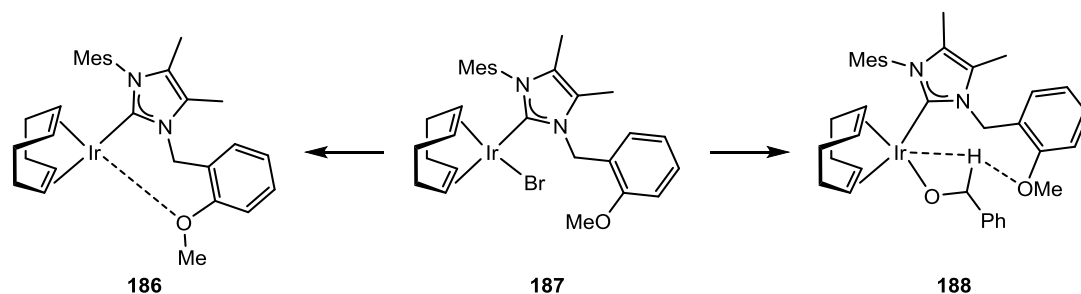
When we compared the activity of **32** and **185** to that of our optimised catalyst **164**, we were pleased to see that under our mild room temperature conditions, the activity of **164** exceeded its smaller and unsubstituted analogues (Table 2.8).

Table 2.8



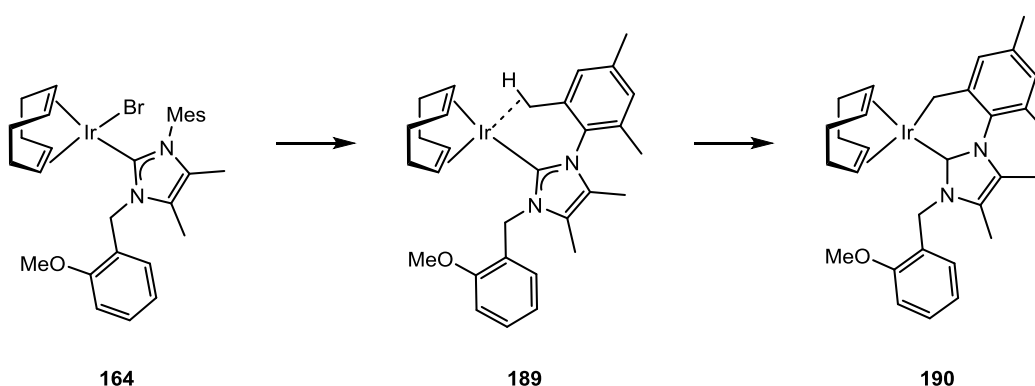
Entry	Catalyst	Yield / %
1	164	76
2	32	26
3	185	15

These results demonstrated two key points. Firstly, comparing **164** with **185** showed that the presence of an electron-donating substituent at the *ortho*- position was essential for the high reactivity observed. Secondly, it can be seen that the bulky mesityl group present in catalyst **164** has a notable positive effect on catalyst activity when compared to catalyst **32**, which has a smaller methyl substituent. It has been proposed that the success of catalysts featuring donor-functionalised NHC ligands can be, in part, attributed to the ligands' hemilabile nature and the ability of the donor group to coordinate to the metal centre.^{137–140} It is likely that this is the cause of **164**'s increased activity compared to **185**, with the methoxy oxygen coordinating to the iridium centre and stabilising any coordinatively unsaturated intermediates, as shown in Scheme 2.50. Additionally, and as shown below, hydrogen bonding interactions can assist in the abstraction of a hydride from the alcohol hydrogen donor.



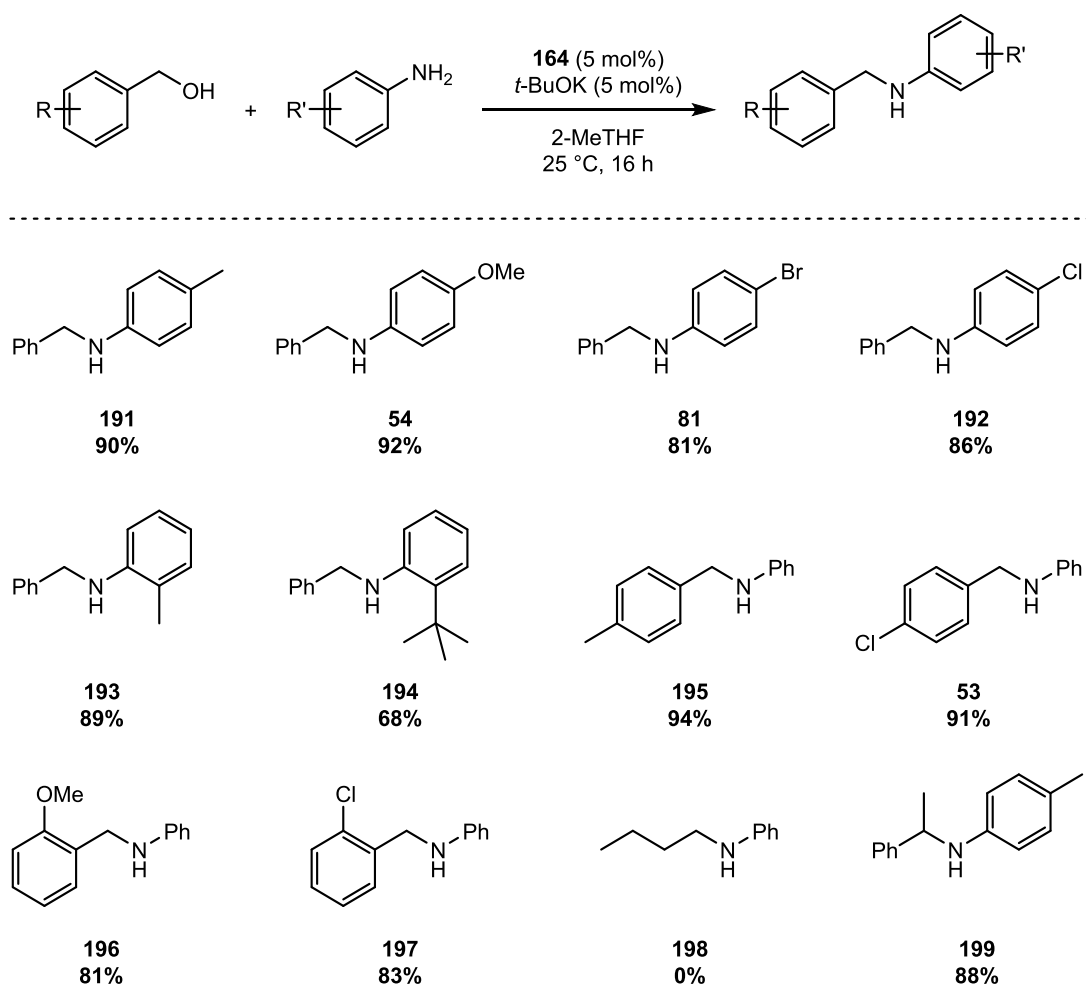
Scheme 2.50

The increased activity of **164** compared to **32** could be a result of the ligand's increased steric demands; Gülcemal and co-workers have demonstrated that complexes with highly bulky NHC ligands can perform excellently as transfer hydrogenation catalysts.⁴² However, if, as discussed above, the mechanism involves the formation of coordinatively unsaturated intermediates, additional stabilisation could be offered *via* interaction with one of the *ortho*-methyl groups on the mesityl unit, as depicted in Scheme 2.51. It has been demonstrated numerous times that C–H activation of NHC ligands can occur at iridium, rhodium, and ruthenium centres.^{141–144} While insertion into one of the methyl C–H bonds may be irreversible and lead to a loss of activity, an agostic interaction between the C–H bond and the metal centre could stabilise any vacant coordination sites during catalysis.



Scheme 2.51

Having developed a remarkably mild and efficient method for the *N*-benzylation of aniline *via* hydrogen borrowing, we applied our optimised conditions to a series of alternative substrates (Scheme 2.52). We were delighted to see that good functional group tolerance was observed for a series of substituted anilines and benzyl alcohols, with reactions proceeding well for substrates bearing electron-donating and electron-withdrawing groups. Particularly impressive was the success observed for anilines bearing bulky substituents at the *ortho*-position (**193** and **194**). Similarly, *ortho*-substituted benzyl alcohols also underwent the reaction efficiently. The alkylation of aniline was attempted with an unactivated, straight chain alcohol (**198**) but none of the desired product was observed. Lastly, the reaction proceeded smoothly with α -methylbenzyl alcohol to afford product **199** in excellent yield. Furthermore, recent work within the Kerr group has extended this methodology, demonstrating that the *N*-alkylation of anilines can be carried out efficiently with a wide range of secondary alcohols.¹⁴⁵



Scheme 2.52

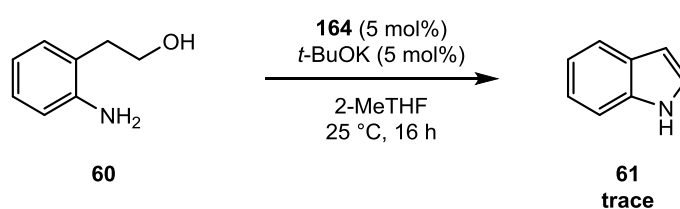
Synthesis of *N*-Heterocycles *via* Hydrogen Borrowing

We were pleased at this stage of the project to have developed a mild and high-yielding method for the formation of C–N bonds *via* a hydrogen borrowing process, and our attention now turned to the expansion of this methodology. We considered that developing an intramolecular version of our *N*-alkylation procedure could offer expedient access to useful heterocyclic compounds.

As discussed in more detail in Chapter 1, *N*-heterocycles are among the most important scaffolds in modern medicinal chemistry.^{146,147} Indeed, a 2014 study showed that 59% of small molecule drugs approved by the FDA contain at least one nitrogen heterocycle.¹⁴⁸ As such, they represent essential building blocks and efficient methods for their synthesis are of enormous relevance to the pharmaceutical and agrochemical industries.

We were first interested in investigating the reaction of 2-aminophenethyl alcohol **60** under our reaction conditions; recent reports have demonstrated that under transfer hydrogenation conditions, **60** can be converted to indole **61**.^{83,90} While there are numerous methods for indole synthesis, which have been comprehensively reviewed,^{149–151} the indole moiety is of enormous relevance in modern drug discovery and thus the development of new indole synthesis methodology remains a desirable target.

As an initial test, **60** was subjected to our previously optimised conditions for *N*-alkylation (Scheme 2.53). We were disappointed, however, to observe only trace amounts of the desired indole product.

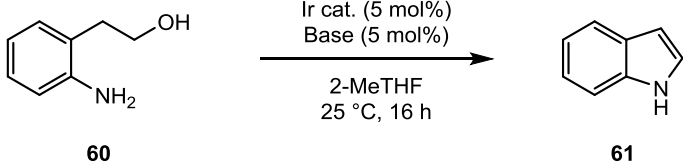


Scheme 2.53

It thus appeared that **60** could be a more challenging substrate, and wanting to increase our chances of achieving an initial hit, we repeated the above reaction with a slightly elevated temperature of 50 °C. Catalysts **158** and **164** were both tested, since so far only slight differences in activity had been observed between these chloride and bromide complexes. Additionally, the reactions were carried out with a carbonate and an alkoxide base.

The results of this screening are shown in Table 2.9. Unfortunately, in all cases, conversions of less than 20% were achieved. Although we considered it promising that **158** and **164** were displaying some activity, the levels observed here suggested that in order to be of utility, our reaction conditions would need to be altered significantly.

Table 2.9

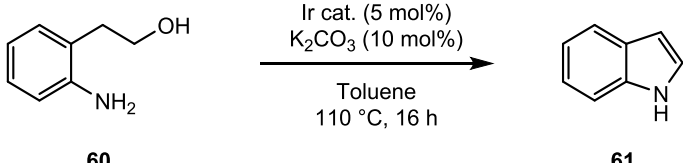


Entry	Catalyst	Base	Conversion* / %
1	158	<i>t</i> -BuOK	13
2	158	K ₂ CO ₃	18
3	164	<i>t</i> -BuOK	9
4	164	K ₂ CO ₃	14

* Calculated by LCMS analysis

At this stage, we decided to abandon the reaction conditions optimised for the intermolecular reaction, and instead run a test reaction based on conditions used in the literature. In a 2002 paper, Yamaguchi and co-workers reported on the synthesis of **61** from **60** using a [Cp*IrCl₂]₂ catalyst.⁸³ We were interested to see whether **158** or **164** would show activity under these harsher conditions. Table 2.10 shows the results. Pleasingly, both our catalysts showed moderate activity under these conditions, with conversions of 48% and 37% achieved.

Table 2.10

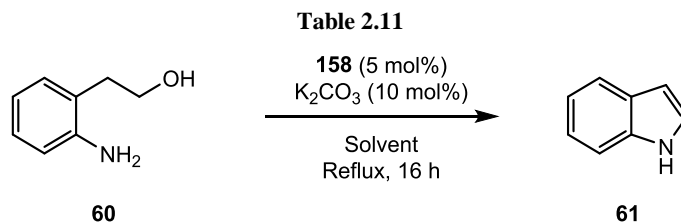


Entry	Catalyst	Conversion* / %
1	158	48
2	164	37

* Calculated using LCMS analysis

While the results shown in Table 2.10 were promising, it was evident that additional optimisation was still required, and we chose to use chloride catalyst **158** for our further investigations. We next carried out a solvent screen; as it appeared likely at this stage that high temperatures were necessary, the reaction was carried out under reflux in a series of

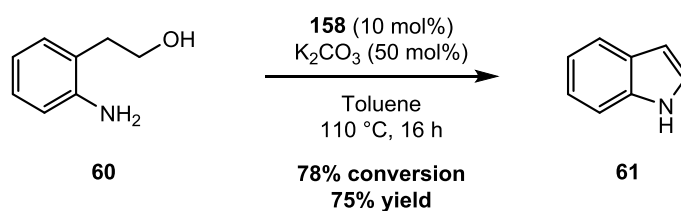
high boiling point solvents. One run was also carried out neat (Entry 7). As shown in Table 2.11, the reaction was seen to proceed most efficiently in toluene and dioxane, and we chose to continue our optimisation using toluene.



Entry	Solvent	Temp. / ° C	Yield / %
1	Toluene	110	48
2	Dioxane	101	46
3	DCE	80	<10
4	2-MeTHF	80	26
5	CPME	106	38
6	<i>t</i> -AmOH	100	29
7	-	100	21

* Calculated using LCMS analysis

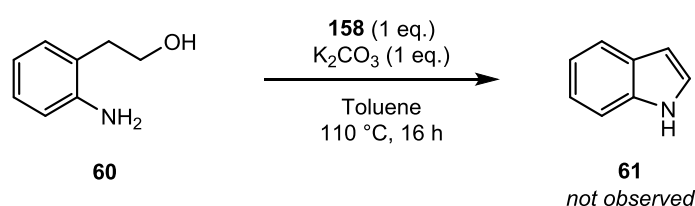
Having chosen our preferred catalyst and solvent, further optimisation of the reaction was carried out using Design of Experiments.^{152,153} A 2-level, 4-factorial design was used to investigate the effects of temperature (20–110 °C), catalyst loading (0.25–10 mol%), base loading (0.25–50 mol%) and solvent volume (0.7–13 mL/mmol). The half-normal plot generated suggested that reaction efficiency was dependent on all the variables investigated, as well as on several two-factor interactions. The largest effects came from alteration of the temperature and catalyst loading; in both cases, higher values led to higher conversion. We also observed that increasing the quantity of base to 0.5 equivalents had a beneficial effect on the reaction. Our DOE-optimised conditions are shown in Scheme 2.54.



Scheme 2.54

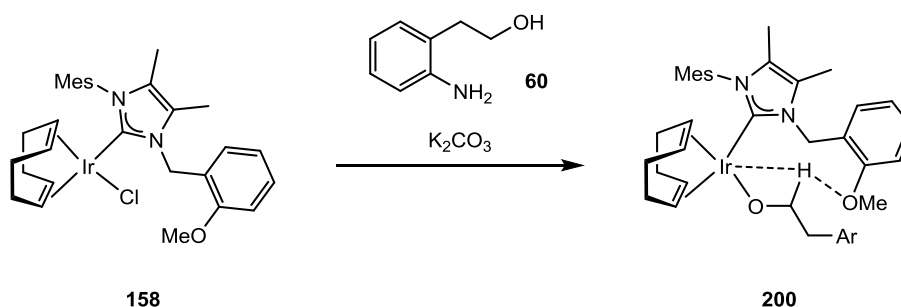
We were pleased that the synthesis of indole **61** was now proceeding in yields as high as 75%. Given, however, that the conditions required are notably harsher than those used in our intermolecular hydrogen borrowing methodology, we considered a number of strategies that would increase conversions while offering us insight into the factors affecting the reaction.

Since our Design of Experiments had demonstrated that catalyst loading was the most important variable in determining reaction efficiency, the reaction was repeated with stoichiometric quantities of catalyst and base (Scheme 2.55). Unfortunately, while numerous new peaks were observed by LCMS analysis, no appreciable conversion to the desired product was observed and we were unable to isolate any product from the reaction mixture.



Scheme 2.55

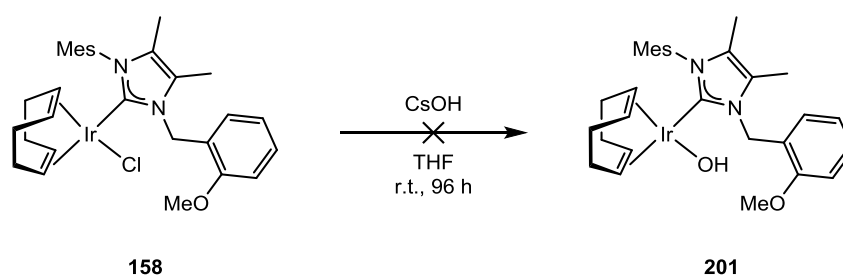
Based on the mechanism proposed by Jiménez and co-workers for transfer hydrogenation of catalysed by iridium(I) complexes with hemilabile NHC ligands,¹⁵⁴ we surmised that the first step of our hydrogen borrowing mechanism involves the formation of an alkoxide intermediate with loss of the halide ligand, as shown in Scheme 2.56.



Scheme 2.56

We considered that alkoxide formation could be hindering reaction speed and proposed two potential solutions. Firstly, it was considered that the use of a hydroxide analogue of chloride complex **158** could facilitate easier formation of the iridium alkoxide species. We

sought, therefore, to prepare hydroxide complex **201** following a procedure reported by Nolan and co-workers (Scheme 2.57).¹⁵⁵



Scheme 2.57

Unfortunately, none of the desired product **201** was observed or isolated. In their paper describing the synthesis of iridium NHC/hydroxide complexes, Nolan and co-workers reported that long reaction times were necessary to obtain even moderate to good yields, so the reaction was left for 96 h. NMR monitoring of the reaction, however, showed only decomposition of complex **158**.

Undeterred, we instead explored the possibility of using a halide abstractor to remove the chloride ligand and encourage formation of the alkoxide complex. The reaction of 2-(2-aminophenyl)ethanol **60** was therefore carried out with the addition of a range of silver and sodium salts that are able to act as halide abstractors (Table 2.12).

Table 2.12

60

$\xrightarrow[\text{Toluene, 110 } ^\circ\text{C, 16 h}]{\text{158 (10 mol\%)}, \text{K}_2\text{CO}_3 \text{ (50 mol\%)}, \text{Additive (10 mol\%)}}$

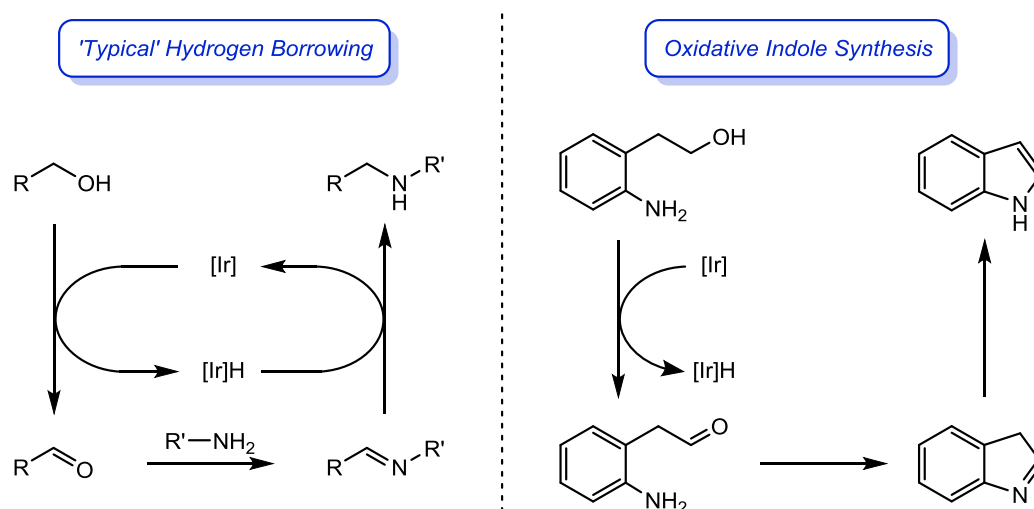
61

Entry	Additive	Conversion* / %
1	AgOTf	56
2	AgBF ₄	93
3	AgPF ₆	82
4	NaBAr _F	89

* Calculated using LCMS analysis

We were delighted to see that silver tetrafluoroborate, silver hexaphosphate, and sodium tetrakis[3,5-bis(trifluoromethyl)phenyl]borate all caused notable increases in conversion, with AgBF_4 having the largest effect and achieving an excellent conversion of 93%.

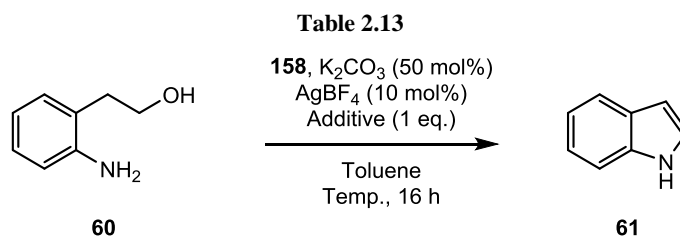
While the addition of a silver salt had allowed us to achieve greatly improved conversions, the conditions being used were still considerably harsher than desirable. We proposed that one source of this could be the fact that when our hydrogen borrowing reaction is used for indole synthesis, there is no formal reduction process taking place. As shown in Scheme 2.58, the formation of C–N bonds *via* hydrogen borrowing typically involves three key steps; after iridium-catalysed alcohol oxidation, imine condensation occurs through a non-catalytic process. The iridium hydride species generated in the first step is then responsible for the reduction of the imine to the desired amine product. In the reaction of 2-aminophenyl ethanol, however, after intramolecular condensation, the generated imine rearomatizes instead of undergoing reduction. This renders the overall process an oxidative cyclisation.



Scheme 2.58

Yamaguchi and co-workers have suggested that the reaction of the *in situ*-generated iridium hydride species with another equivalent of the alcohol substrate releases hydrogen and regenerates the active iridium alkoxide species.⁸³ We considered, however, that the lack of a formal reduction process in the catalytic cycle could be responsible for the sluggish activity observed, and proposed that the addition of a sacrificial reduction substrate could offer improved catalytic efficiency.

A series of reactions were carried out with one equivalent of a ketone or alkene additive (Table 2.13). In all cases, either the catalyst loading or temperature used was lower than our previously optimised conditions. Since we had already achieved conversions up to 93%, our aim here was to obtain comparable results with milder reaction conditions.



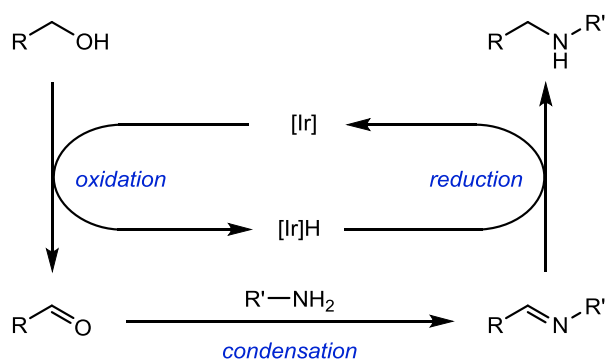
Entry	Additive	Catalyst Loading / mol%	Temp. / °C	Conversion* / %
1	Acetone	10	80	52
2	Acetone	10	60	35
3	Acetone	1	60	>10
4	Cyclohexene	10	80	72
5	Cyclohexene	10	60	32
6	Cyclohexene	1	60	>10
7	Styrene	10	80	81
8	Styrene	10	60	76
9	Styrene	5	60	58
10	Styrene	2.5	60	51
11	Styrene	1	60	46

* Calculated using LCMS analysis

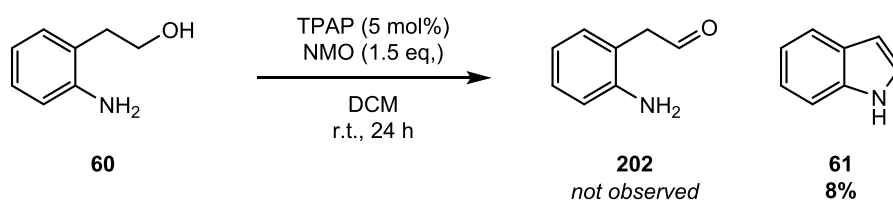
Of the three additives tested, styrene was shown to have the most positive effect, even allowing moderate activity at a catalyst loading of 1 mol% (Entry 11). Our Design of Experiments showed that catalyst loading had the most significant effect on catalyst efficiency, so we were pleased with this result, especially when compared to Entries 3 and 6, in which conversions drop to less than 10%. Of particular interest to us were Entries 7 and 8, which demonstrate that good conversions can be obtained at temperatures as low as 60 °C. While none of the conditions tested above achieved conversions quite as high as seen in our previously optimised conditions, the feasibility of the reaction at lower temperatures offers

an attractive set of alternative conditions for substrates that might be sensitive to harsh conditions.

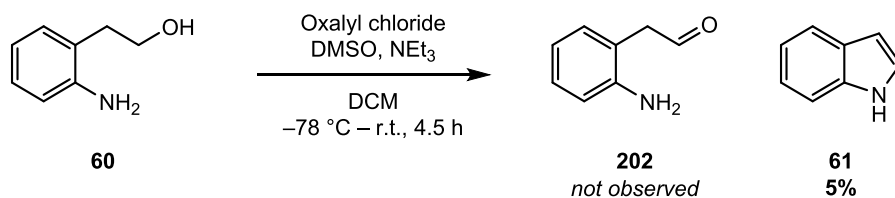
Through a series of rigorous optimisation studies, we were delighted to now be achieving yields comparable to those seen for our intermolecular *N*-alkylation reactions. We were keen, however, to investigate the factors that made this process so much more sluggish. As discussed previously, the formation of C–N bonds *via* hydrogen borrowing involves three key steps, as shown in Scheme 2.59, and we looked to determine which of these was responsible for the difficulties we had encountered. It was postulated that comparing the relative rates of reaction of alcohol substrate **60** and its aldehyde would offer an insight into whether the initial oxidation state was rate-determining.



The synthesis of aldehyde **202** from alcohol **60** was first attempted *via* oxidation with tetrapropylammonium perruthenate (TPAP) (Scheme 2.60). None of the desired aldehyde **202** was observed whatsoever, and a small amount of indole **61** was observed.

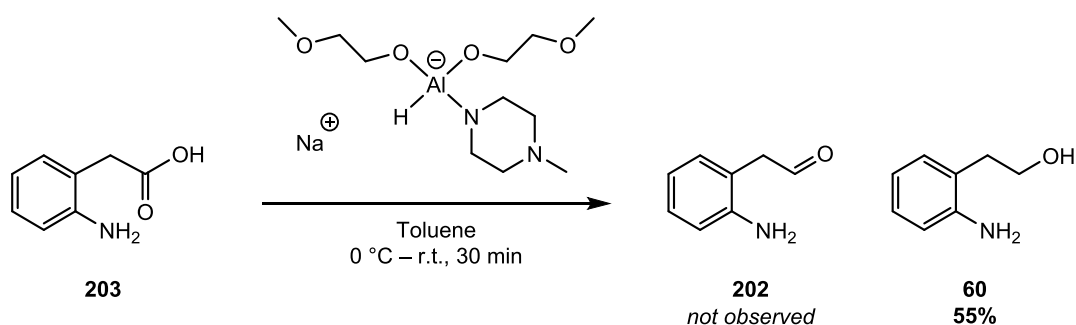


A similar result was obtained when the oxidation was instead attempted *via* Swern oxidation (Scheme 2.61). Once again, the desired aldehyde was not observed and LCMS analysis confirmed formation of a small amount of indole **61**.



Scheme 2.61

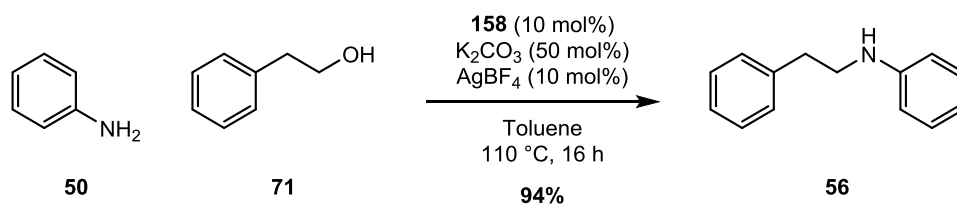
The formation of indole **61** (albeit in small quantities) was believed to occur as a result of spontaneous intramolecular cyclisation of aldehyde **202** followed by rearomatisation. In case this was dependent on the oxidative conditions used, a last attempt was made to prepare **61** *via* partial reduction of acid **203** using an NMP-modified sodium bis(2-methoxyethoxy) aluminium hydride (RedAl) reagent.¹⁵⁶ Again, no aldehyde was observed, with 55% of the fully reduced product **60** having formed within 30 minutes.



Scheme 2.62

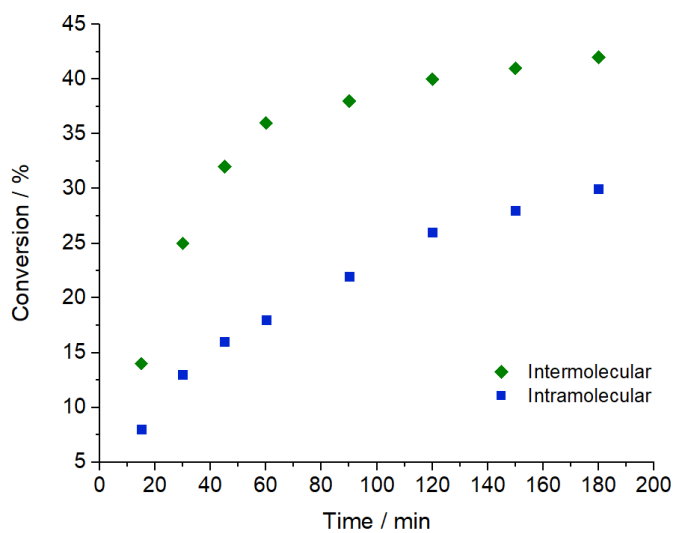
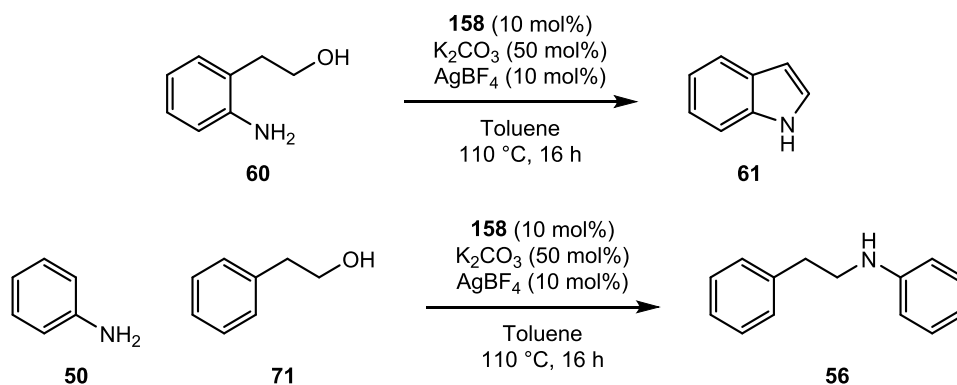
While we were disappointed not to have succeeded in preparing **202**, the fact that it appeared to be immediately and spontaneously reacting *in situ* to form indole **61** lent support to the idea that the initial oxidation process was likely to be rate-determining.

In order to understand why the oxidation of **60** was so challenging, we carried out the equivalent intermolecular hydrogen borrowing reaction, in which the alcohol unit of **71** should be similarly disposed towards oxidation. As shown in Scheme 2.63, the reaction proceeded smoothly in 94% yield.



Scheme 2.63

We now looked to compare the rates of reaction for the inter- and intramolecular variants of the above reaction. Time-point monitoring of both reactions was carried out and, as shown in Graph 2.2, the intermolecular variant was seen to proceed faster than its intramolecular counterpart.

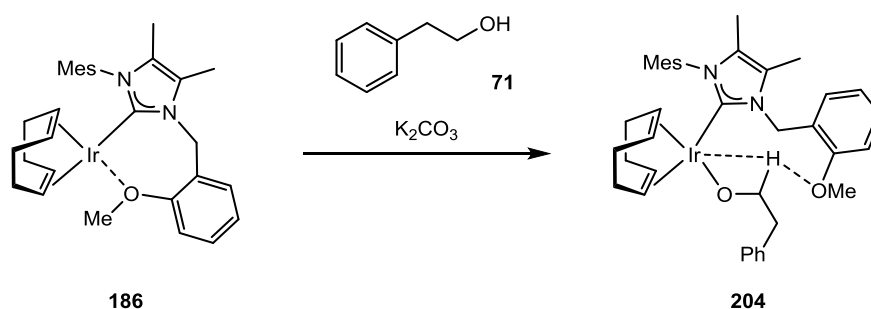


Graph 2.2

This result was surprising to us, since it would typically be expected for an intramolecular reaction to proceed more quickly, and our attention turned to the use of computational studies to investigate the reasoning for this behaviour.

As discussed previously, the reaction is believed to proceed *via* a key alkoxide intermediate, **204**, in which interaction of the NHC methoxy group activates the substrate to hydride abstraction. We first calculated the optimised geometries of the iridium alkoxide species generated from the reaction of catalyst **158** with substrate **60** or **71**.

For the intermolecular reaction involving substrate **71**, our calculations showed that from intermediate complex **186**, in which the vacant coordination site left by chloride abstraction is stabilised by the NHC methoxy group, complexation occurs to form intermediate **204**. Analysis of the optimised geometry confirmed the presence of an interaction between the methoxy oxygen and the alcohol hydrogen.



Scheme 2.64

However, when the calculations were run with amino-substituted **60**, the substrate was shown to interact with the iridium centre in a bidentate manner, with a formal Ir–O bond observed, as well as a loose coordination between the amine nitrogen and the metal centre. Figure 2.12 shows the two lowest energy isomers of the substrate-bound complex. Compound **205** is further stabilised by not only an Ir–N interaction, but also by a hydrogen bonding interaction between the amine nitrogen and the methoxy oxygen atom. In complex **206**, which is the lowest energy isomer of those calculated, while there is also an iridium–nitrogen interaction, the substrate is positioned in a way that the alcohol hydrogen can still interact with the methoxy oxygen, as with complex **204** (*vide supra*).

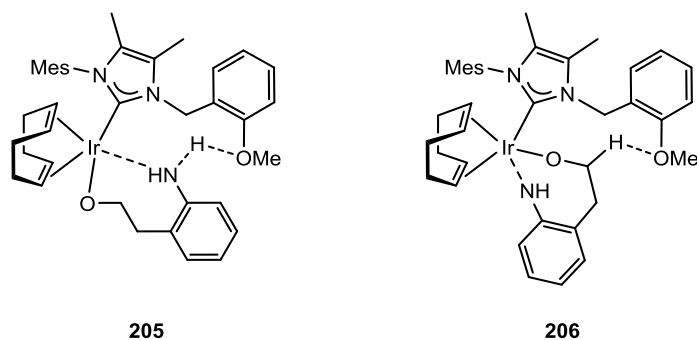


Figure 2.12

Having compared the geometries of the relative substrate-bound intermediates, we next looked to model the pathway for hydride abstraction from the alcohol carbon, and it was here that notable differences between the two substrates were observed. Complex **204** was seen to facilitate oxidation following a pathway similar to that described by Jiménez and co-workers, with the interaction between the hydride and the methoxy interaction serving to activate the substrate. The bidentate substrate binding seen in complexes **205** and **206**, on the other hand, increases the rigidity of the complex and renders formation of the necessary Ir–H interaction significantly more challenging.

The problems associated with oxidation from complexes **205** and **206** are summarised in Figure 2.13. In each of the complexes shown, formation of the Ir–H bond requires the hydride to move in the direction indicated by the blue arrow. For complex **205**, the bidentate coordination of the substrate means that the steric bulk of the nearby amino group, which is held in place by the methoxy oxygen, hinders movement of the alcohol hydrogen. Additionally, the arrangement of the substrate means that there is no activation of the alcohol C–H bond by the methoxy group. In complex **206**, while the alcohol hydrogen can be activated by the methoxy oxygen, the increased rigidity of the substrate due to amine coordination means that rotation of the substrate's alkyl chain is severely restricted, and approach to the iridium centre is sterically hindered. In comparison, complex **204**, with phenyl ethanol as the substrate, is significantly less hindered. Free rotation of the alkyl chain and increased rotation of the Ir–O bond mean that the barrier for approach to the metal centre is more facile.

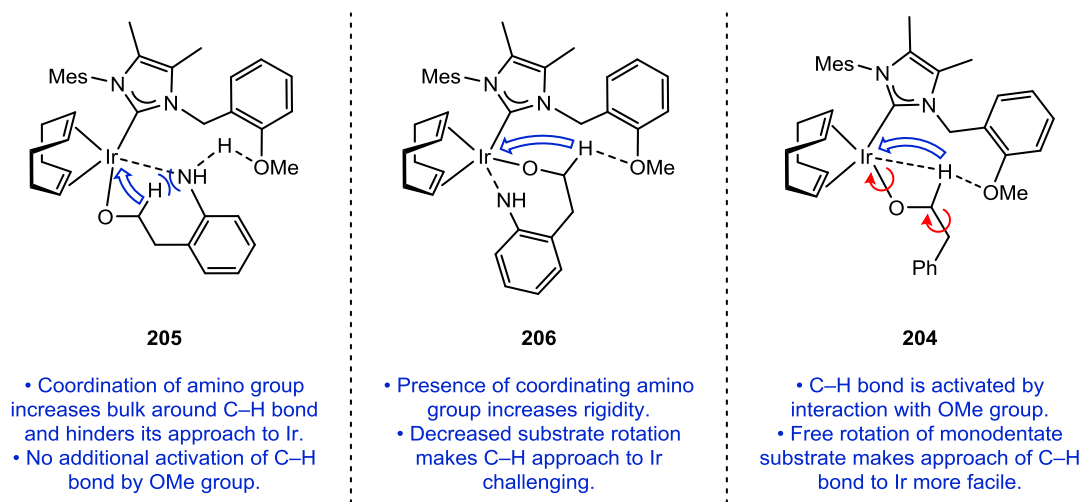
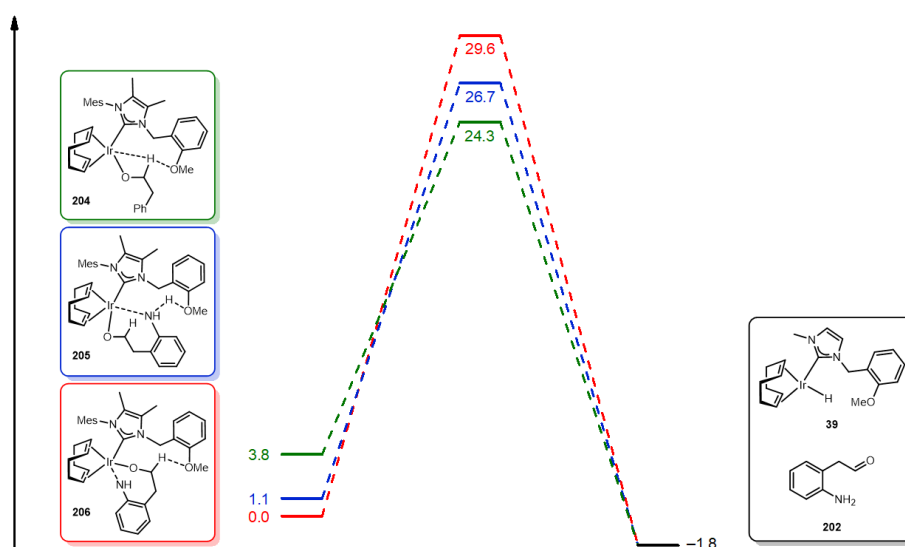


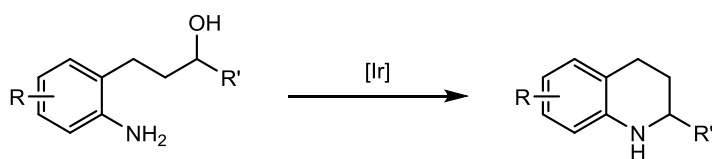
Figure 2.13

Graph 2.3 shows the energy barriers for hydride abstraction with all three modelled alkoxide complexes. While alkoxide complexes **205** and **206** are both lower in energy than **204**, it can be seen that they both have significantly higher energy barriers. **206** has the highest activation barrier of 29.6 kcal/mol, and is unlikely to predominate as a pathway. Oxidation of substrate **60** is therefore believed to proceed *via* intermediate **204**; while this has a much more feasible barrier of 20.5 kcal/mol, it is still significantly higher than the barrier for the reaction of substrate **71** in the intermolecular process. We therefore propose that the harsher conditions required to achieve high conversions for the synthesis of indole **61** from **60** are a result of the increased energy barrier compared to the analogous intermolecular reaction.



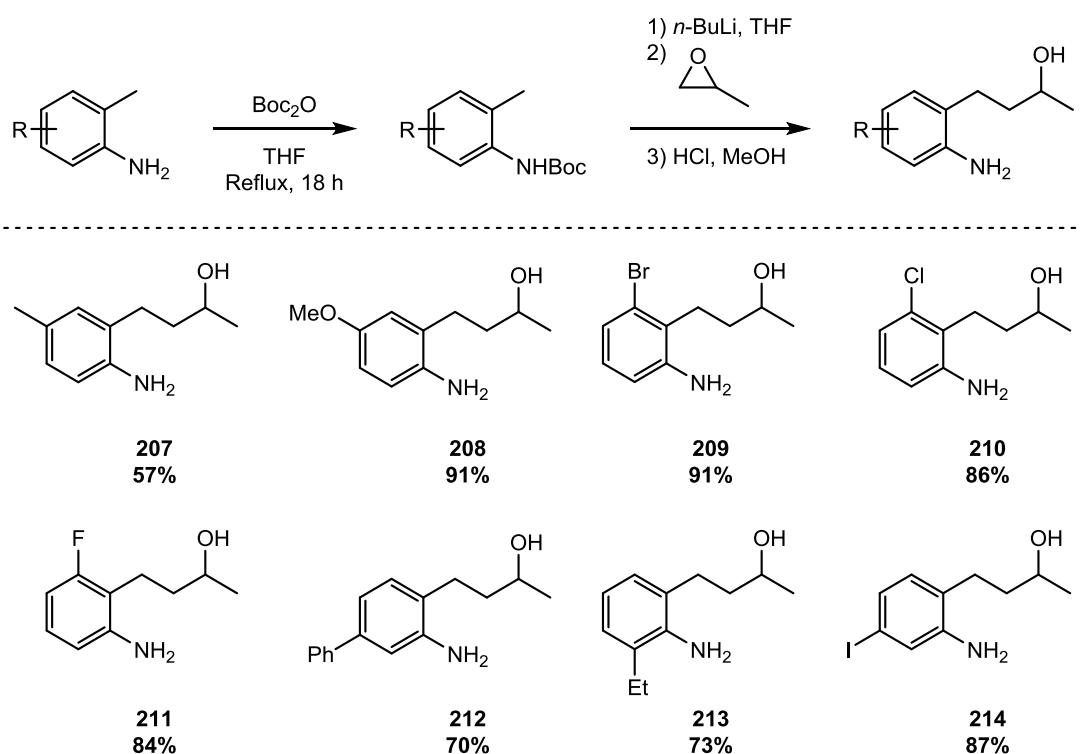
Graph 2.3

Having now developed an amenable set of conditions for indole synthesis *via* *N*-alkylation of amines with alcohols, and having explored the mechanistic aspects of this intramolecular reaction, we next sought to expand the scope of our heterocycle synthesis methodology. So far, reactions had been carried out to synthesise indole **61** through an oxidative cyclisation method. In expanding our substrate scope, however, we looked to the synthesis of an alkyl *N*-heterocycle and decided to focus on the synthesis of tetrahydroquinoline derivatives, from the homologated analogues of substrate **60**, as shown in Scheme 2.65. Our reasons for selecting this reaction were threefold. Firstly, the requisite substrates can be easily made from commercial starting materials, whereas analogues of **60** are significantly harder to prepare. Additionally, the preparation of an alkyl *N*-heterocycle would proceed *via* a true hydrogen borrowing process, *i.e.* with reduction of the imine generated *in situ* from condensation of the alcohol oxidation product. This could avoid some of the difficulties we faced when developing our indole synthesis methodology. Lastly, the easy modification of the alkyl chain would allow us to investigate the reaction of secondary alcohols. This is an attractive target in itself, but would also enable us to investigate the possibility of developing an asymmetric variant of this methodology.



Scheme 2.65

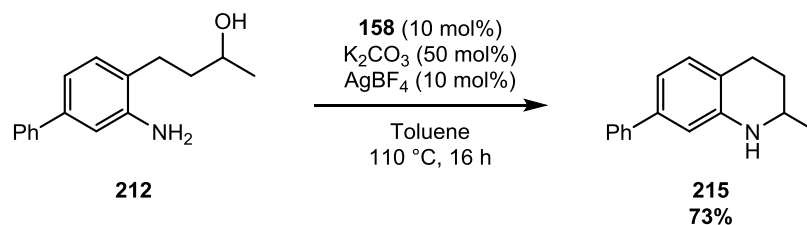
A series of substrates were prepared in good to excellent yields as shown in Scheme 2.66. After Boc protection of the requisite 2-methylanilines, deprotonation with *n*-butyllithium followed by epoxide ring opening was used to introduce the extended alcohol chain. Boc deprotection was carried out *in situ* to furnish the desired substrates.



NB Yields are reported over both steps

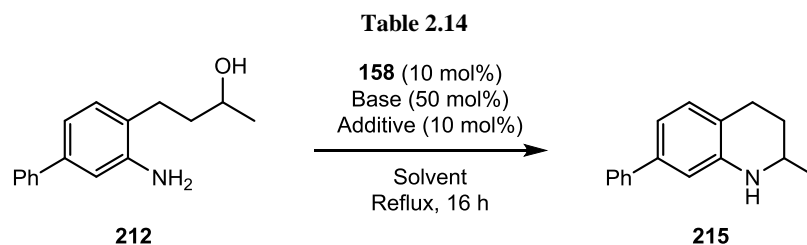
Scheme 2.66

With a series of substrates in hand, we were eager to attempt the hydrogen borrowing reaction. **212** was chosen as a test substrate and was first subjected to our optimised conditions for the reaction of **60** (Scheme 2.67). The alkene additive was removed due to the fact that we expected the generated imine to undergo a reduction process, as opposed to the rearomatisation seen for **60**. We were pleased to see that this initial reaction yielded **215** in 73% yield, despite the fact that we were using a secondary alcohol, which would typically be expected to be a more challenging substrate.



Scheme 2.67

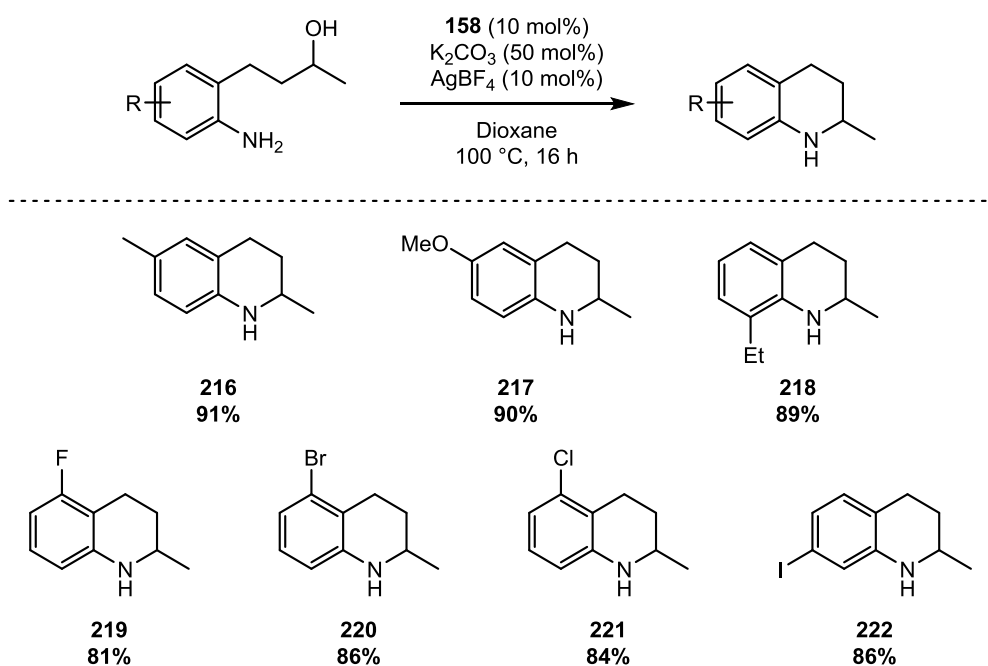
A short screening of our previously most successful bases, additives, and solvents showed that a switch to refluxing dioxane offered an increase in yield to 83% (Table 2.14, Entry 4). These conditions were carried forward for our substrate scope.



Entry	Additive	Base	Solvent	Conversion* / %
1	AgBF ₄	<i>t</i> -BuOK	Toluene	64
2	NaBAr _F	K ₂ CO ₃	Toluene	66
3	AgBF ₄	<i>t</i> -BuOK	Dioxane	69
4	AgBF ₄	K ₂ CO ₃	Dioxane	83
5	NaBAr _F	<i>t</i> -BuOK	Dioxane	58
6	NaBAr _F	K ₂ CO ₃	Dioxane	73

* Calculated using LCMS analysis

Substrates **207–214** were subjected to our optimised conditions (Scheme 2.68). We were delighted to see that excellent functional group tolerance was observed, with substrates bearing electron-withdrawing and electron-donating groups reacting equally well, in the range of 81–91%.



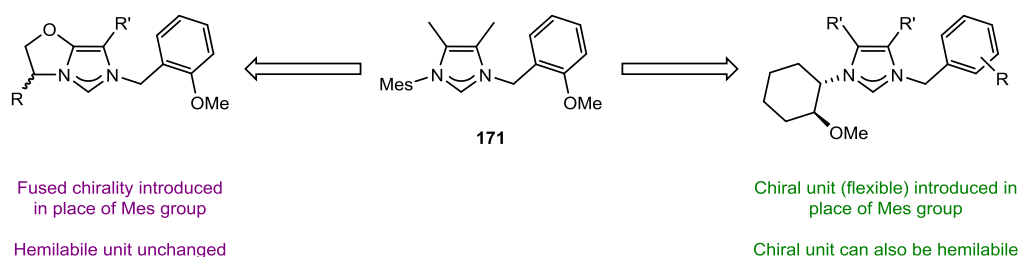
Scheme 2.68

To summarise, in a fruitful extension of our iridium-catalysed *N*-alkylation methodology, we have now successfully developed procedures for the intramolecular synthesis of indoles and tetrahydroquinolines *via* transfer hydrogenation. The challenging nature of these reactions when compared to our intermolecular borrowing hydrogen methodology has been rationalised using computational studies, which highlighted the formation of an O,N chelate motif upon substrate binding to iridium and the corresponding increased energy barrier for alcohol oxidation. The scope of our methodology has been extended to a series of tetrahydroquinoline derivatives, and the successful reaction of a range of secondary alcohols puts us in good stead for a rational progression of our studies into the development of methodology for asymmetric C–N bond formation.

Ligand Design for Asymmetric Transfer Hydrogenation

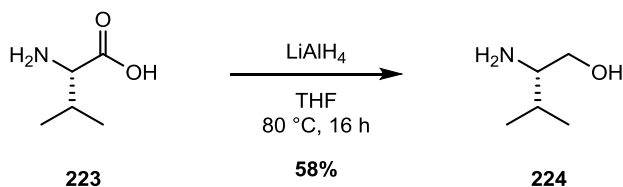
Having successfully developed two methods for the *N*-alkylation of amines with alcohols, both inter- and intramolecularly, we were now keen to further develop our range of complexes in order to expand their reactivity. As discussed previously, the increased interest in 3D drug scaffolds from the pharmaceutical industry means that the preparation of chiral amines remains an important challenge in synthetic chemistry. Recent work within the Kerr group has involved the synthesis of a range of chiral iridium NHC/phosphine complexes, which have been successfully applied in the asymmetric hydrogenation of olefins.¹³⁰ Having had so much success with our hydrogen borrowing methodology, our thoughts turned to the possibility of developing a chiral ligand system that would allow us to develop asymmetric variants of these processes.

Our work so far had shown that the presence of a methoxy substituent on one arm of the NHC was essential for the high reactivity observed. Looking to include this key substituent in any new ligand motifs, two strategies for the development of a chiral NHC ligand were proposed, as depicted in Scheme 2.69. Our first strategy, shown on the left, was to maintain the use of a 2-methoxybenzyl substituent as one arm of the NHC. However, the aryl substituent normally present in our unsymmetrical NHCs would be replaced by an oxazoline unit, fused to the NHC ring. Fused NHC/oxazoline systems have shown excellent activity in a range of asymmetric transformations, including those developed within the group,^{130,157} and we were confident that the presence of a bulky R group could be a good source of asymmetric induction. Our alternative strategy, shown on the right of Scheme 2.69, focused on the inclusion of the donor substituent as part of the chiral portion of the NHC. Douthwaite and co-workers have demonstrated that the use of chiral amino-substituted cyclohexyl NHCs can be highly effective,¹¹⁰ so we postulated that a similar system, with a chiral cyclohexyl substituted with a methoxy group, could be an effective alternative. The other arm of the NHC could be alkylated with a benzyl group, either with or without a donor substituent.



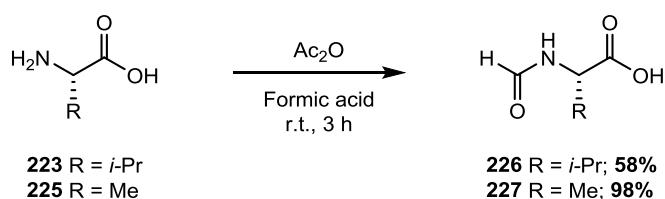
Scheme 2.69

Initially, we looked to explore our first strategy and investigate the synthesis of an NHC–oxazoline fused system. This was carried out using a method described by Yoshida and co-workers.¹⁵⁸ Since the starting materials were amino acids, this strategy would offer good opportunities for modification at a later date, if necessary. In the first instance, the reduction of L-valine with lithium aluminium hydride was carried out (Scheme 2.70).



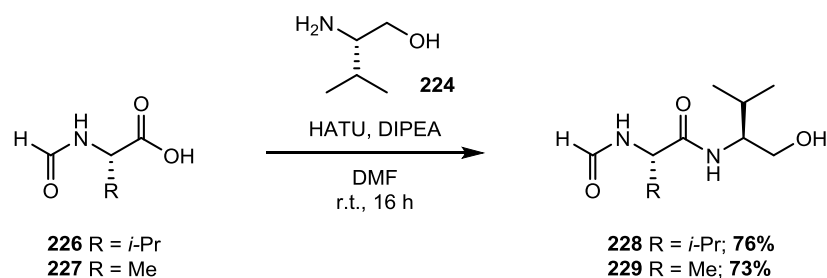
Scheme 2.70

In order to construct the oxazoline/NHC ring system, L-valinol **224** would be coupled with the relevant *N*-formyl amino acid. To investigate the effect of both methyl and *iso*-propyl substituents on the NHC backbone, the formylation of L-alanine and L-valine was carried out, as shown in Scheme 2.71. We were pleased to see that both reactions proceeded smoothly, affording **226** and **227** in good to excellent yields.



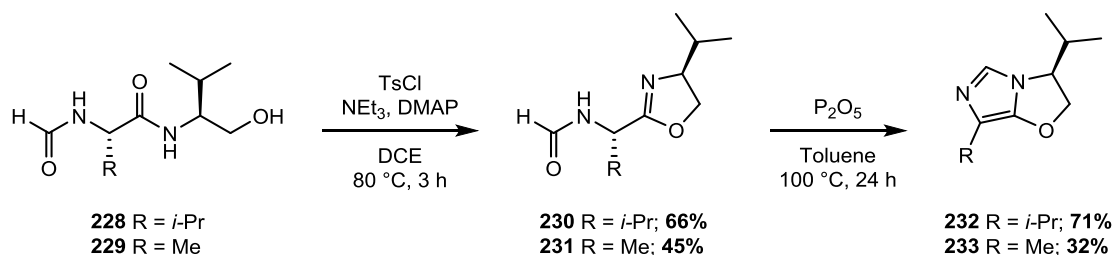
Scheme 2.71

Products **226** and **227** were next coupled with L-valinol using HATU, as shown in Scheme 2.72. Again, both reactions were successful, giving good yields of dipeptides **228** and **229**.



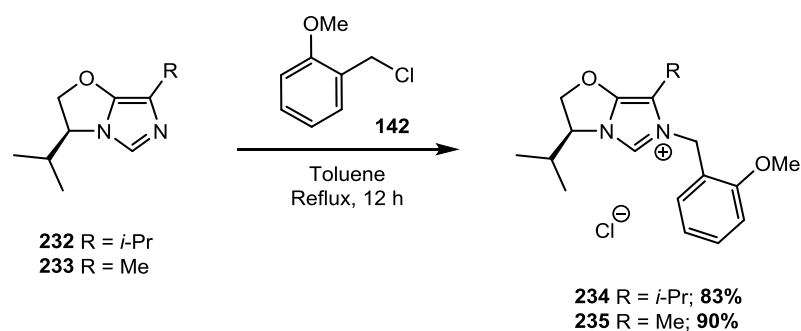
Scheme 2.72

With dipeptides **228** and **229** in hand, we could now attempt the two cyclisation reactions required to build up the oxazoline and NHC ring systems. Firstly, tosyl chloride was used to induce the intramolecular cyclisation of **228** and **229**. Oxazoline products **230** and **231** then underwent a second cyclisation, mediated by P_2O_5 , to afford fused imidazole/oxazoline compounds **232** and **233** (Scheme 2.73). While the yields were lower than expected for the methyl-substituted system, we were delighted to have prepared both bicyclic systems in sufficient quantities for further investigation.



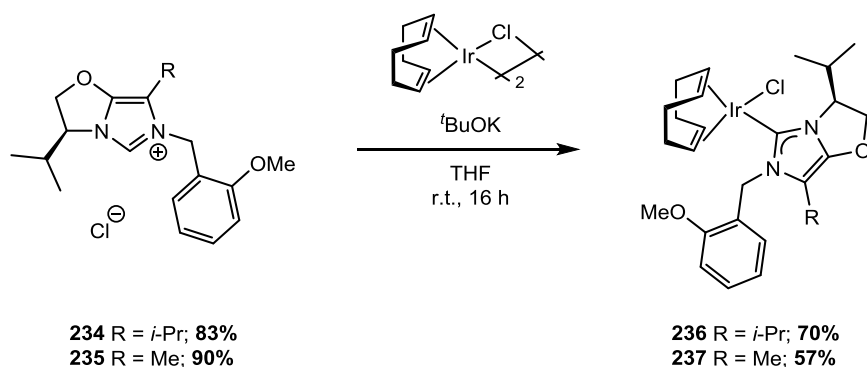
Scheme 2.73

Having successfully prepared two bicyclic imidazole/oxazoline compounds, we were keen to prepare the corresponding imidazolium salts, ready for complexation to iridium. Using the same procedure used for our achiral NHC ligands, **232** and **233** smoothly underwent alkylation with benzyl chloride **142** to afford imidazolium chlorides **234** and **235** in excellent yields, as shown in Scheme 2.74.



Scheme 2.74

Lastly, **234** and **235** were complexed to iridium using our standard procedure (Scheme 2.75). We were delighted to see that both reactions proceeded efficiently, affording chiral iridium complexes **236** and **237** in good yields.

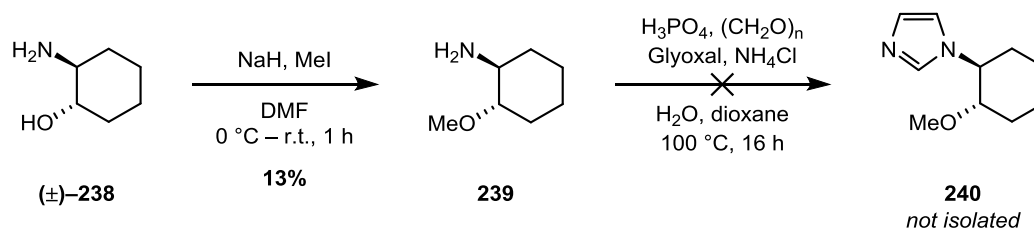


Scheme 2.75

With two NHC/oxazoline complexes now in hand, we looked to investigate our second ligand strategy, with the synthesis of a chiral cyclohexyl-substituted NHC. Due to the high cost of the chiral starting material, this synthesis was carried out using the racemate of *trans*-2-aminocyclohexanol **238**. Since the ligand we were targeting here was significantly different in structure to any that we had prepared previously, it was thought that this would allow us to first investigate the complex's activity, before continuing with a chiral synthesis if the desired catalytic activity was achieved.

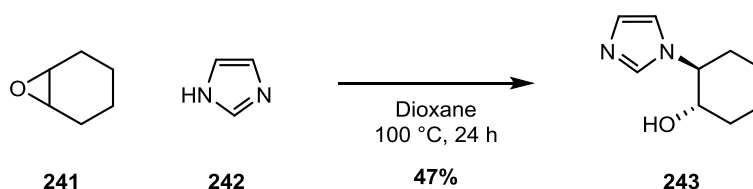
In the first instance, the *O*-methylation of 2-aminocyclohexanol **238** and the subsequent formation of the corresponding imidazole was targeted (Scheme 2.76). We quickly met, however, with some practical difficulties. Upon workup of the methylation reaction, a complex mixture of products was observed, presumably due to a mixture of *N*- and *O*-

alkylation having taken place. This made for a complex purification, but we were able to isolate a small amount of the desired *O*-methyl product. Upon using this in the subsequent imidazole formation, however, we were disappointed to isolate none of the desired product.



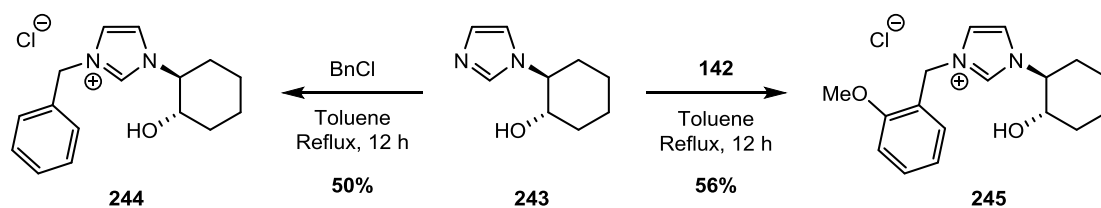
Scheme 2.76

At this stage, we considered an alternative strategy to avoid the problems associated with non-selective alkylation. As shown in Scheme 2.77, it was decided to prepare the hydroxy-substituted cyclohexyl imidazole from epoxide **241**. This could then be taken through to the imidazolium salt before undergoing methylation at a later stage. As well as avoiding a challenging methylation reaction at this stage, this route had the added advantage of not requiring an imidazole formation; these reactions typically involve difficult purifications and low yields. As such, we were more than satisfied with the 47% yield of **243** obtained.



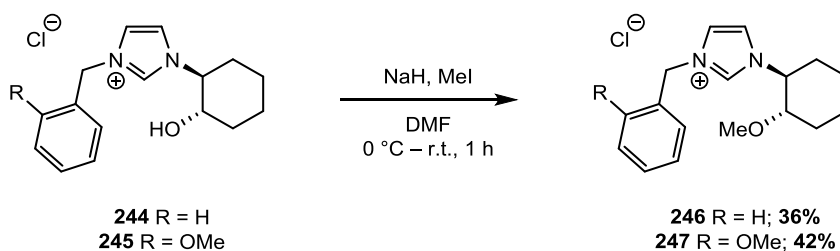
Scheme 2.77

Imidazole **243** was next submitted to two *N*-alkylation reactions, as shown in Scheme 2.78. We chose to use both 2-methoxybenzyl chloride, as in our previous work, as well as an unsubstituted analogue. This would allow us to investigate the difference between ligands with one and two donor substituents. Pleasingly, both alkylation reactions proceeded smoothly.



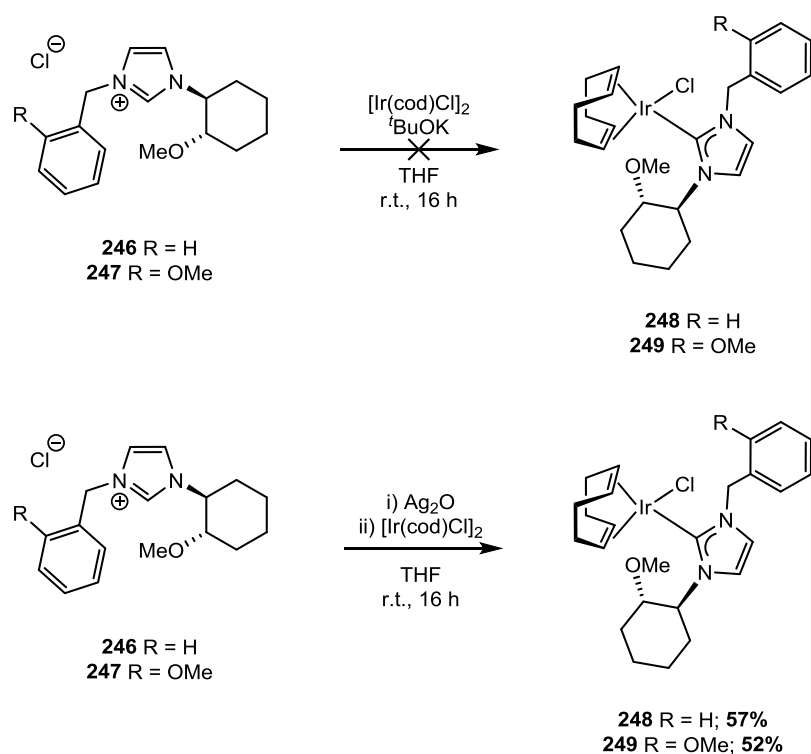
Scheme 2.78

Finally, the *O*-methylation reaction was attempted on **244** and **245** (Scheme 2.79). While the yields obtained were relatively low, we were nevertheless pleased to isolate both of the desired methoxy-substituted ligands.



Scheme 2.79

With two novel imidazolium salts in hand, complexation reactions were next carried out. These were first attempted using our standard conditions, shown at the top of Scheme 2.80. Disappointingly, however, that neither of the desired complexes could be isolated. Pleasingly, however, using an alternative route, which proceeds *via* a silver carbene, worked well, and we were delighted to isolate complexes **248** and **249**.

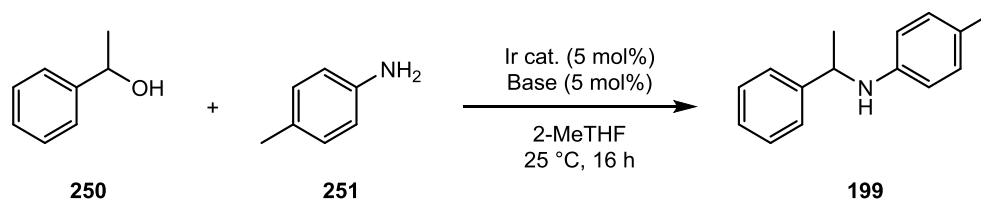


Scheme 2.80

At this stage in the project, we looked to test our complexes **236**, **237**, **248**, and **249** as catalysts in a hydrogen borrowing reaction. As a benchmark reaction, we looked to the alkylation of 4-methylaniline with α -methylbenzyl alcohol. The achiral version of this reaction was shown to proceed efficiently with catalyst **164** in our earlier studies, and the choice of substrate meant that while a chiral centre is formed adjacent to the nitrogen, the steric bulk should not be large enough to hinder reactivity.

We first screened our four new complexes under our previously optimised conditions for *N*-alkylation. Reactions were screened with both alkoxide and carbonate bases, and our initial results are shown in Table 2.15. Initially, we were delighted to see reactivity from catalysts **236** and **237** (Entries 1–4). Upon repetition of the reaction, however, it quickly became apparent that these results were not reproducible, with three runs of each set of conditions delivering vastly different results. Moreover, chiral HPLC analysis confirmed that even in the reactions that had proceeded, the product was completely racemic. Even more disappointingly, cyclohexyl-derived complexes **248** and **249** were found to exhibit no reactivity whatsoever (Entries 5–8).

Table 2.15



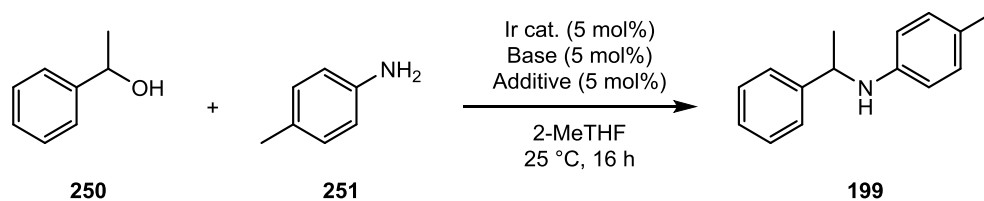
Entry	Catalyst	Base	Conversion / %			<i>e.e.*</i> / %
			Run 1	Run 2	Run 3	
1	236	^t BuOK	42	55	47	<5
2	236	K ₂ CO ₃	52	<5	38	<5
3	237	^t BuOK	29	38	20	<5
4	237	K ₂ CO ₃	31	22	8	<5
5	248	^t BuOK	<5	-	-	-
6	248	K ₂ CO ₃	<5	-	-	-
7	249	^t BuOK	<5	-	-	-
8	249	K ₂ CO ₃	<5	-	-	-

* Based on material isolated from Run 1.

At this stage, we decided to screen a number of alternative reaction conditions. It was decided to test both elevated temperatures – which could improve reactivity – and low temperatures, which could be more conducive to enantioinduction. Reactions were also carried out in the presence of silver tetrafluoroborate, which was previously shown to increase catalyst activity for challenging intramolecular cyclisation reactions. The results of our extensive screening are summarised in Table 2.16.

The addition of silver tetrafluoroborate to the previously screened conditions (Entries 1–4 and 13–16) offered improvement to neither the reproducibility of the reaction nor the reactivity. In the case of catalysts **236** and **237**, an increase in temperature to 100 °C led to complete decomposition of the catalyst and the formation of an inseparable mixture of compounds (Entries 5–8). On the other hand, a decrease in temperature to 0 °C hindered almost all reactivity. While no decomposition of **248** and **249** was observed at high temperatures, reactivity remained minimal.

Table 2.16



Entry	Catalyst	Base	Additive	Solvent	Temp. / °C	Conversion / %			<i>e.e.</i> * / %
						1	2	3	
1	236	^t BuOK	AgBF ₄	2-MeTHF	25	58	12	46	<5
2	236	K ₂ CO ₃	AgBF ₄	2-MeTHF	25	47	30	34	<5
3	237	^t BuOK	AgBF ₄	2-MeTHF	25	36	18	22	<5
4	237	K ₂ CO ₃	AgBF ₄	2-MeTHF	25	29	44	8	<5
5	236	^t BuOK	AgBF ₄	Toluene	100	Decomp.			-
6	236	K ₂ CO ₃	AgBF ₄	Toluene	100	Decomp.			-
7	237	^t BuOK	AgBF ₄	Toluene	100	Decomp.			-
8	237	K ₂ CO ₃	AgBF ₄	Toluene	100	Decomp.			-
9	236	^t BuOK	AgBF ₄	2-MeTHF	0	<5	-	-	-
10	236	K ₂ CO ₃	AgBF ₄	2-MeTHF	0	<5	-	-	-
11	237	^t BuOK	AgBF ₄	2-MeTHF	0	<5	-	-	-
12	237	K ₂ CO ₃	AgBF ₄	2-MeTHF	0	<5	-	-	-
13	248	^t BuOK	AgBF ₄	2-MeTHF	25	<5	-	-	-
14	248	K ₂ CO ₃	AgBF ₄	2-MeTHF	25	<5	-	-	-
15	249	^t BuOK	AgBF ₄	2-MeTHF	25	<5	-	-	-
16	249	K ₂ CO ₃	AgBF ₄	2-MeTHF	25	<5	-	-	-
17	248	^t BuOK	AgBF ₄	Toluene	100	<5	-	-	-
18	248	K ₂ CO ₃	AgBF ₄	Toluene	100	<5	-	-	-
19	249	^t BuOK	AgBF ₄	Toluene	100	<5	-	-	-
20	249	K ₂ CO ₃	AgBF ₄	Toluene	100	<5	-	-	-

* Based on material isolated from Run 1.

The results obtained in this screening were, of course, disappointing. While moderate reactivity had been observed in some cases, issues with reproducibility were arising, and no enantioselectivity whatsoever had been observed. Our results suggested that while catalysts **236** and **237** were indeed active in the alkylation reaction, the lack of consistency was likely due to the thermal instability of the complexes. Indeed, both complexes were found not to be

bench stable, degrading within 1-2 weeks of their synthesis. The complete decomposition observed at 100 °C supports this idea.

In order to investigate whether a ligand bearing a bulky aryl unit could offer an alternative solution, the reaction was carried out with complexes **252** and **253**, which have been employed within the group in asymmetric hydrogenation reactions, delivering high yields and enantioselectivities.¹³⁰ The results are shown in Table 2.17. Both complexes tested showed no reactivity whatsoever under our tested conditions.

Table 2.17

252

253

Entry	Catalyst	Base	Additive	Solvent	Temp. / °C	Conversion / %			<i>e.e.</i> * / %
						1	2	3	
1	252	K ₂ CO ₃	-	2Me-THF	25	0	-	-	-
2	252	K ₂ CO ₃	AgBF ₄ -	2Me-THF	25	0	-	-	-
3	253	K ₂ CO ₃	-	2Me-THF	25	0	-	-	-
4	253	K ₂ CO ₃	AgBF ₄	2Me-THF	25	0	-	-	-

Due to time constraints, no further investigations into asymmetric hydrogen borrowing could be carried out. It should be noted, however, that although no sufficient activity was obtained with our prepared complexes, the reactivity exhibited by **236** and **237** is highly promising, and further investigations into the catalyst stability could well enable the reaction to proceed more reliably. The lack of enantioselectivity observed is disheartening, however the synthesis of **236** and **237**, from commercial amino acids, means that the preparation of analogues, bearing larger substituents, should also be possible.

Overall, the work described within this final section represents an important step into the design and preparation of chiral ligands. While preliminary attempts at asymmetric hydrogen borrowing met with limited success, the behaviour of these novel functionalised ligands remains largely unexplored, and the structures described herein could find activity in a number of synthetically useful asymmetric transformations. The synthetic routes devised will offer access to a diverse range of analogues, allowing future work to include a full investigation of substituent effects, and, similarly, the iridium halide complexes prepared can be used as starting materials for the synthesis of alternative iridium complexes.

Conclusions

The work described in this chapter represents an important new area of reactivity for iridium catalysts developed within the Kerr group. In the first section, the synthesis of a new family of *N*-heterocyclic carbene ligands, strategically designed for use in hydrogen borrowing catalysis, was targeted. A series of 12 imidazolium salts, based on novel NHC motifs functionalised with one or more donor substituents, were prepared; these were successfully complexed to iridium to yield 12 neutral iridium(I) NHC/halide compounds. To complement the preparation of these complexes, a range of techniques were used to explore the electronic and steric properties of our NHC motifs in the context of several known and commonly used NHC ligands.

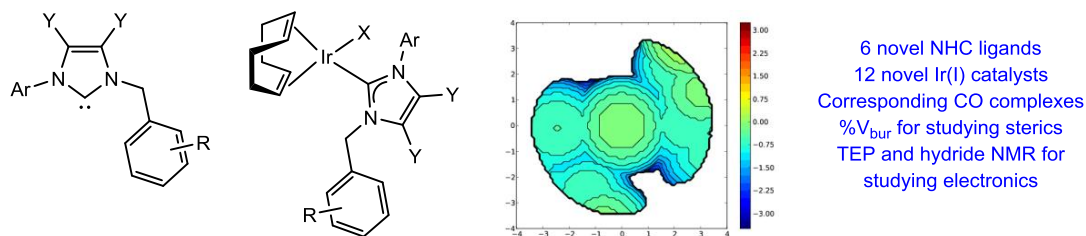
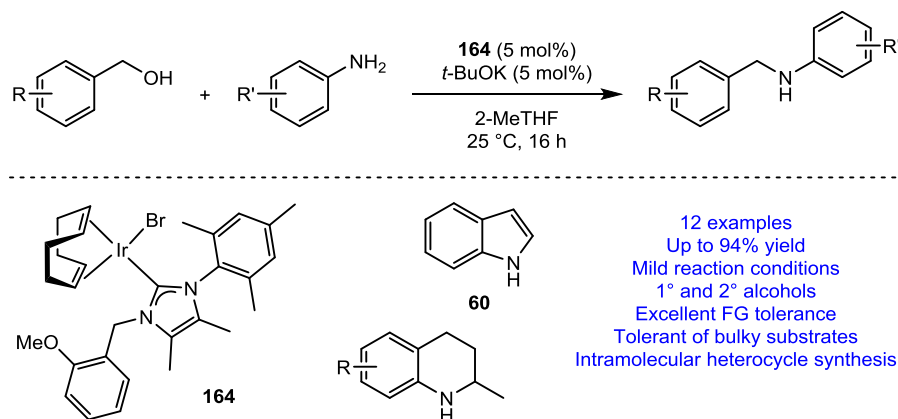


Figure 2.14

Our new complexes were tested as catalysts in the *N*-alkylation of aniline *via* hydrogen borrowing. All of the developed complexes showed catalytic activity, and two were taken forward for further optimisation. In a key development, complex **158** was found to be a highly efficient catalyst for the *N*-benzylation of aniline at room temperature; this offers significant practical advantages over the high temperatures often required for similar procedures. Our hydrogen borrowing methodology was then applied to a series of benzyaniline derivatives with great success. Comparison of analogous complexes, along with computational studies, demonstrated that the presence of a hemilabile methoxy substituent and of a bulky aryl group on the NHC are both key to the high catalytic activity observed.

Our alkylation methodology has also been expanded to include the synthesis of *N*-heterocycles *via* intramolecular C–N bond formation. It was quickly established that this was significantly more challenging than our previous *N*-benzylation work, and that the elevated temperatures we had avoided so far would be necessary here. Nevertheless, through thorough optimisation, we were able to develop a highly efficient cyclisation method for the

synthesis of a series of indoles and tetrahydroquinolines. Rate studies and computational investigations highlighted that the intramolecular C–N bond formation is hindered by bidentate substrate binding, which is avoided in the intermolecular variant.



Scheme 2.81

Lastly, our recent work has involved further expansion of our range of iridium complexes to include those bearing chiral NHC ligands. Once again, a series of ligands were strategically designed, incorporating hemilabile donor substituents alongside bulky chiral oxazoline units, and their synthesis was targeted. A small series of donor-functionalised, chiral fused NHC–oxazoline ligands were successfully prepared through a 5-step process, and the corresponding iridium complexes synthesised. While our preliminary attempts at asymmetric *N*-alkylation with secondary alcohols were unsuccessful, the ligands prepared herein represent a new class of functionalised NHC motifs, and ongoing work aims to further explore their behaviour.

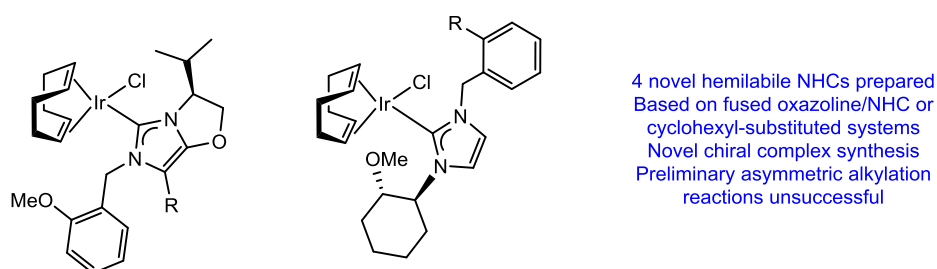


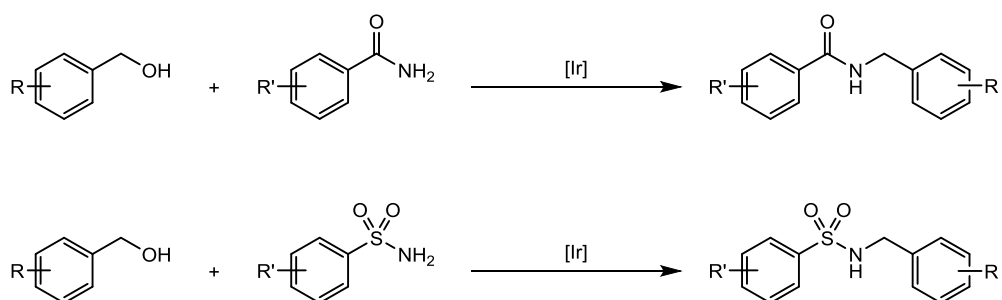
Figure 2.15

Overall, the preparation of a number of new ligands and iridium complexes, and the development of two efficient *N*-alkylation methods represent a new field of research for Kerr

group catalysts, and offers the organic chemistry community expedient access to a wide range of useful amine-containing compounds.

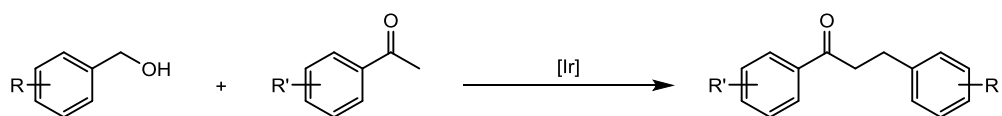
Future Work

The NHCs designed and prepared within this chapter represent a new class of ligand, and there remains enormous scope for further investigation of their activity in a number of reactions. In terms of the hydrogen borrowing methodology developed herein, a number of applicable substrates can be considered. Recent work within the group has discovered that the *N*-alkylation of alkyl amines with our new catalysts was unsuccessful, most likely due to irreversible substrate binding caused by the increased Lewis basicity of the nitrogen atom.¹⁴⁵ An alternative area of interest, however, is the use of amide or sulfonamide substrates, as shown in Scheme 2.82. In this case, it would be essential to monitor the effect of the carbonyl or sulfonyl groups present; since both these groups are known to coordinate to iridium, it is key that their presence does not cause poisoning of the catalyst through irreversible coordination.



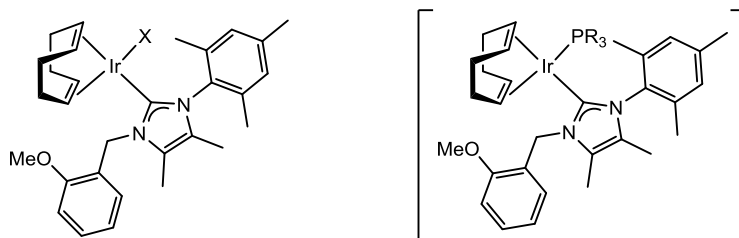
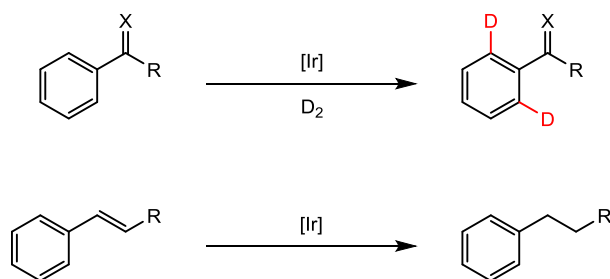
Scheme 2.82

Also of interest to us is the application of our hydrogen borrowing methodology in the direct α -alkylation of ketones with alcohols (Scheme 2.83). This system proceeds *via* a similar mechanism to the *N*-alkylation methods described within this thesis, with the carbonyl species generated *in situ* being attacked by an enolate nucleophile instead of an amine. There are several reports in the literature of such a reaction proceeding under iridium catalysis,³² and the application of our catalysts to this system could offer a mild and convenient route to the formation of new C–C bonds.



Scheme 2.83

Lastly, there remains the possibility of exploring the behaviour of our novel iridium NHC/halide complexes, and their cationic phosphine analogues, in the hydrogen isotope exchange and hydrogenation processes carried out with other Kerr group catalysts. This would allow us to assess the effect of unsymmetrical NHC ligands, and in particular those with weakly-coordinating donor substituents, in the context of a number of catalysts whose activity is more well understood.



Scheme 2.84

In terms of the asymmetric processes investigated within this chapter, a more thorough investigation into the properties of our novel chiral ligands will be essential. The two key issues faced within this section were the low activity and/or thermal instability of the complexes, as well as the lack of asymmetric induction. The first problem can be investigated with derivatisation of the complexes involved; is a more bulky aryl substituent required? Would a less labile ligand than a halide be more effective? Do we need to alter the NHCs' electronic properties? With regards to the lack of asymmetric induction, computational studies could offer enormous insight, and allow us to screen a library of ligand analogues before attempting their synthesis. A full theoretical understanding of the

mechanism of asymmetric hydrogen borrowing, combined with determination of the ligands' steric properties, could allow us to develop a predictive model for asymmetric induction.

Experimental

General Information

All reagents were obtained from commercial suppliers (Alfa Aesar, Sigma Aldrich, Apollo Scientific or Strem) and used without further purification, unless otherwise stated. Purification was carried out according to standard laboratory methods.¹⁵⁹

Tetrahydrofuran was purified by heating to reflux over sodium wire, using benzophenone ketyl as an indicator, before distilling under nitrogen. Dichloromethane was purified by heating to reflux over calcium hydride, before distilling under nitrogen. Diethyl ether and toluene were obtained from a PureSolv SPS-400-5 Solvent Purification System. Triphenylphosphine was purified by recrystallisation from ethanol, followed by drying under vacuum.

Thin layer chromatography was carried out using Camlab silica plates coated with fluorescent indicator UV254. The plates were analysed using a Mineralight UVGL-25 lamp, or developed using vanillin or KMnO_4 solution.

Flash column chromatography was carried out using Prolabo silica gel (230-400 mesh).

IR spectra were obtained on a Shimadzu IRAffinity-1 Spectrophotometer machine and are reported in cm^{-1} unless stated otherwise.

^1H , ^{13}C , ^{19}F , and ^{31}P NMR spectra were recorded on a Bruker DPX 400 spectrometer at 400 MHz, 101 MHz, 376 MHz, and 162 MHz, respectively. Chemical shifts are reported in ppm. Coupling constants are reported in Hz, and refer to $^3J_{\text{H-H}}$ interactions unless otherwise stated.

LCMS analysis was carried out with a Waters ZQ LCMS system with an Acquity UPLC CSH C18 column (50 mm \times 2.1 mm) with a flow rate of 1 mL/min. An A:B gradient of 97:3 to 3:97 was used, where mobile phase A = 10 mmol Ammonium Bicarbonate in water adjusted to pH 10, and mobile phase B = Acetonitrile.

High resolution mass spectrometry was carried out by the EPSRC National Mass Spectrometry Facility at the University of Swansea.

General Procedures

General Procedure A – Preparation of Aryl Dimethylimidazoles with 2,3-Butanedione

Carried out following a literature procedure.¹⁶⁰ To a solution of the relevant aniline (12 mmol) as a solution in chloroform (20 mL) was added 2,3-butanedione (875 μ L, 10 mmol), acetic acid (571 μ L, 10 mmol), ammonium acetate (771 mg, 10 mmol), paraformaldehyde (300 mg, 10 mmol), and water (0.5 mL). The mixture was heated at reflux for 16 h before being concentrated *in vacuo*. The residue was dissolved in diethyl ether (50 mL), cooled in an ice bath, and basified to pH 4 with 40% aqueous potassium hydroxide solution. The mixture was extracted with diethyl ether (3 \times 80 mL), washed with water and brine, and dried over sodium sulfate. The solvent was removed *in vacuo* and the resulting residue was purified by flash column chromatography to afford the desired imidazole.

General Procedure B – N-Alkylation of N-Substituted Imidazoles with Benzyl Halides

A solution of the 2-methoxybenzyl halide (3 mmol) in toluene (6 mL) was prepared and heated to 40 °C. The relevant aryl imidazole (3 mmol) was added and the resulting solution was heated to reflux and stirred for 18 h. The reaction was left to cool and concentrated *in vacuo*. The residue was dissolved in ethyl acetate and extracted with water (4 \times 50 mL), before being concentrated *in vacuo*. The residue was purified by column chromatography with DCM as the eluent to afford the desired imidazolium salt.

General Procedure C – Preparation of [Ir(cod)Cl(NHC)] Complexes

Bis(1,5-cyclooctadiene)diiridium(I) dichloride (1 eq.) and potassium *tert*-butoxide (2 eq.) were added to a flame-dried and Ar-cooled Schlenk tube and stirred under vacuum for 10 min. THF (20 mL / mmol) was added and the mixture stirred for 10 min. The relevant imidazolium chloride (2 eq.) was added and the resulting solution stirred at room temperature for 18 h. The solvent was removed *in vacuo*, and column chromatography (50% ethyl acetate in petrol) afforded the title compound.

General Procedure D – Preparation of [Ir(cod)Br(NHC)] Complexes

Carried out according to a literature procedure.¹²⁹ An oven-dried and nitrogen-cooled flask was charged with a solution of the relevant imidazolium bromide salt (1 eq.), bis(1,5-cyclooctadiene)diiridium(I) dichloride (0.5 eq.), and sodium bromide (2 eq.) in THF (20 mL / mmol). The solution was cooled to -78 °C and potassium hexamethyldisilazide (1.15 eq.)

was added as a solution in toluene (15%, 0.7 M). The reaction mixture was held at $-78\text{ }^{\circ}\text{C}$ for 30 min, and then was allowed to warm to room temperature and stirred for 16 h. The solvent was removed *in vacuo* and the product was purified by flash column chromatography, eluting with 50% ethyl acetate in petrol. Concentration *in vacuo* afforded the desired complex.

General Procedure E – Formation of Iridium Dicarbonyl Complexes

A flame-dried and argon-cooled Schlenk flask was charged with a solution of the relevant Ir(I) complex (0.02 mmol) in DCM (1 mL). Under an argon atmosphere, the mixture was cooled to $-78\text{ }^{\circ}\text{C}$ while stirring. The flask was evacuated and backfilled with CO gas from a balloon; this procedure was repeated twice. The reaction mixture was allowed to warm to room temperature and was stirred for 30 min. The reaction volume was reduced by half *in vacuo*, and diethyl ether was added dropwise to triturate the desired complex.

General Procedure F – Formation of MeCN-stabilised Iridium(III) Hydride Complexes

An NMR tube was charged with a solution of the relevant Ir(I) complex (0.01 mmol) in acetonitrile- d_3 (0.6 mL), before being sealed with a rubber septum and cooled to $0\text{ }^{\circ}\text{C}$. The tube was fitted with a H_2 balloon and an exit needle. H_2 gas was bubbled through the mixture for 3 min at $0\text{ }^{\circ}\text{C}$, during which a colour change from orange to pale yellow was observed. The tube was sealed under 1 atm of H_2 and placed in a Bruker DPX 400 spectrometer with the sample temperature set to 298 K. The resulting hydride intermediates were analysed by ^1H (wide spectrum: sw = 60 ppm, o1p = -20 ppm) and ^{31}P NMR spectra.

General Procedure G – N-Alkylation of Anilines with Benzyl Alcohols

A microwave vial with stirrer bar was charged with the relevant iridium catalyst and base, and sealed with a rubber septum. The relevant alcohol was added *via* syringe as a solution in the reaction solvent, followed by the aniline, also as a solution. The reaction mixture was heated to the appropriate temperature and stirred for 16 h. The mixture was concentrated *in vacuo* and the crude residue was purified by column chromatography to give the desired product.

General Procedure H – Intramolecular N-Heterocycle Synthesis via N-Alkylation

A microwave vial with stirrer bar was charged with the relevant iridium catalyst and base, and sealed with a rubber septum. The relevant substrate was added as a solution in the desired reaction solvent. The reaction mixture was heated to the appropriate temperature and stirred for 16 h. The reaction mixture was concentrated *in vacuo* and conversions were calculated using LCMS analysis of the crude reaction mixture. Isolated yields were obtained by column chromatography of the residue to afford the desired product.

General Procedure I – Intramolecular N-Alkylation with Halide Abstrator Additives

A vial with stirrer bar was charged with the relevant iridium complex. The reaction solvent (1 mL) was added, followed by the appropriate additive. The resulting suspension was passed through a filtration frit into a reaction vial with stirrer bar. The relevant base was added, followed by the substrate as a solution in the appropriate reaction solvent, and the sacrificial hydrogen acceptor if necessary. The reaction was heated to the relevant temperature and stirred for 16 h. The reaction mixture was concentrated *in vacuo* and conversions were calculated using LCMS analysis of the crude reaction mixture. Isolated yields were obtained by column chromatography of the residue to afford the desired product.

General Procedure J – N-Boc Protection of 2-Methylanilines

Carried out following a literature procedure.¹⁶¹ To a flame-dried and argon-cooled flask fitted with a condenser was added THF (5 mL), di-*tert*-butyl dicarbonate (697 μ L, 3 mmol), and the relevant aniline (2.73 mmol). The resulting solution was heated to reflux for 18 h, after which it was allowed to cool to room temperature. The reaction mixture was concentrated *in vacuo* to afford the desired Boc-protected aniline.

General Procedure K – Alkylation and in situ Deprotection of 2-Methyl-N-Boc-anilines

Carried out according to a literature procedure.⁸³ A solution of the relevant *N*-Boc aniline (2 mmol) in THF (6 mL) was prepared under nitrogen and cooled to 0 °C. *n*-Butyllithium (2.000 mL, 5.00 mmol) (2.6 M in hexane) was added dropwise *via* syringe and the reaction mixture was stirred at 0 °C for 2 h. The solution was then cooled to –78 °C and 2-methyloxirane (0.420 mL, 6.00 mmol) was added. The reaction mixture was stirred overnight at 0 °C, after which it was quenched with water and extracted with ethyl acetate. The organic layer was washed with brine, dried through a hydrophobic frit, and concentrated

in vacuo. The residue was dissolved in methanol (5 mL) and hydrochloric acid (4 mL, 12.00 mmol) (3M in water) was added. The resulting solution was stirred for 24 h at room temperature, before being neutralised by careful addition to aqueous sodium hydroxide solution. The product was extracted with ethyl acetate, washed with brine and saturated sodium bicarbonate solution, dried through a hydrophobic frit, and concentrated *in vacuo*.

General Procedure L – N-Formylation of Amino Acids

Carried out according to a literature procedure.¹⁶² A solution of the relevant amino acid (56 mmol) in formic acid (50 mL) was prepared and cooled to 0 °C. Acetic anhydride (42.3 mL, 448 mmol) was added and the reaction mixture was allowed to reach room temperature. After stirring for 3 h, water (20 mL) was added and the mixture was concentrated *in vacuo* to afford the desired product.

General Procedure M – Coupling of N-Formylamino Acids and Amino Alcohols with HATU

The relevant *N*-formylamino acid (4.84 mmol) was dissolved in dry DMF (45 mL). 1-[Bis(dimethylamino)methylene]-1H-1,2,3-triazolo[4,5-b]pyridinium-3-oxide hexafluorophosphate (HATU) (2.024 g, 5.32 mmol) was added and the mixture was stirred at room temperature for 15 min. L-valinol (500 mg, 4.84 mmol) was added and the solution was stirred for 20 mins, after which di-*iso*-propylethylamine (DIPEA) (2.53 mL, 14.52 mmol) was added. The reaction was stirred for 16 h at room temperature, after which a saturated solution of sodium chloride was added. The mixture was cooled to 5 °C, and the resulting precipitate was collected by filtration and washed with water.

General Procedure N – Intramolecular Oxazoline Cyclisation with Tosyl Chloride

Carried out following a literature procedure.¹⁵⁸ The relevant dipeptide (2 mmol) and *N,N*-dimethyl-4-aminopyridine (DMAP) (4 mg, 0.03 mmol) were suspended in dichloroethane (16 mL). Triethylamine (1.2 mL, 0.87 mmol) was added, followed by a solution of *p*-toluenesulfonyl chloride (400 mg, 2.1 mmol) in DCE (8 mL). The mixture was allowed to stir at room temperature for 40 minutes, before being heated to 80 °C for 3 h. A saturated solution of sodium bicarbonate was added, and the aqueous layer was then extracted with DCM. The organic layers were dried over sodium sulfate and concentrated *in vacuo*. Column chromatography, eluting with EtOAc, afforded the desired product.

General Procedure O – Intramolecular Imidazole Cyclisation with Phosphorous Pentoxide

Carried out following a literature procedure.¹⁵⁸ A suspension of the relevant starting material (1 mmol) and phosphorous pentoxide (577 mg, 4 mmol) in toluene (5 mL) was prepared and heated to 100 °C for 24 h. The solvent was removed by decantation, and 1 M HCl (4 mL) was added to the residue. Saturated KOH solution was added until the mixture was approximately pH 12, before DCM was added and the organic layer extracted with DCM (3 × 10 mL). The organic layers were dried over sodium sulfate and concentrated *in vacuo*. Column chromatography, eluting with EtOAc, afforded the desired product.

General Procedure P – Methylation of Hydroxy-substituted Imidazolium Salts

A solution of the relevant imidazolium salt (1 mmol) in DMF (5 mL) was prepared and cooled to 0 °C. Sodium hydride (60% in mineral oil) (50 mg, 1 mmol) was added and the mixture was allowed to warm to room temperature. After stirring for 1 h, the reaction mixture was cooled once again to 0 °C and iodomethane (50 µL, 1 mmol) was added. The mixture was stirred at room temperature for 16 h, after which it was concentrated *in vacuo*. After addition of water, the organics were extracted into ethyl acetate (3 × 10 mL), dried over sodium sulfate and concentrated *in vacuo*.

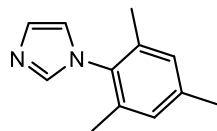
General Procedure Q – Preparation of [Ir(cod)Cl(NHC)] Complexes with Ag₂O

The relevant imidazolium halide salt (1 eq.) was added to a flame-dried and Ar-cooled Schlenk tube along with THF and silver oxide (1 eq.), and the resulting mixture was allowed to stir for 1 h. Bis(1,5-cyclooctadiene)diiridium(I) dichloride (1 eq.) was added and the resulting solution stirred at room temperature for 16 h. The solvent was removed *in vacuo*, and column chromatography (50% ethyl acetate in petrol) afforded the title compound.

Design and Synthesis of Novel Ligands and Complexes

Scheme 2.38

1-(2,4,6-Trimethylphenyl)-1H-imidazole **133**¹⁶³



A solution of aqueous formaldehyde (37%, 10.7 mL, 143 mmol), aqueous glyoxal (40%, 16.3 mL, 143 mmol), and acetic acid (34 mL) was prepared in a round-bottom flask and heated to 70 °C. A solution of ammonium acetate (11 g, 143 mmol), 2,4,6-trimethylaniline (18.3 mL, 130 mmol), and water (2 mL) in acetic acid (34 mL) was prepared and added to the flask over a 20 minute period. The reaction was stirred at 70 °C for 16 h, before being carefully poured into a saturated solution of sodium bicarbonate (1 L). After stirring for 1 h, a brown precipitate was formed, which was collected by filtration and washed with water. The crude product was purified by column chromatography, eluting with DCM, followed by recrystallisation from hexane to afford **133** as brown crystals (10.65 g, 44% yield).

¹H NMR (400 MHz, CDCl₃) δ 7.51 (s, 1H), 7.46 (t, *J* = 1.2 Hz, 1H), 7.23 (t, *J* = 1.2 Hz, 1H), 6.98 (s, 2H), 2.34 (s, 3H, CH₃), 1.99 (s, 6H, CH₃).

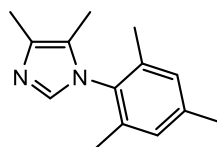
¹³C NMR (100 MHz, CDCl₃) δ 138.9, 137.7, 135.5, 133.5, 129.6, 129.0, 120.4, 21.2, 17.4.

IR (ATR, cm⁻¹) 2980, 2902, 2289, 1748, 1458.

MP (°C) 114–116 (lit. 116–118).¹⁶⁴

Scheme 2.39

1-(2,4,6-Trimethylphenyl)-4,5-dimethyl-1H-imidazole **134**¹²⁸



Prepared according to *General Procedure A*.

Amount of 2,4,6-trimethylaniline: 1.684 mL, 12 mmol.

Product yield: 0.964 g, 45%.

Product appearance: brown crystals.

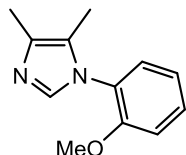
¹H NMR (400 MHz, CDCl₃) δ 7.27 (s, 1H), 6.97 (s, 2H), 2.34 (s, 3H), 2.25 (s, 3H), 1.94 (s, 6H), 1.85 (s, 3H).

^{13}C NMR (101 MHz, CDCl_3) δ .138.2, 135.6, 133.9, 133.3, 131.9, 128.4, 29.2, 20.5, 16.9
12.5, 7.7.

IR (ATR, cm^{-1}) 2918, 2851, 2355, 1730, 1589, 1460.

MP ($^{\circ}\text{C}$) 133–135 (lit. 130–131).¹⁶⁵

1-(2-Methoxyphenyl)-4,5-dimethyl-1H-imidazole 135¹⁶⁰



Prepared according to *General Procedure A*.

Amount of 2-methoxyaniline: 1.381 mL, 12 mmol.

Product yield: 1.172 g, 58%.

Product appearance: light brown crystals.

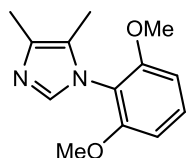
^1H NMR (400 MHz, CDCl_3) δ 7.44–7.39 (m, 1H), 7.38 (s, 1H), 7.16 (d, $J = 7.0$ Hz, 1H),
7.06–7.00 (m, 2H), 3.78 (s, 3H), 2.25 (s, 3H), 1.98 (s, 3H).

^{13}C NMR (101 MHz, CDCl_3) δ .155.0, 135.7, 133.2, 130.0, 128.5, 125.6, 123.9, 120.8,
112.0, 55.6, 12.9, 8.7.

IR (ATR, cm^{-1}) 3160, 2928, 2849, 1674, 1460.

MP ($^{\circ}\text{C}$) 76–78 (lit. 79–80).¹⁶⁰

1-(2,6-Dimethoxyphenyl)-4,5-dimethyl-1H-imidazole 136



Prepared according to *General Procedure A*.

Amount of 2,6-Dimethoxyaniline: 1.838 g, 12 mmol.

Product yield: 1.091 g, 47%.

Product appearance: light brown crystals.

^1H NMR (400 MHz, CDCl_3) δ 7.34 (s, 1H), 7.17 (t, $J = 7.3$ Hz, 1H), 6.86 (d, $J = 7.3$ Hz,
2H), 3.87 (s, 6H), 2.32 (s, 3H), 2.13 (s, 3H).

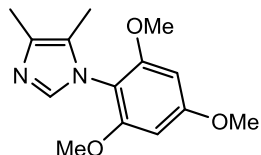
^{13}C NMR (101 MHz, CDCl_3) δ 147.9, 135.4, 134.3, 130.2, 123.5, 108.1, 107.8, 55.9, 12.4,
9.7.

IR (ATR, cm^{-1}) 3159, 2861, 1676, 1458.

HRMS (EI) m/z calculated for $C_{13}H_{16}N_2O_2$ $[M]^+$: 232.1212; found: 232.1216.

MP ($^{\circ}C$) 142–144.

1-(2,4,6-Trimethoxyphenyl)-4,5-dimethylimidazole 137¹²⁸



Prepared according to *General Procedure A*.

Amount of 2,4,6-Trimethoxyaniline: 2.198 g, 12 mmol.

Product yield: 1.180 g, 45%.

Product appearance: light brown powder.

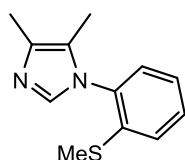
1H NMR (400 MHz, $CDCl_3$) δ 7.23 (s, 1H), 6.20 (s, 2H), 3.83 (s, 3H), 3.72 (s, 6H), 2.18 (s, 6H).

^{13}C NMR (101 MHz, $CDCl_3$) δ 159.9, 148.1, 135.6, 134.4, 123.2, 100.4, 95.3, 55.8, 12.7, 9.9.

IR (ATR, cm^{-1}) 2944, 2853, 1689, 1463.

MP ($^{\circ}C$) 138–141 (lit. 138–140).¹²⁸

1-(2-Thiomethylphenyl)-4,5-dimethylimidazole 138¹⁶⁰



Prepared according to *General Procedure A*.

Amount of 2-thiomethylaniline: 1.502 mL, 12 mmol.

Product yield: 1.463 g, 67%.

Product appearance: light brown powder.

1H NMR (400 MHz, $CDCl_3$) δ 7.46–7.43 (m, 1H), 7.35 (s, 1H), 7.28 (d, $J = 7.2$ Hz, 1H), 7.21 (dt, $J = 7.2$, $^4J = 1.6$ Hz, 1H), 7.14 (dd, $J = 7.2$, $^4J = 1.6$ Hz, 1H), 2.36 (s, 3H), 2.23 (s, 3H), 1.94 (s, 3H).

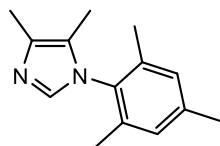
^{13}C NMR (101 MHz, $CDCl_3$) δ 138.6, 135.2, 134.3, 133.8, 129.6, 128.5, 125.6, 125.2, 123.4, 14.6, 12.9, 8.6.

IR (ATR, cm^{-1}) 2926, 2848, 1660, 1580, 1458.

MP ($^{\circ}C$) 98–101 (lit. 101–102).¹⁶⁰

Scheme 2.40

Large-scale Synthesis of 134



Prepared according to *General Procedure A*, with the quantities increased as below.

Amount of 2,4,6-trimethylaniline: 24.860 mL, 216 mmol.

Amount of 2,3-butanedione: 15.764 mL, 180 mmol.

Amount of paraformaldehyde: 5.405 g, 180 mmol.

Amount of ammonium acetate: 13.874 g, 180 mmol.

Amount of acetic acid: 10.278 mL, 180 mmol.

Amount of H₂O: 10 mL.

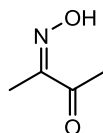
Amount of chloroform: 330 mL.

Product yield: 4.243 g, 11%.

Spectral data as reported above.

Scheme 2.41

2,3-Butanedione monooxime 140¹⁶⁶



Prepared according to a literature procedure.¹⁶⁶ To a solution of 2,3-butanedione in methanol was added hydroxylamine hydrochloride (1 eq.). Pyridine (1.1 eq.) was added dropwise and the reaction mixture was stirred at room temperature for 2 h. The reaction mixture was concentrated *in vacuo*, extracted with ethyl acetate, the extracts washed with water, and dried over sodium sulfate. After removal of the solvent *in vacuo*, the product was purified by column chromatography (5% ethyl acetate in petrol) to give the product **140** as a white fluffy powder.

Run 1: Amount of 2,3-butanedione: 2.633 mL, 30 mmol.

Amount of hydroxylamine hydrochloride: 2.084 g, 30 mmol.

Amount of pyridine: 2.658 mL, 33 mmol.

Amount of methanol: 60 mL.

Product yield: 3.021 g, >99%.

Run 2: Amount of 2,3-butanedione: 35.102 mL, 400 mmol.

Amount of hydroxylamine hydrochloride: 27.796 g, 400 mmol.

Amount of pyridine: 35.441 mL, 440 mmol.

Amount of methanol: 500 mL.

Product yield: 40.121 g, >99%.

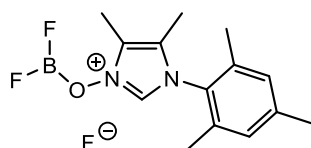
$^1\text{H NMR}$ (400 MHz, CDCl_3) δ 8.37 (br. s, 1H), 2.37 (s, 3H), 1.98 (s, 3H).

$^{13}\text{C NMR}$ (101 MHz, CDCl_3) δ 197.2, 157.6, 25.2, 8.2.

IR (ATR, cm^{-1}) 3270, 3201, 2921, 2865, 1666.

MP ($^\circ\text{C}$) 75–77 (lit. 75–76).¹⁶⁶

3-((difluoroboryl)oxy)-1-mesityl-4,5-dimethyl-1H-imidazol-3-ium fluoride **141**¹²⁸



A solution of butane-2,3-dione monooxime **140** in acetic acid was prepared. Boron trifluoride diethyl etherate (1.1 eq.), formaldehyde (1 eq., 40% aq.) and 2,4,6-trimethylaniline (1 eq.) were then added *via* syringe. The mixture was stirred for 16 h at 50 $^\circ\text{C}$, after which the acetic acid was removed *in vacuo* to give a black tarry residue. The residue was purified *via* column chromatography (2% methanol in DCM) to afford **141** as dark brown crystals.

Run 1: Amount of 2,3-butanedione monooxime **140**: 1.011 g, 10 mmol.

Amount of boron trifluoride diethyl etherate: 1.234 mL, 11 mmol.

Amount of formalin: 744 μL , 10 mmol.

Amount of 2,4,6-trimethylaniline: 1.404 mL, 10 mmol.

Amount of acetic acid: 10 mL.

Product yield: 2.683 g, 90%.

Run 2: Amount of 2,3-butanedione monooxime **140**: 20.22 g, 200 mmol.

Amount of boron trifluoride diethyl etherate: 24.68 mL, 220 mmol.

Amount of formalin: 14.880 mL, 200 mmol.

Amount of 2,4,6-trimethylaniline: 28.08 mL, 200 mmol.

Amount of acetic acid: 200 mL.

Product yield: 50.084 g, 84%.

$^1\text{H NMR}$ (400 MHz, CDCl_3) δ 8.17–8.12 (m, 1H), 7.05 (s, 2H), 2.41 (s, 3H), 2.37 (s, 3H), 2.00 (s, 6H), 1.95 (s, 3H).

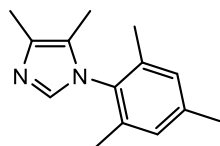
^{13}C NMR (101 MHz, CDCl_3) δ 139.8, 135.4, 128.8, 126.3, 124.1, 121.6, 50.2, 20.5, 16.8, 8.0, 7.0.

^{19}F NMR (376 MHz, CDCl_3) δ -157.91.

IR (ATR, cm^{-1}) 3128, 3063, 2973, 2859, 1628, 1486.

MP ($^{\circ}\text{C}$) 173–176 (lit. 174–176).¹²⁸

Alternative Synthesis of **134**



A solution of 3-((difluoroboryl)oxy)-1-mesityl-4,5-dimethyl-1H-imidazol-3-ium fluoride **141** in acetic acid was prepared, and iron powder (15 eq.) was added. The resulting mixture was heated to reflux and stirred for 2 h, after which it was cooled and poured into water (50 mL / mmol). The iron residue was removed by filtration and the filtrate extracted with chloroform (3 \times 50 mL). The organic extracts were washed with potassium carbonate solution (5% aq.) until the aqueous layer reached pH 8, then washed with brine, dried over sodium sulfate, filtered, and concentrated *in vacuo* to give a dark brown residue. The crude product was purified by column chromatography (2% methanol in DCM) to afford **134**.

Run 1: Amount of **141**: 1.192 g, 4 mmol.

Amount of iron powder: 3.351 g, 60 mmol.

Amount of acetic acid: 6 mL.

Product yield: 603 mg, 81%.

Run 2: Amount of **141**: 47.68 g, 160 mmol.

Amount of iron powder: 134.04 g, 2.4 mol.

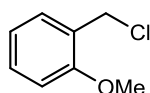
Amount of acetic acid: 500 mL.

Product yield: 24.735 g, 83%.

Spectral data as reported above.

Scheme 2.42

2-Methoxybenzyl chloride **142**¹⁶⁷



A solution of 2-methoxybenzyl alcohol (962 μL , 7.24 mmol) in DCM (25 mL) was prepared in a flame-dried and argon-cooled round bottom flask and was cooled to 0 $^{\circ}\text{C}$. Thionyl

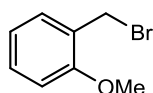
chloride (1.09 mL, 15 mmol) was added over a period of 20 minutes. The reaction mixture was allowed to warm to room temperature and was stirred for 3 h. The reaction was quenched *via* careful addition of 1 M aqueous sodium bicarbonate solution and then washed with saturated sodium bicarbonate solution, water, and brine. The organic phase was dried over sodium sulfate and concentrated *in vacuo* to yield **142** as a colourless liquid (1.102 g, 97% yield).

¹H NMR (400 MHz, CDCl₃) δ 7.39 (dd, *J* = 7.5, ⁴*J* = 1.6 Hz, 1H), 7.37–7.32 (m, 1H), 6.98 (m, 1H), 6.94 (d, *J* = 8.3 Hz, 1H), 4.70 (s, 2H), 3.92 (s, 3H).

¹³C NMR (101 MHz, CDCl₃) δ 167.9, 145.5, 131.8, 128.1, 124.1, 20.2, 17.2, 15.2.

IR (ATR, cm⁻¹) 3001, 2962, 2836, 1587, 1461.

2-Methoxybenzyl bromide **144**¹⁶⁸



Prepared following a literature procedure.¹⁶⁹ A solution of 2-methoxybenzyl alcohol (962 μL, 7.24 mmol) in toluene (25 mL) was prepared in a flame-dried and argon-cooled round bottom flask and was heated to 40 °C. Phosphorous tribromide (240 μL, 0.35 mmol) was added with stirring. The reaction mixture was heated to 100 °C and stirred for 30 min, after which it was allowed to cool to room temperature. The mixture was quenched with water (20 mL) and extracted into diethyl ether (3 × 20 mL). The combined organic phases were washed with water and brine, before being dried over sodium sulfate and concentrated *in vacuo* to yield **144** as a colourless liquid (1.454 g, >99% yield).

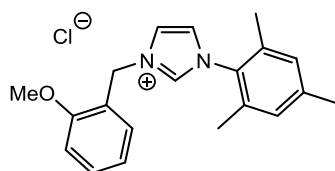
¹H NMR (400 MHz, CDCl₃) δ 7.39–7.32 (m, 2H), 6.96 (m, 1H), 6.93 (d, *J* = 8.3 Hz, 1H), 4.63 (s, 2H), 3.93 (s, 3H).

¹³C NMR (101 MHz, CDCl₃) δ 158.2, 130.6, 130.0, 125.9, 120.5, 110.7, 55.4, 26.8.

IR (ATR, cm⁻¹) 3002, 2960, 2835, 1598, 1464.

Scheme 2.43

1-mesityl-3-(2-methoxybenzyl)-1H-imidazol-3-ium chloride **145**



Prepared according to *General Procedure B*.

Amount of 2-methoxybenzyl chloride **142**: 418 μL , 3 mmol.

Amount of mesityl imidazole **133**: 603 mg, 3 mmol.

Product yield: 802 mg, 78%.

Product appearance: white crystalline solid.

^1H NMR (400 MHz, CDCl_3) δ 10.44 (s, 1H, N-CH-N), 8.07 (d, $J = 1.2$ Hz, 1H, N-CH-CH-N), 7.74 (d, $J = 7.5$ Hz, 1H, ArH), 7.32–7.28 (m, 1H, ArH), 7.07–6.99 (m, 3H, ArH & N-CH-CH-N), 6.90 (s, 2H, ArH), 5.93 (s, 2H, ArCH_2N), 3.85 (s, 3H, OCH_3), 2.35 (s, 6H, ArCH_3), 1.99 (s, 3H, CH_3).

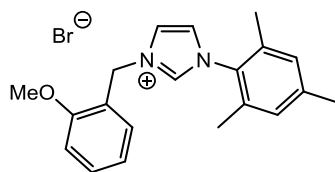
^{13}C NMR (101 MHz, CDCl_3) δ 158.8, 140.6, 138.3, 136.6, 133.2, 133.1, 130.6, 129.3, 128.5, 127.6, 123.1, 115.7, 104.4, 59.9, 53.2, 20.1, 17.1.

IR (ATR, cm^{-1}) 3349, 3145, 3060, 2964, 1543, 1458, 1380.

HRMS (EI) m/z calculated for $\text{C}_{20}\text{H}_{23}\text{N}_2\text{O}$ [M-Cl]: 307.1810; found: 307.1812.

MP ($^\circ\text{C}$) 220–223.

1-mesityl-3-(2-methoxybenzyl)-1H-imidazol-3-ium bromide **146**



Prepared according to *General Procedure B*.

Amount of 2-methoxybenzyl bromide **144**: 603 mg, 3 mmol.

Amount of mesityl imidazole **133**: 603 mg, 3 mmol.

Product yield: 534 mg, 46%.

Product appearance: pale yellow gum.

^1H NMR (400 MHz, CDCl_3) δ 10.40 (s, 1H, N-CH-N), 8.08 (d, 1H, $J = 1.4$ Hz, N-CH-CH-N), 7.74 (d, $J = 7.6$ Hz, 1H, ArH), 7.34–7.29 (m, 1H, ArH), 7.07–7.00 (m, 3H, ArH & N-CH-CH-N), 6.91 (s, 2H, ArH), 5.92 (s, 2H, ArCH_2N), 3.83 (s, 3H, OCH_3), 2.34 (s, 6H, ArCH_3), 2.00 (s, 3H, CH_3).

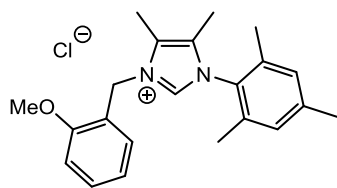
^{13}C NMR (101 MHz, CDCl_3) δ 158.9, 140.6, 136.8, 134.2, 133.2, 133.1, 130.7, 130.1, 129.4, 129.3, 128.5, 127.6, 123.1, 60.0, 53.2, 20.0, 17.1.

IR (ATR, cm^{-1}) 3358, 3146, 3057, 2964, 1544, 1459.

HRMS (EI) m/z calculated for $\text{C}_{20}\text{H}_{23}\text{N}_2\text{O}$ [M-Br]: 307.1810; found: 307.1813.

MP ($^\circ\text{C}$) 213–215.

1-mesityl-3-(2-methoxybenzyl)-4,5-dimethyl-1H-imidazol-3-ium chloride **147**



Prepared according to *General Procedure B*.

Amount of 2-methoxybenzyl chloride **142**: 418 μ L, 3 mmol.

Amount of mesityl dimethylimidazole **134**: 643 mg, 3 mmol.

Product yield: 712 mg, 64%.

Product appearance: light yellow gum.

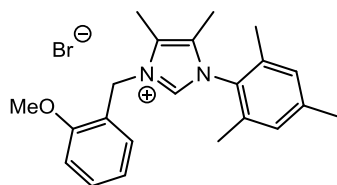
^1H NMR (400 MHz, CDCl_3) δ 10.08 (s, 1H, N-CH-N), 7.44 (d, $J = 7.6$ Hz, 1H, ArH), 7.38–7.30 (m, 1H, ArH), 7.04–6.94 (m, 3H, ArH), 6.90 (d, $J = 8.1$ Hz, 1H, ArH), 5.83 (s, 2H, ArCH₂N), 3.85 (s, 3H, OCH₃), 2.35 (s, 3H, Ar CH₃), 2.25 (s, 3H, NHC CH₃), 2.02 (s, 6H, ArCH₃), 1.90 (s, 3H, NHC CH₃).

^{13}C NMR (101 MHz, CDCl_3) δ 156.9, 130.6, 130.1, 129.7, 126.9, 125.3, 120.3, 120.0, 110.4, 110.1, 59.9, 55.3, 55.1, 54.9, 41.3, 41.1, 34.4, 20.5, 13.7.

IR (ATR, cm^{-1}) 3354, 2960, 2922, 1633, 1589, 1460.

HRMS (EI) m/z calculated for C₂₂H₂₇N₂O [M-Cl]: 335.2123; found: 335.2122.

1-mesityl-3-(2-methoxybenzyl)-4,5-dimethyl-1H-imidazol-3-ium bromide **148**



Prepared according to *General Procedure B*.

Amount of 2-methoxybenzyl bromide **144**: 603 mg, 3 mmol.

Amount of mesityl dimethylimidazole **134**: 643 mg, 3 mmol.

Product yield: 785 mg, 63%.

Product appearance: yellow-orange gum.

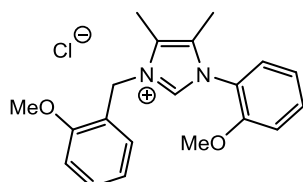
^1H NMR (400 MHz, CDCl_3) δ 10.07 (s, 1H, N-CH-N), 7.46 (d, $J = 7.6$ Hz, 1H, ArH), 7.37–7.29 (m, 1H, ArH), 7.03–6.92 (m, 3H, ArH), 6.91 (d, $J = 8.2$ Hz, 1H, ArH), 5.84 (s, 2H, ArCH₂N), 3.87 (s, 3H, OCH₃), 2.34 (s, 3H, Ar CH₃), 2.23 (s, 3H, NHC CH₃), 2.01 (s, 6H, ArCH₃), 1.92 (s, 3H, NHC CH₃).

^{13}C NMR (101 MHz, CDCl_3) δ 156.1, 130.7, 130.2, 129.7, 126.8, 125.4, 120.4, 119.9, 110.4, 110.0, 59.9, 55.4, 55.2, 54.8, 41.4, 41.0, 34.4, 20.6, 13.7.

IR (ATR, cm^{-1}) 3148, 2959, 2918, 1634, 1587, 1458, 1381.

HRMS (EI) m/z calculated for $\text{C}_{22}\text{H}_{27}\text{N}_2\text{O}$ [M-Br]: 335.2123; found: 335.2121.

3-(2-methoxybenzyl)-1-(2-methoxyphenyl)-4,5-dimethyl-1H-imidazol-3-ium chloride
149



Prepared according to *General Procedure B*.

Amount of 2-methoxybenzyl chloride **142**: 418 μL , 3 mmol.

Amount of 2-methoxyphenyl dimethylimidazole **135**: 606 mg, 3 mmol.

Product yield: 840 mg, 78%.

Product appearance: light yellow gum.

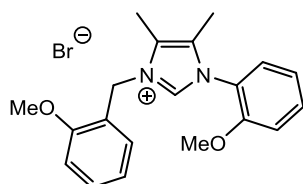
^1H NMR (400 MHz, CDCl_3) δ 10.58 (s, 1H, N-CH-N), 7.46–7.42 (m, 2H, ArH), 7.39 (d, J = 7.2 Hz, 1H, ArH), 7.11–7.02 (m, 2H, ArH), 6.91 (d, J = 7.9 Hz, 1H, ArH), 5.72 (s, 2H, ArCH₂N), 3.84 (s, 3H, OCH₃), 3.79 (s, 3H, OCH₃), 2.28 (s, 3H, NHC CH₃), 1.96 (s, 3H, NHC CH₃).

^{13}C NMR (101 MHz, CDCl_3) δ 159.3, 151.6, 136.4, 131.3, 131.2, 129.8, 129.2, 128.6, 127.9, 127.3, 126.4, 123.0, 120.8, 113.3, 111.3, 56.9, 49.3, 12.4, 11.4.

IR (ATR, cm^{-1}) 3348, 3098, 2952, 2923, 1646, 1560, 1459, 1352.

HRMS (EI) m/z calculated for $\text{C}_{20}\text{H}_{23}\text{N}_2\text{O}_2$ [M-Cl]: 323.1760; found: 323.1756.

3-(2-methoxybenzyl)-1-(2-methoxyphenyl)-4,5-dimethyl-1H-imidazol-3-ium bromide
150



Prepared according to *General Procedure B*.

Amount of 2-methoxybenzyl bromide **144**: 603 mg, 3 mmol.

Amount of 2-methoxyphenyl dimethylimidazole **135**: 606 mg, 3 mmol.

Product yield: 823 mg, 68%.

Product appearance: yellow gum.

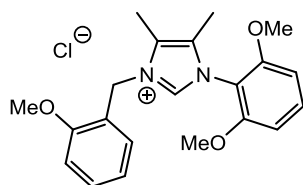
¹H NMR (400 MHz, CDCl₃) δ 10.50 (s, 1H, N-CH-N), 7.45–7.41 (m, 2H, ArH), 7.39–7.36 (m, 1H, ArH), 7.09–6.99 (m, 2H, ArH), 6.92 (d, *J* = 7.8 Hz, 1H, ArH), 5.73 (s, 2H, ArCH₂N), 3.85 (s, 3H, OCH₃), 3.78 (s, 3H, OCH₃), 2.26 (s, 3H, NHC CH₃), 1.95 (s, 3H, NHC CH₃).

¹³C NMR (101 MHz, CDCl₃) δ 159.4, 151.4, 136.5, 131.3, 131.2, 129.9, 129.2, 128.5, 127.9, 127.4, 126.5, 123.0, 120.9, 113.3, 111.4, 57.0, 49.4, 12.4, 11.3.

IR (ATR, cm⁻¹) 3349, 2964, 2922, 1670, 1558, 1461, 1354.

HRMS (EI) *m/z* calculated for C₂₀H₂₃N₂O₂ [M-Br]: 323.1760; found: 323.1766.

1-(2,6-dimethoxyphenyl)-3-(2-methoxybenzyl)-4,5-dimethyl-1H-imidazol-3-ium chloride 151



Prepared according to *General Procedure B*.

Amount of 2-methoxybenzyl chloride **142**: 418 μL, 3 mmol.

Amount of 2,6-dimethoxyphenyl dimethylimidazole **136**: 697 mg, 3 mmol.

Product yield: 945 mg, 81%.

Product appearance: yellow solid.

¹H NMR (400 MHz, CDCl₃) δ 10.58 (s, 1H, N-CH-N), 7.56 (d, *J* = 7.1 Hz, 1H, ArH), 7.37–7.32 (m, 1H, ArH), 7.18 (t, *J* = 7.2 Hz, 1H, ArH), 7.04–7.00 (m, 2H, ArH), 6.89 (d, *J* = 7.2 Hz, 2H, ArH), 5.66 (s, 2H, ArCH₂N), 3.85 (s, 3H, OCH₃), 3.73 (s, 6H, OCH₃), 2.25 (s, 3H, NHC CH₃), 1.98 (s, 3H, NHC CH₃).

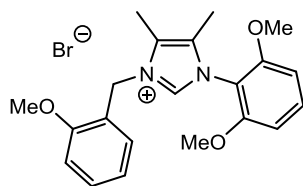
¹³C NMR (101 MHz, CDCl₃) δ 159.2, 137.4, 135.9, 131.4, 131.2, 129.2, 128.7, 128.2, 127.7, 123.0, 120.9, 111.3, 109.7, 56.9, 49.3, 12.4, 11.3.

IR (ATR, cm⁻¹) 3055, 2960, 2918, 1650, 1549, 1462, 1348.

HRMS (EI) *m/z* calculated for C₂₁H₂₅N₂O₃ [M-Cl]: 353.1865; found: 353.1862.

MP (°C) 104–107.

**1-(2,6-dimethoxyphenyl)-3-(2-methoxybenzyl)-4,5-dimethyl-1H-imidazol-3-ium
bromide 152**



Prepared according to *General Procedure B*.

Amount of 2-methoxybenzyl bromide **144**: 603 mg, 3 mmol.

Amount of 2,6-dimethoxyphenyl dimethylimidazole **136**: 697 mg, 3 mmol.

Product yield: 923 mg, 71%.

Product appearance: yellow gum.

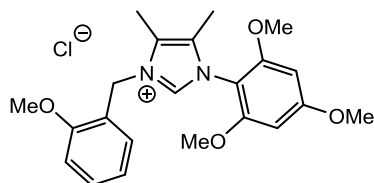
¹H NMR (400 MHz, CDCl₃) δ 10.50 (s, 1H, N-CH-N), 7.55 (d, *J* = 7.2 Hz, 1H, ArH), 7.34 (dd, *J* = 8.1, ⁴*J* = 1.6 Hz, 1H, ArH), 7.17 (t, *J* = 7.2 Hz, 1H, ArH), 7.04–6.99 (m, 2H, ArH), 6.87 (d, *J* = 7.2 Hz, 2H, ArH), 5.65 (s, 2H, ArCH₂N), 3.85 (s, 3H, OCH₃), 3.71 (s, 6H, OCH₃), 2.24 (s, 3H, NHC CH₃), 1.97 (s, 3H, NHC CH₃).

¹³C NMR (101 MHz, CDCl₃) δ 159.1, 137.2, 135.9, 131.3, 131.0, 129.1, 128.7, 128.3, 127.7, 123.1, 120.9, 111.4, 109.8, 56.8, 49.3, 12.5, 11.3.

IR (ATR, cm⁻¹) 3340, 3132, 2952, 2920, 1656, 1546, 1470, 1356.

HRMS (EI) *m/z* calculated for C₂₁H₂₅N₂O₃ [M–Br]: 353.1865; found: 353.1869.

**3-(2-methoxybenzyl)-4,5-dimethyl-1-(2,4,6-trimethoxyphenyl)-1H-imidazol-3-ium
chloride 153**



Prepared according to *General Procedure B*.

Amount of 2-methoxybenzyl chloride **142**: 418 μL, 3 mmol.

Amount of 2,4,6-trimethoxyphenyl dimethylimidazole **137**: 787 mg, 3 mmol.

Product yield: 766 mg, 61%.

Product appearance: pale yellow solid.

¹H NMR (400 MHz, CDCl₃) δ 10.22 (s, 1H, N-CH-N), 7.42 (d, *J* = 7.1 Hz, 1H, ArH), 7.37–7.34 (m, 1H, ArH), 7.31 (s, 2H, ArH), 7.07–7.02 (m, 2H, ArH), 5.57 (s, 2H, ArCH₂N), 3.84

(s, 3H, OCH₃), 3.69 (s, 6H, OCH₃), 3.57 (s, 3H, OCH₃), 2.19 (s, 3H, NHC CH₃), 1.92 (s, 3H, NHC CH₃).

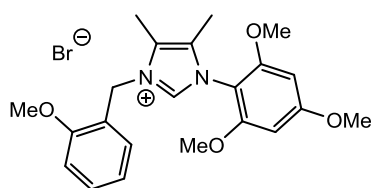
¹³C NMR (101 MHz, CDCl₃) δ 162.9, 159.6, 158.8, 135.9, 131.5, 131.2, 129.2, 128.6, 127.8, 120.9, 118.0, 111.4, 104.7, 95.4, 57.2, 49.3, 12.4, 11.3.

IR (ATR, cm⁻¹) 3146, 2948, 2918, 1650, 1540, 1459, 1352.

HRMS (EI) *m/z* calculated for C₂₂H₂₇N₂O₄ [M-Cl]: 383.1971; found: 383.1977.

MP (°C) 136–140.

3-(2-methoxybenzyl)-4,5-dimethyl-1-(2,4,6-trimethoxyphenyl)-1H-imidazol-3-ium bromide **154**



Prepared according to *General Procedure B*.

Amount of 2-methoxybenzyl bromide **144**: 603 mg, 3 mmol.

Amount of 2,4,6-trimethoxyphenyl dimethylimidazole **137**: 787 mg, 3 mmol.

Product yield: 806 mg, 58%.

Product appearance: yellow solid.

¹H NMR (400 MHz, CDCl₃) δ 10.18 (s, 1H, N-CH-N), 7.40 (dd, *J* = 7.1, ⁴*J* = 1.2 Hz, 1H, ArH), 7.36–7.34 (m, 1H, ArH), 7.26 (s, 2H, ArH), 7.06–7.00 (m, 2H, ArH), 5.57 (s, 2H, ArCH₂N), 3.85 (s, 3H, OCH₃), 3.69 (s, 6H, OCH₃), 3.53 (s, 3H, OCH₃), 2.20 (s, 3H, NHC CH₃), 1.91 (s, 3H, NHC CH₃).

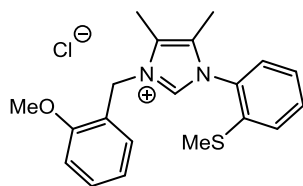
¹³C NMR (101 MHz, CDCl₃) δ 163.0, 159.7, 158.8, 135.8, 131.6, 131.3, 129.2, 128.7, 127.8, 121.0, 117.9, 111.5, 104.5, 95.5, 57.3, 49.3, 12.4, 11.2.

IR (ATR, cm⁻¹) 3342, 3130, 2952, 2916, 1651, 1544, 1462.

HRMS (EI) *m/z* calculated for C₂₂H₂₇N₂O₄ [M-Br]: 383.1971; found: 383.1966.

MP (°C) 124–126.

3-(2-methoxybenzyl)-4,5-dimethyl-1-(2-(methylthio)phenyl)-1H-imidazol-3-ium chloride 155



Prepared according to *General Procedure B*.

Amount of 2-methoxybenzyl chloride **142**: 418 μ L, 3 mmol.

Amount of 2-thiomethylphenyl dimethylimidazole **138**: 655 mg, 3 mmol.

Product yield: 794 mg, 77%.

Product appearance: pale yellow gum.

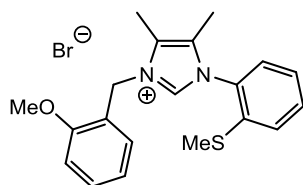
^1H NMR (400 MHz, CDCl_3) δ 9.96 (s, 1H, N-CH-N), 7.46–7.40 (m, 2H, ArH), 7.36 (d, J = 7.2 Hz, 1H, ArH), 7.28 (d, J = 7.2 Hz, 1H, ArH), 7.22 (dt, J = 7.6, 4J = 1.6 Hz, 1H, ArH), 7.12 (dd, J = 7.2, 4J = 1.6 Hz, 1H, ArH), 7.05–6.98 (m, 2H, ArH), 5.61 (s, 2H, ArCH₂N), 3.82 (s, 3H, OCH₃), 2.37 (s, 3H, SCH₃), 2.25 (s, 3H, NHC CH₃), 2.00 (s, 3H, NHC CH₃).

^{13}C NMR (101 MHz, CDCl_3) δ 159.2, 141.0, 136.6, 131.3, 131.1, 129.0, 128.4, 128.2, 127.4, 126.8, 126.4, 125.4, 120.8, 111.0, 56.8, 49.0, 16.4, 12.0, 11.1.

IR (ATR, cm^{-1}) 3240, 2995, 2930, 2870, 1638, 1558, 1460.

HRMS (EI) m/z calculated for $\text{C}_{20}\text{H}_{23}\text{N}_2\text{OS}$ [M-Cl]: 339.1531; found: 339.1526.

3-(2-methoxybenzyl)-4,5-dimethyl-1-(2-(methylthio)phenyl)-1H-imidazol-3-ium bromide 156



Prepared according to *General Procedure B*.

Amount of 2-methoxybenzyl chloride **144**: 418 μ L, 3 mmol.

Amount of 2-thiomethylphenyl dimethylimidazole **138**: 655 mg, 3 mmol.

Product yield: 1.053 g, 84%.

Product appearance: light yellow solid.

^1H NMR (400 MHz, CDCl_3) δ 10.04 (s, 1H, N-CH-N), 7.43–7.39 (m, 2H, ArH), 7.35 (d, J = 7.1 Hz, 1H, ArH), 7.28–7.25 (m, 1H, ArH), 7.23 (d, J = 7.6 Hz, 1H, ArH), 7.10 (dd, J =

7.1, $^4J = 1.5$ Hz, 1H, ArH), 7.06–7.00 (m, 2H, ArH), 5.63 (s, 2H, ArCH₂N), 3.84 (s, 3H, OCH₃), 2.36 (s, 3H, SCH₃), 2.25 (s, 3H, NHC CH₃), 1.99 (s, 3H, NHC CH₃).

^{13}C NMR (101 MHz, CDCl₃) δ 159.4, 141.1, 136.7, 131.3, 131.2, 129.2, 128.6, 128.2, 127.5, 126.8, 126.5, 125.4, 120.9, 111.1, 56.9, 49.1, 16.6, 12.2, 11.2.

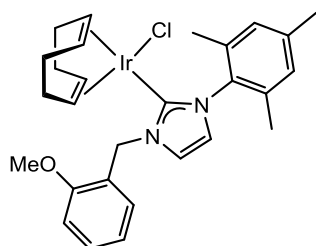
IR (ATR, cm⁻¹) 3251, 3002, 2918, 2868, 1639, 1554, 1462.

HRMS (EI) m/z calculated for C₂₀H₂₃N₂OS [M–Br]: 339.1531; found: 339.1540.

MP (°C) 96–100.

Scheme 2.44

(1,5-cyclooctadiene)(1-mesityl-3-(2-methoxybenzyl)imidazol-2-ylidene)iridium(I) chloride 157



Prepared according to *General Procedure C*.

Amount of bis(1,5-cyclooctadiene)diiridium(I) dichloride: 100 mg, 0.149 mmol.

Amount of potassium *tert*-butoxide: 33.4 mg, 0.298 mmol.

Amount of 1-mesityl-3-(2-methoxybenzyl)-1H-imidazol-3-ium chloride **145**: 102 mg, 0.298 mmol.

Product yield: 134 mg, 70%.

Product appearance: yellow solid.

^1H NMR (400 MHz, CDCl₃) δ 8.07 (d, 1H, $J = 1.2$ Hz, N-CH-CH-N), 7.74 (d, $J = 7.5$ Hz, 1H, ArH), 7.32–7.28 (m, 1H, ArH), 7.07–6.99 (m, 3H, ArH & N-CH-CH-N), 6.90 (s, 2H, ArH), 5.93 (s, 2H, ArCH₂N), 4.14–4.10 (m, 2H, COD CH), 3.85 (s, 3H, OCH₃), 2.94–2.88 (m, 2H, COD CH), 2.35 (s, 6H, ArCH₃), 1.99 (s, 3H, CH₃), 1.76–1.61 (m, 4H, COD CH₂), 1.30–1.14 (m, 4H, COD CH₂).

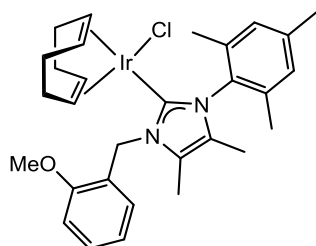
^{13}C NMR (101 MHz, CDCl₃) δ 158.8, 140.6, 136.6, 133.2, 133.1, 130.6, 129.7, 129.3, 128.5, 128.2, 128.1, 127.6, 126.9, 123.1, 59.9, 53.2, 29.6, 28.7, 28.4, 27.9, 20.1, 17.1.

IR (ATR, cm⁻¹) 2925, 2820, 1605, 1578, 1460.

HRMS (EI) m/z calculated for C₂₈H₃₄IrN₂O [M–Cl]: 607.2301; found 607.2320.

MP (°C) decomp. >200.

(1,5-cyclooctadiene)(1-mesityl-3-(2-methoxybenzyl)-4,5-dimethylimidazol-2-ylidene)iridium(I) chloride 158



Prepared according to *General Procedure C*.

Amount of bis(1,5-cyclooctadiene)diiridium(I) dichloride: 100 mg, 0.149 mmol.

Amount of potassium *tert*-butoxide: 33.4 mg, 0.298 mmol.

Amount of 1-mesityl-3-(2-methoxybenzyl)-4,5-dimethyl-1H-imidazol-3-ium chloride **147**: 116 mg, 0.298 mmol.

Product yield: 174 mg, 87%.

Product appearance: yellow solid.

¹H NMR (400 MHz, CDCl₃) δ 7.30-7.24 (m, 1H, ArH), 7.07-7.04 (m, 1H, ArH), 6.96-6.86 (m, 3H, ArH), 6.71-6.67 (m, 1H, ArH), 6.52 (d, ²J = 17.1 Hz, 1H, ArCH₂OCH₃), 5.21 (d, ²J = 17.4 Hz, 1H, ArCH₂OCH₃), 4.40-4.28 (m, 2H, COD CH), 3.93 (s, 3H, OCH₃), 2.96-2.90 (m, 1H, COD CH), 2.78-2.72 (m, 1H, COD CH), 2.38 (s, 3H, NHC CH₃), 2.33 (s, 3H, NHC CH₃), 1.99 (s, 3H, ArCH₃), 1.89 (s, 3H, ArCH₃), 1.84-1.78 (m, 1H, COD CH₂), 1.77 (s, 3H, ArCH₃), 1.76-1.67 (m, 1H, COD CH₂), 1.53-1.42 (m, 2H, COD CH₂), 1.39-1.25 (m, 3H, COD CH₂), 1.14-1.05 (m, 1H, COD CH₂).

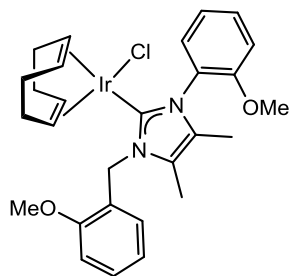
¹³C NMR (101 MHz, CDCl₃) δ 156.7, 129.7, 128.2, 128.1, 126.9, 125.9, 125.7, 120.7, 110.2, 82.2, 81.9, 55.5, 52.6, 51.0, 47.6, 34.3, 32.7, 29.6, 28.7, 21.3, 19.6, 18.0, 9.3, 9.1.

IR (ATR, cm⁻¹) 2920, 2866, 2824, 1601, 1589, 1491, 1425.

HRMS (EI) *m/z* calculated for C₃₀H₃₈IrN₂O [M-Cl]: 635.2614; found 635.2608.

MP (°C) decomp. >190.

(1,5-cyclooctadiene)(1-(2-methoxyphenyl)-3-(2-methoxybenzyl)-4,5-dimethylimidazol-2-ylidene)iridium(I) chloride 159



Prepared according to *General Procedure C*.

Amount of bis(1,5-cyclooctadiene)diiridium(I) dichloride: 100 mg, 0.149 mmol.

Amount of potassium *tert*-butoxide: 33.4 mg, 0.298 mmol.

Amount of 3-(2-methoxybenzyl)-1-(2-methoxyphenyl)-4,5-dimethyl-1H-imidazol-3-ium chloride **149**: 107 mg, 0.298 mmol.

Product yield: 137 mg, 70%.

Product appearance: yellow solid.

¹H NMR (400 MHz, CDCl₃) δ 10.58 (s, 1H, N-CH-N), 7.46–7.42 (m, 2H, ArH), 7.39 (d, *J* = 7.2 Hz, 1H, ArH), 7.11–7.02 (m, 4H, ArH), 6.91 (d, *J* = 7.9 Hz, 1H, ArH), 5.72 (s, 2H, ArCH₂N), 4.14–4.10 (m, 2H, COD CH), 3.84 (s, 3H, OCH₃), 3.79 (s, 3H, OCH₃), 2.94–2.88 (m, 2H, COD CH), 2.28 (s, 3H, NHC CH₃), 1.96 (s, 3H, NHC CH₃), 1.76–1.61 (m, 4H, COD CH₂), 1.30–1.14 (m, 4H, COD CH₂).

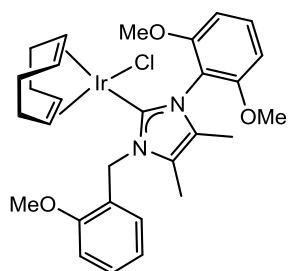
¹³C NMR (101 MHz, CDCl₃) δ 159.3, 151.6, 136.4, 131.3, 131.2, 129.8, 129.3, 129.3, 128.9, 128.6, 128.4, 128.2, 127.9, 127.3, 126.4, 123.0, 120.8, 113.3, 111.3, 56.9, 49.3, 12.4, 11.4.

IR (ATR, cm⁻¹) 2918, 2820, 1606, 1581, 1488.

HRMS (EI) *m/z* calculated for C₂₈H₃₄IrN₂O₂ [M-Cl]: 623.2250; found 623.2279.

MP (°C) decomp. >200.

(1,5-cyclooctadiene)(1-(2,6-dimethoxyphenyl)-3-(2-methoxybenzyl)-4,5-dimethylimidazol-2-ylidene)iridium(I) chloride 160



Prepared according to *General Procedure C*.

Amount of bis(1,5-cyclooctadiene)diiridium(I) dichloride: 100 mg, 0.149 mmol.

Amount of potassium *tert*-butoxide: 33.4 mg, 0.298 mmol.

Amount of 1-(2,6-dimethoxyphenyl)-3-(2-methoxybenzyl)-4,5-dimethyl-1H-imidazol-3-ium chloride **151**: 116 mg, 0.298 mmol.

Product yield: 168 mg, 82%.

Product appearance: yellow solid.

¹H NMR (400 MHz, CDCl₃) δ 7.56 (d, *J* = 7.1 Hz, 1H, ArH), 7.37–7.32 (m, 1H, ArH), 7.18 (t, *J* = 7.2 Hz, 1H, ArH), 7.04–7.00 (m, 1H, ArH), 6.89 (d, *J* = 7.2 Hz, 2H, ArH), 5.66 (s, 2H, ArCH₂N), 4.40–4.28 (m, 2H, COD CH), 3.85 (s, 3H, OCH₃), 3.73 (s, 6H, OCH₃), 2.96–2.90 (m, 2H, COD CH), 2.25 (s, 3H, NHC CH₃), 1.98 (s, 3H, NHC CH₃) 1.76–1.53 (m, 4H, COD CH₂), 1.39–1.25 (m, 3H, COD CH₂), 1.14–1.05 (m, 1H, COD CH₂)..

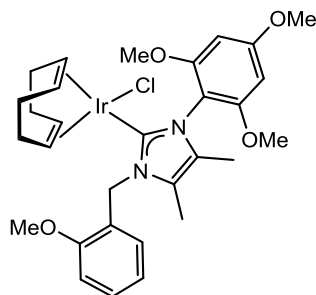
¹³C NMR (101 MHz, CDCl₃) δ 159.2, 137.4, 135.9, 131.4, 131.2, 129.5, 129.3, 128.9, 128.4, 128.2, 128.1, 128.0, 127.7, 123.0, 120.9, 111.3, 109.7, 56.9, 49.3, 12.4, 11.3.

IR (ATR, cm⁻¹) 2922, 2885, 2816, 1604, 1578, 1480.

HRMS (EI) *m/z* calculated for C₂₉H₃₆IrN₂O₃ [M–Cl]: 653.2355; found 653.2370.

MP (°C) decomp. >200.

(1,5-cyclooctadiene)(1-(2,4,6-trimethoxyphenyl)-3-(2-methoxybenzyl)-4,5-dimethylimidazol-2-ylidene)iridium(I) chloride 161



Prepared according to *General Procedure C*.

Amount of bis(1,5-cyclooctadiene)diiridium(I) dichloride: 100 mg, 0.149 mmol.

Amount of potassium *tert*-butoxide: 33.4 mg, 0.298 mmol.

Amount of 3-(2-methoxybenzyl)-4,5-dimethyl-1-(2,4,6-trimethoxyphenyl)-1H-imidazol-3-ium chloride **153**: 125 mg, 0.298 mmol.

Product yield: 131 mg, 61%.

Product appearance: yellow solid.

¹H NMR (400 MHz, CDCl₃) δ 7.42 (d, *J* = 7.1 Hz, 1H, ArH), 7.37–7.34 (m, 1H, ArH), 7.31 (s, 2H, ArH), 7.07–7.02 (m, 2H, ArH), 5.57 (s, 2H, ArCH₂N), 4.14–4.10 (m, 2H, COD CH), 3.84 (s, 3H, OCH₃), 3.69 (s, 6H, OCH₃), 3.61 (s, 3H, OCH₃), 2.94–2.88 (m, 2H, COD CH), 2.19 (s, 3H, NHC CH₃), 1.92 (s, 3H, NHC CH₃), 1.76–1.53 (m, 2H, COD CH₂), 1.53–1.42 (m, 2H, COD CH₂), 1.30–1.14 (m, 4H, COD CH₂).

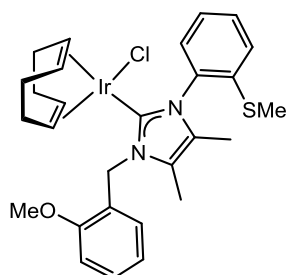
¹³C NMR (101 MHz, CDCl₃) δ 162.9, 159.6, 158.8, 135.9, 131.5, 131.2, 129.2, 128.6, 128.3, 127.9, 127.8, 127.4, 126.8, 120.9, 118.0, 111.4, 95.4, 57.2, 49.3, 29.6, 28.7, 28.4, 27.9, 12.4, 11.3.

IR (ATR, cm⁻¹) 2920, 2822, 1598, 1576, 1456.

HRMS (EI) *m/z* calculated for C₃₀H₃₈IrN₂O₄ [M–Cl]: 683.2461; found 683.2471.

MP (°C) decomp. >180.

(1,5-cyclooctadiene)(1-(2-(methylthio)phenyl)-3-(2-methoxybenzyl)-4,5-dimethylimidazol-2-ylidene)iridium(I) chloride 162



Prepared according to *General Procedure C*.

Amount of bis(1,5-cyclooctadiene)diiridium(I) dichloride: 100 mg, 0.149 mmol.

Amount of potassium *tert*-butoxide: 33.4 mg, 0.298 mmol.

Amount of 3-(2-methoxybenzyl)-4,5-dimethyl-1-(2-(methylthio)phenyl)-1H-imidazol-3-ium chloride **155**: 112 mg, 0.298 mmol.

Product yield: 137 mg, 68%.

Product appearance: yellow solid.

¹H NMR (400 MHz, CDCl₃) δ 7.46–7.40 (m, 2H, ArH), 7.36 (d, *J* = 7.2 Hz, 1H, ArH), 7.28 (d, *J* = 7.2 Hz, 1H, ArH), 7.22 (dt, *J* = 7.6, ⁴*J* = 1.6 Hz, 1H, ArH), 7.12 (dd, *J* = 7.2, ⁴*J* = 1.6 Hz, 1H, ArH), 7.05–6.98 (m, 2H, ArH), 5.61 (s, 2H, ArCH₂N), 4.14–4.10 (m, 2H, COD CH), 3.82 (s, 3H, OCH₃), 2.96–2.90 (m, 2H, COD CH), 2.37 (s, 3H, SCH₃), 2.25 (s, 3H, NHC CH₃), 2.00 (s, 3H, NHC CH₃), 1.84–1.78 (m, 1H, COD CH₂), 1.76–1.66 (m, 1H, COD CH₂), 1.53–1.42 (m, 2H, COD CH₂), 1.39–1.25 (m, 3H, COD CH₂), 1.14–1.05 (m, 1H, COD CH₂).

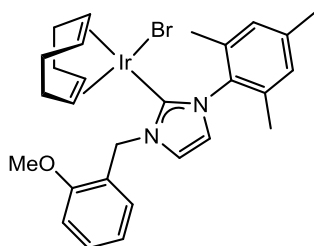
^{13}C NMR (101 MHz, CDCl_3) δ 159.2, 141.0, 136.6, 131.3, 131.1, 129.6, 129.3, 128.9, 128.8, 128.5, 128.4, 128.2, 127.4, 126.8, 126.4, 125.4, 120.8, 111.0, 56.8, 49.0, 29.6, 28.7, 28.4, 27.9, 16.4, 12.0, 11.1.

IR (ATR, cm^{-1}) 2918, 2816, 1608, 1560, 1468, 1426.

HRMS (EI) m/z calculated for $\text{C}_{28}\text{H}_{34}\text{IrN}_2\text{OS}$ [M-Cl]: 639.2021; found 639.2038.

MP ($^\circ\text{C}$) decomp. >200.

(1,5-cyclooctadiene)(1-mesityl-3-(2-methoxybenzyl)imidazol-2-ylidene)iridium(I) bromide 163



Prepared according to *General Procedure D*.

Amount of bis(1,5-cyclooctadiene)diiridium(I) dichloride: 100 mg, 0.149 mmol.

Amount of potassium hexamethyldisilazide (0.7 M in toluene): 0.49 mL, 0.343 mmol.

Amount of sodium bromide: 61 mg, 0.596 mmol.

Amount of 1-mesityl-3-(2-methoxybenzyl)-1H-imidazol-3-ium bromide **146**: 116 mg, 0.298 mmol.

Product yield: 123 mg, 60%.

Product appearance: yellow solid.

^1H NMR (400 MHz, CDCl_3) δ 8.08 (d, 1H, $J = 1.4$ Hz, N-CH-CH-N), 7.74 (d, $J = 7.6$ Hz, 1H, ArH), 7.34–7.29 (m, 1H, ArH), 7.07–7.00 (m, 3H, ArH & N-CH-CH-N), 6.91 (s, 2H, ArH), 5.92 (s, 2H, ArCH₂N), 4.14–4.10 (m, 2H, COD CH), 3.83 (s, 3H, OCH₃), 2.94–2.88 (m, 2H, COD CH), 2.34 (s, 6H, ArCH₃), 2.00 (s, 3H, CH₃), 1.76–1.61 (m, 4H, COD CH₂), 1.30–1.14 (m, 4H, COD CH₂).

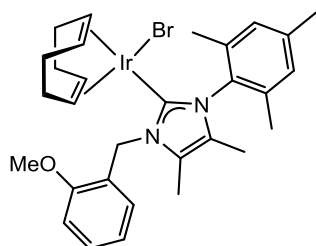
^{13}C NMR (101 MHz, CDCl_3) δ 158.9, 140.6, 136.8, 134.2, 133.2, 133.1, 130.7, 130.1, 129.4, 129.3, 128.5, 127.6, 123.1, 60.0, 53.2, 29.6, 28.7, 28.4, 27.9, 20.0, 17.1.

IR (ATR, cm^{-1}) 2925, 2820, 1605, 1578, 1459.

HRMS (EI) m/z calculated for $\text{C}_{28}\text{H}_{34}\text{IrN}_2\text{O}$ [M-Br]: 607.2301; found 607.2289.

MP ($^\circ\text{C}$) decomp. >180.

(1,5-cyclooctadiene)(1-mesityl-3-(2-methoxybenzyl)-4,5-dimethylimidazol-2-ylidene)iridium(I) bromide 164



Prepared according to *General Procedure D*.

Amount of bis(1,5-cyclooctadiene)diiridium(I) dichloride: 100 mg, 0.149 mmol.

Amount of potassium hexamethyldisilazide (0.7 M in toluene): 0.49 mL, 0.343 mmol.

Amount of sodium bromide: 61 mg, 0.596 mmol.

Amount of 1-mesityl-3-(2-methoxybenzyl)-4,5-dimethyl-1H-imidazol-3-ium bromide **148**: 124 mg, 0.298 mmol.

Product yield: 121 mg, 57%.

Product appearance: yellow solid.

¹H NMR (400 MHz, CDCl₃) δ 7.32-7.26 (m, 1H, ArH), 7.07-7.04 (m, 1H, ArH), 6.97-6.87 (m, 3H, ArH), 6.71-6.67 (m, 1H, ArH), 6.56 (d, ²*J* = 17.2 Hz, 1H, Ar-CH₂-OCH₃), 5.18 (d, ²*J* = 17.3 Hz, 1H, ArCH₂OCH₃), 4.51-4.44 (m, 1H, COD CH), 4.42-4.35 (m, 1H, COD CH), 3.94 (s, 1H, OCH₃), 3.01-2.95 (m, 1H, COD CH), 2.85-2.79 (m, 1H, COD CH), 2.38 (s, 6H, NHC CH₃), 2.00 (s, 3H, ArCH₃), 1.90 (s, 3H, ArCH₃), 1.79 (s, 3H, ArCH₃), 1.76-1.69 (m, 1H, COD CH₂), 1.54-1.44 (ddd, ²*J* = 13.9 Hz, *J* = 10.0, 7.1 Hz, 2H, COD CH₂), 1.37-1.27 (m, 3H, COD CH₂), 1.21-1.12 (m, 1H, COD CH₂), 1.07-0.96 (m, 1H, COD CH₂).

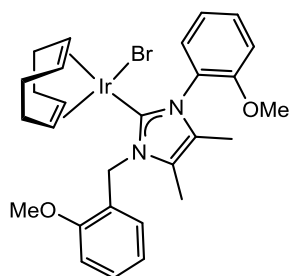
¹³C NMR (101 MHz, CDCl₃) δ 138.8, 138.5, 136.3, 134.6, 129.7, 129.3, 128.9, 128.4, 128.2, 127.1, 123.5, 82.7, 51.7, 33.7, 29.6, 29.2, 28.7, 28.4, 27.9, 21.3, 19.9, 18.4.

IR (ATR, cm⁻¹) 2920, 2825, 1600, 1588, 1491, 1425.

HRMS (EI) *m/z* calculated for C₃₀H₃₈IrN₂O [M-Br]: 635.2614; found 635.2623.

MP (°C) decomp. >200.

(1,5-cyclooctadiene)(1-(2-methoxyphenyl)-3-(2-methoxybenzyl)-4,5-dimethylimidazol-2-ylidene)iridium(I) bromide 165



Prepared according to *General Procedure D*.

Amount of bis(1,5-cyclooctadiene)diiridium(I) dichloride: 100 mg, 0.149 mmol.

Amount of potassium hexamethyldisilazide (0.7 M in toluene): 0.49 mL, 0.343 mmol.

Amount of sodium bromide: 61 mg, 0.596 mmol.

Amount of 3-(2-methoxybenzyl)-1-(2-methoxyphenyl)-4,5-dimethyl-1H-imidazol-3-ium bromide **150**: 120 mg, 0.298 mmol.

Product yield: 117 mg, 56%.

Product appearance: yellow solid.

¹H NMR (400 MHz, CDCl₃) δ 7.45–7.41 (m, 2H, ArH), 7.39–7.36 (m, 1H, ArH), 7.09–6.99 (m, 4H, ArH), 6.92 (d, *J* = 7.8 Hz, 1H, ArH), 5.73 (s, 2H, ArCH₂N), 4.40–4.28 (m, 2H, COD CH), 3.85 (s, 3H, OCH₃), 3.78 (s, 3H, OCH₃), 2.96–2.90 (m, 2H, COD CH), 2.26 (s, 3H, NHC CH₃), 1.95 (s, 3H, NHC CH₃), 1.76–1.61 (m, 4H, COD CH₂), 1.39–1.25 (m, 3H, COD CH₂), 1.14–1.05 (m, 1H, COD CH₂).

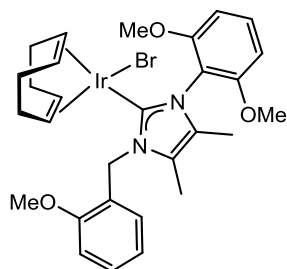
¹³C NMR (101 MHz, CDCl₃) δ 159.4, 151.4, 136.5, 131.3, 131.2, 129.9, 129.4, 129.3, 128.9, 128.4, 128.2, 128.0, 127.9, 127.4, 126.5, 123.0, 120.9, 113.3, 111.4, 57.0, 49.4, 12.4, 11.3.

IR (ATR, cm⁻¹) 2920, 2816, 1610, 1578, 1488.

HRMS (EI) *m/z* calculated for C₂₈H₃₄IrN₂O₂ [M–Br]: 623.2250; found 623.2268.

MP (°C) decomp. >200.

(1,5-cyclooctadiene)(1-(2,6-dimethoxyphenyl)-3-(2-methoxybenzyl)-4,5-dimethylimidazol-2-ylidene)iridium(I) bromide 166



Prepared according to *General Procedure D*.

Amount of bis(1,5-cyclooctadiene)diiridium(I) dichloride: 100 mg, 0.149 mmol.

Amount of potassium hexamethyldisilazide (0.7 M in toluene): 0.49 mL, 0.343 mmol.

Amount of sodium bromide: 61 mg, 0.596 mmol.

Amount of 1-(2,6-dimethoxyphenyl)-3-(2-methoxybenzyl)-4,5-dimethyl-1H-imidazol-3-ium bromide **152**: 129 mg, 0.298 mmol.

Product yield: 157 mg, 72%.

Product appearance: yellow solid.

¹H NMR (400 MHz, CDCl₃) δ 7.55 (d, $J = 7.2$ Hz, 1H, ArH), 7.34 (dd, $J = 8.1$, $^4J = 1.6$ Hz, 1H, ArH), 7.17 (t, $J = 7.2$ Hz, 1H, ArH), 7.04–6.99 (m, 2H, ArH), 6.87 (d, $J = 7.2$ Hz, 2H, ArH), 5.65 (s, 2H, ArCH₂N), 4.14–4.10 (m, 2H, COD CH), 3.85 (s, 3H, OCH₃), 3.71 (s, 6H, OCH₃), 2.94–2.88 (m, 2H, COD CH), 2.24 (s, 3H, NHC CH₃), 1.97 (s, 3H, NHC CH₃), 1.76–1.61 (m, 4H, COD CH₂), 1.39–1.25 (m, 3H, COD CH₂), 1.14–1.02 (m, 1H, COD CH₂).

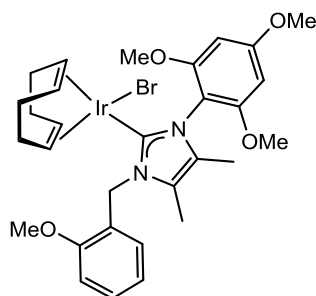
¹³C NMR (101 MHz, CDCl₃) δ 159.1, 137.2, 135.9, 131.3, 131.0, 130.1, 129.3, 128.9, 128.4, 128.2, 127.7, 127.3, 126.7, 123.1, 120.9, 111.4, 109.8, 56.8, 49.3, 12.5, 11.3.

IR (ATR, cm⁻¹) 2919, 2881, 1606, 1580, 1458.

HRMS (EI) m/z calculated for C₂₉H₃₆IrN₂O₃ [M–Br]: 653.2355; found 653.2375.

MP (°C) decomp. >200.

(1,5-cyclooctadiene)(1-(2,4,6-trimethoxyphenyl)-3-(2-methoxybenzyl)-4,5-dimethylimidazol-2-ylidene)iridium(I) bromide 167



Prepared according to *General Procedure D*.

Amount of bis(1,5-cyclooctadiene)diiridium(I) dichloride: 100 mg, 0.149 mmol.

Amount of potassium hexamethyldisilazide (0.7 M in toluene): 0.49 mL, 0.343 mmol.

Amount of sodium bromide: 61 mg, 0.596 mmol.

Amount of 3-(2-methoxybenzyl)-4,5-dimethyl-1-(2,4,6-trimethoxyphenyl)-1H-imidazol-3-ium bromide **154**: 138 mg, 0.298 mmol.

Product yield: 134 mg, 59%.

Product appearance: yellow solid.

¹H NMR (400 MHz, CDCl₃) δ 7.40 (dd, *J* = 7.1, ⁴*J* = 1.2 Hz, 1H, ArH), 7.36–7.34 (m, 1H, ArH), 7.26 (s, 2H, ArH), 7.06–7.00 (m, 2H, ArH), 5.57 (s, 2H, ArCH₂N), 4.40–4.28 (m, 2H, COD CH), 3.85 (s, 3H, OCH₃), 3.69 (s, 6H, OCH₃), 3.60 (s, 3H, OCH₃), 2.94–2.88 (m, 2H, COD CH), 2.20 (s, 3H, NHC CH₃), 1.91 (s, 3H, NHC CH₃) 1.76–1.61 (m, 4H, COD CH₂), 1.30–1.14 (m, 4H, COD CH₂).

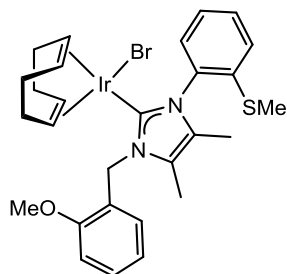
¹³C NMR (101 MHz, CDCl₃) δ 163.0, 159.7, 158.8, 135.8, 131.6, 131.3, 129.6, 129.2, 128.7, 127.8, 126.4, 126.2, 125.8, 121.0, 117.9, 111.5, 95.5, 57.3, 49.3, 12.4, 11.2.

IR (ATR, cm⁻¹) 2920, 2821, 1600, 1574, 1448.

HRMS (EI) *m/z* calculated for C₃₀H₃₈IrN₂O₄ [M–Br]: 683.2461; found 683.2474.

MP (°C) decomp. >200.

(1,5-cyclooctadiene)(1-(2-(methylthio)phenyl)-3-(2-methoxybenzyl)-4,5-dimethylimidazol-2-ylidene)iridium(I) bromide 168



Prepared according to *General Procedure D*.

Amount of bis(1,5-cyclooctadiene)diiridium(I) dichloride: 100 mg, 0.149 mmol.

Amount of potassium hexamethyldisilazide (0.7 M in toluene): 0.49 mL, 0.343 mmol.

Amount of sodium bromide: 61 mg, 0.596 mmol.

Amount of 3-(2-methoxybenzyl)-4,5-dimethyl-1-(2-(methylthio)phenyl)-1H-imidazol-3-ium bromide **156**: 125 mg, 0.298 mmol.

Product yield: 129 mg, 60%.

Product appearance: yellow solid.

¹H NMR (400 MHz, CDCl₃) δ 7.43–7.39 (m, 2H, ArH), 7.35 (d, *J* = 7.1 Hz, 1H, ArH), 7.28–7.25 (m, 1H, ArH), 7.23 (d, *J* = 7.6 Hz, 1H, ArH), 7.10 (dd, *J* = 7.1, ⁴*J* = 1.5 Hz, 1H, ArH), 7.06–7.00 (m, 2H, ArH), 5.63 (s, 2H, ArCH₂N), 4.40–4.28 (m, 2H, COD CH), 3.84 (s, 3H, OCH₃), 2.96–2.90 (m, 1H, COD CH), 2.78–2.72 (m, 1H, COD CH), 2.36 (s, 3H, SCH₃), 2.25 (s, 3H, NHC CH₃), 1.99 (s, 3H, NHC CH₃), 1.76–1.53 (m, 2H, COD CH₂), 1.53–1.42 (m, 2H, COD CH₂), 1.39–1.25 (m, 3H, COD CH₂), 1.14–1.05 (m, 1H, COD CH₂).

¹³C NMR (101 MHz, CDCl₃) δ 159.4, 141.1, 136.7, 131.3, 131.2, 129.6, 129.3, 128.9, 128.4, 128.2, 127.6, 127.2, 126.5, 125.8, 124.5, 125.4, 120.9, 111.1, 56.9, 49.1, 16.6, 12.2, 11.2.

IR (ATR, cm⁻¹) 2919, 1602, 1558, 1462.

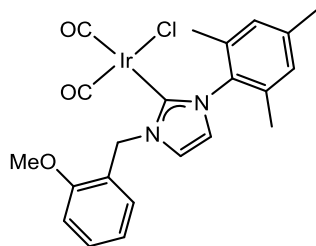
HRMS (EI) *m/z* calculated for C₂₈H₃₄IrN₂OS [M–Br]: 639.2021; found 639.2010.

MP (°C) decomp. >200.

Scheme 2.45

In all cases, clear ^{13}C spectra could not be acquired and therefore are not reported. This is in line with observations reported by Hope and co-workers.¹⁷⁰ Attempts to obtain high resolution mass spectrometry data for complexes **176–181** were unsuccessful due to the air sensitivity of the complexes. For clarity, only the key $\nu(\text{CO})_{\text{DCM}}$ stretching frequencies, used to calculate TEP, are reported.

Dicarbonyl(1-mesityl-3-(2-methoxybenzyl)imidazol-2-ylidene)iridium(I) chloride 176



Prepared according to *General Procedure E*.

(1,5-cyclooctadiene)(1-mesityl-3-(2-methoxybenzyl)imidazol-2-ylidene)iridium(I) chloride

157: 12.8 mg, 0.02 mmol.

Product yield: 9.4 mg, 80%.

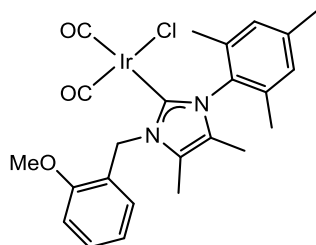
Product appearance: yellow solid.

^1H NMR (400 MHz, CDCl_3) δ 8.08 (d, 1H, $J = 1.4$ Hz, N-CH-CH-N), 7.74 (d, $J = 7.6$ Hz, 1H, ArH), 7.34–7.29 (m, 1H, ArH), 7.07–7.00 (m, 3H, ArH & N-CH-CH-N), 6.91 (s, 2H, ArH), 5.92 (s, 2H, ArCH_2N), 3.83 (s, 3H, OCH_3), 2.34 (s, 6H, ArCH_3), 2.00 (s, 3H, CH_3).

IR (DCM, cm^{-1}) 2021.9.

MP ($^\circ\text{C}$) decomp. >60 .

Dicarbonyl(1-mesityl-3-(2-methoxybenzyl)-4,5-dimethylimidazol-2-ylidene)iridium(I) chloride 177



Prepared according to *General Procedure E*.

Amount of (1,5-cyclooctadiene)(1-mesityl-3-(2-methoxybenzyl)imidazol-2-ylidene)iridium(I) chloride **158**: 13.4 mg, 0.02 mmol.

Product yield: 7.35 mg, 58%.

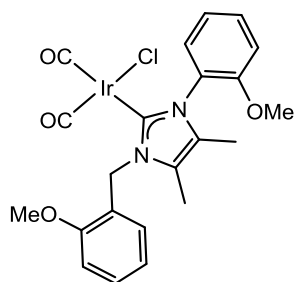
Product appearance: yellow solid.

¹H NMR (400 MHz, CDCl₃) δ 7.46 (d, *J* = 7.6 Hz, 1H, ArH), 7.37–7.29 (m, 1H, ArH), 7.03–6.92 (m, 3H, ArH), 6.91 (d, *J* = 8.2 Hz, 1H, ArH), 5.84 (s, 2H, ArCH₂N), 3.87 (s, 3H, OCH₃), 2.34 (s, 3H, Ar CH₃), 2.23 (s, 3H, NHC CH₃), 2.01 (s, 6H, ArCH₃), 1.92 (s, 3H, NHC CH₃).

IR (DCM, cm⁻¹) 2018.5.

MP (°C) decomp. >60.

Dicarbonyl(1-(2-methoxyphenyl)-3-(2-methoxybenzyl)-4,5-dimethylimidazol-2-ylidene)iridium(I) chloride 178



Prepared according to *General Procedure E*.

Amount of (1,5-cyclooctadiene)(1-(2-methoxyphenyl)-3-(2-methoxybenzyl)-4,5-dimethylimidazol-2-ylidene)iridium(I) chloride **159**: 13.2 mg, 0.02 mmol.

Product yield: 8.4 mg, 69%.

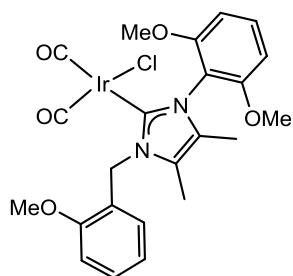
Product appearance: yellow solid.

¹H NMR (400 MHz, CDCl₃) δ 7.45–7.41 (m, 2H, ArH), 7.39–7.36 (m, 1H, ArH), 7.09–6.99 (m, 4H, ArH), 6.92 (d, *J* = 7.8 Hz, 1H, ArH), 5.73 (s, 2H, ArCH₂N), 3.85 (s, 3H, OCH₃), 3.78 (s, 3H, OCH₃), 2.26 (s, 3H, NHC CH₃), 11.95 (s, 3H, NHC CH₃).

IR (DCM, cm⁻¹) 2019.1.

MP (°C) decomp. >60.

Dicarbonyl(1-(2,6-dimethoxyphenyl)-3-(2-methoxybenzyl)-4,5-dimethylimidazol-2-ylidene)iridium(I) chloride 179



Prepared according to *General Procedure E*.

Amount of (1,5-cyclooctadiene)(1-(2,6-dimethoxyphenyl)-3-(2-methoxybenzyl)-4,5-dimethylimidazol-2-ylidene)iridium(I) chloride **160**: 13.8 mg, 0.02 mmol.

Product yield: 8.9 mg, 70%.

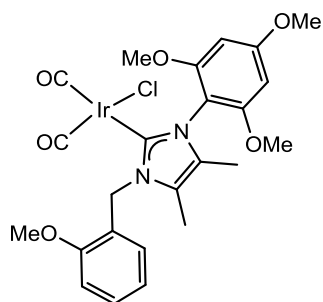
Product appearance: yellow solid.

¹H NMR (400 MHz, CDCl₃) δ 7.55 (d, $J = 7.2$ Hz, 1H, ArH), 7.34 (dd, $J = 8.1$, $^4J = 1.6$ Hz, 1H, ArH), 7.17 (t, $J = 7.2$ Hz, 1H, ArH), 7.04–6.99 (m, 2H, ArH), 6.87 (d, $J = 7.2$ Hz, 2H, ArH), 5.65 (s, 2H, ArCH₂N), 3.85 (s, 3H, OCH₃), 3.71 (s, 6H, OCH₃), 2.24 (s, 3H, NHC CH₃), 1.97 (s, 3H, NHC CH₃).

IR (DCM, cm⁻¹) 2018.6.

MP (°C) decomp. >60.

Dicarbonyl(1-(2,4,6-trimethoxyphenyl)-3-(2-methoxybenzyl)-4,5-dimethylimidazol-2-ylidene)iridium(I) chloride 180



Prepared according to *General Procedure E*.

Amount of (1,5-cyclooctadiene)(1-(2,4,6-trimethoxyphenyl)-3-(2-methoxybenzyl)-4,5-dimethylimidazol-2-ylidene)iridium(I) chloride **161**: 14.4 mg, 0.02 mmol.

Product yield: 10.9 mg, 82%.

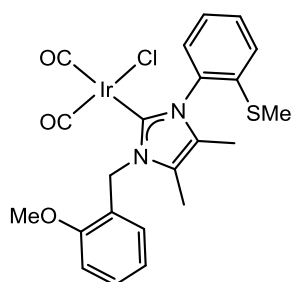
Product appearance: yellow solid.

¹H NMR (400 MHz, CDCl₃) δ 7.40 (dd, *J* = 7.1, ⁴*J* = 1.2 Hz, 1H, ArH), 7.36–7.34 (m, 1H, ArH), 7.26 (s, 2H, ArH), 7.06–7.00 (m, 2H, ArH), 5.57 (s, 2H, ArCH₂N), 3.85 (s, 3H, OCH₃), 3.69 (s, 6H, OCH₃), 3.62 (s, 3H, OCH₃), 2.20 (s, 3H, NHC CH₃), 1.91 (s, 3H, NHC CH₃).

IR (DCM, cm⁻¹) 2018.3.

MP (°C) decomp. >60.

Dicarbonyl(1-(2-(methylthio)phenyl)-3-(2-methoxybenzyl)-4,5-dimethylimidazol-2-ylidene)iridium(I) chloride 181



Prepared according to *General Procedure E*.

Amount of (1,5-cyclooctadiene)(1-(2-(methylthio)phenyl)-3-(2-methoxybenzyl)-4,5-dimethylimidazol-2-ylidene)iridium(I) chloride **162**: 13.5 mg, 0.02 mmol.

Product yield: 7.6 mg, 61%.

Product appearance: yellow solid.

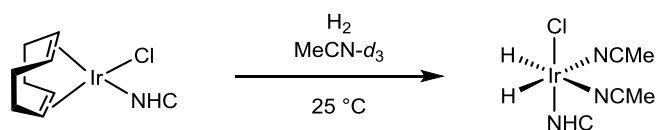
¹H NMR (400 MHz, CDCl₃) δ 7.43–7.39 (m, 2H, ArH), 7.35 (d, *J* = 7.1 Hz, 1H, ArH), 7.28–7.25 (m, 1H, ArH), 7.23 (d, *J* = 7.6 Hz, 1H, ArH), 7.10 (dd, *J* = 7.1, ⁴*J* = 1.5 Hz, 1H, ArH), 7.06–7.00 (m, 2H, ArH), 5.63 (s, 2H, ArCH₂N), 3.84 (s, 3H, OCH₃), 2.36 (s, 3H, SCH₃), 2.25 (s, 3H, NHC CH₃), 1.99 (s, 3H, NHC CH₃).

IR (DCM, cm⁻¹) 2020.3.

MP (°C) decomp. >60.

Scheme 2.46 / Table 2.4

Complex Activation and Observation of Iridium(III) Hydride Intermediates



Carried out according to General Procedure F.

While full analysis of ^1H and ^{13}C NMR data is not provided for each derivative studied, a clear loss of the COD olefinic proton signals was observed in all cases.

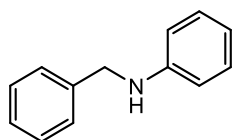
Entry	Catalyst	δH / ppm
1	157	-22.52
2	158	-22.80
3	159	-22.60
4	160	-22.70
5	161	-22.96
6	162	n/a*

* Hydride signal not observed.

***N*-Alkylation of Amines via Hydrogen Borrowing**

Table 2.5

***N*-Benzyl-*N*-phenylamine 51¹⁷¹**



Product appearance: yellow low-melting solid.

^1H NMR (400 MHz, CDCl_3) δ 7.42–7.36 (m, 4H, ArH), 7.32–7.25 (m, 1H, ArH), 7.22–7.17 (m, 2H, ArH), 6.77–6.71 (m, 1H, ArH), 6.69–6.65 (m, 2H, ArH), 4.36 (s, 2H, CH_2), 4.18 (br. s, 1H, NH).

^{13}C NMR (101 MHz, CDCl_3) δ 148.3, 139.6, 129.3, 128.9, 127.7, 127.3, 117.7, 113.0, 48.4.

IR (ATR, cm^{-1}) 3023, 2921, 2844, 1603, 1512.

MP ($^\circ\text{C}$) 33–35 (lit. 34–35).¹⁷¹

Reactions carried out following *General Procedure G*.

Reaction temperature: 110 °C.

Amount of aniline: 20 mg, 0.215 mmol.

Amount of benzyl alcohol: 23 mg, 0.215 mmol.

Amount of toluene: 2.5 mL.

Entry	Catalyst	Amount of Catalyst		Base	Amount of Base		Product Yield	
		mmol	mg		mmol	mg	mg	%
1	157	0.01075	6.9	K ₂ CO ₃	0.01075	1.5	23.2	59
2	158	0.01075	7.2	K ₂ CO ₃	0.01075	1.5	31.5	80
3	159	0.01075	7.1	K ₂ CO ₃	0.01075	1.5	29.8	71
4	160	0.01075	7.4	K ₂ CO ₃	0.01075	1.5	19.7	50
5	161	0.01075	7.7	K ₂ CO ₃	0.01075	1.5	18.1	46
6	162	0.01075	7.2	K ₂ CO ₃	0.01075	1.5	2.4	6
7	163	0.01075	7.4	K ₂ CO ₃	0.01075	1.5	20.9	53
8	164	0.01075	7.7	K ₂ CO ₃	0.01075	1.5	32.3	82
9	165	0.01075	7.6	K ₂ CO ₃	0.01075	1.5	27.6	70
10	166	0.01075	7.9	K ₂ CO ₃	0.01075	1.5	20.1	51
11	167	0.01075	8.2	K ₂ CO ₃	0.01075	1.5	20.5	52
12	168	0.01075	7.7	K ₂ CO ₃	0.01075	1.5	3.2	8
13	157	0.01075	6.9	^t BuOK	0.01075	1.2	25.2	64
14	158	0.01075	7.2	^t BuOK	0.01075	1.2	35.9	91
15	159	0.01075	7.1	^t BuOK	0.01075	1.2	32.7	83
16	160	0.01075	7.4	^t BuOK	0.01075	1.2	22.9	58
17	161	0.01075	7.7	^t BuOK	0.01075	1.2	23.2	59
18	162	0.01075	7.2	^t BuOK	0.01075	1.2	7.1	18
19	163	0.01075	7.4	^t BuOK	0.01075	1.2	26.0	66
20	164	0.01075	7.7	^t BuOK	0.01075	1.2	38.2	97
21	165	0.01075	7.6	^t BuOK	0.01075	1.2	31.9	81
22	166	0.01075	7.9	^t BuOK	0.01075	1.2	24.4	62
23	167	0.01075	8.2	^t BuOK	0.01075	1.2	23.6	60
24	168	0.01075	7.7	^t BuOK	0.01075	1.2	6.3	16

Table 2.6

Reactions carried out following *General Procedure G*.

Amount of aniline: 20 mg, 0.215 mmol.

Amount of benzyl alcohol: 23 mg, 0.215 mmol.

Amount of potassium *tert*-butoxide: 1.2 mg, 0.01075 mmol.

Amount of solvent: 2.5 mL.

Spectral data for N-benzyl-N-phenylamine 5I as reported above.

Entry	Catalyst	Amount of Catalyst		Solvent	Temp. / °C	Product Yield	
		mmol	mg			mg	%
1	158	0.01075	7.2	Toluene	110	35.9	91
2	158	0.01075	7.2	Dioxane	101	36.2	92
3	158	0.01075	7.2	CPME	106	3.5	9
4	158	0.01075	7.2	MTBE	55	5.9	15
5	158	0.01075	7.2	2-MeTHF	80	36.6	93
6	164	0.01075	7.7	Toluene	110	38.2	97
7	164	0.01075	7.7	Dioxane	101	37.4	95
8	164	0.01075	7.7	CPME	106	3.9	10
9	164	0.01075	7.7	MTBE	55	7.1	18
10	164	0.01075	7.7	2-MeTHF	80	37.0	94

Table 2.7

Reactions carried out following *General Procedure G*.

Amount of aniline: 20 mg, 0.215 mmol.

Amount of benzyl alcohol: 23 mg, 0.215 mmol.

Amount of potassium *tert*-butoxide: 1.2 mg, 0.01075 mmol.

Amount of 2-MeTHF: 2.5 mL.

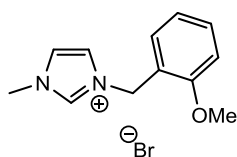
Spectral data for N-benzyl-N-phenylamine 5I as reported above.

Entry	Catalyst	Amount of Catalyst		Temp. / °C	Product Yield	
		mmol	mg		mg	%
1	158	0.01075	7.2	60	37.0	94
2	164	0.01075	7.7	60	37.8	96
3	158	0.01075	7.2	40	35.9	91

Entry	Catalyst	Amount of Catalyst		Temp. / °C	Product Yield	
		mmol	mg		mg	%
4	164	0.01075	7.7	40	37.0	94
5	158	0.01075	7.2	25	29.9	76
6	164	0.01075	7.7	25	36.6	93

Scheme 2.48

3-(2-methoxybenzyl)-1-methyl-1H-imidazol-3-ium bromide 183⁵⁰



Prepared according to *General Procedure B*.

Amount of 2-methoxybenzyl bromide **144**: 603 mg, 3 mmol.

Amount of 1-methylimidazole **182**: 239 μ L, 3 mmol

Product yield: 799 mg, 94%.

Product appearance: off-white solid.

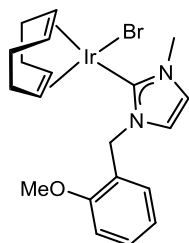
¹H NMR (400 MHz, CDCl₃) δ 10.34 (s, 1H, N-CH-N), 7.60 (dd, $J = 7.5$, $^4J = 1.4$ Hz, 1H, ArH), 7.52–7.37 (m, 1H, ArH), 6.97 (td, $J = 7.5$, $^4J = 1.0$ Hz, 1H, ArH), 6.93 (s, 1H, N-CH-CH-N), 6.89 (s, 1H, N-CH-CH-N), 5.49 (s, 2H, CH₂), 4.11 (s, 3H, OCH₃), 3.91 (s, 3H, NHC CH₃).

¹³C NMR (101 MHz, CDCl₃) δ 157.7, 137.6, 131.7, 131.6, 123.5, 122.2, 121.4, 121.3, 111.1, 55.9, 48.9, 36.9.

IR (ATR, cm⁻¹) 3132, 2922, 2830, 1540, 1456.

MP (°C) 101–104.

(1,5-cyclooctadiene)(1-methyl-3-(2-methoxybenzyl)imidazol-2-ylidene)iridium(I) bromide 32⁵⁰



Prepared according to *General Procedure D*.

Amount of bis(1,5-cyclooctadiene)diiridium(I) dichloride: 100 mg, 0.149 mmol.

Amount of potassium hexamethyldisilazide (0.7 M in toluene): 0.49 mL, 0.343 mmol.

Amount of sodium bromide: 61 mg, 0.596 mmol.

Amount of 3-(2-methoxybenzyl)-1-methylimidazolium bromide **183**: 84 mg, 0.298 mmol.

Product yield: 116 mg, 67%.

Product appearance: yellow solid.

¹H NMR (400 MHz, CDCl₃) δ 7.35–7.20 (m, 2H, ArH), 6.96–6.81 (m, 2H, ArH), 6.72 (d, *J* = 1.6 Hz, 1H, N-*HC-CH-N*), 6.67 (d, *J* = 1.6 Hz, 1H, N-*HC-CH-N*), 5.71 (d, *J* = 14.9 Hz, 1H, CH₂), 5.52 (d, *J* = 14.8 Hz, 1H, ArCH₂N), 4.59–4.51 (m, 2H, COD CH), 3.88 (s, 3H, OCH₃), 3.79 (s, 3H, NHC CH₃), 2.99–2.94 (m, 2H, COD CH), 2.12–2.02 (m, 4H, COD CH₂), 1.72–1.36 (m, 4H, COD CH₂).

¹³C NMR (101 MHz, CDCl₃) δ 155.4, 129.3, 127.3, 124.9, 123.5, 121.2, 120.6, 110.4, 83.9, 83.0, 55.4, 52.6, 52.2, 49.3, 37.6, 33.6, 32.4, 29.7, 28.2 (Imidazole N-C-N not observed).

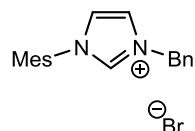
IR (ATR, cm⁻¹) 3095, 2950, 2918, 2820, 1560, 1448.

HRMS (EI) *m/z* calculated for C₂₀H₂₆N₂OIr [M-Br]: 503.1675; found: 503.1689.

MP (°C) decomp. >180.

Scheme 2.49

3-Benzyl-1-methyl-1H-imidazol-3-ium bromide **184**¹⁷²



Prepared according to *General Procedure B*.

Amount of 2-methoxybenzyl bromide **144**: 603 mg, 3 mmol.

Amount of 1-mesitylimidazole **133**: 559 mg, 3 mmol

Product yield: 922 mg, 86%.

Product appearance: colourless gum.

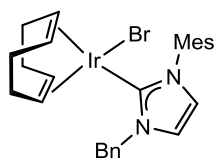
¹H NMR (400 MHz, CDCl₃) δ 10.58 (s, 1H, N-*CH-N*), 7.63–7.54 (m, 3H, ArH), 7.44–7.38 (m, 3H, ArH & N-*CH-CH-N*), 7.14 (s, 1H, N-*CH-CH-N*), 6.98 (s, 2H, ArH), 5.98 (s, 2H, ArCH₂N), 2.35 (s, 3H, CH₃), 2.08 (s, 6H, CH₃).

¹³C NMR (101 MHz, CDCl₃) δ 142.1, 137.9, 134.4, 133.6, 130.9, 130.0, 129.5, 129.3, 123.4, 123.2, 53.4, 21.2, 17.8.

IR (ATR, cm⁻¹) 2920, 2818, 2378, 1612, 1470.

MP (°C) 234–237 (lit. 237–238).¹⁷²

(1,5-cyclooctadiene)(1-methyl-3-(2-methoxybenzyl)imidazol-2-ylidene)iridium(I) bromide **185**⁵⁰



Prepared according to *General Procedure D*.

Amount of bis(1,5-cyclooctadiene)diiridium(I) dichloride: 100 mg, 0.149 mmol.

Amount of potassium hexamethyldisilazide (0.7 M in toluene): 0.49 mL, 0.343 mmol.

Amount of sodium bromide: 61 mg, 0.596 mmol.

Amount of 3-Benzyl-1-methyl-1H-imidazol-3-ium bromide **184**: 106 mg, 0.298 mmol.

Product yield: 63 mg, 59%.

Product appearance: yellow solid.

¹H NMR (400 MHz, CDCl₃) δ 7.58–7.51 (m, 4H, ArH), 7.43–7.36 (m, 3H, ArH & N-CH-CH-N), 7.17 (s, 1H, N-CH-CH-N), 6.97 (s, 2H, ArH), 5.77 (d, $J = 15.0$ Hz, 1H, ArCH₂N), 4.60–4.49 (m, 2H, COD CH), 3.02–2.96 (m, 2H, COD CH), 2.35 (s, 3H, ArCH₃), 2.10–1.99 (m, 10H, COD CH₂ & 2 ArCH₃), 1.60–1.24 (m, 4H, COD CH₂).

¹³C NMR (101 MHz, CDCl₃) δ 137.9, 137.5, 135.4, 132.9, 129.4, 129.1, 128.9, 128.0, 126.5, 125.9, 123.4, 116.3, 52.4, 29.1, 28.7, 22.5, 17.7 (Imidazole N-C-N not observed).

IR (ATR, cm⁻¹) 2918, 2890, 2820, 1604, 1458.

HRMS (EI) m/z calculated for C₂₇H₃₂IrN₂ [M-Br]: 577.2195; found: 577.2180.

MP (°C) decomp. >190.

Table 2.8

Reactions carried out following *General Procedure G*.

Reaction temperature: 25 °C.

Amount of aniline: 20 mg, 0.215 mmol.

Amount of benzyl alcohol: 23 mg, 0.215 mmol.

Amount of potassium *tert*-butoxide: 1.2 mg, 0.01075 mmol.

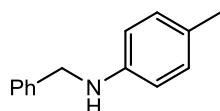
Amount of 2-MeTHF: 2.5 mL.

Spectral data for N-benzyl-N-phenylamine 51 as reported above.

Entry	Catalyst	Amount of Catalyst		Product Yield	
		mmol	mg	mg	%
1	163	0.01075	7.4	29.9	76
2	32	0.01075	6.3	10.2	26
3	185	0.01075	7.1	5.9	15

Scheme 2.52

***N*-benzyl-4-methylaniline 191**¹⁷³



Prepared according to *General Procedure G*.

Reaction temperature: 25 °C.

Amount of 4-methylaniline: 23 mg, 0.215 mmol.

Amount of benzyl alcohol: 23 mg, 0.215 mmol.

Amount of catalyst **164**: 7.7 mg, 0.01075 mmol.

Amount of potassium *tert*-butoxide: 1.2 mg, 0.01075 mmol.

Amount of 2-MeTHF: 2.5 mL.

Product yield: 38 mg, 90%.

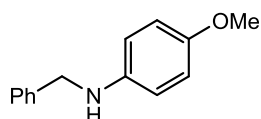
Product appearance: yellow oil.

¹H NMR (400 MHz, CDCl₃) δ 7.42–7.32 (m, 4H, ArH), 7.30–7.25 (m, 1H, ArH), 7.01 (d, *J* = 7.2 Hz, 2H, ArH), 6.63 (d, *J* = 7.8 Hz, 2H, ArH), 4.31 (s, 2H, ArCH₂N), 3.99 (br. s, 1H, NH), 2.26 (s, 3H, CH₃).

¹³C NMR (101 MHz, CDCl₃) δ 146.3, 140.0, 130.1, 128.8, 127.6, 127.5, 127.0, 113.4, 49.1, 20.6.

IR (ATR, cm⁻¹) 3410, 3035, 2358, 1620, 1518.

***N*-benzyl-4-methoxyaniline 54**¹⁷³



Prepared according to *General Procedure G*.

Reaction temperature: 25 °C.

Amount of 4-methoxyaniline: 23 mg, 0.215 mmol.

Amount of benzyl alcohol: 23 mg, 0.215 mmol.

Amount of catalyst **164**: 7.7 mg, 0.01075 mmol.

Amount of potassium *tert*-butoxide: 1.2 mg, 0.01075 mmol.

Amount of 2-MeTHF: 2.5 mL.

Product yield: 42 mg, 92%.

Product appearance: light yellow solid.

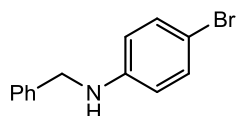
¹H NMR (400 MHz, CDCl₃) δ 7.40–7.31 (m, 4H, ArH), 7.29–7.24 (m, 1H, ArH), 6.80 (d, *J* = 8.3 Hz, 2H, ArH), 6.62 (d, *J* = 8.3 Hz, 2H, ArH), 4.30 (s, 2H, ArCH₂N), 3.78 (s, 3H, OCH₃).

¹³C NMR (101 MHz, CDCl₃) δ 151.9, 142.6, 139.7, 128.8, 127.5, 127.2, 115.0, 114.2, 55.7, 49.3.

IR (ATR, cm⁻¹) 3414, 3028, 2834, 1520, 1453.

MP (°C) 52–55 (lit. 55–56).¹⁷⁴

***N*-benzyl-4-bromoaniline **81**¹⁷⁵**



Prepared according to *General Procedure G*.

Reaction temperature: 25 °C.

Amount of 4-bromoaniline: 37 mg, 0.215 mmol.

Amount of benzyl alcohol: 23 mg, 0.215 mmol.

Amount of catalyst **164**: 7.7 mg, 0.01075 mmol.

Amount of potassium *tert*-butoxide: 1.2 mg, 0.01075 mmol.

Amount of 2-MeTHF: 2.5 mL.

Product yield: 46 mg, 81%.

Product appearance: light brown solid.

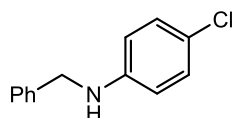
¹H NMR (400 MHz, CDCl₃) δ 7.27–7.20 (m, 5H, ArH), 7.14 (d, *J* = 8.3 Hz, 2H, ArH), 6.42 (d, *J* = 8.3 Hz, 2H, ArH), 4.22 (s, 2H, ArCH₂N), 3.92 (br. s, 1H, NH).

¹³C NMR (101 MHz, CDCl₃) δ 145.8, 137.5, 130.6, 127.5, 126.2, 114.9, 113.5, 108.0, 47.1.

IR (ATR, cm⁻¹) 3390, 3018, 2918, 2353, 1628.

MP (°C) 49–52 (lit. 45–46).¹⁷⁵

***N*-benzyl-4-chloroaniline 192**¹⁷⁵



Prepared according to *General Procedure G*.

Reaction temperature: 25 °C.

Amount of 4-chloroaniline: 27 mg, 0.215 mmol.

Amount of benzyl alcohol: 23 mg, 0.215 mmol.

Amount of catalyst **164**: 7.7 mg, 0.01075 mmol.

Amount of potassium *tert*-butoxide: 1.2 mg, 0.01075 mmol.

Amount of 2-MeTHF: 2.5 mL.

Product yield: 40 mg, 86%.

Product appearance: yellow low-melting solid.

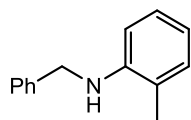
¹H NMR (400 MHz, CDCl₃) δ 7.26–7.20 (m, 5H, ArH), 7.03 (d, *J* = 8.7 Hz, 2H, ArH), 6.44 (d, *J* = 8.7 Hz, 2H, ArH), 4.16 (s, 2H, ArCH₂N), 3.87 (br. s, 1H, NH).

¹³C NMR (101 MHz, CDCl₃) δ 145.4, 137.7, 127.9, 126.2, 126.0, 120.6, 115.1, 112.7, 47.0.

IR (ATR, cm⁻¹) 3394, 3010, 2920, 2354, 1622.

MP (°C) 42–46 (lit.46–47).¹⁷⁶

***N*-benzyl-2-methylaniline 193**¹⁷³



Prepared according to *General Procedure G*.

Reaction temperature: 25 °C.

Amount of 2-methylaniline: 23 mg, 0.215 mmol.

Amount of benzyl alcohol: 23 mg, 0.215 mmol.

Amount of catalyst **164**: 7.7 mg, 0.01075 mmol.

Amount of potassium *tert*-butoxide: 1.2 mg, 0.01075 mmol.

Amount of 2-MeTHF: 2.5 mL.

Product yield: 38 mg, 89%.

Product appearance: light yellow solid.

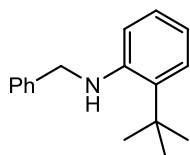
¹H NMR (400 MHz, CDCl₃) δ 7.44–7.33 (m, 2H, ArH), 7.32–7.27 (m, 1H, ArH), 7.14–7.08 (m, 2H, ArH), 6.72–6.65 (m, 2H, ArH), 6.63 (dd, *J* = 8.0, ⁴*J* = 1.1 Hz, 2H, ArH), 4.40 (s, 2H, ArCH₂N), 3.77 (br. s, 1H, NH), 2.20 (s, 3H, CH₃).

¹³C NMR (101 MHz, CDCl₃) δ 146.3, 139.8, 130.4, 128.9, 127.9, 127.5, 127.4, 112.3, 117.7, 110.4, 48.6, 17.9.

IR (ATR, cm⁻¹) 3395, 3025, 2918, 2354, 1624, 1518.

MP (°C) 57–70 (lit. 59–60).¹⁷⁶

***N*-benzyl-2-*tert*-butylaniline 194**¹⁷⁷



Prepared according to *General Procedure G*.

Reaction temperature: 25 °C.

Amount of 2-*tert*-butylaniline: 32 mg, 0.215 mmol.

Amount of benzyl alcohol: 23 mg, 0.215 mmol.

Amount of catalyst **164**: 7.7 mg, 0.01075 mmol.

Amount of potassium *tert*-butoxide: 1.2 mg, 0.01075 mmol.

Amount of 2-MeTHF: 2.5 mL.

Product yield: 35 mg, 68%.

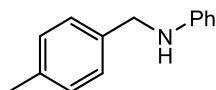
Product appearance: yellow oil.

¹H NMR (400 MHz, CDCl₃) δ 7.48–7.39 (m, 2H, ArH), 7.36–7.32 (m, 2H, ArH), 7.19–7.13 (m, 1H, ArH), 6.76 (td, *J* = 7.8, ⁴*J* = 1.2 Hz, 2H, ArH), 6.70 (dd, *J* = 8.0, ⁴*J* = 1.1 Hz, 2H, ArH), 4.45 (s, 2H, ArCH₂N), 4.18 (br. s, 1H, NH), 1.53 (s, 9H, C(CH₃)₃).

¹³C NMR (101 MHz, CDCl₃) δ 146.1, 139.5, 133.2, 129.4, 128.6, 127.4, 127.2, 126.2, 117.1, 112.0, 48.7, 34.1, 29.7.

IR (ATR, cm⁻¹) 2925, 1602, 1578, 1450.

***N*-(4-methylbenzyl)aniline 195**¹⁷⁵



Prepared according to *General Procedure G*.

Reaction temperature: 25 °C.

Amount of aniline: 20 mg, 0.215 mmol.

Amount of 4-methylbenzyl alcohol: 24 mg, 0.215 mmol.

Amount of catalyst **164**: 7.7 mg, 0.01075 mmol.

Amount of potassium *tert*-butoxide: 1.2 mg, 0.01075 mmol.

Amount of 2-MeTHF: 2.5 mL.

Product yield: 40 mg, 94%.

Product appearance: yellow low-melting solid.

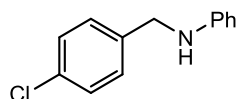
¹H NMR (400 MHz, CDCl₃) δ 7.27 (d, *J* = 7.8 Hz, 2H, ArH), 7.24–7.18 (m, 4H, ArH), 6.76 (t, *J* = 7.2 Hz, 1H, ArH), 6.67 (d, *J* = 7.8 Hz, 2H, ArH), 4.33 (s, 2H, ArCH₂N), 3.91 (br. s, 1H, NH), 2.39 (s, 3H, CH₃).

¹³C NMR (101 MHz, CDCl₃) δ 148.2, 136.6, 136.2, 129.1, 129.0, 117.3, 112.6, 48.0, 20.9.

IR (ATR, cm⁻¹) 3395, 2996, 2920, 2356, 1628, 1520.

MP (°C) 38–41 (lit. 40–41).¹⁷⁵

***N*-(4-chlorobenzyl)aniline **53**¹⁷⁵**



Prepared according to *General Procedure G*.

Reaction temperature: 25 °C.

Amount of aniline: 20 mg, 0.215 mmol.

Amount of 4-chlorobenzyl alcohol: 31 mg, 0.215 mmol.

Amount of catalyst **164**: 7.7 mg, 0.01075 mmol.

Amount of potassium *tert*-butoxide: 1.2 mg, 0.01075 mmol.

Amount of 2-MeTHF: 2.5 mL.

Product yield: 42 mg, 91%.

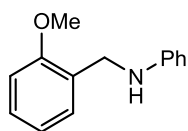
Product appearance: pale yellow oil.

¹H NMR (400 MHz, CDCl₃) δ 7.37–7.32 (m, 4H, ArH), 7.26–7.22 (m, 2H, ArH), 6.78 (t, *J* = 7.1 Hz, 1H, ArH), 6.66 (d, *J* = 8.1 Hz, 2H, ArH), 4.34 (s, 2H, ArCH₂N), 3.97 (br. s, 1H, NH).

¹³C NMR (101 MHz, CDCl₃) δ 148.0, 138.3, 133.0, 131.2, 129.6, 128.9, 128.8, 118.0, 113.2, 47.9.

IR (ATR, cm⁻¹) 3394, 3005, 2916, 2650, 1624.

***N*-(2-methoxybenzyl)aniline 196**¹⁷⁸



Prepared according to *General Procedure G*.

Reaction temperature: 25 °C.

Amount of aniline: 20 mg, 0.215 mmol.

Amount of 2-methoxybenzyl alcohol: 30 mg, 0.215 mmol.

Amount of catalyst **164**: 7.7 mg, 0.01075 mmol.

Amount of potassium *tert*-butoxide: 1.2 mg, 0.01075 mmol.

Amount of 2-MeTHF: 2.5 mL.

Product yield: 37 mg, 81%.

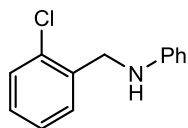
Product appearance: pale yellow oil.

¹H NMR (400 MHz, CDCl₃) δ 7.32–7.26 (m, 2H, ArH), 7.22–7.11 (m, 2H, ArH), 6.94–6.90 (m, 2H, ArH), 6.79–6.72 (m, 3H, ArH), 4.33 (s, 2H, ArCH₂N), 3.85 (s, OCH₃).

¹³C NMR (101 MHz, CDCl₃) δ 157.3, 146.4, 129.2, 129.1, 128.5, 126.1, 120.4, 118.7, 114.4, 110.2, 55.1, 44.2.

IR (ATR, cm⁻¹) 3398, 3024, 2830, 1518, 1449.

***N*-(2-chlorobenzyl)aniline 197**¹⁷⁸



Prepared according to *General Procedure G*.

Reaction temperature: 25 °C.

Amount of aniline: 20 mg, 0.215 mmol.

Amount of 2-chlorobenzyl alcohol: 31 mg, 0.215 mmol.

Amount of catalyst **164**: 7.7 mg, 0.01075 mmol.

Amount of potassium *tert*-butoxide: 1.2 mg, 0.01075 mmol.

Amount of 2-MeTHF: 2.5 mL.

Product yield: 39 mg, 83%.

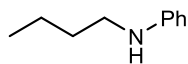
Product appearance: pale yellow oil.

¹H NMR (400 MHz, CDCl₃) δ 7.32–7.26 (m, 2H, ArH), 7.21–7.10 (m, 4H, ArH), 6.74–6.67 (m, 1H, ArH), 6.64–6.58 (m, 2H, ArH), 4.43 (s, 2H, ArCH₂N), 4.02 (br. s, 1H, NH).

^{13}C NMR (101 MHz, CDCl_3) δ 147.2, 136.6, 133.1, 129.4, 129.2, 129.0, 128.1, 126.7, 117.6, 112.7, 45.6.

IR (ATR, cm^{-1}) 3394, 3022, 2924, 2346, 1618.

N-*n*-butylaniline **198**



Synthesis attempted according to *General Procedure G*.

Reaction temperature: 25 °C.

Amount of aniline: 20 mg, 0.215 mmol.

Amount of *n*-butyl alcohol: 16 mg, 0.215 mmol.

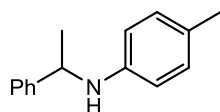
Amount of catalyst **164**: 7.7 mg, 0.01075 mmol.

Amount of potassium *tert*-butoxide: 1.2 mg, 0.01075 mmol.

Amount of 2-MeTHF: 2.5 mL.

None of the desired product observed or isolated.

4-Methyl-(1-phenylethyl)aniline 199¹⁷⁹



Prepared according to *General Procedure G*.

Reaction temperature: 25 °C.

Amount of 4-methylaniline: 23 mg, 0.215 mmol.

Amount of phenylethanol: 26 mg, 0.215 mmol.

Amount of catalyst **164**: 7.7 mg, 0.01075 mmol.

Amount of potassium *tert*-butoxide: 1.2 mg, 0.01075 mmol.

Amount of 2-MeTHF: 2.5 mL.

Product yield: 40 mg, 88%.

Product appearance: pale yellow solid.

^1H NMR (400 MHz, CDCl_3) δ 7.42–7.20 (m, 5H, ArH), 6.91 (d, $J = 8.1$ Hz, 2H, ArH), 6.48 (d, $J = 8.1$ Hz, 2H, ArH), 4.46 (q, $J = 6.7$ Hz, 1H, $\text{NCH}(\text{CH}_3)\text{Ar}$), 2.21 (s, 3H, ArCH_3), 1.52 (d, $J = 6.7$ Hz, 3H, $\text{NCH}(\text{CH}_3)\text{Ar}$).

^{13}C NMR (101 MHz, CDCl_3) δ 145.4, 144.9, 129.6, 128.6, 126.7, 126.3, 125.7, 113.3, 53.7, 25.0, 20.3.

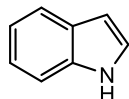
IR (ATR, cm^{-1}) 3022, 2920, 2854, 1602, 1580, 1462.

MP (°C) 68–70 (lit. 68–69).¹⁸⁰

Synthesis of *N*-Heterocycles via Hydrogen Borrowing

Scheme 2.53

1-*H*-Indole **61**¹⁸¹



Synthesis attempted according to *General Procedure H*.

Reaction temperature: 25 °C.

Amount of 2-(2-aminophenyl)ethanol **60**: 20 mg, 0.146 mmol.

Amount of catalyst **164**: 5.2 mg, 0.007 mmol.

Amount of potassium *tert*-butoxide: 0.8 mg, 0.007 mmol.

Amount of 2-MeTHF: 1.5 mL.

Conversion was calculated using LCMS analysis, integrating the peak at $t_R = 0.90$ mins (**61**, $[M-H] = 116.2$) against the peak at $t_R = 0.56$ mins (**60**, $[M-H] = 138.1$).

Conversion to **61**: trace (<3%).

Table 2.9

Reactions carried out according to *General Procedure H*.

Reaction temperature: 25 °C.

Amount of 2-(2-aminophenyl)ethanol **60**: 20 mg, 0.146 mmol.

Amount of 2-MeTHF: 1.5 mL.

Entry	Catalyst	Amount of Catalyst		Base	Amount of Base		LCMS Conversion / %
		mmol	mg		mmol	mg	
1	158	0.007	4.9	<i>t</i> -BuOK	0.007	0.8	13
2	158	0.007	4.9	K ₂ CO ₃	0.007	1.0	18
3	164	0.007	5.2	<i>t</i> -BuOK	0.007	0.8	9
4	164	0.007	5.2	K ₂ CO ₃	0.007	1.0	14

Table 2.10

Reactions carried out according to *General Procedure H*.

Reaction temperature: 110 °C.

Amount of 2-(2-aminophenyl)ethanol **60**: 20 mg, 0.146 mmol.

Amount of toluene: 1.5 mL.

Entry	Catalyst	Amount of Catalyst		Base	Amount of Base		LCMS Conversion / %
		mmol	mg		mmol	mg	
1	158	0.007	4.9	K ₂ CO ₃	0.014	2.0	48
2	164	0.007	5.2	K ₂ CO ₃	0.014	2.0	37

Table 2.11

Reactions carried out according to *General Procedure H*.

Amount of 2-(2-aminophenyl)ethanol **60**: 20 mg, 0.146 mmol.

Amount of catalyst **158**: 4.9 mg, 0.007 mmol.

Amount of potassium carbonate: 2.0 mg, 0.014 mmol.

Amount of solvent: 1.5 mL.

Entry	Catalyst	Temp. / °C	LCMS Conversion / %
1	Toluene	110	48
2	Dioxane	101	46
3	DCE	80	<10
4	2-MeTHF	80	26
5	CPME	106	38
6	<i>t</i> -AmOH	100	29
7	<i>none</i>	100	21

Scheme 2.54 – Reaction Optimisation using Design of Experiments (DOE).

The effects of catalyst loading, base loading, temperature, and solvent volume were assessed using Design of Experiments (DOE).^{152,153} Design-Expert™ software v9.0.3 (Stat-Ease Inc., Minneapolis, MN) was used to generate a set of 12 experiments as part of a 2-level factorial design. For each factor, a range of values was specified; the eight combinations of high and low values were then run as individual experiments. Additionally, four centre point runs were carried out in order to: (a) assess any curvature in the response to changes of the variables, and (b) ensure reproducibility of the reaction. This design gave a total of 12 experiments, with entries 4, 7, 9, and 10 representing the centre points. LCMS conversion to **61** was used as the response.

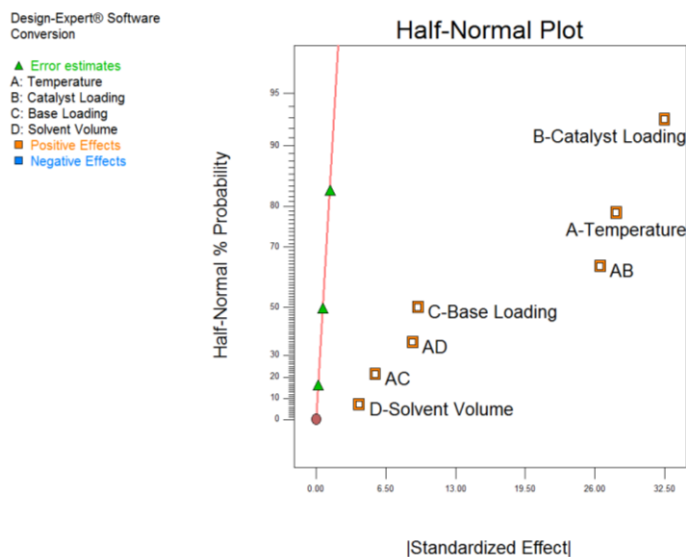
Reactions carried out according to *General Procedure H*.

Amount of 2-(2-aminophenyl)ethanol **60**: 20 mg, 0.146 mmol.

Run	Factor A: Temperature / °C	Factor B: Catalyst Loading / mol%	Factor C: Base Loading / mol%	Factor D: Solvent Volume / mL	Response: LCMS Conversion / %
1	20	10	50	0.1	11
2	110	0.25	50	0.1	3
3	110	0.25	0.25	2	1
4[‡]	65	5.215	25.125	1.05	10
5	20	10	0.25	2	2
6	110	10	0.25	0.1	47
7[‡]	65	5.215	25.125	1.05	9
8	20	0.25	50	2	0
9[‡]	65	5.215	25.125	1.05	8
10[‡]	65	5.215	25.125	1.05	11
11	110	10	50	2	78
12	20	0.25	0.25	0.1	1

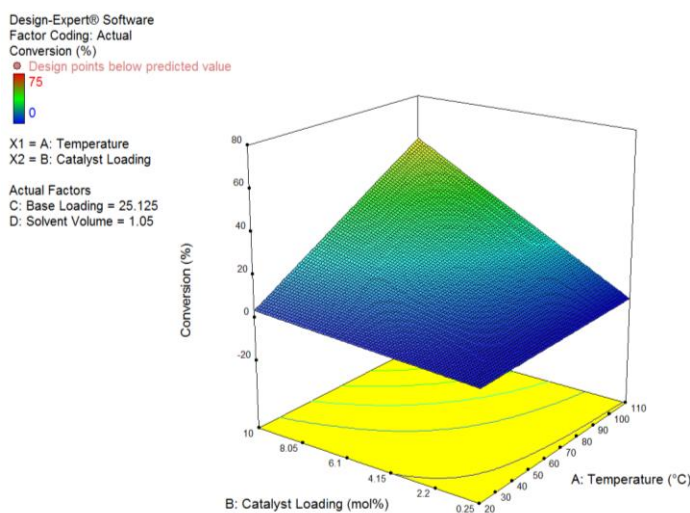
[‡]These entries represent centre points.

The responses were entered into the same design program, and used to generate a half-normal plot (Graph 2.4), which suggested that all variables had notable effects on reaction efficacy, with catalyst loading having the largest effect.



Graph 2.4

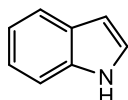
A numerical optimization model was then used to search the factor space for the best combination of variables to achieve the maximum response. The optimised conditions were selected from the top left of the plot shown in Graph 2.5, and in fact were the conditions used in Run 11 (10 mol% catalyst loading, 50 mol% base, 110 °C, 2 mL solvent).



Graph 2.5

Lastly, since we had so far used LCMS conversions to analyse reaction efficiency, the optimised reaction mixture was purified as per *General Procedure G* in order to ensure consistency between conversions and isolated yields.

1-*H*-Indole **61**¹⁸¹



Product yield: 13 mg, 75%.

Product appearance: white crystalline solid.

¹H NMR (400 MHz, CDCl₃) δ 8.21 (br s, 1H, NH), 7.70–7.66 (d, *J* = 7.5 Hz, 1H, C⁷H), 7.45–7.41 (d, *J* = 7.5 Hz, 1H, C²H), 7.28–7.20 (m, 2H, ArH), 7.17–7.14 (m, 1H, C⁵H), 6.60–6.57 (m, 1H, C³H).

¹³C NMR (100 MHz, CDCl₃) δ 135.9, 128.3, 124.6, 122.0, 121.3, 120.1, 111.4, 102.7, 101.9.

IR (ATR, cm⁻¹) 3478, 3330, 3040, 1546, 1480.

MP (°C) 50–53 (lit. 51–54).¹⁸¹

Scheme 2.55

Carried out according to *General Procedure H*.

Reaction temperature: 110 °C.

Amount of 2-(2-aminophenyl)ethanol **60**: 2.7 mg, 0.2 mmol.

Amount of catalyst **158**: 13 mg, 0.2 mmol.

Amount of potassium *tert*-butoxide: 2.8 mg, 0.2 mmol.

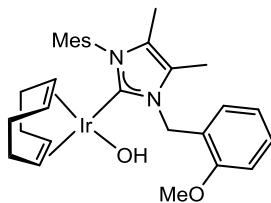
Amount of toluene: 1 mL.

Conversion was calculated using LCMS analysis, integrating the peak at *t*_R = 0.90 mins (**61**, [*M*–*H*] = 116.2) against the peak at *t*_R = 0.56 mins (**60**, [*M*–*H*] = 138.1).

Conversion to **61**: 0%.

Scheme 2.57

(1,5-cyclooctadiene)(1-mesityl-3-(2-methoxybenzyl)-4,5-dimethylimidazol-2-ylidene)iridium(I) hydroxide **201**



Carried out according to a literature procedure.¹⁵⁵ A round-bottom flask with stirrer bar was charged with (1,5-cyclooctadiene)(1-mesityl-3-(2-methoxybenzyl)-4,5-dimethylimidazol-2-

ylidene)iridium(I) chloride **158** (100 mg, 0.149 mmol) and tetrahydrofuran (10 mL) under nitrogen. Once all the Ir complex had dissolved, cesium hydroxide monohydrate (187 mg, 0.891 mmol) was added. The reaction was stirred for 96 h at room temperature. The bright green solution was filtered through celite and concentrated *in vacuo*. The resulting solid was washed with cold *n*-pentane to afford a dark green solid (66 mg), which quickly turned a green-brown colour. NMR analysis showed decomposition of the starting material and confirmed that none of the desired product was observed.

Table 2.12

Reactions carried out according to *General Procedure I*.

Reaction temperature: 110 °C.

Amount of 2-(2-aminophenyl)ethanol **60**: 20 mg, 0.146 mmol.

Amount of catalyst **158**: 10.1 mg, 0.015 mmol.

Amount of potassium carbonate: 10.4 mg, 0.073 mmol.

Amount of toluene: 2 mL.

Entry	Additive	Amount of Additive		LCMS Conversion / %
		mmol	mg	
1	AgOTf	0.015	3.9	56
2	AgBF ₄	0.015	2.9	93
3	AgPF ₆	0.015	3.8	82
4	NaBAR _F	0.015	13.3	89

Table 2.13

Reactions carried out according to *General Procedure I*.

Reaction temperature: 110 °C.

Amount of 2-(2-aminophenyl)ethanol **60**: 20 mg, 0.146 mmol.

Amount of potassium carbonate: 10.4 mg, 0.073 mmol.

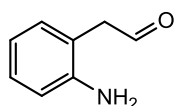
Amount of silver tetrafluoroborate: 2.9 mg, 0.015 mmol.

Amount of toluene: 2 mL.

Entry	Additive	Amount of Additive		Amount of Catalyst 158		Temp. / °C	LCMS Conversion / %
		mmol	mg	mmol	mg		
1	Acetone	0.146	8.5	0.015	10.1	80	52
2	Acetone	0.146	8.5	0.015	10.1	60	35
3	Acetone	0.146	8.5	0.0015	1.0	60	>10
4	Cyclohexene	0.146	12.0	0.015	10.1	80	72
5	Cyclohexene	0.146	12.0	0.015	10.1	60	32
6	Cyclohexene	0.146	12.0	0.0015	1.0	60	>10
7	Styrene	0.146	15.2	0.015	10.1	80	81
8	Styrene	0.146	15.2	0.015	10.1	60	76
9	Styrene	0.146	15.2	0.0075	5.1	60	58
10	Styrene	0.146	15.2	0.0038	2.5	60	51
11	Styrene	0.146	15.2	0.0015	1.0	60	46

Scheme 2.60

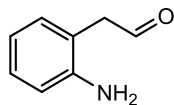
2-(2-aminophenyl)acetaldehyde 202



NMO (256 mg, 2.187 mmol) was dissolved in DCM (1 mL) under nitrogen and stirred with magnesium sulfate for 20 min. The dry solution was then transferred *via* syringe to a solution of 2-(2-aminophenyl)ethanol (200 mg, 1.458 mmol) in DCM (3 mL), and powdered 4Å molecular sieves (800 mg) were added, followed by tetra-*n*-propylammonium perruthenate(vii) (25.6 mg, 0.073 mmol). The black reaction mixture was left to stir at room temperature and the reaction was followed by LCMS. The crude mixture was passed through a plug of silica, eluting with ethyl acetate, and concentrated *in vacuo*. Crude LCMS analysis after 18 h showed 88% of starting material remaining and 8% indole, presumed to have formed as a result of intramolecular cyclisation of the product aldehyde. NMR analysis confirmed that none of the desired aldehyde product was present. The reaction was abandoned without workup.

Scheme 2.61

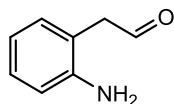
2-(2-aminophenyl)acetaldehyde 202



A solution of oxalyl chloride (137 μ L, 1.6 mmol) in DCM (6 mL) was prepared and cooled to -78 $^{\circ}$ C. DMSO (227 μ L 3.19 mmol) was added to the solution slowly and the mixture was stirred for 20 min. A solution of 2-(2-aminophenyl)ethanol (200 mg, 1.46 mmol) in DCM (1 mL) was prepared and added to the solution of activated DMSO. After stirring for 15 min, triethylamine (1.046 mL, 7.5 mmol) was added, and the reaction mixture was allowed to warm to room temperature. The mixture was quenched with aqueous 10% ammonium chloride solution, and extracted with ethyl acetate (3×5 mL). The organic phase was washed with water, dried over sodium sulfate, and concentrated *in vacuo*. NMR and LCMS analysis showed that none of the desired alcohol was present, and confirmed the presence of 5% of indole **61**. The reaction mixture was disposed of without further purification.

Scheme 2.62

2-(2-aminophenyl)acetaldehyde 202

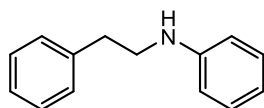


Carried out according to a literature procedure.¹⁵⁶ A solution of sodium bis(2-methoxyethoxy) aluminium hydride (RedAl) (2.101 mL, 7.00 mmol) (65 wt% in toluene) in toluene (4 mL) was prepared and cooled to 0 $^{\circ}$ C. 1-methylpiperazine (0.972 mL, 8.76 mmol) was added dropwise, with the temperature being maintained below 10 $^{\circ}$ C. The resulting mixture was stirred for 30 mins to give a solution of RedAl-NMP in toluene (approx. 1.1 M). A solution of 2-(2-aminophenyl)acetic acid (0.605 g, 4 mmol) was prepared in toluene (20 mL) and cooled to 0 $^{\circ}$ C, and the solution of RedAl-NMP was added dropwise. The reaction was stirred for 30 minutes. The reaction mixture was quenched with water and extracted with ethyl acetate. The organic portions were combined, washed with water, and dried through a hydrophobic frit before being concentrated *in vacuo*. The resulting solid was collected by filtration and dried *in vacuo* to afford a dark purple oil. LCMS and NMR

analysis confirmed this to be 2-(2-aminophenyl)ethanol. None of the desired aldehyde product was observed.

Scheme 2.63

***N*-phenethylaniline 56**¹⁸²



Prepared according to *General Procedure I*.

Reaction temperature: 110 °C.

Amount of aniline: 14 mg, 0.15 mmol.

Amount of 2-phenylethanol: 18 mg, 0.15 mmol.

Amount of catalyst **158**: 10.1 mg, 0.015 mmol.

Amount of potassium carbonate: 10.4 mg, 0.073 mmol.

Amount of silver tetrafluoroborate: 2.9 mg, 0.015 mmol.

Amount of toluene: 2 mL.

Product yield: 28 mg, 96%.

Product appearance: yellow low-melting solid.

¹H NMR (400 MHz, CDCl₃) δ 7.36 (t, *J* = 7.1 Hz, 2H, ArH), 7.30–7.27 (m, 3H, ArH), 7.26–7.23 (m, 2H, ArH), 6.76 (t, *J* = 7.3 Hz, 1H, ArH), 6.67 (d, *J* = 7.3 Hz, 2H, ArH), 3.88 (br. s, 1H, NH), 3.44 (t, *J* = 7.1 Hz, 2H, NCH₂CH₂Ar), 2.94 (t, *J* = 7.1 Hz, 2H, NCH₂CH₂Ar).

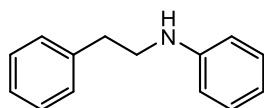
¹³C NMR (101 MHz, CDCl₃) δ 148.4, 139.6, 129.4, 128.8, 128.7, 126.6, 117.7, 113.1, 45.3, 35.8.

IR (ATR, cm⁻¹) 3402, 3030, 2925, 2854, 1602, 1510, 1478.

MP (°C) 43–46 (lit. 45–46).¹⁸²

Graph 2.2

Intermolecular Formation of *N*-phenethylaniline 56 – Rate Study



Carried out according to *General Procedure I*.

Reaction temperature: 110 °C.

Amount of aniline: 14 mg, 0.15 mmol.

Amount of 2-phenylethanol: 18 mg, 0.15 mmol.

Amount of catalyst **158**: 10.1 mg, 0.015 mmol.

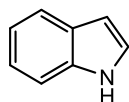
Amount of potassium carbonate: 10.4 mg, 0.073 mmol.

Amount of silver tetrafluoroborate: 2.9 mg, 0.015 mmol.

Amount of toluene: 2 mL.

Entry	Time / min	Conversion / %
1	15	14
2	30	25
3	45	32
4	60	36
5	90	38
6	120	40
7	150	41
8	180	42

Intramolecular Formation of Indole 61 – Rate Study



Prepared according to *General Procedure I*.

Reaction temperature: 110 °C.

Amount of 2-(2-aminophenyl)ethanol **60**: 20 mg, 0.146 mmol.

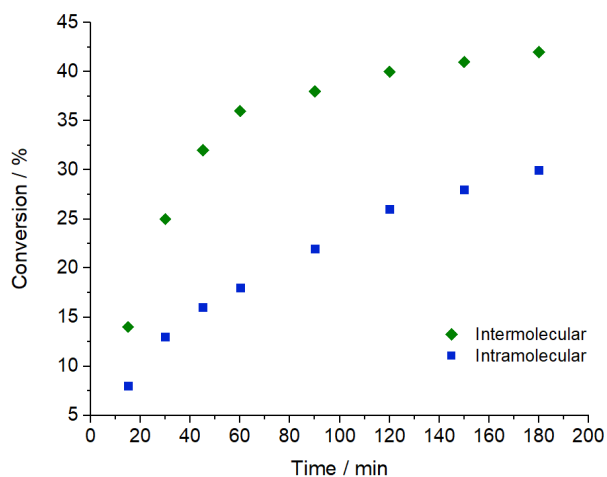
Amount of catalyst **158**: 10.1 mg, 0.015 mmol.

Amount of potassium carbonate: 10.4 mg, 0.073 mmol.

Amount of silver tetrafluoroborate: 2.9 mg, 0.015 mmol.

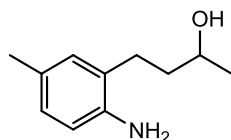
Amount of toluene: 2 mL.

Entry	Time / min	Conversion / %
1	15	8
2	30	13
3	45	16
4	60	18
5	90	22
6	120	26
7	150	28
8	180	30



Scheme 2.66

4-(2-amino-5-methylphenyl)butan-2-ol 207



Prepared according to *General Procedures J* and *K*

Amount of 2,4-dimethylaniline: 330 mg, 2.73 mmol.

N-Boc protection yield: 543 mg, 90%.

Alkylation/deprotection yield: 226 mg, 63%.

Yield over 2 steps: 57%.

Product appearance: pale yellow solid.

$^1\text{H NMR}$ (400 MHz, CDCl_3) δ 7.46 (br. s, 2H, NH), 6.91–6.86 (m, 2H, ArH), 6.58 (d, $J = 8.3$ Hz, 1H, ArH), 3.72 (q, $J = 6.1$ Hz, 1H, CHOH), 2.68–2.62 (m, 2H, ArCH₂), 2.23 (s, 3H, ArCH₃), 1.74 (td, $J = 6.2, 7.2$ Hz, 2H, ArCH₂CH₂), 1.22 (d, $J = 6.1$ Hz, 3H, CHOHCH₃).

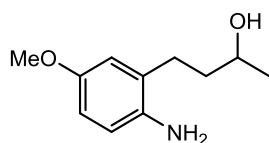
$^{13}\text{C NMR}$ (101 MHz, CDCl_3) δ 144.2, 132.4, 129.3, 129.0, 123.8, 116.8, 77.2, 51.4, 24.2, 21.9, 17.9.

IR (ATR, cm^{-1}) 3396, 3035, 2920, 2353, 1630, 1548, 1470.

LCMS $t_R = 1.06$ min, $[\text{M}+\text{H}] = 178.3$.

MP ($^\circ\text{C}$) 102–106.

4-(2-amino-5-methoxyphenyl)butan-2-ol 208



Prepared according to *General Procedures J* and *K*

Amount of 2-methyl-4-methoxyaniline: 374 mg, 2.73 mmol.

N-Boc protection yield: 615 mg, 95%.

Alkylation/deprotection yield: 375 mg, 96%.

Yield over 2 steps: 91%.

Product appearance: colourless oil.

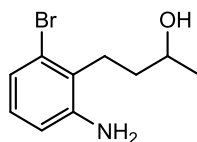
$^1\text{H NMR}$ (400 MHz, CDCl_3) δ 7.60 (br. s, 2H, NH_2), 7.22 (d, $J = 7.2$ Hz, 1H, ArH), 6.72 (m, 1H, ArH), 6.62 (dd, $J = 7.2$, $^4J = 1.2$ Hz, 1H, ArH), 3.83 (q, $J = 6.4$ Hz, 1H, CHOH), 3.77 (s, 3H, OCH_3), 2.57–2.53 (m, 2H, ArCH_2), 1.72 (td, $J = 6.2$, 7.1 Hz, 2H, ArCH_2CH_2), 1.24 (d, $J = 6.2$ Hz, 3H, CHOHCH_3).

$^{13}\text{C NMR}$ (101 MHz, CDCl_3) δ 150.8, 136.6, 131.0, 118.6, 116.2, 111.4, 72.7, 57.4, 30.8, 24.7, 23.4.

IR (ATR, cm^{-1}) 3306, 3020, 2914, 2351, 1616, 1560, 1458.

LCMS $t_{\text{R}} = 0.92$ min, $[\text{M}+\text{H}] = 196.3$.

4-(2-amino-6-bromophenyl)butan-2-ol 209



Prepared according to *General Procedures J* and *K*

Amount of 2-methyl-3-bromoaniline: 507 mg, 2.73 mmol.

N-Boc protection yield: 765 mg, 98%.

Alkylation/deprotection yield: 454 mg, 93%.

Yield over 2 steps: 91%.

Product appearance: yellow-orange solid.

$^1\text{H NMR}$ (400 MHz, CDCl_3) δ 6.93 (dd, $J = 8.0$, 7.8 Hz, 1H, ArH) 6.78 (d, $J = 7.8$ Hz, 1H, ArH), 6.56 (d, $J = 8.0$ Hz, 1H, ArH), 4.86 (s, 1H, OH), 3.87 (q, $J = 6.0$ Hz, 1H, CHOH), 2.56 (t, $J = 6.1$ Hz, 2H, ArCH_2), 1.78 (td, $J = 6.2$, 6.1 Hz, 2H, ArCH_2CH_2), 1.25 (d, $J = 6.0$ Hz, 3H, CHOHCH_3).

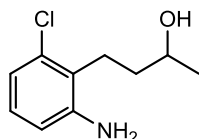
^{13}C NMR (101 MHz, CDCl_3) δ 146.7, 134.6, 127.6, 124.5, 120.2, 114.7, 68.9, 30.8, 24.0, 20.7.

IR (ATR, cm^{-1}) 3395, 2854, 2351, 1617, 1567, 1465.

LCMS $t_{\text{R}} = 1.18$ min, $[\text{M}+\text{H}] = 245.1$.

MP ($^{\circ}\text{C}$) 85–88.

4-(2-amino-6-chlorophenyl)butan-2-ol 210



Prepared according to *General Procedures J* and *K*

Amount of 2-methyl-3-chloroaniline: 387 mg, 2.73 mmol.

N-Boc protection yield: 594 mg, 90%.

Alkylation/deprotection yield: 383 mg, 96%.

Yield over 2 steps: 86%.

Product appearance: yellow oil.

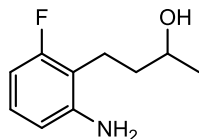
^1H NMR (400 MHz, CDCl_3) δ 7.52 (br. s, 2H, NH_2), 7.00 (t, $J = 7.9$ Hz, 1H, ArH) 6.94 (d, $J = 7.9$ Hz, 2H, ArH), 6.60 (d, $J = 8.0$ Hz, 1H, ArH), 4.01 (q, $J = 6.0$ Hz, CHOH), 2.53 (t, $J = 6.0$ Hz, 2H, ArCH_2), 1.75 (td, $J = 6.0, 6.1$ Hz, 2H, ArCH_2CH_2), 1.25 (d, $J = 6.0$ Hz, 3H, CHOHCH_3).

^{13}C NMR (101 MHz, CDCl_3) δ 146.7, 134.2, 128.2, 126.5, 119.5, 114.2, 67.9, 30.9, 23.6, 19.2.

IR (ATR, cm^{-1}) 3390, 2908, 2344, 1618, 1520, 1468.

LCMS $t_{\text{R}} = 1.19$ min, $[\text{M}+\text{H}] = 200.7$.

4-(2-amino-6-fluorophenyl)butan-2-ol 211



Prepared according to *General Procedures J* and *K*

Amount of 2-methyl-3-fluoroaniline: 342 mg, 2.73 mmol.

N-Boc protection yield: 547 mg, 89%.

Alkylation/deprotection yield: 344 mg, 94%.

Yield over 2 steps: 84%.

Product appearance: pale yellow oil.

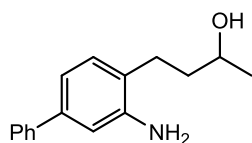
¹H NMR (400 MHz, CDCl₃) δ 7.60 (br. s, 2H, NH₂), 7.02–6.96 (m, 2H, ArH), 6.46 (d, *J* = 8.1 Hz, 1H, ArH), 4.99 (br. s, 1H, OH), 4.01 (q, *J* = 6.1 Hz, CHOH), 2.56 (t, *J* = 6.0 Hz, 2H, ArCH₂), 1.74 (td, *J* = 6.0, 6.1 Hz, 2H, ArCH₂CH₂), 1.23 (d, *J* = 6.0 Hz, 3H, CHOHCH₃).

¹³C NMR (101 MHz, CDCl₃) δ 160.9 (d, ¹*J*_{CF} = 234.3 Hz), 148.0, 128.3, 112.9 (d, ²*J*_{CF} = 23.4 Hz), 111.8, 108.6 (d, ²*J*_{CF} = 21.6 Hz), 70.0, 32.2, 24.6, 19.6.

IR (ATR, cm⁻¹) 3396, 3035, 2920, 2353, 1630, 1548.

LCMS *t*_R = 1.17 min, [M+H] = 184.2.

3-amino-[1,1'-biphenyl]-4-yl)butan-2-ol 212



Prepared according to *General Procedures J* and *K*

Amount of 4-methyl-[1,1'-biphenyl]-3-amine: 500 mg, 2.73 mmol.

N-Boc protection yield: 768 mg, 99%.

Alkylation/deprotection yield: 428 mg, 70%.

Yield over 2 steps: 70%.

Product appearance: off-white solid.

¹H NMR (400 MHz, CDCl₃) δ = 8.09 (br. s, 1H, OH), 7.65 (d, *J* = 7.3 Hz, 2H, ArH), 7.50 (br. s, 2H, NH₂), 7.44 (m, 3H, ArH), 7.38–7.27 (m, 2H, ArH), 7.23 (d, *J* = 8.1 Hz, 1H, ArH), 3.78 (q, *J* = 6.0 Hz, 1H, CHOH), 2.88–2.68 (m, 2H, ArCH₂), 1.79 (td, *J* = 6.3, 7.3 Hz, 2H, ArCH₂CH₂), 1.26 (d, *J* = 6.3 Hz, 3H, CHOHCH₃).

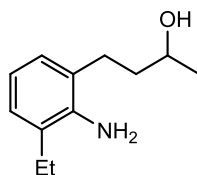
¹³C NMR (101 MHz, CDCl₃) δ 152.5, 140.6, 137.7, 132.3, 132.8, 128.8, 126.1, 123.8, 119.6, 91.2, 80.9, 28.3, 27.4, 17.4.

IR (ATR, cm⁻¹) 3394, 2916, 2349, 1618, 1545, 1470.

LCMS *t*_R = 1.28 min, [M+H] = 242.1.

MP (°C) 116–118.

4-(2-amino-3-ethylphenyl)butan-2-ol 213



Prepared according to *General Procedures J and K*

Amount of 2-methyl-6-ethylaniline: 369 mg, 2.73 mmol.

N-Boc protection yield: 629 mg, 98%.

Alkylation/deprotection yield: 289 mg, 75%.

Yield over 2 steps: 73%.

Product appearance: yellow-orange solid.

¹H NMR (400 MHz, CDCl₃) δ 6.94–6.89 (m, 2H, ArH), 6.74 (t, *J* = 7.8 Hz, 1H, ArH), 3.83 (q, *J* = 6.1 Hz, 1H, CHOH), 3.55 (br. s, 2H, NH₂), 2.55–2.49 (m, 4H, ArCH₂), 1.75 (td, *J* = 6.1, 6.2 Hz, 2H, ArCH₂CH₂), 1.25 (d, *J* = 6.1 Hz, 3H, CHOHCH₃), 1.17 (t, *J* = 6.6 Hz, ArCH₂CH₃).

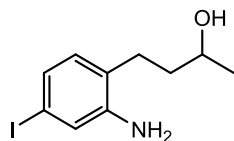
¹³C NMR (101 MHz, CDCl₃) δ 143.4, 127.8, 126.7, 125.5, 122.6, 118.3, 67.7, 31.2, 24.2, 24.1, 22.9, 14.4.

IR (ATR, cm⁻¹) 3364, 2905, 2643, 1645, 1587, 1474.

LCMS *t*_R = 1.09 min, [M+H] = 194.3.

MP (°C) 78–81.

4-(2-amino-4-iodophenyl)butan-2-ol 214



Prepared according to *General Procedures J and K*

Amount of 2-methyl-5-iodoaniline: 636 mg, 2.73 mmol.

N-Boc protection yield: 839 mg, 92%.

Alkylation/deprotection yield: 553 mg, 95%.

Yield over 2 steps: 87%.

Product appearance: yellow oil.

¹H NMR (400 MHz, CDCl₃) δ 7.60 (br. s, 2H, NH₂), 7.05–7.02 (m, 2H, ArH), 6.83 (d, *J* = 8.2 Hz, 1H, ArH), 3.90 (q, *J* = 6.1 Hz, CHOH), 2.54 (t, *J* = 6.0 Hz, 2H, ArCH₂), 1.74 (td, *J* = 6.0, 6.1 Hz, 2H, ArCH₂CH₂), 1.23 (d, *J* = 6.1 Hz, 3H, CHOHCH₃).

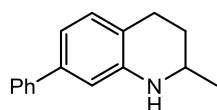
¹³C NMR (101 MHz, CDCl₃) δ 146.2, 131.0, 127.4, 124.9, 124.2, 91.8, 69.2, 31.0, 24.1, 23.2.

IR (ATR, cm⁻¹) 3398, 2918, 2345, 1628, 1564.

LCMS *t*_R = 1.10 min, [M+H] = 292.0.

Scheme 2.67

2-methyl-7-phenyl-1,2,3,4-tetrahydroquinoline 215



Prepared according to *General Procedure I*.

Reaction temperature: 110 °C.

Amount of 3-amino-[1,1'-biphenyl]-4-yl)butan-2-ol **212**: 36 mg, 0.15 mmol.

Amount of catalyst **158**: 10.1 mg, 0.015 mmol.

Amount of potassium carbonate: 10.4 mg, 0.073 mmol.

Amount of silver tetrafluoroborate: 2.9 mg, 0.015 mmol.

Amount of toluene: 2 mL.

Product appearance: colourless oil.

Product yield: 24 mg, 73%.

¹H NMR (400 MHz, CDCl₃) δ 7.73 (d, *J* = 7.3 Hz, 2H, ArH), 7.51–7.48 (m, 3H, ArH & NH), 7.42 (t, *J* = 7.8 Hz, 1H, ArH), 7.29 (d, *J* = 8.1 Hz, 1H, ArH), 6.82–6.77 (m, 2H, ArH), 3.30–3.28 (m, 1H, CH(CH₃)), 2.89–2.73 (m, 2H, ArCH₂), 1.87–1.83 (m, 1H, ArCH₂CH₂), 1.63–1.58 (m, 1H, ArCH₂CH₂), 1.17 (t, *J* = 6.3 Hz, 3H, CH₃).

¹³C NMR (101 MHz, CDCl₃) δ 146.0, 141.2, 137.5, 129.5, 129.3, 128.0, 127.5, 121.0, 116.4, 112.0, 63.4, 32.8, 23.6, 20.7.

IR (ATR, cm⁻¹) 3395, 2970, 2922, 2846, 1605, 1587, 1480.

LCMS *t*_R = 1.18 min, [M+H] = 224.1.

Table 2.14

Reactions carried out according to *General Procedure I*.

Amount of 3-amino-[1,1'-biphenyl]-4-yl)butan-2-ol **212**: 36 mg, 0.15 mmol.

Amount of catalyst **158**: 10.1 mg, 0.015 mmol.

Amount of solvent: 2 mL.

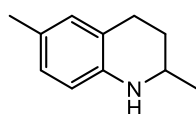
Conversion was calculated using LCMS analysis, integrating the peak at *t*_R = 1.18 mins (**215**, [M+H] = 224.1) against the peak at *t*_R = 1.29 mins (**212**, [M-H] = 240.1).

Entry	Additive	Amount of Additive	Base	Amount of Base	Solvent	LCMS Conversion
-------	----------	--------------------	------	----------------	---------	-----------------

		mmol	mg		mmol	mg		/ %
1	AgBF ₄	0.015	3.9	<i>t</i> -BuOK	0.075	8.4	Toluene	64
2	NaBAr _F	0.015	13.3	K ₂ CO ₃	0.075	10.4	Toluene	66
3	AgBF ₄	0.015	3.9	<i>t</i> -BuOK	0.075	8.4	Dioxane	69
4	AgBF ₄	0.015	3.9	K ₂ CO ₃	0.075	10.4	Dioxane	83
5	NaBAr _F	0.015	13.3	<i>t</i> -BuOK	0.075	8.4	Dioxane	58
6	NaBAr _F	0.015	13.3	K ₂ CO ₃	0.075	10.4	Dioxane	73

Scheme 2.68

2,6-dimethyl-1,2,3,4-tetrahydroquinoline 216¹⁸³



Prepared according to *General Procedure I*.

Reaction temperature: 100 °C.

Amount of 4-(2-amino-5-methylphenyl)butan-2-ol **207**: 27 mg, 0.15 mmol.

Amount of catalyst **158**: 10.1 mg, 0.015 mmol.

Amount of potassium carbonate: 10.4 mg, 0.073 mmol.

Amount of silver tetrafluoroborate: 2.9 mg, 0.015 mmol.

Amount of dioxane: 2 mL.

Product appearance: colourless oil.

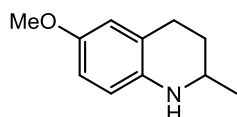
Product yield: 22 mg, 91%.

¹H NMR (400 MHz, CDCl₃) δ 6.72 (m, 2H, ArH), 6.35 (d, *J* = 8.1 Hz, 1H, ArH), 3.30–3.28 (m, 1H, CH(CH₃)), 3.14–2.96 (m, 2H, ArCH₂), 2.10 (s, 3H, ArCH₃), 1.87–1.83 (m, 1H, ArCH₂CH₂), 1.49 (ddd, ²*J* = 16.6, *J* = 6.2, 5.0 Hz, 1H, ArCH₂CH₂), 1.14 (d, *J* = 6.3 Hz, 3H, CH₃).

¹³C NMR (101 MHz, CDCl₃) δ 142.6, 130.1, 127.3, 126.5, 121.3, 114.5, 47.6, 30.3, 26.5, 22.6, 20.5.

IR (ATR, cm⁻¹) 3397, 2960, 2922, 1603, 1578, 1486.

2-methyl-6-methoxy-1,2,3,4-tetrahydroquinoline 217¹⁸⁴



Prepared according to *General Procedure I*.

Reaction temperature: 100 °C.

Amount of 4-(2-amino-5-methoxyphenyl)butan-2-ol **208**: 29 mg, 0.15 mmol.

Amount of catalyst **158**: 10.1 mg, 0.015 mmol.

Amount of potassium carbonate: 10.4 mg, 0.073 mmol.

Amount of silver tetrafluoroborate: 2.9 mg, 0.015 mmol.

Amount of dioxane: 2 mL.

Product appearance: colourless oil.

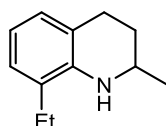
Product yield: 24 mg, 90%.

¹H NMR (400 MHz, CDCl₃) δ 6.62–6.58 (m, 2H, ArH), 6.40 (d, *J* = 8.12 Hz, 1H, ArH), 3.76 (s, 3H, OCH₃), 3.36–3.31 (m, 1H, CH(CH₃)), 2.87–2.82 (m, 1H, ArCH₂), 2.72–2.68 (m, 1H, ArCH₂), 1.87–1.83 (m, 1H, ArCH₂CH₂), 1.54 (ddd, ²*J* = 15.9, *J* = 6.1, 4.8 Hz, 1H, ArCH₂CH₂), 1.18 (d, *J* = 6.2 Hz, 3H, CH₃).

¹³C NMR (101 MHz, CDCl₃) δ 155.3, 139.1, 122.9, 115.7, 114.9, 113.2, 56.2, 47.8, 30.6, 27.2, 22.8.

IR (ATR, cm⁻¹) 2960, 2820, 1500, 1446, 1260.

8-ethyl-2-methyl-1,2,3,4-tetrahydroquinoline 218



Prepared according to *General Procedure I*.

Reaction temperature: 100 °C.

Amount of 4-(2-amino-3-ethylphenyl)butan-2-ol **213**: 29 mg, 0.15 mmol.

Amount of catalyst **158**: 10.1 mg, 0.015 mmol.

Amount of potassium carbonate: 10.4 mg, 0.073 mmol.

Amount of silver tetrafluoroborate: 2.9 mg, 0.015 mmol.

Amount of dioxane: 2 mL.

Product appearance: colourless oil.

Product yield: 23 mg, 89%.

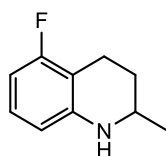
¹H NMR (400 MHz, CDCl₃) δ 6.96–6.90 (m, 3H, ArH), 3.02–2.99 (m, 1H, CH(CH₃)), 2.75–2.67 (m, 2H, ArCH₂), 2.53 (q, *J* = 6.7 Hz, 2H, ArCH₂CH₃), 1.92–1.93 (m, 1H, ArCH₂CH₂), 1.66 (ddd, ²*J* = 15.6, *J* = 5.9, 4.9 Hz, 1H, ArCH₂CH₂), 1.19 (d, *J* = 6.2 Hz, 3H, CH₃), 1.12 (t, *J* = 6.6 Hz, 3H, ArCH₂CH₃).

¹³C NMR (101 MHz, CDCl₃) δ 143.0, 127.6, 122.7, 122.4, 122.0, 117.1, 58.9, 31.8, 24.2, 23.5, 20.9, 14.6.

IR (ATR, cm⁻¹) 3395, 2950, 2918, 1605, 1580, 1480.

LCMS *t*_R = 0.98 min, [M+H] = 176.1.

5-fluoro-2-methyl-1,2,3,4-tetrahydroquinoline 219



Prepared according to *General Procedure I*.

Reaction temperature: 100 °C.

Amount of 4-(2-amino-6-fluorophenyl)butan-2-ol **211**: 27 mg, 0.15 mmol.

Amount of catalyst **158**: 10.1 mg, 0.015 mmol.

Amount of potassium carbonate: 10.4 mg, 0.073 mmol.

Amount of silver tetrafluoroborate: 2.9 mg, 0.015 mmol.

Amount of dioxane: 2 mL.

Product appearance: light yellow solid.

Product yield: 20 mg, 81%.

¹H NMR (400 MHz, CDCl₃) δ 7.10–7.02 (m, 2H, ArH), 6.36 (d, *J* = 7.9 Hz, 1H, ArH), 3.06–3.02 (m, 1H, CH(CH₃)), 2.84–2.73 (m, 2H, ArCH₂), 1.93–1.89 (m, 1H, ArCH₂CH₂), 1.66 (ddd, ²*J* = 15.7, *J* = 5.9, 4.9 Hz, 1H, ArCH₂CH₂), 1.19 (d, *J* = 6.1 Hz, 3H, CH₃).

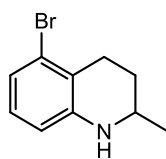
¹³C NMR (101 MHz, CDCl₃) δ 160.8 (d, ¹*J*_{CF} = 232.4 Hz), 147.4, 128.2, 110.6 (d, ²*J*_{CF} = 30.6 Hz), 106.5, 103.4 (d, ²*J*_{CF} = 24.7 Hz), 62.2, 32.0, 20.9, 18.8.

IR (ATR, cm⁻¹) 2960, 2818, 1504, 1448, 1258.

LCMS *t*_R = 1.01 min, [M+H] = 166.1.

MP (°C) 66–69.

5-bromo-2-methyl-1,2,3,4-tetrahydroquinoline 220



Prepared according to *General Procedure I*.

Reaction temperature: 100 °C.

Amount of 4-(2-amino-6-bromophenyl)butan-2-ol **209**: 37 mg, 0.15 mmol.

Amount of catalyst **158**: 10.1 mg, 0.015 mmol.

Amount of potassium carbonate: 10.4 mg, 0.073 mmol.

Amount of silver tetrafluoroborate: 2.9 mg, 0.015 mmol.

Amount of dioxane: 2 mL.

Product appearance: yellow oil.

Product yield: 29 mg, 86%.

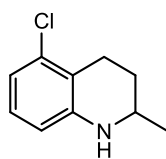
$^1\text{H NMR}$ (400 MHz, CDCl_3) δ 6.96–6.86 (m, 2H, ArH), 6.54 (dd, $J = 8.1$, $^4J = 1.2$ Hz, 1H, ArH), 3.03–2.97 (m, 1H, $\text{CH}(\text{CH}_3)$), 2.85–2.74 (m, 2H, ArCH_2), 1.90 (ddd, $^2J = 15.7$, $J = 6.1$, 4.8 Hz, 1H, ArCH_2CH_2), 1.67 (ddd, $^2J = 15.7$, $J = 5.9$, 4.9 Hz, 1H, ArCH_2CH_2), 1.19 (d, $J = 6.0$ Hz, 3H, CH_3).

$^{13}\text{C NMR}$ (101 MHz, CDCl_3) δ 147.0, 132.4, 128.1, 126.6, 121.1, 109.9, 60.1, 31.5, 22.7, 21.0.

IR (ATR, cm^{-1}) 2968, 2816, 1498, 1442, 1276.

LCMS $t_{\text{R}} = 1.00$ min, $[\text{M}+\text{H}] = 226.0$.

5-chloro-2-methyl-1,2,3,4-tetrahydroquinoline 221



Prepared according to *General Procedure I*.

Reaction temperature: 100 °C.

Amount of 4-(2-amino-6-chlorophenyl)butan-2-ol **210**: 30 mg, 0.15 mmol.

Amount of catalyst **158**: 10.1 mg, 0.015 mmol.

Amount of potassium carbonate: 10.4 mg, 0.073 mmol.

Amount of silver tetrafluoroborate: 2.9 mg, 0.015 mmol.

Amount of dioxane: 2 mL.

Product appearance: colourless oil.

Product yield: 23 mg, 84%.

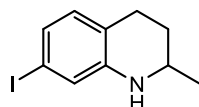
¹H NMR (400 MHz, CDCl₃) δ 7.08–7.03 (m, 2H, ArH), 6.49 (d, *J* = 7.8 Hz, 1H, ArH), 3.06–3.02 (m, 1H, CH(CH₃)), 2.85–2.76 (m, 2H, ArCH₂), 1.95–1.91 (m, 1H, ArCH₂CH₂), 1.68–1.65 (m, 1H, ArCH₂CH₂), 1.18 (d, *J* = 6.2 Hz, 3H, CH₃).

¹³C NMR (101 MHz, CDCl₃) δ 147.1, 136.1, 128.6, 123.8, 117.2, 108.9, 60.0, 31.5, 21.0, 20.7.

IR (ATR, cm⁻¹) 2918, 2820, 1504, 1448, 1260.

LCMS *t*_R = 1.04 min, [M+H] = 182.1.

7-iodo-2-methyl-1,2,3,4-tetrahydroquinoline 222



Prepared according to *General Procedure I*.

Reaction temperature: 100 °C.

Amount of 4-(2-amino-4-iodophenyl)butan-2-ol **214**: 44 mg, 0.15 mmol.

Amount of catalyst **158**: 10.1 mg, 0.015 mmol.

Amount of potassium carbonate: 10.4 mg, 0.073 mmol.

Amount of silver tetrafluoroborate: 2.9 mg, 0.015 mmol.

Amount of dioxane: 2 mL.

Product appearance: yellow-orange solid.

Product yield: 35 mg, 86%.

¹H NMR (400 MHz, CDCl₃) δ 7.01 (d, *J* = 7.9 Hz, 1H, ArH), 6.92–6.87 (m, 2H, ArH), 3.00–2.96 (m, 1H, CH(CH₃)), 2.85–2.75 (m, 2H, ArCH₂), 1.91–1.88 (m, 1H, ArCH₂CH₂), 1.66 (ddd, ²*J* = 16.0, *J* = 6.2, 4.9 Hz, 1H, ArCH₂CH₂), 1.19 (d, *J* = 6.1 Hz, 3H, CH₃).

¹³C NMR (101 MHz, CDCl₃) δ 146.6, 130.8, 126.4, 123.0, 121.4, 92.3, 60.6, 32.0, 23.9, 21.0.

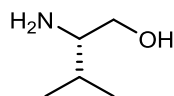
IR (ATR, cm⁻¹) 2958, 2816, 1504, 1448, 1314.

LCMS *t*_R = 0.94 min, [M+H] = 274.0.

Ligand Design for Asymmetric Transfer Hydrogenation

Scheme 2.70

L-Valinol 224



A 1 L round-bottom flask, fitted with a condenser, was flame-dried and charged with lithium aluminium hydride (6.45 g, 170 mmol), and THF (175 mL). The mixture was cooled to 0 °C and L-valine (10 g, 85 mmol) was added portionwise over 2 h. The reaction mixture was heated to 80 °C for 16 h, after which it was cooled to 0 °C. Saturated aqueous sodium sulfate was added dropwise until no more gas was released, and the mixture was stirred for a further 2 h. The mixture was filtered and concentrated *in vacuo*. Kugelrohr distillation (3 mbar, 120 °C) afforded the product as a colourless oil (5.081 g, 58% yield).

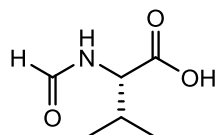
$^1\text{H NMR}$ (400 MHz, CDCl_3) δ 3.62 (dt, $J = 10.6, 3.8$ Hz, 1H, CH_2OH), 3.28 (dd, $J = 10.5, 8.7$ Hz, 1H, CH_2OH), 2.59–2.49 (m, 1H, NH_2CH), 1.63–1.50 (m, 1H, $\text{CH}(\text{CH}_3)_2$), 0.95–0.85 (m, 6H, CH_3).

$^{13}\text{C NMR}$ (101 MHz, CDCl_3) δ 64.9, 58.6, 31.5, 19.4, 18.5.

IR (ATR, cm^{-1}) 3360, 3290, 2958, 2876, 1595, 1468.

Scheme 2.71

N-Formyl-L-valine 226¹⁸⁵



Prepared according to *General Procedure L*.

Amount of L-valine: 6.560 g, 56 mmol.

Product appearance: White fluffy solid.

Product yield: 4.174 g, 58%

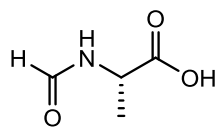
$^1\text{H NMR}$ (400 MHz, DMSO) δ 12.52 (s, 1H, NH), 7.96 (d, $J = 8.4$ Hz, 1H, CHO), 4.34 (dd, $J = 8.5, 5.8$ Hz, 1H, NCH), 1.87 (m, 1H, $\text{CH}(\text{CH}_3)_2$), 0.87 (dt, $J = 10.5, 5.2$ Hz, 6H, CH_3).

$^{13}\text{C NMR}$ (101 MHz, DMSO) δ 172.9, 169.2, 56.9, 29.5, 17.8.

IR (ATR, cm^{-1}) 3415, 3290, 2995, 2930, 2470, 1605, 1470.

MP (°C) 150–151 (lit. 150–151).¹⁸⁵

***N*-Formyl-L-alanine 227¹⁶²**



Prepared according to *General Procedure L*.

Amount of L-alanine: 5 g, 56 mmol.

Product appearance: White fluffy solid.

Product yield: 6.454 g, 98%

¹H NMR (400 MHz, DMSO) δ 12.63 (s, 1H, NH), 8.36 (d, J = 6.8 Hz, 1H, OH), 7.99 (d, J = 4.7 Hz, 1H, CHO), 4.30–4.24 (m, 1H, CHCH₃), 1.27 (d, J = 7.3 Hz, 3H, CH₃). N.B. Peaks at 8.36 and 7.99 appear as doublets due to rotameric splitting.

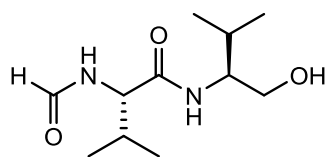
¹³C NMR (101 MHz, DMSO) δ 174.0, 160.9, 46.3, 17.5.

IR (ATR, cm⁻¹) 3380, 2428, 1918, 1605.

MP (°C) 126–128 (lit. 127–128).¹⁶²

Scheme 2.72

(*S*)-2-formamido-*N*-((*S*)-1-hydroxy-3-methylbutan-2-yl)-3-methylbutanamide 228



Prepared according to *General Procedure M*.

Amount of *N*-formyl-L-valine **226**: 702 mg, 4.84 mmol.

Product appearance: Pale yellow fluffy solid.

Product yield: 847 mg, 76%.

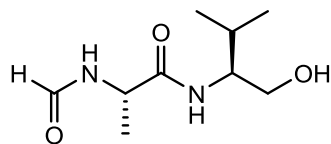
¹H NMR (400 MHz, DMSO) δ 14.02 (s, 1H, NH), 8.34 (s, 1H, NH), 8.01 (s, 1H, CHO), 4.84 (s, 1H, OH), 4.34 (dd, J = 8.6, 5.8 Hz, 1H, NCH), 3.51–3.42 (m, 2H, NCH & CH₂OH), 3.24 (dd, J = 10.5, 8.8 Hz, 1H, CH₂OH), 2.76–2.69 (m, 1H, CH(CH₃)₂), 2.24–2.18 (m, 1H, CH(CH₃)₂), 0.94–0.86 (m, 12H, CH₃).

¹³C NMR (101 MHz, DMSO) δ 171.0, 162.4, 63.3, 62.8, 61.9, 30.3, 29.2, 19.5, 18.2.

IR (ATR, cm⁻¹) 3415, 3290, 2980, 2872, 2460, 1601, 1470.

MP (°C) 168–172.

(S)-2-formamido-N-((S)-1-hydroxy-3-methylbutan-2-yl)propenamide 229



Prepared according to *General Procedure M*.

Amount of *N*-formyl-L-alanine **227**: 566 mg, 4.84 mmol.

Product appearance: White fluffy solid.

Product yield: 714 mg, 73%.

¹H NMR (400 MHz, DMSO) δ 14.23 (s, 1H, NH), 8.18 (s, 1H, NH), 8.00 (s, 1H, CHO), 4.66 (m, 1H, CHCH₃), 4.48 (s, 1H, OH), 3.49–3.40 (m, 2H, NCH & CH₂OH), 3.26 (dd, *J* = 10.3, 8.6 Hz, 1H, CH₂OH), 2.22–2.16 (m, 1H, CH(CH₃)₂), 1.47 (d, *J* = 7.0 Hz, 3H, CH₃), 0.89 (d, *J* = 6.6 Hz, 6H, CH(CH₃)₂).

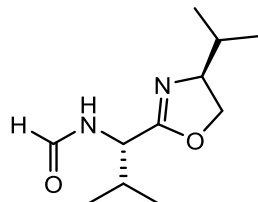
¹³C NMR (101 MHz, DMSO) δ 171.6, 162.0, 63.0, 62.8, 52.2, 30.1, 19.9, 18.2.

IR (ATR, cm⁻¹) 3390, 2975, 2868, 2458, 1596, 1462.

MP (°C) 156–160.

Scheme 2.73

***N*-((S)-1-((S)-4-isopropyl-4,5-dihydrooxazol-2-yl)-2-methylpropyl)formamide 230**



Prepared according to *General Procedure N*.

Amount of **228**: 461 mg, 2 mmol.

Product appearance: White solid.

Product yield: 280 mg, 66%.

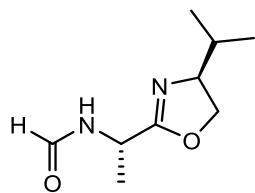
¹H NMR (400 MHz, CDCl₃) δ 14.20 (s, 1H, NH), 8.04 (s, 1H, CHO), 3.62–3.46 (m, 4H, NCH & oxazolineH), 2.40–2.35 (m, 1H, CH(CH₃)₂), 1.77–1.73 (m, 1H, CH(CH₃)₂), 0.95 (d, *J* = 7.3 Hz, 6H, CH₃), 0.89 (d, *J* = 7.1 Hz, 6H, CH₃).

¹³C NMR (101 MHz, CDCl₃) δ 168.2, 160.8, 72.3, 71.9, 59.0, 32.8, 29.5, 20.1, 20.0.

IR (ATR, cm⁻¹) 3301, 2928, 2890, 1765, 1643, 1582, 1492.

MP (°C) 88–91.

N-((S)-1-((S)-4-isopropyl-4,5-dihydrooxazol-2-yl)ethyl)formamide 231



Prepared according to *General Procedure N*.

Amount of **229**: 404 mg, 2 mmol.

Product appearance: Colourless gummy solid.

Product yield: 166 mg, 45%.

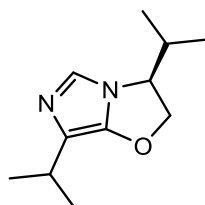
¹H NMR (400 MHz, CDCl₃) δ 14.33 (s, 1H, NH), 8.02 (s, 1H, CHO), 3.81–3.78 (m, 1H, CHCH₃), 3.65–3.44 (m, 3H, oxazoline), 1.68–1.64 (m, 1H, CH(CH₃)₂), 1.21 (d, *J* = 6.6 Hz, 3H, CH₃), 0.88 (d, *J* = 7.1 Hz, 3H, CH₃), 0.89 (d, *J* = 7.1 Hz, 3H, CH₃).

¹³C NMR (101 MHz, CDCl₃) δ 167.9, 161.0, 72.4, 48.2, 32.6, 20.1, 13.0.

IR (ATR, cm⁻¹) 2930, 2878, 1740, 1640, 1576, 1488.

MP (°C) 78–81.

(S)-3,7-diisopropyl-2,3-dihydroimidazo[5,1-b]oxazole 232



Prepared according to *General Procedure O*.

Amount of **230**: 212 mg, 1 mmol.

Product appearance: White crystalline solid.

Product yield: 138 mg, 71%.

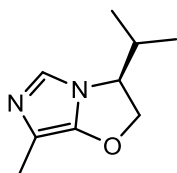
¹H NMR (400 MHz, CDCl₃) δ 8.04 (s, 1H, NCHN), 4.51–4.47 (m, 1H, oxazoline CH₂), 4.27–4.23 (m, 1H, oxazoline CH₂), 4.04–3.97 (m, 1H, oxazoline CH), 3.40–3.35 (m, 1H, CH(CH₃)₂), 1.97–1.93 (m, 1H, CH(CH₃)₂), 1.30 (d, *J* = 7.0 Hz, 6H, CH₃), 0.88 (d, *J* = 6.8 Hz, 6H, CH₃).

¹³C NMR (101 MHz, CDCl₃) δ 138.1, 126.7, 75.1, 68.0, 31.4, 26.9, 22.4, 18.7 (bridgehead carbon not observed).

IR (ATR, cm⁻¹) 2920, 2848, 2310, 1570, 1440, 1329.

MP (°C) 96–98.

(S)-3-isopropyl-7-methyl-2,3-dihydroimidazo[5,1-b]oxazole 233



Prepared according to *General Procedure O*.

Amount of **231**: 184 mg, 1 mmol.

Product appearance: White solid.

Product yield: 53 mg, 32%.

¹H NMR (400 MHz, CDCl₃) δ 7.99 (s, 1H, NCHN), 4.49–4.45 (m, 1H, oxazoline CH₂), 4.24–4.20 (m, 1H, oxazoline CH₂), 4.00–3.95 (m, 1H, oxazoline CH), 2.27 (s, 3H, CH₃), 1.77–1.72 (m, 1H, CH(CH₃)₂), 0.86 (d, *J* = 7.0 Hz, 3H, CH₃).

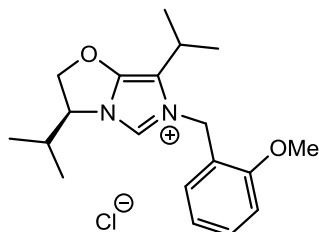
¹³C NMR (101 MHz, CDCl₃) δ 137.5, 114.0, 74.4, 66.5, 26.3, 18.1, 9.1 (bridgehead carbon not observed).

IR (ATR, cm⁻¹) 2918, 2820, 1568, 1450, 1328.

MP (°C) 101–104.

Scheme 2.74

(S)-3,7-diisopropyl-6-(2-methoxybenzyl)-2,3-dihydroimidazo[5,1-b]oxazol-6-ium chloride 234



Prepared according to *General Procedure B*.

Amount of **232**: 97 mg, 0.5 mmol.

Amount of 2-methoxybenzyl chloride **142**: 70 μL, 0.5 mmol.

Product appearance: White solid.

Product yield: 145 mg, 83%.

¹H NMR (400 MHz, CDCl₃) δ 10.04 (s, 1H, NCHN), 7.40 (dd, *J* = 7.5, ⁴*J* = 1.6 Hz, 1H, ArH), 7.14–7.06 (m, 2H, ArH), 6.94 (d, *J* = 8.3 Hz, 1H, ArH), 5.46 (s, 2H, CH₂), 4.51–4.47 (m, 1H, oxazoline CH₂), 4.24–4.20 (m, 1H, oxazoline CH₂), 4.01–3.95 (m, 1H,

oxazoline CH), 3.78 (s, 3H, OCH₃), 3.40–3.35 (m, 1H, CH(CH₃)₂), 1.97–1.93 (m, 1H, CH(CH₃)₂), 1.30 (d, *J* = 7.0 Hz, 6H, CH₃), 0.89 (d, *J* = 6.8 Hz, 6H, CH₃).

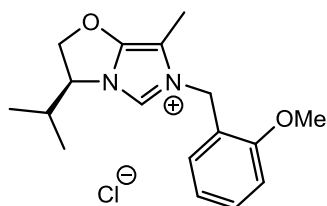
¹³C NMR (101 MHz, CDCl₃) δ 159.1, 143.0, 142.6, 137.8, 128.0, 126.8, 125.9, 121.1, 75.5, 68.2, 57.2, 45.6, 27.2, 26.6, 23.0, 18.7 (bridgehead carbon not observed).

IR (ATR, cm⁻¹) 2925, 2840, 2305, 1558, 1452, 1320.

HRMS (EI) *m/z* calculated for C₁₉H₂₇N₂O₂ [M–Cl]: 315.2073; found: 315.2060.

MP (°C) 66–69.

(S)-3-isopropyl-6-(2-methoxybenzyl)-7-methyl-2,3-dihydroimidazo[5,1-b]oxazol-6-ium chloride 235



Prepared according to *General Procedure G*.

Amount of **233**: 83 mg, 0.5 mmol.

Amount of 2-methoxybenzyl chloride **142**: 70 μL, 0.5 mmol.

Product appearance: White solid.

Product yield: 145 mg, 90%.

¹H NMR (400 MHz, CDCl₃) δ 10.12 (s, 1H, NCHN), 7.39–7.32 (m, 2H, ArH), 7.04–6.93 (m, 2H, ArH), 5.34 (s, 2H, CH₂), 4.50–4.45 (m, 1H, oxazoline CH₂), 4.27–4.23 (m, 1H, oxazoline CH₂), 4.00–3.95 (m, 1H, oxazoline CH), 3.83 (s, 3H, OCH₃), 2.89 (s, 3H, CH₃), 1.77–1.74 (m, 1H, CH(CH₃)₂), 0.90 (d, *J* = 6.8 Hz, 6H, CH₃).

¹³C NMR (101 MHz, CDCl₃) δ 157.9, 143.5, 142.9, 138.1, 128.0, 127.6, 126.2, 121.3, 113.0, 75.2, 68.1, 56.4, 45.1, 27.0, 18.9, 7.4 (bridgehead carbon not observed).

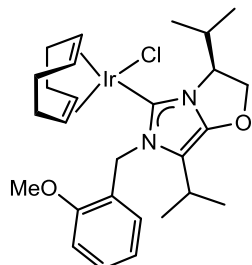
IR (ATR, cm⁻¹) 2920, 2838, 1560, 1448, 1318.

HRMS (EI) *m/z* calculated for C₁₇H₂₃N₂O₂ [M–Cl]: 287.1760; found: 287.1748.

MP (°C) 78–80.

Scheme 2.75

(1,5-cyclooctadiene)((S)-3,7-diisopropyl-6-(2-methoxybenzyl)-2,3-dihydrooxazoimidazol-5-ylidene)iridium(I) chloride 236



Prepared according to *General Procedure C*.

Amount of bis(1,5-cyclooctadiene)diiridium(I) dichloride: 100 mg, 0.149 mmol.

Amount of potassium *tert*-butoxide: 33.4 mg, 0.298 mmol.

Amount of **234**: 105 mg, 0.298 mmol.

Product yield: 136 mg, 70%.

Product appearance: yellow solid.

¹H NMR (400 MHz, CDCl₃) δ 7.38 (dd, *J* = 7.5, ⁴*J* = 1.4 Hz, 1H, ArH), 7.14–7.06 (m, 2H, ArH), 6.96 (d, *J* = 8.1 Hz, 1H, ArH), 5.38 (s, 2H, CH₂), 4.51–4.46 (m, 1H, oxazoline CH₂), 4.24–4.20 (m, 1H, oxazoline CH₂), 4.15–4.11 (m, 2H, COD CH), 4.01–3.94 (m, 1H, oxazoline CH), 3.81 (s, 3H, OCH₃), 3.40–3.35 (m, 1H, CH(CH₃)₂), 2.97–2.92 (m, 2H, COD CH), 1.97–1.93 (m, 1H, CH(CH₃)₂), 1.75–1.61 (m, 4H, COD CH₂), 1.34–1.17 (m, 10H, COD CH₂ & 2 CH₃), 0.89 (d, *J* = 6.8 Hz, 6H, CH₃).

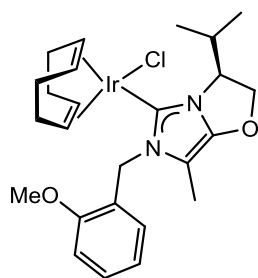
¹³C NMR (101 MHz, CDCl₃) δ 138.8, 138.5, 136.3, 134.6, 129.7, 128.6, 128.4, 128.3, 123.5, 82.7, 51.7, 33.7, 29.2, 28.6, 28.4, 21.3, 19.9, 18.4.

IR (ATR, cm⁻¹) 3005, 2958, 2830, 1578, 1440.

HRMS (EI) *m/z* calculated for IrC₂₇H₃₈N₂O [M–Cl]: 599.2613; found: 599.2621.

MP (°C) decomp. >180.

(1,5-cyclooctadiene)((S)-3-isopropyl-6-(2-methoxybenzyl)-7-methyl-2,3-dihydrodihydrooxazoimidazol-5-ylidene) iridium(I) chloride 237



Prepared according to *General Procedure C*.

Amount of bis(1,5-cyclooctadiene)diiridium(I) dichloride: 100 mg, 0.149 mmol.

Amount of potassium *tert*-butoxide: 33.4 mg, 0.298 mmol.

Amount of **235**: 96 mg, 0.298 mmol.

Product yield: 106 mg, 57%.

Product appearance: yellow solid.

¹H NMR (400 MHz, CDCl₃) δ 7.39–7.32 (m, 2H, ArH), 7.04–6.91 (m, 2H, ArH), 5.37 (s, 2H, CH₂), 4.52–4.43 (m, 1H, oxazoline CH₂), 4.27–4.22 (m, 1H, oxazoline CH₂), 4.17–4.12 (m, 2H, COD CH), 4.00–3.95 (m, 1H, oxazoline CH), 3.84 (s, 3H, OCH₃), 2.99–2.92 (m, 2H, COD CH), 2.89 (s, 3H, CH₃), 1.76–1.53 (m, 5H, COD CH₂ & CH(CH₃)₂), 1.34–1.17 (m, 4H, COD CH₂), 0.92 (d, *J* = 6.6 Hz, 6H, CH₃).

¹³C NMR (101 MHz, CDCl₃) δ 157.9, 143.5, 142.9, 138.1, 129.7, 128.6, 128.4, 128.3, 128.0, 127.6, 126.2, 121.3, 113.0, 75.2, 68.1, 56.4, 45.1, 29.2, 28.6, 28.4, 28.2, 27.0, 18.9, 7.4.

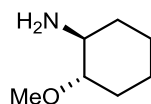
IR (ATR, cm⁻¹) 2954, 2829, 1606, 1568, 1450.

HRMS (EI) *m/z* calculated for IrC₂₅H₃₄N₂O [M–Cl]: 571.2300; found: 571.2286.

MP (°C) decomp. >190.

Scheme 2.76

Trans*-2-methoxycyclohexan-1-amine **239*



A solution of the *trans*-2-hydroxycyclohexan-1-amine (576 mg, 5 mmol) in DMF (15 mL) was prepared and cooled to 0 °C. Sodium hydride (60% in mineral oil) (200 mg, 5 mmol) was added and the mixture was allowed to warm to room temperature. After stirring for 1 h, the reaction mixture was cooled once again to 0 °C and iodomethane (250 μL, 5 mmol) was added. The mixture was stirred at room temperature for 16 h, after which it was concentrated *in vacuo*. After addition of water, the organic layers were extracted into ethyl acetate (3 × 50

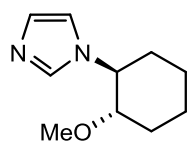
mL), and the combined organic layers dried over sodium sulfate and concentrated *in vacuo*. Column chromatography (2% EtOAc in petrol) afforded **239** as a yellow oil (84 mg, 13% yield).

¹H NMR (400 MHz, CDCl₃) δ 3.68 (s, 3H, OCH₃), 3.20–3.15 (m, 1H, CHOCH₃), 2.80–2.77 (m, 1H, CHNH₂), 1.70–1.64 (m, 2H, CH₂), 1.53–1.41 (m, 4H, CH₂), 1.24–1.20 (m, 1H, CH₂), 1.12–1.09 (m, 1H, CH₂).

¹³C NMR (101 MHz, CDCl₃) δ 85.9, 60.4, 58.1, 30.9, 29.3, 25.4, 24.6.

IR (ATR, cm⁻¹) 3115, 2926, 2871, 1612, 1576.

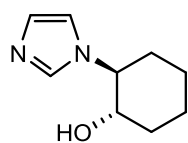
1-(*Trans*-2-methoxycyclohexyl)-1H-imidazole **240**



Reaction attempted following a literature procedure.¹⁸⁶ *Trans*-2-methoxycyclohexan-1-amine **239** (50 mg, 0.38 mmol) was mixed with 1 mL water, and phosphoric acid (85% eq.) was added until a pH of 2 was reached. Paraformaldehyde (12 mg, 0.38 mmol), glyoxal (22 mg, 0.38 mmol), and water (2 mL) were added, followed by dioxane (1 mL). The reaction was heated to 100 °C and saturated ammonium chloride solution (0.5 mL) was added dropwise. The reaction was allowed to stir for 16 h, after which it was cooled to 0 °C and basified to pH 12 with the addition of sodium hydroxide. The organic products were extracted with diethyl ether (3 × 5 mL) and concentrated *in vacuo*. NMR spectroscopic analysis of the residue showed that none of the desired compound had been formed.

Scheme 2.77

1-(*Trans*-2-hydroxycyclohexyl)-1H-imidazole **243**¹⁸⁷



Prepared according to a literature procedure.¹⁸⁷ A solution of cyclohexane oxide (1.534 g, 15.63 mmol) and imidazole (851 mg, 12.5 mmol) in dioxane (5 mL) was prepared and heated to 100 °C for 24 h. The reaction mixture was then cooled and concentrated *in vacuo*. Column chromatography (5% methanol in DCM) afforded the title compound as an off-white powder (1.227 g, 47% yield).

¹H NMR (400 MHz, CDCl₃) δ 7.36 (s, 1H, NCHN), 6.91 (s, 1H, NCHCHN), 6.88 (s, 1H, NCHCHN), 4.06 (s, 1H, OH), 3.73–3.57 (m, 1H, CHN), 2.21–2.10 (m, 1H, CHOH), 2.09–

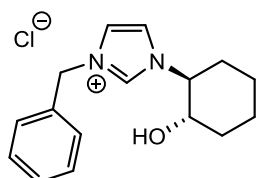
2.01 (m, 1H, CH₂), 1.90–1.78 (m, 2H, CH₂), 1.74–1.62 (m, 1H, CH₂), 1.49–1.30 (m, 4H, CH₂).

¹³C NMR (101 MHz, CDCl₃) δ 136.3, 128.8, 117.2, 73.3, 64.1, 34.1, 32.3, 25.2, 24.4.

IR (ATR, cm⁻¹) 3220, 2980, 2861, 1491.

MP (°C) 130–133 (lit. 132–133).¹⁸⁷

3-benzyl-1-(*trans*-2-hydroxycyclohexyl)-1H-imidazol-3-ium chloride **244**¹⁸⁸



Prepared according to *General Procedure B*.

Amount of **243**: 332 mg, 2 mmol.

Amount of benzyl chloride: 230 μL, 2 mmol.

Product appearance: White solid.

Product yield: 293 mg, 50%.

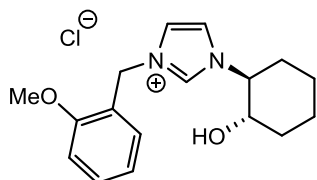
¹H NMR (400 MHz, CDCl₃) δ 10.12 (s, 1H, NCHN), 7.36–7.31 (m, 5H, ArH), 7.05 (s, 1H, NCHCHN), 7.02 (s, 1H, NCHCHN), 5.47 (d, 1H, ²J = 14.8 Hz, CH₂), 5.44 (d, 1H, ²J = 14.8 Hz, CH₂), 4.29–4.26 (m, 1H, CHOH) 3.69–3.61 (m, 1H, CHN), 2.18–2.09 (m, 2H, CH₂), 1.84–1.78 (m, 2H, CH₂), 1.61–1.51 (m, 2H, CH₂), 1.40–1.34 (m, 2H, CH₂).

¹³C NMR (101 MHz, CDCl₃) δ 136.2, 133.4, 129.5, 129.2, 129.0, 121.4, 121.2, 72.3, 65.9, 53.4, 34.7, 31.5, 24.6, 24.2.

IR (ATR, cm⁻¹) 3250, 2925, 2880, 1606, 1580, 1491.

MP (°C) 151–154 (lit. 153–155).¹⁸⁹

1-(*trans*-2-hydroxycyclohexyl)-3-(2-methoxybenzyl)-1H-imidazol-3-ium chloride **245**



Prepared according to *General Procedure B*.

Amount of **243**: 332 mg, 2 mmol.

Amount of 2-methoxybenzyl chloride **142**: 278 μL, 2 mmol.

Product appearance: White solid.

Product yield: 362 mg, 56%.

¹H NMR (400 MHz, CDCl₃) δ 10.06 (s, 1H, NCHN), 7.49 (dd, *J* = 7.8, ⁴*J* = 1.2 Hz, 1H, ArH), 7.09–7.02 (m, 2H, ArH), 7.03 (s, 1H, NCHCHN), 6.99 (s, 1H, NCHCHN), 6.36 (d, *J* = 8.0 Hz, 1H, ArH), 5.43 (d, 1H, ²*J* = 14.9 Hz, CH₂), 5.41 (d, 1H, ²*J* = 14.8 Hz, CH₂), 4.09–4.04 (m, 1H, CHOH), 3.67 (s, 3H, OCH₃), 3.65–3.60 (m, 1H, CHN), 2.12–2.03 (m, 2H, CH₂), 1.79–1.73 (m, 2H, CH₂), 1.57–1.45 (m, 2H, CH₂), 1.43–1.37 (m, 2H, CH₂).

¹³C NMR (101 MHz, CDCl₃) δ 157.8, 138.2, 136.3, 129.6, 129.1, 121.4, 121.3, 117.0, 104.6, 72.7, 66.1, 57.2, 53.6, 34.8, 31.6, 24.8, 24.5.

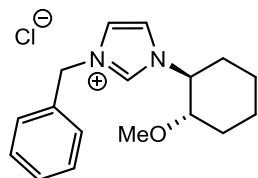
IR (ATR, cm⁻¹) 3246, 2990, 2918, 1604, 1575, 1458.

HRMS (EI) *m/z* calculated for C₁₇H₂₃N₂O₂ [M–Cl]: 287.1759; found: 287.1770.

MP (°C) 162–164.

Scheme 2.79

3-benzyl-1-(*trans*-2-methoxycyclohexyl)-1H-imidazol-3-ium chloride 246



Prepared according to *General Procedure P*.

Amount of **244**: 292 mg, 1 mmol.

Product appearance: White solid.

Product yield: 110 mg, 36%.

¹H NMR (400 MHz, CDCl₃) δ 10.01 (s, 1H, NCHN), 7.65 (s, 1H, NCHCHN), 7.59 (s, 1H, NCHCHN), 7.51–7.44 (m, 5H, ArH), 5.87 (d, 1H, ²*J* = 14.9 Hz, CH₂), 5.83 (d, 1H, ²*J* = 14.8 Hz, CH₂), 4.29–4.26 (m, 1H, CHOCH₃), 3.71 (s, 3H, OCH₃), 3.62–3.59 (m, 1H, CHN), 2.10–2.02 (m, 2H, CH₂), 1.74–1.68 (m, 2H, CH₂), 1.53–1.40 (m, 4H, CH₂).

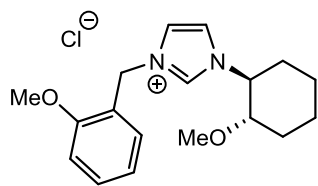
¹³C NMR (101 MHz, CDCl₃) δ 136.1, 133.2, 129.4, 129.0, 128.7, 121.1, 121.0, 81.0, 63.4, 58.2, 56.5, 26.9, 28.4, 26.0, 24.6.

IR (ATR, cm⁻¹) 2922, 2878, 1610, 1576, 1468.

HRMS (EI) *m/z* calculated for C₁₇H₂₃N₂O₂ [M–Cl]: 287.1759; found: 287.1770.

MP (°C) 89–91.

1-(*trans*-2-methoxycyclohexyl)-3-(2-methoxybenzyl)-1H-imidazol-3-ium chloride 247



Prepared according to *General Procedure P*.

Amount of **245**: 332 mg, 1 mmol.

Product appearance: White solid.

Product yield: 141 mg, 42%.

¹H NMR (400 MHz, CDCl₃) δ 10.02 (s, 1H, NCHN), 7.48–7.44 (m, 1H, ArH), 7.03–6.95 (m, 2H, ArH), 7.11 (s, 1H, NCHCHN), 7.06 (s, 1H, NCHCHN), 6.28 (d, $J = 7.9$ Hz, 1H, ArH), 5.72 (d, 1H, $^2J = 14.9$ Hz, CH₂), 5.69 (d, 1H, $^2J = 14.8$ Hz, CH₂), 3.67 (s, 3H, OCH₃), 3.65–3.60 (m, 1H, CHN), 3.48 (s, 3H, OCH₃), 3.30–3.26 (m, 1H, CHOCH₃), 2.08–1.96 (m, 2H, CH₂), 1.75–1.98 (m, 2H, CH₂), 1.55–1.41 (m, 4H, CH₂).

¹³C NMR (101 MHz, CDCl₃) δ 148.1, 136.1, 133.2, 129.2, 128.8, 121.4, 121.1, 117.4, 104.9, 81.2, 63.7, 58.5, 57.2, 56.7, 26.9, 28.6, 26.3, 24.2.

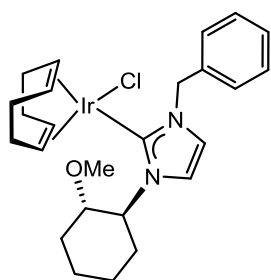
IR (ATR, cm⁻¹) 2995, 2920, 1606, 1578, 1460.

HRMS (EI) m/z calculated for C₁₈H₂₅N₂O₂ [M–Cl]: 301.1916; found: 301.1912.

MP (°C) 96–99.

Scheme 2.80 – top

(1,5-cyclooctadiene)(1-(*trans*-2-methoxycyclohexyl)-3-benzyl-1H-imidazol-2-ylidene)iridium(I) chloride 248



Synthesis attempted according to *General Procedure C*.

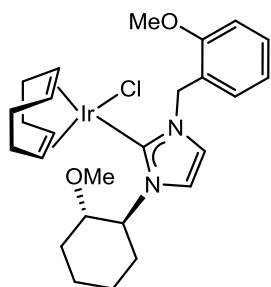
Amount of bis(1,5-cyclooctadiene)diiridium(I) dichloride: 100 mg, 0.149 mmol.

Amount of potassium *tert*-butoxide: 33.4 mg, 0.298 mmol.

Amount of **246**: 91 mg, 0.298 mmol.

None of the desired product isolated.

(1,5-cyclooctadiene)(1-(*trans*-2-methoxycyclohexyl)-3-(2-methoxybenzyl)-1H-imidazol-2-ylidene)iridium(I) chloride **249**



Synthesis attempted according to *General Procedure C*.

Amount of bis(1,5-cyclooctadiene)diiridium(I) dichloride: 100 mg, 0.149 mmol.

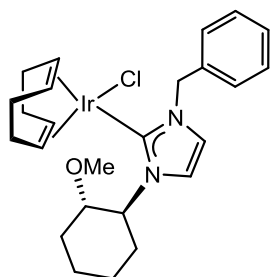
Amount of potassium *tert*-butoxide: 33.4 mg, 0.298 mmol.

Amount of **247**: 100 mg, 0.298 mmol.

None of the desired product isolated.

Scheme 2.80 – bottom

(1,5-cyclooctadiene)(1-(*trans*-2-methoxycyclohexyl)-3-benzyl-1H-imidazol-2-ylidene)iridium(I) chloride **248**



Prepared according to *General Procedure Q*.

Amount of bis(1,5-cyclooctadiene)diiridium(I) dichloride: 100 mg, 0.149 mmol.

Amount of silver oxide: 69 mg, 0.298 mmol.

Amount of **246**: 91 mg, 0.298 mmol.

Product yield: 103 mg, 57%.

Product appearance: yellow solid.

¹H NMR (400 MHz, CDCl₃) δ 7.65 (s, 1H, NCHCHN), 7.62 (s, 1H, NCHCHN), 7.51–7.42 (m, 5H, ArH), 5.58 (d, 1H, ²J = 14.9 Hz, CH₂), 5.53 (d, 1H, ²J = 14.9 Hz, CH₂), 4.30–4.26 (m, 1H, CHOCH₃), 4.14–4.10 (m, 2H, COD CH), 3.76 (s, 3H, OCH₃), 3.62–3.57 (m, 1H, CHN), 2.94–2.88 (m, 2H, COD CH), 2.10–2.02 (m, 2H, CH₂), 1.76–1.61 (m, 6H, CH₂ & COD CH₂), 1.53–1.40 (m, 4H, CH₂), 1.30–1.14 (m, 4H, COD CH₂).

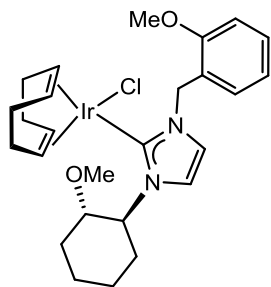
^{13}C NMR (101 MHz, CDCl_3) δ 136.1, 133.2, 129.4, 129.0, 128.7, 128.4, 128.2, 128.1, 127.9, 121.1, 121.0, 81.0, 63.4, 58.2, 56.5, 26.9, 28.9, 28.6, 28.4, 28.3, 28.0, 26.0, 24.6.

IR (ATR, cm^{-1}) 3004, 2970, 2826, 1604, 1566, 1442.

HRMS (EI) m/z calculated for $\text{IrC}_{25}\text{H}_{34}\text{N}_2\text{O}$ [M-Cl]: 571.2300; found: 571.2316.

MP ($^\circ\text{C}$) decomp. >200.

(1,5-cyclooctadiene)(1-(*trans*-2-methoxycyclohexyl)-3-(2-methoxybenzyl)-1H-imidazol-2-ylidene)iridium(I) chloride 249



Prepared according to *General Procedure Q*.

Amount of bis(1,5-cyclooctadiene)diiridium(I) dichloride: 100 mg, 0.149 mmol.

Amount of silver oxide: 69 mg, 0.298 mmol.

Amount of **247**: 100 mg, 0.298 mmol.

Product yield: 99 mg, 52%.

Product appearance: yellow solid.

^1H NMR (400 MHz, CDCl_3) δ 7.48–7.42 (m, 2H, ArH & NCHCHN), 7.39 (s, 1H, NCHCHN), 6.98–6.15 (m, 2H, ArH), 6.26 (d, $J = 7.8$ Hz, 1H, ArH), 5.67 (d, 1H, $^2J = 14.4$ Hz, CH_2), 5.62 (d, 1H, $^2J = 14.9$ Hz, CH_2), 4.14–4.10 (m, 2H, COD CH), 4.09–4.03 (m, 1H, CHOCH_3), 3.78 (s, 3H, OCH_3), 3.66 (s, 3H, OCH_3), 3.62–3.57 (m, 1H, CHN), 2.94–2.88 (m, 2H, COD CH), 2.07–1.94 (m, 2H, CH_2), 1.76–1.61 (m, 6H, CH_2 & COD CH_2), 1.55–1.41 (m, 4H, CH_2), 1.32–1.15 (m, 4H, COD CH_2).

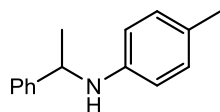
^{13}C NMR (101 MHz, CDCl_3) δ 148.1, 136.1, 133.2, 129.2, 128.8, 128.7, 128.5, 128.3, 128.0, 121.4, 121.1, 81.2, 63.7, 58.5, 56.7, 26.9, 29.0, 28.9, 28.6, 28.4, 28.3, 26.3, 24.2.

IR (ATR, cm^{-1}) 2996, 2928, 2830, 1595, 1557, 1458.

HRMS (EI) m/z calculated for $\text{IrC}_{25}\text{H}_{36}\text{N}_2\text{O}_2$ [M-Cl]: 589.2406; found: 589.2420.

MP ($^\circ\text{C}$) decomp. >190.

Table 2.15

4-Methyl-(1-phenylethyl)aniline 199¹⁷⁹

Prepared according to *General Procedure G*.

Reaction temperature: 25 °C.

Amount of 4-methylaniline: 23 mg, 0.215 mmol.

Amount of phenylethanol: 26 mg, 0.215 mmol.

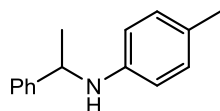
Amount of 2-MeTHF: 2.5 mL.

Spectral data as reported above.

HPLC analysis (Column = OD-H; hexane : isopropanol = 99 :1; UV detection at $\lambda = 210$ nm) was used to establish e.e., where applicable: $t_R^1 = 20.78$ mins, $t_R^2 = 26.48$ mins.

Entry	Catalyst	Amount of Catalyst		Base	Amount of Base		Conversion / %			e.e. / %
		mmol	mg		mmol	mg	1	2	3	
1	236	0.01075	7.0	^t BuOK	0.01075	1.2	42	55	47	<5
2	236	0.01075	7.0	K ₂ CO ₃	0.01075	1.5	52	<5	38	<5
3	237	0.01075	6.7	^t BuOK	0.01075	1.2	29	38	20	<5
4	237	0.01075	6.7	K ₂ CO ₃	0.01075	1.5	31	22	8	<5
5	248	0.01075	6.5	^t BuOK	0.01075	1.2	<5	-	-	-
6	248	0.01075	6.5	K ₂ CO ₃	0.01075	1.5	<5	-	-	-
7	249	0.01075	6.8	^t BuOK	0.01075	1.2	<5	-	-	-
8	249	0.01075	6.8	K ₂ CO ₃	0.01075	1.5	<5	-	-	-

Table 2.16

4-Methyl-(1-phenylethyl)aniline 199¹⁷⁹

Prepared according to *General Procedure G*.

Reaction temperature: 25 °C.

Amount of 4-methylaniline: 23 mg, 0.215 mmol.

Amount of phenylethanol: 26 mg, 0.215 mmol.

Amount of silver tetrafluoroborate: 2.1 mg, 0.01075 mmol.

Amount of solvent: 2.5 mL.

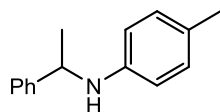
Spectral data as reported above.

HPLC analysis (Column = OD-H; hexane : isopropanol = 99 :1; UV detection at $\lambda = 210$ nm) was used to establish e.e., where applicable: $t_R^1 = 20.78$ mins, $t_R^2 = 26.48$ mins.

Entry	Catalyst	Amount of Catalyst		Base	Amount of Base		Solvent	Temp. / °C	Conversion / %			e.e. / %
		mmol	mg		mmol	mg			1	2	3	
1	236	0.01075	7.0	^t BuOK	0.01075	1.2	2-MeTHF	25	58	12	46	<5
2	236	0.01075	7.0	K ₂ CO ₃	0.01075	1.5	2-MeTHF	25	47	30	34	<5
3	237	0.01075	6.7	^t BuOK	0.01075	1.2	2-MeTHF	25	36	18	22	<5
4	237	0.01075	6.7	K ₂ CO ₃	0.01075	1.5	2-MeTHF	25	29	44	8	<5
5	236	0.01075	7.0	^t BuOK	0.01075	1.2	Toluene	100	Decomp.			-
6	236	0.01075	7.0	K ₂ CO ₃	0.01075	1.5	Toluene	100	Decomp.			-
7	237	0.01075	6.7	^t BuOK	0.01075	1.2	Toluene	100	Decomp.			-
8	237	0.01075	6.7	K ₂ CO ₃	0.01075	1.5	Toluene	100	Decomp.			-
9	236	0.01075	7.0	^t BuOK	0.01075	1.2	2-MeTHF	0	<5	-	-	-
10	236	0.01075	7.0	K ₂ CO ₃	0.01075	1.5	2-MeTHF	0	<5	-	-	-
11	237	0.01075	6.7	^t BuOK	0.01075	1.2	2-MeTHF	0	<5	-	-	-
12	237	0.01075	6.7	K ₂ CO ₃	0.01075	1.5	2-MeTHF	0	<5	-	-	-
13	248	0.01075	6.5	^t BuOK	0.01075	1.2	2-MeTHF	25	<5	-	-	-
14	248	0.01075	6.5	K ₂ CO ₃	0.01075	1.5	2-MeTHF	25	<5	-	-	-
15	249	0.01075	6.8	^t BuOK	0.01075	1.2	2-MeTHF	25	<5	-	-	-
16	249	0.01075	6.8	K ₂ CO ₃	0.01075	1.5	2-MeTHF	25	<5	-	-	-
17	248	0.01075	6.5	^t BuOK	0.01075	1.2	Toluene	100	<5	-	-	-
18	248	0.01075	6.5	K ₂ CO ₃	0.01075	1.5	Toluene	100	<5	-	-	-
19	249	0.01075	6.8	^t BuOK	0.01075	1.2	Toluene	100	<5	-	-	-
20	249	0.01075	6.8	K ₂ CO ₃	0.01075	1.5	Toluene	100	<5	-	-	-

Table 2.17

4-Methyl-(1-phenylethyl)aniline 199¹⁷⁹



Prepared according to *General Procedure G*.

Reaction temperature: 25 °C.

Amount of 4-methylaniline: 23 mg, 0.215 mmol.

Amount of phenylethanol: 26 mg, 0.215 mmol.

Amount of silver tetrafluoroborate: 2.1 mg, 0.01075 mmol.

Amount of 2-MeTHF: 2.5 mL.

Spectral data as reported above.

HPLC analysis (Column = OD-H; hexane : isopropanol = 99 :1; UV detection at $\lambda = 210$ nm) was used to establish e.e., where applicable: $t_R^1 = 20.78$ mins, $t_R^2 = 26.48$ mins.

Entry	Catalyst	Amount of Catalyst		Base	Amount of Base		Conversion / %			e.e. / %
		mmol	mg		mmol	mg	1	2	3	
1	251	0.01075	6.5	K ₂ CO ₃	0.01075	1.5	0	-	-	-
2	251	0.01075	6.5	K ₂ CO ₃	0.01075	1.5	0	-	-	-
3	252	0.01075	6.7	K ₂ CO ₃	0.01075	1.5	0	-	-	-
4	252	0.01075	6.7	K ₂ CO ₃	0.01075	1.5	0	-	-	-

References

- (1) *Modern Reduction Methods*; Andersson, P. G., Munslow, I. J., Eds.; Wiley-VCH Verlag GmbH & Co. KGaA: Weinheim, Germany, 2008.
- (2) *The Handbook of Homogeneous Hydrogenation*; de Vries, J. G., Elsevier, C. J., Eds.; Wiley-VCH Verlag GmbH: Weinheim, Germany, 2006.
- (3) Wang, D.; Astruc, D. *Chem. Rev.* **2015**, *115*, 6621–6686.
- (4) Braude, E. A.; Linstead, R. P. *J. Chem. Soc.* **1954**, 3544–3547.
- (5) Knoevenagel, E.; Bergdolt, B. *Berichte der Dtsch. Chem. Gesellschaft* **1903**, *36*, 2857–2860.
- (6) Meerwein, H.; Schmidt, R. *Justus Liebig's Ann. der Chemie* **1925**, *444*, 221–238.
- (7) Verley, A. *Bull. Soc. Chim. Fr.* **1925**, *37*, 537–542.
- (8) Ponndorf, W. *Zeitschrift für Angew. Chemie* **1926**, *39*, 138–143.
- (9) Cohen, R.; Graves, C. R.; Nguyen, S. T.; Martin, J. M. L.; Ratner, M. A. *J. Am. Chem. Soc.* **2004**, *126*, 14796–14803.
- (10) Oppenauer, R. V. *Recl. des Trav. Chim. des Pays-Bas* **1937**, *56*, 137–144.
- (11) Knauer, B.; Krohn, K. *Liebigs Ann.* **1995**, *1995*, 677–683.
- (12) Namy, J. L.; Girard, P.; Kagan, H. B. *Nouv. J. Chim.* **1977**, *1*, 5.
- (13) Chuah, G.; Jaenicke, S.; Zhu, Y.; Liu, S. *Curr. Org. Chem.* **2006**, *10*, 1639–1654.
- (14) Henbest, H. B.; Mitchell, T. R. B. *J. Chem. Soc. C* **1970**, 785–791.
- (15) Trocha-Grimshaw, J.; Henbest, H. B. *Chem. Commun. (London)* **1967**, 544–544.
- (16) Sasson, Y.; Blum, J. *Tetrahedron Lett.* **1971**, *12*, 2167–2170.
- (17) Blum, J.; Sasson, Y.; Iflah, S. *Tetrahedron Lett.* **1972**, *13*, 1015–1018.
- (18) Sasson, Y.; Blum, J. *J. Org. Chem.* **1975**, *40*, 1887–1896.
- (19) Chowdhury, R. L.; Bäckvall, J.-E. *J. Chem. Soc., Chem. Commun.* **1991**, 1063–1064.
- (20) *Based on a survey of Web of Science results for the topic "Transfer Hydrogenation" (April 2017).*
- (21) Mikhailine, A. A.; Morris, R. H. *Inorg. Chem.* **2010**, *49*, 11039–11044.
- (22) Mazza, S.; Scopelliti, R.; Hu, X. *Organometallics* **2015**, *34*, 1538–1545.
- (23) Horn, S.; Gandolfi, C.; Albrecht, M. *Eur. J. Inorg. Chem.* **2011**, *2011*, 2863–2868.
- (24) Zieliński, G. K.; Samojłowicz, C.; Wdowik, T.; Grela, K. *Org. Biomol. Chem.* **2015**, *13*, 2684–2688.
- (25) Dombay, T.; Helleu, C.; Darcel, C.; Sortais, J.-B. *Adv. Synth. Catal.* **2013**, *355*, 3358–3362.
- (26) Zhang, G.; Hanson, S. K. *Chem. Commun.* **2013**, *49*, 10151–10153.

- (27) Hauwert, P.; Boerleider, R.; Warsink, S.; Weigand, J. J.; Elsevier, C. J. *J. Am. Chem. Soc.* **2010**, *132*, 16900–16910.
- (28) Hauwert, P.; Dunsford, J. J.; Tromp, D. S.; Weigand, J. J.; Lutz, M.; Cavell, K. J.; Elsevier, C. J. *Organometallics* **2013**, *32*, 131–140.
- (29) Ikhile, M. I.; Nyamori, V. O.; Bala, M. D. *Tetrahedron Lett.* **2012**, *53*, 4925–4928.
- (30) Chong, C. C.; Hirao, H.; Kinjo, R. *Angew. Chemie Int. Ed.* **2014**, *53*, 3342–3346.
- (31) Saidi, O.; Williams, J. M. J. In *Topics in Organometallic Chemistry*; Andersson, P. G., Ed.; Springer Berlin Heidelberg, 2011; pp 77–106.
- (32) Bower, J. F.; Krische, M. J. In *Topics in Organometallic Chemistry*; Andersson, P. G., Ed.; Springer Berlin Heidelberg, 2011; pp 107–138.
- (33) Foubelo, F.; Nájera, C.; Yus, M. *Tetrahedron: Asymmetry* **2015**, *26*, 769–790.
- (34) Ito, J.; Nishiyama, H. *Tetrahedron Lett.* **2014**, *55*, 3133–3146.
- (35) Mestroni, G.; Zassinovich, G.; Camus, A. *J. Organomet. Chem.* **1977**, *140*, 63–72.
- (36) Mestroni, G.; Zassinovich, G.; Camus, A.; Martinelli, F. *J. Organomet. Chem.* **1980**, *198*, 87–96.
- (37) Clarke, Z. E.; Maragh, P. T.; Dasgupta, T. P.; Gusev, D. G.; Lough, A. J.; Abdur-Rashid, K. *Organometallics* **2006**, *25*, 4113–4117.
- (38) Sakaguchi, S.; Yamaga, T.; Ishii, Y. *J. Org. Chem.* **2001**, *66*, 4710–4712.
- (39) Hillier, A. C.; Lee, H. M.; Stevens, E. D.; Nolan, S. P. *Organometallics* **2001**, *20*, 4246–4252.
- (40) Albrecht, M.; Miecznikowski, J. R.; Samuel, A.; Faller, J. W.; Crabtree, R. H. *Organometallics* **2002**, *21*, 3596–3604.
- (41) Pontes da Costa, A.; Viciano, M.; Sanaú, M.; Merino, S.; Tejada, J.; Peris, E.; Royo, B. *Organometallics* **2008**, *27*, 1305–1309.
- (42) Gülcemal, S.; Gökçe, A. G.; Çetinkaya, B. *Inorg. Chem.* **2013**, *52*, 10601–10609.
- (43) Altenhoff, G.; Goddard, R.; Lehmann, C. W.; Glorius, F. *Angew. Chemie Int. Ed.* **2003**, *42*, 3690–3693.
- (44) Würtz, S.; Glorius, F. *Acc. Chem. Res.* **2008**, *41*, 1523–1533.
- (45) Collado, A.; Balogh, J.; Meiries, S.; Slawin, A. M. Z.; Falivene, L.; Cavallo, L.; Nolan, S. P. *Organometallics* **2013**, *32*, 3249–3252.
- (46) Altenhoff, G.; Goddard, R.; Lehmann, C. W.; Glorius, F. *J. Am. Chem. Soc.* **2004**, *126*, 15195–15201.
- (47) Normand, A. T.; Cavell, K. J. *Eur. J. Inorg. Chem.* **2008**, *2008*, 2781–2800.
- (48) Hameury, S.; de Frémont, P.; Braunstein, P. *Chem. Soc. Rev.* **2017**, *46*, 632–733.

- (49) Binobaid, A.; Iglesias, M.; Beetstra, D.; Dervisi, A.; Fallis, I.; Cavell, K. J. *Eur. J. Inorg. Chem.* **2010**, *2010*, 5426–5431.
- (50) Jiménez, M. V.; Fernández-Tornos, J.; Pérez-Torrente, J. J.; Modrego, F. J.; Winterle, S.; Cunchillos, C.; Lahoz, F. J.; Oro, L. A. *Organometallics* **2011**, *30*, 5493–5508.
- (51) Samec, J. S. M.; Bäckvall, J.-E.; Andersson, P. G.; Brandt, P. *Chem. Soc. Rev.* **2006**, *35*, 237–248.
- (52) Handgraaf, J.-W.; Reek, J. N. H.; Meijer, E. J. *Organometallics* **2003**, *22*, 3150–3157.
- (53) Pàmies, O.; Bäckvall, J.-E. *Chem. - A Eur. J.* **2001**, *7*, 5052–5058.
- (54) Zhao, J.; Hesslink, H.; Hartwig, J. F. *J. Am. Chem. Soc.* **2001**, *123*, 7220–7227.
- (55) Tojo, G.; Fernández, M. *Oxidation of Alcohols to Aldehydes and Ketones*; Basic Reactions in Organic Synthesis; Springer-Verlag: New York, 2006.
- (56) Crabtree, R. H.; Felkin, H.; Morris, G. E. *J. Organomet. Chem.* **1977**, *141*, 205–215.
- (57) Tejel, C.; Ciriano, M. A. In *Organometallic Oxidation Catalysis*; Meyer, F., Limberg, M. A., Eds.; Springer Berlin Heidelberg, 2006; pp 97–124.
- (58) Suzuki, T. *Chem. Rev.* **2011**, *111*, 1825–1845.
- (59) Nait Ajjou, A. *Tetrahedron Lett.* **2001**, *42*, 13–15.
- (60) Ajjou, A. N.; Pinet, J.-L. *Can. J. Chem.* **2005**, *83*, 702–710.
- (61) Fujita, K.; Furukawa, S.; Yamaguchi, R. *J. Organomet. Chem.* **2002**, *649*, 289–292.
- (62) Hanasaka, F.; Fujita, K.; Yamaguchi, R. *Organometallics* **2005**, *24*, 3422–3433.
- (63) Hanasaka, F.; Fujita, K.; Yamaguchi, R. *Organometallics* **2006**, *25*, 4643–4647.
- (64) Fujita, K.; Tanino, N.; Yamaguchi, R. *Org. Lett.* **2007**, *9*, 109–111.
- (65) Royer, A. M.; Rauchfuss, T. B.; Wilson, S. R. *Inorg. Chem.* **2008**, *47*, 395–397.
- (66) Suzuki, T.; Morita, K.; Tsuchida, M.; Hiroi, K. *J. Org. Chem.* **2003**, *68*, 1601–1602.
- (67) Suzuki, T.; Morita, K.; Tsuchida, M.; Hiroi, K. *Org. Lett.* **2002**, *4*, 2361–2363.
- (68) Hamid, M. H. S. A.; Allen, C. L.; Lamb, G. W.; Maxwell, A. C.; Maytum, H. C.; Watson, A. J. A.; Williams, J. M. J. *J. Am. Chem. Soc.* **2009**, *131*, 1766–1774.
- (69) Hamid, M. H. S. A.; Slatford, P. A.; Williams, J. M. J. *Adv. Synth. Catal.* **2007**, *349*, 1555–1575.
- (70) Leonard, J.; Blacker, A. J.; Marsden, S. P.; Jones, M. F.; Mulholland, K. R.; Newton, R. *Org. Process Res. Dev.* **2015**, *19*, 1400–1410.
- (71) Ma, X.; Su, C.; Xu, Q. *Top. Curr. Chem.* **2016**, *374*, 27.
- (72) Guillena, G.; J Ramón, D.; Yus, M. *Chem. Rev.* **2010**, *110*, 1611–1641.
- (73) McGrath, N. A.; Brichacek, M.; Njardarson, J. T. *J. Chem. Educ.* **2010**, *87*, 1348–

1349.

- (74) Salvatore, R. N.; Yoon, C. H.; Jung, K. W. *Tetrahedron* **2001**, *57*, 7785–7811.
- (75) Watanabe, Y.; Tsuji, Y.; Ohsugi, Y. *Tetrahedron Lett.* **1981**, *22*, 2667–2670.
- (76) Watanabe, Y.; Tsuji, Y.; Ige, H.; Ohsugi, Y.; Ohta, T. *J. Org. Chem.* **1984**, *49*, 3359–3363.
- (77) Del Zotto, A.; Baratta, W.; Sandri, M.; Verardo, G.; Rigo, P. *Eur. J. Inorg. Chem.* **2004**, *2004*, 524–529.
- (78) Grigg, R.; Mitchell, T. R. B.; Sutthivaiyakit, S.; Tongpenyai, N. *J. Chem. Soc. Chem. Commun.* **1981**, 611–612.
- (79) Tsuji, Y.; Takeuchi, R.; Ogawa, H.; Watanabe, Y. *Chem. Lett.* **1986**, *15*, 293–294.
- (80) Fujita, K.; Yamaguchi, R. *Synlett* **2005**, 560–571.
- (81) Fujita, K.; Li, Z.; Ozeki, N.; Yamaguchi, R. *Tetrahedron Lett.* **2003**, *44*, 2687–2690.
- (82) Fujita, K.; Enoki, Y.; Yamaguchi, R. *Tetrahedron* **2008**, *64*, 1943–1954.
- (83) Fujita, K.; Yamamoto, K.; Yamaguchi, R. *Org. Lett.* **2002**, *4*, 2691–2694.
- (84) Fujita, K.; Fujii, T.; Yamaguchi, R. *Org. Lett.* **2004**, *6*, 3525–3528.
- (85) Miao, L.; DiMaggio, S. C.; Shu, H.; Trudell, M. L. *Org. Lett.* **2009**, *11*, 1579–1582.
- (86) Zhu, M.; Fujita, K.; Yamaguchi, R. *Org. Lett.* **2010**, *12*, 1336–1339.
- (87) Saidi, O.; Blacker, A. J.; Lamb, G. W.; Marsden, S. P.; Taylor, J. E.; Williams, J. M. *J. Org. Process Res. Dev.* **2010**, *14*, 1046–1049.
- (88) Cami-Kobeci, G.; Slatford, P. A.; Whittlesey, M. K.; Williams, J. M. *J. Bioorg. Med. Chem. Lett.* **2005**, *15*, 535–537.
- (89) Blank, B.; Michlik, S.; Kempe, R. *Chem. - A Eur. J.* **2009**, *15*, 3790–3799.
- (90) Li, J.-Q.; Andersson, P. G. *Chem. Commun.* **2013**, *49*, 6131–6133.
- (91) Blaser, H.-U.; Pugin, B.; Spindler, F. In *Topics in Organometallic Chemistry*; Beller, M., Blaser, H.-U., Eds.; Springer Berlin Heidelberg, 2012; pp 65–102.
- (92) Ohkuma, T.; Kitamura, M.; Noyori, R. In *Catalytic Asymmetric Synthesis*; John Wiley & Sons, Inc.: Hoboken, NJ, USA, 2005; pp 1–110.
- (93) Malacea, R.; Poli, R.; Manoury, E. *Coord. Chem. Rev.* **2010**, *254*, 729–752.
- (94) Foubelo, F.; Yus, M. *Chem. Rec.* **2015**, *15*, 907–924.
- (95) Hollmann, D. *ChemSusChem* **2014**, *7*, 2411–2413.
- (96) Gladiali, S.; Alberico, E. *Chem. Soc. Rev.* **2006**, *35*, 226–236.
- (97) Palmer, M. J.; Wills, M. *Tetrahedron: Asymmetry* **1999**, *10*, 2045–2061.
- (98) Wang, C.; Wu, X.; Xiao, J. *Chem. - An Asian J.* **2008**, *3*, 1750–1770.
- (99) Müller, D.; Umbricht, G.; Weber, B.; Pfaltz, A. *Helv. Chim. Acta* **1991**, *74*, 232–240.

- (100) Murata, K.; Ikariya, T.; Noyori, R. *J. Org. Chem.* **1999**, *64*, 2186–2187.
- (101) Mashima, K.; Abe, T.; Tani, K. *Chem. Lett.* **1998**, *27*, 1199–1200.
- (102) Chen, J.; Li, Y.; Dong, Z.; Li, B.; Gao, J. *Tetrahedron Lett.* **2004**, *45*, 8415–8418.
- (103) Li, Y.-Y.; Zhang, H.; Chen, J.-S.; Liao, X.-L.; Dong, Z.-R.; Gao, J.-X. *J. Mol. Catal. A Chem.* **2004**, *218*, 153–156.
- (104) Dong, Z.-R.; Li, Y.-Y.; Chen, J.-S.; Li, B.-Z.; Xing, Y.; Gao, J.-X. *Org. Lett.* **2005**, *7*, 1043–1045.
- (105) Debono, N.; Besson, M.; Pinel, C.; Djakovitch, L. *Tetrahedron Lett.* **2004**, *45*, 2235–2238.
- (106) Paredes, P.; Díez, J.; Gamasa, M. P. *Organometallics* **2008**, *27*, 2597–2607.
- (107) McManus, H. A.; Barry, S. M.; Andersson, P. G.; Guiry, P. J. *Tetrahedron* **2004**, *60*, 3405–3416.
- (108) Fuentes, J. A.; France, M. B.; Slawin, A. M. Z.; Clarke, M. L. *New J. Chem.* **2009**, *33*, 466–470.
- (109) Maire, P.; Breher, F.; Schönberg, H.; Grützmacher, H. *Organometallics* **2005**, *24*, 3207–3218.
- (110) Dyson, G.; Frison, J.-C.; Whitwood, A. C.; Douthwaite, R. E. *Dalt. Trans.* **2009**, *100*, 7141–7151.
- (111) Petra, D. G. I.; Kamer, P. C. J.; Spek, A. L.; Schoemaker, H. E.; van Leeuwen, P. W. N. M. *J. Org. Chem.* **2000**, *65*, 3010–3017.
- (112) He, W.; Zhang, B.-L.; Jiang, R.; Liu, P.; Sun, X.-L.; Zhang, S.-Y. *Tetrahedron Lett.* **2006**, *47*, 5367–5370.
- (113) Lundgren, R. J.; Stradiotto, M. *Chem. - A Eur. J.* **2008**, *14*, 10388–10395.
- (114) Lovering, F.; Bikker, J.; Humblet, C. *J. Med. Chem.* **2009**, *52*, 6752–6756.
- (115) Nugent, T. C.; El-Shazly, M. *Adv. Synth. Catal.* **2010**, *352*, 753–819.
- (116) Ros, A.; Magriz, A.; Dietrich, H.; Ford, M.; Fernández, R.; Lassaletta, J. M. *Adv. Synth. Catal.* **2005**, *347*, 1917–1920.
- (117) Haraguchi, N.; Tsuru, K.; Arakawa, Y.; Itsuno, S. *Org. Biomol. Chem.* **2009**, *7*, 69–75.
- (118) Wang, D.-W.; Zeng, W.; Zhou, Y.-G. *Tetrahedron: Asymmetry* **2007**, *18*, 1103–1107.
- (119) Rong, Z.-Q.; Zhang, Y.; Chua, R. H. B.; Pan, H.-J.; Zhao, Y. *J. Am. Chem. Soc.* **2015**, *137*, 4944–4947.
- (120) Brown, J. A.; Irvine, S.; Kennedy, A. R.; Kerr, W. J.; Andersson, S.; Nilsson, G. N.

- Chem. Commun.* **2008**, 1115–1117.
- (121) Bennie, L. S.; Fraser, C. J.; Irvine, S.; Kerr, W. J.; Andersson, S.; Nilsson, G. N. *Chem. Commun.* **2011**, *47*, 11653–11655.
- (122) Kerr, W. J.; Mudd, R. J.; Paterson, L. C.; Brown, J. A. *Chem. - A Eur. J.* **2014**, *20*, 14604–14607.
- (123) Brown, J. A.; Cochrane, A. R.; Irvine, S.; Kerr, W. J.; Mondal, B.; Parkinson, J. A.; Paterson, L. C.; Reid, M.; Tuttle, T.; Andersson, S.; Nilsson, G. N. *Adv. Synth. Catal.* **2014**, *356*, 3551–3562.
- (124) Kerr, W. J.; Lindsay, D. M.; Reid, M.; Atzrodt, J.; Derdau, V.; Rojahn, P.; Weck, R. *Chem. Commun.* **2016**, *52*, 6669–6672.
- (125) Kerr, W. J.; Reid, M.; Tuttle, T. *ACS Catal.* **2015**, *5*, 402–410.
- (126) Kennedy, A. R.; Kerr, W. J.; Moir, R.; Reid, M. *Org. Biomol. Chem.* **2014**, *12*, 7927–7931.
- (127) Reid, M. PhD Thesis, University of Strathclyde, 2015.
- (128) Mityanov, V. S.; Perevalov, V. P.; Tkach, I. I. *Chem. Heterocycl. Compd.* **2013**, *48*, 1793–1800.
- (129) Valdés, H.; Poyatos, M.; Peris, E. *Organometallics* **2014**, *33*, 394–401.
- (130) Mudd, R. J. PhD Thesis, University of Strathclyde, 2016.
- (131) Clavier, H.; Nolan, S. P. *Chem. Commun.* **2010**, *46*, 841–861.
- (132) Falivene, L.; Credendino, R.; Poater, A.; Petta, A.; Serra, L.; Oliva, R.; Scarano, V.; Cavallo, L. *Organometallics* **2016**, *35*, 2286–2293.
- (133) Kelly, R. A.; Clavier, H.; Giudice, S.; Scott, N. M.; Stevens, E. D.; Bordner, J.; Samardjiev, I.; Hoff, C. D.; Cavallo, L.; Nolan, S. P. *Organometallics* **2008**, *27*, 202–210.
- (134) Gusev, D. G. *Organometallics* **2009**, *28*, 6458–6461.
- (135) Nelson, D. J.; Collado, A.; Manzini, S.; Meiries, S.; Slawin, A. M. Z.; Cordes, D. B.; Nolan, S. P. *Organometallics* **2014**, *33*, 2048–2058.
- (136) Henderson, R. K.; Jiménez-González, C.; Constable, D. J. C.; Alston, S. R.; Inglis, G. G. A.; Fisher, G.; Sherwood, J.; Binks, S. P.; Curzons, A. D. *Green Chem.* **2011**, *13*, 854.
- (137) Jiménez, M. V.; Fernández-Tornos, J.; Pérez-Torrente, J. J.; Modrego, F. J.; Winterle, S.; Cunchillos, C.; Lahoz, F. J.; Oro, L. A. *Organometallics* **2011**, *30*, 5493–5508.
- (138) Blanco, M.; Álvarez, P.; Blanco, C.; Jiménez, M. V.; Fernández-Tornos, J.; Pérez-Torrente, J. J.; Oro, L. A.; Menéndez, R. *ACS Catal.* **2013**, *3*, 1307–1317.

- (139) Riener, K.; Bitzer, M. J.; Pöthig, A.; Raba, A.; Cokoja, M.; Herrmann, W. A.; Kühn, F. E. *Inorg. Chem.* **2014**, *53*, 12767–12777.
- (140) Slone, C. S.; Weinberger, D. A.; Mirkin, C. A. John Wiley & Sons, Inc.; pp 233–350.
- (141) Crudden, C. M.; Allen, D. P. *Coord. Chem. Rev.* **2004**, *248*, 2247–2273.
- (142) Huang, J.; Stevens, E. D.; Nolan, S. P. *Organometallics* **2000**, *19*, 1194–1197.
- (143) Chilvers, M. J.; Jazzar, R. F. R.; Mahon, M. F.; Whittlesey, M. K. *Adv. Synth. Catal.* **2003**, *345*, 1111–1114.
- (144) Danopoulos, A. A.; Winston, S.; Hursthouse, M. B. *J. Chem. Soc., Dalton Trans.* **2002**, 3090–3091.
- (145) Steele, K. Final Year Thesis, University of Strathclyde, 2017.
- (146) Gomtsyan, A. *Chem. Heterocycl. Compd.* **2012**, *48*, 7–10.
- (147) Taylor, A. P.; Robinson, R. P.; Fobian, Y. M.; Blakemore, D. C.; Jones, L. H.; Fadeyi, O. *Org. Biomol. Chem.* **2016**, *14*, 6611–6637.
- (148) Vitaku, E.; Smith, D. T.; Njardarson, J. T. *J. Med. Chem.* **2014**, *57*, 10257–10274.
- (149) Taber, D. F.; Tirunahari, P. K. *Tetrahedron* **2011**, *67*, 7195–7210.
- (150) Guo, T.; Huang, F.; Yu, L.; Yu, Z. *Tetrahedron Lett.* **2015**, *56*, 296–302.
- (151) Humphrey, G. R.; Kuethe, J. T. *Chem. Rev.* **2006**, *106*, 2875–2911.
- (152) Brereton, R. *Applied Chemometrics for Scientists*; John Wiley & Sons, Ltd.: West Sussex, U.K., 2008.
- (153) Leardi, R. *Anal. Chim. Acta* **2009**, *652*, 161–172.
- (154) Jiménez, M. V.; Fernández-Tornos, J.; Pérez-Torrente, J. J.; Modrego, F. J.; García-Orduña, P.; Oro, L. A. *Organometallics* **2015**, *34*, 926–940.
- (155) Truscott, B. J.; Nelson, D. J.; Lujan, C.; Slawin, A. M. Z.; Nolan, S. P. *Chem. - A Eur. J.* **2013**, *19*, 7904–7916.
- (156) Hagiya, K.; Mitsui, S.; Taguchi, H. *Synthesis (Stuttg.)* **2003**, *2003*, 823–828.
- (157) Glorius, F.; Altenhoff, G.; Goddard, R.; Lehmann, C. *Chem. Commun.* **2002**, 2704–2705.
- (158) Yoshida, K.; Horiuchi, S.; Takeichi, T.; Shida, H.; Imamoto, T.; Yanagisawa, A. *Org. Lett.* **2010**, *12*, 1764–1767.
- (159) Armarego, W. L. F.; Chai, C. L. L. *Purification of Laboratory Chemicals*; Elsevier, 2009.
- (160) Kuriyama, M.; Matsuo, S.; Shinozawa, M.; Onomura, O. *Org. Lett.* **2013**, *15*, 2716–2719.
- (161) Lood, C. S.; Koskinen, A. M. P. *European J. Org. Chem.* **2014**, *2014*, 2357–2364.

- (162) Pirali, T.; Tron, G. C.; Zhu, J. *Org. Lett.* **2006**, *8*, 4145–4148.
- (163) Zhao, Y.; Gilbertson, S. R. *Org. Lett.* **2014**, *16*, 1033–1035.
- (164) Kumar, M. R.; Park, K.; Lee, S. *Adv. Synth. Catal.* **2010**, *352*, 3255–3266.
- (165) Kuriyama, M.; Hamaguchi, N.; Yano, G.; Tsukuda, K.; Sato, K.; Onomura, O. *J. Org. Chem.* **2016**, *81*, 8934–8946.
- (166) Gutiérrez, R. U.; Rebollar, A.; Bautista, R.; Pelayo, V.; Várgas, J. L.; Montenegro, M. M.; Espinoza-Hicks, C.; Ayala, F.; Bernal, P. M.; Carrasco, C.; Zepeda, L. G.; Delgado, F.; Tamariz, J. *Tetrahedron: Asymmetry* **2015**, *26*, 230–246.
- (167) Standley, E. A.; Jamison, T. F. *J. Am. Chem. Soc.* **2013**, *135*, 1585–1592.
- (168) Doni, E.; Mondal, B.; O’Sullivan, S.; Tuttle, T.; Murphy, J. A. *J. Am. Chem. Soc.* **2013**, *135*, 10934–10937.
- (169) Danthi, S. N.; Hill, R. A. *J. Heterocycl. Chem.* **1997**, *34*, 835–844.
- (170) Fawcett, J.; Harding, D. A. J.; Hope, E. G.; Singh, K.; Solan, G. A. *Dalt. Trans.* **2010**, *39*, 10781–10789.
- (171) Hanson, S. S.; Doni, E.; Traboulsee, K. T.; Coulthard, G.; Murphy, J. A.; Dyker, C. *A. Angew. Chemie Int. Ed.* **2015**, *54*, 11236–11239.
- (172) Flahaut, A.; Roland, S.; Mangeney, P. *J. Organomet. Chem.* **2007**, *692*, 5754–5762.
- (173) Zhou, W.; Fan, M.; Yin, J.; Jiang, Y.; Ma, D. *J. Am. Chem. Soc.* **2015**, *137*, 11942–11945.
- (174) Gülcemal, D.; Gülcemal, S.; Robertson, C. M.; Xiao, J. *Organometallics* **2015**, *34*, 4394–4400.
- (175) Zou, Q.; Wang, C.; Smith, J.; Xue, D.; Xiao, J. *Chem. - A Eur. J.* **2015**, *21*, 9656–9661.
- (176) Zhu, X.; Su, L.; Huang, L.; Chen, G.; Wang, J.; Song, H.; Wan, Y. *European J. Org. Chem.* **2009**, 635–642.
- (177) Neumann, J. J.; Rakshit, S.; Dröge, T.; Glorius, F. *Angew. Chemie Int. Ed.* **2009**, *48*, 6892–6895.
- (178) Rawlings, A. J.; Diorazio, L. J.; Wills, M. *Org. Lett.* **2015**, *17*, 1086–1089.
- (179) Castro, L. C. M.; Sortais, J.-B.; Darcel, C. *Chem. Commun.* **2012**, *48*, 151–153.
- (180) Sakai, N.; Takahashi, N.; Ogiwara, Y. *European J. Org. Chem.* **2014**, *2014*, 5078–5082.
- (181) Kanchupalli, V.; Joseph, D.; Katukojvala, S. *Org. Lett.* **2015**, *17*, 5878–5881.
- (182) Youn, S. W.; Kim, Y. H. *Org. Lett.* **2016**, *18*, 6140–6143.
- (183) Zhang, Y.; Zhu, J.; Xia, Y.-T.; Sun, X.-T.; Wu, L. *Adv. Synth. Catal.* **2016**, *358*,

3039–3045.

- (184) Wu, J.; Wang, C.; Tang, W.; Pettman, A.; Xiao, J. *Chem. - A Eur. J.* **2012**, *18*, 9525–9529.
- (185) Dydio, P.; Rubay, C.; Gadzikwa, T.; Lutz, M.; Reek, J. N. H. *J. Am. Chem. Soc.* **2011**, *133*, 17176–17179.
- (186) Perry, M. C.; Cui, X.; Powell, M. T.; Hou, D.-R.; Reibenspies, J. H.; Burgess, K. *J. Am. Chem. Soc.* **2003**, *125*, 113–123.
- (187) Porcar, R.; Ríos-Lombardía, N.; Busto, E.; Gotor-Fernández, V.; Gotor, V.; Garcia-Verdugo, E.; Isabel Burguete, M.; Luis, S. V. *Catal. Sci. Technol.* **2013**, *3*, 2596–2601.
- (188) Ray, L.; Katiyar, V.; Barman, S.; Raihan, M. J.; Nanavati, H.; Shaikh, M. M.; Ghosh, P. *J. Organomet. Chem.* **2007**, *692*, 4259–4269.
- (189) Allegue, A.; Albert-Soriano, M.; Pastor, I. M. *Appl. Organomet. Chem.* **2015**, *29*, 624–632.